Copyright is owned by the Author of the thesis. Permission is given for a copy to be downloaded by an individual for the purpose of research and private study only. The thesis may not be reproduced elsewhere without the permission of the Author.

Modelling the impact of temperature on microalgae productivity during outdoor cultivation

A thesis presented in partial fulfilment of the requirements for the degree of

Doctor of Philosophy

in Environmental Engineering

at Massey University, Palmerston North, New Zealand.

Quentin Béchet

2014

Abstract

Accurate predictions of algal productivity during outdoor cultivation are critically needed to assess the economic feasibility and the environmental impacts of full-scale algal cultivation. The literature shows that current estimations of full-scale productivities are mainly based on experimental data obtained during lab-scale experiments conducted under conditions poorly representative of outdoor conditions. In particular, the effect of temperature variations on algal productivity is often neglected. The main objective of this thesis was to develop a model able to predict algal productivity under the dynamic conditions of temperature and light representative of full-scale cultivation. In a first step, models were developed to predict broth temperature as a function of climatic, operational, and design parameters. The model developed for open ponds could predict temperature at an accuracy of $\pm 2.6^{o}C$ when assessed against experimental data collected in New Zealand over one year. The temperature model developed for closed photobioreactors was accurate at $\pm 4.3^{o}C$ when compared to experimental data collected in Singapore and New Zealand over a total of 6 months of cultivation. This second temperature model was then applied at different climatic locations to demonstrate that actively controlling temperature would seriously threaten the economics and sustainability of full-scale cultivation in photobioreactors.

To quantify the impact of temperature variations on biomass productivity, a productivity model was developed using *Chlorella vulgaris* as a representative commercial species. To determine the best methodology, a review of more than 40 models described in the literature revealed that an approach accounting for light gradients combined with an empirical function of temperature for photosynthesis and first-order kinetics for respiration would offer the most pragmatic compromise between accuracy and complexity. The model was parameterized using short-term indoor experiments and subsequently validated using independent bench-scale indoor (> 160 days) and pilot-scale outdoor (> 140 days) experiments, showing prediction accuracies of ± 13%. The outdoor data set was obtained from 13 different experiments performed in 4 different reactors operated under various regimes and climatic conditions. The productivity model was found to be accurate enough to significantly refine previous assessments of the economics and the environmental impacts of full-scale algal cultivation.

The productivity model was then used in different case studies in order to investigate the impact of location/climate, design (pond depth or reactor diameter), and operation (hydraulic retention time or HRT) on productivity and water demand. Although the qualitative impact of the HRT on process was already known, this application enabled the first quantification of the HRT value on the productivity. Low HRT values around 3 days were found to maximize productivity at most locations investigated but these operating conditions were associated with a large water demand, illustrating a poorly acknowledged trade-off between sustainability and revenues. The model was also used to demonstrate that actively controlling the pond depth can increase the productivity by up to 23% while minimizing the water demand by up to 46%. This thesis therefore revealed that the choice of a location for algal full-scale production must be based on the comparison of optimized systems, contrarily to current assessments assuming the same design and operation at different locations.

Preface

In the 90s, the terrestrial plant *Jatropha curcus* was considered as a prime candidate for biofuel production. For example, Foidl et al. (1996) concluded that "for developing countries […] *Jatropha curcus* seems to be a very promising energy plant. The plant can be grown on very poor soil and gives a high yield of seeds". Driven by these initial observations, the cultivation of Jatropha was encouraged by India and China on a large scale. In 2008, Jatropha was cultivated on 900,000 hectares of land (Kant and Wu, 2011). However, the actual productivities were far below expectations, for reasons that Kant and Wu (2011) qualified as "nothing out of the ordinary and [which] should have been anticipated". Indeed, the initial studies were carried under conditions that did not represent full-scale cultivation conditions. In particular, even if Jatropha can survive in a dry environment, the seed production only happens when the plant is cultivated in wet and warm conditions that are often not met on marginal lands (Weyerhaeuser et al., 2007).

With the same objective to replace fossil fuels with sustainable fuels, microalgae received the same enthusiasm than Jatropha two decades earlier. For example, Chisti (2008) claimed that "biodiesel from microalgae seems to be the only renewable biofuel that has the potential to completely displace petroleum-derived transport fuel without adversely affecting supply of food and other crop products." Similar claims were made by Leite et al. (2013): "The production of biofuels using microalgae is promising since of all photosynthetic organisms they have the highest growth rates, and they can be cultivated using non-arable land with wastewater as a source of nutrients." However, the assessments of the biofuel production from microalgae are based on observations in indoor laboratories where algae were cultivated under ideal conditions that do not represent full-scale conditions. Moving to full-scale algal cultivation for biofuel production may therefore lead to reproduce the "extraordinary collapse of Jatropha" denounced by Kant and Wu (2011). This is the main motivation for the work undertaken in this thesis.

Acknowledgments

First, I want to sincerely thank my main supervisor Professor Benoit Guieysse for his great supervision, his guidance, and his endless flow of ideas. Benoit's humility and never-ending enthusiasm have been a constant inspiration during all my PhD. I would also like to acknowledge and thank my co-supervisor Professor Andy Shilton for his excellent advice, his wise management and his patience, especially with regard to my English writing skills. I am very thankful to Benoit and Andy for treating me as one of their peers in spite of my tendency to constantly disagree with them.

Many thanks to all the staff at Massey; in particular, Ann-Marie Jackson was extremely patient despite of the fact I was sometimes a "difficult child". I will also always remember all the working sessions with John Edwards who, among other things, taught me to properly use a screwdriver. Many thanks also to Julia Good for her help which always came with a smile, Judy Farrand-Collins, Anthony Wade, Bruce Collins, John Sykes, and all the team of the SEAT workshop (Kerry Griffiths, Ian Thomas, and Clive Davis). A special attention goes to Guillaume Guizard (LBE, Narbonne) who showed me the crucial importance of designing properly experimental set-ups. I also would like to thank Glenda Rosoman, Fiona Falconer and Linda Lowe for their extremely efficient and always friendly help with the administrative aspects of my PhD.

I wish also to thank Oliver Fringer (Stanford University, California) and the National Technological University of Singapore for contributing to preliminary work of this PhD. I also would like to thank Filipa Lopes and Arsène Isembert for welcoming me to the reputed LGPM laboratory of Ecole Centrale Paris in 2010. Many thanks also go to Olivier Bernard who allowed me to enjoy the outstanding working conditions of the LOV laboratory (France) in 2011. NIWA (Hamilton, New Zealand) and the LBE (Narbonne, France) must also be acknowledged for their assistance for providing data for model validation.

I wish to thank Massey University for their financial support through the Massey University Doctoral Scholarship.

Many thanks go to my PhD colleagues who shared with me the joys of the PhD thesis (in particular Matthew Chung, Maxence Plouviez, Zane Norvill, and Roland Schaap). I will also keep in my memory all the interns who came to share our enthusiasm for research. In

particular I wish to thank Laura Etienne, Ivan Feurgard, Nicolas Dumont, Paul Chambonnière, Alexandre Camuel, and Mégan Trémelot who accepted me as an unexperienced supervisor.

I am very thankful to all my friends and my partner for their support during my PhD. Finally, I could never express enough the gratitude to my mother and my father for their limitless trust and their continuous support.

Table of contents

List of illustrations

List of Tables

Structure of the thesis

This thesis is based on six scientific articles attached as appendix at the end of this thesis (four of which have been published). The content of these articles supports the conclusions provided in this thesis. To avoid redundancy (especially the description of materials and methods) or discussion of information not strictly relevant to this thesis (e.g. water footprint in Article 6), the chapters were organized and written based on the articles rather than from the articles. Key results and findings are referred to corresponding articles wherever relevant.

List of Articles and contribution

Article 1: Béchet Q, Shilton A, Guieysse B. 2013. Modelling the effects of light and temperature on algae growth: State of the art and critical assessment for productivity prediction during outdoor cultivation. Biotechnology Advances 31(8): 1648-1663. (2012 Impact factor: 9.599; Number of citations[1]: 5)

Contribution to the article: Q Béchet was the main contributor to the review. In particular, the classification of productivity models was originally proposed by Q Béchet.

Article 2: Béchet Q, Shilton A, Park JBK, Craggs RJ, Guieysse B. 2011. Universal temperature model for shallow algal ponds provides improved accuracy. Environmental Science & Technology 45(8): 3702-3709. (2012 Impact factor: 5.257; Number of citations: 15)

Contribution to the article: Q Béchet was the main contributor to the article. He constructed and numerically implemented the temperature model. The experimental data used for model validation were provided by the New Zealand National Institute for Water and Atmospheric Research (NIWA).

Article 3: Béchet Q, Shilton A, Fringer OB, Muñoz R, Guieysse B. 2010. Mechanistic modeling of broth temperature in outdoor photobioreactors. Environmental Science & Technology 44 (6): 2197-2203. (2012 Impact factor: 5.257; Number of citations: 25)

Contribution to the article: Q Béchet was the main contributor to the article. He constructed and numerically implemented the temperature model. He also collected the experimental data used for model validation.

Article 4: Béchet Q, Chambonnière P, Shilton A, Guizard G, Guieysse B. Algal productivity modeling: a step toward accurate assessments of full-scale algal cultivation (submitted).

[1] According to Google Scholar Citations on the 02/07/2014

Contribution to the article: Q Béchet supervised the student P Chambonnière who performed most of the experimental work for model parameterization and the associated data analysis. Q Béchet did the experimental work for model validation and associated simulations. He also wrote most of the article.

Article 5: Béchet Q, Shilton A, Guieysse B. Full-scale validation of a model of algal productivity (submitted).

Contribution to the article: Q Béchet was the main contributor of the article. He carried the experimental work and analyzed the results (including the numerical implementation of the model). He also wrote most of this article.

Article 6: Guieysse B, Béchet Q, Shilton A. 2013. Variability and uncertainty in water demand and water footprint assessments of fresh algae cultivation based on case studies from five climatic regions. Bioresource Technology 128: 317–323. (2012 Impact factor: 4.750; Number of citations: 10)

Contribution to the article: Q Béchet performed the calculations of water demand and water footprint of algal cultivation in open ponds by using the code he developed for Article 2.

Note: Even if Article 6 discusses the water footprint of algal cultivation, this metric will not be discussed in this thesis as its relevance is uncertain (see the discussion section of Article 6 for further details). In this thesis, only the water demand will be considered to discuss the environmental impacts of full-scale cultivation.

Thesis Introduction

Billions of dollars have been invested in research on algal biofuels in the past decade (Mascarelli, 2009). At the origin of this "green rush" were optimistic estimations of productivity suggesting that biofuels from microalgae could beat current technologies of biofuel production (bio-ethanol) while being more sustainable. For instance, Chisti (2008) estimated that 123 m^3 of algal-based oil could be produced per hectare per year, meaning that "only" 3% of the US cropping area would need to be allocated for algae cultivation to meet the demand of transport fuel in the US. These first estimations were based on the assumption that fast algal growth could occur simultaneously with high lipid production. This has been subsequently challenged (Walker, 2009) and current estimates place the oil production at around 33-44 m^3 of oil per hectare and per year (Stephenson et al., 2010; assuming an oil density of 900 kg/m^3). However, these estimations are based on experimental results observed in laboratory and there is still no evidence that this level of productivity can be reached at full-scale. This is of significant concern as overestimating the productivity at full-scale may have important consequences on the assessment of the cost-efficiency of the process (e.g. overestimation of projected revenues). In addition, the environmental impacts of full-scale cultivation cannot be precisely assessed without accurate productivity predictions (e.g. water resources[2]).

A particularly neglected area of concern is the potential impact of temperature on productivity because most of the light energy received by the algae is converted into heat. Indeed, as temperature cannot be economically controlled at full-scale as further discussed in Article 3, the absorption of light energy can cause significant temperature fluctuations over time (Tredici and Materassi, 1992). Table I.1 thus shows that out of eleven recent feasibility assessments of full-scale algal cultivation, only three studies considered the impact of temperature on productivity. These three studies predicted productivities 2 to 3 times lower than the other eight assessments. Although the modelling approaches used by these three studies to account for temperature were relatively simplistic, these significant differences indicate that temperature may have a high impact on productivity. Yet, there is currently no

[2] In the entire thesis, the water demand associated with full-scale algae cultivation is used to represent the environmental impacts of the technology as water was identified as a critical resource by previous studies (Clarens et al., 2009; Murphy and Allen, 2011; Sander and Murthy, 2010; Sun et al., 2011).

suitable engineering tool available to quantify the impact of temperature on algal productivity in outdoor systems.

Table I.1: Characteristics of recent assessments of full-scale algal cultivation for biofuel productions.

Study	**Location/Climate**	**Productivity (kg/m^2-yr)**	**Was temperature considered?**
Batan et al. (2013)	Arizona	5.3	Yes
	California	5.3	
	Colorado	3.6	
	Montana	2.9	
	Nebraska	3.4	
	Nevada	3.8	
	New Mexico	4.7	
	Texas	4.7	
	Utah	3.9	
	Wyoming	3.3	
Wigmosta et al. (2011)	United States	1.05-3.8	Yes
Yang et al. (2011)	United States[1]	4.9	Yes
Campbell et al. (2011)	Australia	11.0	No
Lardon et al. (2009)	Mediterranean climate	7.3 – 11.0	No
Pate et al. (2011)	South west of US	11.3	No
	Midwest of US	7.0	
	South-East of US	7.7	
	Nineteen Lower-Tier State of US	9.1	
Rogers et al. (2013)	New Mexico	5.5	No
Slade and Bauen (2013)	NS	3.6-14.6	No
Stephenson et al. (2010)	United Kingdom	10	No
Sun et al. (2011)	NS	7.3	No
Wang et al. (2013)	Japan	14.2 – 16.0 23.7 – 31.6	No

[1]Value representing the average value over 28 states of the US.

The literature already contains numerous examples of productivity models but the majority of these models were developed under conditions that do not represent full-scale conditions. This limitation is extensively discussed in Chapter 1 (see Table 1.1 summarizing the characteristics of the modelling studies existing in the literature). This thesis was therefore undertaken with

the objective to develop, validate, and apply a model of algal productivity in outdoor cultivation systems. To develop such a model, the following steps were required:

- To develop mathematical models for prediction of broth temperature during algae cultivation in closed photobioreactors and open ponds.
- To develop a model predicting outdoor algal productivity under transient conditions of light and temperature.
- To validate this productivity model against outdoor data.

Chapter 1 critically discusses prior modelling approaches of algal productivity and highlights their limitations for productivity predictions in full-scale cultivation systems. Chapter 2 describes the design and operation of typical algal cultivation systems and defines the scope of this thesis. Chapter 3 describes how the temperature models in closed photobioreactors and open ponds were developed and validated. Chapter 4 shows how the productivity model was developed and validated against full-scale data. Chapter 5 presents how these different models can be used to optimize design and operation to maximize productivity and minimize environmental impacts during full-scale cultivation.

Chapter 1: Literature review

Preface

With the objective to develop an engineering tool suitable for the assessment of full-scale algal cultivation, this chapter reviews previous approaches for modelling algal productivity. The first objective of this review was to discuss the ability of these existing models to predict productivity in full-scale systems. The second objective was to determine the best modelling approach to use in this thesis.

1.1. Introduction

The economics of microalgae cultivation largely depends on the area of land and amounts of resources needed to support a target productivity (Pate et al., 2011; Sun et al., 2011). In particular, the land area required depends on the amount of sunlight reaching the ground surface at the selected location and the fraction of this sunlight that the algae can convert into biomass during photosynthesis. In order to minimize land use (e.g. capital costs), algal growth should therefore be only limited by light. In practice, maintaining the pH at its optimal value can be done by CO_2 injection and nutrient concentrations can be maintained at saturation (Grobbelaar, 2009). Concentration gradients can occur under poor mixing conditions and cause local nutrient limitation (e.g. CO_2) or oxygen inhibition (Keymer et al., 2013; Mata et al., 2010). These can generally be prevented via adequate design and operation (Benemann et al., 1987). By contrast, temperature cannot be easily (economically) controlled at full-scale, meaning that algae experience significant temperature change over time (see Figure 1 of Article 2 and Figure 2 of Article 3 for an illustration). It results that any meaningful assessment of full-scale algae cultivation should consider the impact of both light and temperature on productivity. This chapter therefore focuses on the modelling approaches that account for the impact of light and temperature on productivity.

Biomass productivity can be expressed as the difference between the rate of biomass production through photosynthesis and the rate of biomass loss due to endogenous respiration (referred to as "respiration" in the rest of the thesis). Photosynthesis enables the conversion of photons into chemical energy in the form of ATP and NADPH molecules. A fraction of this energy is directly used by cells as an energy source during day-time respiration. The other fraction of these ATP and NADPH molecules is used to convert CO_2 into organic material during the Calvin Cycle (Madigan and Martinko, 2006). The resulting organic material is then used either as a carbon source during biomass production or as an energy source during night-time respiration.

The first section (1.2) describes how light and temperature qualitatively impact the rates of photosynthesis and respiration at the cell level. The second section (1.3) discusses how this theoretical knowledge was used to develop models of productivity in the literature. This section proposes a classification of the existing modelling approaches based on the mechanisms that these models can theoretically account for. The third section of this review (1.4) describes the practical issues encountered when using these modelling approaches to

predict productivity of full-scale cultivation systems. From the knowledge gaps identified, the last section (1.5) provides recommendations on the modelling approach to predict algal productivity at full-scale. For clarity, key-terms relevant to this chapter are defined in Box 1.1.

Box 1.1: Definition of key terms

Endogenous respiration (or respiration): Photosynthesis generates chemical energy in the form of ATP, NADPH, and organic material. Respiration is defined as the consumption of this chemical energy (for maintenance and other non-growth related processes).

Net photosynthesis: Difference between the rate of gross photosynthesis (or photosynthesis) and the rate of respiration (expressed in kg O_2/s).

Algal productivity: Rate of net biomass production expressed as the difference between the rate of biomass production and the rate of biomass loss (in kg/s).

Photosynthetic unit (PSU): Cell component responsible for the photosynthetic process leading to the generation of ATP and NADPH (as defined by Camacho Rubio et al., 2003).

Light-inhibition: The degradation of key proteins at high light intensities causes a decrease of the rate of photosynthesis over time. For light-inhibition to become significant, algae cells must be exposed to inhibitive light intensities for a time period in the order of one minute (Ferris and Christian, 1991). Light-inhibition can impact productivity after exposure to high light intensities because damaged cells need time to recover.

Light-acclimation: Change of cellular physiology associated with photosynthesis, such as the change of pigment content in the cell (Bernard, 2011; Crill, 1977; Geider and MacIntyre, 1996; Sakshaug et al., 1991). Light-acclimation occurs on a timescale longer than light-inhibition and can take several hours to days to cause significant changes in pigment content (Crill, 1977).

Flashing-light effect: Following the capture of photons, the photosynthetic units (PSUs) of algae cells need approximately 100 milliseconds to convert light energy into NADPH and ATP. During this time, any photon reaching 'excited' PSUs is wasted. As a result, cells exposed to flashing light with a light/dark cycle close to 100 milliseconds waste less light energy than cells exposed to continuous light (Grobbelaar, 1991, 1994; Janssen et al., 2003; Luo and Al-Dahhan, 2004). The increase of photosynthetic efficiency resulting from cell exposure to flashing light is called the flashing-light effect.

1.2. The effect of light and temperature on algal productivity at the cell level

1.2.1. The PI relationships

The fundamental relationship between light intensity and photosynthesis for individual cells is often represented by 'PI relationships' (P for photosynthetic rate and I for light intensity) depicting three distinct light regimes, as shown by Figure 1.1:

i) At low light intensities, the rate of photosynthesis is usually proportional to light intensity because photosynthesis is limited by the rate of capture of photons.
ii) When light intensity reaches a saturation threshold (I_k), algae become 'light-saturated' because their photosynthetic rate is now limited by the rate of the reactions following the capture of photons (Crill, 1977). Under this condition, the rate of photosynthesis is usually maximal and independent of light intensity.
iii) If light intensity further increases beyond an inhibitory threshold (I_{inhib}), the rate of photosynthesis starts to decrease with light intensity due to the deactivation of key proteins in the photosynthetic units (Camacho Rubio et al., 2003).

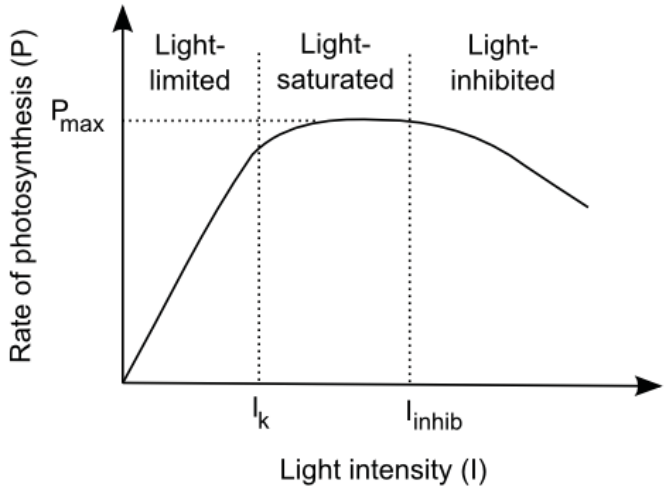

Figure 1.1: Typical PI relationship showing the light-limited ($I < I_k$), light-saturated ($I_k < I < I_{inhib}$), and light-inhibited ($I > I_{inhib}$) regimes of microalgae light response – *Extracted from Article 1*.

Mathematical expressions of PI relationships

There is no clear consensus on the most suitable mathematical expression to describe PI relationships (Table 1 of Article 1). For example, Jassby and Platt (1976) tested eight mathematical expressions and concluded that a hyperbolic tangent model was the best formula. By contrast, Lee et al. (1987) demonstrated that a simplified light-inhibition model provided a better fit against other models. Alternatively, Monod-like models derived by analogy to bacterial growth on organic material have also been used to model PI relationships. These models consider light as a substrate for algal photosynthesis and the rate of photosynthesis is modelled as:

$$P = P_m \frac{I}{I_k + I} X \quad (1.1)$$

where P is the specific rate of photosynthesis (kg O_2/s), P_m is the maximum specific rate of photosynthesis (kg O_2/kg-s), I is the light intensity reaching the cells (W/m^2), I_k is the half-saturation constant (W/m^2), and X is the algal concentration (kg/m^3). A mechanistic justification to Monod-like kinetics was provided by Han (2001) who considered photosynthesis as a two-step process involving the subsequent activation and deactivation of photosynthetic units (see Box 1.1 for definition). Alternative models assume that the rate at which photons 'strike' photosynthetic units follows a Poisson distribution, leading to the following expression for the rate of photosynthesis:

$$P = P_m \left(1 - \exp\left(1 - \frac{I}{I_k} \right) \right) X \quad (1.2)$$

where the different symbols are defined similarly to the symbols in Equation 1.1.

PI relationships and light-inhibition

The level of light-inhibition experienced by cells does not only depend on the instantaneous light intensity, as depicted in typical PI relationships, but also on pre-exposure to high or low irradiances due to light-inhibition and light-acclimation (see Box 1.1 for definitions). For example, Beardall and Morris (1976) and Falkowski and Owens (1978) showed that algae cells pre-exposed to a high light intensity had a lower productivity than cells pre-exposed to dark conditions (which is called the 'hysteresis effect'). The dynamic effects of light-inhibition are often not accounted for in the determination of PI relationships (Table 1.1), which implies that the use of simple PI-based models may overestimate productivity during outdoor cultivation. To account for light-inhibition, Denman and Marra (1986) considered

that the rate of photosynthesis of *Lauderia borealis* for a given light intensity could vary between two values corresponding to a fully-inhibited state and a non-inhibited state. The actual rate of photosynthesis at a given light intensity was then determined based on the level of light-inhibition experienced by the algae using a dynamic model accounting for light variation.

1.2.2. Effect of temperature on photosynthesis and respiration

This paragraph is mostly based on the study of Davison (1991) who thoroughly reviewed the literature to describe the impact of temperature on photosynthesis and respiration. In the short-term, temperature has different impacts on the rate of photosynthesis depending if the cells are light-limited, light-saturated or light-inhibited. When cells are light-limited, the light reactions associated with the capture of photons by photosynthetic pigments are usually assumed to be temperature-independent. As a result, the rate of photosynthesis of light-limited cells can be assumed to be independent on temperature. However, Davison (1991) also reports that even at low light intensities, the rate of photosynthesis can be limited by associated aspects of photosynthesis (transport enzymes, etc.) which can be impacted by temperature. This temperature dependence for the algal species *Chlorella vulgaris* used in this thesis is further discussed in Chapter 4. When cells are light-saturated, the rate of photosynthesis of cells is limited by biochemical reactions in the electron transport chain following the capture of photons (the "Z-scheme") or in the carbon capture process (the "Calvin Cycle"; Madigan and Martinko, 2006). As the rates of these reactions are controlled by enzymes, the rate of photosynthesis of light-saturated algae is dependent of temperature. As discussed by Borowitzka (1998), the light intensity at which algal cells are light-inhibited is also a function of temperature. For instance, the inhibitive light intensity I_{inhib} (Figure 1.1) was shown to increase with temperature for the algal species *Phormidium bohneri*. This dependence is due to the fact that biological mechanisms associated with light-inhibition are regulated by enzymes and are therefore temperature dependent. The occurrence of light-inhibition in the algal species *Chlorella vulgaris* used in this thesis is further discussed in Chapter 4.

In the long-term, algae tend to adapt their biochemistry to the temperature of the culture medium although this ability remains limited to a certain temperature range. For example, de-Bashan et al. (2008) showed *Chlorella sorokiniana* can grow at high temperature (40^{o}C) after a period of five days of acclimation at this temperature. The capacity of algal cells to

acclimate to temperature also depends on the species. For example, Kvíderová and Lukavský (2005) compared different strains of the algal species *Stichococcus* originating from localities with different temperature profiles. The strains from "cold" localities were able to grow at relatively cold temperatures, but all the strains were found to have the same maximal temperature limit. Temperature also impacts the rate of respiration as the consumption of the energy generated through photosynthesis is controlled by enzymes. For example, the study of Collins and Boylen (1982) showed that the specific rate of respiration of *A. variabilis* increased by a factor 5 when temperature varied from 10^{o}C to 40^{o}C. This strong dependence on temperature suggests that it is necessary to account for temperature in productivity models.

1.3. Current modelling approaches to predict algal productivity

The objective of this section is to critically review the various modelling approaches developed by prior studies to predict productivities in full-scale cultivation systems. The first section (1.3.1) describes the biological mechanisms that should be accounted for in full-scale cultivation systems. The second section (1.3.2) details how these mechanisms were accounted for in prior modelling approaches. The four following sections critically discuss the previous modelling approaches in order to determine the best model for the engineering purposes of this thesis. In detail, Sections 1.3.3 and 1.3.4 focus on modelling the rate of photosynthesis, Section 1.3.5 examines existing models of light distribution and Section 1.3.6 discusses models of respiration. Finally, Section 1.3.7 summarizes the modelling approach that was followed in this thesis.

1.3.1. Predicting productivity at full-scale: challenges

Predicting the rate of biomass production at full-scale is challenging, even under the assumption that light and temperature are the only factors impacting productivity. First, algal concentration should be kept high enough to ensure that all the light entering the system is captured by the algae. High algal concentrations should therefore maximize algal productivity and minimize capital and harvesting costs (Sánchez Mirón et al., 1999). These high concentrations cause light gradients to occur and individual cells experience different light intensities depending on their location in the system. Another consequence from light gradients in well-mixed systems is that individual algae cells experience short light cycles when they travel from high-light zones to near-dark zones. This cycling may reduce light-inhibition and enable the flashing-light effect (as defined in Box 1.1). Secondly, algae cultures cultivated outdoors are exposed to changing conditions of light and temperature. Acclimation processes are therefore expected to impact the light and temperature responses of algae across seasons. The accuracy of models described in the literature should therefore reflect the ability of the modelling approach to account for the impact of light gradients, short light cycles and acclimation processes.

1.3.2. Modelling algal productivity: state of the art

Table 1.1 classifies the experimental conditions used by prior modelling studies to generate data sets used for model development and/or validation according to six main criteria:

- *Outdoor*: "Yes" means that cultivation was carried out outdoors;
- *Dynamic*: "Yes" means that cultivation was carried out under dynamic conditions of light and/or temperature;
- *Time*: duration of the experiment;
- *Dense*: "Yes" means that cultivation was carried out at an algal concentration high enough to generate light gradients and short-light cycles in the algal broth;
- *Data set*: "Yes" means that the model was tested against data that was not used to determine the kinetic parameters of the model;
- *Measurement*: Experimental technique used to measure productivities (O_2: oxygen production/consumption rates, C: carbon release/fixation rate; CC: cell counts, OD: optical density; DW: dry weight; T: turbidity).

Table 1.1 shows that most of the previous modelling studies have not been independently validated[3] and/or validated against outdoor cultivation data (*Outdoor* and *Data set* criteria). This lack of validation is problematic as most models were developed under conditions that do not represent full-scale cultivation conditions. In particular, the impact of light-acclimation was rarely accounted for as most of experiments were performed over short periods of time (*Time* criteria) or simply under constant light and temperature conditions (*Dynamic* criteria). As a result, it is challenging to estimate the accuracy of these modelling approaches for outdoor cultivation. This point is further discussed in Section 1.4 detailing the practical issues associated with model development. Table 1.1 also shows that the majority of modelling studies developed models for dense cultures and therefore needed to account for light gradients in the culture broth (*Dense* criteria). Based on these observations, the classification of models proposed in the following section (1.3.3) was based on the theoretical ability of the models to account for light gradients and associated short light cycles.

[3] Two levels of model validation can be defined. A first level consists on checking that the model can fit one set of data. In a second level of validation, the kinetic parameters of the model are first determined on a first data set and the resulting model is then tested against a second data set.

Table 1.1: Experimental conditions used during algae cultivation performed to generate data sets used for model development and/or validation (table adapted from Article 1).

Model	Outdoor	Dynamic	Time	Dense	Data set	Meas.
Chalker, 1980	No	No	hours[a]	NS	No	O_2
Sakshaug et al., 1991	No	No	1 h	No	No	CC
Geider et al., 1997	No	No	3-4 h	No	No	C
Megard et al., 1984	No	No	1 h	NS	No	O_2
Pahl-Wostl and Imboden, 1990	No	Yes	1 d	NS	Yes	O_2
Bernard and Rémond, 2012	No	No	1-15 d[b]	NA[f]	No	CC
Dermoun et al., 1992	No	No	NS	No	No	OD
Talbot et al., 1991	No	No	NS	No	No	OD/DW
Collins and Boylen, 1982	No	No	NS	NS	No	DW
Kiefer and Mitchell, 1983	No	No	NS	Yes	No	CC
Kurano and Miyachi, 2005	No	No	NS	NS	No	OD
Carvahlo and Malcata, 2003	No	No	15-40 d	NS	No	CC
Haario et al., 2009	Yes	Yes	8 yrs	Yes	Yes	CC
Jeon et al., 2005	No	No	hours[a]	Yes	No	O_2
Bordel, 2009	No	No	1-9 d[c]	Yes	Yes	NS
Lee at al., 1987	No	No	NS	Yes	No	OD/DW
Molina Grima et al., 1994	No	No	days[d]	Yes	Yes	NS
Ogbonna et al., 1995	No	No	NS	Yes	Yes	DW
Ragonese and Williams, 1968	No	No	3-11d	Yes	No	CC
Rabe and Benoit, 1962	No	No	NS	Yes	No	NS
Molina Grima et al., 1996	No	No	4 d[e]	Yes	No	DW
Acién Fernández et al., 1998	Yes	Yes	1 yr	Yes	Yes	OD
Bosma et al., 2007	Yes	Yes	2-3 mths	Yes	Yes	T
Cornet et al., 1995	No	No	NS	Yes	Yes	OD
Cornet and Dussap, 2009	No	No	NS	Yes	Yes	NS
Evers, 1991	No	No	NS	No	No	NS
Grobbelaar, 1990	Yes	Yes	16 mths	Yes	No	DW
Guterman et al., 1990	Yes	Yes	18 mths	Yes	No	O_2
Muller-Feurga et al., 2003	No	No	3 wks	Yes	Yes	DW
Yun and Park, 2003	No	No	hours[a]	Yes	No	O_2
Camacho Rubio et al., 2003	No	Yes	1 d	NS	No	NS
Crill, 1977	No	No	NS	NS	No	NS
Duarte, 1995	No	No	hours[a]	NS	No	O_2
Wu and Merchuk, 2001	No	Yes	10 d	No	No	CC
Fasham and Platt, 1983	No	No	NS	NS	No	C
Wu and Merchuk, 2002	No	Yes	seconds	No	No	CC
Luo and Al-Dahhan, 2004	No	No	10 d	Yes	Yes	CC
Merchuk and Wu, 2003	NA	NA	NA	NA	NA	CC
Pruvost et al., 2002	No	No	NS	Yes	Yes	DW
Pruvost et al., 2008	No	No	NS	Yes	No	DW
Wu and Merchuk, 2004	No	No	9 d	Yes	Yes	CC
Ketheesan and Nirmalakhandan, 2013	Yes	Yes	3 wks	Yes	Yes	DW
Quinn et al., 2011	Yes	Yes	9 wks	Yes	Yes	DW/OD
Costache et al., 2013	Yes	Yes	1 day	Yes	Yes	O_2

(NS: not specified; NA: not applicable)

[a] Although the duration was not specified, the measurement of the photosynthetic rate based on oxygen accumulation suggests a short duration (i.e. hours).

[b] This study used experimental data from previous studies and the duration of 1-15 d corresponds to the experimental studies we could access from the literature.

[c] Although the duration was not specified, the data set used to develop and validate this model was obtained from a continuous culture monitored during near steady-state for a minimum duration of 2 HRTs.

[d] Although the duration was not specified, the results provided suggest an experiment of at least 200 hours.

[e] Validation was carried under a steady state regime maintained for at least 4 days.

[f] This study used experimental data from previous studies. Some of these studies were conducted at high algal concentrations.

1.3.3. Modelling the effect of light on photosynthesis

This section presents the classification of models based on their ability to account for the light gradients and the short light cycles experienced by algae during full-scale cultivation. For the sake of discussion, three categories of model were defined. Type I models predict the rate of photosynthesis of the entire culture as a function of the incident or the average light intensity reaching the culture. Type II models determine the rate of photosynthesis as the sum of localized rates of photosynthesis within the cultivation broth without consideration of short light cycles. Type III models account for both light gradients and short light cycles. This classification was defined by the authors of Article 1 and does not refer to any official classification of models.

Type I models

A first sub-category of Type I models expresses the rate of photosynthesis of the entire culture as a function of the irradiance (I_0) reaching the external surface of the system (Table 2 or Article 1). For example, Jeon et al. (2005) modelled the rate of photosynthesis of a culture of *Haematococcus pluvialis* using a Monod-like function described as:

$$P = P_m \frac{I_0}{I_k + I_0} \cdot XV \qquad (1.3)$$

where P is the rate of photosynthesis of the entire culture (kg O_2/s), P_m is the maximum specific rate of photosynthesis (kg O_2/kg-s), I_0 is the irradiance (W/m^2), I_k is the half-saturation constant (W/m^2), X is the algal concentration (kg/m^3), and V is the culture volume (m^3). A second sub-category of Type I models expresses the rate of photosynthesis of well-mixed cultures as a function of the average light intensity within the broth I_{av}. For example, Bordel et al. (2009) expressed the specific growth rate μ (in s^{-1}) of *Chlorella sorokiniana* as a function of the average light intensity by using a Monod-like function described as:

$$\mu = \mu_m \frac{I_{av}}{I_k + I_{av}} \qquad (1.4)$$

where μ_m is the maximum specific growth rate (kg/kg-s^{-1}) and I_{av} is the average light intensity in the culture (W/m^2). The average light intensity I_{av} was determined by using a Beer-Lambert law in this study (see Section 1.3.4 for further details).

Type I models are in practice relatively simple to develop and apply as the incident and average light intensities can be obtained through simple measurements and/or calculations. However, the kinetic parameters of Type I models were experimentally found to depend on

the algal concentration, the light intensity, and the geometry of the cultivation system (see Box 2 of Article 1 for details). At full-scale, the algal concentration and the light intensity are expected to change significantly over time. The kinetic parameters of Type I models would therefore need to be determined for a large range of algal concentrations and light intensities before the model can be confidently applied to full-scale cultivation systems. Using Type I models for productivity predictions during full-scale cultivation would therefore be unpractical as they require important laboratory work.

Type II models

Type II models account for the impact of light gradients on the local rate of photosynthesis. These models are constructed by 1) quantifying the light distribution within the broth, 2) selecting a biological model that expresses the local rate of photosynthesis as a function of the local light intensity, and 3) summing the local rates of photosynthesis to obtain the overall rate of photosynthesis. For example, Cornet et al. (1995) developed a Type II model by expressing the local rate of photosynthesis as a Monod-like function of the local light intensity I_{loc} (W/m^2). The rate of photosynthesis of the system P was then determined by integrating the local rates of photosynthesis over the system volume as (Cornet et al., 1995):

$$P = \int_V P_m \frac{I_{loc}}{I_k + I_{loc}} X \cdot dV \qquad (1.5)$$

where P_m is the maximum volumetric rate of photosynthesis (kg/kg-s), I_k is a saturation constant (W/m^2), V is the culture volume (m^3), X is the algal concentration (kg/m^3), and dV is the volume of the discrete elements (m^3). Evidence from the literature suggests that Type II models can accurately predict algal productivity under a broad range of operational conditions and designs. For example, Yun and Park (2003) were able to accurately predict the rate of photosynthesis of *Chlorella vulgaris* under different incident light intensities and algal concentrations using the Type II model described by Equation 1.5. Similarly, Cornet and Dussap (2009) showed that a Type II model was able to predict the rate of photosynthesis of *Arthrospira platensis* in eight photobioreactors with different geometries with a level of accuracy of ±15%.

Type II models can account for light-inhibition by adding a term proportional to the light intensity to the square in at the denominator in Equation 1.5, as done by Muller-Feurga et al. (2003) (see Table 3 of Article 1 for further details). However, a potential shortcoming of Type II models is their inability to account for the effect of short light cycles. The degree of light-

inhibition experienced by cells in a well-mixed dense culture is theoretically influenced by the cycling of individual algae cells between high-irradiance zones near the surface and low-light zones in deep areas. This cycling allows cells to recover from short-term exposure to inhibitory light intensities, which attenuates the overall impact of light-inhibition on the rate of photosynthesis. As pointed by Bosma et al. (2007), the use of Type II models for the prediction of productivity during full-scale algae cultivation outdoors may therefore overestimate the impact of light-inhibition.

Type III models

By contrast with Type II models, Type III models were developed to account for the impact of short light cycles on the rate of photosynthesis. Type III models consider that the rate of photosynthesis of an individual algae cell is a function of its 'light story', i.e. the light intensity experienced by an algae cell over time as it moves in the system. Type III modelling thus involves 1) determining the light distribution in the broth; 2) computing the trajectories of single cells; 3) based on 1 and 2, determining the light story of algae cells; 4) based on their light stories, determining the rate of photosynthesis of individual algae cells using a dynamic biological model; and 5) summing the rates of productivity of individual algae cells to calculate the total rate of photosynthesis in the cultivation system (see Section 3.3 of Article 1 for a full description of Type III models).

Because Type III models were developed to account for short light cycles, these models are theoretically capable of predicting productivity during full-scale algae cultivation outdoors. However, the compounded inaccuracies of the three sub-models needed for this approach (for light distribution, cells trajectories, and biological response) may significantly impact the accuracy of the overall prediction of Type III models. Finally, the benefit brought about by the ability to account for the impact of short-light cycles is contested in the context of full-scale cultivation because the massive mixing energy required for the algae to benefit from the flashing-light effect would damage cells and significantly increase operational costs (Benemann, 1987).

Conclusion on the "best" modelling approach

Whereas Type I models are easy to implement, they are theoretically not applicable outside the range of experimental conditions used for their development. This is potentially limiting

for prediction of cultivation outdoors if the model was parameterized using experiments conducted under low light intensity, at a different algal concentration, or in a reactor of different geometry. By contrast, Type III models offer significant refinement but the complexity of the inputs needed currently restricts their practical application. It was therefore proposed in Article I that Type II models currently offer the best compromise between accuracy and practicability for full scale engineering applications. The Type II modelling approach was therefore used in this thesis in order to predict algal productivity in full-scale cultivation systems.

1.3.4. Modelling light distribution in dense cultures

The application of Type II models requires determining the light distribution in the culture broth. This subsection reviews the different modelling approaches existing in the literature for the determination of the light distribution in algal cultures.

The Beer-Lambert law

During algae cultivation, light distribution is often estimated using the Beer-Lambert law which assumes an exponential decay of the light intensity from the external surface of the cultivation system (Table 6 of Article 1), as represented by the following equation:

$$I_{loc}(l) = I_0 \exp(-\sigma X l) \quad (1.6)$$

where $I_{loc}(l)$ is the local light intensity (W/m^2), l is the distance from the external surface of the system to the position under consideration (m), I_0 is the irradiance (W/m^2), σ is the extinction coefficient (m^2/kg), and X is the algal concentration (kg/m^3).

To apply the Beer-Lambert law, the culture medium must be isotropic (i.e. the optical properties of the broth must be independent of the light direction) and algae cells must not scatter light. Even if the first condition is often met in well-mixed outdoor cultivation systems, algae cells do scatter light (Acién Fernández et al., 1997). Various empirical expressions have therefore been developed to account for scattering such as, for example:

$$I_{loc}(l) = I_0 \exp\left(-\frac{k_1 X l}{k_2 + X}\right) \quad (1.7)$$

where $I_{loc}(l)$, l, I_0 and X are defined as in Equation 1.6 and k_1 and k_2 are empirical constants. These empirical formulas have shown good agreement with experimental data (Acién Fernández et al., 1997; Katsuda et al., 2000; Suh and Lee, 2003) but are species-dependent.

As a result, an empirical light distribution should ideally be determined over a suitable range of algal concentrations for each algal species studied.

The two-flux model and the radiative transfer equation

An alternative to the Beer-Lambert approach involves solving the radiative transfer equation (RTE) in three dimensions (see Houf and Incropera, 1980 for more details). The RTE can be derived by considering a small element of broth and performing a radiation balance on this element, considering the incident, absorbed, transmitted, and scattered sources of radiation. The determination of the light distribution by solving the RTE can be computationally intensive and different attempts were made to simplify the RTE while maintaining an acceptable level of accuracy. For example, by assuming that light scattering is one-directional, Cornet et al. (1992) developed a 'two-flux model' enabling the determination of the light distribution with a set of two ordinary differential equations (Table 6 of Article 1). Using this approach, Acién Fernández et al. (1997) demonstrated that the Beer-Lambert law overestimated the level of light attenuation in a cylindrical photobioreactor by a factor 2, while the prediction of the two-flux model was in good agreement with the measured light distribution.

While the Beer-Lambert law was found to be too simplistic to determine the light gradient in algal cultures by previous studies, the complexity of the radiative transfer equation limits its practical application. Alternative approaches such as the modified Beer-Lambert law and the two flux model were shown to accurately predict the light distribution in algal solutions. For the engineering purposes of this thesis, a modified Beer-Lambert law was used to determine the light distribution in algal broth.

1.3.5. Modelling the effect of temperature on photosynthesis

Uncoupled models

A first approach to model the effect of temperature on photosynthesis is to consider light and temperature as two independent factors. These 'uncoupled' models express the rate of photosynthesis as the product of two distinct functions of light intensity and temperature. For example, the Type II model of Guterman et al. (1990) multiplies the local light intensity by a

parabolic function of temperature to express the local specific growth rate μ_{loc} (s^{-1}) of *Spirulina platensis*:

$$\mu_{loc} = qI_{loc}\left(1-\left(\frac{T-T_{opt}}{T_{\max}-T_{\min}}\right)^2\right) \qquad (1.8)$$

where q is a constant (m^2-s/W), T is the broth temperature (^oC), and $T_{min}/T_{max}/T_{opt}$ are respectively the minimal, maximal and optimal temperatures for algal growth (^oC). Different mathematical expressions were used in the literature with no clear consensus on the best formula (see Section 4 of Article 1 for further details).

Coupled models

Uncoupled approaches are unable to account for the fact that the light-response of algae is dependent on temperature. 'Coupled' models aim to account for the coupled effects of light and temperature on the rate of photosynthesis (Butterwick et al., 2005; Fawley, 1984, see Section 1.2.2). For example, in the model developed by Dermoun et al. (1992), the parameters of the 'light-inhibition model' described in Table 1 of Article 1 were all made functions of temperature and the specific growth rate μ (s^{-1}) was expressed as follows:

$$\mu = 2\mu_m(T)(1+\beta_I)\frac{I/I_{opt}(T)}{1+2\beta_I I/I_{opt}(T)+(I/I_{opt}(T))^2} \qquad (1.9)$$

where $\mu_m(T)$ is the maximum specific growth rate at the temperature T (s^{-1}), β_I is a constant, I is the light intensity (W/m^2), and $I_{opt}(T)$ is the optimum light intensity for photosynthesis at the temperature T (W/m^2).

Although coupled models theoretically better represent the impact of temperature than uncoupled models, the interdependence of light and temperature on photosynthesis is not always significant (Davison, 1991). In addition, coupled models require a large number of parameters to be fitted experimentally (e.g. nine in the model depicted by Equation 1.9). The main risk associated a high number of parameters is that an apparent good fit to experimental data may only be due to a good adjustment of the set of parameters. This issue, usually referred to as 'overfitting', can impact the accuracy of the prediction, because the model is parameterized to describe noise in addition to/rather than important trends (Hawkins, 2004).

1.3.6. Modelling day-time and night-time respiration

Falkowski and Owens (1978) showed that short-term respiration during day time can consume up to 25% of the chemical energy (ATP, NADPH) generated during photosynthesis. This consumption can be assumed to be directly proportional to the rate of photosynthesis (García Camacho et al., 2012). Accordingly, Geider et al. (1997) assumed that the rate of day-time respiration (ER_{day}, in g C/s) could be expressed as:

$$ER_{day} = -\zeta \mu X V \quad (1.10)$$

where ζ is a dimensionless constant, μ is the specific growth rate (s^{-1}), X is the algal concentration (g C/m^3), and V is the system volume (m^3). Alternatively, other modelling studies assumed that the rate of respiration was constant and equal to the rate of respiration at night-time (e.g. Evers, 1991; Guterman et al., 1990; Yun and Park, 2003). This absence of clear consensus on the best modelling approach for day-time respiration therefore requires individual studies for each algal species.

Long-term night-time respiration

Long-term respiration at night time associated with the consumption of stored carbohydrates can cause significant biomass losses during algae cultivation (Torzillo et al., 1991). The rate of night-time respiration ER_{night} (kg/s) is usually modelled using first-order kinetics with regards to algal concentration as described by:

$$ER_{ntight} = -\lambda X V \quad (1.11)$$

where λ is the maintenance coefficient (s^{-1}), X is the algal concentration (kg/m^3) and V is the system volume (m^3). This approach assumes that night-time respiration is only associated with normal maintenance functions and that, therefore, its specific rate λ is constant over time. However, in full-scale cultivation systems, assuming a constant rate of night-time respiration may cause inaccuracy for several reasons:

- Temperature: In the modelling study of Collins and Boylen (1982), the specific rate of respiration of *A. variabilis* was shown to increase from 0.2 to 1.0 g carbon/g biomass-d when temperature varied from 10°C to 40°C. As temperature can drop by more than 10°C at night during outdoor cultivation (see for example Figure 1 of Article 2), the impact of temperature on night-time respiration must be considered. Few models however account for the temperature effect on night-time respiration. For this purpose,

Grobbelaar (1990) proposed to multiply the specific rate respiration λ by a Van't Hoff function by analogy with chemical reactions (Table 2 of Article 1).

- Cellular composition: Torzillo et al. (1991) observed that the magnitude of night-time biomass loss in outdoor cultivation systems depended on the light intensity and temperature during the previous day. This dependence was explained by the fact that the respiration rate was a function of the carbohydrate content of cells.

As first-order kinetics was experimentally proved to describe night-time respiration by various studies (see Section 5 of Article 1), this approach was used in this thesis. Furthermore, to account for the impact of temperature on the rate of endogenous respiration, the decay coefficient λ was expressed as an empirical function of temperature.

1.3.7. Conclusions on the modelling approach used in this thesis to predict algal productivity at full-scale

The reviewed modelling approaches predicting algal productivity are summarized in Figure 1.2. Because model refinement must be weighed against the increasing uncertainty brought by increased complexity, we conclude that the currently most pragmatic modelling methodology for engineering assessments of full-scale systems would combine the following approaches (Figure 1.2):

1) For the rate of photosynthesis, Type II models provide a compromise between practicability and universality.
2) Empirical functions of temperature should be used in conjunction with Type II models to account for the effect of temperature on photosynthesis.
3) In order to predict the net productivity, the above should be used in conjunction with a decay term for respiration that empirically accounts for temperature effects.

To the best of our knowledge, no model following this approach was fully validated against full-scale data.

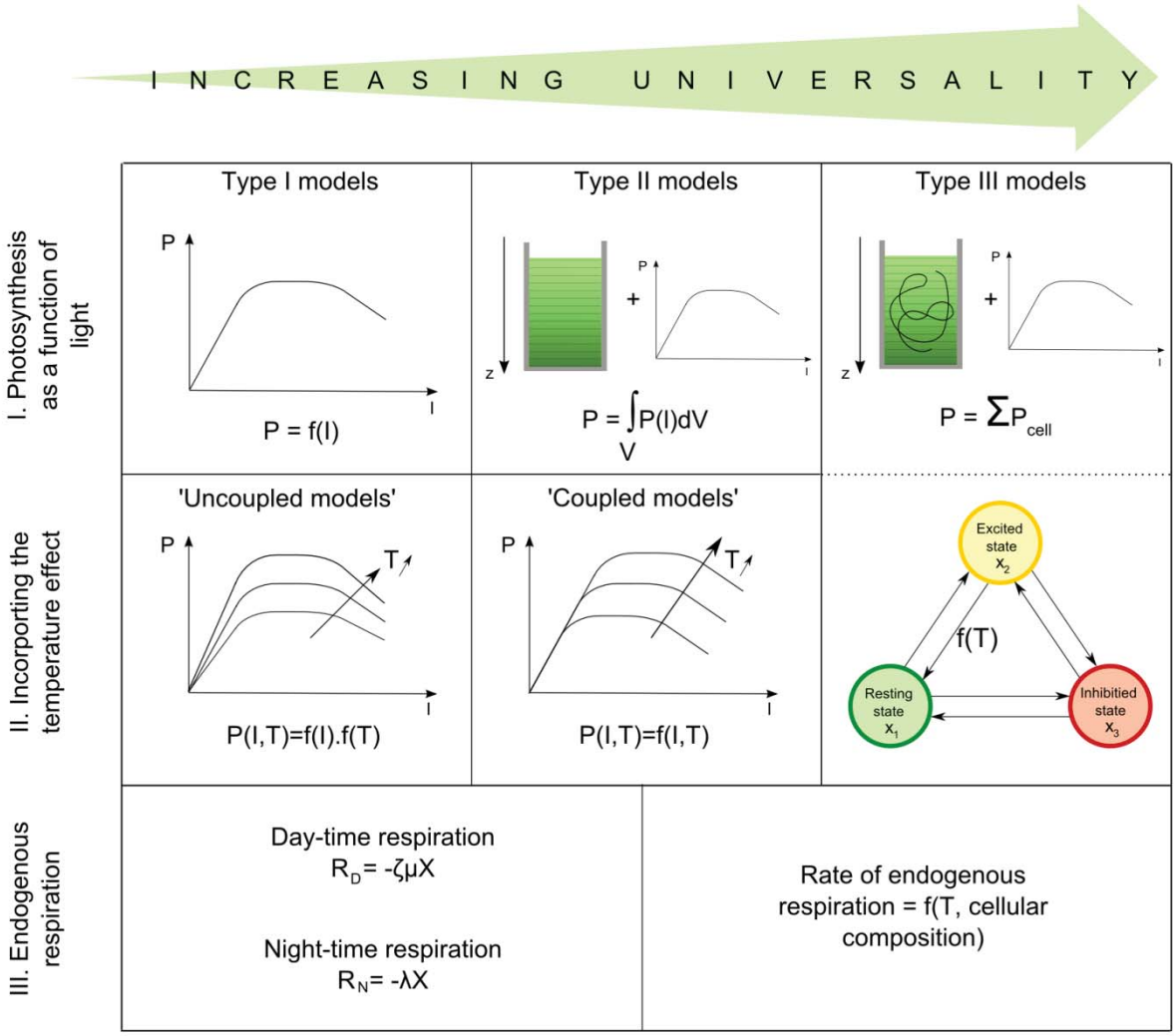

Figure 1.2: Summary of the different categories of models (*I*: light intensity; *T*: temperature; R_D: rate of day-time respiration; μ: specific rate of photosynthesis; *X*: algal concentration; ζ: proportionality constant; R_N: rate of night-time maintenance; λ: maintenance coefficient) – *Extracted from Article 1*.

1.4. Practical issues during model development

This section explains the practical issues encountered when determining the kinetic parameters of productivity models. Traditionally, the determination of model parameters is performed by experimentally measuring the algal rates of photosynthesis and respiration when algae are exposed to different light intensities and temperatures. However, the conditions typically used during indoor cultivation are not fully representative of the conditions experienced by microalgae during full-scale cultivation, for mainly three reasons:

1. The majority of models hitherto described were developed using indoor data collected over only hours to days of cultivation (*Time* criteria in Table 1.1). As a result, the resulting models cannot theoretically account for long-term acclimation processes that are likely to occur at full-scale.
2. Most of the models hitherto described were developed using indoor cultivation data generated under constant light and temperature conditions (*Dynamic* criteria in Table 1.1). The effect of diurnal cycles and especially the change of biomass composition at night observed at full-scale (Torzillo et al., 1991) therefore cannot be accounted by these models.
3. A wide range of light sources, going from 'Cool White' fluorescent tubes (Collins and Boylen, 1982), to tungsten lamps (Katsuda et al., 2000) and natural sunlight (Bosma et al., 2007) have been used in previous experimental studies. Yet, the light response of algae cells is also a function of the light spectrum because photosynthetic pigments have preferential wavelengths for light absorption (Jeon et al., 2005). As most light sources have a spectrum different from sunlight, models validated from indoor data may not be directly applicable to outdoor cultures.

In addition, several proxies were measured to quantify the rate of photosynthesis during modelling studies (Table 1.1). Examples include the rate of oxygen production or inorganic carbon uptake (e.g. Chalker, 1980; Cullen, 1990), the dry weight (DW) concentration (e.g. Bosma et al., 2007), or the broth optical density (OD, e.g. Acién Fernández et al., 1997). Unfortunately, biomass composition and other cell properties depend on species and cultivation conditions (Posten, 2009), meaning that predicting biomass productivity based on a proxy to biomass weight can generate considerable uncertainty.

The usual experimental techniques used to determine the kinetic parameters may lead to inaccuracy of the productivity predictions in full-scale systems. Yet, there no easy practical way of determining coefficients in conditions that represent outdoor cultivation conditions. In particular, cultivating algae over long periods of time or under variable temperature and light conditions is unpractical as it requires important laboratory work. In addition, it is technically challenging to mimic solar light spectrum with artificial light bulbs. In order to estimate how the indoor cultivation conditions affect the accuracy of productivity predictions, models should be validated against full-scale cultivation data. However, as stated in Section 1.3, the large majority of models found in the literature were either not validated against full-scale data or were only validated against the data set for model development (*Data set* criteria in Table 1.1). To the best of our knowledge, only four modelling studies assessed the accuracy of productivity models against outdoor data. However, three of these outdoor studies were performed under some degree of temperature-control (Bosma et al., 2007; Ketheesan and Nirmalakhandan, 2013; Quinn et al., 2011). Out of these four studies, only Costache et al. (2013) validated a productivity model on an outdoor non-temperature controlled system. However, this model generates estimates of oxygen productivity rather than in biomass productivity, which limits its use for engineering purposes. There is therefore a critical need for a complete validation of biomass productivity models against full-scale data.

1.5. Conclusions on the modelling approach followed in this thesis

At full-scale, both light and temperature have a significant impact on algal productivity. Numerous models of algal productivity exist in the literature but, to the best of our knowledge, no modelling approach predicting biomass productivity was validated against full-scale conditions. In particular, different knowledge gaps were identified in this review:

- The temperature variations and their influence on algal productivity were neglected in most of models whereas temperature can significantly vary during full-scale cultivation.
- Most of the existing models were developed using data generated under conditions that do not fully represent full-scale cultivation conditions (e.g. temperature-controlled cultivation, artificial lighting). The accuracy of these models for full-scale predictions therefore still needs to be assessed.

In order to fill the gaps of knowledge identified in this review, the following approach was followed:

1) A mathematical model predicting the temperature in full-scale cultivation systems was developed.
2) A productivity model accounting for the effect of both light and temperature was constructed from the guidelines determined in Section 1.3.7 and parameterized from indoor data.
3) The productivity model was independently assessed against full-scale outdoor cultivation data.

Chapter 2: Cultivation systems and methods

Preface

Even if there is currently no full-scale algal cultivation for biofuel production, there are guidelines on the geometry and operating conditions of open ponds and closed photobioreactors. This chapter aims to describe how these guidelines were used to define the scope and identify the limitations of the modelling approach developed in this thesis.

2.1. Cultivation systems

Full-scale algal cultivation systems are traditionally classified in two categories: open systems (e.g. ponds) and closed systems (e.g. photobioreactors). No clear consensus has been reached concerning the best system for full-scale cultivation (Del Campo, 2007; Grobbelaar 2009): open ponds are usually considered cheaper to build and operate but closed systems supposedly allow a better control of cultivation conditions. In order to design and assess the costs of full-scale algal cultivation systems, it was therefore important to ensure that the model developed in this thesis could predict productivity regardless of the system geometry.

2.1.1. Open ponds

Open ponds used for full-scale algal cultivation are usually shallow to avoid large dark zones in the cultivation broth, with a depth varying between 0.1m and 0.5m (Benemann et al., 1987; Del Campo et al., 2007; Leite et al., 2013; Makareviciene et al., 2013). This range was used in this thesis. In an early review, Benemann et al. (1987) recommended the use of paddle wheels in shallow ponds as an efficient way to ensure completely mixed conditions (Figures 2.1 and 2.2). Following the guidelines provided by Del Campo et al. (2007), the Reynolds number characterizing the flow of an open raceway pond should vary between 56,000 and 290,000, which is higher than the value of 4,000 ensuring turbulent conditions (pond width: 2-10 m; pond depth: 0.15-0.3 m; water velocity: 0.2-0.5 m/s). In the rest of this thesis, it was therefore assumed that cultivation broth in open ponds was well-mixed, ensuring homogenous algal concentration, nutrient concentration, pH and temperature. The homogeneity of the temperature was experimentally verified on the open ponds used for the validation of the temperature model described in Chapter 3 by measuring the temperature of the broth at various depths.

Figure 2.1: Open raceway ponds used for the validation of the temperature model – NIWA, Hamilton, New Zealand.

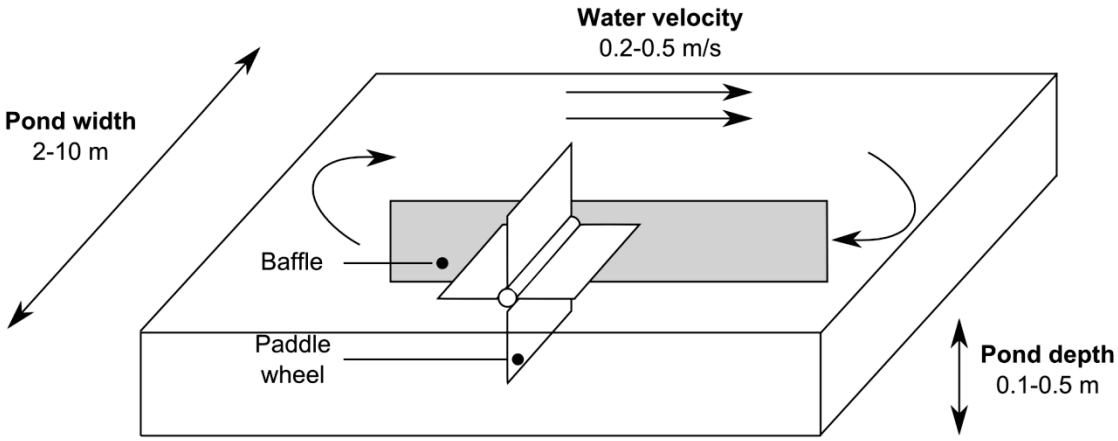

Figure 2.2: Key characteristics of open ponds.

2.1.2. Closed photobioreactors

Vertical, horizontal, spiral tubular, flat-plate, ring, dome and pyramide-shaped closed photobioreactors geometries have been described in the literature (Makareviciene, 2013). As there is no clear consensus on the best photobioreactor geometry, a vertical cylindrical geometry was chosen in this thesis due to its simplicity of construction and operation and low energy requirement for mixing (Figure 2.3). Indeed, Béchet et al. (2013) showed that a mixing input for bubbling of only 7.5 W/m^3 was sufficient to ensure good mixing conditions (no algal sedimentation) in an outdoor vertical cylindrical photobioreactor used for *Chlorella* cultivation. The well-mixed assumption was experimentally verified in the photobioreactors operated for model validation described in Chapters 3 and 4 by placing temperature sensors at five different depths in the reactors. No significant temperature differences were observed, demonstrating homogenous temperature in the reactors. In addition, no algal sedimentation was observed after several months of cultivation of *Chlorella vulgaris* in the outdoor reactors used for model validation (Experiment 1, Chapter 4), suggesting that algal concentration was homogenous. Finally, it was assumed biofouling did not significant reduce light transmittance (no significant fouling occurred).

Figure 2.3: Quentin Béchet operating a vertical cylindrical photobioreactor used for model validation.

2.2. Cultivation conditions

As discussed in Chapter 1, in order to maximize the profit of full-scale algal cultivation, it is generally important to ensure that no other factor than light supply and temperature affects algal productivity. Nutrient saturation can be easily be avoided by maintaining high nutrient concentrations in the cultivation broth (Grobbelaar, 2009) while CO_2 injection ensures saturating CO_2 conditions and pH control (Del Campo et al., 2007). Although the occurrence of inhibitive oxygen concentrations has been observed during intense periods of photosynthesis at full-scale (Grobbelaar, 2009; Tredici and Materassi, 1992), oxygen inhibition was assumed to not significantly affect full-scale productivity, which was experimentally verified as discussed below.

In order to reproduce full-scale conditions during model validation, the outdoor photobioreactors presented in Chapter 3 were operated under the following conditions:

- A phosphate-buffered BG-11 (see Béchet et al. 2013 for full description) was experimentally shown to ensure nutrient saturation and pH control (6.8-7.5) under the conditions used in this study.
- Air enriched in CO_2 (2%) was bubbled in all the photobioreactors used for model validation, in order to ensure CO_2 saturation and well-mixed conditions.
- The oxygen concentration was continuously monitored to ensure that inhibitive levels were never reached (a maximum of 140% of saturation was observed in the closed photobioreactors).

Batch versus continuous operation

There is no clear consensus on the best operational regime for full-scale cultivation according to Mata et al. (2010). As a result, the productivity model was developed with the objective to predict algal productivity under various batch and fed-batch operations.

2.3. Algae species

The modelling approach developed in this thesis is in theory applicable to a large range of algal species. Due to time constrains, this thesis focused on *Chlorella vulgaris*, a commercially relevant species (Makareviciene et al., 2013; Spolaore et al., 2006) that is endemic to New Zealand (no biohazard) and therefore adapted to its climate. The *Chlorella vulgaris* strain used in this thesis was obtained from Landcare Research and isolated in New Zealand. Cellular death is seldom considered during algae productivity modelling and the viable/total cell fraction was experimentally verified to remain above 95% during all experiments. As discussed in Chapter 4, biomass loss was therefore assumed to be caused by endogenous respiration (see Box 1.1 for definition).

2.4. Algal productivity and experimental measurement

Productivity was defined as the gain in biomass over time (expressed in kg biomass per year) and measured using dry weight measurements during model validation. Dry weight tests were performed by filtering a known volume of algal broth on a pre-weighted filter. The filters were then dried at 105^{o}C for 1 hour and weighted again. Dry weight concentration was then obtained by measuring the difference in the filter weights. While dry weight measurement is the experimental technique the most commonly used to assess biomass productivity in the field, this technique is limited by the fact that dissolved organic matter can be excreted by cells and is not accounted for in the measurement.

2.5. Simulations

To illustrate how the productivity model can be used as an engineering tool, simulations were performed at five locations representing different climatic conditions. These locations and their meteorological characteristics (yearly averages of solar irradiance, air temperature, etc.) are shown on Figure 2.4.

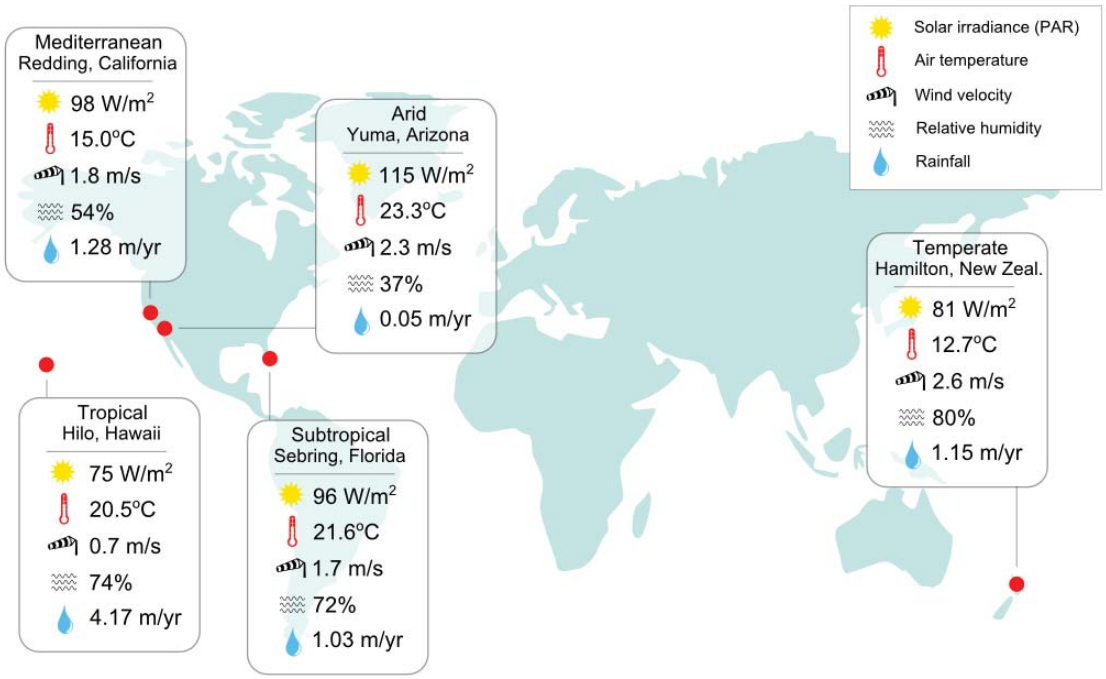

Figure 2.4: Meteorological conditions at the five climatic locations used in the different case studies in this thesis (yearly averages)[4].

[4] Meteorological data from the US National Climate Data Centre (NCDC) and from the New Zealand National Institute for Water and Atmospheric Research (NIWA). The climates at the five locations were determined from the classification of Peel et al. (2007).

Chapter 3: Temperature models

Preface

As demonstrated in Chapter 1, there is nowadays a critical lack of knowledge on how to predict the magnitude of temperature variations experienced during full-scale cultivation systems and how these changes impact productivity. There is also no modelling tool available to conduct the simulations necessary to gain from this knowledge and provide guidelines for design and operational practices. This chapter describes how the temperature model was developed and validated during this thesis. As discussed in Chapter 1, productivity depends on location, system design and operation. For this reason, the temperature model was derived from theoretical considerations rather than site-specific formulas. In addition, the temperature model was developed to account for the differences of geometry of open ponds and closed photobioreactors.

3.1. Introduction

Open and closed systems are exposed to the same heat flows (solar heat flow, air convection, etc.) but the expression of these heat flows changes with the system design, a significant difference being the evaporative heat flow. Conversely to open systems, closed systems are usually not in contact with ambient air, which limits the rate of evaporation from these systems. In addition, the expression of the heat flows depends on the system geometry. For instance, a fraction of the radiation reaching the ground surface is reflected onto closed photobioreactors, while there is no radiative interaction between the ground surface and open ponds. As a result, two distinct temperature models are presented in this chapter. The first section reviews temperature models previously developed for prediction in outdoor systems similar to algal ponds. The second section describes how the temperature model in open ponds was constructed and validated. The third section focuses on the temperature prediction in vertical column closed photobioreactors.

3.2. Literature review on temperature models

As discussed in Chapter 1, and to the best of our knowledge, no temperature model was specifically developed for full-scale algal cultivation systems before this thesis. However, several studies focused on the prediction of temperature in open water bodies with geometries and optical properties similar to that of algae ponds. In particular, the temperature of wastewater treatment ponds has been the object of multiple studies because temperature variation has a significant influence on biological kinetics during wastewater treatment (Rittman and McCarty, 2001). These temperature models are all based on heat balances represented by the following equation:

$$\rho_w Cp_w V \frac{dT}{dt} = \sum Q_i \qquad (3.1)$$

where ρ_w and Cp_w are the density (kg/m^3) and thermal heat capacity of water (J/kg-K), respectively, V is the system volume (m^3), T is the system temperature (K) at the time t (s), and Q_i represents the different heat flows reaching the system (W). The heat flows Q_i considered in the heat balance and their expressions varied across studies. This section aims to detail how these heat flows were expressed in prior models. Special emphasis was given to evaporation models given the impact of this mechanism on the water demand associated with full-scale algal cultivation.

3.2.1. Heat flows reaching open water bodies

Seven heat flows are generally considered in the heat balances used to predict temperature in open water bodies (Table 3.1):

- **Solar radiation**: Previous temperature models focused on opaque water bodies, meaning that all the solar light entering the water is converted into heat. Most studies expressed solar radiation from on-site solar irradiance data (in W per m^2 of horizontal ground surface).
- **Air radiation**: Water bodies capture long-wave radiation emitted by the atmosphere. The existing models all expressed this heat flow by considering the atmosphere as a "grey body", meaning that this heat flow is proportional to the atmosphere temperature to the fourth power (Howell et al., 2011).

- **Water radiation**: Water bodies emit long-wave radiation that is also usually modelled by assuming that the top surface of water bodies is ‘grey’.
- **Evaporation**: Water evaporation is associated with a heat loss. There is a large range of formulas available in the literature to predict the rate of evaporation from open water bodies. Most of these formulas are empirically derived and are therefore specific to the system they were derived from (see Section 3.2.2 for further discussion).
- **Convection:** As water bodies are usually at a temperature different from the ambient air, convective heat transfer occurs between the water body and the ambient air.
- **Conduction**: As open bodies are in contact with the ground surface, heat can be transferred between the water body and the ground. The ground can be seen as a temperature buffer: at day-time, heat is transferred from the water body to the ground; at night-time, the heat stored during day-time is transferred back into the water body.
- **Inflow**: Water inflow into the system can be responsible for a heat loss or a heat gain if the inflow temperature is lower or higher than the water body temperature, respectively.

Another heat flow that is not accounted for in the studies reviewed in Table 3.1 is associated with rainfall, as the temperatures of rainwater and water body usually differ.

Table 3.1 shows that empirical formulas were often used to express the heat flows reaching outdoor systems. Yet, empirical formulas are usually too system-specific to be applied to a large range of systems. For example, most of the approaches used to predict the rate of evaporation from open water bodies did not account for the size of the system. However, as air flows over the water surface, the relative humidity of the air increases, which in returns decreases the rate of evaporation (Sartori, 2000). The average evaporation rate from an open water body is therefore lower for large water bodies (e.g. lake) than for small open ponds. As described in this chapter preface, the temperature model must predict temperature at different meteorological locations for different system designs and operations. As a result, the temperature model developed in this thesis used theoretical expressions instead of system-specific formulas to express the different heat flows reaching full-scale cultivation systems.

Table 3.1: Characteristics of models predicting the temperature in systems similar to algal ponds (**Theo.**: T
Expression derived from an empirical study: **NA**: Not applicable, **Neg.**: Neglected; **From H_s** means that th
site solar irradiance data) – *Table extracted from Article 2*.

Model	System	Solar rad.	Pond rad.	Air rad.	Conv.	Evap.	Cond.
1	Open roof pond	Theo.	Theo.	Theo.	*	*	Theo.
2	Stabilization pond	Theo.	Theo.	Theo.	Emp.	Emp.	Neg.
3	Shallow pond	From H_s	Theo.	Theo.	Emp.	Emp.	Theo.
4	Aeration-basin / Wastewater treatment pond	Theo.	Theo.	Theo.	Emp.	Emp.	Theo.
5	Aquaculture pond	From H_s	Theo.	Theo	Emp.	Emp.	Neg.
6	Open tank	NA	Theo.	Theo.	Theo.	Emp.	NA
7	Fish pond	From H_s	Theo.	Theo.	Emp.	Emp.	Neg.
8	Aquaculture pond	From H_s	Theo.	Theo.	Emp.	Emp.	Theo.
9	Cooling pond	Theo.	Theo.	Theo.	Emp.	Emp.	NA

*The authors did not specify the origin of the heat flux expression

3.2.2. Modelling free-surface evaporation

The bubbling of gas unsaturated in water causes evaporation during algae cultivation (this supply is required to provide CO_2 and mixing while removing O_2 in closed systems, but is also often needed to prevent pH raise during peak hours in open ponds). The associated heat flow is however minor in the heat balance as demonstrated in Section 3.4.2. This section therefore focuses on the modelling of free-surface evaporation in open ponds as this flow impacts both the pond temperature and the water demand associated with the process (see Article 6 for further discussion).

Table 3.2 summarizes various formulas used to predict the rate of evaporation from free water surfaces. Table 3.2 shows that past studies have been either based on empirical formulas expressing the rate of evaporation as a function of readily available evaporation data such as pan evaporation (*Pan evaporation, Lake evaporation model, Penman equation* in Table 3.2) or semi-empirical models expressing the rate of evaporation as a function of the water temperature (referred to as *Models 1 to 5* in Table 3.2). With respect to the 'empirical formulas', approaches based on the rate of evaporation from a Class-A pan ($m_{e,PAN}$) should be used with caution in the context of algae cultivation for various reasons: First, a lower amount of the visible light reaching the water is converted into heat in Class-A pans than in the algal pond because the water used in Class-A pans is clear. Secondly, the edges of Class-A pans shelter the water surface from wind, which reduces evaporation. Thirdly, the small size of Class-A pans influences the rate of evaporation because the relative humidity of the layer of air above the water surface varies with the surface area. The other formulas listed in Table 3.2 were empirically derived from studies on various systems. As a result, these formulas may be too system-specific to be applied to open ponds. For example, a typical lake has more thermal inertia than a shallow pond and consequently experiences lower temporal temperature variations, which also reduces peak evaporation rates. Hence, the use of lake-based formula may cause an underestimation of evaporation rates and peak temperature events during algae cultivation. As a result, a theoretical approach based on mass transfer theory was specifically developed in this thesis.

Table 3.2: Formulas of water evaporation from free water surfaces (Symbols are defined at the end of the

	Name	System	Equation	
Empirical formulas	Pan evaporation	Class A Pan	$m_e = m_{e,PAN}$	(3.2
	Lake evaporation model	Lake	$m_e = 0.75 m_{e,PAN}$	(3.3
	Penman equation	Shallow water bodies	$m_e = \frac{\Delta I_0 + \gamma L_w \rho_w K_E v_h (P_w - RHP_a)}{L_w \rho_w (\Delta + \gamma)}$	(3.4
Semi-empirical models	Model 1	Small open pond	$m_e = \frac{(0.2253 + 0.24644 v_{0.55})(P_w - RHP_a)^{0.82}}{L_w}$	(3.5
	Model 2	Aquaculture Pond	$m_e = 4.34.10^{-8}(1 + 0.22 v_{8.2})(P_w - RHP_a)$	(3.6
	Model 3	Lake Hefner	$m_e = \frac{0.038 v_2 (P_w - RHP_a)}{L_w}$	(3.7
	Model 4	Aeration basin	$m_e = \frac{4.8.10^{-5} \cdot f_m \cdot e^{0.0604(T_a - 273.15)} S_p^{-0.05} v_6}{L_w}$	(3.8a
			where $f_m = 1.15.10^6 (1 - RH) + 6.86.10^4 (T_w - T_a)$	(3.8b
	Model 5	Large water bodies	$m_e = \frac{(9.2 + 0.46 v_7^2)(P_w - RHP_a)}{L_w}$	(3.9

Symbols: m_e: rate of evaporation (m^3/m^2-d); $m_{e,PAN}$: rate of evaporation in a Class-A pan (m^3/m^2-day); Δ: slope of the saturated v (Pa/°C); I_0: solar irradiance (W/m^2); γ: psychometric constant (Pa/°C); ρ_w: water density (kg/m^3); K_E: mass transfer coefficient d heat of vaporization of water (J/kg); v_h: wind velocity at h meters above the ground surface (m/s); P_w: saturated vapor pressure (saturated vapor pressure (Pa) at the air temperature T_a (K), RH: air relative humidity; S_p: pond surface area (m^2).

3.3. Temperature model in open ponds

3.3.1. Heat balance in open ponds

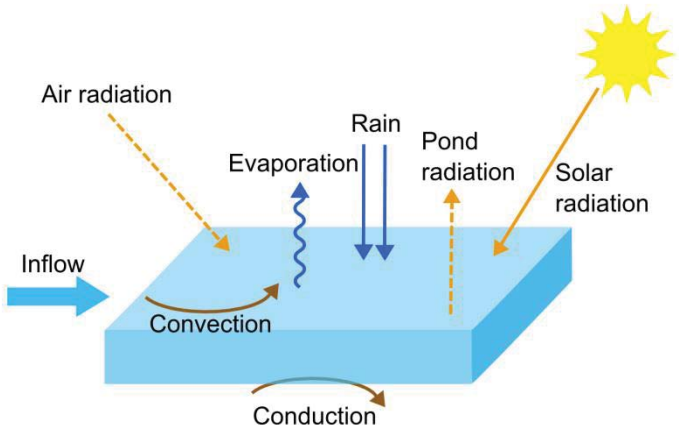

Figure 3.1: Different heat flows reaching an open pond.

Based on the eight heat flows shown in Figure 3.1, the dynamic prediction of temperature in open ponds was achieved by solving the following heat balance:

$$\rho_w V Cp_w \frac{dT_p}{dt} = Q_{ra,p} + Q_{ra,s} + Q_{ra,a} + Q_{ev} + Q_{conv} + Q_{cond} + Q_i + Q_r \quad (3.10)$$

where ρ_w is the water density (kg/m^3), V is the pond volume (m^3), Cp_w is the water heat capacity (J/kg-K), T_p is the pond temperature (K), $Q_{ra,p}$ is the radiation from the pond surface (W), $Q_{ra,s}$ is the solar radiation (W), $Q_{ra,a}$ is the radiation from the air (W), Q_{ev} is the evaporative heat flow (W), Q_{conv} is the convective heat flow (W), Q_{cond} is the conductive heat flow (W), Q_i is the inflow heat flow (W), and Q_r is the rain heat flow (W). Theoretical expressions were used to express each heat flow as shown in Table 3.3. In particular:

- **Air radiation** was modelled based on a theoretical calculation of the air emissivity ε_a as suggested by Taine et al. (2008) (see Supplementary information S3 of Article 2 for a detailed calculation). The air emissivity was assumed to be constant for simplicity in spite of its well-known dependence on various environmental factors (Marthews et al., 2012).
- **Evaporation and Convection** were modelled based on the application of the Buckingham theorem (Taine et al, 2008). As heat and mass transfers obey the same

physical laws, these two heat flows were expressed by using the same modelling approach.

- **Conduction** was modelled by predicting the temperature profile in the layer of ground beneath the pond by solving the following partial differential equation:

$$\frac{\partial T_s}{\partial t} = \alpha_s \frac{\partial^2 T_s}{\partial z^2} \quad (3.11)$$

Where T_s is the ground temperature (K) at the depth z (m) and the time t (s), and α_s is the soil thermal diffusivity (m^2/s). The two partial differential equations 3.10 and 3.11 were numerically solved by using a first-order Euler forward algorithm for the time variable and a second-order scheme for the depth. A time step of 1000 seconds and a soil element thickness of 0.08m ensured no significant numerical error of the temperature prediction (see Article 2 for more details).

Table 3.3: Equations used to express each heat flow in the temperature model for open ponds – *Formulas extracted from Article 2.*

Heat flow	**Equation**	
Pond radiation	$Q_{ra,p} = -\varepsilon_w \sigma S T_p^4$	(3.12)
Solar radiation	$Q_{ra,s} = (1 - f_a) H_s S$	(3.13)
Air radiation	$Q_{ra,a} = \varepsilon_w \varepsilon_a \sigma T_a^4$	(3.14)
Evaporation	$Q_{evap} = -K_{evap}\left(\frac{P_w}{T_p} - \frac{RH \times P_a}{T_a}\right)\frac{M_w}{R} L_w S$	(3.15a)
	$K_{evap} = C_{evap}(\mathrm{Re}_L)^{\beta}(Sch)^{\delta}$	(3.15b)
Convection	$Q_{conv} = K_{conv} S(T_a - T_p)$	(3.16a)
	$K_{conv} = C_{conv}(\mathrm{Re}_L)^{\beta}(\mathrm{Pr})^{\delta}$	(3.16b)
Conduction	$Q_{cond} = -k_s S \frac{dT_s}{dz}\Big\vert_{z=0}$	(3.17)
Inflow	$Q_i = \rho_w Cp_w q_i (T_i - T_p)$	(3.18)
Rain	$Q_r = \rho_w Cp_w q_r (T_i - T_p) S$	(3.19)

Symbols: Q: heat flows reaching the pond as defined in Section 3.3.1; $\varepsilon_w/\varepsilon_a$: water/air emissivity; σ: Boltzmann constant ($W/K^4\text{-}m^2$); S: pond surface area (m^2); T_p/T_a pond/air temperature (K); f_a: fraction of sunlight converted in chemical energy through photosynthesis; H_s: solar irradiance (W/m^2); P_w: Saturated vapor pressure at T_p (Pa); P_a: saturated vapor pressure at T_a (Pa); M_w: molar weight of water (kg/mol); RH: relative humidity; R: ideal-gas constant ($Pa\text{-}m^3/mol\text{-}K$); K_{conv}: convection coefficient ($W/m^2\text{-}K$); L_w: water latent heat (J/kg); Re_L: Reynolds number, calculated for the pond length L (m); Sch: Schmidt number; Pr: Prandtl number; C_{evap}: constant (m/s); C_{conv}: constant ($W/K\text{-}m^2$); β, γ: constants; k_s: soil thermal conductivity (W/m-K), T_i: inflow temperature (K); T_s: soil temperature; q_i: inflow rate (m^3/s); q_r: rainwater flow (m/s); z: depth in the ground (m); ρ_w: water density (kg/m^3); C_{pw}: water thermal capacity (J/kg-K).

3.3.2. List of parameters

As shown in Table 3.3, it is necessary to determine the value of a significant number of variables and parameters to predict the temperature of an open pond. However, most of these inputs are universal constants, such as air or water properties, and the values of these parameters can be found in Article 2. All the other parameters and variables that need to be determined for each specific location, geometry and operation are (Figure 3.2):

- Weather variables that can be obtained from a weather station (for example by using the data freely available from NIWA in New Zealand or NCDC in the US as done in Articles 2 and 3).
- Operational parameters that can be adjusted to optimize algal productivity and minimize water demand (see Chapter 5);
- Geometrical parameters;
- The latitude of the location considered;
- The parameters characterizing the 'environment around the pond' shown in Figure 3.2 and influencing the wind profile (Gipe, 2004);
- The fraction of solar energy converted into chemical energy through photosynthesis (in general taken at 2.5% and having an insignificant impact on temperature predictions as shown in Article 2);
- Ground characteristics that are tabulated for different soil types (Miller, 1981).

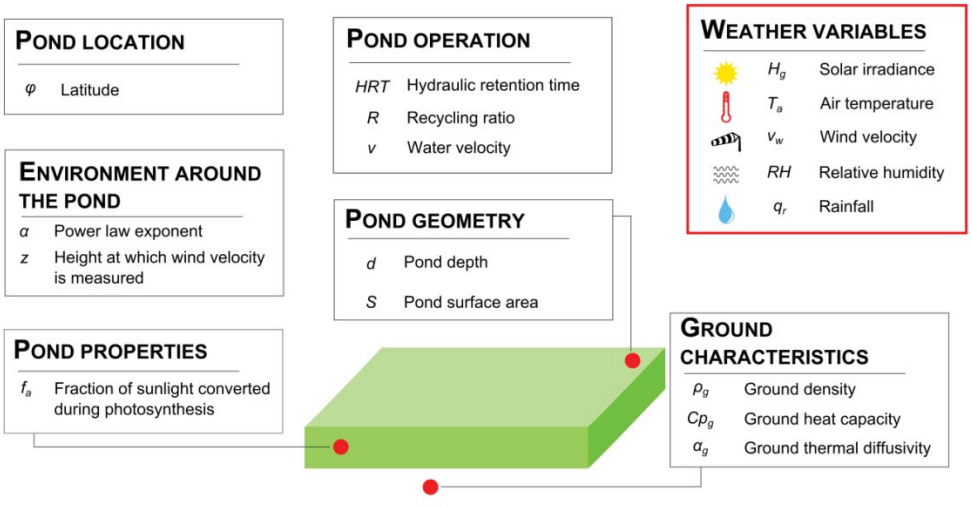

Figure 3.2: Specific inputs necessary for the prediction of temperature in an open pond.

3.3.3. Accuracy of the temperature model for open ponds

The model predictions were compared to experimental data from a shallow open pond operated outdoor for one year in Hamilton, New Zealand. This pond (depth: 0.25m; surface area: 32m^2) was used for wastewater treatment and was therefore opaque (i.e. all the light entering the pond was captured by the water). As a result, the temperature profile in this open pond should be the same as in a shallow open pond for algal cultivation. The pond was operated continuously (hydraulic retention time of 4 to 8 days) and the accuracy of the model was assessed using 33,221 data points representing a full year of operation. A complete description of this pond can be found in the materials and methods section of Article 2.

Figure 3.3 illustrates the excellent fit between the experimental and predicted temperature profiles for a typical month (with all other months shown in the Supplementary information S5 of Article 2). The overall accuracy of the model prediction when compared to experimental data was defined as the maximum temperature difference between the predicted and measured temperatures for 95% of data points[5]. The overall accuracy for the entire year 2009 was estimated to ±2.6^{o}C. In addition, peak temperatures in cultivation systems may cause cellular death, and being able to predict these temperature maxima is crucial to assess the feasibility of algal cultivation at certain hot locations. This error on peak temperatures was defined as the average difference between the predicted and the measured peak temperatures at midday (in absolute value). The average error in the estimation of the afternoon peak for the year 2009 temperature was 1.3^{o}C.

[5] For example, an overall accuracy of 1^{o}C means that the difference between the predicted and measured temperature was lower than 1^{o}C for 95% of data points.

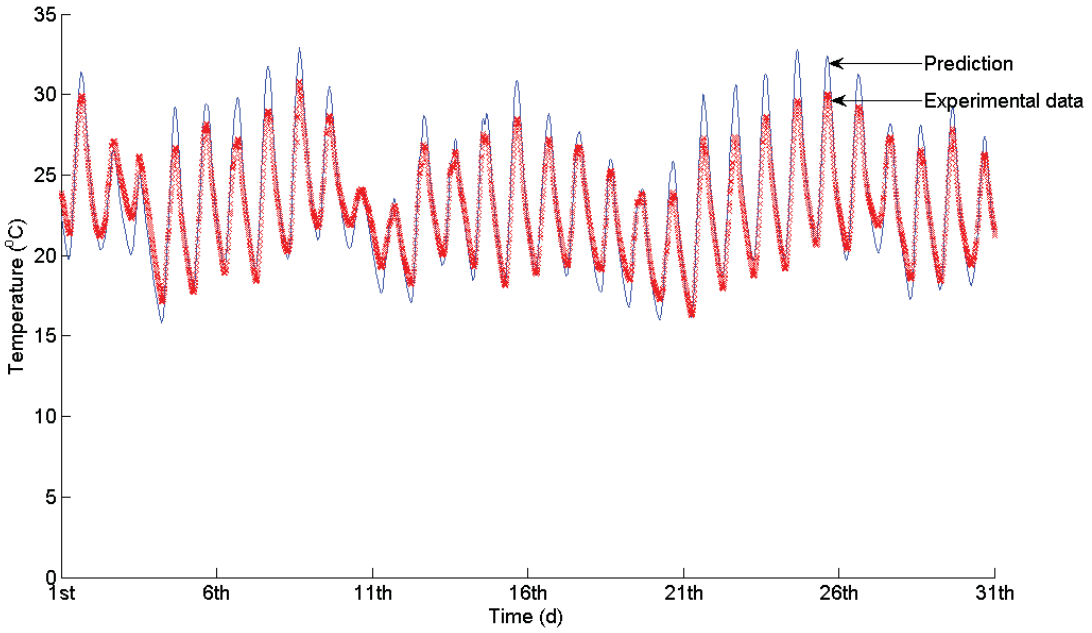

Figure 3.3: Predicted (blue line) and measured (red crosses) temperature profile in the high-rate algal pond in Hamilton (New Zealand) over the month of January 2009 – *Extracted from Article 2*.

The daily peak temperatures were overestimated and the temperature during winter months was underestimated by the model as shown in the supplementary information S5 of Article 2. Two possible explanations for these trends are that (1) air emissivity was assumed to be constant through time, although it is actually a function of meteorological parameters (Culf and Gash, 1993) and (2) the impact of the paddle wheel on shading and evaporation in the pilot-scale pond used for validation was neglected. Figure 3.4 shows that, on a yearly basis, the air radiation and pond radiation generally compensate each other. The pond radiation is proportional to the pond temperature to the fourth, while the air radiation is proportional to the air temperature to the fourth (Table 3.3, Equations 3.12 and 3.14). As the pond and air temperatures generally differed by less than 10^{o}C, their values in Kelvin are relatively similar, and the two heat flows tend to balance themselves. Therefore, solar radiation was mainly responsible for temperature raise at daytime, whereas conduction and evaporation were the main drivers to temperature decrease at night. In addition, reflection of solar radiation at the water surface is higher in winter than in summer due to higher incident angles. As a result, the solar heat flow in winter may be overestimated. These different contributions may explain

why the model was slightly less accurate during winter, because there is less inaccuracy on the prediction of the solar heat flow than other heat flows.

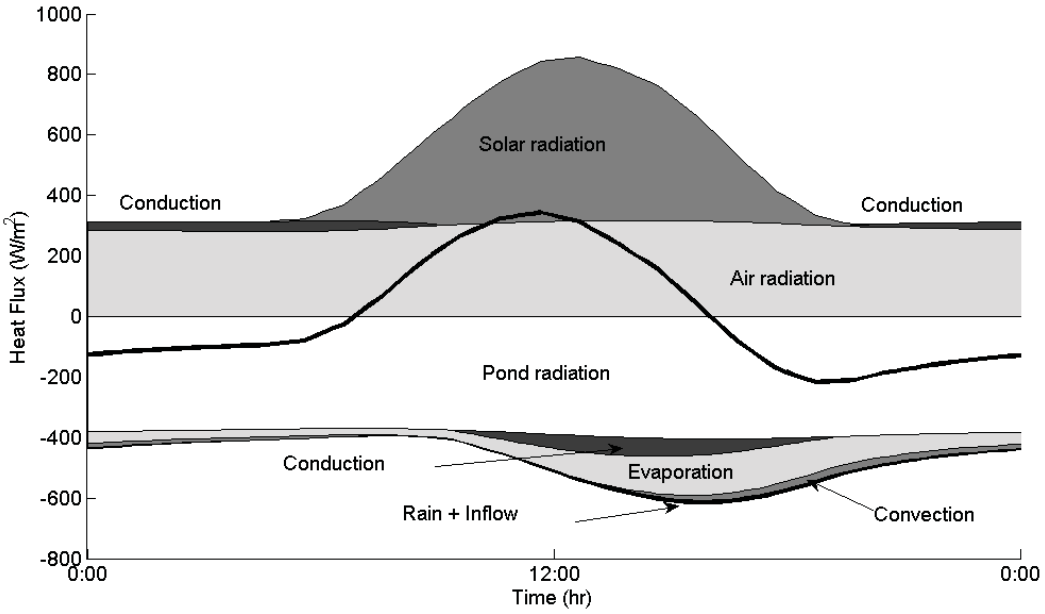

Figure 3.4: Changes in heat fluxes (annual average) reaching the high rate algal pond. The thick plain line represents the total heat flux. The value of each heat flux at time *t* was computed as the average of the heat flux over the year at this time – *Extracted from Article 2*.

It may have been possible to adjust key inputs parameters to improve the accuracy of the temperature prediction for the specific open pond in New Zealand. However, the temperature model was developed with the objective to predict temperature on a large range of system designs as explained in the preface of this chapter. As a result, specific adjustments were thus avoided in order to keep the temperature model universal. Although the impact of these systematic errors on the overall predicted productivity should be minor considering the magnitude and duration of these events; this potential effect should be quantified when the full biological model is available.

3.3.4. Theoretical expressions against empirical expressions in the temperature model for open ponds

As described in Section 3.3.1, the expressions of the eight heat flows reaching the open pond were all based on theoretical considerations. The objective of this section is to demonstrate that using empirical formulas instead leads to lower levels of accuracy. For this purpose, alternative heat flow expressions used in nine prior models were systematically substituted into our model and evaluated against the experimental data. As can be seen in Table 3.4, the accuracy of Models 1-5 for evaporation and convection (see Table 3.2) was generally lower than the accuracy of the theoretical model[6] (Model 3 showed similar accuracy given the uncertainty of the input parameters). As previously discussed, the equations expressing pond radiation, air radiation, and the heat flow associated with the inflow in the new universal model have been used in prior models. With regard to the other heat flows our analysis showed the following:

- The evaporative heat flow represented up to 22% of the total heat loss (Figure 3.4). Consequently, the poor representativeness of empirically-based expressions of convection and evaporation derived from different systems (e.g., mechanically agitated ponds) likely explain the lower accuracy of these approaches (Table 3.4).
- Conduction was found to contribute little to the total heat balance (Figure 3.4). Therefore, assuming the ground temperature to be a linear function of soil depth or even neglecting the conductive heat flow had minor impacts on accuracy (Table 3.4).
- The heat flow associated with rain was minimal (Figure 3.4) and could be neglected from the model with little loss of accuracy (Table 3.4).

[6] The term “theoretical” is used here only by contrast to prior approaches that were based on empirical formulas. However, it can be noted that some physical parameters of our “theoretical model” (e.g. thermal properties) were determined experimentally.

Table 3.4: Accuracy of temperature prediction and water evaporation (annual average) using models constructed by replacing selected heat flows with alternative expressions used in prior models – *Extracted from Article 2*.

Heat flow	Expression	Overall accuracy (^{o}C)	Error on the peak temperature (^{o}C)	Evap. (mm/d)
Evaporation[a] /Convection	Model 1	4.3	1.5	3.2
	Model 2	4.0	1.4	3.0
	Model 3	2.9	1.4	2.3
	Model 4	5.5	1.4	3.0
	Model 5	3.2	1.1	2.8
Conduction	Simple	3.1	1.6	2.3
	Neglected	3.1	1.5	2.3
Rain	Neglected	2.7	1.3	2.2
Theo. Model		**2.6**	**1.3**	**2.2**

[a] See Table 3.2 for a description of evaporation Models 1 to 5.

Previous studies showed the impact of temperature during outdoor algal cultivation. For example, Richmond et al. (1990) showed that heating a *Spirulina* culture in the morning increased productivity in a raceway pond by 20%. Furthermore, Zhang et al. (1999) achieved a 50% increase in productivity by maintaining temperature in its optimal range (37−43 °C) during *Chlorella sorokiniana* outdoor cultivation instead of letting the temperature fluctuate with the ambient temperature (20−44°C). As shown by Table 3.4, the empirically-based model leading to the highest level of inaccuracy (Model 4) exhibited overall inaccuracy higher than 5°C. Because it is generally accepted that the growth rate of microalgae doubles when temperature increases by 10 °C within a certain range (e.g., 10−30 °C for most commercial algal species; Davison, 1991), this error of 5°C could translate into a productivity prediction inaccuracy of approximately 40%. The recent cost-analysis of Rogers et al. (2013) investigated the case of algal cultivation in open ponds in New Mexico. The productivity value assumed in this study was 5.5 kg/m^2-yr, which was used as a conservative value when compared to previous studies (See Table 0.1). In the sensitivity analysis also performed in the Rogers et al. (2013), a drop in productivity by 30% was shown to increase the cost of biofuel from 3.21 $/L to approximately 4.8 US$/L. If we extrapolate this result linearly, an error of 5^{o}C in the temperature prediction may lead to underestimate the price of biofuel by 2 $US/L.

As a result, accounting for temperature variation in full-scale systems is crucial to assess the economics of biodiesel production from microalgae.

This example only illustrates the impact of inaccurate temperature predictions in the worst-case scenario and empirically-based models such as Model 3 could also provide accurate predictions of temperature. However, using the theoretically-based equations listed in Table 3.3 rather than empirically-derived formulas does not significantly increase the level of complexity of the model. Indeed, the computational time for a simulation was the same regardless of the equations chosen. In addition, using the equations listed in Table 3.3 rather than empirically-based equations does not require additional model calibration as most of the input parameters are universal constants as discussed in Section 3.3.2. As the new temperature model was found more accurate than prior approaches with no significant increase in the complexity of the model inputs, the theoretical modelling approach was used in the rest of this thesis.

3.4. Temperature models in closed photobioreactors

3.4.1. Heat balance in photobioreactors

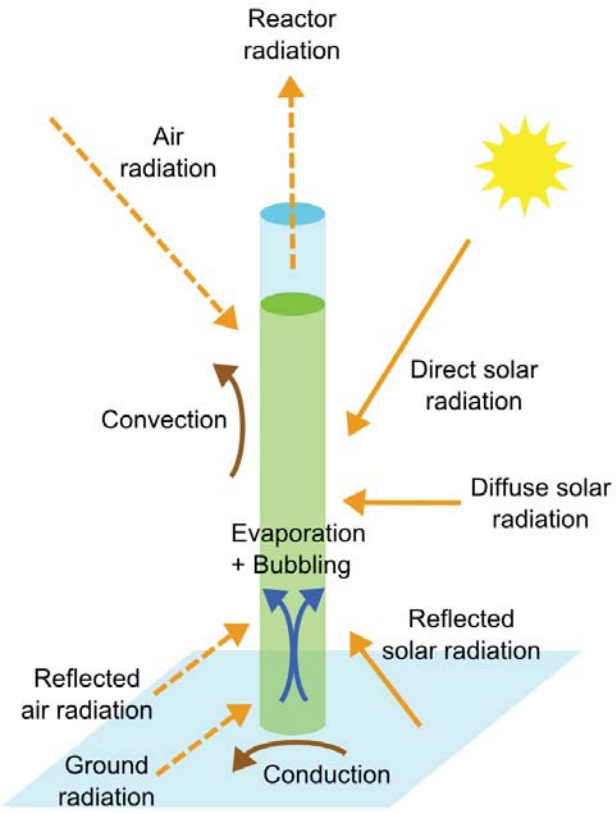

Figure 3.5: Different heat flows reaching the algae in an outdoor photobioreactor.

The temperature model for the closed photobioreactor was developed based on the heat flows identified in Section 3.2.1. Due to the vertical geometry of the photobioreactor, the temperature model was however adapted as follows:

- The fraction of radiation (air and solar radiation) reflected onto the ground surface was accounted for in the heat balance (Figure 3.5);
- The contributions of the direct and diffuse solar radiations were segregated: direct solar radiation has a direction fixed by the sun position and reaches only the half of the reactor surface exposed to the sun. In comparison, diffuse solar radiation reaches the reactor on its entire surface.

- The model accounted for the fraction of the long-wave radiation emitted by the ground surface captured by the reactor.
- The evaporation of the reactor was assumed to be mainly due to the bubbling of air in the culture.
- The expression of convective flow was adapted to the cylindrical geometry of the reactor.
- The thermal mass of the reactor wall was neglected compared to the thermal mass of the liquid culture.

A total of 11 heat flows were considered in the heat balance, which was expressed by the following equation:

$$\rho_w V_r Cp_w \frac{dT_r}{dt} = Q_{ra,r} + Q_{ra,d} + Q_{ra,D} + Q_{re,s} + Q_{ra,a} + Q_{re,a} + Q_{ra,g} + Q_c + Q_{ev} + Q_b + Q_{cond} \quad (3.20)$$

where ρ_w is the density of water (kg/m^3), V_r is the reactor volume (m^3), Cp_w is the water heat capacity (J/kg-K), T_r is the bioreactor temperature (K), $Q_{ra,r}$ is the radiation from the reactor (W), $Q_{ra,d}$ is the solar diffuse radiation (W), $Q_{ra,D}$ is the direct solar radiation (W), $Q_{re,s}$ is the solar radiation reflected on the ground (W), $Q_{ra,a}$ is the air radiation (W), $Q_{re,a}$ is the reflected air radiation (W), $Q_{ra,g}$ is the ground radiation (W), Q_c is the convection (W), Q_{ev} is the evaporative heat flow (W), Q_b is the heat flow associated with bubbling (W), and Q_{cond} is the conduction (W).

Table 3.5 summarizes the expressions of the different heat flows considered in the heat balance for the reactor. Further details on the derivation of these equations and associated assumptions can be found in the materials and methods section of Article 3.

Table 3.5: Expression of the different heat flows reaching the closed photobioreactor – *Formulas were extracted from Article 3*.

Heat flow	Equation	
Reactor radiation	$Q_{ra,r} = -\sigma\tau\varepsilon_r\left(\pi R_r^2 + 2\pi R_r L_r\right)T_r^4$	(3.21)
Diffuse solar radiation	$Q_{ra,d} = \tau\varepsilon_r K_d H_g\left(\pi R_r^2 + \pi R_r L_r\right)$	(3.22)
Direct solar radiation	$Q_{ra,D} = \tau\varepsilon_r\left(1-K_d\right)H_g\left(\pi R_r^2 + 2R_r L_r \tan\theta_z\right)f(t)$	(3.23)
Reflected solar radiation	$Q_{re,s} = \tau\varepsilon_r r_g H_g \pi R_r L_r f(t)$	(3.24)
Air radiation	$Q_{ra,a} = \tau\varepsilon_r\varepsilon_a\sigma T_a^4\left(\pi R_r^2 + \pi R_r L_r\right)$	(3.25)
Reflected air radiation	$Q_{re,a} = \tau\varepsilon_r r_g\varepsilon_a\sigma T_a^4\pi R_r L_r$	(3.26)
Ground radiation	$Q_{ra,g} = \tau\varepsilon_r\varepsilon_g\sigma T_g^4\pi R_r L_r$	(3.27)
Convection	$Q_c = h_c\left(T_a - T_r\right)2\pi R_r L_r$	(3.28)
Evaporation	$Q_{ev} = -\left(1-RH\right)X_a F_b L_w$	(3.29)
Bubbling	$Q_b = -Cp_a\left(T_r - T_a\right)\rho_a F_b$	(3.30)
Conduction	$Q_{cond} = -k_{wall}\dfrac{T_r - T_g}{l_{wall}}\pi R_r^2$	(3.31)

Symbols: σ: Boltzmann constant (W/m^2-K^4); τ: wall transmittance; $\varepsilon_r/\varepsilon_a$: reactor/air emissivity; R_r/L_r: reactor radius/height (m); T_r: reactor temperature (K); K_d: diffuse fraction of the solar irradiance; H_g: solar irradiance (W/m^2); θ_z: angle between the sun and a vertical axis; *f(t)*; shadow function equal to 0 if the reactor is in the shadow of a building and 1 otherwise; r_g: ground reflectivity; T_a: air temperature (K); T_g: ground temperature (K); h_c: convective coefficient (W/m^2-K); *RH*: relative humidity of the incoming air; X_a: water concentration in saturated air (kg/m^3); F_b: bubble flow rate (m^3/s); L_w: water latent heat (J/kg); Cp_a: air thermal capacity (J/kg-K); ρ_a: air density (kg/m^3); k_{wall}: reactor wall thermal conductivity (W/m-K); l_{wall}: reactor wall thickness (m).

3.4.2. List of variables and parameters

As shown in Table 3.5, numerous variables and parameters must be determined to predict the temperature of a closed photobioreactor. While most of these model inputs are universal constants, a significant number of parameters and variables must be determined for each specific location, reactor geometry and reactor operation (Figure 3.6):

- Weather variables that can be obtained from a weather station (for example by using the data freely available from NIWA in New Zealand or NCDC in the US; see Articles 2 and 3).
- Operational parameters that can be adjusted to optimize algal productivity and minimize water demand (see Chapter 5);
- Geometrical parameters;
- The latitude of the location considered;
- The parameters characterizing the 'environment around the reactor' shown in Figure 3.6 influencing the wind profile (Gipe, 2004);
- The ground characteristics that influence the fraction of reflected solar radiation reaching the algae;
- The fraction of solar energy converted into chemical energy through photosynthesis (in general taken at 2.5%);
- The transmittance of the reactor τ that was determined experimentally on the photobioreactors used for model validation (see Section 3.4.4 for details).

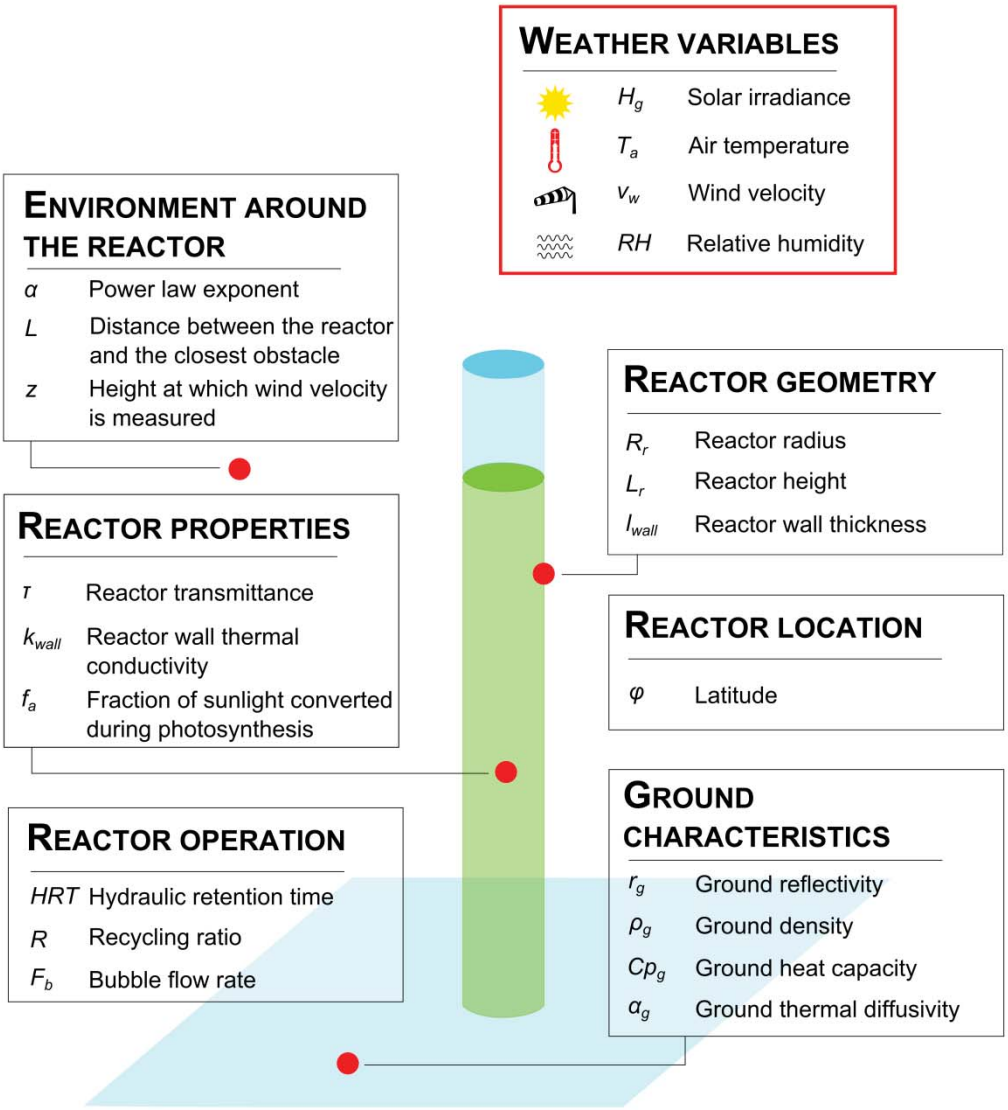

Figure 3.6: Inputs of the temperature model for closed photobioreactors which are specific to the location, the reactor geometry and the reactor operation.

3.4.3. Accuracy of the temperature model for photobioreactors

The accuracy of the temperature model for closed photobioreactors was assessed against experimental data collected from an outdoor photobioreactor located in Singapore (reactor radius: 0.095m, height: 1.8m, working volume: 50L). The reactor was operated as a batch system for the cultivation of *Chlorella sorokiniana*. A complete description of the reactor and its operation can be found in the materials and methods section of Article 3. The experimental data used to validate the model was not recorded continuously and, as a result, only the overall accuracy was used to compare the predicted temperature to experimental data (and not the error on the afternoon peak temperature, defined in the case of the open ponds in Section 3.3.3).

Figure 3.7 illustrates the good fit of the temperature model to the experimental data collected during a typical day of cultivation. Over the entire cultivation period, the model predicted the temperature of the culture broth of a photobioreactor operated in Singapore with an accuracy of ±2.45°C (N = 107, Figure 3.8). The homogeneous distribution of error shown by Figure 3.8 suggests that the model did not systematically overestimate or underestimate temperatures over the range measured (23-41°C). In consequence, the assumptions made to simplify modelling can be considered as acceptable (a detailed discussion on these assumptions can be found in the materials and methods section of Article 3).

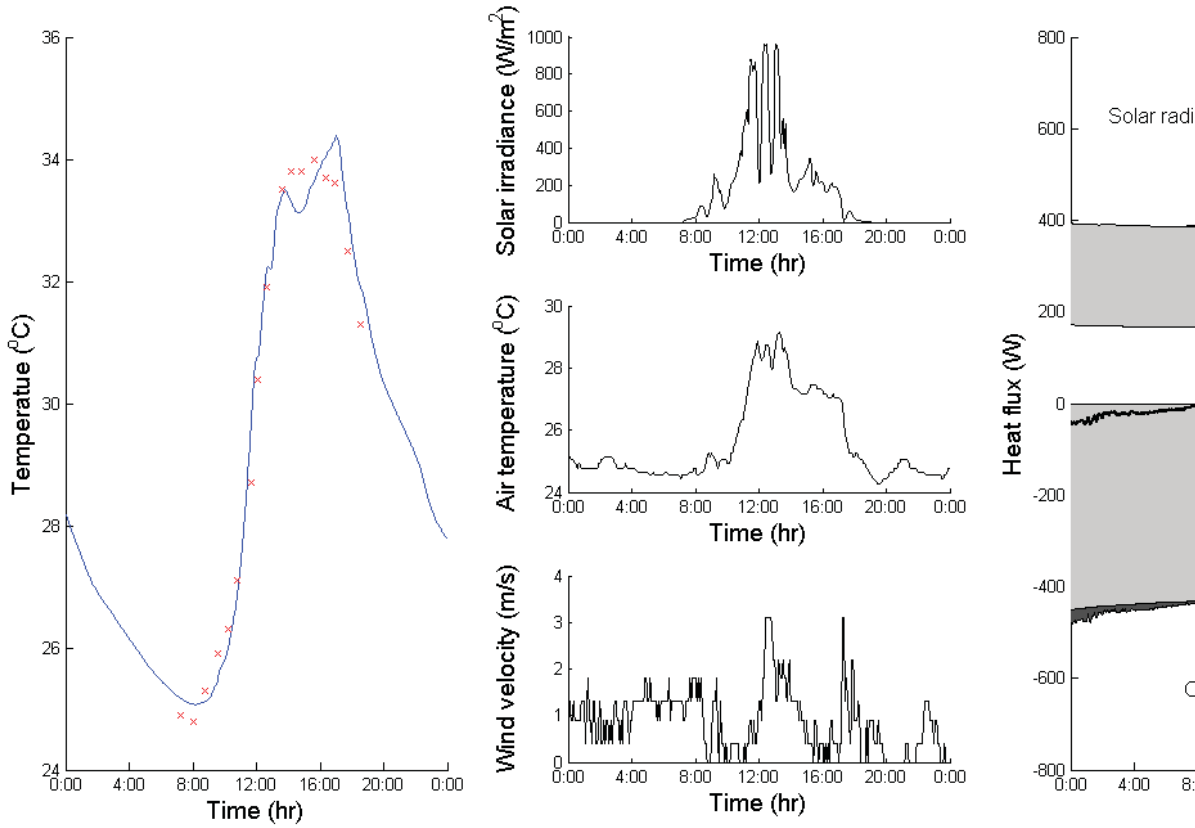

Figure 3.7: *Left*: Change in experimental (crosses) and predicted (plain line) temperatures inside a cl (August 22, 2008) during outdoor operation in Singapore. *Middle*: Meteorological data on the same day. *R* photobioreactor on the same day (the bold line represents the total heat flow)

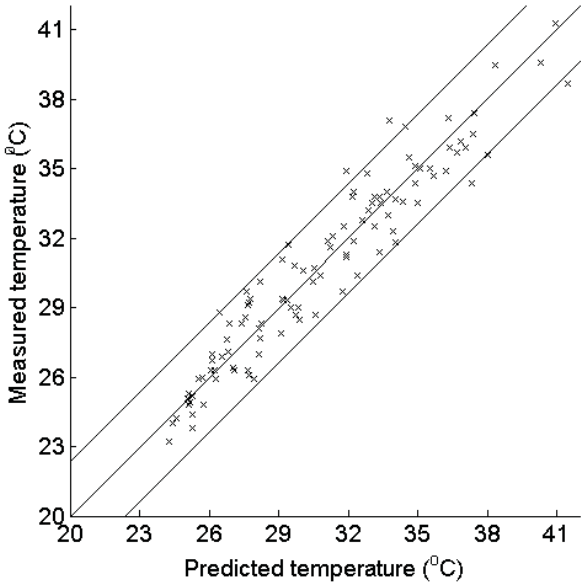

Figure 3.8: Comparison of experimental and predicted temperatures inside a column photobioreactor during outdoor cultivation in Singapore – *Extracted from Article 3*.

As can be seen in Figure 3.7, Five flows typically dominate the heat balance: radiation from the air, radiation from the ground, radiation from the reactor, solar radiation (including direct, diffuse, and reflected radiations), and convection. Evaporation from the top surface, cooling by bubbling, and conduction to the soil were not significant (<10 W). The positive heat flows from ground radiation (180-220 W) and air radiation (180-220 W) are within the same range as radiation losses from the reactor (-360 to -440 W). These ground, air, and reactor radiative flows are relatively constant with respect to time because their proportionality to temperature is to the fourth power (the ground surface, the air, and the reactor temperatures fluctuated within less than 10% when expressed in K). Thus, changes in the reactor broth temperature were mainly due to significant fluctuations in solar radiation (0-200 W) and convective flow (-30 to 50 W), the latter being correlated to the difference between the air and the reactor temperatures. Losses from convection could not compensate the solar heat flow during daytime, which caused temperature to increase. However, convection was the main flow contributing to temperature decrease at night. On the basis of these observations, a simplified model was constructed using only solar radiation and convection in the heat balance and the model was fitted over the entire set of experimental data (see results and discussion section of Article 3). The simplified model was able to predict temperature with an accuracy of ±4.7°C.

This approach underestimated cooling at night and the predicted temperature at sunrise of the following day was overestimated by 2°C. This can be explained by the fact that the difference between the radiation from the surroundings (air and ground) and from the reactor is, although small, not negligible compared to convection at night.

3.4.4. Refinement of the temperature model for photobioreactors

The temperature model for the photobioreactors was developed in the early stage of this PhD thesis. As described in the previous section, the model was able to predict temperature in an outdoor photobioreactor with a satisfying level of accuracy. Yet, simplistic assumptions were made to determine the amount of solar radiation entering the reactor. As accurate estimations of the amount of light entering the reactor were crucial for productivity predictions, the expressions of the solar heat flows were later refined. The objective of this section is to detail how the model was refined. The following section (3.4.5) describes how these refinements impacted the accuracy of the temperature prediction.

First, the diffuse fraction of the solar radiation reaching the reactor was assumed to be constant in the original version of the model. However, according to Duffie and Beckman (2006), the diffuse fraction of solar radiation (K_d) is a function of multiple meteorological variables and can vary from 0.165 (clear sky conditions) to 1 (overcast conditions). Béchet et al. (2013) demonstrated that assuming a constant K_d fraction may cause an inaccuracy of up to 40% on the amount of light reaching the algae (Béchet et al. 2013). In order to refine the expression of the K_d coefficient, the Erbs correlation was used as described in the supplementary information S2 of Article 5 (Duffie and Beckman, 2006).

The second improvement on the temperature model was on the expression of the amount of radiation reflected on the wall surface. In the original version of the model, it was assumed that 10% of the radiation reaching the reactor was reflected on the reactor wall. However, this reflected fraction is theoretically a function of the angle between the incident light and the reactor wall. In the case of the direct solar radiation, this angle changes over time with the sun position. The angular dependence was accounted for in the updated version of the model by using the reflection laws of Fresnel (see Supplementary information S2 in Article 5).

Finally, the expression of the air emissivity was also changed from the original version of the model. The air emissivity was originally taken equal to 1 for simplicity but theoretical

calculations performed later showed that this value was most likely closer to 0.8 than 1 (see the supplementary information S3 of Article 2).

3.4.5. Comparison of the original and refined versions of the temperature model for photobioreactors

In order to compare the original and the refined versions of the temperature model, the two temperature predictions were compared to different data sets. The first data set was extracted from the outdoor photobioreactor in Singapore described in Section 3.4.3. The other experimental data were taken from outdoor photobioreactors having the same geometry than in Singapore but operated in New Zealand. A detailed description of these reactors and their operation can be found in Section 2.1 of Article 5.

As shown by Table 3.6, the refinement of the temperature model for the closed photobioreactor did not systematically contribute to increase the accuracy of the temperature prediction. As discussed in the study of Béchet et al. (2013), the uncertainty on key inputs of the model such as the ground reflectivity can cause a significant inaccuracy on the temperature prediction. It is therefore challenging to reach a level of accuracy higher than the level of approximately 3^{o}C already obtained with the original model for the closed photobioreactor. The refined model was nevertheless preferred in the subsequent simulations (including productivity) because the ability to theoretically determine the light reaching the algae should generate a more accurate prediction of the productivity[7].

Table 3.6: Overall accuracy of temperature predictions by the 'original' and 'refined' versions of the model (*N*: Number of data points).

Data set	**Original model**	**Refined model**	***N***
Singapore (August-September 2008)	2.45	3.46	107
New Zealand (April-May 2011)	3.33	3.90	5181
New Zealand (March 2012)	4.22	4.27	283
New Zealand (April 2012)	5.45	5.33	415
New Zealand (June 2012)	4.48	2.62	1009

[7] In the following, the term 'temperature model' for the photobioreactors will refer to the refined version of the model.

3.4.6. Temperature control in closed photobioreactors

As shown in Figure 3.7, important temperature variations can be observed in closed photobioreactors operated in hot locations such as Singapore. These temperature variations were also observed at different locations such as Italy where the temperature of an outdoor vertical panel photobioreactor was shown to reach levels as high as 48^{o}C (Tredici and Materassi, 1992). Yet, the maximal temperature tolerated by most algal species is around 35^{o}C (Wigmosta et al., 2011). A potential strategy to avoid high temperature events would consist on controlling the reactor temperature. Replacing a fraction of the culture volume by fresh medium has a minimal impact on temperature for typical values of hydraulic retention times (see Section 3.3.3). As a result, this strategy cannot provide efficient temperature control. This section aims to illustrate how the knowledge of temperature variation in closed photobioreactors can be used to assess the feasibility of active temperature control strategies.

As a case study, the temperature model for a single closed photobioreactor was used to quantify the amount of cooling necessary to maintain the temperature of a photobioreactor under or at 35^{o}C. In order to perform these calculations, hourly meteorological data from the five climatic locations shown in Figure 2.4 were used as input of the temperature model. It was also assumed that the closed photobioreactor had the same geometry as the reactor used for the model validation in Singapore (reactor radius: 0.095m, height: 1.8m, working volume: 50L). Figure 3.9 shows the energy demand necessary for controlling the reactor temperature below 35^{o}C.

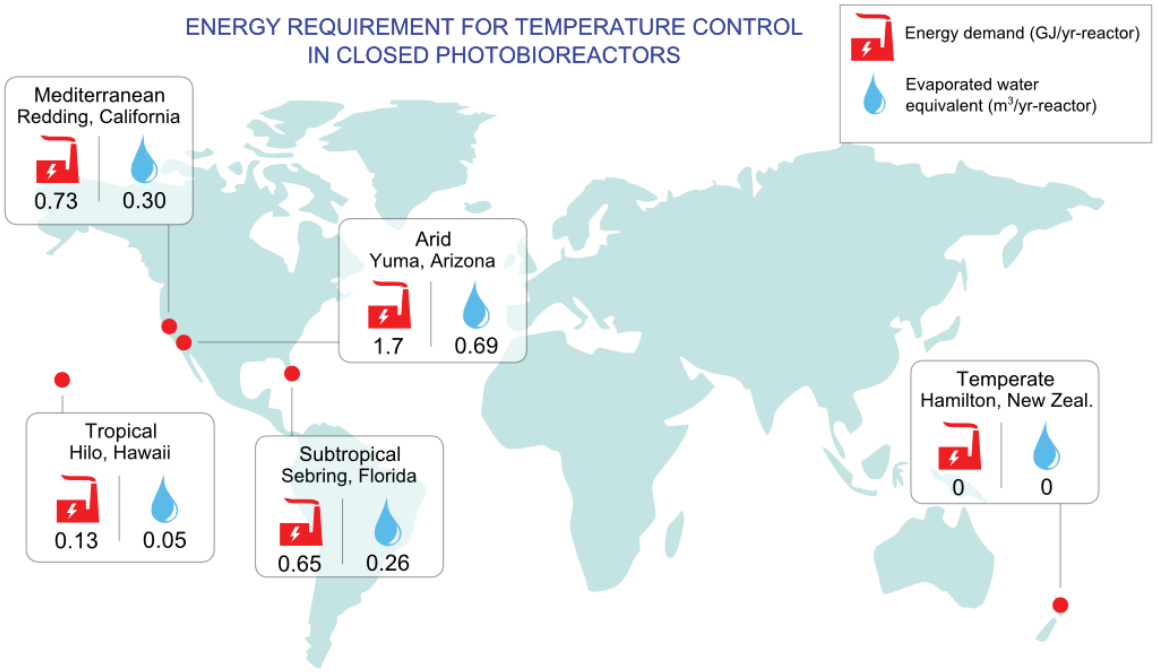

Figure 3.9: Amount of energy and water equivalent necessary to maintain a closed photobioreactor at or below 35°C.

Figure 3.9 shows that maintaining broth temperature under or at 35°C in a closed photobioreactor could require extracting up to 1.7 GJ of heat per year for every reactor, depending on the location. To illustrate the potential environmental and economic implications of temperature-control, the feasibility of cooling the reactors using water evaporation at the surface of the reactor walls was investigated as this strategy is commonly proposed in the literature (Singh and Sharma, 2012; Torzillo et al., 1986; Tredici, 2004). If cooling was thus performed, 0.69 m^3 of fresh water would be needed per year to cool a single 50L-closed photobioreactor located in Arizona. To put this figure into perspective, it would be necessary to collect all the yearly rainfall on 14 m^2 just to cool down a single reactor during one year at this location. An alternative to rainwater would be using brackish water that would need to be first purified to avoid deposition of salts on the reactor wall which would cause significant shading. In this case, if reverse osmosis was used to remove salts from water, the cost of water purification would represent US $0.55 dollars per reactor/year in Arizona (assuming a RO cost of US $0.8 m^{-3} based on the US $0.26-1.33 m^{-3} range for full-scale brackish water given by Karagiannis and Soldatos, 2008). Based on productivity values of 5.3 kg/m^2-yr in Arizona in a temperature-controlled photobioreactor (Batan et al., 2013) and by

assuming a reactor density of 1 to 2 reactor(s)/m^2, the cost of water purification would represent US $0.10-0.20 per kg of algae. RO treatment would therefore be uneconomical for reactors cooling since Chisti (2008) estimated that the total cost of algae biomass cultivation should not exceed US $0.34 kg^{-1} to be competitive with oil at US $100 a barrel. Of course, it is not impossible that targeted temperature-control strategies may support significant productivity gain at affordable energy inputs under specific conditions. However, the calculations shown above do not account for inefficiencies in heat transfer and algal biofuel generation. In conclusion, the economic and environmental costs of active temperature control therefore seriously threaten the feasibility of algal cultivation at hot locations.

Chapter 4: Productivity model

Preface

The previous chapter focuses on the prediction of temperature in full-scale cultivation systems. In order to assess how the temperature variation impacts algal productivity in these systems, a model predicting algal productivity as a function of light and temperature was developed. Chapter 4 describes the approach used to develop and validate this productivity model. This approach involved three main steps as can be seen in Figure 4.1. First, the kinetic parameters of the productivity model were obtained for *Chlorella vulgaris* from short-term indoor experiments. Secondly, the model was validated against experimental data collected from indoor bench-scale reactors operated under constant light and temperature. Thirdly, the model predictions were compared to biomass productivities measured in outdoor pilot-scale reactors.

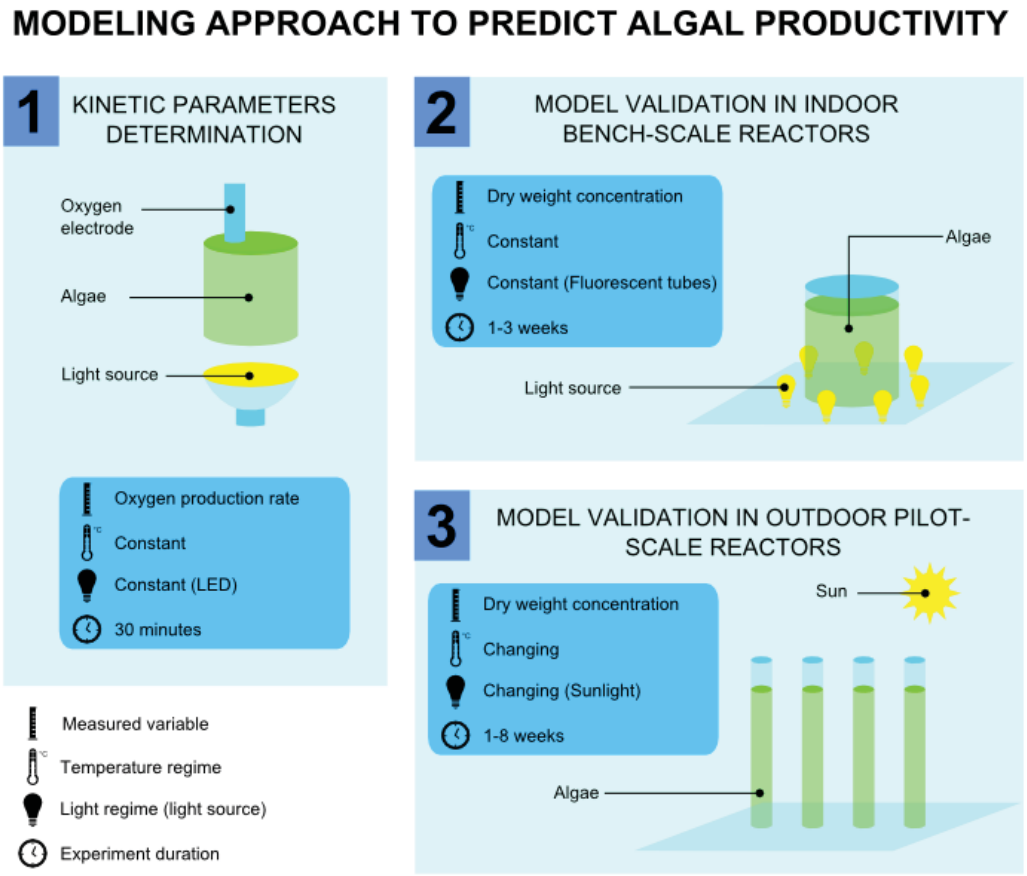

Figure 4.1: Modelling approach to predict algal productivity

4.1. Introduction

This chapter describes how the productivity model developed in this thesis was developed and validated against experimental data. Section 4.2 presents the mathematical expression of the productivity model. Section 4.3 describes how the kinetic parameters of the productivity model were experimentally determined. Section 4.4 discusses scale-up issues associated with the application of this model to predict the productivity of full-scale cultivation systems. Sections 4.5 and 4.6 detail how the model was validated against indoor and outdoor cultivation data, respectively. The objective of these validations was to determine the level of accuracy of the productivity predictions. Section 4.7 discusses if this level of accuracy is high enough to assess the economics and environmental impacts of full-scale cultivation. Section 4.8 demonstrates the necessity of using hourly temperature predictions for achieving meaningful assessments of algal productivity at full-scale.

4.2. Mathematical expression of the productivity model

As defined in Section 1.1, algal productivity P_{net} (kg O_2/s) is the difference between the rate of photosynthesis P (kg O_2/s) minus the rate of respiration ER (kg O_2/s). Based on the guidelines established in Chapter 1 (see Section 1.3.7 for a summary), the productivity model was developed by using the following approach. First, the overall rate of photosynthesis of an algae culture P (kg O_2/s) was expressed as the sum of the rates of photosynthesis in each volume element dV of the culture:

$$P = \int_V P_{loc}\left(\sigma_X I_{loc}, T, X\right) \cdot dV \quad (4.1)$$

where P_{loc} is the local volumetric rate of photosynthesis in each volume element (kg O_2/m^3-s), σ_X is the extinction coefficient (m^2/kg), I_{loc} is the local light intensity in each volume element (W/m^2), T is the temperature (^oC), X is the algal concentration (kg/m^3), and V is the culture volume (m^3).

Secondly, the local light intensity I_{loc} in each volume element was determined by using a modified Beer-Lambert law described as follows:

$$I_{loc}(l) = I_0 \exp\left(-\sigma_X X l\right) \quad (4.2)$$

where I_0 is the irradiance external to reactor (W/m^2), X is the algal concentration (kg/m^3), and l is the light path from the outside of the reactor to the volume element (m).

Thirdly, the rate of respiration at night-time[8] in the entire reactor ER_{night} (kg O_2/s) was expressed using first-order kinetics:

$$ER_{night} = -\lambda X V \quad (4.3)$$

where λ is the maintenance coefficient (kg O_2/kg-s).

[8] As there is no consensus on the best approach to model the rate of respiration at day-time in the literature, only the rate of respiration at night-time is discussed in this section. See Section 4.3.5 for a discussion on the rate of day-time respiration.

4.3. Determination of the model kinetic parameters

To the best of our knowledge, no prior model of productivity was developed for the species *Chlorella vulgaris* for a complete range of light intensities and temperatures. The objective of this section is therefore to detail how the kinetic parameters of the productivity model were obtained. Section 4.3.1 first presents the design of the vessels used for the determination of the kinetic parameters. Section 4.3.2 focuses on how the light distribution was modelled using a modified Beer-Lambert law as described by Equation 4.2. Section 4.3.3 compares different mathematical formulas to express the local rate of photosynthesis P_{loc} in Equation 4.1 as a function of the local light intensity I_{loc}. Section 4.3.4 discusses the variation of the model parameters with temperature. Section 4.3.5 details how the model of respiration was developed. Section 4.3.6 details how the kinetic parameters were converted from oxygen to biomass production rates. Finally, Sections 4.3.7 and 4.3.8 summarize the equations and the inputs of the productivity model, respectively.

4.3.1. Experimental device used to determine kinetic parameters

The device used to determine the model kinetic parameters was composed of six cylindrical vessels placed above LED lamps which full specifications are given in Article 3 (Figure 4.2). The side and the top of the vessels were made of aluminium and were therefore opaque, while the bottom was made of transparent plastic. The plastic material was shown not to impact the light spectrum through spectrophotometry analysis. The vessels were equipped with a mixing device ensuring homogenous oxygen concentration in the cultivation broth. The vessels were also gas-tight and mainly constructed of aluminium; the impact of oxygen absorption onto the plastic material at the vessel bottom was therefore neglected. Each vessel was equipped with a dissolved oxygen electrode connected to a computer. Dissolved oxygen electrodes were calibrated in the vessels filled with well-aerated BG-11 at equilibrium with the atmosphere and oxygen-free BG-11 enriched in more than 5g/L sodium sulphite. At the start of an experiment, the LED lamps underneath each vessel were turned on and the recording of the dissolved oxygen concentration and temperature in each vessel started. The rate of oxygen production was computed by linear regression of the dissolved concentration over time. When the dissolved concentration reached more than 80 to 90% of the saturation value in any vessel, the lights were turned off. Indeed, reaching levels higher than 100% caused oxygen degasing

in the vessel and therefore inaccurate measurements of the oxygen productivity. The consequential rate of oxygen consumption was then measured as the algae switched from photosynthesis to respiration[9]. Temperature was maintained constant (at approximately ±1.5^{o}C) during the entire experiment by circulating air between the LED lamps and the vessels (Figure 4.2). Experiments were performed at different temperatures by placing the entire device in a temperature-controlled incubator. The algae used during model parameterization were extracted from bench-scale photobioreactors (shown in Figure 4.3) cultivated for around 7 days in a fed batch regime under high light intensities (65 W/m^2 and 49.9 W/m^2) at 30^{o}C. These cultivation conditions ensured that algae were adapted to cultivation conditions similar to outdoor conditions.

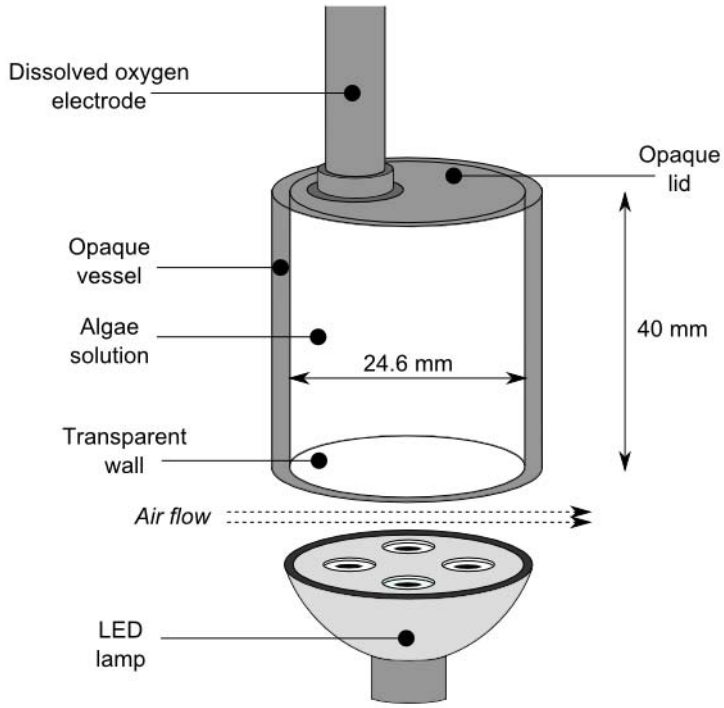

Figure 4.2: A vessel of the device used for model development – *Extracted from Article 4.*

[9] The rate of respiration in the dark was assumed to represent the rate of respiration at night-time.

4.3.2. Light distribution in the device vessels

As explained in Section 1.3.4, a modified Beer-Lambert law was used to determine the light distribution in the culture broth (Equation 4.2). This type of equation is empirical and specific to each algal species. This section explains how the extinction coefficient in Equation 4.2 was empirically expressed as a function of the algal concentration X[10].

The amount of light transmitted through the device vessels shown in Figure 4.2 was measured for different algal concentrations and light intensities. The extinction coefficient σ_X was then expressed as a function of transmittance by reversing Equation 4.2. Figure 4.3 shows how the measured extinction coefficient σ_X changes with the algal concentration. As shown in Figure 4.3, the variation of σ_X could be described by a power law[11] of the algal concentration, expressed as:

$$\sigma_X = AX^B \qquad (4.4)$$

where A and B are the empirical coefficients shown in Figure 4.3. Using Equation 4.4 was subsequently used to determine the light distribution in culture broth.

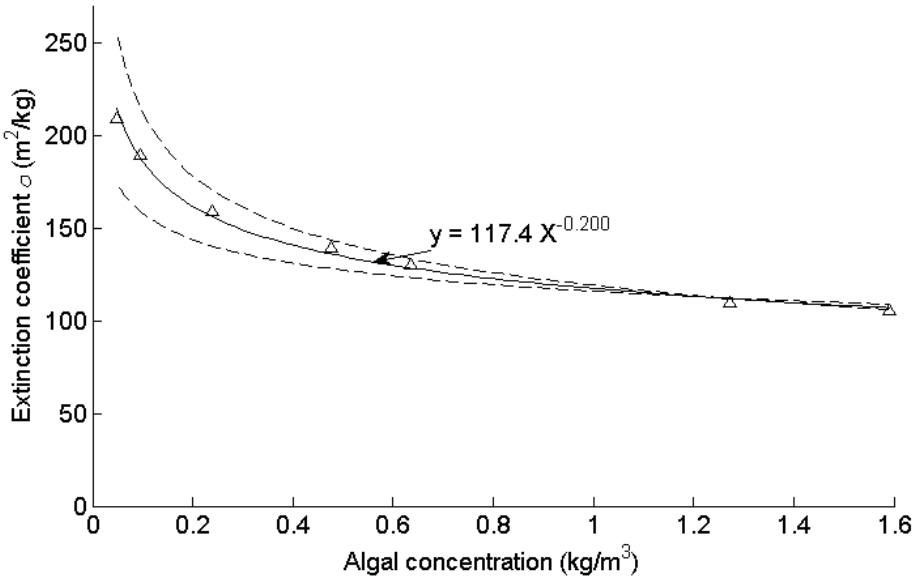

[10] The extinction coefficient was represented by the symbol σ_X in the rest of this thesis to represent its dependence with respect to the algal concentration X.
[11] Interestingly and to the best of our knowledge, this formula has never been used in prior studies.

Figure 4.3: Relationship between the extinction coefficient σ and the algal concentration (plain line). The dash-line represents the confidence interval on σ (see supplementary information S2 of Article 4 for more details) – *Extracted from Article 4*.

4.3.3. Expressing the local rate of photosynthesis as a function of local light intensity

As concluded earlier in Section 1.3.3, Type II models appear to be a good compromise between accuracy and complexity. As can be seen through Equation 4.1, using a Type II model requires expressing the local rate of photosynthesis of algae cells as a function of the local light intensity in small volume elements *dV*. No decrease of the rate of photosynthesis was observed when algae were exposed to high light intensities equivalent to full sunlight. As a result, the equation used to express the local rate of photosynthesis as a function of local light intensity only covered the light-limited and light-saturated regimes shown in Figure 1.1. Previous modelling studies demonstrated the ability of the Monod formula to predict the rate of photosynthesis of algae cultures in different cultivation systems (see Table 3 of Article 1). In particular, Yun and Park (2003) demonstrated that the Monod formula accurately predicted the rate of photosynthesis of *Chlorella vulgaris* under a large range of light intensities and algal concentrations. However, there is no consensus on the best mathematical formula to describe how the local rate of photosynthesis changes with local light intensity. In addition to the Monod formula, two other formulas are commonly used in the literature: the hyperbolic tangent formula and the Poisson formula (Table 4.1). The objective of this section is to determine which of these three mathematical formulas describes best the relationship between the local rate of photosynthesis and the local light intensity.

Table 4.1: Mathematical formulas of the local rate of photosynthesis (P_{loc}, in kg O_2/m^3-s) as a function of the local light intensity (I_{loc}, in W/m^2), the extinction coefficient σ_X, and the algal concentration X (kg/m^3). P_m (kg O_2/kg-s) represents the maximum specific rate of photosynthesis and K/σ_X (W/m^2) represents the half-saturating light intensity (the extinction coefficient σ_X was determined from Equation 4.4) – *Extracted from Article 4*.

Formula	Equation	References
Monod	$P_{loc} = P_m \frac{\sigma_X I_{loc}}{K + \sigma_X I_{loc}} X$ (4.6)	Bordel et al. (2009) Carvahlo and Malcata (2003) Collins and Boylen (1982) Kiefer and Mitchell (1983) Cornet and Dussap (2009) Cornet et al. (1995) Evers (1991) Haario et al. (2009) Jeon et al. (2005) Yun and Park (2003)
Tangent hyperbolic	$P_{loc} = P_m \tanh\left(\frac{\sigma_X I_{loc}}{K}\right) X$ (4.6)	Chalker (1980) Kurano and Miyachi (2005) Pahl-Wostl (1992) Pahl-Wostl and Imboden (1990)
Poisson	$P_{loc} = P_m\left(1 - \exp\left(-\frac{\sigma_X I_{loc}}{K}\right)\right) X$ (4.7)	Cullen (1990) Geider (1990) Geider and McIntyre (1996) Geider et al. (1998) Palhow (2005) Sakshaug et al. (1991)

In order to determine which of the three formulas in Table 4.1 describes the best the relationship between the rate of photosynthesis and the light intensity, the rate of photosynthesis was measured for different light intensities and algal concentrations. The Type II model was then fitted to this experimental data by determining the two parameters P_m and K that minimized the least-square error[12] by replacing P_{loc} in Equation 4.1 by each of the

[12] The least-square error was defined as the sum of the differences between each data point and model prediction to the square.

formulas in Table 4.1. Figure 4.4 shows the experimental data (blue dots) and the fit obtained with these three formulas (black lines). Figure 4.4 shows that the Monod, the Poisson and the hyperbolic tangent formulas were all able to fit the experimental data for different light intensities and algal concentrations. It was therefore not possible to conclude on the formula providing the best fit and consequently the choice of the formula was based on the literature. As the Monod formula is the most commonly used in the literature (Table 4.1) and was used by Yun and Park (2003) for *Chlorella vulgaris*, this formula was selected to express the local rate of photosynthesis P_{loc} as a function of the local light intensity I_{loc}.

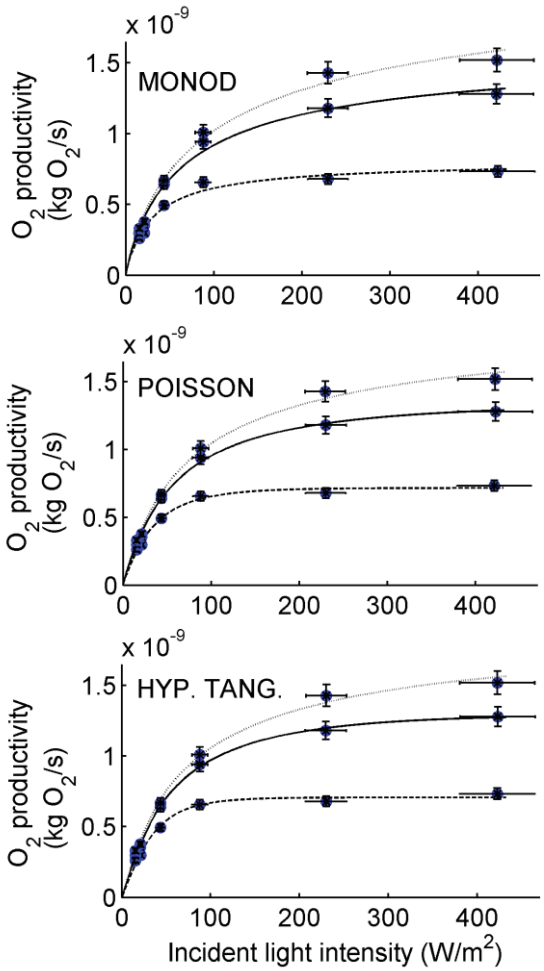

Figure 4.4: Experimental (dots) and fitted oxygen productivities in the vessels used for model parameterization (point-line: X = 0.19 kg/m^3; plain line: X = 0.43 kg/m^3; dash-line: X = 0.64 kg/m^3). The error bars represent the levels of confidence at 95% on the measured rates of photosynthesis and light intensity (see Supplementary Information S6 of Article 4 for details) - *Extracted from Article 4*

When combining Equations 4.1 and 4.2 with the Monod formula (Equation 4.5) to express the local rate of photosynthesis, the total rate of photosynthesis in the vessel used for model parameterization (Figure 4.2) can be expressed as follows (see Article 4 for details):

$$P_{O2} = \frac{P_m S}{\sigma_X} \ln\left(\frac{K + \sigma_X I_0}{K + \sigma_X I_0 \cdot \exp\left(-\sigma_X XL\right)} \right) \quad (4.8)$$

where S is the surface area of the vessel (m^2). This analytical expression was used in the following section to determine by fitting the values of P_m and K at different temperatures.

4.3.4. Values of the model parameters K and P_m at different temperatures

This section focuses on the determination of the kinetic parameters of the model formula P_m and K (Table 4.1) at different temperatures. The rates of photosynthesis of *Chlorella vulgaris* were measured in the devices shown in Figure 4.2 for different light intensities and temperatures. The kinetic parameters P_m and K were then obtained by fitting this experimental data to the theoretical expression given by Equation 4.1. As shown by Figure 4.5, the values of K and P_m follow the same evolution with temperature. Their values first increase with temperature until approximately 38°C before a rapid drop to 0 for higher temperatures.

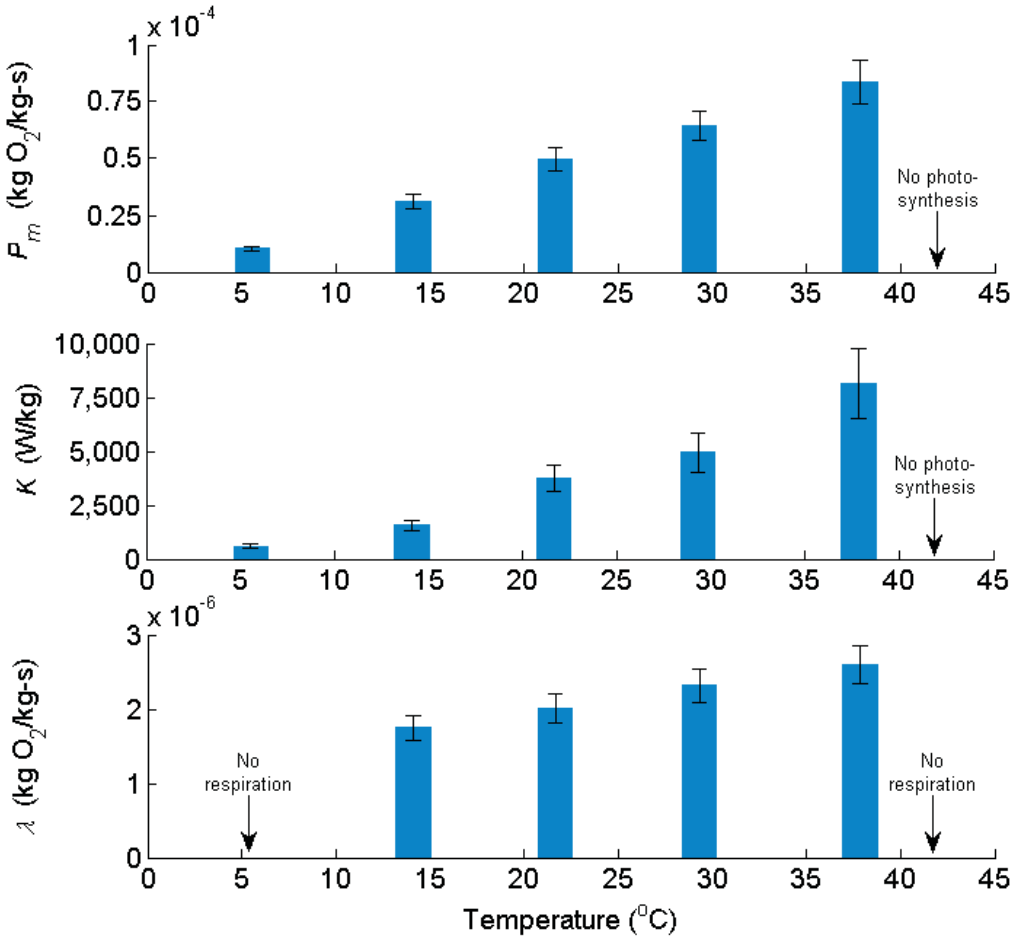

Figure 4.5: Values of P_m, K, and λ at different temperatures. The error bars represent the 95% confidence interval determined by Monte-Carlo simulations (see the supplementary information S6 of Article 4 for details) - *Extracted from Article 4*.

First, as discussed by Bernard and Rémond (2012), the trend showed in Figure 4.5 is commonly observed for microalgae. The initial increase of the rate of photosynthesis with increasing temperature is explained by the increasing activity of the key enzymes of the photosynthetic process. Whereas the Monod-like model used in this study is the mathematical representation of very complex cellular mechanisms, the impact of temperature on P_m and K can be discussed with regards to mechanistic considerations. In particular, P_m 'represents' the maximum ability of the algae to convert CO_2 into organic carbon; K 'represents' the light flow above which the rate of photon processed by PSII start to exceed the ability of the cell to use this reducing power for CO_2 fixation. Consequently, the values of both P_m and K are determined by the activity of key enzymes in the Calvin cycle. Below a specific threshold

(e.g. 38°C for *Chlorella vulgaris*), the activities of key enzymes involved in the conversion of CO_2 into biomass increase with temperature, which explains the positive dependence of P_m and K with temperature. At temperatures higher than this threshold, key enzymes are denatured, which results in the abrupt decrease of P_m and K. In the absence of clear consensus on the best mathematical formula to express the coefficients P_m and K as a function of temperature, the data showed in Figure 4.5 was not fitted to a specific formula (e.g. Arrhenius formula or the formula proposed by Bernard and Rémond (2012). Hence, the values of the kinetic parameters were obtained by linear interpolation between the values shown in Figure 4.5.

Secondly, the similarity in shapes of P_m and K as a function of temperature shown in Figure 4.5 suggests a close to linear relationship between P_m and K, which is confirmed by Figure 4.6. This linearity is explained by the fact that the rate of photosynthesis of light-limited cells is not impacted by temperature (Davison, 1991). Indeed, the rate of photosynthesis of light-limited cells (i.e. when $\sigma I_{loc} << K$) can be expressed as follows:

$$P_{loc} \cong \frac{P_m}{K} \sigma I_{loc} \quad (4.9)$$

Equation 4.9 shows that the temperature-independence of light limited cells is equivalent to the ratio P_m/K being temperature-independent. The good agreement with previous observations from the literature suggests that the technique used to determine the model parameters was appropriate.

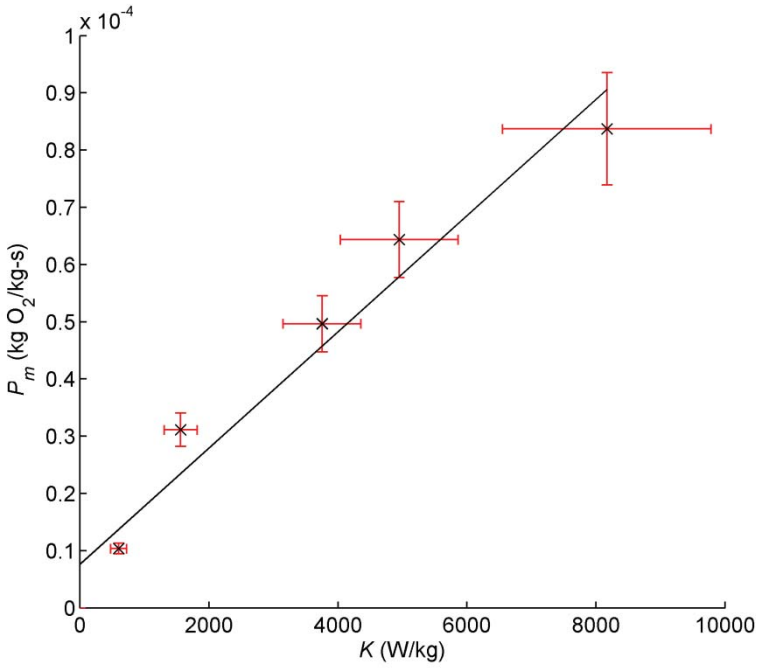

Figure 4.6: P_m values vs. K values at different temperatures. The error bars represent the 95% confidence interval determined by Monte-Carlo simulations (see the supplementary information S6 of Article 4 for details) – *Extracted from Article 4*.

4.3.5. Rates of night-time and day-time respiration

As discussed in Section 1.3.6, endogenous respiration can have an important impact on the total productivity. While the night-time respiration was modelled by most studies using first-order kinetics (Equation 4.3), there is no consensus on the best modelling approach for day-time respiration. The objectives of this section are to describe how the decay coefficients λ in Equation 4.3 were obtained for different temperatures T from empirical measurements and how the model of day-time respiration was developed.

Night-time respiration

It was experimentally demonstrated that the respiration rate at night during the first 15 minutes after light-exposure represents the rate of night-time respiration for several hours (data not shown). The decay coefficients λ were therefore determined from the measurement of the respiration rates measured immediately after light exposure. Figure 4.5 shows that the evolution of the decay coefficient λ with temperature is similar to the evolution of the kinetic parameters P_m and K with temperature. These trends are commonly reported in the literature

(Collins and Boylen, 1982; Grobbelaar, 1990; Le Borgne and Pruvost, 2013) and are explained by the temperature-dependence of key enzymatic reactions. Again, these similarities with previous observations indicate that the experimental technique used to determine the decay coefficients is appropriate.

There is no clear consensus on the literature on how to mathematically express the respiration coefficient λ as a function of temperature. The data showed in Figure 4.5 was therefore not fitted to a specific formula (e.g. Arrhenius equation). In the rest of this thesis, the values of λ at any temperatures were obtained by linear extrapolation of the experimental values shown in Figure 4.5.

Day-time respiration

In various modelling studies, the rate of day-time respiration was assumed to be proportional to the rate of photosynthesis (García Camacho et al., 1999, Geider et al., 1997). However, Figure 4.7 shows that the rate of respiration measured directly after light exposure was not clearly correlated with the rate of photosynthesis during light exposure. This lack of correlation suggests that the rates of respiration at day-time and night-time should be similar. Assuming that day-time and night-time respiration rates are equal is in fact a common assumption in the literature (Quinn et al., 2011). Following this assumption, the rate of day-time respiration was expressed as:

$$ER_{day} = \lambda XV \quad (4.10)$$

where the values of the decay coefficients λ at different temperatures are shown in Figure 4.5.

It should be noted that simple mathematical expression 'hides' the complex effects of temperature, as can be seen by influence of temperature on the relationship between the rates of respiration and photosynthesis seen in Figure 4.8. Temperature acclimation was not systematically performed and this may have influenced the productivity predictions.

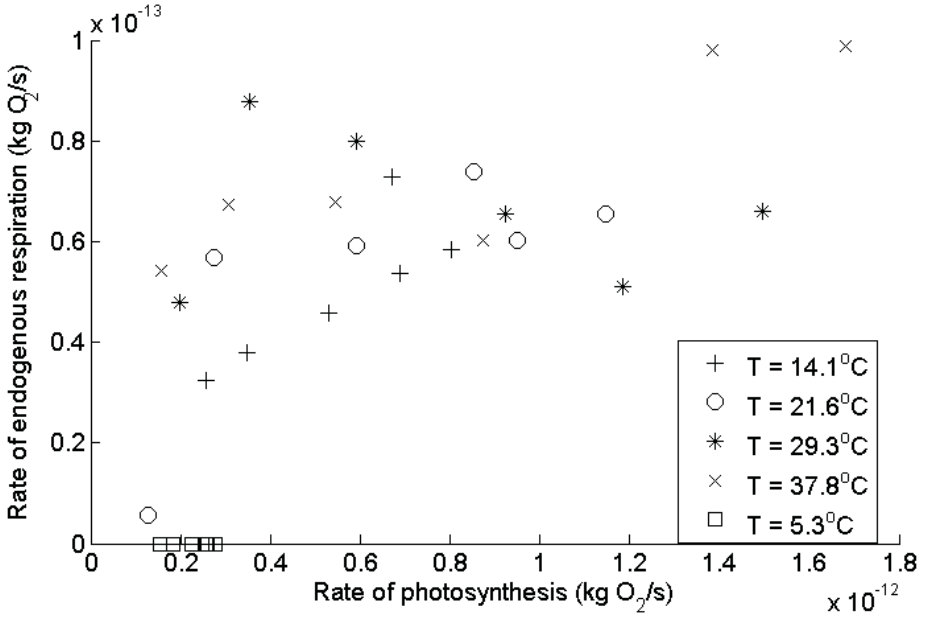

Figure 4.7: Rate of respiration after light exposure vs. rate of photosynthesis – *Extracted from Supplementary information S8 of Article 4*.

4.3.6. Conversion from oxygen production rates to biomass productivities

For the engineering purposes of this thesis, it was necessary to convert the kinetic parameters P_m and λ from oxygen–based units (kg O_2/kg-s) into actual biomass production rates (kg/kg-s). The general equation representing photosynthesis is (Madigan and Martinko, 2006):

$$6CO_2 + 6H_2O \rightarrow C_6H_{12}O_6 + 6O_2$$

The glucose generated for photosynthesis can then be assumed to be used by the algae for three main purposes (Burris, 1981): i) energy source for respiration; ii) carbon and energy source for generating new cellular material; and iii) energy storage in various forms. The calculation of the conversion coefficients were based on the assumptions that 1) half of the glucose generated during day-time was stored and that 2) the average lipid, carbohydrate and protein contents of *C. vulgaris* were those determined by the studies of Illman et al. (2000) and Becker et al. (2007). In order to account for the uncertainty on the fraction of glucose used for storage (taken here equal to 0.5), this fraction was made vary between 0.25 and 0.75 in the sensitivity analysis performed during model validation. These assumptions enabled the determination of the following conversion coefficients (see supplementary information S5 of Article 4 for detailed calculations):

- P_m' [kg/kg-s] = 0.76 (±0.09) P_m [kg O_2/kg-s]
- λ' [kg/kg-s] = 0.76 (±0.09) λ [kg O_2/kg-s] at day-time
- λ' [kg/kg-s] = 0.94 λ [kg O_2/kg-s] at night-time

Caution should be taken when using the model to predict the productivity of algae encouraged to accumulate large amounts of lipid (cultivation is however often done under nutrient starvation for this purpose, a condition outside the scope of this thesis).

4.3.7. Summary of equations of the productivity model

Table 4.2 summarizes the various equations of the model which were derived in Section 4.3.

Table 4.2: Summary of equations in the productivity model

	Equation		**Symbol definition**
Biomass productivity $P_{biomass}$ (kg/s)	$P_{biomass} = \int_V P_m \frac{\sigma_X I_{loc}}{K + \sigma_X I_{loc}} X \cdot dV - \lambda XV$	(4.11)	P_m: maximum specific rate of photosynthesis (in kg/kg-s) σ_X:extinction coefficient (m^2/kg) I_{loc}: local light intensity (W/m^2) K: constant (W/kg) X: algal concentration (kg/m^3) V: system volume (m^3) λ: decay coefficient (kg/kg-s)
Extinction coefficient σ_X (m^2/kg)	$\sigma_X = AX^B$	(4.12)	A: constant (117.4 m^2/kg) B: constant (-0.200)
Local light intensity I_{loc} (W/m^2)	$I_{loc}(l) = I_0 \exp(-\sigma_X Xl)$	(4.13)	I_0: irradiance (W/m^2) l: light path (m)

4.3.8. Application of the productivity model to full-scale cultivation systems

This section describes how the modelling approach can be applied to predict the productivity of full-scale open ponds and photobioreactors. Algal productivity varies over time due to the fluctuations of irradiance and temperature in the cultivation system. In order to determine the yearly productivity achieved in a photobioreactor or open pond, it is therefore necessary to determine the instantaneous productivity over time during an entire year and integrate these instantaneous productivities over time. In this thesis, this integration was done numerically by using a forward-Euler algorithm with a time step of 1000s. The prediction of the instantaneous productivity $P_{biomass}$ at t was a three-step approach:

1. The temperature of the cultivation system at t was determined by using the temperature models described in Chapter 3. The biological coefficients P_m, K and λ at this instant t were then determined by linearly extrapolating the experimental values obtained during the model parameterization described in Sections 4.3.4 and 4.3.5.
2. The light distribution in the cultivation broth was expressed from the extinction coefficient of the broth (see Equation 4.4), the system geometry and the solar irradiance. The derivation of the light distribution in a photobioreactor and an open pond are fully described in the Article 5 and in appendix.
3. The instantaneous productivity at t was obtained by integrating Equation 4.11 over the entire cultivation broth.

Figures 4.8 and 4.9 summarize the variables and inputs needed for the application of the productivity model in an open pond and a closed photobioreactor, respectively.

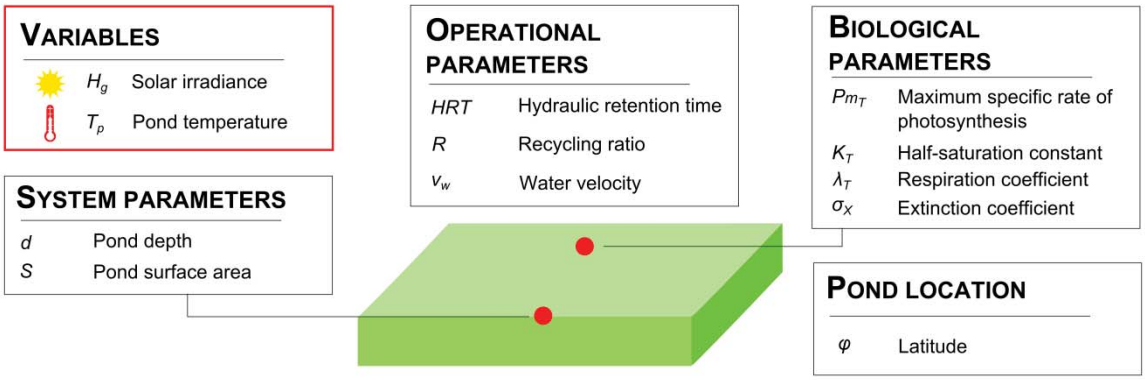

Figure 4.8: Variables and parameters necessary to determine the productivity in full-scale open ponds (additional inputs necessary to determine the pond temperature as shown in Figure 3.2).

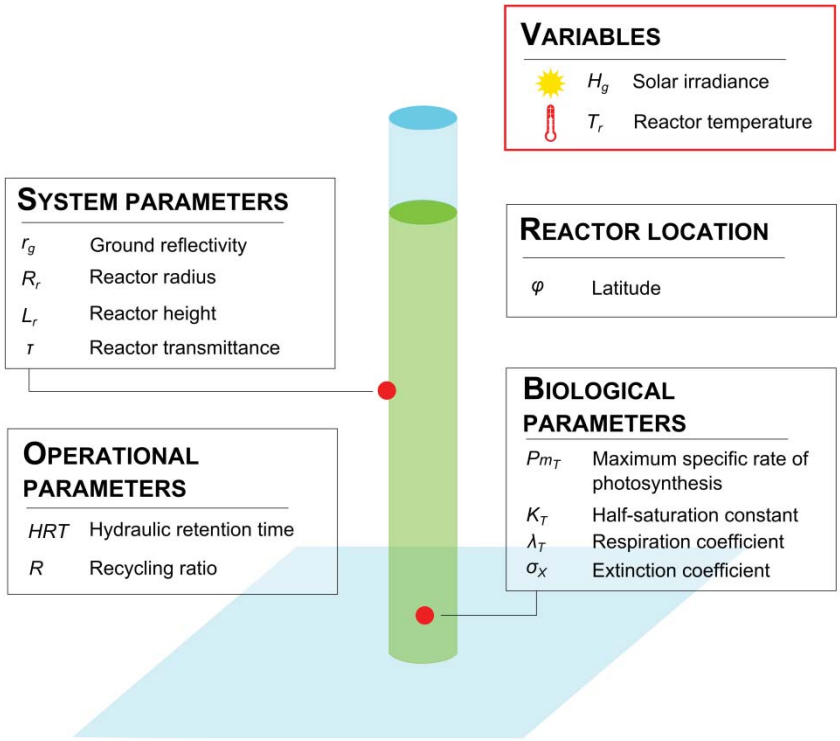

Figure 4.9: Variables and parameters necessary to determine the productivity in full-scale photobioreactors (additional inputs necessary to determine the reactor temperature as shown in Figure 3.6).

4.4. Application of the productivity model to full-scale cultivation systems: Scale-up

The kinetic parameters of the productivity model were derived from short-term measurements of oxygen production rates conducted under constant light and temperature. As discussed in Chapter 1, the following questions must therefore be addressed with regards to predictions under full-scale conditions:

1. How accurate is the conversion from oxygen productivity into biomass productivity?
2. Can the model accurately predict yearly productivities? i.e. Does acclimation matter?
3. Can the model accurately predict algae response to sunlight? i.e. Is the algae response significantly impacted by the light source spectrum?

In order to answer these questions, a validation procedure in two steps was performed:

- The accuracy of the model was first assessed against experimental biomass productivities recorded in indoor bench-scale reactors operated under constant light and temperature. This first validation step should address the first two questions.
- The accuracy of the model was then assessed against full-scale data collected from pilot-scale outdoor photobioreactors. This should allow the verification of all the assumptions.

A single-step validation procedure would be risky because of potential compensatory effects. For example, a systematic error on the conversion factors could be compensated by the influence of the light spectrum on photosynthesis, leading to an apparent good fit. The validation in two steps undertaken in this study aimed to minimize this risk, by validating the productivity models against data obtained under various cultivation conditions (Table 4.3).

Table 4.3: Comparison of cultivation conditions in the device used for model development, the indoor reactors and the outdoor reactors used for model validation.

	System	Productivity metric	Duration	Light source	Light and temperature regime
Model development	Small vessels	Oxygen	15-30 minutes	LEDs	Constant
Model validation	Indoor reactors	Biomass	1-3 weeks	Fluorescent light bulbs	Constant
	Outdoor reactors	Biomass	1 week – 2 months	Sunlight	Variable

4.5. Productivity model validation using bench-scale indoor reactors

As a first validation step, the productivity model was tested against indoor cultivation data obtained by cultivating *Chlorella vulgaris* in bench-scale reactors for several weeks under constant light intensity and constant temperature. Section 4.5.1 describes the geometry of the reactors and the operational conditions used. The measured and predicted productivities in the indoor reactors are compared in Section 4.5.2.

4.5.1. Bench-scale reactors used for productivity model validation

The experimental set-up was composed of four bench-scale reactors operated at the same temperature and exposed to different light intensities (Figure 4.10). The reactors were made of two concentric transparent plastic tubes (height: 25cm; diameters: 7cm and 9.5cm, working volume: 2L). The temperature of the cultures in each reactor was maintained constant by circulating water between the inner and outer tubes. The outer tubes were surrounded by 14 light bulbs (Figure 4.10) which continuously illuminated the reactors. In order to expose the reactors to different light intensities, each reactor was surrounded by light bulbs of different wattage. The irradiance entering each reactor was measured using a lux meter in the empty reactors at 4 heights and 20 angular positions on the reactor wall, representing a total of 80 measurement points. By assuming a conversion factor of 2.7 between klux and W/m^2 (Lang et al., 1981), the average incident light intensities reaching the algae in each reactor were 26.8 W/m^2, 44.7 W/m^2, 49.9 W/m^2, and 65.0 W/m^2 (as photosynthetically active radiation or 'PAR'). Air enriched in CO_2 (2%) was bubbled in the reactors (2.5 L/min) to ensure that CO_2 saturation was maintained and that the dissolved oxygen concentration did not inhibit algal productivity. Air bubbling in the reactor also ensured completely mixed conditions in the reactors. Reactors were operated in a batch regime until algal concentration reached 0.5 kg/m^3 (shaded area in Figure 4.11). Operation was then switched to a semi-continuous regime by replacing every day a fraction of the culture with freshly prepared pH-buffered BG-11 medium. Various preliminary tests were conducted to ensure there was no nutrient limitation. The dry weight concentration of the culture was measured after each sampling. A total of five experiments at different temperatures were performed (10°C, 20°C, 25°C, 30°C, and 35°C). More details on the bench-scale reactors and their operation can be found in the materials and methods section of Article 4.

The model of productivity described in Section 4.2 was adapted to the specific geometry of the indoor photobioreactors as described in the supplementary information S2 and S4 of Article 4. The inputs necessary to apply the model to the bench-scale photobioreactors were:

- The irradiance profile and the reactor temperature;
- The biological parameters P_m, K, λ, and σ_X were determined by linear interpolation between the values shown in Figure 4.5.
- The system geometry (reactor radius and working height);
- The operational parameters (volume change, etc.)

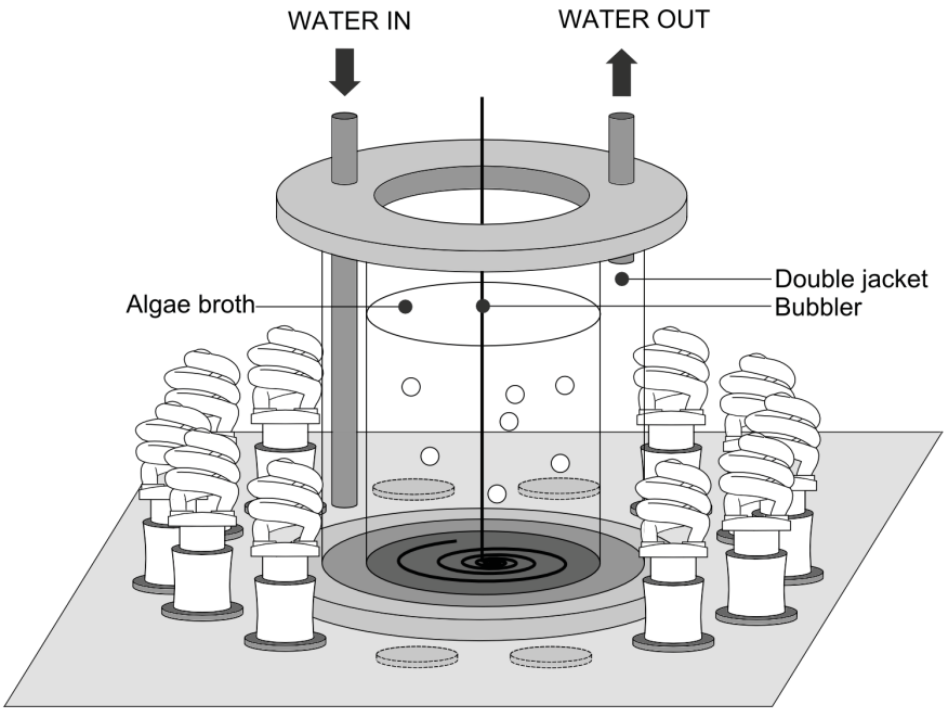

Figure 4.10: Bench-scale reactor used for validation. The reactors were surrounded by 14 light bulbs each, and temperature was controlled by re-circulating water in the double jacket – *Extracted from Article 4*.

4.5.2. Comparison between predicted and measured productivities in the bench-scale reactors

Figure 4.10 shows the cumulative productivities over time in the four indoor reactors exposed to four different light intensities and for five different temperatures. Figure 4.10 shows that for temperatures lower than 30°C, the model prediction (plain blue line) fits the experimental data (red crosses) over the entire period of cultivation (the dash-lines represent the level of accuracy of model predictions due to uncertainty of model inputs[13]). However, at a temperature of 35°C, the model was unable to predict algal productivity for a period of time longer than 1 or 2 days due to the subsequent culture collapse. This suggests that the optimal temperature for photosynthesis (around 38°C, Section 4.3) is not the same as the optimal temperature for biomass production. This difference is explained by the fact that photosynthesis and biomass production are processes regulated by different enzymes (Davison, 1991). These differences of temperature optima will be further discussed in Chapter 5. Due to this culture collapse, the experimental data at 35°C was not considered in the assessments of the model accuracy.

The overall accuracy of the model was defined as the relative difference between the measured and predicted cumulative productivities in all the reactors (in absolute value, expressed in %)[14]. Over the entire period of cultivation (representing 163 days of operation), the model was able to predict productivity with an accuracy of ±13%. Figure 4.12 directly compares the measured and predicted cumulative productivities over the entire period of cultivation in the indoor reactors. Figure 4.12 confirms that model predictions and experimental data are in good agreement.

The good fit of the model prediction to the experimental data was obtained under a broad range of conditions and in particular for different light intensities. Any model inaccuracies therefore appear to originate from measurement error and uncertainty in the model inputs, represented by the error bars in Figure 4.12 (e.g. light intensity, extinction coefficient, etc.), and not from the assumptions made in the model development. In particular, the conversion factors discussed in Section 4.3.6 and the differences in light spectrum between the device shown in Figure 4.2 and the bench-scale reactors do not appear to significantly and systematically impact productivity. In addition, the good fit of the model suggests that the

[13] See supplementary information S6 of Article 5 for a detailed description of the Monte-Carlo simulations used to determine the confidence intervals on model predictions.
[14] The data at 35°C was not included due to the culture collapse observed at these temperatures (Figure 4.11).

level of dissolved oxygen in the cultivation broth did not significantly impact productivity. As the model was able to predict productivities over several weeks, it seems also that light acclimation mechanisms do not have a significant impact on algal productivity over this timescale.

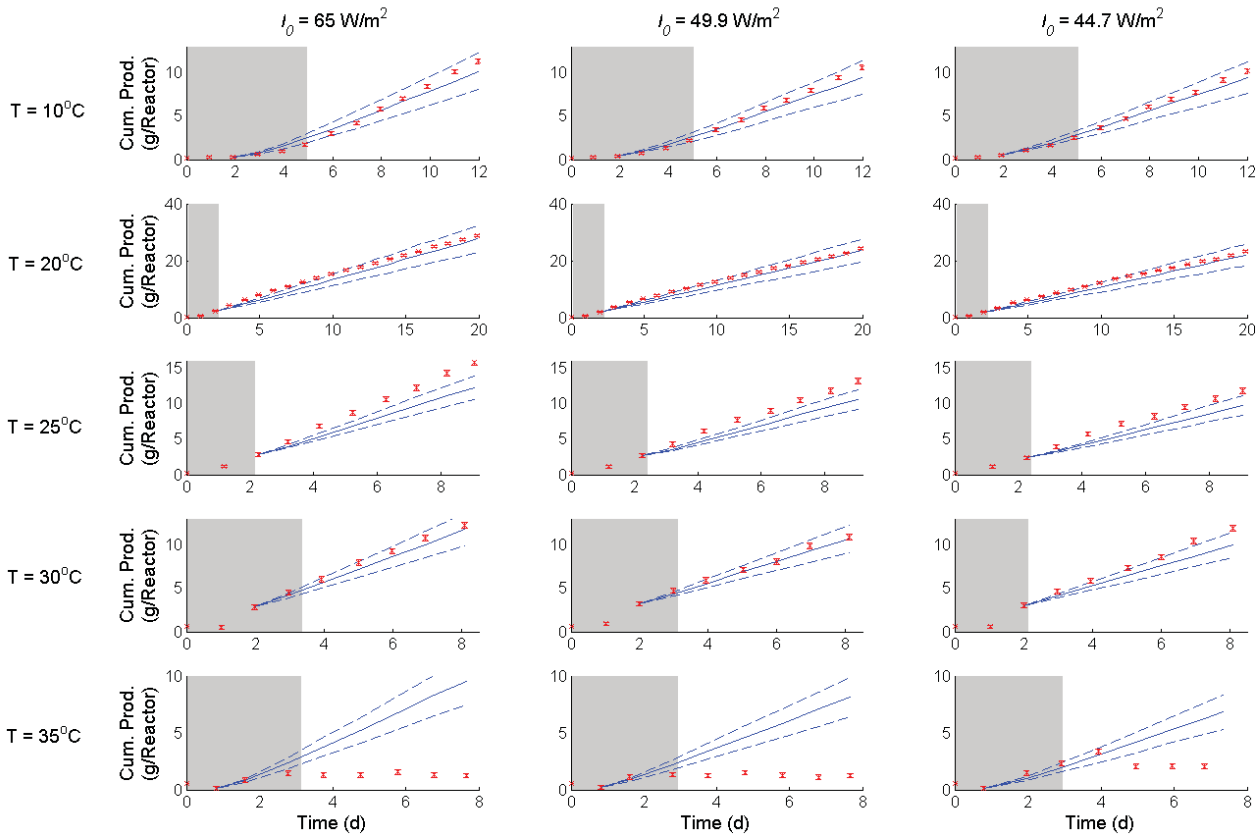

Figure 4.11: Cumulative productivity in the indoor bench-scale reactors operated under different light i
model prediction; blue dash-line: prediction inaccuracy due to uncertainty of inputs; red crosses: experim
the period of time when the reactors were operated as batch systems. The higher cumulative productivit
longer cultivation time at this temperature – *Extracted from Article 4*.

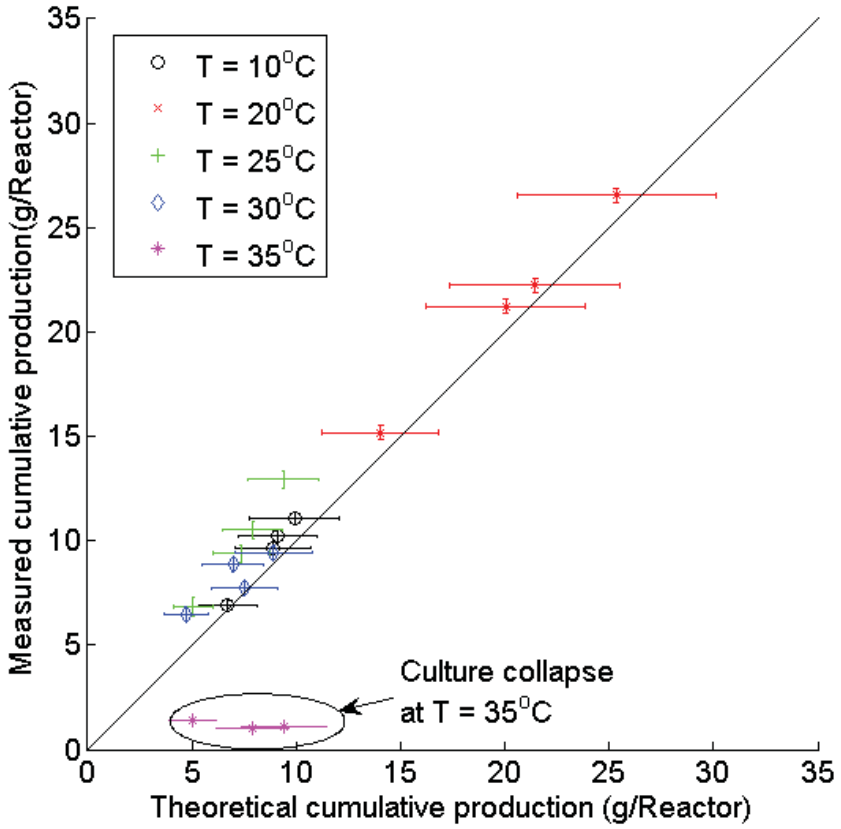

Figure 4.12: Predicted and measured cumulative productivities over the entire experiment. The higher cumulative productivities at 20°C are the consequence of the longer cultivation time at this temperature – *Extracted from Supplementary information S9 of Article 5*.

As discussed in Section 4.4, even though the model was validated on bench-scale photobioreactors, there is still a risk that two systematic errors tend to compensate each other. For example, a systematic error on the conversion factors may compensate the error on the impact of the light spectrum on productivity and cause an 'apparent' but accidental good fit. In order to ensure that these compensation effects do not explain the high level of accuracy of ±13% observed in this section, the model was also tested against experimental data collected in outdoor photobioreactors. This validation is detailed in the next section.

4.6. Validation of the productivity model in outdoor photobioreactors

In a second validation step, the model predictions were compared to experimental data collected from pilot-scale photobioreactors continuously operated in outdoor conditions in New Zealand.

4.6.1. Outdoor pilot-scale photobioreactors used for model validation

In order to validate the productivity model against full-scale experimental data, *Chlorella vulgaris* was cultivated in outdoor photobioreactors in New Zealand (Figure 4.13). In order to assess the model predictions against different climatic conditions, outdoor cultivation was performed at different seasons and under both temperature-controlled and non-temperature controlled conditions. A total of four outdoor experiments[15], each involving between 1 to 4 photobioreactor(s), were carried out between summer 2011 and winter 2012. In total, 141 days of experimental data were obtained from all the reactors combined. Table 4.4 describes the date of operation, the number of reactors involved, the operation mode, and the light and temperature conditions of each experiment. The study of Béchet et al. (2013) demonstrated that the algae species *Chorella sorokiniana* can grow in outdoor vertical photobioreactors in Singapore with a good photosynthetic efficiency (on average 4.8% of the light reaching the algae was converted into biomass). For this reason, the same reactor design and operation were used in this thesis for the validation of the productivity model.

[15] A fifth set of experimental data was collected after the submission of this thesis and was therefore not included in this thesis. This data is however used in Article 5.

Table 4.4: Characteristics of the outdoor experiments used for model validation (TC: temperature-control) – *Extracted from Article 5*.

	Number of reactors	Date of operation	Operation mode	Av./Max. Solar irradiance (W/m^2, PAR)	Reactor temperature range (^oC)
Exp. 1	1	29 Mar – 27 May 2011	Batch/Semi-continuous[a]	48/374	5.5 – 34
Exp. 2	4	28 Mar – 5 Apr 2012	Batch No temperature control	76/366	12 – 29
Exp. 3	3	18 Apr – 25 Apr 2012	Batch No temperature control	62/280	8 – 28
Exp. 4	4	25 May – 18 Jun 2012	Batch/Semi-continuous[a] TC in 2 reactors only	31/202	No TC: 0 – 26 TC: 18 – 26

'Semi-continuous' means that a fraction of the cultivation broth was changed daily.

Figure 4.13: Four pilot-scale photobioreactors used for the outdoor validation of the model (winter 2012) – *Extracted from Article 5*.

The four outdoor reactors were vertical transparent columns (height 2m; diameter: 0.19m; working volume: 50L). Two of the reactors were equipped with heaters to maintain the temperature higher than 18^{o}C during the experiment undertaken in winter 2012 (Experiment 4, Table 4.4). Air enriched in CO_2 (2%) was bubbled in each reactor (1 L/min) to ensure that CO_2 supply did not limit algal growth and that dissolved oxygen concentration did not inhibit algal growth. Bubbling was also used to ensure good mixing conditions in the reactors. Reactors were initially operated as batch systems to enable the algal concentration to initially reach values higher than 0.5 g/L. Reactors were then operated as semi-continuous systems on a daily basis by replacing 5L of culture by fresh BG-11. The medium used was phosphate-buffered in order to control the pH at values close to 7.2.

The model of productivity described in Section 4.2 was adapted to the specific geometry of the outdoor photobioreactors (see the supplementary information S5 and S6 of Article 5 for more details). In addition, the productivity model was coupled to the temperature model presented in Chapter 3 to predict the productivity in the pilot-scale photobioreactors. The meteorological data used as inputs of the temperature model was uploaded from a weather station located at a distance of 1.2 km from the reactors (NIWA, Weather station number: 21963, latitude -40.38195; longitude 175.60915). Dry weight concentration was measured daily in the early morning and late evening. The temperature in the reactors was continuously monitored at 30 minute intervals.

4.6.2. Comparison of predicted and measured productivities in the outdoor reactors

Figures 4.14 to 4.17 compare the predicted (blue plain line) and measured (red cross-line) cumulative productions in outdoor photobioreactors for the four experiments described in Table 4.4. The model was unable to predict the low productivities achieved during the first days which was most likely caused by brutal change of cultivation conditions from laboratory to outdoor environment. For this reason, only the experimental data collected after several days of cultivation was used in the model validation. As can be seen in Figure 4.17 (bottom-left plot), a culture collapse was observed in one of the reactors in winter 2012 (Experiment 4). The corresponding data was therefore not used in the assessment of the model accuracy. The overall level of accuracy was defined as for the bench-scale photobioreactors (see Section 4.5.2). Over the four experiments (representing a total of 141 days of cultivation), the model was able to predict productivity within an accuracy of ±13%. Table 4.5 summarizes the levels

of accuracy on the productivity predictions for each data set. Table 4.5 shows that the average error decreases with the duration of the experiment. This is likely due to the fact that the measured cumulative productivity over short periods of time was more inaccurate due to error in algal concentration measurements. As discussed in supplementary information S6 of Article 4, this experimental error was unavoidable due to the technique used to measure the dry weight concentration of the algal broth.

The model was able to predict productivity in the outdoor reactors for a large range of temperatures and light intensities and for different types of operation. Furthermore, accurate predictions were obtained with and without temperature-control (Table 4.4). This good fit over broad meteorological and operating conditions suggests that there is no systematic error due to light spectrum differences, conversion factors, inhibition due to high dissolved oxygen concentration, or acclimation processes. The level of accuracy of ±13% is likely explained by uncertainty on model inputs rather than error in the assumptions made during the development of the model. Indeed, the experimental measurements fall within the confidence interval of the model predictions (represented by the dash lines in Figures 4.14 to 4.17[16]).

Table 4.5: Error on productivities calculated by dividing the difference between the predicted and the measured cumulative productivities over the entire period of cultivation. "TC" indicates temperature control.

Experiment	Reactor	Length of cultivation (d)	Average error (g/reactor-d)	Average productivity (g/reactor/d)
1	1	51.7	0.23	4.0
2	1	2.5	0.14	5.2
	2		3.3	2.0
	3		0.40	5.0
	4		3.2	2.3
3	1	1.6	1.1	2.3
	2		0.61	2.8
	3		0.34	3.1
4	1	18.6	0.54	3.3
	2 (TC)		0.35	3.6
	4 (TC)		0.53	3.8

[16] See Supplementary information S6 Article 5 for a detailed description of the Monte-Carlo simulations used to determine the confidence intervals of model predictions.

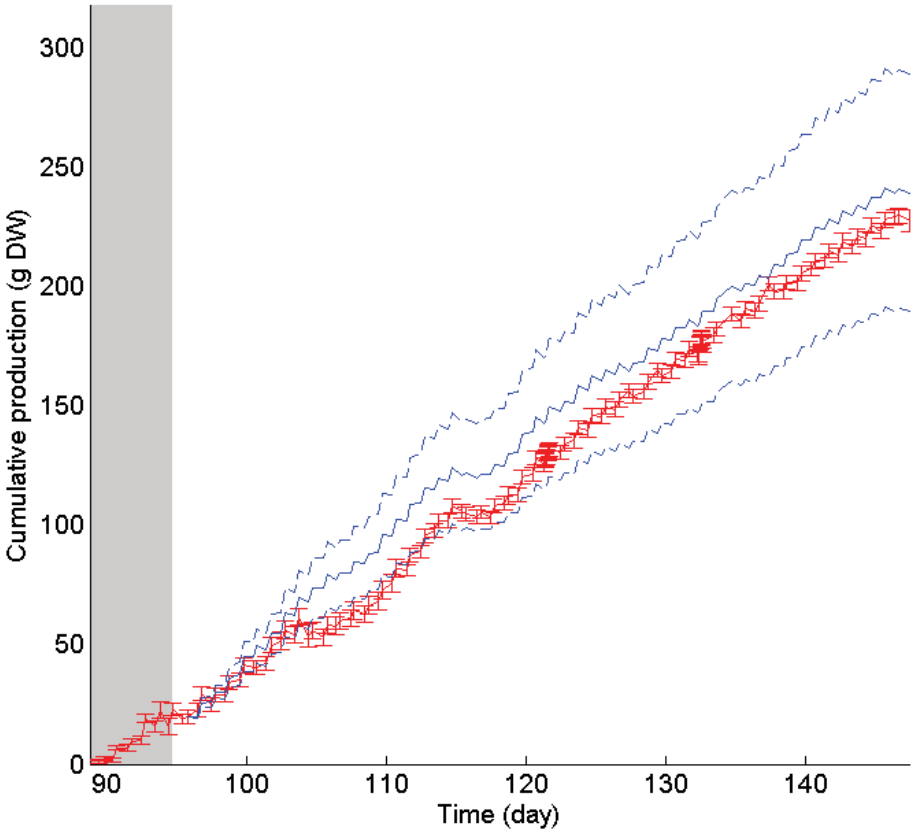

Figure 4.14: Experiment 1 - Cumulative production in the outdoor reactor in fall 2011 (red-crossed line: experimental data; blue plain line: prediction; blue dash-lines: upper and lower boundaries of the confidence intervals of the prediction). The grey shaded area represents the period of time over which the reactor was operated in batch regime – *Extracted from Article 5*.

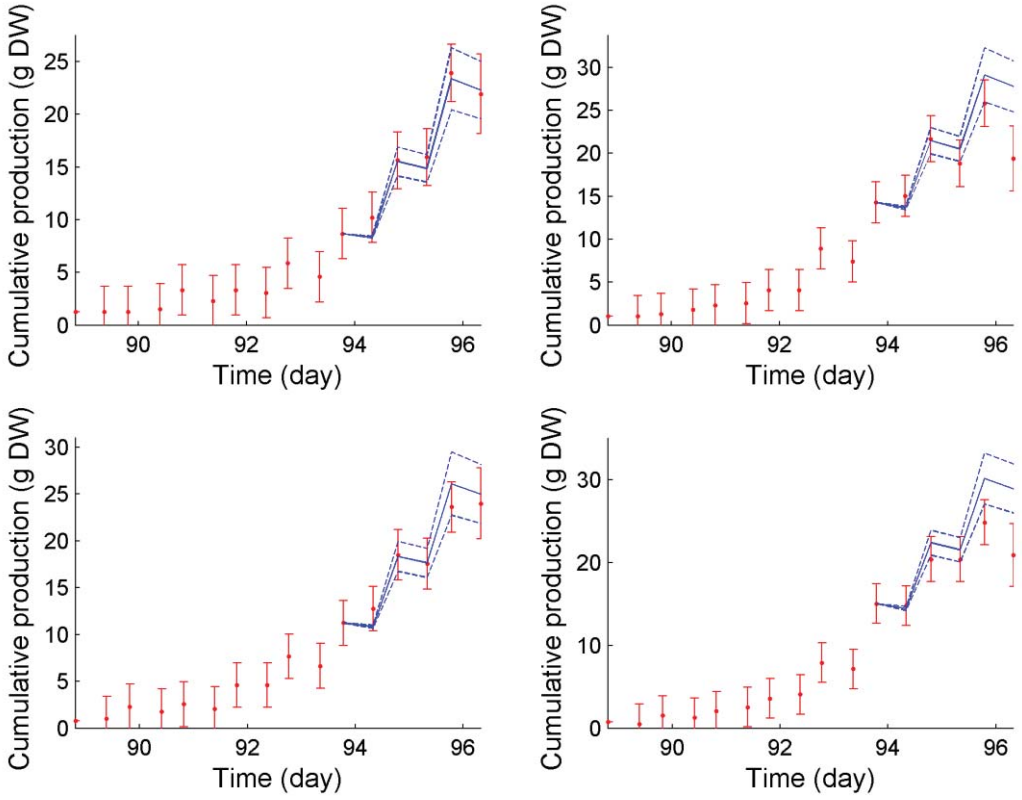

Figure 4.15: Experiment 2 - Cumulative production in the outdoor reactors in summer 2012 (red-crossed line: experimental data; blue plain line: prediction; blue dash-lines: upper and lower boundaries of the confidence intervals of the prediction).

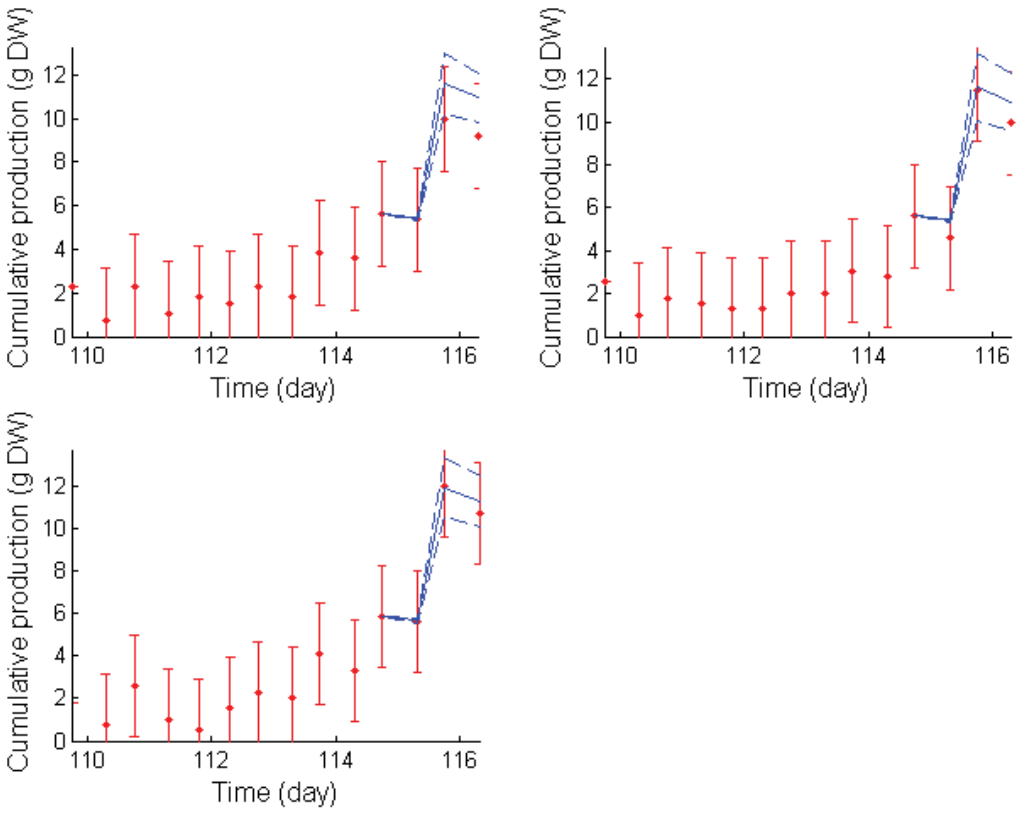

Figure 4.16: Experiment 3 - Cumulative production in the outdoor reactors in fall 2012 (red-crossed line: experimental data; blue plain line: prediction; blue dash-lines: upper and lower boundaries of the confidence intervals of the prediction).

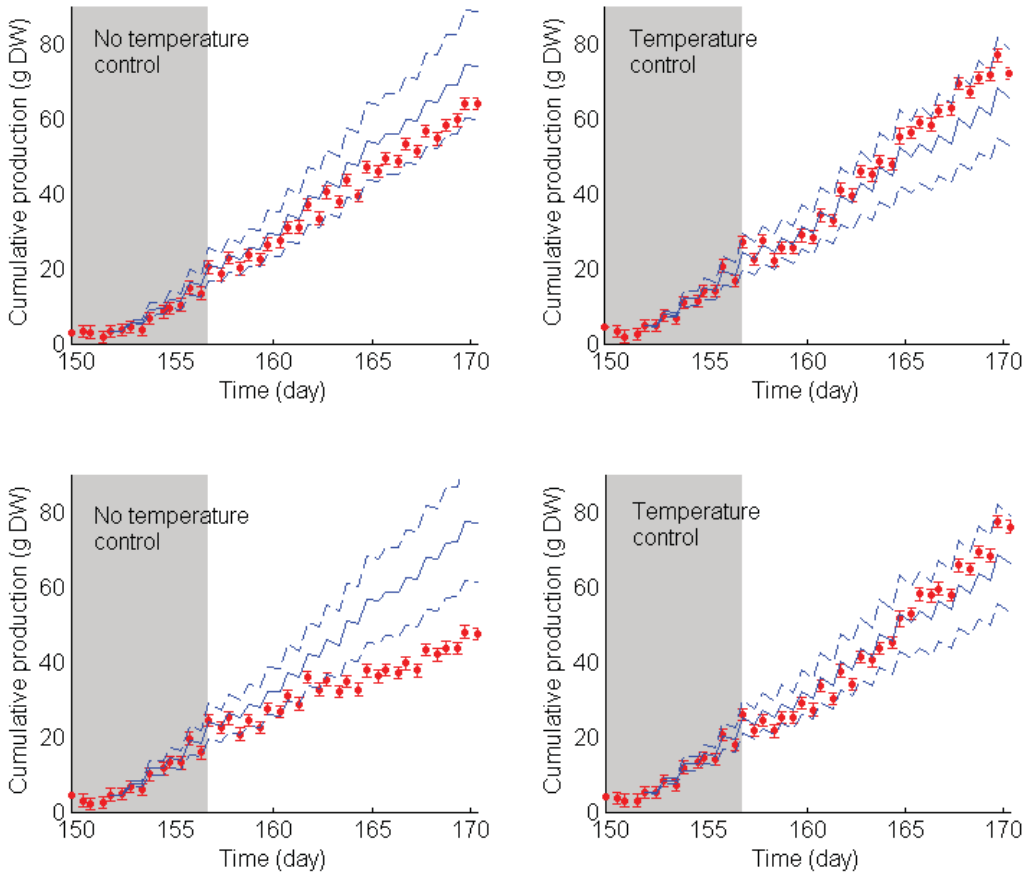

Figure 4.17: Experiment 4 - Cumulated production in the outdoor reactors in winter 2012. red-crossed line: experimental data; blue plain line: prediction; blue dash-lines: upper and lower boundaries of the confidence intervals of the prediction. The grey shaded area represents the period of time over which the reactors were operated in batch regime – *Extracted from Article 5*.

4.7. What level of accuracy is required to make the productivity model fit for the purpose of assessing the economics and environmental impacts of full-scale algal cultivation?

In the two previous sections, algal productivity was predicted in indoor and outdoor cultivation systems with accuracies of ±13%. The objective of this section is to investigate if this level of accuracy of ±13% is high enough to assess the economics and environmental impacts of full-scale algal cultivation.

One of the objectives of the model is to assess the economic feasibility of full-scale cultivation systems. Because of the uncertainty on productivity values used in previous studies, prior assessments were unable to precisely determine the cost of biofuel from microalgae. For example, in the recent study of Rogers et al. (2013), the cost of biofuel from microalgae cultivated in open ponds located in New Mexico was estimated at 3.21$ US per litre, by assuming a productivity of 5.5 kg/m^2-yr. However, this estimation was shown to be highly sensitive on the productivity value assumed in the calculation. Rogers et al. (2013) thus showed that the cost of algal biofuel would increase by 1.60$ US if the productivity dropped to 3.7 kg/m^2-yr. The level of accuracy of ±13% on the productivity predictions therefore translates to an uncertainty of approximately ±0.35 $ US/litre. This level of uncertainty is comparable to the level of uncertainty caused by the variable price of CO_2 or the price of nutrients as shown by Rogers et al. (2013). The current level of accuracy of the productivity model developed in this thesis is therefore high enough to assess the cost-efficiency of the process.

The model also aims to estimate the impact of full-scale algal cultivation on the environment. In Article 6, the water demand of algae cultivation was estimated at the five locations showed in Figure 2.4. For example, the water demand in a Mediterranean climate was estimated at 5.44 m^3/m^2-yr. However, a sensitivity analysis revealed that uncertainty on the hydraulic retention time (HRT) caused an inaccuracy on the water demand of ±3.3m^3/m^2-yr (Figure 3 of Article 6). The HRT indicates what fraction of the pond broth is extracted for harvesting every day. At full-scale, the HRT would therefore be used to adjust the algal concentration in the cultivation system. For example, in order to maintain an optimal algal concentration X_{opt} (kg/m^3), the HRT (d) should be set at the following value (see materials and methods section of Article 6 for details):

$$HRT = \frac{d \cdot X_{opt}}{P_{net}} \qquad (4.14)$$

where d is the pond depth (m) and P_{net} is the productivity (kg/m^2-d). In Article 6, a large range of HRT values was used for the sensitivity analysis mostly because of uncertainties on the optimal algal concentrations and productivities values (see Figure 3 of Article 6). With a level of accuracy of ±13% on the productivity prediction, the range of possible HRT values at full-scale should be refined within ±1 day (according to Equation 4.14). As shown in Article 6 (Figure 3), an uncertainty of ±1 day on the HRT causes an inaccuracy on the water demand of ±0.5 m^3/m^2-yr, which is comparable to the uncertainty caused by water leaks. Further improvement of the productivity accuracy is therefore unlikely to refine the assessments of the environmental impacts of full-scale cultivation systems.

4.8. The need for temperature modelling for accurate productivity predictions

Numerous assessments of full-scale algae cultivation for biofuel production can be found in the literature. Table 4.6 summarizes the main assumptions used in eleven 'key' studies on the cost and environmental impact assessment of large scale algae cultivation, cumulating more than 1,000 citations in less than 3 years[17]. Out of the 11 assessments reviewed, only 3 studies considered the impact of temperature on productivity (Batan et al., 2013; Wigmosta et al., 2011; Yang et al., 2011) whereas the remaining eight studies used productivity values obtained during lab-scale experiments conducted under poorly representative conditions (e.g. constant temperature of 25^{o}C, see Table 4.6). Interestingly, the productivities used in the studies considering the impact of temperature were 2-3 folds lower than the productivity values used in the other eight studies. This section aims to investigate how neglecting the influence of temperature variations at full-scale impacts productivity predictions. For this purpose, the productivities of single photobioreactors operated continuously for one year at five different climatic conditions were compared in two scenarios. In the first scenario, the productivity was predicted by using the temperature prediction from the model described in Chapter 3 (no temperature-control). In the second scenario, the productivity was computed by assuming that the temperature of the reactor was constantly maintained at 25^{o}C, which is a temperature often used during indoor algal cultivation.

[17] As reported by Google Scholar in January 2014.

Table 4.6: Characteristics of recent assessments of full-scale algae cultivation for biofuel productions – *Ex*

Study	Context of the study	Algae species	Cultivation system	Location/Climate
Batan et al. (2013)	Water footprint of microalgae biofuel production	*Nannochloropsis salina*	Photobioreactor	Arizona California Colorado Montana Nebraska Nevada New Mexico Texas Utah Wyoming
Wigmosta et al. (2011)	Assessment of microalgae biofuel potential and resource demand	NS	Open pond	United States
Yang et al. (2011)	Life-cycle analysis on biodiesel production from microalgae: water footprint and nutrients balance	*Chlorella vulgaris*	Open pond	US[1] Arizona California Florida Hawaii
Campbell et al. (2011)	Life-cycle assessment of biodiesel production from microalgae	NS	Open pond	Australia

NS: not specified

[1]Average over 28 states

Study	Context of the study	Algae species	Cultivation system	Location/Climate
Lardon et al. (2009)	Life cycle assessment of biodiesel production from microalgae	*Chlorella vulgaris*	Open pond	Mediterranean climate
Pate et al. (2011)	Assessment of resource demand for microalgae cultivation	NS	NS	Southwest of US
Rogers et al. (2013)	Cost-analysis of algae biofuels	NS	Open pond	New Mexico
Slade and Bauen (2013)	Assessment of the cost, energy balance and environmental impacts of biofuel production from microalgae	NS	Photobioreactor/ Open pond	NS
Stephenson et al. (2010)	Life cycle assessment of algal biodiesel	*Chlorella vulgaris*	Photobioreactor/ Open pond	United Kingdom
Sun et al. (2011)	Cost-analysis of algal oil production for biofuels	NS	Open pond	NS
Wang et al. (2013)	Assessment of algae-based biofuel production	*Chlorella vulgaris*	Photobioreactor/ Open pond	Japan

NS: not specified

Figure 4.18 shows the productivity predictions in single photobioreactors located at five climatic locations in the cases of no temperature-control (dark blue bar) and temperature-control (light grey bar). This figure shows that maintaining broth temperature at 25°C during full-scale cultivation can significantly impact the productivity predictions. For example, temperature-control can boost productivity by 58% in the arid climate as shown in Figure 4.18. This increase is due to the fact that, without temperature-control, temperature is expected to be higher than the maximal temperature for photosynthesis (42°C) for 158 days a year at this location. Accounting for the impact of temperature on algal productivity is therefore crucial to accurately assess the sustainability of biofuels from microalgae.

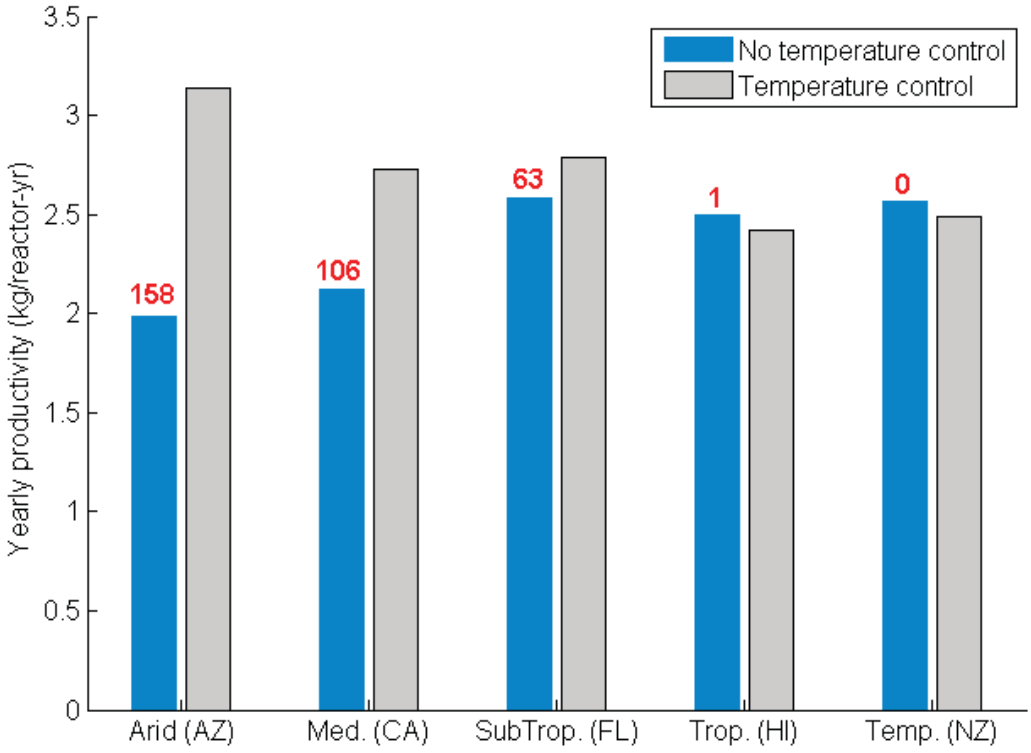

Figure 4.18: Predicted productivities with temperature control and no temperature control in closed photobioreactors. The numbers on the blue bars are the number of days per year where temperature is higher than 42°C in the case of temperature-control.

4.9. Conclusions

- The kinetic parameters of the productivity model were first determined from short-term lab-scale experiments. The variation of the kinetic parameters with temperature was in agreement with prior observations, which indirectly validates the original experimental technique used to determine these kinetic parameters.
- The accuracy of the model was assessed against biomass productivities measured in indoor bench-scale reactors operated under constant light and temperature conditions. The accuracy of the model was found to be ±13%, the error of the prediction being most likely due to uncertainty on the model inputs.
- The model was also validated against pilot-scale data collected from outdoor photobioreactors operated outdoor in New Zealand. Over 141 days of outdoor cultivation, the average accuracy of the productivity prediction was found to be ±13%. The productivity model developed in this thesis is, to the best of our knowledge, the first model to be fully validated against outdoor data.
- These good levels of accuracy were obtained in spite of the assumptions made to apply the productivity model developed from lab-scale experiments to full-scale cultivation systems.
- Calculations based on prior assessments in the literature showed that the level of accuracy achieved by our model was high enough to provide an accurate tool to estimate the cost-efficiency and environmental impacts of the full-scale algal cultivation.
- Neglecting the impact of temperature variations on productivity at full-scale has the potential to significantly impact the productivity predictions and hence the conclusions on the sustainability of full-scale algal cultivation.

Chapter 5: Engineering applications

Preface

The modelling approach used in this thesis was selected to ensure accuracy over a large range of climatic conditions, system designs, and operational regimes. For this reason, the expressions of all the heat flows in the temperature models were based on theoretical considerations rather than empirically-derived formulas. In addition, productivity was predicted based on a 'Type II' model previously shown to be applicable over a large range of algal concentrations, light intensities and system geometries. Finally, the model thus constructed was independently validated against full-scale data obtained under a broad range of relevant cultivation conditions. To the best of our knowledge, this effort thus produced the first predictive tool of algal productivity to be fully validated against full-scale data. The objective of this chapter is to demonstrate how this predictive model can be used to optimize process and operation to maximize the algal productivity while minimizing the environmental impacts of full-scale algal cultivation.

5.1. Introduction

As discussed in Chapter 3, active temperature control can boost productivity but requires tremendous amounts of energy, which jeopardizes the sustainability and economics of the process. Alternative strategies can be investigated to maximize productivity: Mitchels et al. (2013) for example investigated the impact of the algal concentration on the productivity. This study thus experimentally demonstrated that a concentration of 0.7 g/L was optimal for the cultivation of *Tetraselmis suecica* in outdoor photobioreactors operated in the Netherlands. Below this concentration, a fraction of the light reaching the cultivation system was not captured by the algae. Above this concentration, respiration caused significant decrease of net productivity. In practice, algal concentration can be controlled at its optimal value by changing the water inflow/outflow of the system. As algal productivity varies with meteorological conditions, maintaining the algal concentration at a fixed value requires adjusting constantly the water inflow. For example, Muñoz-Tamayo et al. (2013) used the temperature model for open ponds developed in this thesis (Article 2) coupled with a productivity model to optimize the water inflow of an open pond to maximize productivity. Another alternative strategy to maximize productivity consists on optimizing the design of the cultivation system. For example, Ritchie and Larkum (2012) investigated how the depth of shallow ponds impacted the algal productivity and Slegers et al. (2013b) attempted to optimize the relative positioning of reactors in a farm of photobioreactors to maximize productivity. Except for the study of Muñoz-Tamayo et al. (2013), the optimization studies undertaken in the literature did not account for the impact of temperature on productivity. In addition, emphasis was given to maximizing productivity, irrespective of potential environmental impacts. The main objective of this chapter is to demonstrate how the productivity model can be used to overcome the limitations of previous optimization studies.

The demonstration of the ability of the productivity model developed in this thesis to optimize cultivation systems was demonstrated through simulations at different climatic locations. Section 5.2 presents the assumptions made for the simulations. In a first case-study (Section 5.3), the productivity achieved in photobioreactors is predicted at different climatic locations and under various system designs (radius) and operational regimes. In a second case-study (Section 5.4), the productivity achieved in open ponds was simulated under different climatic and operational conditions and for different designs. This second case-study demonstrates how the model can be used to optimize the pond depth to maximize productivity and minimize water demand.

5.2. Methodology followed in the case-studies

This methodology section details the assumptions made on the operation and design of cultivation systems in the case-studies discussed in this chapter. The climatic locations at which these simulations were performed are described in Figure 2.4. As the results shown in this chapter were not published, the methods used in the case-studies developed in this chapter are fully detailed in this section.

5.2.1. Calculation of the yearly water demand

Figure 5.1 shows the different water flows entering and exiting a cultivation system (open pond or photobioreactor). In the two case-studies discussed in this chapter, a fraction of the water outflow will be considered to be recycled back into the system after harvesting the algae (the recycling ratio R being defined as the fraction of water recycled back into the system).

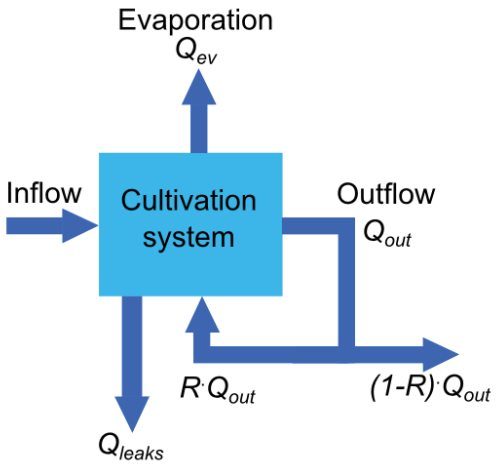

Figure 5.1: Different water flows during the operation of an algal cultivation systems (R: recycling ratio; Q_{ev}: evaporation rate (m^3/s); Q_{out}: outflow rate (m^3/s); Q_{leaks}: leaks rate (m^3/s).

From Figure 5.1, the water demand (WD, m^3/yr) can be calculated by summing the rate of water lost by evaporation (Q_{ev}, m^3/yr), the rate of water outflow not recycled back into the system and the rate of water lost through leaks (Q_{leaks}, m^3/yr):

$$WD = Q_{ev} + (1-R) \cdot Q_{out} + Q_{leaks} \qquad (5.1)$$

In the following, the rate of water lost by leaks was neglected in order to focus on the impact of the climatic location and process operation on the water demand. The amount of water exiting the system is usually characterized by using the hydraulic retention time (HRT). The HRT is defined as the average period of time that a particle of water spends in the system before exiting the system[18]. From this definition, the water outflow Q_{out} (m^3/yr) can be expressed as a function of the culture volume V (m^3) and the system HRT (d) by assuming 365 days of operation a year:

$$Q_{out} = 365\frac{V}{HRT} \quad (5.2)$$

HRT values ranging from 2 to 33 days have been proposed during algae cultivation (Cooney et al., 2011). A narrower range of 2–10 days was however used in this study to maintain yearly-averaged algae effluent concentrations within operational guidelines (Supplementary information S5 of Article 6). The value of 7 days was used as base-case. There is no clear consensus on the maximal recycling ratio R that can be achieved during full-scale cultivation. A ratio of 0.75 was selected as a representative value based on data from the literature on similar cultivation systems (see supplementary information S1 of Article 6 for further details).

5.2.2. Calculation of the yearly algal productivity

The productivity in the two cultivation systems was calculated by combining the hourly predictions of temperature (obtained as described in Chapter 3) and the productivity model described in Chapter 4. Details on the application of the productivity model in open ponds (including the determination of the light distribution) can be found in Appendix A. In order to ensure that all the light entering the cultivation broth was captured by the algae at all times, the initial algal concentration was set to 0.1 g/L in all simulations (this threshold was experimentally observed to ensure complete light adsorption at 10 cm under typical conditions). Yet this value did not significantly impact the predictions of yearly productivities. The cultivation systems were assumed to be operated in a semi-continuous regime from the first day of operation. In order to minimize biomass loss at night, the daily change of medium was performed at 7 pm.

[18] For example, a HRT value of 4 days means that in average molecules of water spend four days in the system before exiting the system. In a system operated continuously, the amount of water exiting the system in one day would therefore represent 25% of the system volume.

As discussed in Chapter 4, the productivity predictions may be inaccurate in the case where the cultivation broth reaches hot temperatures. Indeed, the productivity model predicts that the optimal temperature for photosynthesis is around 38°C (Section 4.3). However, long-term cultivation in indoor bench-scale reactors revealed that *Chlorella vulgaris* was unable to maintain growth for more than 24 to 48 hours at a constant temperature of 35°C (Section 4.5). It is therefore challenging to predict the productivity when temperature is higher than 35°C for long periods of time. For this reason, the predicted productivities given in this analysis were associated with a 'temperature risk factor' (TRF) defined as the amount of daytime that algae are exposed to temperatures higher than 35°C. In addition, the productivity model demonstrated that there is no photosynthesis and respiration at temperatures higher than 42°C. As discussed in Chapters 1 and 4, high temperatures are likely to cause cellular death. For this reason, it was considered in the simulations that temperatures higher than 42°C caused algae death. It was also considered that the system was then re-inoculated the day after such high temperature events at an initial concentration of 0.1 g/L.

Following this operation mode, the yearly productivity of a cultivation system P_{year} (kg/yr) was expressed as follows:

$$P_{year} = \left(X_{end} - X_{ini}\right) \cdot V + \sum_{i=1}^{365} X_{s,i} \cdot V_{s,i} - N_r \cdot X_{ini} \cdot V \quad (5.3)$$

where X_{end} and X_{ini} are the final and initial algal concentrations (kg/m^3), respectively, V is the system volume (m^3), $X_{s,i}$ is the algal concentration at day i at the time of sampling (kg/m^3), $V_{s,i}$ is the volume of water sampled at day i, and N_r is the number of days where re-inoculation was necessary after a hot temperature event (T > 42°C).

5.2.3. Specific assumptions for closed photobioreactors

Reactor design and geometry

A large variety of designs and geometries have been tested in prior studies (Pegallapati et al., 2013) but there are still no clear guidelines on the best geometry for full-scale algal cultivation. In these simulations, the 'base-case' reactor geometry was based on the reactors used for model development and validation (height 1.8m; diameter: 0.19m; working volume: 50L). The materials and the characteristics of the environment around the reactors were also

set based on the photobioreactors operated in New Zealand (see Supplementary information S4 of Article 5 for further details).

Unit for biomass productivity

To express the productivity of photobioreactors per unit ground surface (for example in ton/ha-year) requires knowing the reactor density (defined as the number of reactors per unit surface). In practice, the relative positioning of individual reactors within a photobioreactor farm (which determines the reactor density) must be carefully optimized based on the light supply and inter-reactor shading (Slegers et al., 2013b; Mirón et al., 1999; Zhang et al., 1999; Zitelli et al., 2006). The optimal reactor density therefore varies with location and time as the sun position changes with latitude and time (Slegers et al., 2013b). As the optimization of the reactor positioning is out of the scope of this thesis, the productivity values discussed in this chapter were expressed per unit reactor and were based on the assumption of no light interaction effects between reactors.

5.2.4. Specific assumptions for open ponds

The depth of an open pond has a critical influence on productivity and water demand. Values used in prior studies varied from 0.2m to 0.3m (Clarens et al., 2010; Cooney et al., 2011; Lardon et al., 2009; Murphy and Allen, 2011; Stephenson et al., 2010; Weissman et al., 1989; Wigmosta et al., 2011; Yang et al., 2011). The median depth of 0.25m was used as a base-case value in this case-study. Other model inputs were based on the open pond used for model validation (see materials and methods section of Article 2 for further details). For a given location, the yearly productivity of an open pond is proportional to its surface area. The productivity of open ponds was therefore expressed per unit pond surface per year.

5.3. Photobioreactors - optimization of full-scale algal cultivation

In this first case study, the model was used to predict the productivity of photobioreactors at five climatic locations. The impact of the location on productivity is discussed in the first section (Section 5.3.1). Sections 5.3.2 and 5.3.3 then illustrate how the model can be used to investigate strategies to maximize productivity while minimizing the environmental impacts of full-scale cultivation systems.

5.3.1. Impact of climatic conditions on productivity and water demand in closed photobioreactors

Figure 5.2 shows the different outputs of the model for single closed photobioreactors at five climatic locations: the yearly productivity associated with the temperature risk factor and the water demand.

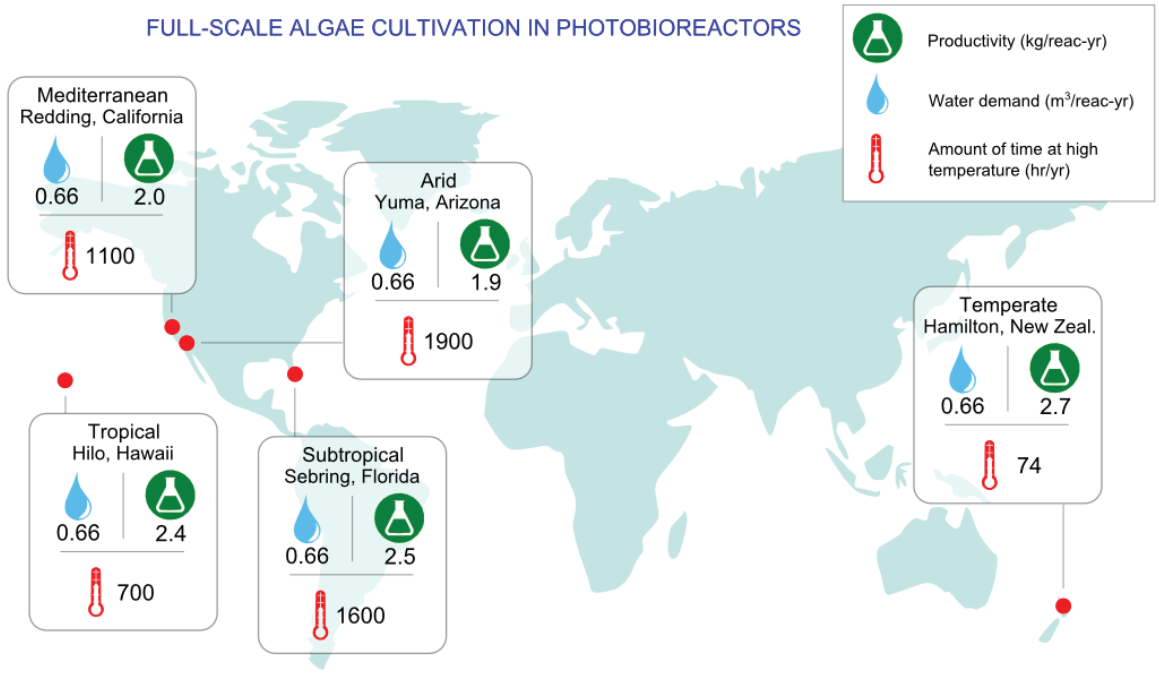

Figure 5.2: Productivity, water demand, and temperature risk factor in photobioreactors at different climatic locations.

Figure 5.2 shows that the predicted productivity varies from 1.9 kg/reactor-year in an arid climate to 2.7 kg/reactor-year in a temperate climate. The two locations with the highest

amounts of solar irradiance (California and Arizona, see Figure 2.4) paradoxically supported the lowest productivities due to the high occurrence of hot temperatures events (e.g. peak temperatures > 42^{o}C were predicted during 158 days and 106 days per year in Arizona and California, respectively). In contrast, the relatively high productivities predicted in a temperate climate are explained by the fact that temperature was predicted to remain between 10 and 35^{o}C for most of the year at these locations (Figure 5.2).

Because the amount of water evaporated by bubbling represented less than 10L of water per year under the conditions described in Chapter 3, the water demand of full-scale algal cultivation in closed photobioreactors was a sole function of the reactor volume and hydraulic retention time. As these parameters were set identical across all locations, the water demand was logically predicted to be independent of climate (0.66 m^{3}/yr; see Figure 5.2). However, the HRT and the reactor radius may need to be locally optimized to account for the specific climatic conditions, which may cause the water demand to differ across locations. The next two sections discuss how these two factors impact the predictions shown in Figure 5.2.

5.3.2. Impact of the hydraulic retention time on productivity and water demand in closed photobioreactors

Optimizing the hydraulic retention time can potentially help to maximize productivity in photobioreactors. Even if the hydraulic retention time has a minimal influence on the temperature (Article 3), this operational parameter can significantly impact the rate of respiration and therefore productivity. Indeed, the HRT influences the quantity of biomass in a photobioreactor (as discussed in Section 5.2.1) and therefore the respiration rate. In previous assessments of full-scale algal production, the influence of HRT on productivity prediction was not accounted for because of the lack of knowledge on respiration. The objective of this section is to demonstrate how the productivity model of this thesis can be used to optimize the HRT.

Figure 5.3 shows how the hydraulic retention time impacts both productivity and water demand at the five climatic locations used in this thesis as case-studies.

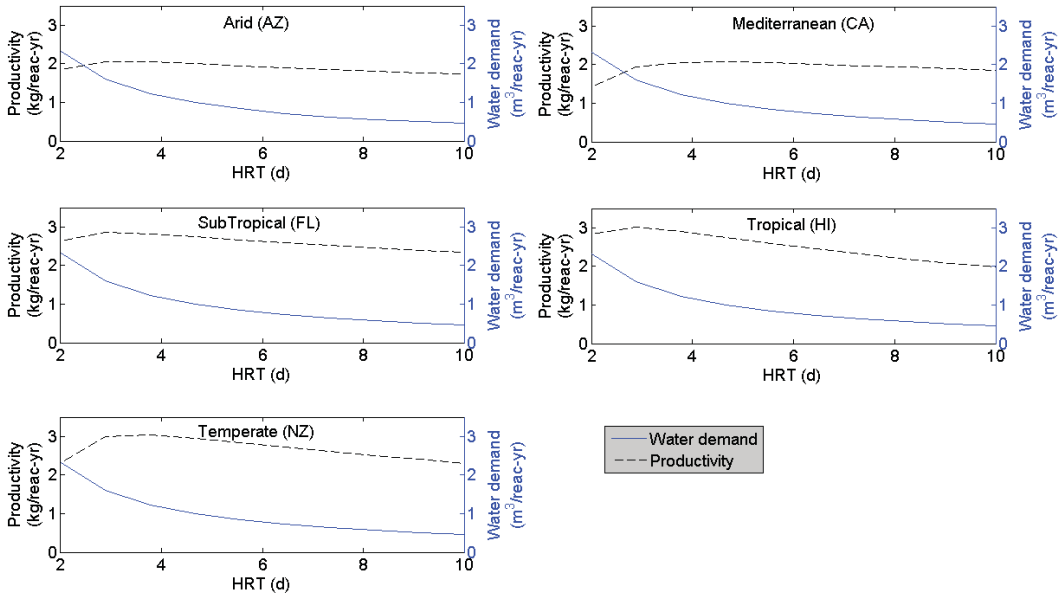

Figure 5.3: Variation of the productivity in full-scale photobioreactors and associated water demand with the hydraulic retention time

Figure 5.3 revealed that increasing the hydraulic retention time results in an increase of productivity for values lower than 3 days and in a decrease afterwards. This trend is explained by the fact that algal concentration increases with HRT. For low HRT values, the increase of concentration is beneficial for productivity as the amount of light captured by the system first increases with algal concentration. At a certain concentration threshold, all the available light is already captured by the algae and a further increase of the HRT does not translate into an increase of productivity. On the contrary, increasing further the algal concentration leads then to higher rates of respiration and consequently to a decrease of productivity. For example, Figure 5.3 shows that increasing the HRT from 3 to 10 days translates into a productivity loss of nearly 25% in a temperate climate. As discussed in the introduction of this chapter, these trends are in agreement with empirical observations in the literature (Mitchels et al., 2013; Silva Benavides et al., 2013).

The simulations revealed that the HRT values maximizing algal productivity for *Chlorella vulgaris* are relatively low (around 3 days, Figure 5.3), which would generate a relatively high water demand (e.g. 1.5 m^3/yr at a HRT value of 3 days). In addition to a potentially important economic cost, this high water demand can have important impact on local water resources as

extensively discussed in Section 4.4 of Article 6. The HRT value should therefore be optimized by considering both productivity and water demand.

5.3.3. Impact of reactor radius on peak temperatures

As discussed in Section 5.3.1, the occurrence of hot temperature events significantly impacts productivity during cultivation in closed photobioreactors. This section aims to investigate if changing the reactor radius can help minimizing the frequency of these hot temperature events.

Reactor geometry (radius in the case of column reactors) can impact temperature in various ways. The solar flow reaching the algae (in W) is roughly proportional to the reactor lateral surface and the thermal capacity of the reactor (in J/K) is proportional to the reactor volume. As a result, a higher reactor radius can theoretically result in lower reactor peak temperatures (Figure 5 of Article 3). However, Figure 5.4 shows that increasing the reactor radius does not significantly reduce the frequency of hot temperature episodes. This low effect is due to the decrease of cooling by natural convection as the reactor radius increases (see the results and discussion section of Article 3 for more details). The radius of the reactors should then be optimized by finding the best compromise between capital costs and productivity. On one side, small reactors are expected to achieve better productivities that big reactors (simply due to their higher surface/volume ratio). On the other side large reactors may be cheaper to build and operate.

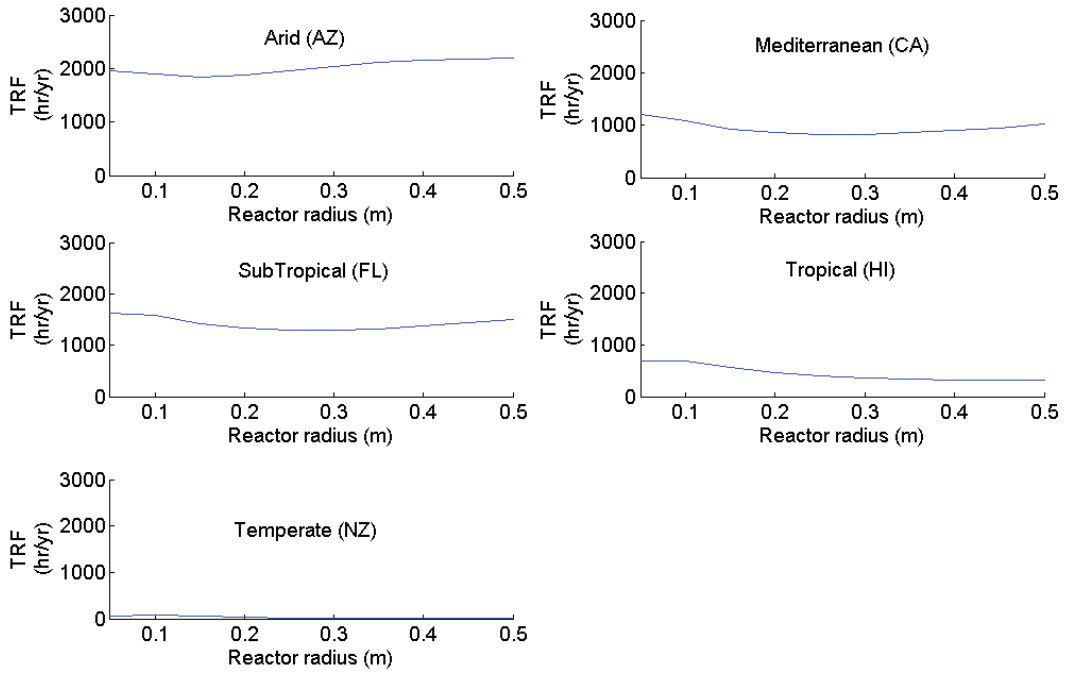

Figure 5.4: Effect of the reactor radius on the risk of overheating ("TRF": Temperature risk factor, defined in Section 5.2.2).

5.3.4. The need for temperature-tolerant species in the arid and Mediterranean locations

As discussed in Section 5.3.1, the productivity model revealed that hot temperatures would significantly impact the productivity at the arid and Mediterranean locations. Active temperature-control was shown to seriously threaten the sustainability of the process (Section 3.4.6) and increasing the reactor radius was proved to be inefficient at reducing the occurrence of hot temperature events (Section 5.3.3). An alternative strategy would consist on shading the photobioreactors during hot hours to avoid hot temperature events. However this strategy would lead to a significant decrease of productivity and further calculations using the model described in this thesis could determine the net benefit (if any) of this strategy. Another strategy would consist on cultivating temperature-tolerant species at hot locations as proposed by Tredici and Materassi (1992) or Morita et al. (2000). As the modelling approach used to develop the productivity model of *Chlorella vulgaris* was fully validated against full-scale data, the next logical step would be to apply the same approach to other algae species. The temperature prediction could then be used to optimize the algal species at each location.

5.4. Open ponds: optimization of full-scale algal cultivation

The case-study discussed in this section investigates the production of *Chlorella vulgaris* in open ponds. The impact of climatic conditions on productivity and water demand will be discussed in Section 5.4.1. The impact of HRT and pond depth will be discussed in Sections 5.4.2 and 5.4.3, respectively. In order to illustrate how the model can be used to optimize cultivation conditions, the pond depth was optimized at different locations to maximize productivity while minimizing the water demand. This optimization is described in Section 5.4.4.

5.4.1. Impact of location on productivity and water demand in open ponds

Figure 5.5 shows how the algal productivity (associated with the temperature risk factor) and the water demand vary across locations for open ponds in the base-case.

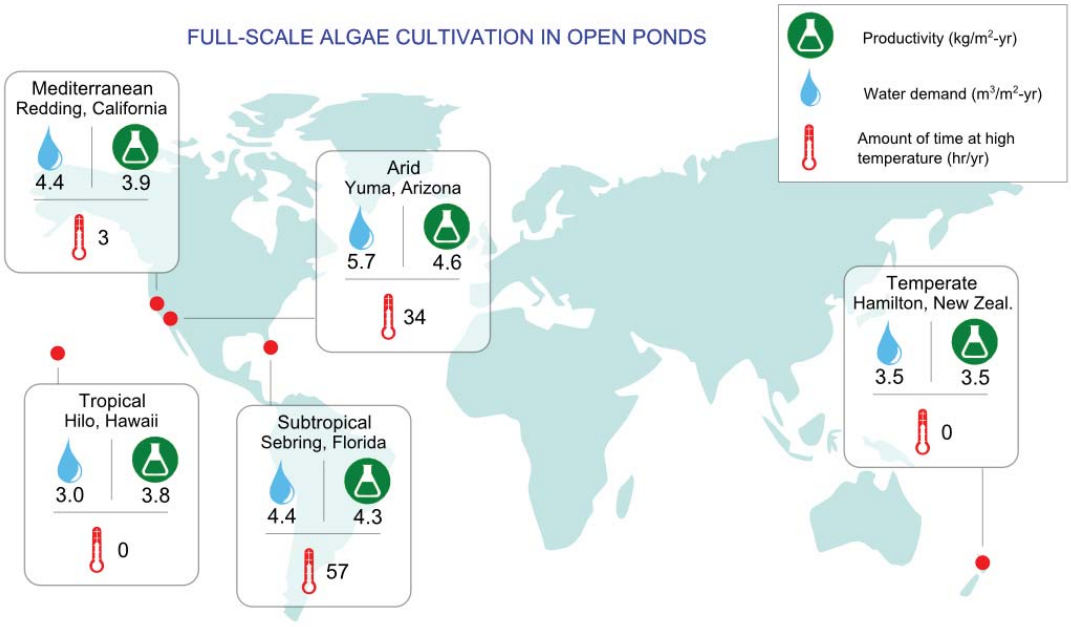

Figure 5.5: Productivity, water demand, and temperature risk factor in open ponds at different climatic locations.

Figure 5.5 shows that temperatures over 35°C were predicted to be relatively rare in open ponds, with a maximum of 57 hours per year in a subtropical climate. This low frequency is mostly due to the higher thermal inertia of ponds compared to photobioreactors. As a result, hot temperatures would be unlikely to cause culture collapse and for this reason, the predicted productivity generally increases with the solar irradiance (Figure 5.6). However, Figure 5.6 also shows that cold temperatures have a significant impact on productivity. For example, the predicted productivity in California is approximately 10% lower than in Florida while the solar irradiances at these two locations differ by less than 2%. This difference is explained by the occurrence of cold temperatures in California where the temperature was predicted to be below 10°C for 1100 hours of daytime per year.

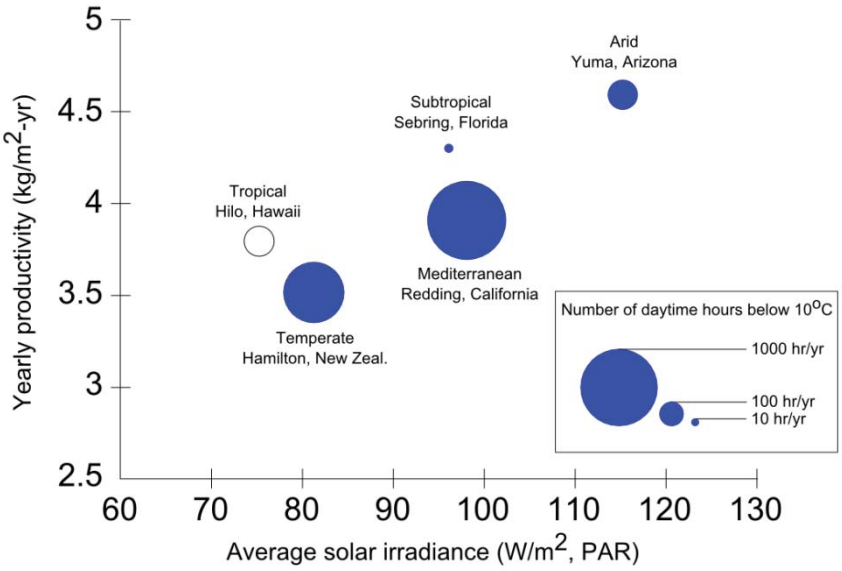

Figure 5.6: Correlation between the yearly productivity of open ponds vs. the solar irradiance (the temperature of a pond located in Hilo, Hawaii was predicted to remain above 10°C all year long).

Interestingly, the outdoor productivities predicted in this thesis for *Chlorella vulgaris* are between 2 to 4 times lower than the values used in prior assessments of biofuel production (Table 4.6). These differences may have an important impact on the conclusions of these studies. In particular, the study of Stephenson et al. (2010) concluded that using biodiesel from microalgae in raceway ponds in the UK rather than fossil fuels would decrease the CO_2

emissions by 78%. This analysis was performed by assuming yearly productivity of *Chlorella vulgaris* of 10 kg/m^2-yr. However, in a temperate climate, the productivity model revealed that productivities should be approximately 3.5 kg/m^2-yr (Figure 5.5). For this productivity value, Stephenson et al. (2010) predicts that using biodiesel from microalgae rather than fossil fuels would decrease CO_2 emissions by 30% instead of 78%. Another example is the assessment of Pate et al. (2011) which aimed to assess the feasibility of biofuel production in the US. The amount of land required to meet the combined US diesel and aviation transport fuel demand (100 billion gallons per year, or BGY) was estimated at 6% of the Southwest of the US. This study was based on algal productivity of 11.3 kg/m^2-yr. However, the simulations using the model developed in this thesis revealed that productivities should be at least two times lower than the levels assumed by the study of Pate et al. (2011). As a result, the amount of land required to produce 100 BGY of biofuel may therefore represent approximately 12% of the Southwest of the US. This overestimation of productivity may therefore change the main conclusion of the study which was that land is the most manageable resource for biofuel production. These two examples illustrate how neglecting the impact of temperature on productivity may impact the conclusions regarding the feasibility and the environmental consequences of full-scale algal cultivation.

On the contrary to closed photobioreactors, significant differences in water demand are observed across locations. While the water demand in a tropical climate was estimated at 3.0 m^3/m^2-yr, the water demand in an arid climate was estimated at 5.6 m^3/m^2-year. These differences are due to the variation of rainfall and evaporation rates across locations. The selection of a location for full-scale algal cultivation in open ponds should therefore account for these differences in water demand, in conjunction with the availability of water resources.

5.4.2. Impact of HRT on the productivity and water demand in open ponds

Figure 5.7 shows that the impact of HRT on productivity and water demand in open ponds is similar to the case of the closed photobioreactors (see Section 5.2). While reducing the HRT value can help to maximize productivity, this strategy also leads to increase the water demand. For example, decreasing the HRT from 10 to 2 days in an arid climate can cause a 2 to 3-fold increase in the water demand against a productivity gain of 'only' 30% (Figure 5.7). These results indicate that the optimization of the HRT should therefore be done by accounting for the water availability at the location considered.

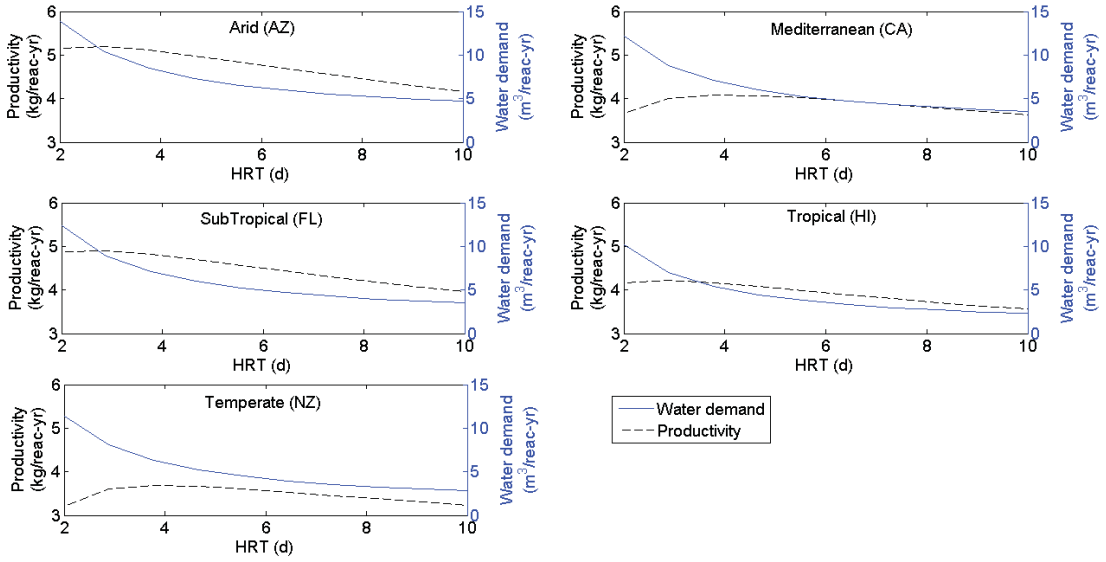

Figure 5.7: Influence of the HRT on the productivity and water demand in open ponds.

5.4.3. Influence of the depth on productivity and water demand in open ponds

This section investigates how the depth of open ponds influences the productivity and water demand in open ponds. The thermal inertia of open ponds is directly proportional to the pond depth, meaning that temperature variation is faster in a shallow pond than in a deep pond. As a result, the pond depth has a high impact on temperature, hence on productivity. In addition, decreasing the pond depth while maintaining the HRT constant has the potential to significantly reduce the water demand of the process. The objective of this section is to illustrate how the model can be used to quantify the impact of the pond depth on productivity and water demand. Figure 5.8 shows the influence on the pond depth on the productivity and water demand in open ponds at different climatic locations.

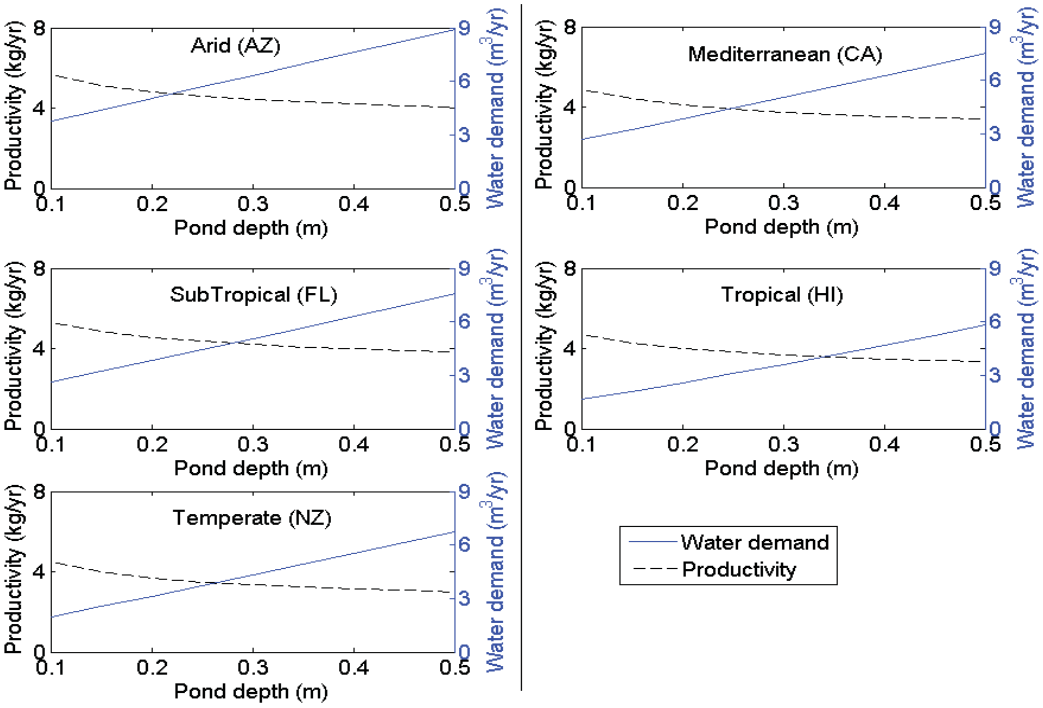

Figure 5.8: Productivity and water demand at different climatic locations as a function of depth.

As shown in Figure 5.8, decreasing the pond depth from 0.5 to 0.1m can theoretically increase the productivity by between 20 to 40% while decreasing the water demand by 60 to 75%, depending on the location considered. This increase of productivity is due to the fact that the day-time pond temperature was predicted to reach values closer to the optimal values of photosynthesis (38^{o}C) as the pond depth decreases. In addition, the decrease of the pond depth is responsible for a faster decrease of temperature at night-time. As a result, respiration rates at night time should decrease with the pond depth, which also favors higher productivities.

Ritchie and Larkum (2012) showed that the optimal pond depth for *Chlorella sp.* cultivation was 0.087m for an open pond located at the tropic of Cancer. However, these authors assumed temperature could be controlled and therefore did not account for the risk of overheating. Indeed, Figure 5.8 shows that the temperature in a 0.087m pond located in Florida (a location close to the Tropic of Cancer) would exceed 35^{o}C for around 350 hours a year. As a result, the optimal pond depth should actually be higher than 0.087m to avoid hot temperature events. Another attempt to consider the impact of the pond depth on temperature was presented by Slegers et al. (2013a). The authors used an empirical model to predict the

temperature of open shallow ponds located in the Netherlands and Algeria. Surprisingly, the temperature model used in this study predicted a maximum temperature around 28°C in Algeria in summer in a 0.1m-deep pond. The climate of Algeria is Mediterranean to arid (depending on the location considered) and Figure 5.9 shows that under this type of climate, the temperature of a 0.1m-deep pond should be higher than 35°C for around 250 hours a year. The conclusions of Ritchie and Larkum (2010) and Sledgers et al. (2013a) illustrate the need for accurate models accounting for the impact of dynamic broth temperature changes when optimizing the process.

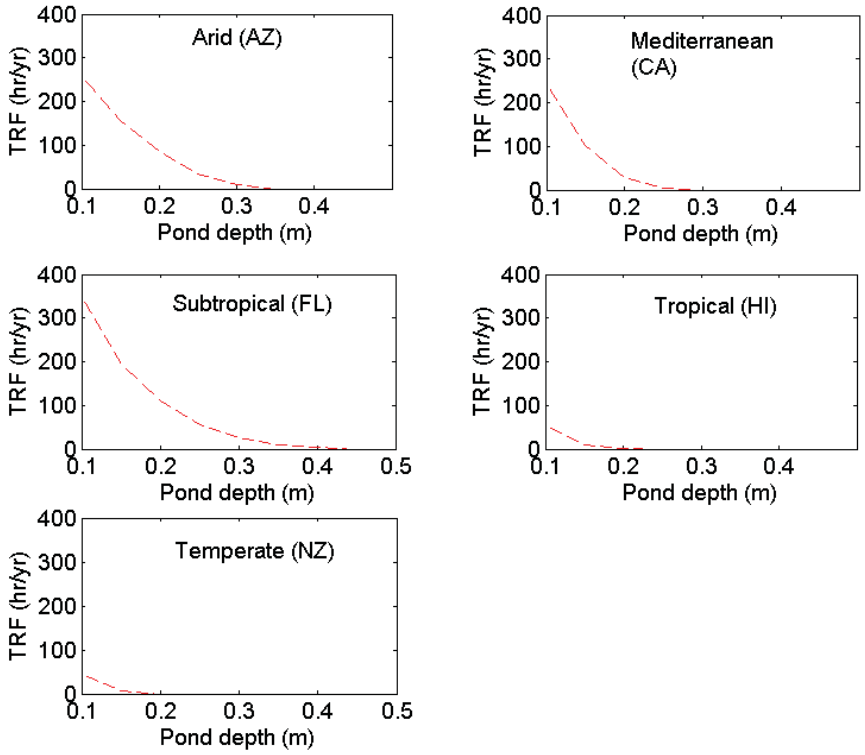

Figure 5.9: Occurrence of hot temperature events as a function of the depth

5.4.4. Optimization of process by active control of the pond depth

As demonstrated in the previous section, decreasing the pond depth (while maintaining the HRT constant) reduces water demand and, under specific circumstances, increases productivity. However, the occurrence of hot temperature events in open ponds is also expected to increase when the pond depth decreases (Figure 5.9). A possible process

optimization would therefore consist on increasing the pond depth in summer to avoid hot temperature events, while decreasing pond depth in winter to minimize the water demand of the process. This section describes how this optimization can be done by using the model developed in this thesis.

Optimization process

The following process was used to maximize productivity while minimizing water demand at the five climatic locations selected in this thesis (Figure 2.4). The pond depth was changed on a monthly basis and, for each month of the year, was set at the lowest value possible ensuring that the temperature would not be higher than 35^{o}C for more than 20 hours per month. The minimal pond depth was set at 0.1m based on Sledgers et al. (2013a). Figure 5.10 shows the pond depth profile thus obtained. A pond depth of 0.35 m was found sufficient to prevent hot temperature occurrences in summer at most climatic locations.

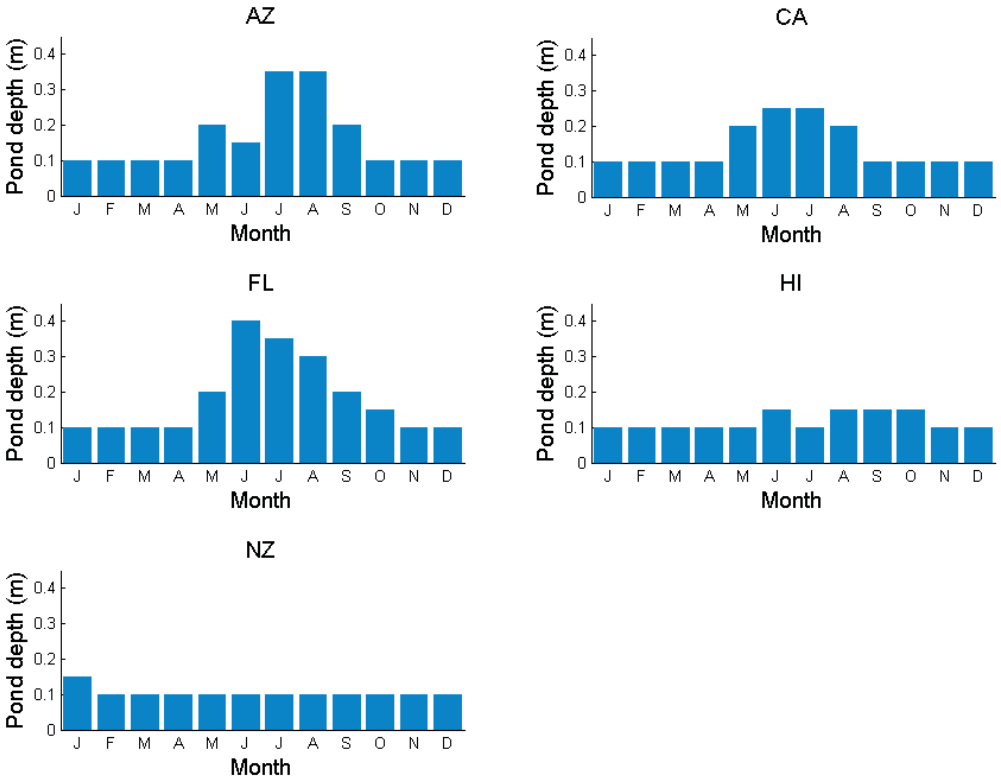

Figure 5.10: Optimized pond depth following the optimization scheme described in Section 5.4.4

Impact of optimization on productivity and water demand

Figure 5.11 illustrates how optimizing pond depth can help to increase productivity by 8% to 23% while the water demand can be reduced by 15% to 46%, depending on location. Interestingly, whereas the 'optimal' productivities predicted in Arizona and New Zealand only differed by 18%, the predicted water demand was 2.4 times higher in Arizona than in New Zealand. These results suggest that temperate locations may actually be more suitable than arid locations where water resources are limited and where their consumption has a more serious impact.

In the current assessments of full-scale production of microalgae, locations are very often compared by using the same assumptions on system design and operation. For example, the study of Yang et al. (2011) investigated how the geographic location influences the water footprint of *Chlorella vulgaris* biodiesel production in open ponds. In this study, locations were compared by assuming that systems would be designed and operated similarly across locations in the US. The conclusion of the study was that "Florida and Hawaii were the most suitable locations for microalgae-based biodiesel production, and Arizona has the third smallest water footprint among all states". However, Figure 5.11 shows that these conclusions would be different if the comparison was based on systems that were optimized specifically for each location[19].

[19] The same limitation applies to our study in Article 6 where the water demand of open ponds located at five different climatic conditions was calculated by assuming the same design and operation at all locations. At the time of the study, the productivity could not be accurately predicted and uncertainty on the productivity caused important inaccuracy on the water demand (Section 4.7).

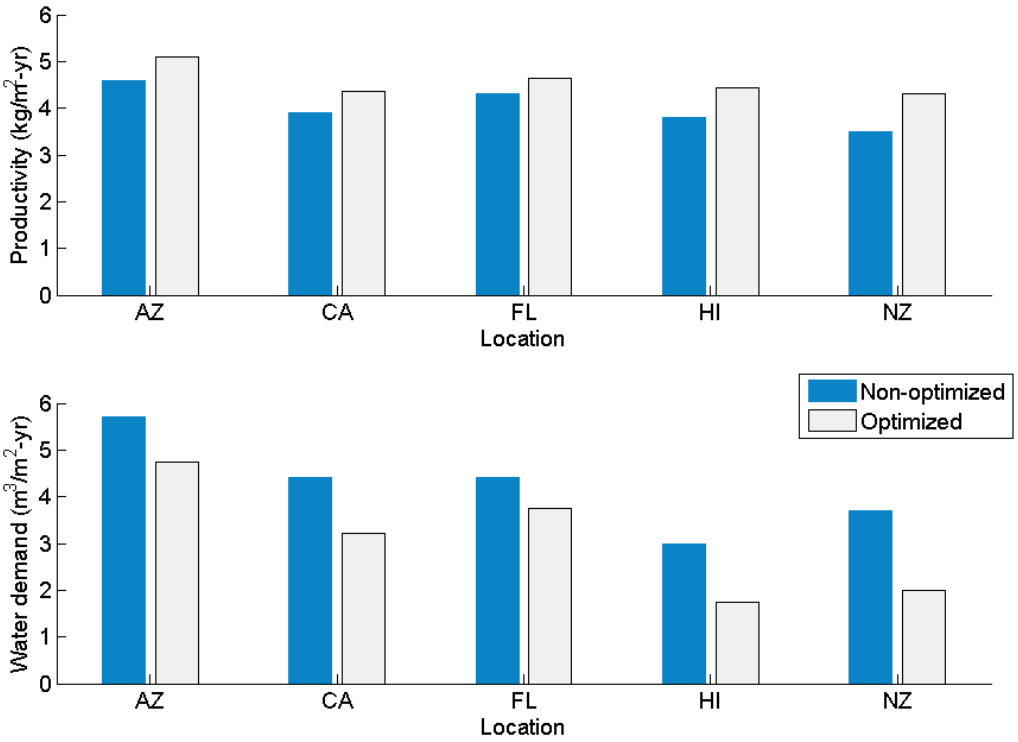

Figure 5.11: Water demand and productivity during optimized and non-optimized process

5.5. Conclusions

- Simulations using the newly developed productivity model demonstrated that hot temperature events (T> 42^{o}C) could significantly impact productivity in arid and Mediterranean climates.
- While active temperature control was shown to be economically prohibitive, manipulating the radius of closed photobioreactors was shown to be inefficient at reducing the frequency of hot temperature events.
- Our simulations revealed that optimal HRT values for both open ponds and photobioreactors are in the order of 3 days at all the locations considered for *Chlorella vulgaris*.
- However, large amounts of water resources may be needed to operate full-scale systems at these low HRT values. Optimizing HRT should therefore be done with consideration of the availability of water resources by coupling the prediction of the model developed in this thesis with the local water resources availability.
- Changing the pond depth was shown to significantly impact algal productivity and water demand in open ponds.
- The model developed in this thesis has a unique ability to account for the impact of the design and operational parameters on the algal productivity and the water demand. The productivity model developed in this thesis is therefore the first engineering tool for process optimization. To illustrate this ability, the pond depth was optimized on a monthly basis to maximize yearly productivities and minimize water demand. Depending on location, the active control of the pond depth was shown to maximize the productivity by 8 to 23% while minimizing the water demand by 15 to 46%.
- Current assessments of full-scale algal cultivation often compare locations by assuming the same design and operation across locations. However, our study revealed that comparing non-optimized processes may lead to erroneous conclusions regarding the best location for full-scale algal cultivation.

Thesis conclusions

- At full-scale, both light and temperature have a significant impact on algal productivity. Numerous models of algal productivity exist in the literature but to the best of our knowledge, no modelling approach predicting biomass productivity was validated against full-scale conditions prior to this thesis. In particular, different knowledge gaps were identified in our initial literature review:
    - The temperature variations and their significant influence on algal productivity were neglected in most of models whereas temperature can significantly vary during full-scale cultivation.
    - Most of the existing models were developed indoor under conditions that do not represent full-scale cultivation conditions. To the best of our knowledge, the accuracy of these models for full-scale predictions has never been fully assessed before this thesis.
- Based on the assessment of more than 40 modelling approaches, we concluded that currently the most pragmatic modelling methodology for engineering assessments of full-scale systems would utilize the following approaches (Figure 1.2):
    - For the rate of photosynthesis, Type II models (expressing the total rate of photosynthesis as the sum of local rates of photosynthesis) provide a pragmatic compromise between practicability and universality.
    - In conjunction with Type II models, empirical functions that account for the effect of temperature on photosynthesis should be used.
    - In order to predict the net productivity, the above should be used in conjunction with a decay term for respiration that empirically accounts for temperature effects.
- The model of temperature for open ponds was found to be accurate within $\pm 2.6^{o}C$ ($p = 0.05$, $N = 33{,}221$) when compared to experimental data collected over an entire year in an open pond in Hamilton (New Zealand).
- The temperature model developed in this thesis was the first model exclusively based on theoretical expressions rather than empirical formulas. This temperature model was demonstrated to be systematically more accurate than prior temperature models which were all partly based on empirical formulas.

- This thesis also presents the first temperature model for vertical column photobioreactors. This temperature model was found to be accurate within 4.2^{o}C when compared against experimental data from Singapore and New Zealand ($p = 0.05$, $N = 6{,}995$).
- Simulations using the temperature model for photobioreactors revealed that high amounts of heat would need to be extracted from photobioreactors to maintain the temperature of the algal culture below 35^{o}C in arid and Mediterranean climates. It was shown that temperature cannot be actively controlled in photobioreactors at these hot locations without threatening the cost-efficiency and sustainability of full-scale algal cultivation.
- The kinetic parameters of the productivity model were first determined from short-term lab-scale experiments. The predictions of the resulting productivity model were then compared to biomass productivities measured in indoor bench-scale reactors operated under constant light and temperature conditions. The accuracy of the model was found to be ±13%, the error of the prediction being mostly due to the uncertainty of experimentally measured model inputs (precision of the light sensors, etc.)
- The model was also validated against pilot-scale data collected from outdoor photobioreactors operated in New Zealand. Over 141 days of outdoor cultivation under various meteorological conditions, the average accuracy of the productivity prediction was found to be ±13%.
- Prior cost-studies and assessments of environmental impacts were often inaccurate due to the uncertainty on the productivity achieved in outdoor cultivation systems (generally taken at ±50%). The level of accuracy of our productivity predictions was found to reduce considerably the uncertainty of these assessments.
- Neglecting the impact of temperature variations on productivity at full-scale can significantly impact the conclusions of the assessments of biofuel production from microalgae, in particular concerning the actual cost of biofuel production.
- The productivity model demonstrated that hot temperature events (above 42^{o}C) would significantly impact the productivity in an arid or a Mediterranean climate in photobioreactors.
- Changing the size of closed photobioreactors was shown to be inefficient at reducing the frequency of hot temperature events. As a result, temperature-resistant algae would be required for cultivation at these hot locations.

- Our simulations revealed that optimal HRT values for both open ponds and photobioreactors are in the order of 3 days at all the locations considered for *Chlorella vulgaris*.
- However, large amounts of water resources may be needed to operate full-scale systems at these low HRT values. Optimizing the HRT should therefore be done with consideration of the availability of water resources by coupling the prediction of the model developed in this thesis with the local water resources availability.
- Changing the pond depth was shown to significantly impact algal productivity and water demand.
- The model developed in this thesis has a unique ability to account for the impact of the design and operational parameters on the algal productivity and the water demand. The productivity model developed in this thesis is therefore the first engineering tool for process optimization. To illustrate this ability, the pond depth was optimized on a monthly basis to maximize yearly productivities and minimize water demand. Depending on location, the active control of the pond depth was shown to maximize the productivity by 8 to 23% while minimizing the water demand by 15 to 46%.
- Current assessments of full-scale algal cultivation often compare locations by assuming the same design and operation across locations. However, our study revealed that comparing non-optimized processes may lead to erroneous conclusions regarding the best location for full-scale algal cultivation.

Future prospects

Even if the productivity model developed in this thesis was validated against a broad range of cultivation conditions, this validation was conducted within a particular scope (e.g. well-mixed conditions; nutrient saturation; and oxygen sub-inhibitory levels). However, full-scale productivity might be affected by factors that were not accounted for, such as contamination in open ponds. In addition, the main assumption behind the productivity model developed in this thesis was that productivity at full-scale should only be affected by light and temperature. In the context of biofuel production, the generation of lipids by the algae must often be triggered by nutrient starvation (Illman et al., 2000). Prior modelling approaches were developed with the purpose to account for nitrogen starvation (Droop, 1968). It would therefore be very interesting to combine the model of productivity developed in this thesis

with the Droop model to refine the productivity predictions in the context of biofuel production. Another limitation of the model is that the impact of dissolved oxygen on productivity was not accounted for. While the level of dissolved oxygen reached during the full-scale cultivation of *Chlorella vulgaris* did not have a significant impact on productivity (Chapter 4), oxygen-inhibition may be observed for different algal species and cultivation systems (Keymer et al., 2013). Future modelling studies should therefore aim to account for the impact of dissolved oxygen on productivity. Despite these limitations, it should be noted that the model prediction of full-scale productivity in open ponds are in good agreement with field data: For example, Moheimani and Borowitzka (2006) achieved a productivity of 5.5 kg/m^2-yr in an open pond located in Western Australia for the algae *Pleurochrysis carterea*, which is similar to the model predictions for *Chlorella vulgaris* in a similar climate (Figure 5.11). An ultimate validation step would consist of assessing the model productivity against cultivation data from open ponds.

The modelling approach presented in this thesis was only developed and validated for *Chlorella vulgaris*. Other algal species are currently receiving attention due to their commercial interest. In particular, the cyanobacteria *Spirulina platensis* was the algae the most produced in 2006 according to Spolaore et al. (2006). The next logical step would therefore be to apply the methodology developed in this thesis to other algae species. Practically, the experimental technique used to parameterize the biological model was developed with the purpose of being practical, which would ease the application of the model to multiple algal species.

Finally, while Chapter 5 investigated the impact of the pond depth on productivity and water demand, the model developed in this thesis can be used for multiple engineering applications. For instance, similarly to the dynamic control of the pond depth investigated in Chapter 5, the model can be used to investigate the dynamic control of the HRT in open ponds to further limit water consumption while increase algal productivity. Other optimization strategies such as partly shading photobioreactors at mid-day in order to avoid overheating can also be investigated.

References

Acién Fernández FG, García Camacho F, Sánchez Pérez JA, Fernández Sevilla JM, Molina Grima E. 1997. A model for light distribution and average solar irradiance inside outdoor tubular photobioreactors for the microalgal mass culture. Biotechnol Bioeng 55(5): 701-714.

Ali, AHH. 2007. Passive cooling of water in uninsulated open tank in hot arid areas. Energy Conv Manag (48): 93-100.

Batan L, Quinn JC, Bradley TH. 2013. Analysis of water footprint of a photobioreactor microalgae biofuel production system from blue, green and lifecycle perspectives. Algal Res 2(3): 196-203.

Beardall J, Morris I. 1976. The concept of light intensity adaptation in Marine Phytoplankton: Some experiments with Phaeodactylum tricornutum. Marine Biol 37: 377-387.

Béchet Q, Muñoz R, Shilton A, Guieysse B. 2013. Outdoor Cultivation of Temperature-Tolerant Chlorella sorokiniana in a Column Photobioreactor Under Low Power-Input. Bioeng Biotechnol 110(1): 118-126.

Becker EW. 2007. Micro-algae as a source of protein. Biotechnol Adv 25(2): 207‑210.

Benemann JR, Tillett DM, Weisman JC. 1987. Microalgae biotechnology. Trends Biotechnol 5(2): 47-53.

Bernard O. 2011. Hurdles and challenges for modelling and control of microalgae for CO_2 mitigation and biofuel production. J Process Control 21:1378–1389.

Bernard O, Rémond B. 2012. Validation of a simple model accounting for light and temperature effect on microalgal growth. Biores Technol 123: 520-527.

Bordel S, Guieysse B, Muñoz R. 2009. Mechanistic model for the reclamation of industrial wastewaters using algal-bacterial photobioreactors. Environ Sci Technol 43(9): 3200–3207.

Borowitzka MA. 1998. Limits to growth. In: Wong YS, Tam NFY (eds) Wastewater treatment with algae. Springer-Verlag Berlin pp 203-226.

Bosma R, van Zessen E, Reith JH, Tramper J, Wijffels RH. 2007. Prediction of volumetric productivity of an outdoor photobioreactor. Biotechnol Bioeng 97(5):1108-1120.

Brady DK, Graves WL, Geyer, JC. 1969. Surface Heat Exchange at Power Plant Cooling Lakes - Report #5, Edison Electric Institute Publication #69-901, New York, NY.

Burris JE. 1981. Effects of oxygen and inorganic carbon concentrations on the photosynthetic quotients of marine algae. Mar Biol 65: 215-219.

Butterwick C, Heaney SI, Talling JF. 2005. Diversity in the influence of temperature on the growth rates of freshwater algae, and its ecological relevance. Freshw Biol 50:291-300.

Camacho Rubio F, García Camacho F, Fernández Sevilla JM, Chisti Y,Molina Grima E. 2003. A mechanistic model of photosynthesis in microalgae. Biotechnol Bioeng 81(4):459-473.

Campbell PK, Beer T, Batten D. 2011. Life Cycle assessment of biodiesel production form microalgae in ponds. Bioresour Technol 102: 50-56.

Carvahlo AP, Malcata FX. 2003. Kinetic modeling of the autotrophic growth of *Pavlova lutheri*: study of the combined influence of light and temperature. Biotechnol Prog 19:1128-1135.

Chalker BE. 1980. Modelling light saturation curves for photosynthesis: an exponential function. J Theor Biol 84: 205-215.

Chisti Y. 2008. Biodiesel from microalgae beats bioethanol. Trends Biotechnol 26(3): 126-131.

Clarens AF, Resurreccion EP, White MA, Colosi LM. 2010. Environmental life cycle comparison of algae to other bioenergy feedstocks. Environ Sci Technol 44: 1813–1819.

Collins CD, Boylen CW. 1982. Physiological responses of *Anabaena variabilis* (cyanophyceae) to instantaneous exposure to various combinations of light intensity and temperature. J Phycol 18:206-211.

Cooney MJ, Young G, Pate R. 2011. Bio-oil from photosynthetic microalgae: case study. Bioresour Technol 102 : 166–177.

Cornet JF, Dussap CG, Dubertret G. 1992. A structured model for simulation of cultures of the cyanobacterium Spirulina platensis in photobioreactors: I. Coupling between light transfer and growth kinetics. Biotechol Bioeng 40:817-825.

Cornet JF, Dussap CG, Gros, JB. 1995. A simplified monodimensional approach for modeling coupling between radiant light transfer and growth kinetics in photobioreactors. Chem Eng Sci 50(9):1489-1500.

Cornet JF, Dussap CG. 2009. A simple and reliable formula for assessment of maximum volumetric productivities in photobioreactors. Biotechnol Prog 25(2):424-435.

Costache TA, Acién Feranández FGA, Morales MM, Fernández-Sevilla JM, Stamatin I, Molina E. 2013. Comprehensive model of microalgae photosynthesis brate as a function of culture conditions in photobioreactors. Appl Microbiol Biotechnol. 97(17): 7627-7637.

Crill, PA. 1977. The photosynthesis-light curve: a simple analog model. J Theor Biol 64: 503-516.

Culberson SD, Piedrahita RH. 1996. Aquaculture pond ecosystem model: temperature and dissolved oxygen prediction – mechanism and application. Ecol Model (89): 231-258.

Culf AD, Gash JHC. 1993. Longwave radiation from clear skies in Niger: a comparison of observations with simple formulas. J Appl Meteor (32): 539-547.

Cullen JJ. 1990. On models of growth and photosynthesis in phytoplankton. Deep Sea Research 37(4): 667-683.

Davison IR. 1991. Environmental effects of temperature on photosynthesis: temperature. J Phycol 2-8.

de-Bashan LE, Trejo A, Huss VAR, Hernandez JP, Bashan Y. 2008. Chlorella sorokiniana UTEX 2805, a heat and intense, sunlight-tolerant microalga with potential for removing ammonium from wastewater. Biores Technol 99:4980-9.

Del Campo JA, García González M, Guerrero MG. 2007. Outdoor cultivation of microalgae for carotenoid production: current state and perspectives. Appl Microbial Biotechnol74:1163-1174.

Denman KL, Marra J. 1986. Modelling the Time Dependent Photoadaptation of Phytoplankton to Fluctuating Light. Elsevier Oceanog Ser 42 (C): 341-359.

Dermoun D, Chaumont D., Thebault JM, Dauta A. 1992. Modelling of growth of *Porphyridium cruentum* in connection with two interdependent factors: light and temperature. Biores Technol 42:113-117.

Droop MR. 1968. Vitamin B12 and marine ecology. The kinetics of uptake growth and inhibition in Monochrysis lutheri. J Mar Biol Assoc 48(3):689–733.

Duarte P. 1995. A mechanistic model of the effects of light and temperature o algal primary productivity. Ecol Model 82:151-160.

Duffie JA, Beckman WA. 2006. Solar engineering of thermal processes, 3rd edition. Hoboken, NJ: Wiley.

Edinger JE, Brady DK, Geyer JC. 1974. Heat Exchange and transport in the environment – Report #14, Edison Electric Institute Publication, New York, NY.

Evers EG. 1991. A model for light-limited continuous cultures: Growth, shading, and maintenance. Biotechnol Bioeng 38(3):254-259.

Falkowski PG, Owens TG. 1978. Effects of light intensity on photosynthesis and dark respiration in six species of marine phytoplankton. Marine Biol 45:289-295.

Farnsworth RK, Edwin ST. 1982. Mean Monthly, seasonal, and annual pan evaporation for the United States. USDC, NOAA, National Weather Service. NOAA Technical Report NWS 34.

Fasham MJR, Platt T. 1983. Photosynthetic response of phytoplankton to light: a physiological model. Proc Royal Soc Lond Ser B, Biol Sci 219(1217): 355-370.

Fawley MW. 1984. Effects of light intensity and temperature interactions on growth characteristics of *Phaeodactylum tricornutum* (bacillariophyceae). J Phycol 20:67-72.

Ferris JM, Christian R. 1991. Aquatic primary production in relation to microalgal responses to changing light: a review. Aquat Sci 53(2/3):187-217.

Foidl N, Foidl G, Sanchez M, Mittelbach M, Hackel S. 1996. Jatropha curcas L. as a source for the production of biofuel in Nicaragua. Biores Technol 58: 77-82.

Frank ED, Han J, Palou-Rivera I, Elgowainy A, Wang MQ. 2011. Life Cycle Analysis of Algal Lipid Fuels with the GREET Model. Argonne National Laboratory, US Department of Energy.

Fritz JJ, Meredith DD, Middleton AC. 1979. Non-steady state bulk temperature determination for stabilization ponds. Water Res (14): 413-420.

García Camacho F, Contreras Gómez A, Acién Fernández FG, Fernández Sevilla J, Molina Grima E. 1999. Use of concentric-tube airlift photobioreactors for microalgal outdoor mass cultures. Enzym Microb Technol 24: 164-172.

García-Camacho F, Sánchez-Mirón A, Molina Grima E, Camacho Rubio F, Merchuck JC. 2012. A mechanistic model of photosynthesis in microalgae including photoacclimation dynamics. J Theor Biol 304:1-15.

Geider RJ. 1990. The relationship between steady state phytoplankton growth and photosynthesis. Limnol Oceanogr 35(4): 971-972.

Geider RJ, MacIntyre HL. 1996. A dynamic model of photoadaptation in phytoplankton. Limnol Oceanogr 41(1): 1-15.

Geider RJ, MacIntyre HL, Kana TM. 1997. Dynamic model of phytoplankton growth and acclimation: responses of the balanced growth rate and the chlorophyll *a*: carbon ratio to light, nutrient-limitation and temperature. Mar Ecol Prog Ser 148:187-200.

Geider RL, MacIntyre HL, Kana TM. 1998. A dynamic regulatory model of phytoplanktonic acclimation to light, nutrients, and temperature. Limnol Oceanogr 43(3):679-694.

Gipe, P. 2004. Wind Power—Renewable Energy for Home, Farm, and Business. Chelsea Green Publishing Co.: White River Junction, VT.

Grobbelaar JU. 1990. Modeling algal productivity in large outdoor cultures and waste treatment systems. Biomass 21:297-314.

Grobbelaar, JU. 1991. The influence of light/dark cycles in mixed algal cultures on their productivity. Biores Technol 38:189-194.

Grobbelaar JU. 1994. Turbulence in mass algal cultures and the role of light/dark fluctuations. J Appl Phycol 6:331-335.

Grobbelaar JU. 2009. Factors governing algal growth in photobioreactors: the “open” versus “closed” debate. J Appl Phycol 21(5): 489-492.

Guterman H, Vonshak A, Ben-Yaakov S. 1990. A macromodel for outdoor algal mass production. Biotechnol Bioeng 35: 809-819.

Haario H, Kalachev L, Laine 2009. M. Reduced models of algae growth. Bull Math Biol 71: 1626-1648.

Han BP. 2001. Photosynthesis-Irradiance response at physiological level: a mechanistic model. J Theor Biol 213:121-127.

Hawkins DM. 2004. The problem of overfitting. J Chem Inf Comput Sci 44: 1-12.

Houf WG, Incropera FP. 1980. An assessment of techniques for predicting radiation transfer in aqueous media. J Quant Spectrosc Radiat Transfer 23: 101-115.

Howell JR, Siegel R, Pinar Mengüç M. 2011. Thermal radiation heat transfer. 5th edition. CRC PressINC.

Illman AM, Scragg AH, Shales SW. 2000. Increase in Chlorella strains calorific values when grown in low nitrogen medium. Enzym Microbial Technol 27: 631–635.

Janssen M, Tramper J, Mur LR, Wijffels RH. 2003. Enclosed outdoor photobioreactors: light regime, photosynthetic efficiency, scale-up, and future prospects. Biotechnol Bioeng 81(2):193-210.

Jassby AD, Platt T. 1976. Mathematical formulation of the relationship between photosynthesis and light for phytoplankton. Limnol Oceanog 21(4): 540-547.

Jeon YC, Cho CW, Yun YS. 2005. Measurement of microalgal photosynthetic activity depending on light intensity and quality. Biochem Eng J 27: 127-131.

Kant P, Wu S. 2011. The extraordinary collapse of Jatropha as a global biofuel. Environ Sci Technol 45: 7114-7115.

Karagiannis I, Soldatos PG. 2008. Water desalination cost literature: review and assessment. Desalination 223: 448-456.

Katsuda T, Arimoto T, Igarashi K, Azuma M, Kato J, Takakuwa S, Ooshima H. 2000. Light intensity distribution in the externally illuminated cylindrical photo-bioreactor and its application to hydrogen production by *Rhodobacter capsulatus*. Biochem Eng 157-164.

Ketheesan B, Nirmalakhandan N. 2013. Modeling microalgal growth in an airlift-driven raceway reactor. Biores Technol 136: 689-696.

Keymer PC, Pratt S, Lant PA. 2013. Development of a Novel Electrochemical System for Oxygen Control (ESOC) to Examine Dissolved Oxygen Inhibition on Algal Activity. Biotechnol Bioeng 110(9): 2405-2411.

Kiefer DA, Mitchell BG. 1983. A simple, steady-state description of phytoplankton growth based on absorption cross section and quantum efficiency. Limnol Oceanog 28(4): 770-776.

Klemetson SL; Rogers GL. 1985. Aquaculture pond temperature modeling. Aquac Eng (4): 191-208.

Krant J, Motzkin F, Gordin H. 1982. Modelling temperatures and salinities of mixed seawater fish ponds. Aquac (27): 377-388.

Kurano N, Miyachi S. 2005. Selection of microalgal growth models for describing specific growth rate-light response using extended information criterion. J Biosci Bioeng 100 (4): 403-408.

Kvíderová J, Lukavský J. 2005. The comparison of ecological characteristics of *Stichococcus* (Chlorophyta) strains isolated from polar and temperate regions. Algological Studies/Archiv für Hydrobiologie, Suuplement Volumes 118: 127-140.

Lang OL, Novel PB, Osmond B, Ziegler H. 1981. Photosynthetically active radiation. In: Physiological plant ecology. Vol. 12A, Encyclopedia of plant physiology (new series).

Lardon L, Helias A, Sialve B, Steyer JP, Bernard O. 2009. Life-cycle assessment of biodiesel production from microalgae. Environ Sci Technol 43: 6475–6481.

Le Borgne F; Pruvost J. 2013. Investigation and modeling of biomass decay rate in the dark and its potential influence on net productivity of solar photobioreactors for microalga *Chlamydomonas reinhardtii* and cyanobacterium *Arthrospira platensis*. Biores Technol 138: 271-276.

Lee HY, Erickson LE, Yang SS. 1987. Kinetics and bioenergetics of light-limited photoautotrophic growth of *Spirulina platensis*. Biotechnol Bioeng 29:832-843.

Leite GB, Abdelaziz AEM, Hallenbeck PC. 2013. Algal biofuels: challenges and opportunities. Biores Technol 145: 134-141.

Lin, SH. 1997. A heat transfer model for biological wastewater treatment system. Heat Mass Transfer (32): 313-316.

Losordo TM, Piedrahita RH. 1991. Modelling temperature and thermal stratification in shallow aquaculture ponds. Ecol Model (54): 189-226.

Luo HP, Al-Dahhan MH. 2004. Analyzing and modeling of photobioreactors by combining first principles of physiology and hydrodynamics. Biotechnol Bioeng 85(4):382-393.

Madigan MT, Martinko JM. 2006. Brock – Biology of microorganisms. 11th Edition. Pearson Prentice Hall. Upper Saddle River, NJ 07458.

Makareviciene V, Skorupskaite V, Andruleviciute V. 2013. Biodiesel fuel from microalgae-promising alternative fuel for the future: a review. Rev Environ Sci Biotechnol 12: 119-130.

Makinia J, Wells SA, Zima P. 2005. Temperature modeling in activated sludge systems: a case study. Water Environ Res 77 (5): 525-532.

Marthews TR, Malhi Y, Iwata H. 2012. Calculating downward longwave radiation under clear and cloudy conditions over a tropical lowland forest site: an evaluation of model schemes for hourly data. Theor Appl Climatol 107:461‑477.

Mascarelli AL. 2009. Algae: fuel of the future? Environ Sci Technol 43 (19): 7160–7161.

Mata TM, Martins AA, Caetano NS. 2010. Microalgae for biodiesel production and other applications: a review. Renew Sustain Energy Rev 14:217-232.

Megard RO, Tonkyn DW, Senft WH. 1984. Kinetics of oxygenic photosynthesis in planktonic algae. J Plankton Res 6(2): 325-337.

Merchuk JC, Wu X. 2003. Modeling of photobioreactors: application to bubble column simulation. J Appl Phycol 15:163-169.

Miller DH. 1981. Energy at the surface of the Earth – An introduction to the energetics of

ecosystems. Academic Press, Inc., New-York.

Mirón AS, Gómez AC, Camacho FG, Grima EM, Chisti Y. 1999. Comparative evaluation of compact photobioreactors for large-scale monoculture of microalgae. J Biotechnol 70: 249–270.

Mitchels MHA, Slegers PM, Vermuë MH, Wijffels RH. 2013. Effect of biomass concentration on the productivity of *Tetraselmis suecica* in a pilot-scale tubular photobioreactor using natural sunlight. Algal Res (2013) http://dx.doi.org/10.1016/j.algal.2013.11.011.

Moheimani NR, Borowitzka MA. 2006. The long-term culture of the coccolithophore Pleurochrysis carterae (Haptophyta) in outdoor raceway ponds. J Appl Phycol 18: 703-712.

Molina Grima E, Camacho Rubio F, Sanchez Pérez JA, Fernandez Sevilla JM, Acién Fernandez FG, Contreras Gomez A. 1994. A mathematical model of microalgal growth in light-limited chemostat culture. J Chem Tech Biotechnol 61:167-173.

Molina Grima E, Fernández Sevilla JM, Sánchez Pérez JA, García Camacho F. 1996. A study on simultaneous photolimitation and photoinhibition in dense microalgal cultures taking into account incident and averaged irradiances. J Biotechnol 45:59-69.

Morita M, Watanabe Y, Saiki H. 2000. High photosynthetic productivity of green microalga Chlorella sorokiniana. Appl Biochem Biotechnol 87: 203-218.

Muller-Feurga A, Le Guédes R, Pruvost J. 2003. Benefits and limitations of modelling for optimization of *Porphyridium cruentum* culture in annular photobioreactor. J. Biotechnol 103:153-163.

Muñoz-Tamayo R, Mairet F, Bernard O. 2013. Optimizing microalgal production in raceway systems. Biotechnol Prog 29(2):543-552.

Murphy CC, Allen DT. 2011. Energy-water nexus for mass cultivation of algae. Environ Sci Technol 45: 5861–5868.

National Climatic Data Center of the US - National Oceanic and Atmospheric Administration. 2012. http://www.ncdc.noaa.gov/crn/report

New Zealand Institute of Water and Atmospheric Research. 2012. http://cliflo.niwa.co.nz

Ogbonna JC, Yada H, Tanaka H. 1995. Kinetic study oh light-limited batch cultivation of photosynthetic cells. J Ferment Bioeng 80(3): 259-264.

Pahlow M. 2005. Linking chlorophyll-nutrient dynamics to the Redfield N:C ratio with a model of optimal phytoplankton growth. Mar Ecol Prog Ser 287: 33-43.

Pahl-Wostl C, Imboden DM. 1990. DYPHORA – a dynamic model for the rate of photosynthesis of algae. J Plankton Res 12(6):1207-1221.

Pahl-Wostl C. 1992. Dynamic versus static models for photosynthesis. Hydrol 238:189-196.

Pate R, Klise G, Wu B. 2011. Resource demand implications for US algae biofuels production scale-up. Appl Energy 88: 3377-3388.

Peel MC, Finlayson BL, McMahon TA. 2007. Updated world map of the Köppen–Geiger climate classification. Hydrol. Earth Syst. Sci. 11: 1633–1644.

Pegallapati AK, Arudchelvam Y, Nirmalakhandan N. 2013. Energetic performance of photobioreactors for algal cultivation. Environ Sci Technol Lett 10.1021/ez400079f

Penman HL. 1948. Natural evaporation from open water, bare soil and grass. Proc Roy Soc London A(194), 120-145.

Posten C. 2009. Design principles of photo-bioreactors for cultivation of microalgae. Eng Life Sci 9(3):165–177.

Pruvost J, Legrand J, Legentillhomme P. Muller-Feuga A. 2002. Simulation of microalgae growth in limiting light conditions: flow effect. Bioeng Food Nat Prod 48(5): 1109-1120.

Pruvost J, Cornet JF, Legrand J. 2008. Hydrodynamics influence on light conversion in photobioreactors: An energetically consistent analysis. Chem Engineer Sci 63: 3679-3694

Quinn J, de Winter L, Bradley T. 2011. Microalgae bulk growth model with application to industrial scale systems. Biores Technol 102: 5083-5092.

Rabe AE, Benoit RJ. 1962. Mean light intensity: a useful concept in correlating growth rates of dense cultures of microalgae. Biotechnol Bioeng 4:377-390.

Ragonese FP, Williams JA. 1968. A mathematical model for the batch reactor kinetics of algae growth. Biotechnol Bioeng 10(1):83-88.

Richmond A, Lichtenberg E, Stahl B, Vonshak A. 1990. Quantitative assessment of the major limitations on productivity of *Spirulina platensis* in open raceways. J Apply Phycol (2): 195-206.

Ritchie RJ, Larkum AWD. 2012. Modelling photosynthesis in shallow algal production ponds. Photosynthetica 50(4): 481-500.

Rittmann BE, McCarty PL. 2001. Environmental biotechnology: principles and applications. McGraw-Hill series in water resources and environmental engineering. McGraw-Hill.

Rogers JN, Rosenberg JN, Guzman BJ, Oh VH, Mimbela LE, Ghassemi A, Betenbaugh MJ, Oyler GA, Donohue MD. 2013. A critical analysis of paddlewheel-driven raceway ponds for algal biofuel production at commercial scales. Algal Research (In press)

Sakshaug E, Johnsen G, Andresen K, Vernet M. 1991. Modeling of light-dependent algal photosynthesis and growth: experiments with the Barents Sea diatoms *Thalassiosira nordenskioeldii* and *Chaetoceros furcellatus*. Deep-Sea Res 38(4): 415-430.

Sánchez Mirón A, Contreras Gómez A, García Camacho F, Molina Grima E, Chisti Y. 1999. Comparative evaluation of compact photobioreactors for large-scale monoculture of microalgae. J Biotechnol 70:249-270.

Sander K, Murthy GS. 2010. Life cycle analysis of algae biodiesel. Int J Life Cycle Assess 15: 704-714.

Sartori E. 2000. A critical review on equations employed for the calculation of the evaporation rate from free water surfaces. Sol Energy 68 (1), 77-89.

Scherfig J, Schleisner L, Brønd S, Kilde N. 1996. Dynamic temperature changes in wastewater treatment plants. Water Environ Res 68(2): 143-150.

Scott CJ; Boriah V. 2010. Modeling Algae Growth in an Open-Channel Raceway. J Comput Biol 17(7): 895-906.

Sedory PE, Strenstrom MK. 1995. Dynamic prediction of wastewater aeration basin temperature. J Environ Eng 121(9): 609-618.

Silva Benavides AM, Torzillo G, Kopecký J, Masojídek J. 2013. Productivity and biochemical composition of *phaeodactylum tricornutum* (Bacillariophyceae) cultures grown outdoor in tubular photobioreactors and open ponds. Biomass Bioenergy 54: 115-122.

Singh RN, Sharma S. 2012. Development of suitable photobioreactor for algae production – A review. Renew Sustain Energ Rev 16: 2347– 2353.

Slade R, Bauen A. 2013. Micro-algae cultivation for biofuels: cost, energy balance, environmental impacts and future prospects. Biomass Bioenergy 53: 29-38.

Slegers PM, Lösing MB, Wijffels RH, van Straten G, van Boxtel AJB. Scenario evaluation of open pond microalgae production. Algal Research (2013), http://dx.doi.org/10.1016/j.algal.2013.05.001.

Slegers PM, van Beveren PJM, Wijffels RH, van Straten G, van Boxtel AJB. 2013. Scenario analysis of large scale algae production in tubular photobioreactors. Appl Energ 105: 395-406.

Sodha MS, Singh U, Srivastava A, Tiwari GN. 1981. Experimental validation of thermal model of open roof pond. Build Env 16(2): 93-98.

Spolaore P, Joannis-Cassan C, Duran E, Isambert A. 2006. Commercial applications of microalgae. J Biosci Bioeng 101(2): 87-96.

Stephenson AL, Kazamia E, Dennis JS, Howe CJ, Scott SA, Smith AG. 2010. Life-cycle assessment of potential algal biodiesel production in the United Kingdom: a comparison of raceways and air-lift tubular bioreactors. Energy Fuels 24: 4062–4077.

Suh IS, Lee SB. 2003. A light distribution model for an internally radiating photobioreactor. Biotechnol Bioeng 82(2):180-189.

Sun A, Davis R, Starbuck M, Ben-Amotz A, Pate R, Pienkos PT. 2011. Comparative cost analysis of algal oil production for biofuels. Energ 36: 5169-5179.

Taine J, Iacona E, Petit JP. 2008. Transferts thermiques – Introduction aux transferts d'énergie. 4th ed; Dunod, Paris.

Talati SN, Stenstrom MK. 1990. Aeration-basin heat loss. J Environ Eng 116 (1): 70-86.

Talbot P, Thébault JM, Dauta A, De La Noüe. 1991. A comparative study and mathematical modelling of temperature, light and growth of three microalgae potentially useful for wastewater treatment. Wat Res 25(4): 465-472.

Tang R, Etzion Y. 2004. Comparative studies of the water evaporation rate from a wetted surface and that from a free water surface. Build Environ (39): 77-86.

Thackston EL, Parker FL. 1972. Geographical influence on cooling ponds. J Water Pollut Control Fed 44(7): 1334-1351.

Torzillo G, Pushparaj B, Bocci F, Balloni W, Materassi R, Florenzano G. 1986. Production of *Spirulina* Biomass in Closed Photobioreactors. Biomass 11: 61-74.

Torzillo G, Sacchi A, Materassi R. 1991. Temperature as an important factor impacting productivity and night biomass loss in *Spirulina platensis* grwon outdoors in tubular photobioreactors. Biores Technol 38(2-3): 95–100.

Tredici MR, Materassi R. 1992. From open ponds to vertical alveolar panels: the Italian experience in the development of reactors for the mass cultivation of phototrophic microorganisms. J Appl Phycol 4: 221-231.

Tredici MR. 2004. Mass production of microalgae: photobioreactors. Handbook of microalgal culture: Biotechnology and applied phycology 1 178-214.

Walker DA. 2009. Biofuels, facts, fantasy, and feasibility. J Appl Phycol 21: 509-517.

Wang T, Yabar H, Higano Y. 2013. Perspective assessment of algae-based biofuel production using recycled nutrient sources: the case of Japan. Bioresour Technol 128: 688-696.

Weissman JC, Tillett DT, Goebel RP. 1989. Design and Operation of an Outdoor Microalgae Test Facility: Final Subcontract Report. SERI/ STR-232-3569. Solar Energy Research Institute, Golden, Colorado.

Weyerhaeuser H, Tennigkeit T, Yufang S, Kahrl F. 2007. Biofuels in China: an analysis of the opportunities and challenges of Jatropha curcas in Southwest China. World Agroforestry Centre – Working paper.

Wigmosta ML, Coleman AM, Skaggs RJ, Huesemann MH, Lane LJ. 2011. National microalgae biofuel production potential and resource demand. Water Resour Res 47.

Wu X, Merchuk JC. 2001. A model integrating fluid dynamics in the photosynthesis and the photoinhibition process. Chem Eng Sci 36: 3527:3538.

Wu X, Merchuk JC. 2002. Simulation of algae growth in a bench-scale bubble column reactor. Biotechnol Bioeng 80(2): 156-168.

Wu X, Merchuk JC. 2004. Simulation of algae growth in a bench scale internal loop airlift reactor. Chem Eng Sci 59: 2899-2912.

Yang J, Xu M, Zhang X, Hu Q, Sommerfeld M, Chen Y. 2011. Life-cycle analysis on biodiesel production from microalgae water footprint and nutrients balance. Bioresour Technol 102: 159–165.

Yun Y.S, Park J.M. 2003. Kinetic modeling of the light-dependent photosynthetic activity of the green microalga *Chlorella vulgaris*. Biotechnol Bioeng 83(3): 303-311.

Zhang K, Kurano N, Miyachi S. 1999. Outdoor culture of a cyanobacterium with a vertical flat-plate photobioreactor: Effects on productivity of the reactor orientation, distance setting between the plates, and culture temperature. Appl Microbiol Biotechnol 52: 781–786.

Zittelli GC, Rodolfi L, Biondi N, Tredici MR. 2006. Productivity and photosynthetic efficiency of outdoor cultures of Tetraselmis suecica in annular columns. Aquaculture 261: 932–943.

Appendix A: Modelling the light distribution and algal productivity in outdoor open ponds – Calculation details

A.1. Introduction

This appendix details the application of the Type II model developed in this thesis to the specific geometry of open ponds. Section A.2 first details how the light distribution was determined in the culture broth of open ponds. Sections A.3 and A.4 describe the equations used to express the productivity in open ponds and how these equations were numerically implemented, respectively.

A.2. Modelling the light distribution in outdoor open ponds

The solar irradiance reaching the algae in an open pond can be divided in two components: the direct radiation and the diffuse radiation. While direct radiation is unidirectional, the diffuse radiation can be assumed to be isotropic (i.e. coming from all the directions). In this study, the impact of sides of the pond on the light distribution was neglected. The local light intensity was therefore assumed to depend only on the depth.

A.2.1. Direct radiation

The local light intensity $I_{loc,dir}$ of the direct radiation reaching an algal cell located at a depth z can be expressed as:

$$I_{loc,dir}(z) = \frac{I_{0,dir}}{\cos\theta_z} \exp\left(-\sigma X \frac{z}{\cos\theta_z}\right) \quad \text{(A-1)}$$

where $I_{0,dir}$ is the irradiance reaching the top surface of the pond, θ_z is the angle between the sun and a vertical axis (Figure A-1), σ is the extinction coefficient (m^2/kg), and X is the algal concentration (kg/m^3).

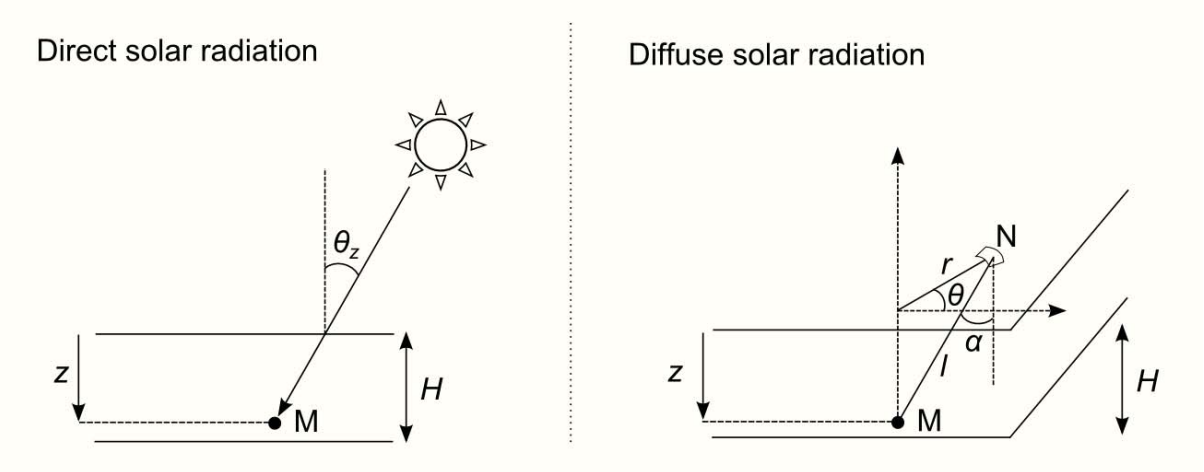

Figure A-1: Different constants used for the calculation of the direct and diffuse components of the solar light intensity

A.3. Diffuse radiation

In order to determine the amount of diffuse radiation reaching a single algae cell located at a depth *z*, the following strategy was followed:

1) The top surface of the pond was discretized in small $rdrd\theta$ elements (Figure A-1);
2) The amount of diffuse radiation going through each infinitesimal element and reaching the considered algal cell was calculated;
3) The total amount of diffuse radiation reaching the considered algae cell was determined by integrating the amount of radiation coming from all these infinitesimal surface elements.

In the following, an infinitesimal element located at the top surface of the reactor with the coordinates (r, θ, z) will be considered. The amount of diffuse radiation that is going through this infinitesimal surface before reaching the single algae cell considered can be expressed as:

$$dI_{loc,dif}(z) = \frac{I_{0,dif}}{\pi \cdot l^2} \cos\alpha \cdot \exp(-\sigma X l) \cdot r dr d\theta \quad \text{(A-2)}$$

where α is the angle between the vector $-\mathbf{e_z}$ and the vector **NM** (Figure A-1), and l the distance NM. l and $\cos\alpha$ can be expressed as:

$$l = \sqrt{r^2 + z^2} \quad \text{(A-3)}$$

$$\cos\alpha = \frac{z}{l} \quad \text{(A-4)}$$

The intensity of diffuse radiation reaching a single algae cell at a depth z can therefore be expressed as:

$$I_{loc,dif}(z) = \int_r \int_\theta \frac{I_{0,dif}}{\pi \cdot l^3} z \cdot \exp(-\sigma X l) \cdot r dr d\theta \quad \text{(A-5)}$$

By differentiating l with respect to r, the following equation can be obtained:

$$l \cdot dl = r \cdot dr \quad \text{(A-6)}$$

This yields the following expression for the local light intensity:

$$I_{loc,dif}(z) = 2 \cdot z \cdot I_{0,dif} \int_{l=z}^{\infty} \frac{1}{l^2} \exp(-\sigma X l) \cdot dl \quad \text{(A-7)}$$

This last integral could not be integrated analytically and was therefore computed numerically. In the following, this integral will be defined as the function "f":

$$f(z, \sigma X) = \int_{l=z}^{\infty} \frac{1}{l^2} \exp(-\sigma X l) \cdot dl \quad \text{(A-8)}$$

A.4. Total productivity in the pond

From the equations derived in the previous section, the total productivity per meter square of pond (P, kg/m^2-s) can be expressed as follows:

$$P = P_m \int_{z=0}^{H} \frac{\sigma\left(I_{loc,dir}\left(z,\theta_z,\sigma X, I_{0,dir}\right)+2\cdot z\cdot I_{0,dif}\cdot f\left(z,\sigma X\right)\right)}{K+\sigma\left(I_{loc,dir}\left(z,\theta_z,\sigma X, I_{0,dir}\right)+2\cdot z\cdot I_{0,dif}\cdot f\left(z,\sigma X\right)\right)} X\cdot dz \quad \text{(A-9)}$$

A.5. Numerical implementation

In order to minimize the computational time for the calculation of the productivity, the values of the function f were pre-calculated for a range of values for the two parameters z and σX. Figure A-2 represents the matrix in which these values were stored.

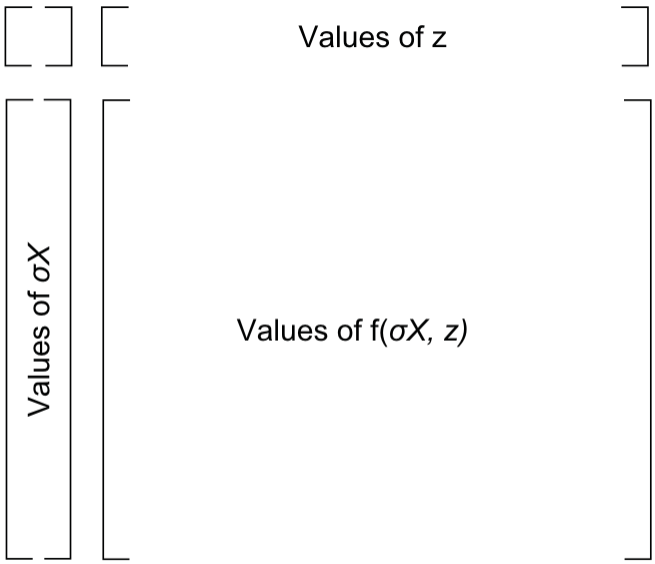

Figure A-2: Representation of the matrix storing the pre-calculated values of the function f for different values of z and σX. The number of values for z and σX (and their corresponding ranges) were respectively 2500 (0 – 1 m) and 400 (1 – 5000 m^{-1}). The number of elements considered for the calculation of the integral in Equation A-8 was N_l = 500, and in the case where the location considered was too close to the pond surface to be valid, a sub-discretization of each element was performed in N_{lim} = 50 elements (see the supplementary information S2 of Article 4 for further details).

A.6. Verification of the equations

A.6.1. Light distribution

The light intensity derived from Equations A-1 and A-7 should exhibit an exponential decay as light propagates through the pond, which is confirmed by Figure A-3. In addition, the rate at which the light decays as it propagates through the pond is an increasing function of the extinction coefficient which is in agreement with theory.

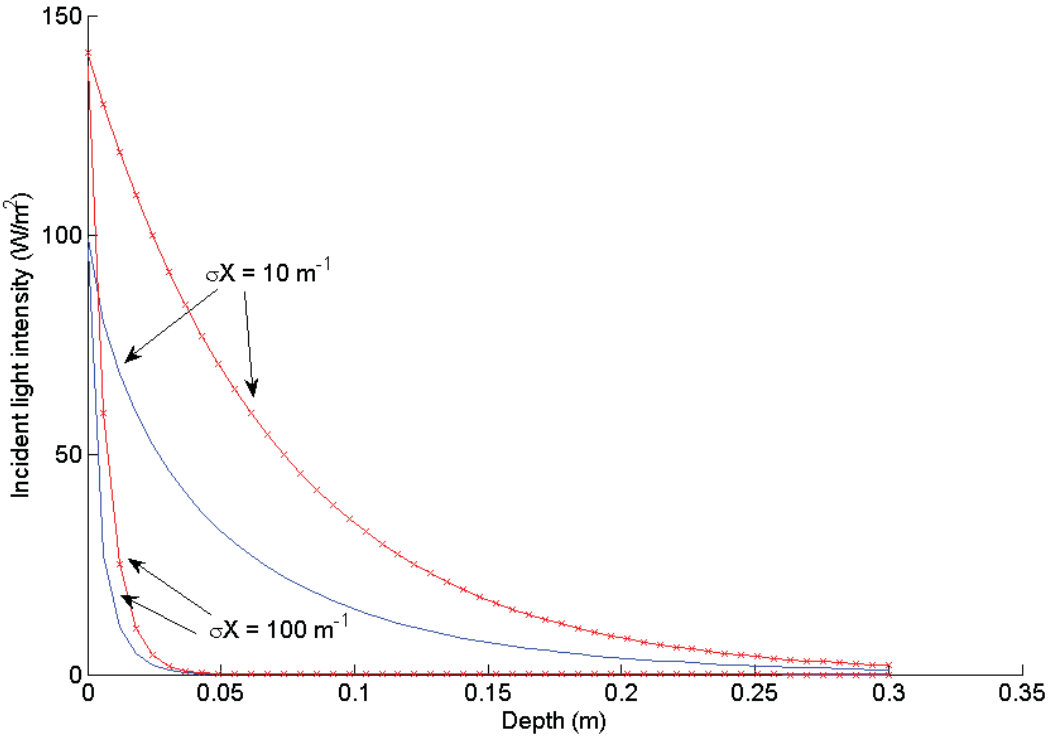

Figure A-3: Light distribution in a pond for the two components of solar light (Red crossed line: direct light intensity; Blue plain line: diffuse light intensity). Parameters values: H = 0.3m; $I_{0,dif}$ = 100 W/m^2; $I_{0,dir}$ = 200 W/m^2; $\theta_z = \pi/4$.

A.6.2. Conservation laws

For high values of cell concentration or high pigment content, all the light entering the pond should be absorbed by the cells. As seen on Figure A-4, no light is going through the pond after a certain value of σX.

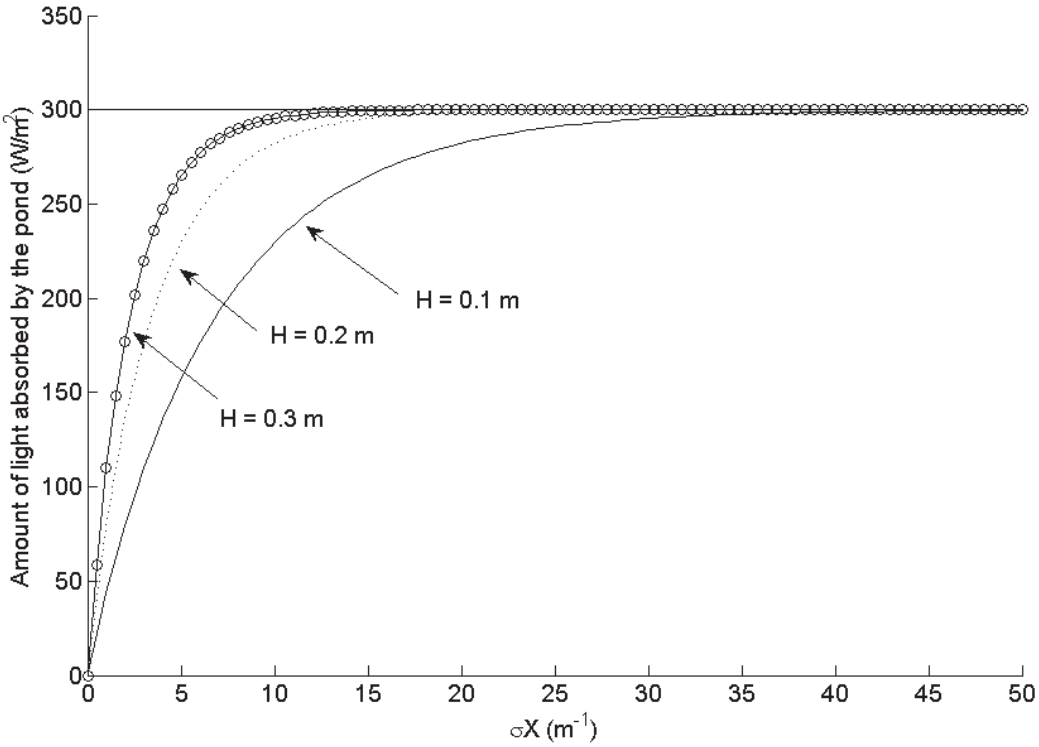

Figure A-4: Evolution of the amount of light absorbed by the pond with the parameter σX for different pond depths. The plain horizontal line represents the amount of light entering the pond. Parameters values: $I_{0,dif}$ = 100 W/m^2; $I_{0,dir}$ = 200 W/m^2; $\theta_z = \pi/4$. The number of "slices" of pond considered for the integration of the light absorbed by the pond was N_z = 300.

A.6.3. Case of high *K* values

For high K values and for high values of the parameter σX, the expression of the total productivity of the pond becomes (Equation A-9):

$$P \cong \frac{P_m}{K}\left(I_{abs}\right) = \frac{P_m}{K}\left(I_{0,dir} + I_{0,dif}\right) \quad \text{(A-10)}$$

Equation A-10 is found to be validated for relatively high values of K as shown by Figure A-5.

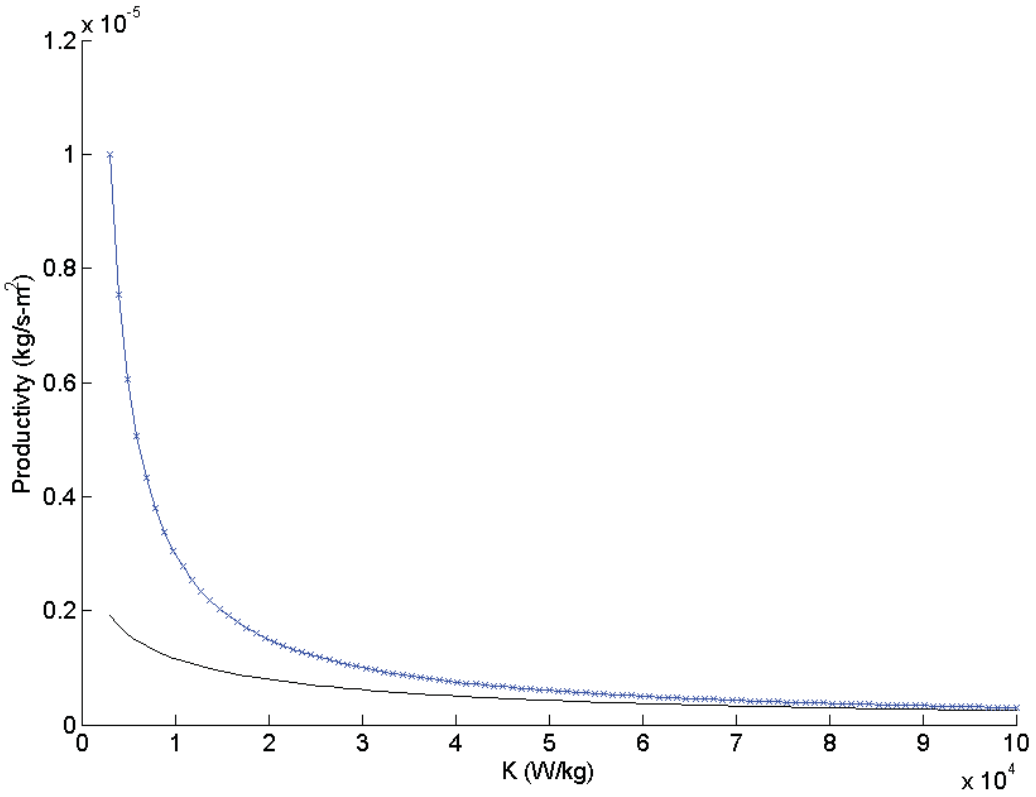

Figure A-5: Evolution of productivity with the parameter K (Blue-crossed line: approximated productivity from Equation A-10; black plain line: computed value of productivity from Equation A-9). Parameter values: H = 0.3m; $I_{0,dif}$ = 100 W/m^2; $I_{0,dir}$ = 200 W/m^2; $\theta_z = \pi/4$; P_m = 10^{-4} kg/kg-s; σ = 100 m^2/kg; X = 1 kg/m^3. The number of "slices" of pond considered for the calculation of the productivity was N_z = 20.

A.6.4. Evolution of the productivity with the extinction coefficient σ

The amount of light captured by each single algae cell is assumed to be proportional to the extinction coefficient σ. If the amount of light captured by cells is higher than what cells can convert into chemical energy through photosynthesis, the extra amount of light is wasted as heat. Productivity should therefore be a decreasing function of σ, as confirmed by Figure A-6.

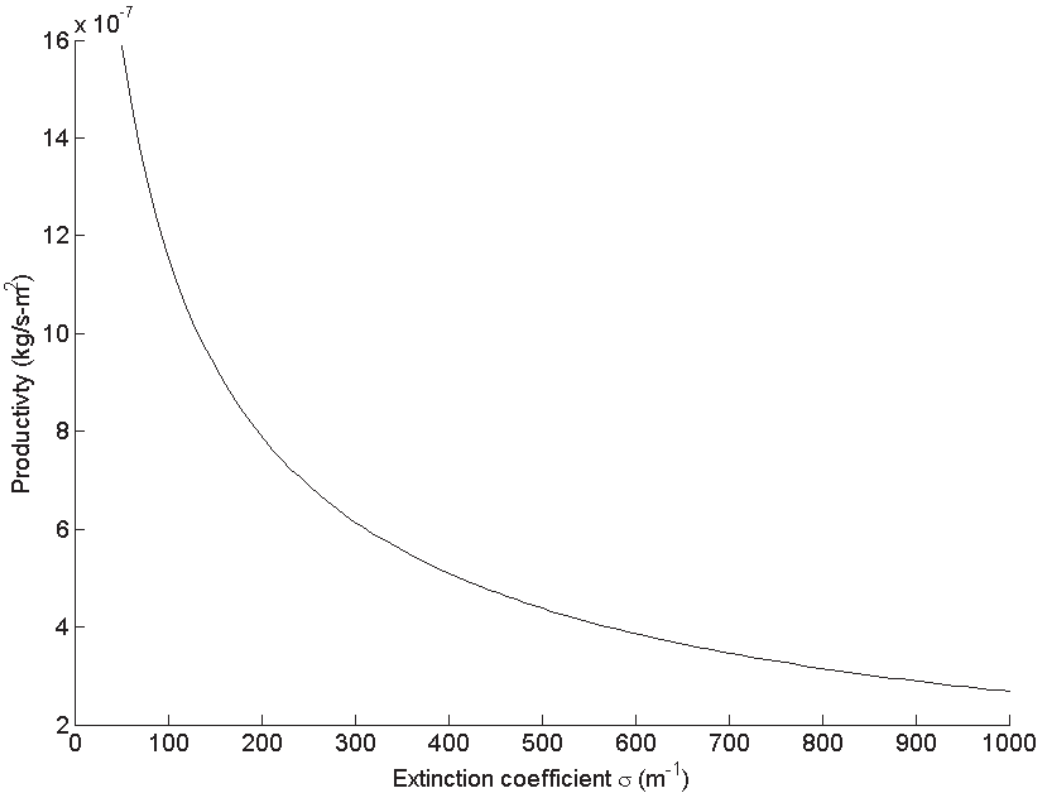

Figure A-6: Evolution of productivity with the pigment content. Parameter values: H = 0.3m; $I_{0,dif}$ = 100 W/m^2; $I_{0,dir}$ = 200 W/m^2; $\theta_z = \pi/4$; $P_m = 10^{-4}$ kg/kg-s; $K = 10^4$ W/kg; X = 1kg/m^3. The number of "slices" of pond considered for the calculation of the productivity was N_z = 20.

A.6.5. Evolution of the productivity with X

The productivity should be an increasing function of the cell concentration until the algal concentration reaches a level at which all the light entering the pond is captured by algae. The productivity should then become a constant function of the algal concentration as shown by Figure A-7.

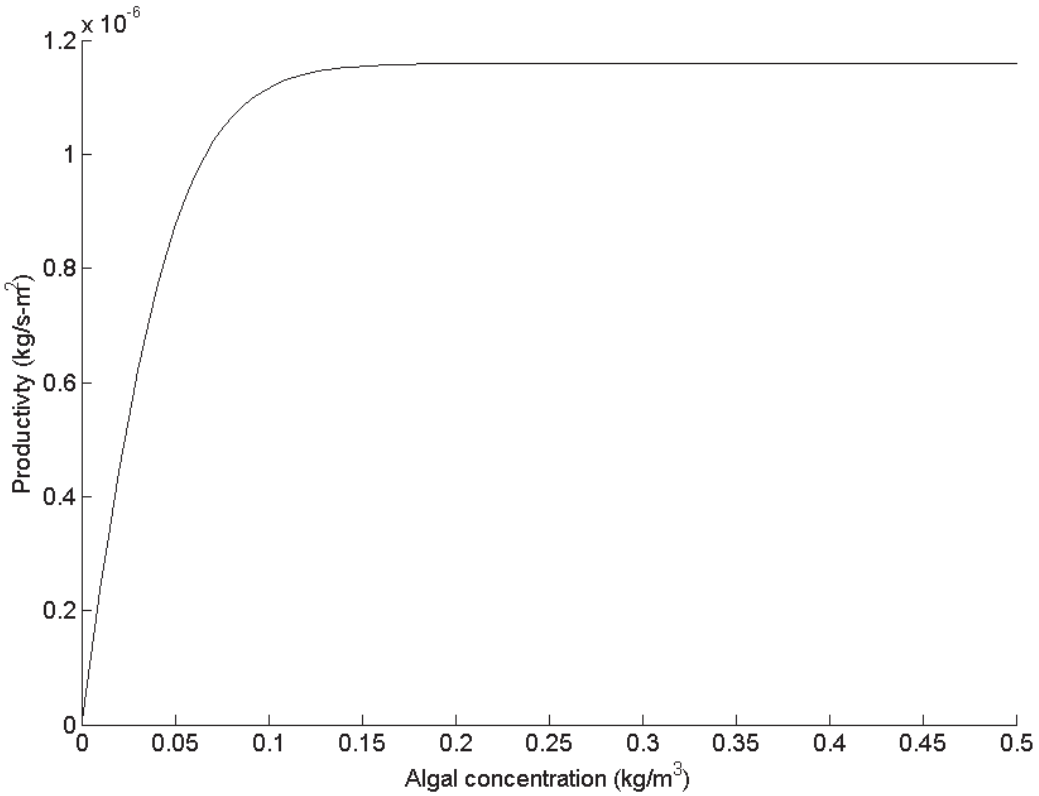

Figure A-7: Evolution of productivity with the algal concentration. Parameter values: H = 0.3m; $I_{0,dif}$ = 100 W/m^2; $I_{0,dir}$ = 200 W/m^2; $\theta_z = \pi/4$; $P_m = 10^{-4}$ kg/kg-s; $K = 10^4$ W/kg; σ = 100 m^2/kg. The number of "slices" of pond considered for the calculation of the productivity was $N_z = 20$.

Article 1

MASSEY UNIVERSITY
GRADUATE RESEARCH SCHOOL

STATEMENT OF CONTRIBUTION TO DOCTORAL THESIS CONTAINING PUBLICATIONS

(To appear at the end of each thesis chapter/section/appendix submitted as an article/paper or collected as an appendix at the end of the thesis)

We, the candidate and the candidate's Principal Supervisor, certify that all co-authors have consented to their work being included in the thesis and they have accepted the candidate's contribution as indicated below in the *Statement of Originality*.

Name of Candidate: Quentin Béchet

Name/Title of Principal Supervisor: Prof Benoit Guieysse

Name of Published Research Output and full reference:

Béchet Q, Shilton A, Guieysse B. Modeling the effects of light and temperature on algae growth: State of the art and critical assessment for productivity prediction during outdoor cultivation. Biotechnol Adv 31(8): 1648-1663.

In which Chapter is the Published Work: 1

Please indicate either:

- The percentage of the Published Work that was contributed by the candidate:

  and / or

- Describe the contribution that the candidate has made to the Published Work:

  Q Béchet was the main contributor to the review. In particular, the classification of productivity models was initially proposed by Q Béchet.

Quentin Béchet
Digitally signed by Quentin Béchet
DN: cn=Quentin Béchet, o=Massey University, ou=SEAT, email=q.bechet@massey.ac.nz, c=NZ
Date: 2014.02.17 18:49:56 +13'00'

Candidate's Signature

17/02/2014
Date

Benoit Guieysse
Digitally signed by Benoit Guieysse
DN: cn=Benoit Guieysse, o=Massey University, ou=SEAT, email=b.j.guieysse@massey.ac.nz, c=NZ
Date: 2014.02.24 11:17:49 +13'00'

Principal Supervisor's signature

24/02/2014
Date

Biotechnology Advances 31 (2013) 1648–1663

Contents lists available at ScienceDirect

Biotechnology Advances

journal homepage: www.elsevier.com/locate/biotechadv

Research review paper

Modeling the effects of light and temperature on algae growth: State of the art and critical assessment for productivity prediction during outdoor cultivation

Quentin Béchet, Andy Shilton, Benoit Guieysse *

School of Engineering and Advanced Technology, Massey University, Private Bag 11 222, Palmerston North 4442, New Zealand

ARTICLE INFO

Article history:
Received 11 December 2012
Received in revised form 12 August 2013
Accepted 17 August 2013
Available online 24 August 2013

Keywords:
Algae
Photosynthesis
Endogenous respiration
Models
Light
Temperature
Photobioreactor
Full-scale
Biofuel

ABSTRACT

The ability to model algal productivity under transient conditions of light intensity and temperature is critical for assessing the profitability and sustainability of full-scale algae cultivation outdoors. However, a review of over 40 modeling approaches reveals that most of the models hitherto described in the literature have not been validated under conditions relevant to outdoor cultivation. With respect to light intensity, we therefore categorized and assessed these models based on their theoretical ability to account for the light gradients and short light cycles experienced in well-mixed dense outdoor cultures. Type I models were defined as models predicting the rate of photosynthesis of the entire culture as a function of the incident or average light intensity reaching the culture. Type II models were defined as models computing productivity as the sum of local productivities within the cultivation broth (based on the light intensity locally experienced by individual cells) without consideration of short light cycles. Type III models were then defined as models considering the impacts of both light gradients and short light cycles. Whereas Type I models are easy to implement, they are theoretically not applicable to outdoor systems outside the range of experimental conditions used for their development. By contrast, Type III models offer significant refinement but the complexity of the inputs needed currently restricts their practical application. We therefore propose that Type II models currently offer the best compromise between accuracy and practicability for full scale engineering application. With respect to temperature, we defined as "coupled" and "uncoupled" models the approaches which account and do not account for the potential interdependence of light and temperature on the rate of photosynthesis, respectively. Due to the high number of coefficients of coupled models and the associated risk of overfitting, the recommended approach is uncoupled models. Most of models do not include the modeling of endogenous respiration and the modeling of light and temperature acclimation in spite of their potential effect on productivity.

© 2013 Elsevier Inc. All rights reserved.

Contents

* Corresponding author. Tel.: +64 6 350 5841; fax: +64 6 350 5604.
E-mail address: B.J.Guieysse@massey.ac.nz (B. Guieysse).

0734-9750/$ – see front matter © 2013 Elsevier Inc. All rights reserved.
http://dx.doi.org/10.1016/j.biotechadv.2013.08.014

1. Introduction

Tremendous research efforts are currently ongoing to develop new algae biotechnologies for biofuel production (Chisti, 2007; Mata et al., 2010). However, the technical feasibility, economics, and environmental benefits of full-scale algal cultivation are still unproven and debated (Chisti, 2008; Guieysse et al., 2013; Murphy and Allen, 2011; Singh and Olsen, 2011). Of particular concern, many economic and life cycle assessments of algae cultivation are based on gross estimates of productivity that do not account for the impacts of process geometry (e.g. pond depth), operation (e.g. hydraulic retention time) and temperature on productivity (Béchet et al., 2010; Guieysse et al., 2013; Sánchez Mirón et al., 1999; Tredici and Materassi, 1992). There is therefore a critical need to accurately forecast algae productivity during outdoor cultivation in order to improve assessment of best location and engineering practice for maximizing revenues and minimizing environmental impacts.

Box 1
Definition of key concepts.

Endogenous respiration: Photosynthesis generates chemical energy in the form of ATP, NADPH, and organic material. Endogenous respiration includes the consumption of chemical energy at day time and the consumption of organic material at night time.
Algal productivity: Rate of net biomass production expressed as the difference of the rate of photosynthesis minus the rate of endogenous respiration.
Photosynthetic unit (PSU): Cell unit responsible for the photosynthetic process leading to the generation of ATP and NADPH (Camacho Rubio et al., 2003).
Light-inhibition: The degradation of key proteins at high light intensities causes a decrease of the rate of photosynthesis over time. For light-inhibition to become significant, algae cells must be exposed to inhibiting light intensities for a time period in the order of 1 min (Ferris and Christian, 1991). Light-inhibition can impact productivity past exposure to high light intensities because damaged cells need time to recover.
Light-acclimation: Change of cellular physiology and biochemistry associated with photosynthesis, such as the change of pigment content in the cell (Bernard, 2011; Crill, 1977; Sakshaug et al., 1991). Light-acclimation occurs on a timescale longer than light-inhibition and can take several hours to days to cause significant changes in pigment content (Crill, 1977).
Flashing-light effect: Following the capture of photons, the photosynthetic units (PSUs) of algae cells need approximately 100 ms to convert light energy into NADPH and ATP. During this time, any photon reaching 'excited' PSUs is wasted. As a result, cells exposed to flashing light with a light/dark cycle close to 100 ms waste less light energy than cells exposed to continuous light (Grobbelaar, 1991, 1994; Janssen et al., 2003; Luo and Al-Dahhan, 2004). The increase of photosynthetic efficiency resulting from cell exposure to flashing light is called the flashing-light effect.

Algal biomass productivity is the net result of photosynthesis and endogenous respiration (Box 1). Predicting the rate of these mechanisms during outdoor cultivation is challenging because algal activity is influenced by numerous factors such as light intensity, temperature, pH, dissolved oxygen concentration, and nutrient availability (Mata et al., 2010). In order to maximize the algal productivity per unit of land area, cultivation systems should ideally be limited by no other factor than the amount of light energy reaching the algae. Maintaining the pH at its optimal value can be done by CO_2 injection and nutrient concentration can be maintained at saturation (Grobbelaar, 2009). Concentration gradients can occur under poor mixing conditions and cause local nutrient limitation (e.g. CO_2) or oxygen inhibition (Mata et al., 2010). These can generally be prevented via adequate design and operation (Benemann et al., 1987). By contrast, temperature cannot be easily (economically) controlled at full-scale, meaning that algae experience significant temperature change over time (Béchet et al., 2010, 2011). This review therefore focuses on the modeling of algal productivity as a function of light and temperature. The review is organized in five sections: 1) description of the fundamental effect of light on photosynthesis; 2) application of this knowledge to well-mixed dense cultures as used in full-scale production systems; 3) inclusion of temperature in models of photosynthesis; 4) models of endogenous respiration; and 5) inaccuracy originating from experimental measurements independent on the modeling approach.

2. Modeling the relationship between light intensity and photosynthesis for individual cells

The fundamental relationship between light intensity and photosynthesis for individual cells is often represented by 'PI relationships' (P for

photosynthetic rate and I for light intensity) depicting three distinct light regimes, as shown by Fig. 1:

1) At low light intensities, the rate of photosynthesis is usually proportional to light intensity because photosynthesis is limited by the rate of capture of photons.
2) When light intensity reaches a saturation threshold (I_k), algae become 'light-saturated' because their photosynthetic rate is now limited by the rate of the reactions following the capture of photons (Crill, 1977). Under this condition, the rate of photosynthesis is usually maximal and independent of light intensity.
3) If light intensity further increases beyond an inhibitory threshold (I_{inhib}), the rate of photosynthesis starts to decrease with light intensity due to the deactivation of key proteins in the photosynthetic units (Camacho Rubio et al., 2003).

2.1. Mathematical expressions of PI relationships

There is no clear consensus on the most suitable mathematical expression to describe PI relationships (Table 1). For example, Jassby and Platt (1976) tested eight mathematical expressions and concluded that a hyperbolic tangent model (Table 1) was the best formula whereas Lee et al. (1987) demonstrated that a simplified light-inhibition model (Table 1) provided a better fit against other models. Monod-like models derived by analogy to chemotrophic bacterial growth have also been used to model PI relationships. These models consider light as a substrate for algal photosynthesis and the rate of photosynthesis is modeled as:

$$P = P_m \frac{I}{I_k + I} \quad (1)$$

where P is the specific rate of photosynthesis, P_m is the maximum specific rate of photosynthesis, I is the light intensity reaching the cells, and I_k is a constant. A mechanistic justification for Monod-like kinetics was provided by Han (2001) who considered photosynthesis as a two-step process involving the subsequent activation and deactivation of photosynthetic units. Alternative models assume that the rate at which photons 'strike' photosynthetic units follows a Poisson distribution (see 'Poisson models' in Table 1).

2.2. PI relationships and light-inhibition

The level of light-inhibition does not only depend on the instantaneous light intensity, as depicted in typical PI relationships, but also on pre-exposure to high or low irradiances (Box 1). Such dynamic effect was demonstrated by Beardall and Morris (1976) and Falkowski and Owens (1978) who showed that algae cells pre-exposed to high light intensity had a lower productivity than cells pre-exposed to dark conditions (called the 'hysteresis effect'). The dynamic effects of light-inhibition are often not accounted for in the determination of PI relationships (Table 1), which implies that the use of simple PI-based models may cause to overestimate productivity during outdoor cultivation. To account for light-inhibition, Denman and Marra (1986) considered that the rate of photosynthesis of *Lauderia borealis* for a given light intensity could vary between a minimum value corresponding to a fully-inhibited state and a maximum value corresponding to a non-inhibited state. The actual rate of photosynthesis at a given light intensity was then determined based on the level of light-inhibition experienced by the algae using a dynamic model accounting for light variation.

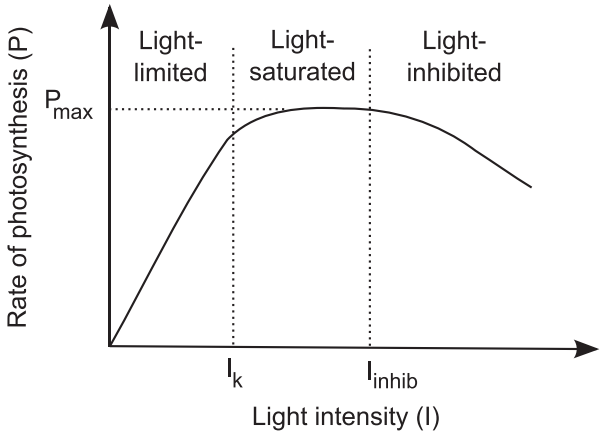

Fig. 1. Typical PI relationship showing the light-limited ($I < I_k$), light-saturated ($I_k < I < I_{inhib}$), and light-inhibited ($I > I_{inhib}$) regimes of microalgae light response.

2.3. Metabolic network analysis

Metabolic models are built by considering the metabolic reactions involved in biomass synthesis. This approach usually requires knowledge of the genome of the algal species in order to predict key metabolites and enzymes (Schmidt et al., 2010). Recent applications to phototrophic organisms include models of *Chlamydomonas reinhardtii* (Boyle and Morgan, 2009; Chang et al., 2011; Cogne et al., 2011), *Arthrospira* (*Spirulina*) *platensis* (Cogne et al., 2003) and *Synechocystis* sp. (Shastri and Morgan, 2005). In these studies, the effect of light intensity was modeled by considering the rate of conversion of light energy into NADPH and ATP molecules via electron transport chain(s) (Shastri and Morgan, 2005). The predictions of the rate of photosynthesis and biomass composition were in good agreement with experimental results. An interesting feature of metabolic network analyses is their ability to model biochemical composition. This is particularly advantageous when algal biotechnologies target specific bio-products.

3. Modeling photosynthesis in well-mixed dense cultures

PI relationships aim to accurately describe the intrinsic relationship between photosynthesis and light intensity. For this reason, light response must be experimentally determined at low cell concentration in order to ensure that all cells are exposed to the same light intensity. By contrast, algal concentration should be kept high during commercial outdoor cultivation in order to maximize algal productivity and minimize capital and harvesting costs (Sánchez Mirón et al., 1999). These high concentrations cause light gradients to occur and individual cells to experience different light intensities depending on their location in the system. Another consequence from light gradients in well-mixed systems is that individual algae cells experience short light cycles when they travel from high-light zones to near dark zones. This cycling may reduce light-inhibition and enable the flashing-light effect (Box 1). The accuracy of models described in the literature should therefore reflect the ability of the modeling approach to account for the impact of light gradients and short light cycles. Our review of over 40 modeling approaches reveals that most models have not been validated under conditions relevant to outdoor cultivation (Table S1). We therefore categorized and assessed these models based on their theoretical ability to account for the light gradients and short light cycles experienced in well-mixed dense outdoor cultures. Type I models predict the rate of photosynthesis of the entire culture as a function of the incident or the average light intensity reaching the culture. Type II models determine productivity as the sum of local productivities within the cultivation broth without consideration of short light cycles. Type III models account for both light gradients and short light cycles.

3.1. Type I models

3.1.1. Type I models using the incident light intensity

A first sub-category of Type I model expresses the rate of photosynthesis of the entire culture as a function of the incident light intensity (I_0) reaching the external surface of the system (Table 2). For example,

Table 1
Examples of different PI relationships (P: specific rate of oxygen production; P_m: maximum specific rate of oxygen production; μ: specific growth rate; μ_m: maximum specific growth rate; I: light intensity; I_{opt}: optimum light intensity for photosynthesis; T: temperature; T_0: standard temperature; T_{opt}/T_{min}/T_{max} optimum/minimum/maximum temperature for photosynthesis; Chl: Chlorophyll concentration; C: carbon concentration; λ: maintenance coefficient). As it is not possible to convert the various units used in the literature into a universal unit, the following parameters are provided in the original units.

Model	Equation	Parameters values	Experimental conditions (I: Light; T: Temperature)	Reference
PI relationships based on the specific rate of oxygen production (P)				
Hyperbolic tangent model	$P = P_m \tanh(\alpha I)$ α: constant	*Gynodinium microadriaticum* $P_m = 36$ mol O_2/h-mol Chl a $\alpha = 4.60$ m^2-h/E	I = 0–1 E/m^2-h T = 27 °C	Chalker (1980)
Poisson model	$P = P_m\left(1-\exp\left(-\frac{\alpha I}{P_m}\right)\right)$ α: constant	*Skeletonema costatum* $P_m = 6.23$ g C/g Chl-h $\alpha = 0.0202$ g C-m^{2}s/g Chl-h-μmol	I = 0.043–4.33 E/m^2-h T = 15 °C	Cullen (1990) Sakshaug et al. (1991) Geider (1990) Geider et al. (1998) Pahlow (2005)
Light-inhibition model	$P = P_s \frac{I}{K_I+I+I^2/K_I'}$ P_sK_I, K_I': constants	(Algae sampled in the Como lake, Minnesota) Temperature: 4 °C $K_I = 0.15$ E/m^2-h $K_I' = 6.7$ E/m^2-h $P_m = 0.21$ mmol O_2/mg Chl-h Temperature: 10 °C $K_I = 0.45$ E/m^2-h $K_I' = 2.2$ E/m^2-h $P_m = 0.38$ mmol O_2/mg Chl-h Temperature: 12 °C $K_I = 0.25$ E/m^2-h $K_I' = 16$ E/m^2-h $P_m = 0.28$ mmol O_2/mg Chl-h Temperature: 19 °C $K_I = 0.90$ E/m^2-h $K_I' = 10$ E/m^2-h $P_m = 0.50$ mmol O_2/mg Chl-h Temperature: 25 °C $K_I = 0.75$ E/m^2-h $K_I' = 12$ E/m^2-h $P_m = 0.54$ mmol O_2/mg Chl-h	I = 0–7 E/m^2-h	Megard et al. (1984)
Modified hyperbolic tangent model	$P = P_m \frac{\tanh(I/I_k)}{1+K(I-I_c)}$ for $I>I_c$ $P = P_m \tan(I/I_k)$ for $I < I_c$ I_k, K, I_c: constants	*Lauderia borealis* $I_k = 825$ μE/m^2-s $K = 52.8 \times 10^{-4}$ m^{2}s/μE $I_c = 250$ μE/m^2-s	I = 100–1500 μE/m^2-s T: unavailable	Pahl-Wostl and Imboden (1990)/Pahl-Wostl (1992)
PI relationships based on specific growth rate (μ)				
Poisson model with light-adaptation	$\mu = \mu_m\left(1-\exp\left(-\frac{\alpha I\theta}{\mu_m}\right)\right)-\lambda$ $\theta = \theta_m\left(\frac{1}{1+\frac{\theta_m \alpha I}{2\mu_m}}\right)$ α, θ_m : constants	Coefficients values not available		Geider and MacIntyre (1996)
	$\mu = \mu_m\left(1-\exp\left(-\frac{\alpha I\theta}{\mu_m}\right)\right)f(T)-\lambda$ $\lambda = \zeta\mu$ $\theta = \theta_m\left(\frac{1}{1+\frac{\theta_m \alpha I}{2\mu_m}}\right)$ $f(T) = \exp\left(-\frac{E_a}{R}\left(\frac{1}{T}-\frac{1}{T_0}\right)\right)$ $\alpha, \zeta, \theta_m, E_a, R$: constants	Coefficients values available for 19 algae species[a]		Geider et al. (1997)
Light-inhibition model with temperature dependence	$\mu = \mu_{opt}(I)\cdot\varphi(T)$ $\mu_{opt}(I) = \mu_m \frac{I}{I+\frac{\mu_m}{\alpha}\left(\frac{I}{I_{opt}}-1\right)^2}$ $\varphi(T) = \frac{(T-T_{max})(T-T_{min})^2}{(T_{opt}-T_{min})\cdot(f(T)-g(T))}$ for $T_{min}<T<T_{max}$ $f(T) = (T_{opt}-T_{min})(T-T_{opt})$ $g(T) = (T_{opt}-T_{max})(T_{opt}+T_{min}-2T)$ α: constant	*C. pyrenoidosa* $T_{min} = 5.2$ °C $T_{opt} = 38.7$ °C $T_{max} = 45.8$ °C $\mu_m = 2.00$ d^{-1} $\alpha = 0.05$ d^{-1} $I_{opt} = 2.75 \times 10^2$ μE/m^2-s *N. oceanica* $T_{min} = -0.2$ °C $T_{opt} = 26.7$ °C $T_{max} = 33.3$ °C $\mu_m = 1.85$ d^{-1} $\alpha = 0.12$ d^{-1} $I_{opt} = 2.03 \times 10^8$ μE/m^2-s	*C. pyrenoidosa* I = 100–2900 ft-candle T = 15–43 °C *N. oceanica* I = 34–80 μmol/m^2-s T = 14.5–35.7 °C	Bernard and Rémond (2012)
	$\mu = 2\mu_m(T)(1+\beta_I)\frac{i}{1+2\beta_I i+i^2}$ $i = \frac{I}{I_{opt}(T)}$ $\mu_m(T) = 2\nu\left(1+\beta_T^{\mu}\right)\frac{x}{1+2\beta_T^{\mu}x+x^2}$ $x = \frac{T-\theta_0^{\mu}}{\theta_{opt}^{\mu}-\theta_0^{\mu}}$ $I_{opt}(T) = 2\rho_I\left(1+\beta_T^{I}\right)\frac{y}{1+2\beta_T^{I}y+y^2}$ $y = \frac{T-\theta_0^{I}}{\theta_{opt}^{I}-\theta_0^{I}}$ $\beta_I, \nu, \beta_T^{\mu}, \theta_0^{\mu}, \theta_{opt}^{\mu}, \rho_I, \beta_T^{I}, \theta_0{}^{I}, \theta_{opt}^{I}$: constants	*Porphyridium cruentum* $\beta_I = 0.5$ $\nu = 1.4$ d^{-1} $\beta_T^{\mu} = 0.02$ $\theta_0{}^{\mu} = 4.7$ °C $\theta_{opt}^{\mu} = 20.5$ °C $\rho_I = 538$ μmol/m^2-s $\beta_T^{I} = 0.56$ $\theta_0{}^{I} = 4.7$ °C $\theta_{opt}^{I} = 12.3$ °C	I = 5–1100 μE/m^2-s T = 5–35 °C	Dermoun et al. (1992)

(continued on next page)

Table 1 (*continued*)

Model	Equation	Parameters values	Experimental conditions (I: Light; T: Temperature)	Reference
PI relationships based on specific growth rate (μ)				
	$\mu = 2\mu_m(T)(1+\beta(T))\frac{i}{1+2\beta(T)i+i^2}$ $i = \frac{I}{I_{opt}(T)}$ The functions $\mu_m(T)$, $\beta(T)$, or $I_{opt}(T)$ are all represented by a $\gamma(T)$ function: $\gamma(T) = \gamma_m\left(\frac{T}{T_{opt}}w^u\right)^{\alpha}$ $w = \frac{T-T_0}{T_{opt}-T_0}$ $u = \frac{T_0-T_{opt}}{T_{opt}}$ γ_m, α: constants	*Oscillatoria agardhii* Function $\mu_m(T)$: $\gamma_m = 0.5\ d^{-1}$; $T_{opt} = 37.0$ °C; $T_0 = 43.0$ °C; $\alpha = 0.3$ Function $\beta(T)$: $\gamma_m = 2.3$; $T_{opt} = 18.0$ °C; $T_0 = 43.0$ °C; $\alpha = 1.9$ Function $I_{opt}(T)$: $\gamma_m = 101.0$ μE/m²-s; $T_{opt} = 24.0$ °C; $T_0 = 43.0$ °C; $\alpha = 1.6$ *Ankistrodesmus falcatus* Function $\mu_m(T)$: $\gamma_m = 1.1\ d^{-1}$; $T_{opt} = 37.0$ °C; $T_0 = 43.0$ °C; $\alpha = 0.2$ Function $\beta(T)$: $\gamma_m = 2.2$; $T_{opt} = 22.0$ °C; $T_0 = 43.0$ °C; $\alpha = 1.5$ Function $I_{opt}(T)$: $\gamma_m = 174.0$ μE/m²-s; $T_{opt} = 29.0$ °C; $T_0 = 43.0$ °C; $\alpha = 1.2$ *Phormidium bohneri* Function $\mu_m(T)$: $\gamma_m = 1.7\ d^{-1}$; $T_{opt} = 37.0$ °C; $T_0 = 43.0$ °C; $\alpha = 2.7$ Function $\beta(T)$: $\gamma_m = 5.4$; $T_{opt} = 23.0$ °C; $T_0 = 43.0$ °C; $\alpha = 5.0$ Function $I_{opt}(T)$: $\gamma_m = 541.0$ μE/m²-s; $T_{opt} = 30.0$ °C; $T_0 = 43.0$ °C; $\alpha = 4.8$	I = 3–650 μE/m²-s T = 5–35 °C	Talbot et al. (1991)
Monod model	$\mu = \mu_m(T)\frac{I}{K(T)+I} - \lambda(T)$ $\mu_m(T) = \mu_{m,0}\exp(\alpha_\mu T)$ $K_I(T) = K_{I,0}\exp(\alpha_K T)$ $\lambda(T) = \lambda_0\exp(\alpha_\lambda T)$ $\mu_{m,0}$, α_μ, $K_{I,0}$, α_K, λ_0, α_λ: constants	*Anabaena variabilis* $\mu_{m,0} = 0.098$ gC/gDW-d $\alpha_\mu = 0.0854\ °C^{-1}$ $K_{I,0} = 32.05$ μE/m²-s $\alpha_K = 0.078\ °C^{-1}$ $\lambda_0 = 0.072$ gC/gDW-d $\alpha_\lambda = 0.067\ °C^{-1}$	I = 0–600 μE/m²-s T = 10–40 °C	Collins and Boylen (1982)
	$\mu = \mu_g - \lambda$ $\mu_g = \varphi_m\frac{Chl}{C}{}^0a_p^*\frac{KI}{K+I}$ $\lambda = a_1 + b_1\mu_g$ K: constant φ_m: maximum photosynthetic yield ${}^0a_p^*$: extinction coefficient a_1, b_1: constants	*Thalassiosira weissflogii* $K = 10$ E/m²-d $\varphi_m = 0.06$ g-atom C/E ${}^0a_p^* = 17\ m^2/g\ Chl\ a$ $a_1 = 0.046\ d^{-1}$ $b_1 = 0.20\ d^{-1}$	I = 4.4–209 μE/m²-s T: unavailable	Kiefer and Mitchell (1983)
Hyperbolic tangent model	$\mu = \mu_m\tanh\left(\frac{I}{K_I}\right)$ K_I: constant	*Chlorococcum littorale* $\mu_m = 0.115\ h^{-1}$ $K_I = 150$ μE/m²-s	I = 2.3–1060 μE/m²-s T = 25 °C	Kurano and Miyachi (2005)[b]

[a] Data available in Geider et al. (1997), Table 2.
[b] The model presented in this table is the model providing the best fit in the study cited.

Jeon et al. (2005) modeled the rate of photosynthesis of a culture of *Haematococcus pluvialis* using a Monod-like function described as:

$$P = P_m\frac{I_0}{I_k + I_0} \quad (2)$$

where P (mg O_2/h-g biomass) is the specific rate of photosynthesis, P_m (mg O_2/h-g biomass) is the maximum specific rate of photosynthesis, I_0 (μmol/m²-s) is the incident light intensity, and I_k (μmol/m²-s) is a constant. Type I models are easy to implement as I_0 is simple to measure but the values of the kinetic parameters depend on the specific operating conditions used to develop and validate the model, which limits the universality of this approach. For example, the kinetic parameters P_m and I_k used in the model of Jeon et al. (2005) were found to be dependent on cell concentration (Table 2). In outdoor cultivation systems, the cell concentration is a function of the net productivity and the cell retention time, and will vary depending on the cultivation system and its operating conditions. Type I models using I_0 should therefore be used with considerable caution for the prediction of outdoor algal productivity outside the range of experimental conditions used for their development.

3.1.2. Type I models using the average light intensity

In order to consider the impact of cell concentration and reactor geometry, a sub-category of Type I models expresses the rate of photosynthesis of well-mixed cultures as a function of the average light intensity within the broth I_{av} (Table 2). The rationale behind this approach is that individual algae cells in a well-mixed system are, on average, exposed to the same light intensity and, therefore, have the same average rate of photosynthesis (Yun and Park, 2003). However, empirical studies have shown that the kinetic parameters associated with these models are actually functions of operating conditions, such as cell concentration, incident light intensity, or system size, as discussed in Box 2. A possible explanation for these observations is the fact that Type I models do not account for the impact of the short light cycles experienced by microalgae in dense cultures (see Section 3.3). In addition, algae cultivated in two systems exposed to different I_0 can experience the same I_{av} depending on cell concentration and system geometry. Consequently, if the same I_{av}-based Type I model is used to predict the rate of photosynthesis in these two systems, the same rate of photosynthesis will also be predicted. In reality, the respective fractions of light-

Table 2
Black-box models (P: specific rate of oxygen production; P_m: maximum specific rate of oxygen production; μ: specific growth rate; μ_m: maximum specific growth rate; I_{av}: average light intensity; I_0: incident light intensity; T: temperature; T_0: standard temperature; λ: maintenance coefficient; λ_m: maximum maintenance coefficient; X: cell concentration). As it is not possible to convert the various units used in the literature into a universal unit, the following parameters are provided in the original units.

Model	Equation	Parameters values	Experimental conditions (I: Light; T: Temperature)	Reference
Black-box models using the incident light intensity (I_0)				
Monod model	$\mu = \mu_m\left(1-\frac{X}{X_m}\right)$ $\mu_m = \frac{K_1 L}{K_2 T+L}\exp\left(-\frac{K_3 L}{RT}\right)$ $X_m = (K_4 + K_5 T)\exp\left(-\frac{K_6 L}{RT}\right)$ $L = \frac{I_0}{I_{max}}$ K_1, K_2, K_3, K_4, K_5, K_6: constants I_{max}: maximum incident light intensity R: ideal-gas constant	*Pavlova lutheri* $K_1 = -2.72\ d^{-1}$ $K_2 = -2.86 \times 10^{-1}\ °C^{-1}$ $K_3 = 129 \times 10^2$ J/mol $K_4 = 1.19 \times 10^8$ cell/mL $K_5 = -3.69 \times 10^5$ cell/mL-°C $K_6 = -1.24 \times 10^1$ J/mol I_{max}: unavailable	I = 0–I_{max} T = 10–26 °C	Carvahlo and Malcata (2003)
	$\mu = \mu_m(P,N)\theta_\mu{}^{T-T_0}\frac{I_0}{K+I_0} - \frac{\lambda_m}{h}\theta_\lambda{}^{T-T_0}$ P, N: phosphorous and nitrogen concentrations, respectively. h: depth of the cultivation system (a lake, in the study of Haario et al., 2009) K, θ_μ, θ_λ: constants	*Diatoms* $\mu_m = 0.0886\ d^{-1}$; $\theta_\mu = 1.14$; $K_I = 61.9$ W/m^2; $\lambda_m = 0.0845$ m/d; $T_0 = 20$ °C; $\theta_\lambda = 1.05$ *Chrysophycea* sp. $\mu_m = 0.0465\ d^{-1}$; $\theta_\mu = 1.07$; $K_I = 115$ W/m^2; $\lambda_m = 0.137$ m/d; $T_0 = 20$ °C; $\theta_\lambda = 1.05$ *N-fixing cyanobacteria* $\mu_m = 0.329\ d^{-1}$; $\theta_\mu = 1.16$; $K_I = 16.4$ W/m^2; $\lambda_m = 0.349$ m/d; $T_0 = 20$ °C; $\theta_\lambda = 1.05$ (The value of μ_m given for each species corresponds to the value under and phosphorous and nitrogen saturations.)	I = 0–400 W/m^2 T = 0–20 °C	Haario et al. (2009)
	$P = P_m\frac{I_0}{I_k+I_0} - \lambda$ I_k: constant	*Haematococcus pluvialis* $\lambda = 3.66$ mg O_2/g-h For $X = 0.215$ g/L $P_m = 43.5$ mg O_2/g-h $I_k = 177.2$ μE/m^2-s For $X = 0.123$ g/L $P_m = 51.7$ mg O_2/g-h $I_k = 254.4$ μE/m^2-s	I = 0–2000 μE/m^2-s T = 25 °C	Jeon et al. (2005)
Black-box models using the average light intensity (I_{av})				
Monod model	$\mu = \mu_m(T)\frac{I_{av}}{K+I_{av}}$ $\mu_m(T) = \mu_{m,0}\exp(-E_a/kT)$ E_a: activation energy k: Boltzmann constant $\mu_{m,0}$: constant	*Chlorella sorokiniana* Parameters values unavailable		Bordel et al. (2009)
Simplified light-inhibition model	$\mu = \frac{I_{av}}{K_1+K_2 I_{av}^2}$ K_1, K_2: constants	*Spirulina platensis* For $X = 0.04$ g/L $K_1 = 177.9$ h-W/m^2 $K_2 = 0.1083$ h-m^2/W For $X = 0.05$ g/L $K_1 = 217.3$ m^2/W-h $K_2 = 0.1193$ m^2/h-W	I = 0–90 W/m^2 T = 33 °C	Lee et al. (1987)[a]
Power model	$\mu = \mu_m\frac{I_{av}^n}{K_I^n+I_{av}^n} - \lambda$ n, I_k: constants	*Isochrysis galbana* $\mu_m = 0.046\ h^{-1}$ $K_I = 9.67 \times 10^{15}$ quanta/cm^2-s $n = 1.7$ $\lambda = 0.00385\ h^{-1}$	I = (4–19) × 10^{15} quanta/cm^2-s T = 20 °C	Molina Grima et al. (1994)
Linear model	$\mu = \mu_s\frac{I_{abs}}{XV} - \lambda_m(1-V_F)$ μ_s: constant V_F: volume fraction of the broth where light intensity is higher than I_c I_{abs}: amount of light absorbed by the culture[c] V: culture volume	*Chlorella pyrenoidosa* $\mu_s = 0.8$ kg/mol $\lambda_m = 0.104\ d^{-1}$ $I_c = 0.66$ mol/m^2-d	I = 26.7–1130 μE/m^2-s T: unavailable	Ogbonna et al. (1995a)
	$\mu = \mu_s\frac{I_{abs}}{X}$ μ_s: constant I_{abs}: amount of light absorbed by the culture[c]	*Chlorella ellipsoida* Parameters values unavailable		Ragonese and Williams (1968)
Log model	$\mu = A\log_{10}(I_{av}) - \lambda$ A: constant	*Chlorella pyrenoidosa* $A = 0.133\ h^{-1}$ $\lambda = 0.356\ h^{-1}$	I = 600–5000 ft-candle T: unavailable	Rabe and Benoit (1962)
Black-box models using both the incident and the average light intensities (I_0, I_{av})				
Photobioreactor model	$\mu = \mu_m\frac{(I_{av})^{n_2/I_0}}{\left(K_I+\left(\frac{I_0}{K'_I}\right)^{n_1}\right)^{n_2/I_0}+I_{av}^{n_2/I_0}} - \lambda$ K_I, K_I', n_1, n_2: constants	*Isochrysis galbana* $\mu_m = 0.0444\ h^{-1}$ $K_I = 170.68$ μE/m^2-s $K_I' = 2217.2$ μE/m^2-s $n_1 = 12.8$	I = 820–3270 μE/m^2-s T = 20 °C	Molina Grima et al. (1996)[a]

(continued on next page)

Table 2 (*continued*)

Model	Equation	Parameters values	Experimental conditions (I: Light; T: Temperature)	Reference
Black-box models using both the incident and the average light intensities (I_0, I_{av})				
	$\mu = \mu_m \frac{(I_{av})^{n_2+n_3/I_0}}{\left(K_I+\left(\frac{I_0}{K'_I}\right)^{n_1}\right)^{n_2+n_3/I_0}+I_{av}^{n_2+n_3/I_0}}$ K_I, K_I', n_1, n_2, n_3: constants	$n_2 = 2728.8$ μE/m^2-s $\lambda = 0.00385$ h^{-1} *Phaeodactylum tricornutum* $\mu_m = 0.063$ h^{-1} $K_I = 94.3$ μE/m^2-s $K_I' = 768.4$ μE/m^2-s $n_1 = 3.04$ $n_2 = 1.209$ $n_3 = 514.6$ μE/m^2-s	I = 0–4000 μE/m^2-s[b] T = 20 °C	Acién Fernández et al. (1998)[a]

[a] The model shown is the model providing the best fit in the study cited.
[b] Experimental studies carried outdoors.
[c] The amount of light absorbed by cells, I_{abs}, can be shown to be proportional to the average light intensity I_{av} (when the Beer–Lambert law is used to describe light distribution). The linear model presented by Ogbonna et al. (1995a) can therefore be considered as a PI curve using I_{av}.

limited, light-saturated, and light-inhibited cells can differ in each system, meaning that the rate of photosynthesis would most likely be different. For prediction of outdoor algal productivity, Type I models using I_{av} should therefore only be used within the range of cell concentration, incident light intensity and system geometry used for their development.

3.2. Type II models

Type II models account for the impact of light gradients on the local rate of photosynthesis. These models are constructed by 1) quantifying the light distribution within the broth, 2) selecting a biological model that expresses the local rate of photosynthesis as a function of the local light intensity, and 3) summing the local rates of photosynthesis to obtain the global rate of photosynthesis.

As example of Type II approach, the local rate of photosynthesis can be calculated using a Monod-like function coupled with the Beer–Lambert law for light distribution (Table 6) described as:

$$P(l) = P_m \frac{I_0 \exp(-\sigma X l)}{I_k + I_0 \exp(-\sigma X l)} \quad (3)$$

where $P(l)$ is the local volumetric rate of photosynthesis at the distance l from the system external boundary, P_m is the maximum volumetric rate of photosynthesis, I_k is a saturation constant, I_0 is the incident light intensity, σ is the extinction coefficient reflecting the level of light absorption of the broth, and X is the cell concentration. The rate of photosynthesis of the entire system P can then be determined by integrating $P(l)$ over the entire system volume as:

$$P = \int_V P(l) \cdot dV \quad (4)$$

where V is the culture volume and dV the volume of the discrete elements. Numerous examples of Type II models can be found in the literature as shown in Table 3.

3.2.1. Universality of Type II models

Evidence from the literature suggests that Type II models can accurately predict algal productivity under a broad range of operational conditions and designs. For example, Yun and Park (2003) were able to accurately predict the rate of photosynthesis of *Chlorella vulgaris* under different incident light intensities and algal concentrations using the Type II model described by Eqs. (3) and (4). Similarly, Cornet and Dussap (2009) showed that a Type II model was able to predict the rate of photosynthesis in eight photobioreactors with different geometries with a level of accuracy of +/− 15%.

3.2.2. Application of Type II models for full-scale outdoor cultivation

As explained above, an accurate prediction of photosynthesis during outdoor cultivation should account for light-inhibition at high light intensities. The degree of light-inhibition experienced by cells in a well-mixed dense culture is theoretically influenced by the cycling of individual algae cells between high-irradiance zones near the surface and low-light zones in deep areas. This cycling allows cells to recover from short-term exposure to inhibitory light intensities, which attenuates the overall impact of light-inhibition on the rate of photosynthesis. The effect of short light cycles is not considered in Type II models. The use of Type II models for the prediction of productivity during full-scale algae cultivation outdoors may therefore overestimate the impact of light-inhibition, as suggested by Bosma et al. (2007).

3.3. Type III models

Type III models consider that the rate of photosynthesis of an individual algae cell is a function of its 'light story' (i.e. the light intensity experienced by an algae cell over time as it moves in the system). Type III modeling thus involves 1) determining the light story of algae cells; 2) based on their light stories, determining the rate of photosynthesis of individual algae cells using a dynamic biological model; and 3) summing the rates of photosynthesis of individual algae cells to calculate the total rate of photosynthesis in the cultivation system.

3.3.1. Determination of the light story of algae cells

In the simplest application, the photobioreactor is divided into a number of zones by judgment. For example, Wu and Merchuk (2004) modeled productivity in an airlift photobioreactor by considering two zones of constant velocity: an outer downcomer exposed to a constant light intensity and a central riser draft pipe in complete darkness. Alternatively, Esposito et al. (2009) considered that individual phytoplankton cells in the ocean had a circular trajectory in the vertical dimension. The models thus constructed provided good accuracy but this type of approach could be limited in more complex system geometries.

An alternative to 'guessing' the hydraulics is building a physical model and directly measuring the flow field, as done by Pruvost et al. (2002) who used particle image velocimetry to determine cell trajectories within their reactor. However, experimentally determining the flow field is laborious. Alternatively, the flow field can be modeled using computational fluid dynamics (CFD) (Merchuk et al., 2011; Perner-Nochta and Posten, 2007; Pruvost et al., 2006). Once the model is defined, multiple variations of flow rate and reactor design can be relatively quickly assessed to determine the flow field in the reactor, and hence

the cell trajectories. However, while CFD appears very fundamental in that it solves the Navier–Stokes equations, it requires judgment in the selection of differencing schemes and its own internal models of turbulence ideally need validation against experimental data for confirmation of accuracy of prediction (Bitog et al., 2011).

3.3.2. Three-population models

In order to predict the rate of photosynthesis of an individual algae cell, most of the biological models included in the Type III approach (step 2, exemplified in Table 5, Column 2) focus on the photosynthetic units (PSUs, Box 1) responsible for the capture of light (Camacho Rubio et al., 2003; Eilers and Peeters, 1988, 1993; Merchuk et al., 2011). These so-called three-population models assume that the conversion of photons into usable energy is a two-step process where PSUs are first hit by photons until they store an amount of energy sufficient for the 'charged PSUs' to produce ATP and NADPH. The rate of photosynthesis is generally assumed to be proportional to the turnover rate from excited state to resting state. PSUs can be inhibited if they are hit by an overflow of photons causing the deactivation of key proteins in the photosynthetic process. Inhibited PSUs are assumed to be unable to process photons and to need time to recover. PSUs can therefore be found in: 1) a resting state, where PSUs are paused but will move to an excited state if they are hit by enough photons; 2) an excited state, where PSUs contain the photochemical energy necessary to generate NADPH and ATP molecules; and 3) an inhibited state, where PSUs cannot process photons until the damaged key proteins are regenerated (recovery process).

When the three-population model is applied under constant and homogenous illumination (Camacho Rubio et al., 2003; García-Camacho et al., 2012), the rate of photosynthesis is predicted as:

$$P = P_s \frac{I}{1 + KI + K'I^2} \tag{5}$$

where P is the rate of photosynthesis, and P_s, K and K' are constants (Eilers and Peeters, 1988). This expression has been shown to accurately describe the rate of photosynthesis of cultures exposed to constant and homogenous light intensity in several experimental studies (Dermoun et al., 1992; Megard et al., 1984; Talbot et al., 1991). The three-population model is theoretically able to predict the flashing-light effect (Box 1), as demonstrated by Camacho Rubio et al. (2003).

An alternative model accounting for the dynamic nature of light-inhibition was developed by Han et al. (2000) who modeled changes in the concentration of the D1 protein, which damage results in light-inhibition (Table 4).

3.3.3. Application of Type III models for full-scale outdoor cultivation

Because Type III models were developed to account for short light cycles, they are theoretically capable of predicting productivity during full-scale algae cultivation outdoors. However, the compounded inaccuracies of three sub-models (for light-distribution, cell trajectories, and biological response) may significantly affect the accuracy of the overall prediction of Type III models. Finally, the benefit brought about by the ability to model the flashing-light effect is in its own right contested in the context of full-scale cultivation because the massive mixing energy required would damage cells and significantly increase operational costs (Benemann et al., 1987).

3.4. Modeling light-acclimation during outdoor cultivation

The pigment content of algae cells can vary significantly during outdoor cultivation (Béchet et al., 2013). This change is caused by light-acclimation: at low light intensity, cells tend to increase their pigment content to maximize the amount of light captured. At high light intensity, cells tend to lower their pigment content to minimize the risks of light-inhibition (Geider et al., 1997).

Light-acclimation occurs at a relatively long time scale (hours to days) and can be modeled independently from other dynamic mechanisms of photosynthesis. Geider and MacIntyre (1996) assumed that the biomass generated during photosynthesis was allocated to either a "photosynthetic apparatus pool" or a "storage pool". These authors then hypothesized that chlorophyll production was inversely proportional to light intensity. This light-acclimation model was later refined by Geider et al. (1997, 1998) and Pahlow (2005) to account for the effects of nutrient-limitation and temperature on light-acclimation.

Neglecting light-acclimation in models of productivity may affect the accuracy of predictions for outdoor cultivation. However, light-acclimation is rarely accounted for in current models of photosynthesis (Zonneveld, 1998) and approaches similar to the approach of Geider may be needed for full-scale prediction.

Box 2

Effect of cell concentration, incident light intensity, and system size on the parameters of Type I models using I_{av}.

1) *Cell concentration*: In the study of Lee et al. (1987), the specific growth rate of *Spirulina platensis* was expressed as a function of the average light intensity as follows:

$$\mu = \frac{I_{av}}{K_1 + K_2 I_{av}^2} \tag{2-1}$$

where μ (h^{-1}) is the specific growth rate, I_{av} (W/m^2) is the average light intensity, and K_1 (W-h/m^2) and K_2 (m^2-h/W) are constants. The values of μ_m, K_1, and K_2 were found to vary significantly with cell concentration (Table 2).

2) *Incident light intensity*: The study of Molina Grima et al. (1994) aimed to model the growth of *Isochrysis galbana* in a closed photobioreactor. Different expressions were tested, including a 'power model' defined as:

$$\mu = \mu_m \frac{I_{av}^n}{I_k^n + I_{av}^n} \tag{2-2}$$

where μ (h^{-1}) is the specific growth rate, μ_m (h^{-1}) is the maximum specific growth rate, I_{av} (quanta/cm^2-s) is the average light intensity within the broth, and I_k (quanta/cm^2-s) and n (–) are constants. The values of the kinetic parameters in Eq. (2-2) were shown to be functions of the incident light intensity I_0. This variation of the parameters μ_m, K, and n led the authors to develop a model expressing these parameters as functions of I_0 and the expression of the specific growth rate became (Table 2):

$$\mu = \mu_m \frac{(I_{av})^{n_2/I_0}}{\left(K + \left(\frac{I_0}{K'}\right)^{n_1}\right)^{n_2/I_0} + (I_{av})^{n_2/I_0}} \tag{2-3}$$

where μ_m (h^{-1}) is the maximum specific growth rate, I_{av} (quanta/cm^2-s) is the average light intensity within the broth, and K, K'(quanta/cm^2-s), n_1, and n_2 (quanta/cm^2-s) are constants. This model was shown to correctly predict the growth of different algae species (Acién Fernández et al., 1998; Molina Grima et al., 1996).

3) *System size*: Ogbonna et al. (1995b) cultivated *Chlorella pyrenoidosa* in cuboidal photobioreactors having different sizes and could not find a universal relationship between the linear growth rates of this algae and I_{av}. These findings indicate that the kinetic parameters associated with a Type I model using I_{av} are only valid for a specific geometry.

Table 3
Type II models for photosynthesis ($I(l)$: local light intensity at a distance l from the external surface of the cultivation system; I_0: incident light intensity; T: temperature; $T_{opt}/T_{min}/T_{max}$: optimum/minimum/maximum temperatures for photosynthesis, respectively; μ: specific growth rate; μ_m: maximum specific growth rate; P: specific rate of photosynthesis; P_m: maximum specific rate of photosynthesis; λ: maintenance coefficient; X: cell concentration; σ: extinction coefficient; E_a: mass absorption coefficient; E_s: mass scattering coefficient). As it is not possible to convert the various units used in the literature into a universal unit, the following parameters are provided in the original units.

System	Biological model	Light distribution model	Parameters values	Experimental conditions (I: Light; T: Temperature)	Reference
Outdoor bubble column	$\mu = Y(16 \cdot 3600 \cdot 10^{-6} I)$ $Y = b_0 + b_1 I + b_2 T + b_3 I^2 + b_4 T^2 + b_5 IT$ b_0, b_1, b_2, b_3, b_4, b_5: constants	Beer–Lambert law $I(l) = I_0 \exp(-\sigma X l)$	*Monodus Subterraneus* $b_0 = -1.70$ g/mol $b_1 = -9.45 \times 10^{-4}$ g-m^2-s/mol-μmol $b_2 = 0.20$ g/mol-°C $b_3 = 3.60 \times 10^{-7}$ g-m^4-s^2/mol-μmol^2 $b_4 = -4.07 \times 10^{-3}$ g/mol-°C^2 b_5: unavailable $\sigma = 214$ m^2/kg	I = 50–1550 μmol/m^2-s T = 17.5–29.5 °C	Bosma et al. (2007)
Indoor reactor of any geometry	Monod model $\mu = \mu_m \frac{I}{K_I + I}$ K_I: light constant	Two-flux model (Table 6)	*Spirulina platensis* $\mu_m = 0.54$ h^{-1} $K_I = 20$ W/m^2 $E_a = 150$ m^2/kg $E_s = 200$ m^2/kg	I = 4–200 W/m^2 T = 36 °C	Cornet et al. (1995)
Indoor photobioreactor	Monod model $\mu = \rho_M \varphi E_a \frac{K_I I}{K_I + I}$ ρ_M: maximum energetic yield for photon conversion φ: mass quantum yield K_I: light constant	Simplified two-flux model $I(l) = I_0 \exp(-\frac{1+\alpha}{2\alpha} E_a X l)\alpha = \sqrt{\frac{E_a}{E_a + 2bE_s}}$ b: back-scattering coefficient	*Arthrospira* (*Spirulina*) *platensis* $\rho_M = 0.8$ $\varphi = 1.85 \times 10^{-9}$ kg DW/μmol $K_I = 90$ μmol/m^2-s $E_a = 162$ m^2/kg $E_s = 640$ m^2/kg $b = 0.030$	I = 30–1600 μmol/m^2-s T = 35–36 °C	Cornet and Dussap (2009)
Cylindrical indoor photobioreactor	Monod model and first-order decay $\mu = \mu_m \frac{I}{K+I} - \lambda$ K: constant	Beer–Lambert law $I(l) = I_0 \exp(-\sigma X l)$ k_1, k_2: constants	*Oscillatoria agardhii* $\mu_m = 0.0431$ h^{-1} $K = 1.72$ W/m^2 $\lambda = 0.0037$ h^{-1} $\sigma = 0.72$ dm^2/kJ biomass	I = 0–40 W/m^2 T: unavailable	Evers (1991)
Outdoor cultivation system	$\mu = \frac{\mu_s(T)}{h} \frac{I}{K(T)+I} (1 - \alpha(T) I) - \frac{\lambda(T)}{h}$ $\mu_s(T) = \mu_0 \theta_\mu^{\frac{T-10}{10}}$ $K_I(T) = K_0 \theta_K^{\frac{T-10}{10}}$ $\alpha(T) = \alpha_0 \theta_\alpha^{\frac{T-10}{10}}$ $\lambda(T) = \lambda_0 \theta_\lambda^{\frac{T-10}{10}}$ μ_0, θ_μ, K_0, θ_K, α_0, θ_α, λ_0, θ_λ: constants	Beer–Lambert law $I(l) = I_0 \exp(-\sigma X l)$	Parameters values unavailable		Grobbelaar (1990)
Outdoor open pond	Linear model and first-order decay $\mu = qI\left(1 - \left(\frac{T - T_{opt}}{T_{max} - T_{min}}\right)^2\right) - \lambda$ $\lambda = (aT + b)\frac{z_D}{h}$ q, a, b, z_D: constants h: pond depth (m)	Beer–Lambert law $I(l) = I_0 \exp(-\sigma X l)$	*Spirulina platensis* $a = -0.0231$ min^{-1} °C^{-1} $b = 0.343$ min^{-1} $q = 5.679$ min^{-1} klux^{-1} $T_{opt} = 33$ °C T_{max}–$T_{min} = 25$ °C	I = 0–full sunlight T = 15–40 °C	Guterman et al. (1990)
Indoor annular photobioreactor	Inhibition model $\mu = \frac{2\mu_s(1-i_c)(i-i_c)}{(1-i_c)^2 + (i-i_c)^2}$ $i = I/I_s$ $i_c = I/I_c$ μ_s, I_c, I_s: constants	Beer–Lambert law $I(l) = I_0 \exp(-\sigma X l)$	*Porphyridium cruentum* $\mu_s = 1.415$ d^{-1} $I_s = 385$ μE/m^2-s $I_c = 3.5$ μE/m^2-s $\sigma = 150$ m^2/kg	I = 0–236 μE/m^2-s T = 25 °C	Muller-Feurga et al. (2003)
Indoor cultivation system	Monod model and first-order decay $P = P_m \frac{I}{K+I} - \lambda$ K: constant	Hyperbolic Beer–Lambert law $I(l) = I_0 \exp\left(-\frac{k_1 X}{k_2 + X} l\right)$	*Chlorella vulgaris* $P_m = 136.4$ mg O_2/g biomass-h $K = 49.0$ μE/m^2-s $\lambda = 4.05$ mg O_2/g biomass-h $k_1 = 1041$ m^{-1} $k_2 = 1.03$ kg/m^3	I = 0–2000 μE/m^2-s T = 27 °C	Yun and Park (2003)[a]

[a] The model shown is the model providing the best fit in the study cited.

3.5. Modeling light distribution

3.5.1. The Beer–Lambert law

During algae cultivation, light distribution is often estimated using the Beer–Lambert law which assumes an exponential decay of the light intensity from the external surface of the cultivation system (Table 6), as represented by the following equation:

$$I(l) = I_0 \exp(-\sigma X l) \quad (6)$$

where $I(l)$ is the local light intensity, l is the distance from the external surface of the system to the position under consideration, I_0 is the incident light intensity, σ is the extinction coefficient, and X the cell concentration.

To apply the Beer–Lambert law, the culture medium must be isotropic (i.e. the optical properties of the broth are independent of the light direction) and algae cells must not scatter light. Unfortunately, if the first condition is often met in well-mixed outdoor cultivation systems, algae cells do scatter light (Acién Fernández et al., 1997). Various

Table 4
Dynamic models for photosynthesis (I: light intensity; T: temperature; P: rate of photosynthesis; μ: specific growth rate; λ: maintenance coefficient; R_i: rates of the different reactions shown in Fig. 2 (i between 1 and 6); x_2: fraction of excited PSU in the three-population model, Fig. 2; θ: relative concentration of D1 protein; τ: turnover time of electron transfer time; σ: cross section of PSU). As it is not possible to convert the various units used in the literature into a universal unit, the following parameters are provided in the original units.

Model	Equations	Parameters values	Experimental conditions (I: Light; T: Temperature)	Reference
Two-stage model (simplification of the three-population model)	$R_1 = \alpha \frac{I}{I_m} \exp\left(1-\frac{I}{I_m}\right)$ $R_2 = \beta \frac{x_2}{K_x+x_2}$ $R_3 = 0$ $R_4 = 0$ $R_5 = 0$ $R_6 = 0$ $P \propto R_2$ α, I_m, β, K_x: constants	Parameters values unavailable		Crill (1977)
Three-population model	$R_1 = k_2 I$ $R_2 = k_3$ $R_3 = k_4 I$ $R_4 = 0$ $R_5 = 0$ $R_6 = k_5$ $P = k_1 \exp(d-\frac{e}{T})$ k_1, k_2, k_3, k_4, k_5, d, e: constants	*Gelidium sesquipedale*[a] $d \in [0.5183; 1.5180]$ $e \in [11.5143; 18.3652]$ °C Values for the other parameters are unavailable.		Duarte (1995)
	$R_1 = \alpha I$ $R_2 = \gamma(T)$ $R_3 = \beta I$ $R_4 = 0$ $R_5 = 0$ $R_6 = \delta(T)$ $P \propto R_2$ α, β: constants $\gamma(T)$ and $\delta(T)$ are temperature functions	*Porphyridium* sp. $\mu = k\gamma x_2 - \lambda$ $\alpha = 1.935 \times 10^{-3}$ m^2/µE $\gamma = 0.1460$ s^{-1} $\beta = 5.7848 \times 10^{-7}$ m^2/µE $\delta = 4.796 \times 10^{-4}$ s^{-1} $k = 3.65 \times 10^{-4}$ $\lambda = 0.05908$ h^{-1}	I = 110–550 µE/m^2-s T = 24 °C	Eilers and Peeters (1988)/ Eilers and Peeters (1993)/ Wu and Merchuk (2002)
	$R_1 = \sigma I$ $R_2 = \tau^{-1}$ $R_3 = k_d \sigma I$ $R_4 = k_r$ $R_5 = 0$ $R_6 = 0$ $P \propto R_1$ τ, k_d, k_r: constants	Parameters values unavailable		Han et al. (2000)
PSU-electron donor model	$U \rightarrow^{k_p I} U^+$ $D + U^+ \rightarrow^{k_d \exp(-\beta I)} D^+ + U$ $D^+ + e^- \rightarrow^{k_r} D$ $P = k_r D^+$ U: non-excited PSU U^+: excited PSU D: proximate electron donor (reduced form) D^+: proximate electron donor (oxidized form) k_p, k_d, k_r, β: constants	Parameters values unavailable		Fasham and Platt (1983)
D1-Protein model	$P = a^* \phi_m \frac{(1-\exp(-\sigma\tau I))}{\sigma\tau}$ $\tau = \frac{\tau_m}{\theta}$ $\frac{d\theta}{dt} = -k_d \sigma I \theta + k_r(1-\theta)$ a^*: light-absorption efficiency ϕ_m: Maximum quantum yield τ_m: minimum turnover time of electron transfer chain k_d: damage constant of D1 protein k_r: recovery rate constant of protein D1	a^*: unavailable ϕ_m: 0.1 mol O_2/E $\tau_m = 3 \times 10^{-3}$ s $\sigma = 2$ nm^2 $k_r = 0.55$ h^{-1} $k_d \in [0;10^{-7}]$	I = 0–7 E/m^2-h T unknown	Han et al. (2000)

[a] The values of the parameters d and e are given for different pre-conditions of illumination.

empirical expressions have therefore been developed to account for scattering (Table 6) such as, for example:

$$I(l) = I_0 \exp\left(-\frac{k_1 X l}{k_2 + X}\right) \quad (7)$$

where $I(l)$, l, I_0 and X are defined as in Eq. (6) and k_1 and k_2 are empirical constants. These empirical formulas have shown good agreement with experimental data (Acién Fernández et al., 1997; Katsuda et al., 2000; Suh and Lee, 2003) but are species-dependent. As a result, an empirical light distribution should ideally be determined over a suitable range of cell concentration for each algal species studied, which can be time-consuming.

3.5.2. The radiative transfer equation

An alternative to the Beer–Lambert approach involves solving the radiative transfer equation (RTE) in three dimensions (see Houf and Incropera, 1980 for more details). The RTE can be derived by considering a small element of broth and performing a radiation balance on this element, considering the incident, absorbed, transmitted, and scattered sources of radiation.

Assuming angular light scattering is fixed on each hemisphere, Cornet et al. (1992a, 1992b) developed a 'two-flux model' enabling the determination of the light distribution with a set of two ordinary differential equations (Table 6). Using this approach, Acién Fernández et al. (1997) demonstrated that the Beer–Lambert law overestimated the level of light attenuation in a cylindrical photobioreactor by a factor

Table 5
Type III models ($I(l)$: local light intensity at a distance l from the external surface of the cultivation system; I_0: incident light intensity; μ: specific growth rate; λ: maintenance coefficient; X: cell concentration; X_p: pigment content; σ: extinction coefficient). As it is not possible to convert the various units used in the literature into a universal unit, the following parameters are provided in the original units.

System	Biological model	Light distribution model	Cell trajectories determination	Parameters values	Experimental conditions (I: Light; T: Temperature)	Study
Bubble column reactor	Three-population model (Fig. 2) and first-order decay associated with shear stress $R_1 = \alpha I$ $R_2 = \gamma$ $R_3 = \beta I$ $R_4 = 0$ $R_5 = 0$ $R_6 = \delta$ $\mu = k\gamma x_2 - \lambda$ $\lambda = \lambda_0 \exp(k_m(\tau - \tau_m))$ for $\tau > \tau_m$ $\lambda = \lambda_0$ for $\tau < \tau_m$ $\alpha, \beta, \gamma, \delta, k, \lambda_0, k_m, \tau_m$: constants	Beer–Lambert law in a non-transparent culture medium $I(l) = I_0 \exp(-(k_w + k_X X)l)$ k_w, k_X: constants	Simple assumptions on the cell trajectories	*Porphyridium* sp. $k = 3.65\ 10^{-4}$ $k_m = 1.6 \times 10^{-3}$ Pa^{-1} $\lambda_0 = 1.64 \times 10^{-5}$ s^{-1} $\alpha = 1.935 \times 10^{-3}$ m^2/μE $\beta = 5.7848 \times 10^{-7}$ m^2/μE $\delta = 4.796 \times 10^{-4}$ s^{-1} $\gamma = 0.1460$ s^{-1} $\tau_m = 2400$ Pa $k_x = 3.0 \times 10^{-6}$ mL/m-cell $k_w = 0.2$ m^{-1}	I = 110–550 μE/m^2-s T = 24 °C	Wu and Merchuk (2002)
Draft tube	Model from Wu and Merchuk, 2002	Model from Wu and Merchuk (2002)	Experimental measurement trajectories (using CARPT experiment)	Values from Wu and Merchuk (2002)	Values from Wu and Merchuk (2002)	Luo and Al-Dahhan (2004)
Indoor bubble column reactor	Three-population model (Fig. 2) and first-order decay $R_1 = \alpha I$ $R_2 = \gamma$ $R_3 = \beta I$ $R_4 = 0$ $R_5 = 0$ $R_6 = \delta$ $\mu = k\gamma x_2 - \lambda$ $\alpha, \beta, \gamma, \delta, k, \lambda$: constants	Beer–Lambert in non-transparent culture medium $I(l) = I_0 \exp(-(k_1 + k_2 X_p)Xl)$ k_1, k_2: constant	Simple assumptions on the trajectories of cells in a bubble column reactor	*Porphyridium* sp. $\alpha = 1.935 \times 10^{-3}$ m^2/μE $\beta = 5.7848 \times 10^{-7}$ m^2/μE $\delta = 4.796 \times 10^{-4}$ s^{-1} $\gamma = 0.1460$ s^{-1} $k = 3.65 \times 10^{-4}$ $\lambda = 0.05908$ h^{-1}	I = 110–550 μE/m^2-s T = 24 °C	Merchuk and Wu (2003)
Indoor 'light-chamber' photobioreactor	Light-inhibition model $\mu = 2\mu_s \frac{(1-i)(i-i_c)}{(1-i_c)^2+(i-i_c)^2}$ $i = I/I_s$ $i_c = I_c/I_s$ μ_s, I_c, I_s: constant	Beer–Lambert law $I(l) = I_0 \exp(-\sigma X l)$	Particle image velocimetry	*Porphyridium purpureum* $\mu_s = 16 \times 10^{-6}$ s^{-1} $I_s = 385$ μE/m^2-s $I_c = 15$ μE/m^2-s σ: Spectral distribution for the extinction coefficient	I = 0–236 μE/m^2-s T = 25 °C	Pruvost et al. (2002)
Indoor torus photobioreactor	Light-inhibition model with first-order decay $\mu = \mu_s \frac{I}{K+I+I^2/K'^2} - \lambda$ μ_s, K, K', λ: constants	Two-flux model with back-scattering	Computational fluid dynamics	*Chlamydomonas reinhardtii* $\mu_s = 0.2479$ h^{-1} $K = 69.75$ μE/m^2-s $K' = 2509.66$ μE/m^2-s $\lambda = 0.0531$ h^{-1} $E_a = 172$ m^2/kg $E_s = 868$ m^2/kg $b = 0.01728$	I = 0–1200 μE/m^2-s T = 25 °C	Pruvost et al. (2008)
Indoor airlift reactor	Model from Wu and Merchuk (2002)	Beer–Lambert in non-transparent culture medium $I(l) = I_0 \exp(-(k_1 + k_2 X_p)Xl)$ k_1, k_2: constants	Simple assumptions on the trajectories of cells in an airlift reactor	Values from Wu and Merchuk, 2002 k_1, k_2: unavailable	Values from Wu and Merchuk (2002)	Wu and Merchuk (2004)

2, while the prediction of the two-flux model was in good agreement with the measured light distribution. Alternatively, by assuming that light propagates in an individual direction, Pruvost and Cornet (2012) were able to generate an algorithm determining light distribution for any type of reactor geometry.

Without simplification, the RTE must be solved numerically, as done by Cornet et al. (1994). This approach was found to generate a more accurate prediction of light distribution than the Beer–Lambert law and the two-flux model (Cornet et al., 1994) but it is computationally intensive. Alternatively, Monte Carlo simulations can be used to numerically determine the light distribution in the solution (Aiba, 1982; Csogör et al., 2001; Dauchet et al., 2013). Ideally, and regardless the approach used, the prediction of light distribution should be validated against in-situ experimental measurement of irradiance.

4. Modeling the impact of temperature on photosynthesis

4.1. Temperature in Type I and Type II models

4.1.1. Uncoupled models

A first approach to model the effect of temperature on photosynthesis is to consider light and temperature as two independent factors. These 'uncoupled' models express the rate of photosynthesis as the product of two distinct functions of light intensity and temperature. For example, the Type I model of Bordel et al. (2009) multiplies a Monod function for light intensity with the Arrhenius equation for temperature as follows:

$$\mu = \mu_{m,0} \exp\left(-\frac{E_a}{kT}\right) \cdot \frac{I_{av}}{K + I_{av}} \tag{8}$$

Table 6
Light distribution equations ($I(l)$: local light intensity at a distance l from the external surface of the cultivation system; I_0: incident light intensity; X: cell concentration; X_p: pigment content). The approaches consisting of solving the radiative transfer equation numerically and using Monte-Carlo methods to determine the light distribution are not given in this table. The reader is referred to the studies of Aiba (1982), Csogör et al. (2001), Dauchet et al. (2013), Houf and Incropera (1980), and Pruvost and Cornet (2012) for examples of implementation of these methods.

Model	Equation	Values	Algae	Reference
Beer–Lambert	$I(l) = I_0\exp(-\sigma X l)$ σ: extinction coefficient	$\sigma = 214$ m^2/kg $\sigma = 0.72$ dm^2/kJ $\sigma = 175$ m^2/kg (graphical reading) $\sigma = 150$ m^2/kg $\sigma = 200$ m^2/kg	*Monodus subterraneus* *Oscillatoria agardhii* *Spirulina platensis* *Porphyridium cruentum* *Chlorella pyrenoidosa*	Bosma et al. (2007) Evers (1991) Lee et al. (1987) Muller-Feurga et al. (2003) Ogbonna et al. (1995b)
Beer–Lambert in non-transparent culture medium	$I(l) = I_0\exp(-(k_w + k_X X)l)$ k_w, k_X: constants	$k_w = 0.2$ m^{-1} $k_X = 3.0 \times 10^{-6}$ mL/cell-m	*Porphyridium* sp.	Luo and Al-Dahhan (2004)
Beer–Lambert with pigment content	$I(l) = I_0\exp(-(k_1 + k_2 X_p)Xl)$ k_1, k_2: constants	$k_1 = 10$ m^2/kg biomass $k_2 = 2990$ m^5/kg pigment-kg biomass	*Phaeodactylum tricornutum*	Acién Fernández et al. (1998), García Camacho et al. (1999)
	$I(l) = I_0\exp(-\sigma X_p l)$ σ: extinction coefficient		*Arthrospira* (*Spirulina*) *platensis*	Janssen et al. (2003)
Hyperbolic Beer–Lambert	$I(l) = I_0\exp\left(-\frac{1}{l_{av}}\frac{k_1 X}{k_2+X} l\right)$ l_{av}: average light path in the culture k_1, k_2: constants	$k_1 = 4.8$–15.1 $k_2 = 2.4$–11.7 kg/m^3	*Phaeodactylum tricornutum*	Acién Fernández et al. (1997)
	$I(l) = I_0\exp\left(-\frac{k_1 X}{(K_X+X)(K_L+l)} l\right)$ k_1, K_X, K_L: constants	$k_1 = 50$ $K_X = 2.7$ kg/m^3 $K_L = 0.047$ m	*Synechoccus* sp.	Suh and Lee (2003)
	$I(l) = I_0\exp\left(-\frac{k_1 X}{k_2+X} l\right)$ k_1, k_2: constants	$k_1 = 1041$ m^{-1} $k_2 = 1.03$ kg/m^3	*Chlorella vulgaris*	Yun and Park (2003)
Two-flux model	$I(l) = F^+(l) + F^-(l)$ $\frac{dF^+}{dl} = -E_a X F^+ + \frac{1}{2}E_s X(F^- - F^+)$ $\frac{dF^-}{dl} = E_a X F^- + \frac{1}{2}E_s X(F^- - F^+)$ l: direction of light propagation (Cartesian coordinates) E_a: mass absorption coefficient E_s: mass scattering coefficient	$E_a = 150$ m^2/kg $E_s = 200$ m^2/kg	*Spirulina platensis*	Cornet et al. (1995)
Two-flux model with back-scattering	$I(l) = F^+(l) + F^-(l)$ $\frac{dF^+}{dl} = -E_a X F^+ - bE_s X(F^+ - F^-)$ $\frac{dF^-}{dl} = E_a X F^- - bE_s X(F^+ - F^-)$ E_a: mass absorption coefficient E_s: mass scattering coefficient b: back-scattering coefficient	$E_a = 172$ m^2/kg $E_s = 868$ m^2/kg b = 0.01728	*Chlamydomonas reinhardtii*	Pottier et al. (2005)
Hyperbolic	$I(l) = \frac{I_0}{(K_L l+1)^{n_1}(K_X X l+1)^{n_2}}$ K_L, K_X, n_1, n_2: constants	$K_L = 21.6$ m^{-1} $n_1 = 1.54$ $K_X = 130$ m^2/kg $n_2 = 1.18$	*Rhodobacter capsulatus*	Katsuda et al. (2000)

where μ is the specific growth rate (h^{-1}), $\mu_{m,0}$ is the maximum specific growth rate (h^{-1}), E_a is the activation energy for photosynthesis (J), k is the Boltzmann constant (J/K), T is the temperature (K), I_{av} is the average light intensity in the culture broth (μmol/m^2-s), and K is a light constant (μmol/m^2-s).

Even if the Arrhenius equation is used in several models (e.g. Bissinger and Montagnes, 2008; Eppley, 1972), this equation was initially developed to predict the impact of temperature on the rate of chemical reactions and cannot predict the negative impact of high temperature on enzymatic activity in biological systems (Ahlgren, 1987). To address this limitation, Roels (1983) modeled the rate of deactivation of enzymes as a function of temperature as:

$$\mu(I) = \mu_{m,0}(I)\frac{\exp\left(-\frac{E_a}{kT}\right)}{1 + K\exp\left(-\frac{E_a'}{kT}\right)} \quad (9)$$

where $\mu(I)$ is the specific growth rate (d^{-1}) at the light intensity I (W/m^2), $\mu_{m,0}$ is maximum specific growth rate (d^{-1}) at the light intensity I, k is the Boltzmann constant (J/K), T is the temperature (K), E_a and E_a' are the activation energy for photosynthesis and enzyme denaturation, respectively (J), and K is a dimensionless constant. Alternatively, Bernard and Rémond (2012) expressed the maximum specific growth rate as a function of the minimum, maximum and optimum temperatures for photosynthesis (T_{min}, T_{max}, and T_{opt}, respectively, Table 1) as follows:

$$\mu(I) = \mu_{m,0}(I)\frac{(T-T_{max})(T-T_{min})^2}{\left(T_{opt}-T_{min}\right)\left[\left(T_{opt}-T_{min}\right)\left(T-T_{opt}\right)-\left(T_{opt}-T_{max}\right)\left(T_{opt}+T_{min}-2T\right)\right]}. \quad (10)$$

4.1.2. Coupled models

In contrast to uncoupled approaches, 'coupled' models aim to account for the potential interdependence of light and temperature on the rate of photosynthesis (Butterwick et al., 2005; Fawley, 1984; Box 3). For example, in the model developed by Dermoun et al. (1992), the parameters of the 'light-inhibition model' described in Table 1 were all made functions of temperature and the specific growth rate μ (d^{-1}) was expressed as:

$$\mu = 2\mu_m(T)(1+\beta_I)\frac{I/I_{opt}(T)}{1 + 2\beta_I I/I_{opt}(T) + \left(I/I_{opt}(T)\right)^2} \quad (11)$$

where $\mu_m(T)$ is the maximum specific growth rate (d^{-1}) at the temperature T (°C), β_I is a constant, I is the light intensity (μmol/m^2-s), and $I_{opt}(T)$ is the optimum light intensity for photosynthesis (μmol/m^2-s) at the temperature T (°C).

Box 3
Temperature effect on photosynthesis.

Short-term effect: Under light-limited conditions (Fig. 1), the rate of photosynthesis is limited by the rate of photon supply (Davison, 1991) and the rate of photon capture is considered as independent of temperature. When algae are light-saturated, temperature impacts the maximum rate at which the dark reactions of photosynthesis can occur and with it, the threshold for light saturation (I_k, Fig. 1).
Long-term effect (temperature-adaptation): cells can acclimatize to temperature (Davison, 1991). For example, de-Bashan et al. (2007) showed that *Chlorella sorokiniana* can grow at high temperature (40 °C) after a period of five days of acclimation at this temperature.

Although coupled models theoretically better represent the impact of temperature than uncoupled models, the limiting step of photosynthesis is not always temperature-dependent. In addition, coupled models require a large number of parameters to be fitted experimentally (e.g. nine in the model depicted by Eq. (11)). Therefore, an apparent good fit during validation may only be due to a good adjustment of the set of parameters. This issue, usually referred to as 'overfitting', can affect the accuracy of the prediction because the model describes noise rather than important trends (Hawkins, 2004).

4.2. Temperature in Type III models

Because Type III models are based on the kinetics of reactions occurring at the cell level, it is possible to model the effect of temperature by considering its impact on the limiting reactions of photosynthesis. For example, the rates of the recovery and de-excitation processes considered in the three-population model (R_2 and R_5, respectively, Fig. 2) are controlled by specific enzymes which activity can be estimated at different temperatures. Duarte (1995) for example assumed that the dependence of these two reaction rates on temperature could be modeled using an Arrhenius law. The reaction rates R_1 and R_3 (Fig. 2) are only functions of the light intensity and can be considered as temperature-independent (Eilers and Peeters, 1988).

Important daily and seasonal temperature fluctuations can be observed during outdoor cultivation (Béchet et al., 2011), meaning that temperature-acclimation may impact productivity (Box 3). This mechanism was however not considered in the models reviewed in this study.

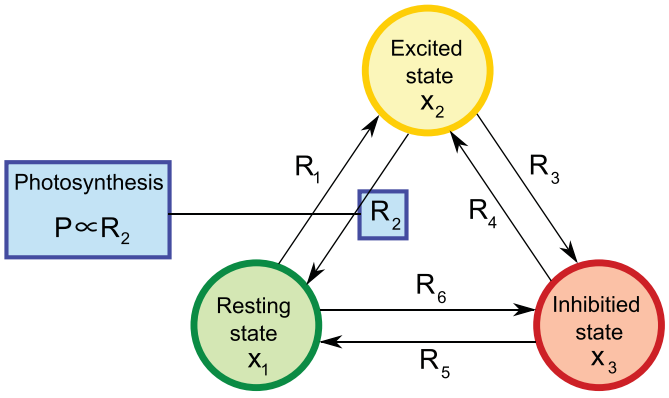

Fig. 2. Three-population model showing the resting, excited, and inhibited states of photosynthetic units (PSUs). R_i (i between 1 and 6) represents the rate of change from one state to another.

5. Modeling endogenous respiration

5.1. Short-term day-time respiration

Falkowski and Owens (1978) showed that short-term respiration during day time can consume up to 25% of the chemical energy (ATP, NADPH) generated during photosynthesis. This consumption can be assumed to be directly proportional to the rate of photosynthesis (García Camacho et al., 1999). For example, Geider et al. (1997) assumed that the rate of day-time respiration (R_D, in g C/s-m^3) could be expressed as:

$$R_D = -\zeta \mu X \tag{12}$$

where ζ is a dimensionless constant, μ the specific growth rate (s^{-1}), and X the cell concentration (g C/m^3). It should be noted that day-time respiration can be inhibited by light in certain cyanobacteria and therefore does not occur when these cells are only exposed to short periods of darkness (Pruvost et al., 2012). For these algal species, the rate of day-time respiration can be assumed to be zero.

5.2. Long-term night-time respiration

Long-term respiration at night time can cause significant biomass losses during algae cultivation (Torzillo et al., 1991). The rate of night-time maintenance R_N (expressed as biomass per unit time and per unit volume) is usually modeled using first-order kinetics with regard to cell concentration as:

$$R_N = -\lambda X \tag{13}$$

where λ is a constant (expressed per unit time) and X is the cell concentration (expressed as biomass per unit volume). This approach assumes that night-time respiration is only associated with normal maintenance functions and that, therefore, its specific rate λ is constant over time. This approach was used by Pruvost et al. (2012) in order to model *A. platensis* growth during outdoor cultivation at constant temperature.

In full-scale cultivation systems, assuming a constant rate of night-time respiration may cause inaccuracy for several reasons:

- Temperature: In the modeling study of Collins and Boylen (1982), the specific rate of respiration of *A. variabilis* was shown to increase from 0.2 to 1.0 g carbon/g biomass-d when temperature varied from 10 °C to 40 °C. As temperature can drop by more than 10 °C at night during outdoor cultivation (Béchet et al., 2011), the impact of temperature on night-time respiration must be considered. Few models however account for the temperature effect on night-time respiration. For this purpose, Grobbelaar (1990) proposed to multiply the specific rate respiration λ by a Van't Hoff function by analogy with chemical reactions (Table 2).
- Cellular composition: Torzillo et al. (1991) observed that the magnitude of night-time biomass loss in outdoor cultivation systems depended on the light intensity and temperature during the previous day. This dependence was explained by the fact that the endogenous respiration rate was a function of the carbohydrate content of cells.

6. Sources of inaccuracy

6.1. Light sources

A wide range of light sources, going from 'Cool White' fluorescent tubes (Collins and Boylen, 1982), to tungsten lamps (Katsuda et al., 2000) and natural sunlight (Bosma et al., 2007) have been used in the experimental studies reviewed in this paper. In most studies, the light source is only characterized by its intensity expressed in units of a flux of photons (μmol/m^2-s) or an energy flux (in W/m^2). Yet, the light response of algae cells is also a

function of the light spectrum because photosynthetic pigments have preferential wavelengths for light absorption, as shown by Jeon et al. (2005) during *Haemetococcus pluvialis* cultivation. As most light sources have a spectrum different from sunlight, models validated from indoor data may not be directly applicable to outdoor cultures. To account for the interaction between the lamp type and the cell pigment content, several studies have determined the absorption and emission spectra of photosynthetic micro-organisms (Pruvost and Cornet, 2012). This approach also requires the experimental determination of the spectral distribution of the light source used for model development.

6.2. Experimental techniques used to measure the rate of photosynthesis

Several proxies can be measured to quantify the rate of photosynthesis during modeling studies and the best parameter to use depends on the purpose of the study. Examples include the rate of oxygen production or the rate of inorganic carbon uptake (e.g. Chalker, 1980; Cullen, 1990), the dry weight (DW) concentration (e.g. Bosma et al., 2007), or the broth optical density (OD, e.g. Acién Fernández et al., 1997). Unfortunately, biomass composition and other cell properties depend on species and cultivation conditions (Posten, 2009), meaning that predicting biomass productivity based on a proxy to biomass weight can generate considerable uncertainty. In particular, careful consideration should be given to the use of the OD in modeling studies aiming to predict productivity in outdoor systems because the OD/DW ratio can fluctuate considerably over time due to changes in chlorophyll content associated with light-acclimation (Béchet et al., 2013). In order to minimize the impact of changes in pigment content on the OD/DW ratio, various studies have measured OD at wavelengths higher than 700 nm (e.g. 750 nm in Cornet et al., 1995; 760 nm in Dermoun et al., 1992; or 720 nm in Kurano and Miyachi, 2005).

6.3. Inaccuracy of light and temperature inputs

The incident light intensity reaching outdoor cultivation systems is challenging to predict and its estimation has a certain level of uncertainty. For example, Béchet et al. (2013) demonstrated that the amount of light reaching the algae cultivated in an outdoor vertical column photobioreactor could vary significantly depending on the wall transmittance (which can vary due to biomass deposition on the reactor wall) or the reflectivity of the ground surface. This level of inaccuracy on the main input of the model may cause inaccuracy on the productivity prediction. Similarly, current models that predict temperature in outdoor cultivation systems are only accurate within a range of 1 to 2 °C (Béchet et al., 2010, 2011), which may also impact the accuracy of the productivity prediction. Yet, very little consideration has hitherto been given to the uncertainty associated with the evaluation of the light

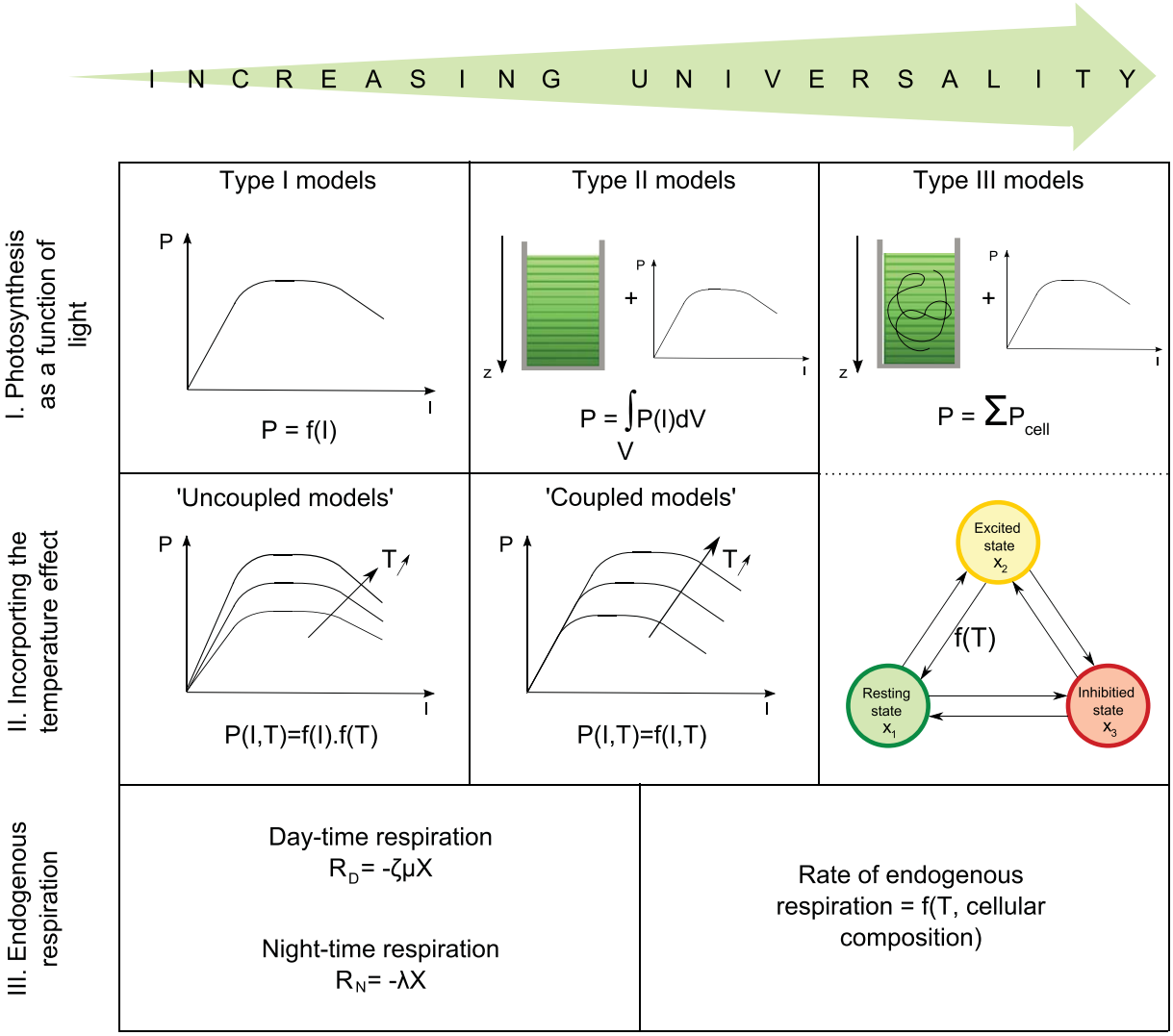

Fig. 3. Schematic representation of models of algal productivity (*P: rate of photosynthesis; I*: light intensity; *T*: temperature; R_D: rate of day-time respiration; μ: specific rate of photosynthesis; *X*: cell concentration; ζ: proportionality constant; R_N: rate of night-time maintenance; λ: maintenance coefficient).

and temperature inputs in the prediction of algal productivity in full-scale systems.

7. Conclusions

To date, over 40 models predicting algae productivity have been described in the literature. Most of these models were not validated against outdoor data and therefore their comparative assessment can only be done by considering the biological mechanisms that the different models can theoretically account for. We therefore categorized and assessed these models based on their theoretical ability to account for biological mechanisms relevant to full-scale systems.

Because model refinement must be weighed against the increasing uncertainty brought by increased complexity, we conclude that the currently most pragmatic modeling methodology for engineering assessments of full-scale systems would utilize the following approaches (Fig. 3):

1) For the rate of photosynthesis, Type II models provide a compromise between practicability and universality.
2) Empirical 'uncoupled models' should be used in conjunction with Type II models to account for the effect of temperature on photosynthesis.
3) In order to predict the *net* productivity, the above should be used in conjunction with a first-order decay term for endogenous respiration that empirically accounts for temperature effects.

Given the current lack of full-scale validation, there is now a critical need to benchmark the accuracy of the modeling approaches discussed in this review against outdoor experimental data. Such research should also determine the level of inaccuracy caused by uncertainty on model parameters and input variables (e.g. light and temperature). Future research should also aim to better quantify the impacts of endogenous respiration and acclimation to light and temperature.

Supplementary data to this article can be found online at http://dx.doi.org/10.1016/j.biotechadv.2013.08.014.

Acknowledgments

Quentin Béchet is supported by a Massey University Doctoral Scholarship. The authors thank Professor Yusuf Chisti from Massey University, New Zealand, for valuable discussions about algal productivity models.

References

Acién Fernández FG, García Camacho F, Sánchez Pérez JA, Fernández Sevilla JM, Molina Grima E. A model for light distribution and average solar irradiance inside outdoor tubular photobioreactors for the microalgal mass culture. Biotechnol Bioeng 1997;55(5):701–14.
Acién Fernández FG, García Camacho F, Sánchez Pérez JA, Fernández Sevilla JM, Molina Grima E. Modeling of biomass productivity in tubular photobioreactors for microalgal cultures: effects of dilution rate, tube diameter, and solar irradiance. Biotechnol Bioeng 1998;58(6):605–16.
Ahlgren G. Temperature functions in biology and their application to algal growth constants. Oikos 1987;49(2):177–90.
Aiba S. Growth kinetics of photosynthetic microorganisms. Adv Biochem Eng 1982;23:85–156.
Beardall J, Morris I. The concept of light intensity adaptation in marine phytoplankton: some experiments with *Phaeodactylum tricornutum*. Mar Biol 1976;37:377–87.
Béchet Q, Shilton A, Fringer O, Munoz R, Guieysse B. Mechanistic modelling of broth temperature in outdoor photobioreactors. Environ Sci Technol 2010;44:2197–203.
Béchet Q, Shilton A, Park JB, Craggs RJ, Guieysse B. Universal temperature model for shallow algal ponds provides improved accuracy. Environ Sci Technol 2011;45(8):3702–9.
Béchet Q, Muñoz R, Shilton A, Guieysse B. Outdoor cultivation of temperature-tolerant *Chlorella sorokiniana* in a column photobioreactor under low power-input. Biotechnol Bioeng 2013;110(1):118–26.
Benemann JR, Tillett DM, Weisman JC. Microalgae biotechnology. Trends Biotechnol 1987;5(2):47–53.
Bernard O. Hurdles and challenges for modelling and control of microalgae for CO_2 mitigation and biofuel production. J Process Control 2011;21:1378–89.
Bernard O, Rémond B. Validation of a simple model accounting for light and temperature effect on microalgal growth. Bioresour Technol 2012;123:520–7.
Bissinger JE, Montagnes DJS. Predicting marine phytoplankton maximum growth rates from temperature: improving on the Eppley curve using quantile regression. Limnol Oceanogr 2008;53(2):487–93.
Bitog JP, Lee IB, Lee CG, Kim KS, Hwang HS, Hong SW, et al. Application of computational fluid dynamics for modeling and designing photobioreactors for microalgae production: a review. Comput Electron Agric 2011;76:131–47.
Bordel S, Guieysse B, Muñoz R. Mechanistic model for the reclamation of industrial wastewaters using algal-bacterial photobioreactors. Environ Sci Technol 2009;43(9):3200–7.
Bosma R, van Zessen E, Reith JH, Tramper J, Wijffels RH. Prediction of volumetric productivity of an outdoor photobioreactor. Biotechnol Bioeng 2007;97(5):1108–20.
Boyle NR, Morgan JA. Flux balance analysis of primary metabolism in *Chlamydomonas reihardtii*. BMC Syst Biol 2009;3:4.
Butterwick C, Heaney SI, Talling JF. Diversity in the influence of temperature on the growth rates of freshwater algae, and its ecological relevance. Freshw Biol 2005;50:291–300.
Camacho Rubio F, García Camacho F, Fernández Sevilla JM, Chisti Y, Molina Grima E. A mechanistic model of photosynthesis in microalgae. Biotechnol Bioeng 2003;81(4):459–73.
Carvahlo AP, Malcata FX. Kinetic modeling of the autotrophic growth of *Pavlova lutheri*: study of the combined influence of light and temperature. Biotechnol Prog 2003;19:1128–35.
Chalker BE. Modelling light saturation curves for photosynthesis: an exponential function. J Theor Biol 1980;84:205–15.
Chang RL, Ghamsari L, Manichaikul A, Hom EFY, Balaji S, Fu W, et al. Metabolic network reconstruction of *Chlamydomonas* offers insight into light-driven algal metabolism. Mol Syst Biol 2011;7:518.
Chisti Y. Biodiesel from microalgae. Biotechnol Adv 2007;25:294–306.
Chisti Y. Biodiesel from microalgae beats bioethanol. Trends Biotechnol 2008;26:126–31.
Cogne G, Gros JB, Dussap CG. Identification of a metabolic network structure representative of *Arthrospira* (*Spirulina*) *platensis* metabolism. Biotechnol Bioeng 2003;84(6):667–76.
Cogne G, Rügen M, Bockmayr A, Titica M, Dussap CG, Cornet JF, et al. A model-based method for investigating bioenergetics processes in autotrophically growing eukaryotic microalgae: application to the green algae *Chlamydomonas reinhardtii*. Biotechnol Prog 2011;27(3):631–40.
Collins CD, Boylen CW. Physiological responses of *Anabaena variabilis* (cyanophyceae) to instantaneous exposure to various combinations of light intensity and temperature. J Phycol 1982;18:206–11.
Cornet JF, Dussap CG. A simple and reliable formula for assessment of maximum volumetric productivities in photobioreactors. Biotechnol Prog 2009;25(2):424–35.
Cornet JF, Dussap CG, Dubertret G. A structured model for simulation of cultures of the cyanobacterium *Spirulina platensis* in photobioreactors: I. Coupling between light transfer and growth kinetics. Biotechnol Bioeng 1992a;40:817–25.
Cornet JF, Dussap CG, Cluzel P, Dubertret G. A structured model for simulation of cultures of the cyanobacterium *Spirulina platensis* in photobioreactors. II. Identification of kinetic parameters under light and mineral limitations. Biotechnol Bioeng 1992b;40:826–34.
Cornet JF, Dussap CG, Gros JB. Conversion of radiant light energy in photobioreactors. AIChe 1994;40:1055–66.
Cornet JF, Dussap CG, Gros JB. A simplified monodimensional approach for modeling coupling between radiant light transfer and growth kinetics in photobioreactors. Chem Eng Sci 1995;50(9):1489–500.
Crill PA. The photosynthesis-light curve: a simple analog model. J Theor Biol 1977;64:503–16.
Csogör Z, Herrenbauer M, Schmidt K, Posten C. Light distribution in a novel photobioreactor—modelling for optimization. J Appl Phycol 2001;13:325–33.
Cullen JJ. On models of growth and photosynthesis in phytoplankton. Deep-Sea Res 1990;37(4):667–83.
Dauchet J, Blanco S, Cornet JF, El Hafi M, Eymet V, Fournier R. The practice of recent radiative transfer Monte Carlo advances and its contribution to the field of micro-organisms cultivation in photobioreactors. J Quant Spectrosc Radiat Transfer 2013;128:52–9.
Davison IR. Environmental effects of temperature on photosynthesis: temperature. J Phycol 1991:2–8.
de-Bashan LE, Trejo A, Huss VAR, Hernandez JP, Bashan Y. Chlorella sorokiniana UTEX 2805, a heat and intense, sunlight-tolerant microalga with potential for removing ammonium from wastewater. Biores Technol 2008;99:4980–9.
Denman KL, Marra J. Modelling the time dependent photoadaptation of phytoplankton to fluctuating light. Elsevier Oceanog. Ser., 42 (C). ; 1986. p. 341–59.
Dermoun D, Chaumont D, Thebault JM, Dauta A. Modelling of growth of *Porphyridium cruentum* in connection with two interdependent factors: light and temperature. Bioresour Technol 1992;42:113–7.
Duarte P. A mechanistic model of the effects of light and temperature on algal primary productivity. Ecol Model 1995;82:151–60.
Eilers PHC, Peeters JCH. A model for the relationship between light intensity and the rate of photosynthesis in phytoplankton. Ecol Model 1988;42:199–215.
Eilers PHC, Peeters JCH. Dynamic behavior of a model for photosynthesis and photoinhibition. Ecol Model 1993;69:113–33.
Eppley RW. Temperature phytoplankton growth in the sea. Fish Bull 1972;70:1063–85.
Esposito S, Botte V, Iudicone D, Ribera d'Alcala M. Numerical analysis of cumulative impact of phytoplankton photoresponses to light variation on carbon assimilation. J Theor Biol 2009;261:361–71.
Evers EG. A model for light-limited continuous cultures: growth, shading, and maintenance. Biotechnol Bioeng 1991;38(3):254–9.
Falkowski PG, Owens TG. Effects of light intensity on photosynthesis and dark respiration in six species of marine phytoplankton. Mar Biol 1978;45:289–95.

Fasham MJR, Platt T. Photosynthetic response of phytoplankton to light: a physiological model. Proc R Soc Lond B Biol Sci 1983;219(1217):355–70.
Fawley MW. Effects of light intensity and temperature interactions on growth characteristics of *Phaeodactylum tricornutum* (bacillariophyceae). J Phycol 1984;20:67–72.
Ferris JM, Christian R. Aquatic primary production in relation to microalgal responses to changing light: a review. Aquat Sci 1991;53(2/3):187–217.
García Camacho F, Contreras Gómez A, Acién Fernández FG, Fernández Sevilla J, Molina Grima E. Use of concentric-tube airlift photobioreactors for microalgal outdoor mass cultures. Enzyme Microb Technol 1999;24:164–72.
García-Camacho F, Sánchez-Mirón A, Molina Grima E, Camacho Rubio F, Merchuck JC. A mechanistic model of photosynthesis in microalgae including photoacclimation dynamics. J Theor Biol 2012;304:1–15.
Geider RJ. The relationship between steady state phytoplankton growth and photosynthesis. Limnol Oceanogr 1990;35(4):971–2.
Geider RJ, MacIntyre HL. A dynamic model of photoadaptation in phytoplankton. Limnol Oceanogr 1996;41(1):1–15.
Geider RJ, MacIntyre HL, Kana TM. Dynamic model of phytoplankton growth and acclimation: responses of the balanced growth rate and the chlorophyll *a*: carbon ratio to light, nutrient-limitation and temperature. Mar Ecol Prog Ser 1997;148:187–200.
Geider RL, MacIntyre HL, Kana TM. A dynamic regulatory model of phytoplanktonic acclimation to light, nutrients, and temperature. Limnol Oceanogr 1998;43(3):679–94.
Grobbelaar JU. Modeling algal productivity in large outdoor cultures and waste treatment systems. Biomass 1990;21:297–314.
Grobbelaar JU. The influence of light/dark cycles in mixed algal cultures on their productivity. Bioresour Technol 1991;38:189–94.
Grobbelaar JU. Turbulence in mass algal cultures and the role of light/dark fluctuations. J Appl Phycol 1994;6:331–5.
Grobbelaar JU. Factors governing algal growth in photobioreactors: the "open" versus "closed" debate. J Appl Phycol 2009;21:489–92.
Guieysse B, Béchet Q, Shilton A. Variability and uncertainty in water demand and water footprint assessments of fresh algae cultivation based on case studies from five climatic regions. Bioresour Technol 2013;128:317–23.
Guterman H, Vonshak A, Ben-Yaakov S. A macromodel for outdoor algal mass production. Biotechnol Bioeng 1990;35:809–19.
Haario H, Kalachev L, Laine M. Reduced models of algae growth. Bull Math Biol 2009;71:1626–48.
Han BP. A mechanistic model of algal photoinhibition induced by photodamage to Photosystem-II. J Theor Biol 2002;214:519–27.
Han BP. Photosynthesis-irradiance response at physiological level: a mechanistic model. J Theor Biol 2001;213:121–7.
Han BP, Virtanen M, Koponen J, Straškraba M. Effect of photoinhibition on algal photosynthesis: a dynamic model. J Plankton Res 2000;22(5):865–85.
Hawkins DM. The problem of overfitting. J Chem Inf Comput Sci 2004;44:1–12.
Houf WG, Incropera FP. An assessment of techniques for predicting radiation transfer in aqueous media. J Quant Spectrosc Radiat Transfer 1980;23:101–15.
Janssen M, Tramper J, Mur LR, Wijffels RH. Enclosed outdoor photobioreactors: light regime, photosynthetic efficiency, scale-up, and future prospects. Biotechnol Bioeng 2003;81(2):193–210.
Jassby AD, Platt T. Mathematical formulation of the relationship between photosynthesis and light for phytoplankton. Limnol Oceanogr 1976;21(4):540–7.
Jeon YC, Cho CW, Yun YS. Measurement of microalgal photosynthetic activity depending on light intensity and quality. Biochem Eng J 2005;27:127–31.
Katsuda T, Arimoto T, Igarashi K, Azuma M, Kato J, Takakuwa S, et al. Light intensity distribution in the externally illuminated cylindrical photo-bioreactor and its application to hydrogen production by *Rhodobacter capsulatus*. Biochem Eng J 2000;2000:157–64.
Kiefer DA, Mitchell BG. A simple, steady-state description of phytoplankton growth based on absorption cross section and quantum efficiency. Limnol Oceanogr 1983;28(4):770–6.
Kurano N, Miyachi S. Selection of microalgal growth models for describing specific growth rate-light response using extended information criterion. J Biosci Bioeng 2005;100(4):403–8.
Lee HY, Erickson LE, Yang SS. Kinetics and bioenergetics of light-limited photoautotrophic growth of *Spirulina platensis*. Biotechnol Bioeng 1987;29:832–43.
Luo HP, Al-Dahhan. Analyzing and modeling of photobioreactors by combining first principles of physiology and hydrodynamics. Biotechnol Bioeng 2004;85(4):382–93.
Mata TM, Martins AA, Caetano NS. Microalgae for biodiesel production and other applications: a review. Renew Sustain Energy Rev 2010;14:217–32.
Megard RO, Tonkyn DW, Senft WH. Kinetics of oxygenic photosynthesis in planktonic algae. J Plankton Res 1984;6(2):325–37.
Merchuk JC, Wu X. Modeling of photobioreactors: application to bubble column simulation. J Appl Phycol 2003;15:163–9.
Merchuk JC, Carcia Camacho F, Molina Grima E. Photobioreactors—models of photosynthesis and related effects. Compr Biotechnol 2011;2:227–47.
Mirón AS, Gómez AC, Camacho FG, Grima EM, Chisti Y. Comparative evaluation of compact photobioreactors for large-scale monoculture of microalgae. J Biotechnol 1999;70:249–70.
Molina Grima E, Camacho Rubio F, Sanchez Pérez JA, Fernandez Sevilla JM, Acién Fernandez FG, Contreras Gomez A. A mathematical model of microalgal growth in light-limited chemostat culture. J Chem Technol Biotechnol 1994;61:167–73.
Molina Grima E, Fernández Sevilla JM, Sánchez Pérez JA, García Camacho F. A study on simultaneous photolimitation and photoinhibition in dense microalgal cultures taking into account incident and averaged irradiances. J Biotechnol 1996;45:59–69.
Muller-Feurga A, Le Guédes R, Pruvost J. Benefits and limitations of modeling for optimization of *Porphyridium cruentum* culture in annular photobioreactor. J Biotechnol 2003;103:153–63.
Murphy CC, Allen DT. Energy–water nexus for mass cultivation of algae. Environ Sci Technol 2011;45:5861–8.
Ogbonna JC, Yada H, Tanaka H. Kinetic study of light-limited batch cultivation of photosynthetic cells. J Ferment Bioeng 1995a;80(3):259–64.
Ogbonna JC, Yada H, Tanaka H. Light-supply coefficient: a new engineering parameter for photobioreactor design. J Ferment Bioeng 1995b;80(4):369–76.
Pahlow M. Linking chlorophyll-nutrient dynamics to the Redfield N:C ratio with a model of optimal phytoplankton growth. Mar Ecol Prog Ser 2005;287:33–43.
Pahl-Wostl C. Dynamic versus static models for photosynthesis. Hydrobiologia 1992;238:189–96.
Pahl-Wostl C, Imboden DM. DYPHORA—a dynamic model for the rate of photosynthesis of algae. J Plankton Res 1990;12(6):1207–21.
Perner-Nochta I, Posten C. Simulations of light intensity variation in photobioreactors. J Biotechnol 2007;131:276–85.
Posten C. Design principles of photo-bioreactors for cultivation of microalgae. Eng Life Sci 2009;9(3):165–77.
Pottier L, Pruvost J, Deremetz J, Cornet JF, Legrand J, Dussap CG. A fully predictive model for one-dimensional light attenuation by *Chlamydomonas reinhardtii* in a torus reactor. Biotechnol Bioeng 2005;91(5):569–82.
Pruvost J, Cornet JF. Knowledge models for the engineering and optimization of photobioreactors. In: Posten C, Walter C, editors. Microalgal biotechnology vol. 1 "Potential and Production". De Gruyter GmbH & Co. KG978-3-11-022501-3; 2012.
Pruvost J, Legrand J, Legentillhomme P, Muller-Feuga A. Simulation of microalgae growth in limiting light conditions: flow effect. Bioeng Food Nat Prod 2002;48(5):1109–20.
Pruvost J, Pottier L, Legrand J. Numerical investigation of hydrodynamic and mixing conditions in a torus photobioreactor. Chem Eng Sci 2006;61:4476–89.
Pruvost J, Cornet JF, Legrand J. Hydrodynamics influence on light conversion in photobioreactors: an energetically consistent analysis. Chem Eng Sci 2008;63:3679–94.
Pruvost J, Cornet JF, Goetz V, Legrand J. Theoretical investigation of biomass productivities achievable in solar rectangular photobioreactors for the cyanobacterium *Arthrospira platensis*. Biotechnol Prog 2012;28:699–714.
Rabe AE, Benoit RJ. Mean light intensity: a useful concept in correlating growth rates of dense cultures of microalgae. Biotechnol Bioeng 1962;4:377–90.
Ragonese FP, Williams JA. A mathematical model for the batch reactor kinetics of algae growth. Biotechnol Bioeng 1968;10(1):83–8.
Roels JA. Energetics and kinetics in biotechnology. Amsterdam: Elsevier Biomedical Press; 1983.
Sakshaug E, Johnsen G, Andresen K, Vernet M. Modeling of light-dependent algal photosynthesis and growth: experiments with the Barents Sea diatoms *Thalassiosira nordenskioeldii* and *Chaetoceros furcellatus*. Deep-Sea Res 1991;38(4):415–30.
Sánchez Mirón A, Contreras Gómez A, García Camacho F, Molina Grima E, Chisti Y. Comparative evaluation of compact photobioreactors for large-scale monoculture of microalgae. J Biotechnol 1999;70:249–70.
Schmidt BJ, Lin-Schmidt XL, Chamberlin A, Salehi-Ashtiani K, Papin JA. Metabolic systems analysis to advance algal biotechnology. Biotechnol J 2010;5:660–70.
Shastri AA, Morgan JA. Flux balance analysis of photoautrophic metabolism. Biotechnol Prog 2005;21:1617–26.
Singh A, Olsen SI. A critical review of biochemical conversion, sustainability and life cycle assessment of algal biofuels. Appl Energy 2011;88:3548–55.
Suh IS, Lee SB. A light distribution model for an internally radiating photobioreactor. Biotechnol Bioeng 2003;82(2):180–9.
Talbot P, Thébault JM, Dauta A, La Noüe De. A comparative study and mathematical modelling of temperature, light and growth of three microalgae potentially useful for wastewater treatment. Water Res 1991;25(4):465–72.
Torzillo G, Sacchi A, Materassi R. Temperature as an important factor affecting productivity and night biomass loss in *Spirulina platensis* grown outdoors in tubular photobioreactors. Bioresour Technol 1991;38(2–3):95–100.
Tredici MR, Materassi R. From open ponds to vertical alveolar panels: the Italian experience in the development of reactors for the mass cultivation of phototrophic microorganisms. J Appl Phycol 1992;4:221–31.
Wu X, Merchuk JC. Simulation of algae growth in a bench-scale bubble column reactor. Biotechnol Bioeng 2002;80(2):156–68.
Wu X, Merchuk JC. Simulation of algae growth in a bench scale internal loop airlift reactor. Chem Eng Sci 2004;59:2899–912.
Yun YS, Park JM. Kinetic modeling of the light-dependent photosynthetic activity of the green microalga *Chlorella vulgaris*. Biotechnol Bioeng 2003;83(3):303–11.
Zonneveld C. Light-limited microalgal growth: a comparison of modeling approaches. Ecol Model 1998;113:41–54.

Supplementary Material – JBA-D-12-0299

Title: **Modeling the effects of light and temperature on algae growth: state of the art and critical assessment for productivity prediction during outdoor cultivation**

Authors: Quentin Béchet, Andy Shilton, Benoit Guieysse

S1 – **Characteristics of modeling studies**

1 Table

3 Pages

S1 - Characteristics of modeling studies

Table S1: Experimental conditions of algae cultivations performed to generate data sets used for model development and/or validation: OUTDOOR ("Yes" means cultivation carried out outdoors); DYNAMIC ("Yes" means cultivation carried out under dynamic conditions of light and temperature); TIME (duration of the experiment); LIGHT GRADIENT ("Yes" means cultivation was carried out at a cell concentration high enough to generate light gradients in the cultivation broth); DATA SET ("Yes" means the model was tested against data that was not used to build the model).

Model	OUTDOOR	DYNAMIC	TIME	LIGHT-GRADIENT	DATA SET
Chalker, 1980	No	No	hours[1]	NS	No
Sakshaug et al., 1991	No	No	1 h	No	No
Geider et al., 1996	No	No	3-4 h	No	No
Megard et al., 1984	No	No	1 h	NS	No
Pahl-Wostl and Imboden, 1990	No	Yes	1 d	NS	Yes
Bernard and Rémond, 2012	No	No	1-15 d[2]	NA[6]	No
Dermoun et al., 1992	No	No	NS	No	No
Talbot et al., 1991	No	No	NS	No	No
Collins and Boylen, 1982	No	No	NS	NS	No
Kiefer and Mitchell, 1983	No	No	NS	Yes	No
Kurano and Miyachi, 2005	No	No	NS	NS	No
Carvahlo and Malcata, 2003	No	No	15-40 d	NS	No
Haario et al., 2009	Yes	Yes	8 yrs	Yes	Yes
Jeon et al., 2005	No	No	hours[1]	Yes	No
Bordel, 2009	No	No	1-9 d[3]	Yes	Yes
Lee at al., 1987	No	No	NS	Yes	No
Molina Grima et al., 1994	No	No	days[4]	Yes	Yes
Ogbonna et al., 1995	No	No	NS	Yes	Yes
Ragonese and Williams, 1968	No	No	3-11d	Yes	No
Rabe and Benoit, 1962	No	No	NS	Yes	No
Molina Grima et al., 1996	No	No	4 d[5]	Yes	No
Acién Fernández et al., 1998	Yes	Yes	1 yr	Yes	Yes
Bosma et al., 2007	Yes	Yes	2-3 mths	Yes	Yes
Cornet et al., 1995	No	No	NS	Yes	Yes
Cornet and Dussap, 2009	No	No	NS	Yes	Yes
Evers, 1991	No	No	NS	No	No
Grobbelaar, 1990	Yes	Yes	16 mths	Yes	No
Guterman et al., 1990	Yes	Yes	18 mths	Yes	No
Muller-Feurga et al., 2003	No	No	3 wks	Yes	Yes
Yun and Park, 2003	No	No	hours[1]	Yes	No
Camacho Rubio et al., 2003	No	Yes	1 d	NS	No
Crill, 1977	No	No	NS	NS	No
Duarte, 1995	No	No	hours[1]	NS	No
Wu and Merchuk, 2001	No	Yes	10 d	No	No
Fasham and Platt, 1983	No	No	NS	NS	No
Wu and Merchuk, 2002	No	Yes	seconds	No	No
Luo and Al-Dahhan, 2004	No	No	10 d	Yes	Yes
Merchuk and Wu, 2003	NA	NA	NA	NA	NA
Pruvost et al., 2002	No	No	NS	Yes	Yes
Pruvost et al., 2008	No	No	NS	Yes	No
Wu and Merchuk, 2004	No	No	9 d	Yes	Yes

(NS: not specified; NA: not applicable)

[1]: Although the duration was not specified, the measurement of the photosynthetic rate based on oxygen accumulation suggests a short duration (i.e. hours).
[2]: This study used experimental data from previous studies and duration of 1-15 d corresponds to the experimental studies we could access from the literature.
[3]: Although the duration was not specified, the data set used to develop and validate this model was obtained from a continuous culture monitored during near steady-state for a minimum duration of 2 HRTs.
[4]: Although the duration was not specified, the results provided suggest an experiment of at least 200 hours.
[5]: Validation was carried under a steady state regime maintained for at least 4 days.
[6]: This study used experimental data from previous studies. Some of these studies were conducted at high cell concentrations.

Article 2

MASSEY UNIVERSITY
GRADUATE RESEARCH SCHOOL

STATEMENT OF CONTRIBUTION TO DOCTORAL THESIS CONTAINING PUBLICATIONS

(To appear at the end of each thesis chapter/section/appendix submitted as an article/paper or collected as an appendix at the end of the thesis)

We, the candidate and the candidate's Principal Supervisor, certify that all co-authors have consented to their work being included in the thesis and they have accepted the candidate's contribution as indicated below in the *Statement of Originality*.

Name of Candidate: Quentin Béchet

Name/Title of Principal Supervisor: Prof Benoit Guieysse

Name of Published Research Output and full reference:

Béchet Q, Shilton A, Park JBK, Craggs RJ, Guieysse B. 2011. Universal temperature model for shallow algal ponds provides improved accuracy. Environ Sci Technol 45(8): 3702-3709.

In which Chapter is the Published Work: 3

Please indicate either:

- The percentage of the Published Work that was contributed by the candidate:

  and / or

- Describe the contribution that the candidate has made to the Published Work:

  Q Béchet was the main contributor to the article. He constructed and numerically implemented the temperature model. The experimental data used for model validation were provided by the New Zealand National Institute for Water and Atmospheric Research (NIWA).

Quentin Béchet
Digitally signed by Quentin Béchet
DN: cn=Quentin Béchet, o=Massey University, ou=SEAT, email=q.bechet@massey.ac.nz, c=NZ
Date: 2014.02.17 18:49:56 +13'00'

Candidate's Signature

17/02/2014
Date

Benoit Guieysse
Digitally signed by Benoit Guieysse
DN: cn=Benoit Guieysse, o=Massey University, ou=SEAT, email=b.j.guieysse@massey.ac.nz, c=NZ
Date: 2014.02.24 11:17:49 +13'00'

Principal Supervisor's signature

24/02/2014
Date

Environmental Science & Technology

ARTICLE

pubs.acs.org/est

Universal Temperature Model for Shallow Algal Ponds Provides Improved Accuracy

Quentin Béchet,[†] Andy Shilton,[†] Jason B. K. Park,[‡] Rupert J. Craggs,[‡] and Benoit Guieysse*[,†]

[†]Center for Environmental Technology and Engineering, School of Engineering and Advanced Technology, Massey University, Private Bag 11 222, Palmerston North 4442, New Zealand

[‡]National Institute of Water and Atmospheric Research (NIWA), P.O. Box 11-115, Hamilton, New Zealand

Supporting Information

ABSTRACT: While temperature is fundamental to the design and optimal operation of shallow algal ponds, there is currently no temperature model universally applicable to these systems. This paper presents a model valid for any opaque water body of uniform temperature profile. This new universal model was tested against 1 year of experimental data collected from a wastewater treatment high rate algal pond. On the basis of 1 year of data collected every 15 min, the average errors of the predicted afternoon peak and predawn minimum were both only 1.3 °C and the average error between these extremes was just 1.2 °C. In order to demonstrate the improvement in accuracy gained, the expressions for heat fluxes used in nine prior temperature models were systematically substituted into the new universal model and evaluated against the experimental data. Errors in the peak and minimum temperatures increased by up to 2.1 and 3.2 °C, respectively, while the error between these extremes increased by up to 2.9 °C. In practical applications, these levels of inaccuracies could lead to an under/overestimation of the algal productivity and the evaporative water loss by approximately 40% and 300%, respectively.

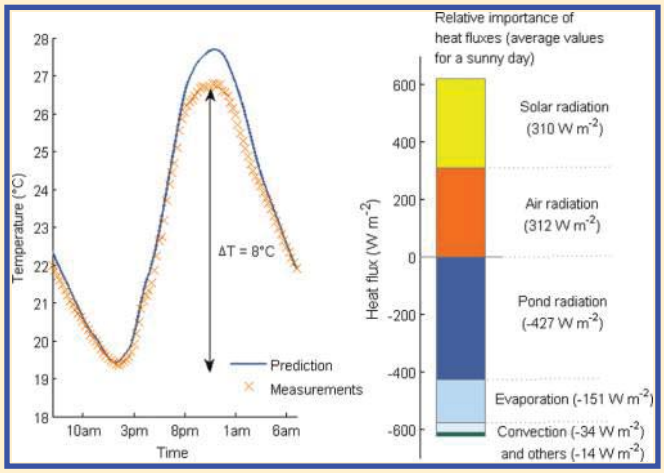

INTRODUCTION

Evaluating the economical feasibility and sustainability of processes incorporating shallow algal ponds requires the ability to forecast the productivity of these systems and their environmental impact. For this purpose, it is necessary to accurately predict the pond water temperature.

In the first instance, accurately predicting the pond temperature is important because temperature influences the rate of various reactions of photosynthesis.[1] This temperature dependence causes

(i) algae to exhibit optimal growth only within a narrow temperature range,
(ii) algae to die above a certain temperature threshold, and
(iii) algal light-saturation to occur at relatively low light intensity at low temperature, for example, in the morning.

Second, an accurate temperature model can also be used to optimize temperature control strategies to maximize algal productivity by estimating the amount of heat to add to or remove from the pond. Examples of temperature control strategies in the literature include

(i) maintaining optimum temperature at all times,[2]
(ii) reducing temperature to prevent growth inhibition at high temperatures,[3] and
(iii) raising temperature in the morning to optimize light utilization efficiency.[4]

Finally, accurate temperature prediction is important because evaporation from shallow algal ponds is positively correlated with the water temperature.[5] This means that the temperature directly affects the green and blue water footprint of these processes, typically defined as the volume of evaporative water loss per unit of biomass produced.[6]

Various models for predicting water temperature in lakes, wastewater treatment ponds, aquaculture ponds, and other similar systems have been described in the literature (e.g., refs 7−10). However, these prior models cannot be universally applied because the expressions of certain heat fluxes, the evaporative heat flux in particular, are derived from empirical relationships specific to the type of system studied.[7−10]

The objective of this paper is to present the first universal model for temperature prediction in shallow algal ponds validated against data obtained from over 1 year of experimental

Received: December 5, 2010
Accepted: March 8, 2011
Revised: March 1, 2011
Published: March 29, 2011

ACS Publications © 2011 American Chemical Society

monitoring of a high rate algal pond. This model is based on eight heat fluxes that use input parameters from readily available field data (meteorological data, site characteristics) and is valid for any opaque water body of a uniform temperature profile. The accuracy of the new universal model is compared to that of prior models published in the literature. The modeling includes a thorough sensitivity analysis conducted to determine the uncertainty generated by various input parameters. Finally, predictions of algal productivity and evaporative water loss using the new universal temperature model are demonstrated to be more accurate than those from using other temperature models.

MATERIALS AND METHODS

The temperature data used to validate the model was collected from a pilot-scale wastewater treatment high rate algal pond at National Institute of Water and Atmospheric Research's (NIWA) Ruakura Research Centre, Hamilton, New Zealand (37°47′S, 175°19′E). The pond had the following dimensions: volume, 8.1 m^3; surface area, 31.8 m^2; and depth, 0.3 m. A paddlewheel ensured complete mixing. The pond was operated on a fed-batch regime with an average hydraulic retention time of 4−8 days, depending on the season. Water was added every hour (for example, 55 L of water per hour was added to the pond for a hydraulic retention time of 6 days). The concentration of suspended solids was on the order of 0.3 g L^{-1} and algae productivity was between 9.0 and 17 g m^{-2} d^{-1}. The soil beneath the pond was a wet clay. The algae raceway pond used for model validation was fed with domestic wastewater, but the influence of the heat released by heterotrophic bacteria during growth was neglected. A more detailed description of the pond, its wastewater treatment performance, and algal productivity can be found in ref 11.

Meteorological data used in the model were taken from a weather station located less than 1 km away from the pond (C75734 Hamilton Ruakura 2EWS Climate Station[12]). Solar irradiance, air temperature, wind velocity, relative humidity, and rainfall were collected hourly and cloud cover daily. Pond temperature was collected and logged at 15 min intervals.

Modeling Approach. The pond was assumed completely mixed and all physical properties were assumed to be that of water under standard conditions. Every radiating body was considered as a gray-diffuse surface. The pond was assumed to be deep enough to absorb all radiative fluxes from the environment. In other words, air and solar radiation were assumed to be fully absorbed by the water before reaching the pond base. This assumption was based on the fact that light only penetrates two-thirds of the actual culture depth under typical algae cultivation field operation.[13] The fraction of solar radiation converted by algae into algal biomass during photosynthesis was assumed to be constant and equal to 2.5%.[14] The model inputs (solar irradiance, air temperature, wind velocity, relative humidity, rainfall, and inflow temperature) are described below with other specific assumptions.

Description of the Model. A heat balance analysis for the pond water can be described as

$$\rho_w V C_{p_w} \frac{dT_p}{dt} = Q_{ra,p} + Q_{ra,s} + Q_{ra,a} + Q_{ev} + Q_{conv} + Q_{cond} + Q_i + Q_r \quad (1)$$

where T_p is the pond temperature (K); ρ_w and C_{p_w} are the density (kg m^{-3}) and the specific heat capacity (J kg^{-1} K^{-1}) of pond water, respectively; V is the pond volume (m^3); $Q_{ra,p}$ is the radiation from the pond surface (W); $Q_{ra,s}$ is the total (direct + diffuse) solar radiation (W); $Q_{ra,a}$ is the radiation from the air to the pond (W); Q_{ev} is the evaporation flux (W); Q_{conv} is the convective flux at the pond surface (W); Q_{cond} is the conductive flux with the ground at the pond bottom (W); Q_i is the heat flux associated with the water inflow (W); and Q_r is the heat flux induced by rain (W) (Supporting Information, S1).

Pond Radiation. Because the water surface is assumed to be gray-diffuse, radiation from the pond surface to the atmosphere is given by Stefan−Boltzmann's fourth power law[15]

$$Q_{ra,p} = -\varepsilon_w \sigma T_p^4 S \quad (2)$$

where ε_w is the emissivity of water (0.97 is used, which is typical for water[9]), σ is the Stefan−Boltzmann constant (W m^{-2} K^{-4}), and S is the pond surface area (m^2).

Solar Radiation. The heat flux received by the pond from solar radiation can be calculated on the basis of the total (direct + diffuse) solar irradiance at ground level, H_s (W m^{-2}):[15]

$$Q_{ra,s} = (1 - f_a) H_s S \quad (3)$$

where f_a is the photosynthetic efficiency (the fraction of sunlight converted by algae into chemical energy during photosynthesis). When the pond is in the shade of external elements, such as trees or buildings, eq 3 can be adjusted by adding a "shadow function" (see ref 16). The component of solar radiation that is reflected was assumed to be negligible (Supporting Information, S2).

Air Radiation. According to the Stefan−Boltzmann's fourth power law, the radiative flux $Q_{ra,a}$ (in W m^{-2}) generated by air at a temperature of T_a (K) is given by[15]

$$Q_{ra,a} = \varepsilon_w \varepsilon_a \sigma T_a^4 S \quad (4)$$

where ε_a is the emissivity of the air (also called the atmospheric coefficient). Determination of the air emissivity is given in the Supporting Information (S3). Water reflectivity was not taken into account in this expression for the same reasons it was neglected in the expression of solar radiation heat flux.

Evaporation. The rate of evaporation m_e (kg s^{-1} m^{-2}) is related to the evaporative heat flux Q_{ev} by

$$Q_{evap} = -m_e L_w S \quad (5)$$

where L_w is the water latent heat (J kg^{-1}). The rate of evaporation from a water surface has been the object of numerous studies in the past.[17] However, the formulas expressing the rate of evaporation have been derived from experimental studies and most of them are too specific to the system studied to be applicable to a general model that will be suitable for ponds operated in different locations and climates.[17] In an alternative theoretical approach based on the application of the Buckingham theorem,[5] the evaporation rate can be shown to depend on three dimensionless numbers

$$\text{the Sherwood number}: \quad Sh = \frac{KL}{D_{w,a}} \quad (6a)$$

$$\text{the Schmidt number}: \quad Sch = \frac{\nu_a}{D_{w,a}} \quad (6b)$$

$$\text{the Reynolds number}: \quad Re_L = \frac{Lv}{\nu_a} \quad (6c)$$

where K is the mass transfer coefficient (m s^{-1}), L is the characteristic pond length (m), $D_{w,a}$ is the mass diffusion coefficient of water vapor in air (m^2 s^{-1}), ν_a is the air kinematic viscosity (m^2 s^{-1}), and v is the wind velocity (m s^{-1}) at a given elevation from the pond surface. The Buckingham theorem links these three parameters as follows:

$$Sh_L = A(Re_L)^{\beta}(Sch)^{\delta} \quad (7)$$

where A, β, and δ are dimensionless coefficients that depend on the surface shape (e.g., cylindrical, horizontal, etc.) and on the nature of the flow (laminar or turbulent). For a horizontal surface, eq 7 becomes:[5]

$$Sh_L = 0.035(\mathrm{Re}_L)^{0.8}(Sch_L)^{1/3} \quad \text{for } Re_L > 5 \times 10^5 \text{ (turbulent flow)} \quad (8a)$$

$$Sh_L = 0.628(Re_L)^{0.5}(Sch_L)^{1/3} \quad \text{for } Re_L < 3 \times 10^5 \text{ (laminar flow)} \quad (8b)$$

The mass transfer coefficient K can be determined using eqs 8a and 8b, and the evaporation rate m_e is given by

$$m_e = K\left(\frac{P_w}{T_p} - \frac{\mathrm{RH} \times P_a}{T_a}\right)\frac{M_w}{R} \quad (9)$$

where T_a is the air temperature (K), P_a and P_w are the saturated vapor pressure (Pa) at T_a and T_p, RH is the relative humidity of the air over the pond surface, M_w is the molecular weight of water (kg mol^{-1}), and R the ideal gas constant (Pa m^3 mol^{-1} K^{-1}). P_a and P_w can be determined using[18]

$$P_i = 3385.5 \exp[-8.0929 + 0.97608(T_i + 42.607 - 273.15)^{0.5}] \quad (10)$$

There is no clear consensus in the literature on which elevation is most appropriate for quantifying the wind velocity used in the above application.[17] Eqs 8a and 8b were derived for situations when the wind is constant with respect to height prior to reaching the edge of a horizontal boundary. Thus, in this theoretical situation the value of wind velocity used in the Reynolds number (eq 6c) is assumed to be equal to this constant value. However, in the real world situation of an outdoor pond, the wind velocity varies with the height above the pond surface. Thus, in practical application the height at which the wind velocity was determined was equal to the boundary layer thickness where the wind velocity is not retarded by surface drag. The height δ_L at which the wind velocity was determined can be calculated as:[19]

$$\delta_L = L(0.381{Re_L}^{-1/5} - 10256{Re_L}^{-1}) \quad (11)$$

In the case of the pond used for validation in the present study, the boundary layer height was estimated to be around half a meter above the pond surface, a value well within the 0.3−2.0 m range proposed by ref 17. Interestingly, when the wind velocity was determined at this elevation, eq 9 predicted almost exactly the same amount of evaporation as the experimental formula derived to predict evaporation from small lakes,[8] which gave further confidence to this approach.

If wind data is not available at the boundary layer height, a power law can be used to determine the wind velocity v at a height z knowing the wind velocity v_0 at a height z_0

$$v(z) = v_0\left(\frac{z}{z_0}\right)^{\alpha} \quad (12)$$

where α is the power law exponent and is a function of obstructions surrounding the pond (e.g., trees, buildings, etc.[20]).

Convection. As heat transfer and mass transfer obey to the same laws, the convective heat flux Q_{conv} can be expressed in a similar manner to the evaporative heat flux. Application of the Buckingham theorem to convection at the pond surface thus yields three dimensionless numbers:[5]

the Nusselt number :

$$Nu_L = \frac{h_{conv}L}{\lambda_a} \quad \text{(analogous to the Sherwood number)} \quad (13a)$$

the Prandtl number :

$$Pr = \frac{\nu_a}{\alpha_a} \quad \text{(analogous to the Schmidt number)} \quad (13b)$$

$$\text{the Reynolds number :} \quad Re_L = \frac{Lv}{\nu_a} \quad (13c)$$

where h_{conv} is the convection coefficient (W m^{-2} K^{-1}), λ_a is the air thermal conductivity (W m^{-1} K^{-1}), and α_a is the air thermal diffusivity (m^2 s^{-1}). As convection and evaporation obey to the same law, the relationship between these three numbers uses the same coefficients A, β, and δ:

$$Nu_L = 0.035(Re_L)^{0.8}(Pr)^{1/3} \quad \text{for } Re_L > 5 \times 10^5 \text{ (turbulent flow)} \quad (14a)$$

$$Nu_L = 0.628(Re_L)^{0.5}(Pr)^{1/3} \quad \text{for } Re_L < 3 \times 10^5 \text{ (laminar flow)} \quad (14b)$$

The convective flux Q_{conv} is given by

$$Q_{conv} = h_{conv}(T_a - T_p)S \quad (15)$$

Conduction. An expression of the conductive heat flux between the pond bottom and the soil beneath it originates from Fourier's law

$$Q_{cond} = k_s S\frac{dT_s}{dz}(z = 0) \quad (16)$$

where k_s is the soil thermal conductivity (W m^{-1} K^{-1}), T_s is the soil temperature (K), and z is the depth (m). To determine the gradient of temperature in the soil under the pond, the soil temperature profile has to be determined by solving the heat equation in the soil beneath the pond, assuming the soil temperature T_s is a function of the depth z and the time t:

$$C_{p_s}\rho_s\frac{dT_s}{dt}(z,t) = k_s\frac{d^2T_s}{dz^2}(z,t) \quad (17)$$

where C_{p_s} is the soil specific heat capacity (J K^{-1} kg^{-1}) and ρ_s is the soil density (kg m^{-3}). The thermal characteristics of several types of soil are found in ref 21.

Table 1. Constants and Parameter Values for the Pond in New Zealand and Input Variables[a]

symbol	definition	unit	value
	Water Constants		
ρ_w	water density	kg m^{-3}	998
C_{p_w}	water heat capacity	J kg^{-1} K^{-1}	4.18 × 10^3
L_w	water latent heat	J kg^{-1}	2.45 × 10^6
ε_w	water emissivity	–	0.97
M_w	water molecular weight	kg mol^{-1}	0.018
	Soil Constants		
k_s	**soil thermal conductivity**	**W m^{-1} K^{-1}**	**1.7**
C_{p_s}	**soil specific heat capacity**	**J kg^{-1} K^{-1}**	**1.25 × 10^3**
ρ_s	**soil density**	**kg m^{-3}**	**1.9 × 10^3**
$T_{s,ref}$	soil temperature at $l_{s,ref}$	°C	13.6
	Air Constants		
ε_a	**air emissivity**	–	**0.8**
ν_a	air kinematics viscosity	m^2 s^{-1}	1.5 × 10^{-5}
λ_a	air thermal conductivity	W m^{-1} K^{-1}	2.6 × 10^{-2}
Pr_a	air Prandtl number	–	0.7
ρ_a	air density	kg m^{-3}	1.2
α_a	air thermal diffusivity	m^2 s^{-1}	2.2 × 10^{-5}
$D_{w,a}$	mass diffusion coefficient of water vapor in air	m^2 s^{-1}	2.4 × 10^{-5}
	Pond constants		
V	pond volume	m^3	8.1
S	pond surface	m^2	31.8
z	**wind velocity height**	**m**	**0.5**
z_0	wind sensor height	m	10
q_i	inflow rate	m^3 s^{-1}	1.5 × 10^{-5}
f_a	**algal absorption fraction**	**%**	**2.5**
L	pond characteristic length	m	10
α	**power law exponent**	**-**	**0.29**
φ	site latitude	deg	−37.9°
	Universal Constants		
σ	Stephan−Boltzmann constant	W m^{-2} K^{-4}	5.67 × 10^{-8}
R	ideal gas constant	Pa m^3 mol^{-1} K^{-1}	8.314
	Input Variables		
T_a	**air temperature**	**°C**	
H_s	**solar irradiance**	**W m^{-2}**	
RH	**relative humidity**	–	
v	**wind velocity**	**m s^{-1}**	
q_r	**rain waterflow**	**m^3 m^{-2} s^{-1}**	

[a] The most uncertain parameters are written in bold characters and were tested in a sensitivity analysis (Figure 3).

The first boundary condition is given by the fact that the temperature at the surface of the soil (at $z = 0$) is equal to the water temperature in the pond (see Supporting Information, S4). The second boundary condition is given by the value of the soil temperature $T_{s,ref}$ at the depth $l_{s,ref}$, where $l_{s,ref}$ is the depth at which the soil temperature is constant over the year. $T_{s,ref}$ is generally assumed to equal the annual average temperature and $l_{s,ref}$ can be estimated with the eq 18[5]:

$$l_{s,\,ref} = 4400(\alpha_s)^{1/2} \tag{18}$$

where α_s is the soil thermal diffusivity (m^2 s^{-1}). Initially, the temperature profile is assumed to be linear, which yields the following set of initial and boundary conditions (Supporting Information, S4):

$$T_s(t, z = 0) = T_p(t) \tag{19a}$$

$$T_s(t, z = l_{s,\,ref}) = T_{s,\,ref} \tag{19b}$$

$$\frac{d^2 T_s}{dz^2}(t = 0) = 0 \tag{19c}$$

Solving the heat equation (eq 17) yields the soil temperature profile $T_s(z,t)$ and therefore the value of the soil temperature gradient under the pond (at $z = 0$).

Inflow Heat flux. The heat flux associated with the water inflow (q_i, $m^3\ s^{-1}$) can be expressed as

$$Q_i = \rho_w C p_w q_i (T_i - T_p) \quad (20)$$

assuming that the water inflow is at temperature T_i and that the outflow is at temperature T_p.

Rain Heat Flux. Rainwater is assumed to be at air temperature. The heat flux Q_r from the rainwater flow (q_r, $m^3\ m^{-2}\ s^{-1}$) can be expressed as

$$Q_r = \rho_w C p_w q_r (T_a - T_p) S \quad (21)$$

Computations and Methods for Results Analysis. The equations described in the model section were computationally integrated in time using MATLAB software (The MathWorks, Natick, MA). A first-order forward Euler algorithm was used with a 1 s time step. A first-order Euler scheme in time and a second-order scheme in space (with a 1 cm length step) were used to solve the heat equation in the soil (eq 17). As an initial value, the pond temperature was set at the experimental temperature measured at midnight at the first day of simulation. Meteorological data were interpolated linearly between the data points. Experimental data were available over nearly an entire year (February 1, 2008 to January 30, 2009). A total of 20 days were excluded from the data set because no pond temperature data was collected (e.g., pond temperature value was 0 for several days, etc.). The details on the data set selection are given in the Supporting Information (S5). The inflow temperature was taken equal to the soil temperature $T_{s,ref}$.

Three criteria were used to define the accuracy of the model: (i) the average error in the estimation of the afternoon peak temperature (absolute value, over the 345 days considered), (ii) the average error in the estimation of the predawn minimum temperature (absolute value, over the 345 days considered), and (iii) the average error in the estimation of the temperature prediction between the afternoon peak and predawn minimum (absolute value, over the 345 days considered) (Supporting Information, S6).

To assess the accuracy of the new universal model compared to nine prior models published in the literature, the alternative expressions of heat fluxes used in the prior models were systematically substituted into the new universal model and evaluated against the experimental data. Because the expressions of pond radiation, air radiation, and the heat flux associated with the water inflow were identical in all the prior models (Supporting Information, S7), this evaluation was limited to considering

(i) one expression for the solar radiation based on a theoretically based calculation of solar irradiance,
(ii) four expressions of the evaporative and convective heat fluxes (these fluxes were considered together because they rely on the same fundamental laws), and
(iii) a simple expression of the conductive flux.

Furthermore, the effect of neglecting the conductive and rainwater fluxes on temperature prediction accuracy was evaluated. A detailed rationale and description of the heat flux expressions selected for comparison can be found in the Supporting Information (S8).

Finally, because various input parameters cannot be determined with a high level of accuracy, a sensitivity analysis was undertaken to quantify their impact on the temperature prediction. The input parameters which were identified as requiring investigation were

(1) the air emissivity, ε_a, which is a function of several meteorological parameters (air temperature, relative humidity, different atmospheric gas concentrations, etc) and thus cannot be tightly defined;[22]
(2) the soil thermal characteristics (k_s and α_s), which are only defined for specific types of soil and there can be a wide range of thermal behaviors between different soil types;[21]
(3) the power law exponent (α), which is a function of the environment (trees, buildings, etc.) and so is a subjective coefficient;[20]
(4) the height z at which the wind velocity must be measured; as discussed in the modeling section, z is not clearly defined in the literature and has a range between 0.3 and 2 m;[17] and
(5) the photosynthetic efficiency (f_a), which varies depending on the cultivation conditions such as light intensity, temperature, etc.

The upper and lower extremes of all the above input parameters were tested in the new universal model, and their influence on the temperature prediction accuracy was quantified. Uncertainty from weather data was also evaluated by varying the solar irradiance, wind velocity, and relative humidity by ±10% and the air temperature by ±1 °C. Table 1 lists the parameters used in the new universal model.

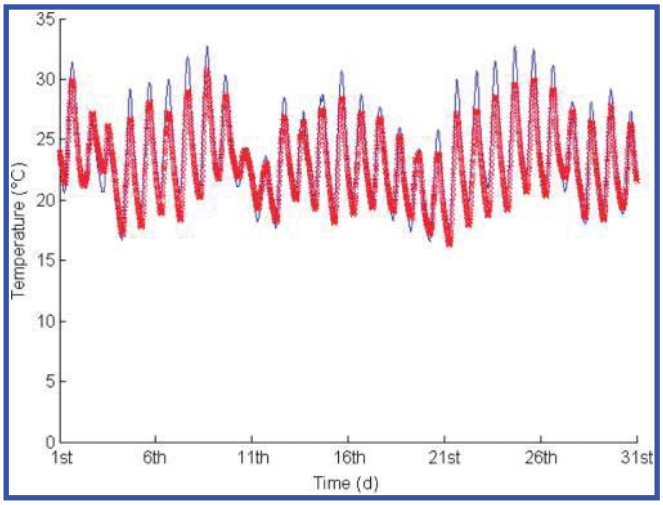

Figure 1. Predicted (blue line) and measured (red crosses) temperature profiles in the high rate algal pond over the month of January 2009.

RESULTS AND DISCUSSION

Model Accuracy. The ability of the new universal model to predict the temperature of the high rate algal pond was determined on the basis of 33 221 data points representing a year of operation. Figure 1 illustrates the excellent fit between the experimental and predicted temperature profiles for the month of January 2009 with all other months shown in the Supporting Information (S5). The average errors in the estimation of the afternoon peak and predawn minimum temperatures were both 1.3 °C, and the average error in the temperature difference between the afternoon peak and predawn minimum was 1.2 °C. The model had a tendency to slightly overestimate daily peak temperature and underestimate temperature during the winter

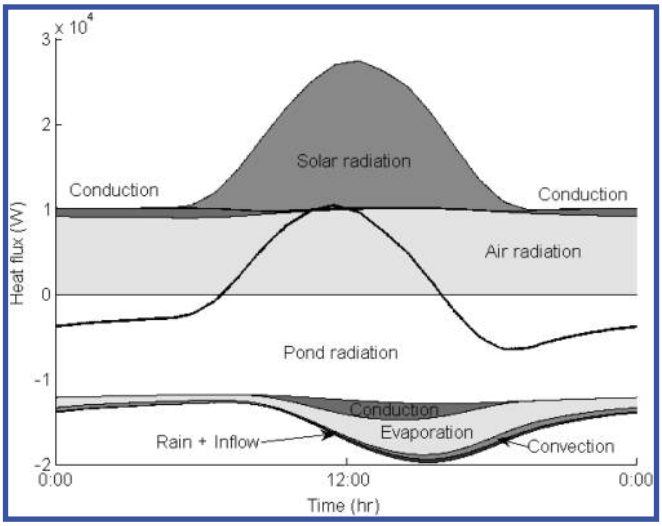

Figure 2. Changes in heat fluxes (annual average) reaching the high rate algal pond. The thick plain line represents the total heat flux. The value of each heat flux at time t was computed as the average of the heat flux over the year at this time.

months (Supporting Information, S5). Two possible explanations for these trends are (1) that air emissivity was assumed to be constant through time, although it is actually a function of meteorological parameters,[22] and (2) the impact of the paddle wheel on shading and evaporation in the pilot-scale pond used for validation was neglected (see Supporting Information, S5, for further explanations). While it is possible to improve the fit of the prediction for the pond located in New Zealand by adjusting key input parameters, this was not attempted because this study aimed to develop a universal model for temperature prediction rather a model optimized for a specific location.

Figure 2 shows that, on a yearly basis, the air radiation and pond radiation generally compensate each other. The pond radiation is proportional to the pond temperature to the fourth, while the air radiation is proportional to the air temperature to the fourth (eqs 2 and 4). As the pond and air temperatures generally differed by less than 10 °C, their values in kelvin are relatively similar, and the two heat fluxes tend to balance themselves. Therefore, solar radiation was mainly responsible for temperature raise at daytime, whereas conduction and evaporation were the main contributors to cooling at dusk. These different contributions may explain why the model was slightly less accurate during winter (Supporting Information, S5) because there is less uncertainty on the prediction of the solar heat flux than other heat fluxes.

Comparison with Other Temperature Models. In order to assess the relative accuracy of the new universal model, alternative heat flux expressions used in nine prior models were systematically substituted into the new universal model and evaluated against the experimental data. Full details are found in the Supporting Information (S8). The average errors in the estimations of the new universal model are compared against the average errors in the estimations of the prior models in Table 2. The errors in the estimated temperatures for the afternoon peak and predawn minimum increased from 1.3 to 2.1 and 3.2 °C respectively, while the error in the temperature difference between the afternoon peak and predawn minimum increased from 1.2 to 2.9 °C.

As previously discussed, the expressions for pond radiation, air radiation, and the heat flux associated with the inflow used in the new universal model have been used in prior models. With regard to the other five heat fluxes our analysis showed the following.

(1) Solar radiation represented 35% of the heat gain in average over the year (Figure 2) and therefore made a high contribution to the overall accuracy. A net improvement in accuracy was therefore obtained by using on-site irradiance data as opposed to an estimate based on cloud cover data (Table 2).
(2) The evaporative heat flux represented up to 22% of the total heat loss (Figure 2). Consequently, modeling convection and evaporation using expressions empirically derived from different systems (e.g., mechanically agitated ponds) significantly reduced accuracy (Table 2).
(3) Conduction was of low importance in the total heat balance (Figure 2). Therefore, assuming the ground temperature to be a linear function of soil depth or even neglecting the conductive heat flux had minor impacts on accuracy (Table 2).
(4) The heat flux associated with rain was minimal (Figure 2) and could be neglected from the model with little loss of accuracy (Table 1).

Sensitivity Analysis. A sensitivity analysis was conducted in order to assess the relative significance of uncertainties in the input parameters, the results of which are presented in Figure 3. Uncertainty regarding the air emissivity (ε_a) generated the greatest variation in the overall temperature prediction. This variation is due to the predominance of the air radiation in the heat balance (more than 60% of the heat gain on average; Figure 2). Uncertainties from other physical parameters and meteorological data tested were of minor importance affecting accuracy by less than 0.5 °C. Because the uncertainty with the air emissivity can cause the temperature prediction to vary by more than 1 °C, it is unlikely that the accuracy of the new universal model could be further improved.

Temperature Prediction Accuracy and Algal Productivity. As discussed in the Introduction, evaluating the economical feasibility and sustainability of processes incorporating shallow algal ponds requires the ability to predict the productivity of these systems and their environmental impact. For example, Richmond et al.[25] showed heating a *Spirulina* culture in the morning increased productivity in a raceway pond by 20%. Furthermore, Zhang et al.[2] achieved a 50% increase in productivity by maintaining temperature in its optimal range (37−43 °C) during *Chlorella sorokiniana* outdoor cultivation instead of letting the temperature fluctuate with the ambient temperature (20−44 °C). As shown in Figure 4, on a daily time scale the prior models regularly exhibited inaccuracies of more than 5 °C. In particular, predicting solar irradiance theoretically[23] caused a significant overestimation of the solar heat flux and the pond temperature (Figure 4). Reversely, determining the evaporative and convective heat fluxes using the empirical expressions from Talati et al.[9] caused an overestimation of the heat losses and therefore an underestimation of pond temperature. Because it is generally accepted that the growth rate of microalgae doubles when temperature increases by 10 °C within a certain range (e.g., 10−30 °C for most commercial algal species[24]), this error of 5 °C could therefore translate into a productivity prediction inaccuracy of approximately 40%.

Temperature Prediction Accuracy and Rate of Water Evaporation. In addition to the need to predict temperature

Table 2. Accuracy of Temperature and Water Evaporation (Annual Average) Using Models Constructed by Replacing Selected Heat Fluxes with Alternative Expressions Used in Prior Models[a]

heat flux	expression (ref)	E_{day} (°C)	E_{night} (°C)	E_{inter} (°C)	evaporation (mm d^{-1})
solar radiation	theoretical (23)	1.8	1.7	1.5	2.6
evaporation/convection	(7)	2.8	2.9	2.9	1.3
	(8)	2.5	2.4	2.6	2.0
	(9)	2.6	2.6	2.5	2.8
	(10)	3.4	4.5	4.1	4.6
conduction	simple	1.7	1.7	1.5	2.3
	neglected	1.8	1.7	1.5	2.3
rain	neglected	1.4	1.3	1.2	2.2
new universal model	see Modeling Approach	1.3	1.3	1.2	2.2

[a] The alternative expressions for each heat flux are detailed in the Supporting Information (S8). E_{day} is the average error in the estimation of the afternoon peak temperature, E_{night} is the average error in the estimation of the pre-dawn minimum temperature and E_{inter} the average error in the temperature difference between the afternoon peak and predawn minimum (Supporting Information, S6).

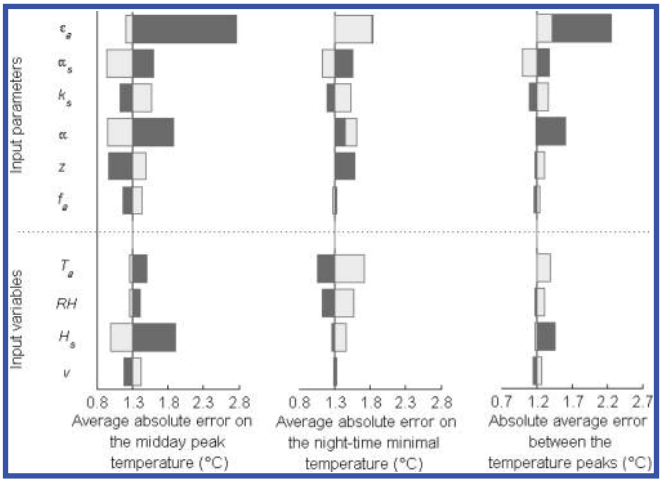

Figure 3. Sensitivity analysis on input parameters and input variables. The dark bars represent the level of accuracy for the maximum value of the parameter and the light bars the level of accuracy for the minimum value of the parameter [air emissivity (ε_a), 0.75−0.95; soil diffusivity (α_s), 10^{-7}−10^{-5} m^2 s^{-1}; soil conductivity (k_s), 0.2−4 W m^{-1} K^{-1}; power law exponent (α), 0.15−0.43; wind velocity height, 0.3−2 m; photosynthetic efficiency (f_a), 0−0.05; air temperature (T_a), ±1 °C; relative humidity (RH), ±10%; solar irradiance (H_s), ±10%; wind velocity (v), ±10%].

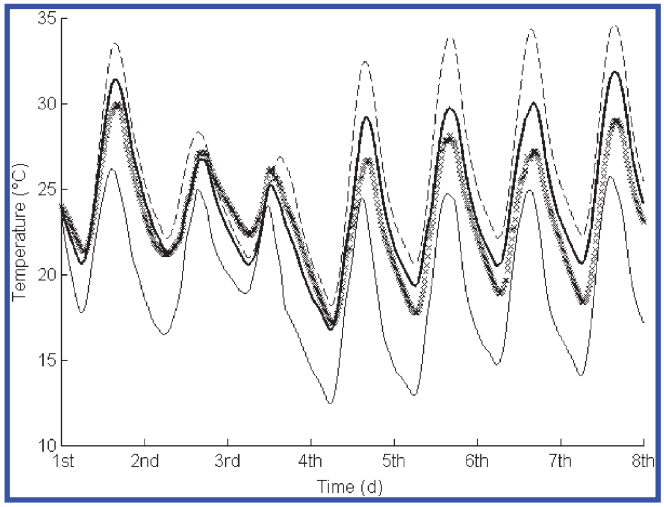

Figure 4. Predicted and measured temperature profiles in the high rate algal pond over the first week of January 2009 (crosses, experimental data; thick solid line, prediction by the new universal model; dashed line, prediction when a theoretical expression is used to determine the solar irradiance instead of on-site data;[23] thin solid line, prediction by the model when the expressions for convective and evaporative heat fluxes are taken from ref 9.

to estimate productivity, accurate temperature prediction is also required to estimate evaporative water loss. When using alternative heat flux expressions used in prior models, the predicted rate of evaporation from the high rate algal pond varied from 1.3 to 4.6 mm d^{-1} (Table 2). Under the temperate climatic conditions of Hamilton, New Zealand, the estimated annual average algal production was 220 kg (dry wt) (19 g m^{-2} d^{-1}) based on the amount of direct solar radiation reaching the pond (considering a photosynthetic efficiency of 2.5% and *Chlorella* biomass heat value of 20 kJ g^{-1} [26]). Thus, depending on the rate of water evaporation predicted by alternative heat flux expressions used in prior models, the estimate of the blue water footprint of the cultivation system varies from 70 to 240 L of water/kg of dry algal biomass. This variation of 300% is obviously problematic if an accurate estimation of the water evaporation losses is required at a high temporal resolution. Improved accuracy would be even more crucial for shallow algal ponds operated in semiarid or arid areas with limited freshwater resources.

In conclusion, the new universal model presented in this paper was validated with a high degree of accuracy with the average error at the afternoon peak and predawn minimum being just 1.3 °C, while the error between the afternoon peak and the predawn minimum was only 1.2 °C. This new universal model is valid for any opaque water body with a uniform temperature profile. Properly accounting for the evaporation appears to be the key to the new universal model and confirms that a theoretical approach is the most relevant to predict the rate of evaporation.[17] The inaccuracy on the temperature prediction introduced by the use of alternative heat flux expressions described in the literature could lead one to overestimate or underestimate algal productivity and the rate of water evaporation by approximately 40% and 300%, respectively.

■ ASSOCIATED CONTENT

Supporting Information. S1, schematic representation of the pond and heat fluxes considered in the heat balance; S2, significance of the solar radiation reflected on the water surface compared with the solar irradiance reaching the pond surface; S3, estimation of the air emissivity; S4, boundary condition of the heat equation in the soil layer under the pond; S5, data selection to determine the accuracy and month-by-month temperature profiles; S6, definition of the criteria for model accuracy; S7, prior temperature models published in the literature for ponds and similar systems; S8, alternative expressions from prior models for the solar heat flux, the evaporative and convective heat fluxes and the conductive heat flux. This material is available free of charge via the Internet at http://pubs.acs.org.

■ AUTHOR INFORMATION

Corresponding Author
*Telephone: +64 6 350 5841; fax: +64 6 350 5604; e-mail B.J.Guieysse@massey.ac.nz.

■ ACKNOWLEDGMENT

Q.B. is supported by a Massey University Doctoral Scholarship. We would like to acknowledge Dr. Marie-Laurence Giorgi (Ecole Centrale Paris, France) for very valuable discussions on thermal heat transfers. The high rate algae pond construction and operation were funded by New Zealand government funded research grant.

■ REFERENCES

(1) Raven, J. A.; Geider, R. J. Temperature and algal growth. *New Phytol.* **1988**, *110* (4), 441–461.

(2) Zhang, K.; Kurano, N.; Miyachi, S. Outdoor culture of a cyanobacterium with a vertical flat plate photobioreactor: Effects on productivity of the reactor orientation, distance setting between the plates, and culture temperature. *Appl. Microbiol. Biotechnol.* **1999**, *52*, 781–786.

(3) Torzillo, G.; Pushparaj, B.; Bocci, F.; Balloni, W.; Materassi, R.; Florenzano, G. Production of *Spirulina* biomass in closed photobioreactors. *Biomass* **1986**, *11*, 61–74.

(4) Vonshak, A.; Torzillo, G.; Masojidek, J.; Boussiba, S. Sub-optimal morning temperature induces photoinhibition in dense outdoor cultures of the alga *Monodus subterraneus* (Eustigmatophyta). *Plant Cell Environ.* **2001**, *24*, 1113–1118.

(5) Taine, J.; Iacona, E.; Petit, J. P. *Transferts Thermiques—Introduction aux Transferts d'Energie*, 4th ed; Dunod: Paris, 2008.

(6) Gerbens-Leenes, W.; Hoekstraa, A. Y.; van der Meerb, T. H. The water footprint of bioenergy. *Proc. Natl. Acad. Sci.U. S. A.* **2009**, *106* (25), 10219–10223.

(7) Losordo, T. M.; Piedrahita, R. H. Modelling temperature variation and thermal stratification in shallow aquaculture ponds. *Ecol. Modell.* **1991**, *54*, 189–226.

(8) Klemetson, S. L; Rogers, G. L. Aquaculture pond temperature modelling. *Aquac. Eng.* **1985**, *4*, 191–208.

(9) Talati, S. N.; Stenstrom, M. K. Aeration-basin heat loss. *J. Environ. Eng.* **1990**, *116* (1), 70–86.

(10) Ali, H. H. A. Passive cooling of water at night in uninsulated open tank in hot arid areas. *Energy Convers. Manag.* **2007**, *48*, 93–100.

(11) Park, J. B. K.; Craggs, R. J. Wastewater treatment and algal production in high rate algal ponds with carbon dioxide addition. *Wat. Sci. Technol.* **2010**, *61*, 633–639.

(12) New-Zealand National Institute of Water and Atmospheric Research Web site, http://www.niwa.co.nz/education-and-training/schools/resources/climate.

(13) Andersen, R. A., Ed. *Algal Culturing Techniques*; Elsevier Academic Press: Amsterdam, 2005.

(14) Hase, R.; Oiakawa, H.; Sasa, C.; Morita, M.; Watanabe, Y. Photosynthetic production of microalgal biomass in a raceway system under greenhouse conditions in Sendai City. *J. Biosci. Bioeng.* **2000**, *89* (2), 157–163.

(15) Howell, J. R; Siegel, R. *Thermal Radiation Heat Transfer*, 4th ed; Taylor & Francis: New York, 2004.

(16) Béchet, Q.; Shilton, A.; Fringer, O. B.; Muñoz, R.; Guieysse, B. Mechanistic modeling of broth temperature in outdoor photobioreactors. *Environ. Sci. Technol.* **2010**, *44*, 2197–2203.

(17) Sartori, E. A critical review on equations employed for the calculation of the evaporation rate from free water surfaces. *Sol. Energy* **2000**, *68* (1), 77–89.

(18) Tang, R.; Etzion, Y. Comparative studies of the water evaporation rate from a wetted surface and that from a free water surface. *Build. Environ.* **2004**, *39*, 77–86.

(19) Holman, J. P. *Heat Transfer*, 10th ed.; MacGraw Hill Higher Education: Boston, 2010.

(20) Gipe, P. *Wind Power—Renewable Energy for Home, Farm, and Business*; Chelsea Green Publishing Co.: White River Junction, VT, 2004.

(21) Miller, D. H., Ed. *Energy at the Surface of the Earth—An Introduction to the Energetics of Ecosystems*; Academic Press: New York, 1981.

(22) Culf, A. D.; Gash, J. H. C. Longwave radiation from clear skies in Niger: a comparison of observations with simple formulas. *J. Appl. Meteor.* **1993**, *32*, 539–547.

(23) Fritz, J. J.; Meredith, D. D.; Middleton, A. C. Non-steady state bulk temperature determination for stabilization ponds. *Water Res.* **1979**, *14*, 413–420.

(24) Davison, I. R. Environmental effects on algal photosynthesis: Temperature. *J. Phycol.* **1991**, *27*, 2–8.

(25) Richmond, A.; Lichtenberg, E.; Stahl, B.; Vonshak, A. Quantitative assessment of the major limitations on productivity of *Spirulina platensis* in open raceways. *J. Appl. Phycol.* **1990**, *2*, 195–206.

(26) Illman, A. M.; Scragg, A. H.; Shales, S. W. Increase in *Chlorella* strains calorific values when grown in low nitrogen medium. *Enzym. Microb. Technol.* **2000**, *27*, 631–635.

Supporting information

ES&T manuscript es-2010-040706

Title: Universal temperature model for shallow algal ponds provides improved accuracy

Authors: Quentin Béchet, Andy Shilton, Jason B. K. Park, Rupert J. Craggs, Benoit Guieysse

S1 - Schematic representation of the pond and heat fluxes considered in the heat balance

S2 - Significance of the solar radiation reflected on the water surface compared with the solar irradiance reaching the pond surface

S3 - Estimation of the air emissivity

S4 - Boundary condition of the heat equation in the soil layer under the pond

S5 - Data selection to determine the accuracy and month-by-month temperature profiles

S6 - Definition of the criteria for model accuracy

S7 - Prior temperature models published in the literature for ponds and similar systems

S8 - Alternative expressions from prior models for the solar heat flux, the evaporative and convective heat fluxes and the conductive heat flux

19 Figures

4 Tables

24 Pages

S1 – Schematic representation of the pond and heat fluxes considered in the heat balance

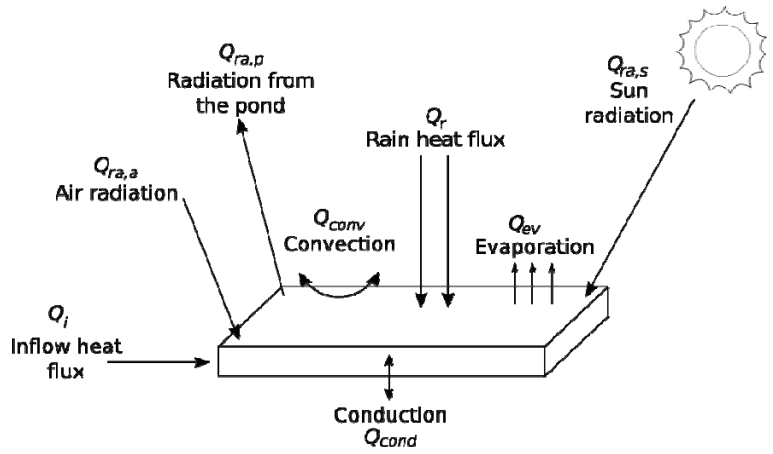

Figure S1-S1 – Schematic representation of the pond and heat fluxes considered in the heat balance

S2 – Significance of the solar radiation reflected on the water surface compared with the solar irradiance reaching the pond surface.

The purpose of this study is to determine the fraction of solar radiation reaching the pond surface that is reflected on the water surface. According to the Fresnel equations (S2-1), the reflectance of a flat water surface is a function of the radiation incident angle as shown by the equation:

$$r_p = \frac{\left(n_{air}\cos\left(\theta_i\right) - n_{water}\cos\left(\theta_t\right)\right)^2 + \left(n_{air}\cos\left(\theta_t\right) - n_{water}\cos\left(\theta_i\right)\right)^2}{2\left(n_{air}\cos\left(\theta_i\right) + n_{water}\cos\left(\theta_t\right)\right)} \quad \text{(S2-1)}$$

, where n_{air} and n_{water} are the air and water refractive index (generally taken equal to 1 and 1.33 at 25°C for visible radiation, respectively (S2-2), and θ_i and θ_t the angles of incident and transmitted radiation, respectively (Figure S2-S1).

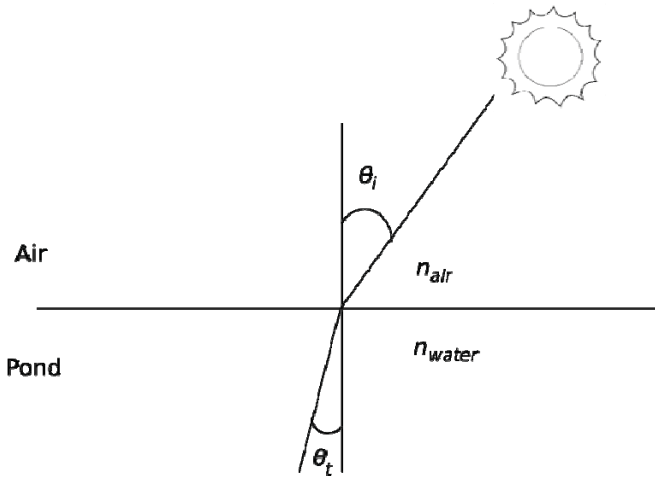

Figure S2-S1: Reflection of a beam of light onto a water surface

Figure S2-S2 shows that most of the radiation reaching the water surface with an incident angle lower than 70 ° is not reflected. As the highest solar irradiance values are recorded in the middle of the day, when the radiation incident angle θ_i between the sun and a vertical axis is small, the fraction of the solar radiation which is reflected by the water surface is small compared with the total solar radiation reaching the ground surface.

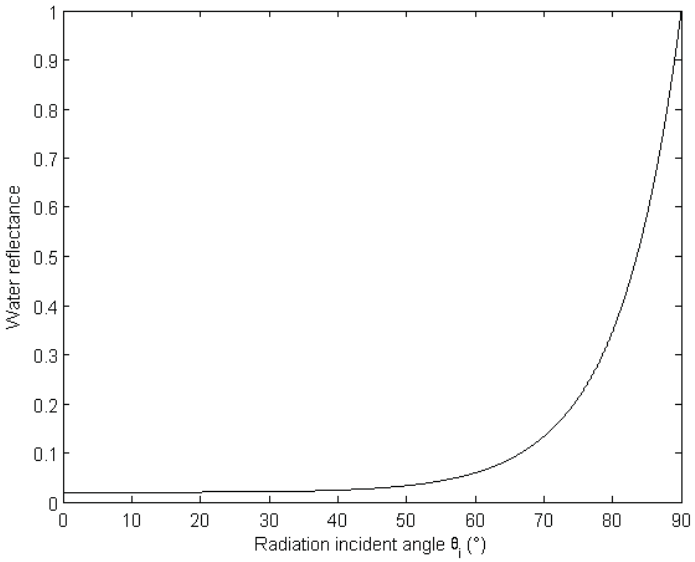

Figure S2-S2: Water reflectance as a function of the radiation incident angle.

Another reason for not considering the partial reflection of the solar radiation onto the water surface was that this would have required knowing the respective fractions of diffuse and direct components in the solar radiation, on which there is a high degree of uncertainty (S2-2). Indeed, as the reflectivity of the water surface is a function of the radiation incident angle, the diffuse and the direct components of the solar radiation are not reflected in the same proportion on the water surface.

References for S2

S2-1. Bass, M.; Enoch, J.M; Decusatis, C.; Lakshminarayanan, V.; Li, G.; MacDonald, C.; Mahajan, V.N.; Van Stryland, E. Handbook of Optics: geometrical and physical optics, polarized light, components and instruments. 3rd, ed; McGraw-Hill, **2010**.

S2-2. Duffie J. A.; Beckman W.A. Solar engineering of thermal processes. 3rd, ed; Wiley, Hoboken, NJ, **2006**.

S3 - Estimation of the air emissivity

In the literature, the air emissivity ε_a (also called atmospheric coefficient) is generally taken equal to an arbitrary value between 0.75 and 0.95 (S3-1). Instead, (S3-2) proposes approach to calculate a value for ε_a where air is assumed as a grey diffuse body either totally transparent (its emissivity is 0) or totally opaque (its emissivity is 1) depending on the wavelength of the radiation. The emissivity of the air over the radiation wavelength is plotted in Figure S3-S1.

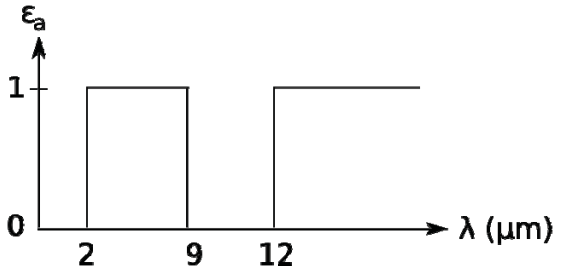

Figure S3-S1: Emissivity of the air over the radiation wavelength

The radiation flux from the air $Q_{ra,air}$ is given by the formula:

$$Q_{ra,air} = \int_0^{\infty} \varepsilon_a(\lambda) L_\lambda^0(T_a) \pi d\lambda \quad \text{(S3-1)}$$

Where T_a is the air temperature and $L_\lambda{}^0(T_a)$ is the luminance of a black body at equilibrium at the temperature T_a. Using the spectral distribution given by Figure S3-1, equation S3-1 becomes:

$$Q_{ra,air} = \int_2^{9} L_\lambda^0(T_a) \pi d\lambda + \int_{12}^{\infty} L_\lambda^0(T_a) \pi d\lambda \quad \text{(S3-2)}$$

As the emission spectrum of a black body is given by the Plank function (S3-2), it is possible to calculate the previous integral, using a "*Z* function" (S3-2) defined as:

$$Z(0,\frac{\lambda_0}{\lambda_m(T)}) = \frac{\int_0^{\lambda_0} L_\lambda^0(T)\pi d\lambda}{\sigma T^4},\ \lambda_m(T)T = 2898\mu mK \quad \text{(S3-3)}$$

This yields:

$$Q_{ra,air} = \sigma T_a^4 \left(Z\left(0,\frac{9}{\lambda_m(T_a)}\right) - Z\left(0,\frac{2}{\lambda_m(T_a)}\right) + 1 - Z\left(0,\frac{12}{\lambda_m(T_a)}\right)\right) \quad \text{(S3-4)}$$

Table S3-S1 presents the results obtained for ε_a at different air temperatures T_a.

Table S3-S1: Air emissivity at different temperatures

T_a (K)	280	290	300	310	320
ε_a	0.813	0.807	0.802	0.798	0.795

In the model, a value of 0.8 was taken for the air emissivity.

References for S3

S3-1. Talati, S. N.; Stenstrom, M. K. Aeration-basin heat loss. *J. Environ. Eng.* **1990**, *116* (1), 70-86.

S3-2. Taine, J.; Iacona, E.; Petit, J. P. Transferts thermiques – Introduction aux transferts d'énergie. 4th, ed; Dunod, Paris, **2008**.

S4 - Boundary condition of the heat equation in the soil layer under the pond

In the soil under the pond, assuming that the soil is homogeneous and that the soil temperature T_s is a function of the depth (z) and the time (t), the equation followed by the soil temperature is:

$$\frac{\partial T_s}{\partial t} = \alpha_s \frac{\partial^2 T_s}{\partial z^2} \quad \text{(S4-1)}$$

where T_s is the soil temperature (K) and α_s the soil thermal diffusivity ($m^2\ s^{-1}$). Solving this equation requires one initial condition (giving the temperature profile at $t=0$) and two boundary conditions. The initial condition is given by assuming a linear temperature profile at $t=0$:

$$\frac{\partial^2 T_s}{\partial z^2}(z, t=0) = 0 \quad \text{(S4-2a)}$$

The first boundary condition is obtained by considering that below a certain depth $l_{s,ref}$ under the soil surface, the soil temperature is no longer affected by variations in the surface temperature and becomes constant over time. This dept $l_{s,ref}$ is given by (S4-1):

$$l_{s,ref} = 4400(\alpha_s)^{1/2} \quad \text{(S4-2b)}$$

This yields the first boundary condition:

$$T_s(z = l_{s,ref}) = T_{s,ref} \quad \text{(S4-2c)}$$

where $T_{s,ref}$ is taken equal to the average of the air temperature over the year (K).

The second boundary layer is given by the continuity of the heat flux at the interfacial surface between the soil and the pond water (see Figure S4-S1). This continuity translates into the equation:

$$k_s \frac{\partial T_s}{\partial z}(z = 0) = h_{w,s}(T_i - T_w) \quad \text{(S4-2d)}$$

, where k_s is the soil thermal conductivity (W m^{-1} K^{-1}), $h_{w,s}$ is the convective coefficient between the pond water and the soil horizontal surface (W m^{-2} K^{-1}) and T_i the temperature (K) at the separation surface ($z=0$).

Unfortunately, there is no simple way to solve equation (S4-1) with this set of initial and boundary conditions. Indeed, the variable T_i introduced by equation (S4-2d) is an unknown. However, in the case that the conductive flux from the soil is slow compared to the convective flux between the water and the soil, the interface temperature T_i can be taken equal to the water temperature. For example, when the soil is warmer than the pond water, the soil gives heat to the water. As water flows over the interfacial surface between the pond and the soil, the heat given by the soil is taken away from the interfacial surface by water. If this flow is "strong enough", the interfacial surface is cooled down instantaneously and the interfacial surface temperature can be taken equal to the water temperature.

To compare the intensities of the convective and conductive fluxes, two characteristic times (for convection and conduction) need to be computed and compared.

First, the characteristic time for convection is:

$$\tau_{conv} = \frac{\rho_s Cp_s dz}{h_{w,s}} \quad \text{(S4-3)}$$

where ρ_s is the soil density (kg m^{-3}), Cp_s the soil specific heat capacity (J kg^{-1} K^{-1}) and dz a specific length (m). To calculate $h_{w,s}$, [S4-2] proposes the following formula:

$$h_{w,s} = 0.027\,\mathrm{Re}_L^{\,4/5}\,\mathrm{Pr}^{1/3} \quad \text{(S4-4)}$$

Taking thermal characteristics of water at 25°C:

$$\tau_{conv} \cong 0.95\,\mathrm{s} \quad \text{(S4-5)}$$

The characteristic time for the conductive flux between the soil and the water is given by:

$$\tau_{cond} = \frac{dz^2}{\alpha_s} \quad \text{(S4-6)}$$

When the soil thermal characteristics are taken equal to the clay characteristics, this yields:

$$\tau_{cond} \cong 140s \quad \text{(S4-7)}$$

Consequently, the conduction is slow compared to the convection and we can assume that the temperature of the interfacial surface is equal to the water temperature.

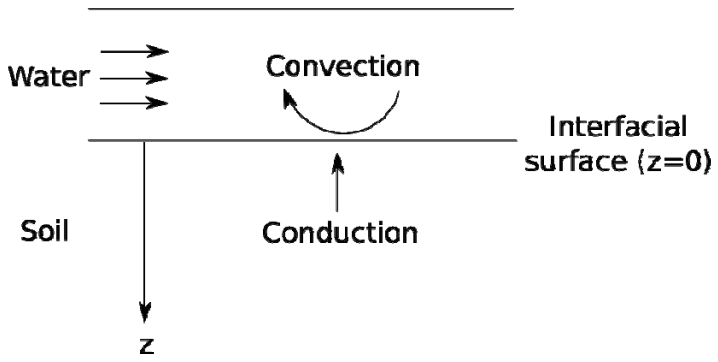

Figure S4-S1: Heat fluxes considered at the bottom of the pond

References for S4

S4-1. Miller, D. H. Energy at the surface of the Earth – An introduction to the energetics of ecosystems. Academic Press, Inc., New-York, **1981**.

S4-2. Taine, J.; Iacona, E.; Petit, J. P. Transferts thermiques – Introduction aux transferts d'énergie. 4th, ed; Dunod, Paris, **2008**.

S5 – Data selection to determine the accuracy and month-by-month temperature profiles

Table S5-S1 summarized the days withdrawn from the initial data set for the calculation of the model accuracy. Figures S5-S1 to S5-S12 show the profiles of the measured and predicted temperature month by month (red crosses: experimental temperature; blue line: predicted temperature). Figure S5-S13 shows the predicted temperature versus the temperature data.

Table S5-S1: Data exclusion for the model accuracy calculation and reasons for its exclusion

Month	Days withdrawn	Reason for withdrawal
February 2008	1st-9th	The pond temperature followed the air temperature (the temperature sensor was likely out of the water)
March 2008	15th, 16th	The pond temperature followed the air temperature (the temperature sensor was likely out of the water)
May 2008	4th, 5th, 6th	The pond temperature exhibited rapid changes of several degrees over a time of 15 minutes
October 2008	20th, 21st, 22nd	Erroneous data (T = 0°C)
November 2008	1st, 2nd	Erroneous data (T = 0°C)

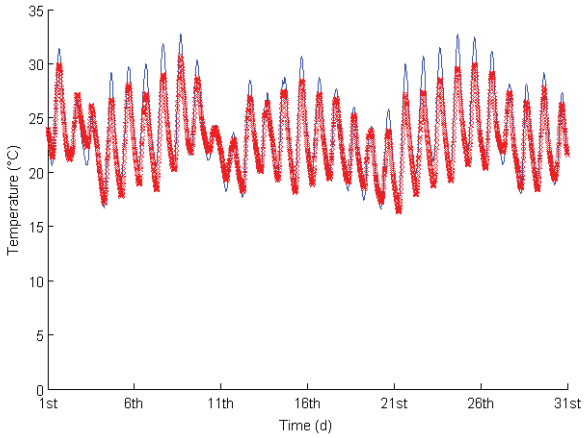

Figure S5-S1: Experimental and measured pond temperature profiles in January 2009

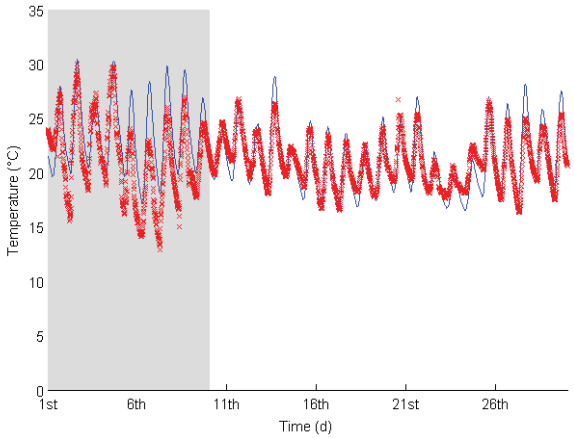

Figure S5-S2: Experimental and measured pond temperature profiles in February 2008

(Shaded area represents the excluded data)

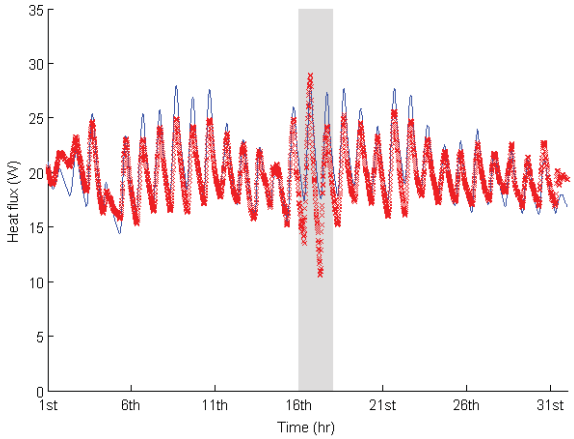

Figure S5-S3: Experimental and measured pond temperature profiles in March 2008 (Shaded area represents the excluded data)

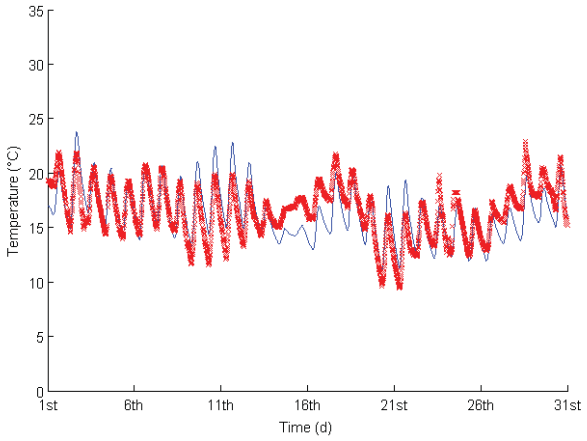

Figure S5-S4: Experimental and measured pond temperature profiles in April 2008

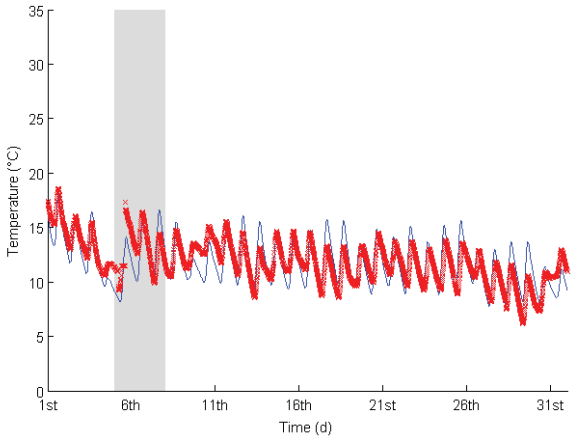

Figure S5-S5: Experimental and measured pond temperature profiles in May 2008 (Shaded area represents the excluded data)

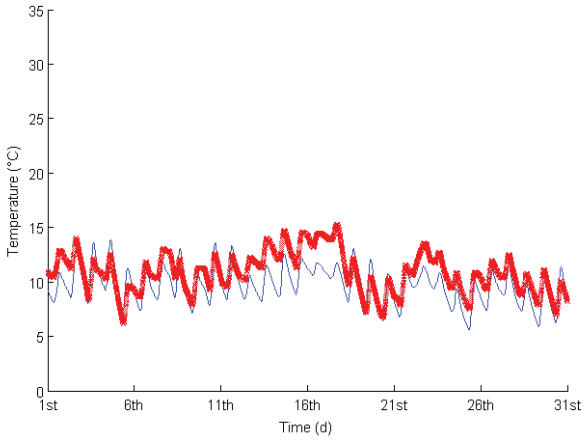

Figure S5-S6: Experimental and measured pond temperature profiles in June 2008

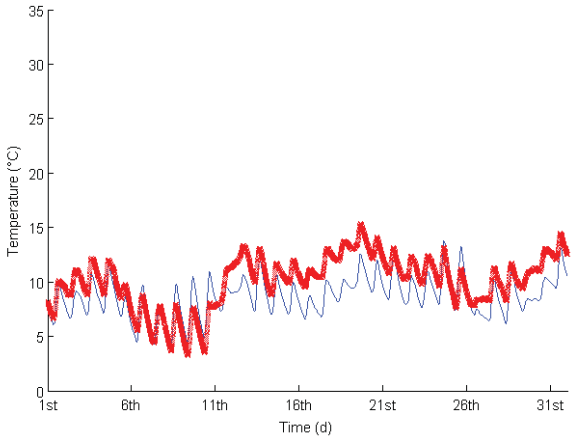

Figure S5-S7: Experimental and measured pond temperature profiles in July 2008

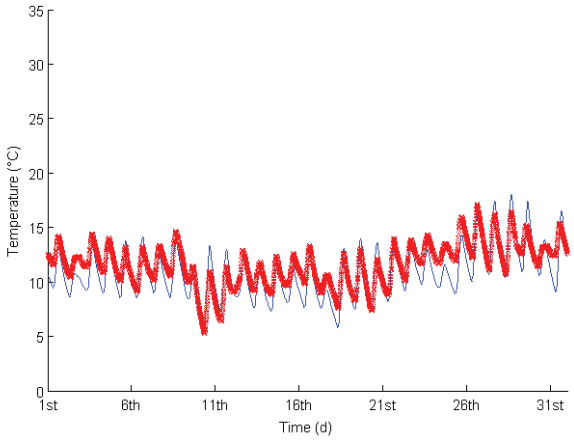

Figure S5-S8: Experimental and measured pond temperature profiles in August 2008

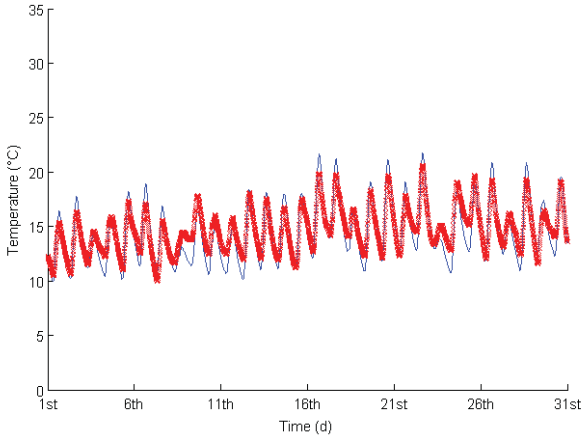

Figure S5-S9: Experimental and measured pond temperature profiles in September 2008

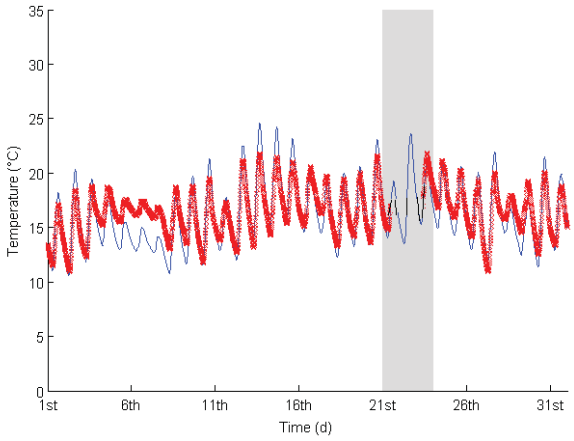

Figure S5-S10: Experimental and measured pond temperature profiles in October 2008

(Shaded area represents the excluded data)

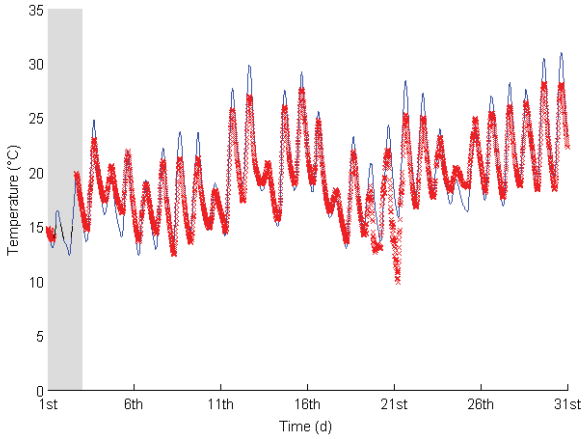

Figure S5-S11: Experimental and measured pond temperature profiles in November 2008

(Shaded area represents the excluded data)

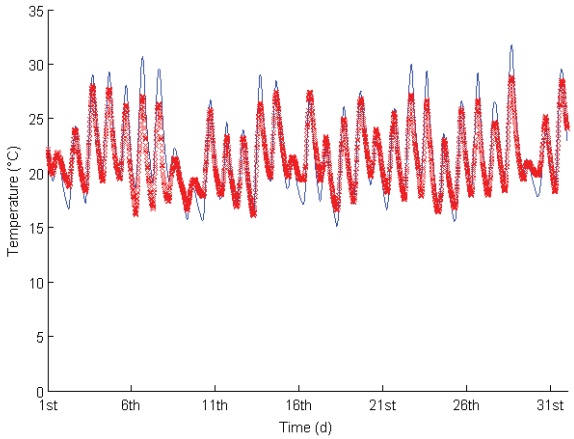

Figure S5-S12: Experimental and measured pond temperature profiles in December 2008

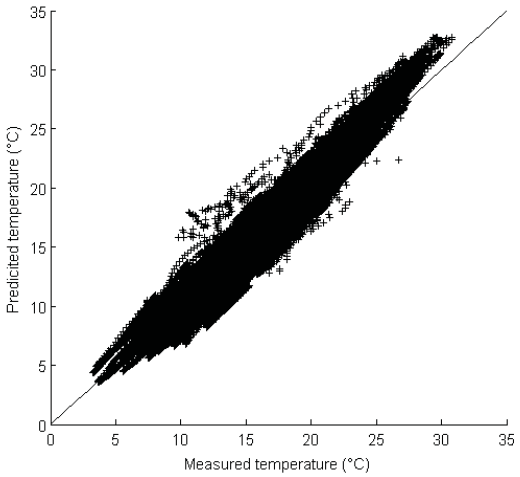

Figure S5-S13: Predicted temperature versus measured temperature (N = 33,221).

Explanation for the overestimation of the peak temperature

In net value, the model overestimated the daily peak temperature by 0.5 °C in average over the year. This trend could be explained by two assumptions in the modeling approach:

- Air emissivity was assumed to be constant in the model although it is actually a function of meteorological parameters (S5-1). Our sensitivity analysis showed uncertainty on ε_a impacted temperature prediction. Inputting a value of 0.75 for ε_a was found to minimize the error on the afternoon peak temperature (data not shown) but the theoretical value of 0.80 (as derived in S3) was preferred to keep the modeling approach as universal as possible.
- The effect of the paddle wheel was neglected. However, the paddle wheel theoretically reduces the pond surface exposed to sunrays by shadowing the pond and enhances evaporation by increasing the exchange surface between the pond and the air. Because of scalability issues, the paddle wheel area (4 m^2) was significant in regards to the pond area at the pilot facilities used to provide experimental data. However, the relative surface area and impacts of the paddle wheel should be negligible at full scale.

Uncertainty on the fraction of radiation converted into chemical energy was unlikely to be the cause for the systematic overestimation of the daily peak temperature: As shown by the sensitivity analysis, the uncertainty on the fraction of sunlight converted into biochemical energy through photosynthetic process cannot explain an uncertainty on temperature prediction by more than 0.2 °C. The photosynthetic efficiency is also more likely to decrease at peak hour due to light and temperature inhibition.

Finally, the overestimation cannot be explained by the assumption that the culture broth is a grey body. Because the fraction of incoming radiation absorbed by chlorophyll is a function of the radiation wavelength, considering a single algae cell as a grey body would be erroneous. However, in the case of a mixed dense culture, light is going through a cell population which behaves as a grey body and it is acceptable to assume that all the sunlight is absorbed by the cells. Thus, regardless the wavelength of the radiation, the cell density is assumed to be high enough to absorb all the light reaching the broth. A fraction of this sunlight is converted into chemical energy through the photosynthetic process (value of 2.5 % set in our study) but most of sunlight reaching the broth is converted into heat (in our case 97.5 %).

Explanation for the poor fit in winter (June-July-August)

Figures S5-S6 to S5-S8 suggests the model predicted temperature with a lower level of accuracy during winter than during summer. The solar heat flux could represent more than 50 % of the daily heat gain in summer compare to less than 10 % in winter. As the expression of the solar heat flux is relatively simple and depends on the solar irradiance as sole input variable, there is less uncertainty on the prediction of the solar heat flux than other heat fluxes

such as the evaporative heat flux (which depends on wind velocity, air temperature, relative humidity). Consequently, temperature prediction is expected to be better in summer where the solar heat flux is predominant than in winter when other fluxes become more significant.

Reference for S5

S5-1: Culf, A. D.; Gash, J. H. C. Longwave radiation from clear skies in Niger: a comparison of observations with simple formulas. *J. Appl. Meteor*. **1993**, *32*, 539-547.

S6 – Definition of the criteria for model accuracy

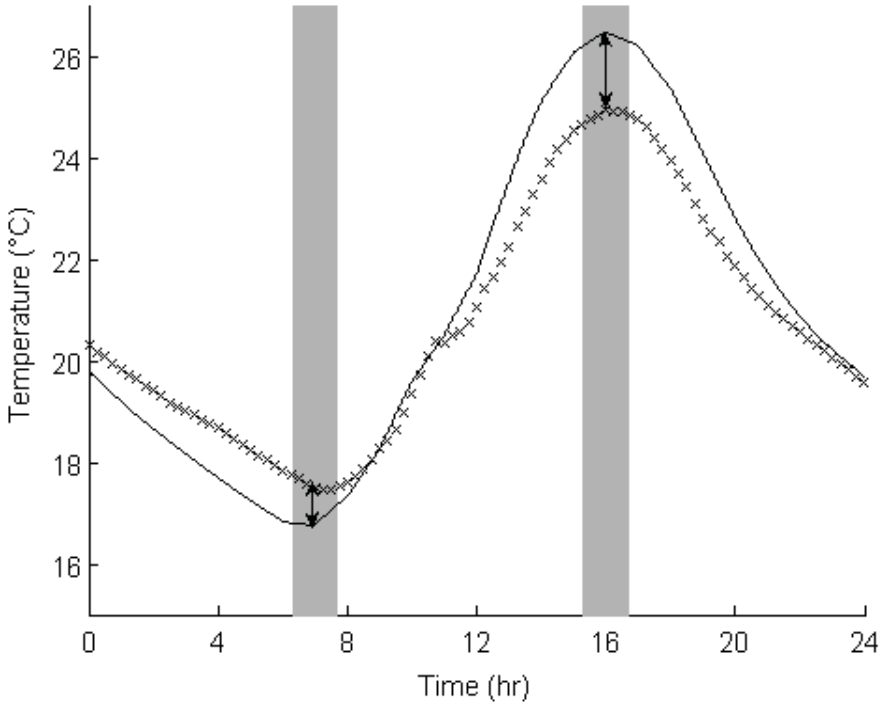

Figure S6-S1: Temperature profile over one day (plain line: predicted temperature; crosses: measured temperature). The arrows represent the errors on the afternoon peak temperature and the pre-dawn minimum temperature. The non-shaded area represent the period of the day considered for the estimation of the error between the two temperature peaks (22 hours).

ed in the literature for ponds and similar systems

g the temperature in systems similar to shallow ponds (**Theo.**: Theoretically modeled; **Emp.**: expression derived from

Neg.: neglected; **From H_s** means that the solar heat flux is calculated from the solar irradiance data).

	Solar rad.	Pond rad.	Air rad.	Conv.	Evap.	Cond.	Inflow	Comments	Reference
	Theo.	Theo.	Theo.	*	*	Theo.	NA		(S7-1)
	Theo.	Theo.	Theo.	Emp.	Emp.	Neg.	Theo.		(S7-2)
	From H_s	Theo.	Theo.	Emp.	Emp.	Theo.	NA	Stratification considered.	(S7-3)
ment pond,	Theo.	Theo.	Theo.	Emp.	Emp.	Theo.	Theo.	+ Aeration considered	(S7-4) (S7-5) (S7-6) (S7-7) (S7-8)
	From H_s	Theo.	Theo	Emp.	Emp.	Neg.	NA		(S7-9)
	NA	Theo.	Theo.	Theo.	Emp.	NA	NA		(S7-10)
	From H_s	Theo.	Theo.	Emp.	Emp.	Neg.	Theo.		(S7-11)
	From H_s	Theo.	Theo	Emp.	Emp.	Theo.	NA	Stratification considered	(S7-12)
	Theo.	Theo.	Theo.	Emp.	Emp.	NA	NA		(S7-13)

n of the heat flux expressions)

References for S7

S7-1: Sodha, M. S.; Singh, U.; Srivastava, A.; Tiwari, G. N. Experimental validation of thermal model of open roof pond. *Build. Env.* **1981**, *16*(2), 93-98.

S7-2: Fritz, J.J.; Meredith, D. D.; Middleton, A. C. Non-steady state bulk temperature determination for stabilization ponds. *Water Reas.* **1979**, *14*, 413-420.

S7-3: Losordo, T. M.; Piedrahita R. H. Modelling temperature and thermal stratification in shallow aquaculture ponds. *Ecol. Model.* **1991**, *54*: 189-226.

S7-4: Talati, S. N.; Strenstrom, M. K. Aeration-basin heat loss. *J. Environ. Eng.* **1990**, *116*(1): 70-86.

S7-5: Scherfig, J.; Schleisner, L.; Brønd, S.; Kilde, N. Dynamic temperature changes in wastewater treatment plants. *Water Environ. Res.* **1996**, *68*(2), 143-150.

S7-6: Sedory, P. E.; Strestrom, M. K. Dynamic prediction of wastewater aeration basin temperature. *J. Environ. Eng.*, **1995,** *121*(9), 609-618.

S7-7: Makinia, J.; Wells, S. A; Zima, P. Temperature modeling in activated sludge systems: a case study. *Water Environ. Res.* **2005**, *77*(5), 525-532.

S7-8: Lin, S. H. A heat transfer model for biological wastewater treatment system. *Heat Mass Transfer*, **1997**, *32*, 313-316.

S7-9: Klemetson, S. L.; Rogers, G. L. Aquaculture pond temperature modeling. *Aquac. Eng.* **1985**, *4*, 191-208.

S7-10: Ali, A. H. H. Passive cooling of water in uninsulated open tank in hot arid areas. *Energy Conv. Manag.* **2007**, *48*, 93-100.

S7-11: Krant, J.; Motzkin, F.; Gordin, H. Modelling temperatures and salinities of mixed seawater fish ponds. *Aquac.* **1982**, *27*: 377-388.

S7-12: Culberson, S. D.; Piedrahita, R. H. Aquaculture pond ecosystem model: temperature and dissolved oxygen prediction – mechanism and application. *Ecol. Model.* **1996**, *89*: 231-258.

S7-13: Thackston, E. L.; Parker, F. L. Geographical influence on cooling ponds. *J. Water Pollut. Control. Fed.* **1972,** *44*(7), 1334-1351.

S8 - Alternative expressions used in prior models for the solar heat flux, the evaporative and convective heat fluxes and the conductive heat flux

S8.1. Solar heat flux: Predicting the solar irradiance from the cloud cover data as a single input

The model described by [S8-1] was used to predict the solar irradiance form the cloud cover data (temperature modeling in stabilization ponds). The following expressions derive from theoretical considerations and empirical relationships.

The solar intensity H_s reaching the ground surface is:

$$H_s = \frac{I_{sc}}{r^2} cos\,\theta_z A_t^m (1 - 0.65CC^2) \quad \text{(S8-1)}$$

, where I_{sc} is the solar constant (taken in this study equal to 1393 W m^{-2}), r the normalized radius of the Earth orbit, θ_z is the solar angle (the determination of θ_z is described in S2), A_t is the atmospheric transmission coefficient, m is the optical air mass (m), and CC is the cloud cover (expressed in tenths).

The normalized radius of the Earth orbit r is given by:

$$r = 1.0 + 0.017 \cos\left(\frac{2\pi}{365}(186 - N)\right) \quad \text{(S8-2)}$$

, where N is the day number (N = 1 on the first of January).

The optical air mass m can be determined from the following expression:

$$m = \frac{1}{\sin(\cos\vartheta_z) + a(\arcsin(\cos\vartheta_z) + b)^{-c}} \left(\frac{288 - 0.0065z}{288}\right)^{5.256} \quad \text{(S8-3)}$$

, where a = 0.15, b = 3.885, c = 1.253 and z is the site altitude (m).

Finally, the atmospheric transmission coefficient A_t is given by:

$$A_t = 0.0685\cos\left(\frac{2\pi}{365}\left(N+10\right)\right)+0.80 \qquad \text{(S8-4)}$$

S8.2. Evaporative and convective heat fluxes: alternative expressions

Different expressions for the convective and evaporative heat fluxes at the top surface of a water body can be found in the literature. This section aims to present in details some of these models. It has to be noted that the models presented in this section are only examples of formulas which can be found in the literature. Four expressions of the evaporative and convective heat fluxes from four different sources were considered together because evaporation and convection rely on the same fundamental laws. The expressions of the evaporative and convective heat fluxes substituted to our universal expressions in our comparative analysis are summarized in Table S8-1.

or convective/evaporative heat fluxes

Evaporative flux (W m^{-2})	Convective flux (W m^{-2})
$(0.2253 + 0.24644 v_{0.55})(P_w - RHP_a)^{0.82}$	$0.075(\frac{k_a}{L})(\frac{v_{0.55} L}{\nu_a})^{0.8} \mathrm{Pr}_a^{0.33}(T_w - T_a)$
$1.1.10^{-8} L_w(1 + 0.22 v_{8.2})(P_w - RHP_a)$	$5.68(0.8 + 0.27 v_{8.2})(T_w - T_a)$
$0.038 v_2(P_w - RHP_a)$	$1.57 v_2(T_w - T_a)$
$4.8.10^{-5}\left[1.15.10^6(1 - RH) + 6.86.10^4(T_w - T_a)\right] \times e^{0.0604(T_a - 273)} S^{-0.05} v_t$	$1.9.10^{-2} \rho_a Cp_a(T_w - T_a) S^{-0.05} v_t$

vel i (in m) above the ground surface. v_t is the wind speed at "tree-top level", taken at 6m in this study.

S8. 3. Conductive heat flux: simplification

Models of temperature in similar systems (aquaculture ponds, lakes, wastewater treatment ponds, etc) generally assume that the conductive flux can be modeled in a simpler manner by assuming that the temperature profile in the ground is a linear function of the depth *z*. In other words, the expression of the gradient of temperature in the soil is taken constant and equal to:

$$-k_s \frac{dT_s}{dt}(z=0) = -k_s \frac{T_{s,ref} - T_p}{l_{s,ref}} \quad \text{(S8-5)}$$

This leads to express the conductive flux Q_{conv} as:

$$Q_{conv} = -k_s \frac{T_{s,ref} - T_p}{l_{s,ref}} S \quad \text{(S8-6)}$$

References for S8

S8-1. Fritz, J. J.; Meredith, D. D.; Middleton, A. C. Non-steady state bulk temperature determination for stabilization ponds. *Water Res.* **1979**, *14*, 413-420.

S8-2. Ali, H. H. A. Passive cooling of water at night in uninsulated open tank in hot arid areas. *Energy Convers. Manag.* **2007**, *48*, 93-100; DOI: 10.1016/j.enconman.2006.05.012

S8-3. Klemetson, S. L; Rogers, G. L. Aquaculture pond temperature modelling. *Aquac. Eng.* **1985**, *4*, 191-208.

S8-4. Losordo, T. M.; Piedrahita, R. H. Modelling temperature variation and thermal stratification in shallow aquaculture ponds. *Ecol. Modell.* **1991**, *54*, 189-226.

S8-5. Talati, S. N.; Stenstrom, M. K. Aeration-basin heat loss. *J. Environ. Eng.* **1990**, *116* (1), 70-86.

Article 3

MASSEY UNIVERSITY
GRADUATE RESEARCH SCHOOL

STATEMENT OF CONTRIBUTION TO DOCTORAL THESIS CONTAINING PUBLICATIONS

(To appear at the end of each thesis chapter/section/appendix submitted as an article/paper or collected as an appendix at the end of the thesis)

We, the candidate and the candidate's Principal Supervisor, certify that all co-authors have consented to their work being included in the thesis and they have accepted the candidate's contribution as indicated below in the *Statement of Originality*.

Name of Candidate: Quentin Béchet

Name/Title of Principal Supervisor: Prof Benoit Guieysse

Name of Published Research Output and full reference:

Béchet Q, Shilton A, Fringer OB, Muñoz R, Guieysse B. 2010. Mechanistic modeling of broth temperature in outdoor photobioreactors. Environ Sci Technol 44 (6): 2197-2203.

In which Chapter is the Published Work: 3

Please indicate either:

- The percentage of the Published Work that was contributed by the candidate:

  and / or

- Describe the contribution that the candidate has made to the Published Work:

  Q Béchet was the main contributor to the article. He constructed and numerically implemented the temperature model. He also collected the experimental data used for model validation.

Quentin Béchet
Digitally signed by Quentin Béchet
DN: cn=Quentin Béchet, o=Massey University, ou=SEAT, email=q.bechet@massey.ac.nz, c=NZ
Date: 2014.02.17 18:49:56 +13'00'

Candidate's Signature

17/02/2014
Date

Benoit Guieysse
Digitally signed by Benoit Guieysse
DN: cn=Benoit Guieysse, o=Massey University, ou=SEAT, email=b.j.guieysse@massey.ac.nz, c=NZ
Date: 2014.02.24 11:17:49 +13'00'

Principal Supervisor's signature

24/02/2014
Date

Environ. Sci. Technol. **2010,** *44,* 2197–2203

Mechanistic Modeling of Broth Temperature in Outdoor Photobioreactors

QUENTIN BÉCHET,[†] ANDY SHILTON,[†] OLIVER B. FRINGER,[‡] RAUL MUÑOZ,[∥] AND BENOIT GUIEYSSE*[,†,§]

School of Engineering and Advanced Technology, Massey University, Private Bag 11 222, Palmerston North 4442, New Zealand, Environmental Fluid Mechanics Laboratory, Stanford University, Stanford, California 94305-4020, School of Civil and Environmental Engineering, Nanyang Technological University, Singapore 639798, Singapore, and Department of Chemical Engineering and Environmental Technology, Valladolid University, Paseo del Prado de la Magdalena, s/n, Valladolid, Spain

Received October 21, 2009. Revised manuscript received January 23, 2010. Accepted February 3, 2010.

This study presents the first mechanistic model describing broth temperature in column photobioreactors as a function of static (location, reactor geometry) and dynamic (light irradiance, air temperature, wind velocity) parameters. Based on a heat balance on the liquid phase the model predicted temperature in a pneumatically agitated column photobioreactor (1 m^2 illuminated area, 0.19 m internal diameter, 50 L gas-free cultivation broth) operated outdoor in Singapore to an accuracy of 2.4 °C at the 95% confidence interval over the entire data set used (104 measurements from 7 different batches). Solar radiation (0 to 200 W) and air convection (−30 to 50 W) were the main contributors to broth temperature change. The model predicted broth temperature above 40 °C will be reached during summer months in the same photobioreactor operated in California, a value well over the maximum temperature tolerated by most commercial algae species. Accordingly, 18 000 and 5500 GJ $year^{-1}$ ha^{-1} of heat energy must be removed to maintain broth temperature at or below 25 and 35 °C, respectively, assuming a reactor density of one reactor per square meter. Clearly, the significant issue of temperature control must be addressed when evaluating the technical feasibility, costs, and sustainability of large-scale algae production.

Introduction

Despite the considerable investment made in algae biofuel research in recent years (*1*), the feasibility and sustainability of full-scale mass algae cultivation remain highly debated because of significant biological limitations and scaling-up issues (*2*–*7*). Processes for algae cultivation are normally classified as photobioreactors or open ponds (*8*–*10*). Typically, photobioreactors support higher photosynthetic efficiencies, and therefore biomass productivities, than ponds whereas open ponds are more economical to build and operate (*3, 8*). Because most of the sunlight reaching the culture is converted into heat, broth temperature can easily reach 40 °C in photobioreactors, a value well over the maximum temperature tolerated by most commercial algae species (*10*). In addition, each algae species operates at its maximum photosynthetic efficiency at an optimal temperature (*11*). Optimizing algal production would therefore require maintenance of broth temperature at its optimum value (*12*). Thus, to be able to predict algal productivity and process economics, we must understand how broth temperature is affected by environmental and process parameters.

This study presents the first fully mechanistic model describing broth temperature in column photobioreactor as a function of static (location, reactor geometry) and dynamic (light irradiance, air temperature, wind velocity) parameters. The model was validated against experimental broth temperature data from a pneumatically agitated column algal photobioreactor operated outdoor in Singapore. Broth temperature changes in a similar photobioreactor located in California were simulated to estimate the annual heat energy that must be removed to maintain the broth temperature below a certain value.

Materials and Methods

Modeling Approach. The photobioreactor broth was assumed completely mixed (all physical properties of the broth were considered uniform). In addition, as the algae dried weight (DW) and nutrient concentrations are generally very low (of the order of 1 g L^{-1}), every solution property (i.e., density, heat capacity, emissivity, etc.) was taken equal to that of water at standard temperature and pressure. For simplicity, every radiating body was considered as a gray-diffuse surface (e.g., its radiative properties do not depend on the wavelength or on the angle of the radiation).

The ground surface and the solution inside the reactor were considered opaque (absorptivity = emissivity). Considering the reactor broth as opaque restricts the model validity to light-limiting conditions. However, light-limited conditions would indeed be expected because (1) it is economically unsound to cultivate algae under nonlight-limiting conditions in large systems; and (2) light-limiting conditions occur at low algae densities in full scale photobioreactors (0.05 g DW/L in our system). The fraction of solar radiation used by algae to carry out photosynthesis (typically less than 4% of total solar radiation (*8*)) and microbial heat release (due to decay) were neglected in the heat balance. The wall surface was assumed to be a partly transparent gray-diffuse body and its transmittance τ was therefore defined as the ratio of the outgoing radiation over the incoming radiation. The fraction of radiation that does not penetrate the plastic wall was assumed reflected; there was therefore no absorption by the wall. Consequently, the emissivity of the wall was negligible and no radiation from the wall was considered. The reactor wall temperature was considered uniform and equal to the solution temperature because convection from the air to the plastic wall is negligible in comparison to the convection from the broth to the plastic wall. Other specific assumptions are described in the following section.

A heat balance analysis fo the liquid solution in the reactor (S1 in Supporting Information) yields

$$\rho_w V_r C p_w \frac{dT_r}{dt} = Q_{ra,r} + Q_{ra,d} + Q_{ra,D} + Q_{re,s} + Q_{ra,a} + Q_{re,a} + Q_{ra,g} + Q_c + Q_{ev} + Q_b + Q_{cond} \quad (1)$$

* Corresponding author phone: +64 6 350 5841; fax: +64 6 350 5604; e-mail: B.J.Guieysse@massey.ac.nz.
[†] Massey University.
[‡] Stanford University.
[∥] Valladolid University.
[§] Nanyang Technological University.

10.1021/es903214u © 2010 American Chemical Society
Published on Web 02/23/2010

where T_r is the reactor broth temperature (K); ρ_w and Cp_w are the density (kg m^{-3}) and the specific heat capacity (J kg^{-1} K^{-1}) of water, respectively; V_r *is* the volume of the broth (m^3); $Q_{ra,r}$ is the radiation from the reactor itself (W); $Q_{ra,D}$ is the direct solar radiation (W); $Q_{ra,d}$ is the diffuse solar radiation (W); $Q_{re,s}$ is the solar radiation reflected from the ground (W); $Q_{ra,a}$ is the radiation from the air surrounding the reactor (W); $Q_{re,a}$ is the air radiation reflected from the ground (W); $Q_{ra,g}$ is the radiation from the ground (W); Q_c is the convective flux (W); Q_{ev} is the evaporation flux (W); Q_b is heat flux into air bubbles (W); and Q_{cond} is the conductive flux with the ground surface at the base surface (W). In eq 1, the heat capacity of the plastic wall (in J K^{-1}) was neglected in the left-hand term because it is negligible compared with the heat capacity of the broth.

Radiation from the Reactor. As water radiates heat over the entire reactor surface, the radiation from the liquid phase based on the Stefan−Boltzmann's fourth power radiation law was expressed as (*13*)

$$Q_{ra,r} = -\sigma\tau\varepsilon_r(\pi R_r^2 + 2\pi R_r L_r) T_r^4 \tag{2}$$

where σ is the Stefan−Boltzmann constant (W m^{-2} K^{-4}); τ is the reactor wall transmittance (−); ε_r is the emissivity of the liquid phase (0.97 is used and is a common value for water); R_r is the reactor radius (m); L_r is the reactor height (water level, in m); and T_r is the reactor temperature (K).

Direct Solar Radiation. The heat flux arising from the direct solar radiation reaching the top of the reactor can be expressed as

$$Q_{ra,D,top} = \varepsilon_r\tau H_D\pi R_r^2 \tag{3}$$

where H_D (W m^{-2}) is the intensity of the direct solar radiation reaching the ground surface in the vertical direction.

The heat flux reaching the lateral surface of the water column $Q_{ra,D,lat}$ is

$$Q_{ra,D,lat} = \varepsilon_r\tau H_D \tan\theta_z 2R_r L_r \tag{4}$$

where θ_z (rad) is the angle between a vector normal to the ground surface and the sun direction (S2 in SI).

The total direct solar flux $Q_{ra,D}$ can then be expressed as

$$Q_{ra,D} = (Q_{ra,D,top} + Q_{ra,D,lat}) f(t) \tag{5}$$

where $f(t)$ is a "shading" function set to 0 when the reactor is not exposed to the Sun and set to 1 otherwise. This function is used when environmental elements (such as buildings, vegetation, etc.) hide the reactor from the sun rays during the day (different shading functions for different surfaces can be used if needed).

The angle between a vector normal to the ground surface and the sun direction, θ_z, is a function of the latitude φ (rad), the solar declination δ (rad) and the solar hour and is expressed as (*14*) (S3)

$$\cos(\theta_z) = \sin\varphi\sin\delta + \cos\varphi\cos\delta\cos\omega \tag{6}$$

where ω is the radial position of the reactor in a geocentric model (rad). ω varies linearly in time from $-\omega_s$ to ω_s ($-\omega_s$ at sunrise and ω_s at sunset), where

$$\cos\ \omega_s = -\tan\delta \times \tan\varphi \tag{7}$$

The solar declination can be calculated as function of the day of the year, N, as (*14*)

$$\delta = 23.35\frac{2\pi}{360}\sin\left(2\pi\frac{284 + N}{365}\right) \tag{8}$$

In most cases, including the present study, total solar irradiance (diffuse plus direct) H_g (W m^{-2}) reaching the ground surface in the vertical direction was experimentally measured. Therefore, the direct and diffuse solar irradiance at the ground level H_D and H_d (W m^{-2}) can be expressed as a function of H_g as

$$H_D = (1 - K_d) H_g \tag{9a}$$

and

$$H_d = K_d H_g \tag{9b}$$

Here, K_d (−) is the fraction of diffuse radiation reaching the ground surface. K_d typically ranges from 0.1 to 0.3 (*14*).

Diffuse Solar Radiation. Diffuse radiation is emitted equally in all space directions and is independent of θ_z. It can be expressed as

$$Q_{ra,d} = \tau\varepsilon_r(\pi R_r^2 + 2\pi R_r L_r) H_d \tag{10}$$

Reflected Solar Radiation. Because the ground surface is considered diffuse, it reflects direct and diffuse solar radiation homogeneously in every direction. The reflectivity of the ground r_g (−) can then be defined as the ratio of the reflected flux over the incoming flux. In addition, as the ground is considered opaque, radiation theory (*13*) gives

$$r_g = 1 - \varepsilon_g \tag{11}$$

where ε_g is the ground surface emissivity. Knowing that H_g is the intensity of the solar flux, the total intensity reflected by the ground integrated over all directions is

$$Q_{re,s,tot} = r_g H_g \tag{12}$$

The fraction of this flux reaching the lateral surface of the reactor can be expressed as

$$Q_{re,s} = \tau r_g \varepsilon_r H_g S_g \tag{13}$$

where $f_{g,lat}$ (−) is the form factor from this surface to the ground and S_g is the ground surface reflecting sunlight (m^2). Applying the form-factor theory gives (*13*)

$$S_g f_{g,lat} = S_{r,lat} f_{lat,g} \tag{14}$$

where $S_{r,lat}$ is the lateral surface of the reactor (m^2) and $f_{lat,g}$ the form factor from the lateral surface to the ground (−). Because the ground surface is assumed to be infinitely large, one-half of the lateral surface can be exposed and $f_{lat,g}$ equals one-half. This yields

$$Q_{re,s} = \tau(1 - \varepsilon_g)\varepsilon_r H_g \pi R_r L_r f(t) \tag{15}$$

Air Radiation. According to the Stefan−Boltzman's fourth power law, the radiative flux (in W m^{-2}) generated by air at a temperature of T_a (K) is given by

$$Q_a = \varepsilon_a \sigma T_a^4 \tag{16}$$

Air radiates on the top surface of the reactor (flux $Q_{ra,a,top}$, in W) and on its lateral surface (flux $Q_{ra,a,lat}$, in W). Using the form-factor theory, these fluxes can be expressed as (*13*)

$$Q_{ra,a,top} = \tau\varepsilon_r Q_a S_{a,top} f_{a,top} \tag{17a}$$

and

$$Q_{ra,a,lat} = \tau\varepsilon_r Q_a S_{a,lat} f_{a,lat} \tag{17b}$$

where $S_{a,top}$ and $S_{a,lat}$ are the air surfaces "seen" by the top surface and the lateral surface (m^2) and $f_{a,top}$ and $f_{a,lat}$ the corresponding form factors equal to one and one-half, respectively. Using the form factor theory, the final expression for the flux $Q_{ra,a}$ is expressed as:

$$Q_{ra,a} = \tau\varepsilon_r\varepsilon_a\sigma T_a^4(\pi R_r^2 + \pi R_r L_r) \tag{18}$$

Reflection of Air Radiation on the Ground Surface. Because the ground surface is exposed to air radiation and is assumed to be gray-diffuse with the reflectivity coefficient r_g, a fraction of the heat flux reaching the ground is reflected on the lateral surface of the reactor. The heat flux $Q_{a\text{-}g}$ (W) radiated from the air reaching the ground surface is

$$Q_{a-g} = \varepsilon_a \sigma T_a^4 S_g \tag{19}$$

where S_g is the ground surface considered (m^2). The fraction of this flux reflected onto the water column lateral surface is

$$Q_{re,a} = r_g Q_{a-g} f_{g,lat} \tag{20}$$

Again, from the form factor theory, this formula can be simplified as

$$Q_{re,a} = \tau \varepsilon_r r_g \varepsilon_a \sigma T_a^4 \pi R_r L_r \tag{21}$$

Radiation from the Ground. As ground surface is exposed to the sun and air radiation, its temperature T_g (K) can reach relatively high values and the ground can radiate back to its environment. The ground surface was assumed to be thin and at a uniform temperature T_g (S4). The fraction of ground radiation reaching the reactor lateral surface can be expressed as

$$Q_{ra,g} = \tau \varepsilon_r \varepsilon_g \sigma T_g^4 S_{g,lat} f_{g-lat} \tag{22}$$

Again, the form factor theory yields

$$Q_{ra,g} = \tau \varepsilon_r \varepsilon_g \sigma T_g^4 \pi L_r R_r \tag{23}$$

Convection. Assuming that the temperature of the air in the bubbles reaching the top surface is at the reactor temperature T_r, there is no convection at the top surface. Therefore, the convection flux Q_c (W) on the wall lateral surface is (*15*)

$$Q_c = h_{co,lat}(T_a - T_r) 2\pi R_r L_r \tag{24}$$

where $h_{co,lat}$ ($W \cdot m^{-2} \cdot K^{-1}$) is the convection coefficient between the lateral surface and the air. Natural (no wind) and forced (wind) convection must be considered. The coefficient for natural convection can be expressed as (*15*)

$$h_{co,lat} = \frac{\lambda_a}{L_r}\left(0.825 + \frac{0.387 \mathrm{Ra}_{Lr}^{1/6}}{\left(1 + \left(\frac{0.492}{\mathrm{Pr}}\right)^{9/16}\right)^{8/27}}\right)^2 \tag{25}$$

where Pr is the Prandtl number for air (0.7 at 25 °C), λ_a is the air thermal conductivity ($W\,m^{-1}\,K^{-1}$), and Ra_{Lr} is the Rayleigh number expressed for L_r (−) as:

$$\mathrm{Ra}_{Lr} = \frac{g|T_r - T_a|L_r^3}{a_a \nu_a T_a} \tag{26}$$

where g is the gravity constant ($m\,s^{-2}$); ν_a is the air kinematics viscosity ($m^2\,s^{-1}$) and a_a is the air diffusivity ($m^2\,s^{-1}$).

The convection coefficient for forced convection can be calculated as (*15*)

$$h_{co,lat} = \frac{\lambda_a}{2R_r}\left(0.3 + \frac{0.62 \mathrm{Re}_{2Rr}^{0.5} \mathrm{Pr}^{1/3}}{\left(1 + \left(\frac{0.4}{\mathrm{Pr}}\right)^{2/3}\right)^{1/4}}\right)\left(1 + \left(\frac{\mathrm{Re}_{2Rr}}{282,000}\right)^{5/8}\right)^{4/5} \tag{27}$$

where Re_{2Rr} is the Reynolds number (−) expressed for the diameter of the reactor as

$$\mathrm{Re}_{2Rr} = \frac{\rho_a 2R_r \nu_w}{\mu_a} \tag{28}$$

where ρ_a is the air density, ν_w is the wind velocity, and μ_a is the air viscosity.

Evaporation. In this model, we assume the air leaving the reactor is saturated in water and at the reactor temperature. There is therefore no evaporation at the top surface of the liquid and the evaporative flux Q_{ev} can be expressed as

$$Q_{ev} = -(1 - RH) X_a F_b L_w \tag{29}$$

where RH is the incoming (i.e., ambient) air relative humidity (unitless) X_a is the concentration of water in saturated air (kg water m^{-3} air), F_b is the bubble flow rate ($m^3 \cdot s^{-1}$), and L_w is the water latent heat content ($J\,kg^{-1}$).

Cooling by Air Bubbling. As previously mentioned, air bubbles were assumed to reach thermal equilibrium with water before they reach the reactor top surface. The heat flux induced by bubbles can then be expressed as

$$Q_b = -Cp_a(T_r - T_a)\rho_a F_b \tag{30}$$

where Cp_a is the air specific capacity ($J\,kg^{-1}\,K^{-1}$) and ρ_a is the air density ($kg\,m^{-3}$).

Conduction. Using Fourier's law, the conductive flux between the liquid phase and the ground can be expressed as

$$Q_{cond} = -k_{wall}\frac{T_r - T_g}{l_{wall}}\pi R_r^2 \tag{31}$$

where k_{wall} is the wall conductivity ($W\,m^{-1}\,K^{-1}$) and l_{wall} is the wall thickness (m).

Validation. Experimental broth temperature data for validation of the model were obtained from a parallel study on *Chlorella sorokiniana* productivity in a column photobioreactor conducted in Singapore. A transparent acrylic cylindrical tank (2 m height × 0.19 m diameter) containing 50 L of gas-free cultivation broth was used as the pilot column photobioreactor. CO_2-enriched air (2−3%) was continuously bubbled at a rate of approximately 1.2 L min^{-1}; the corresponding working (gas bubbles + liquid) and overall volumes (gas bubbles + liquid + headspace) being 51.0 and 56.7 L, respectively. A multiprobe sensor (CyberScan PD650, Eutech, Thermo Fischer) was used for monitoring broth temperature. A complete description of reactor operation and monitoring is provided in S5. Meteorological data (air temperature, solar irradiance in $W\,m^{-2}$, wind speed, and air moisture) were obtained from a Vantage Pro II weather station (Davis Instrument, Hayward, CA) located on a building roof 200 m away from the photobioreactor. Data were recorded at 5 min intervals and are publicly available (*16*). In total, 7 batch experiments were conducted between August 20 and September 17, 2008 and 104 broth temperature measurements were made. Daily volumetric and algae areal productivities averaged 0.20 ± 0.04 g DW/L-d and 10 ± 2 g DW/m^2-d, respectively; algae concentration averaged 0.38 ± 0.05 g/L.

Computations. The equations described above were computationally integrated in time using the software MATLAB (The MathWorks, Natick, MA). A first-order forward Euler algorithm was chosen for its simplicity and the time step size was set to 100 s. Assuming the broth was at thermal equilibrium on the first morning of a batch study at 7 a.m., the initial temperature was taken equal to the air temperature at this time. Meteorological data (solar irradiance, air temperature, and wind velocity) collected every 5 min (*16*) were linearly extrapolated over the entire time interval and used for model validation. The meteorological data of 5 consecutive days during each climatic season (January 25−29, 2009; April 25−29, 2009; July 23−27, 2009; and October 25−29, 2008) at Merced, CA, were obtained from ref *17* and used for simulations. Selected values of physical parameters

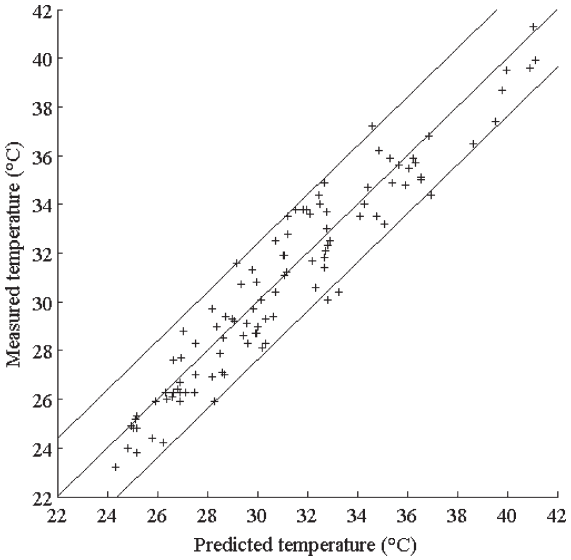

FIGURE 1. Comparison of experimental and predicted temperatures inside a column photobioreactor during outdoor cultivation in Singapore.

are shown in S6. Acuracy was defined as the maximum error between experimental and predicted data at the 95% confidence interval ($n = 104$, no experimental data were excluded).

Results and Discussion

Accuracy of Temperature Prediction. The model predicted the temperature of the culture broth of a photobioreactor operated in Singapore with an accuracy of 2.4 °C (Figure 1). The homogeneous distribution of error suggests the model does not systematically overestimate or underestimate temperatures over the range measured (23−41 °C). The accuracy of the temperature model is further illustrated by the 12-h (Figure 2) and 5-d (S7) predicted versus recorded temperature profiles during typical operation. In consequence, the assumptions made to simplify modeling can be considered as acceptable (a detailed discussion on these assumptions can be found in S8).

Uncertainty was introduced when fixing certain model parameters listed in S6 and when assuming other parameters were constant during operation (for example, wall transmittance can decrease due to dust and algae attachment). A sensitivity analysis was therefore conducted to quantify how varying these parameters would impact the model accuracy. For each parameter, the range of values acceptable to maintain the validation accuracy at 3 °C is shown in Table 1. For instance, it was demonstrated that wind velocity can be measured with an accuracy of 0.2 m s^{-1} against 1 °C for the air temperature and 8% for solar irradiance. By comparison, accuracies of weather station sensors were 0.1 m s^{-1} for the wind velocity, 5% for the solar irradiance, and 0.5 °C for the air temperature.

The sensitivity of time steps was evaluated to determine the frequency of climatic data collection required. It was found that in order to maintain accuracy within 3 °C, light irradiance data must be provided every hour whereas wind velocity and air temperature need to be supplied only every 4 and 8 h, respectively. When all three parameters were monitored every hour, the error was still lower than 3 °C (2.5 °C). This is significant for the use of the model as climatic data is often available on an hourly basis. By comparison, the model was able to predict temperature with an accuracy of 4.2 °C when 12 h-averaged climatic data were used (S9).

Five fluxes typically dominate the heat balance (Figure 3): radiation from the air, radiation from the ground, radiation from the reactor, solar radiation (including direct, diffuse, and reflected radiations), and convection. Evaporation from the top surface, cooling by bubbling, and conduction to the soil were not significant (<10 W). The positive heat fluxes from ground radiation (180−220 W) and air radiation (180−220 W) are within the same range as radiation losses from the reactor (−360 to −440 W). These ground, air, and reactor radiations fluxes are relatively constant (±10%) with respect to time because their proportionality to temperature is to the fourth power (the ground surface, the air, and the reactor temperatures fluctuated within less than 10% when expressed in K). Thus, changes in the reactor broth tem-

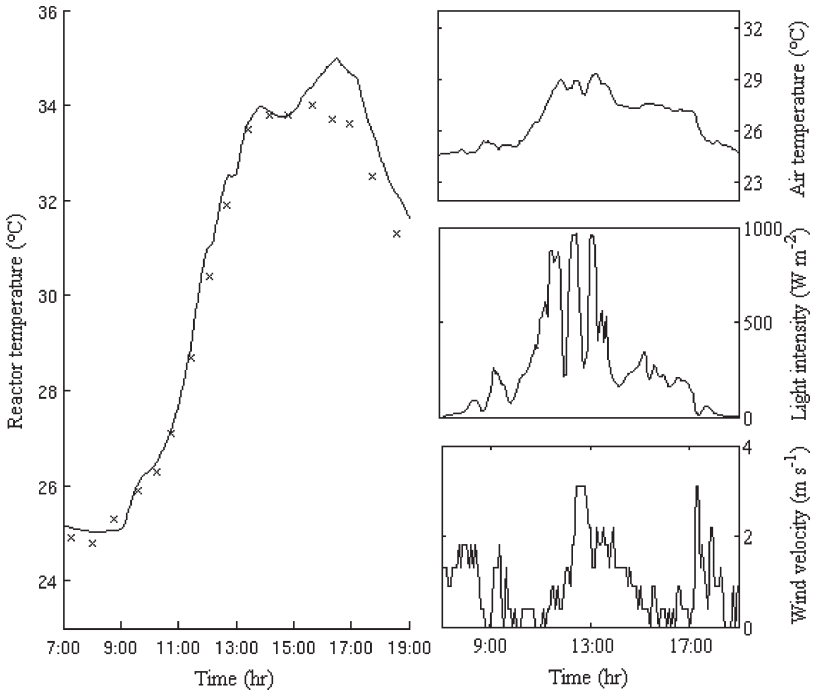

FIGURE 2. Change in experimental (crosses) and predicted (plain line) temperature inside a column photobioreactor on August 22, 2008 during outdoor operation in Singapore. Meteorological data are shown on the right.

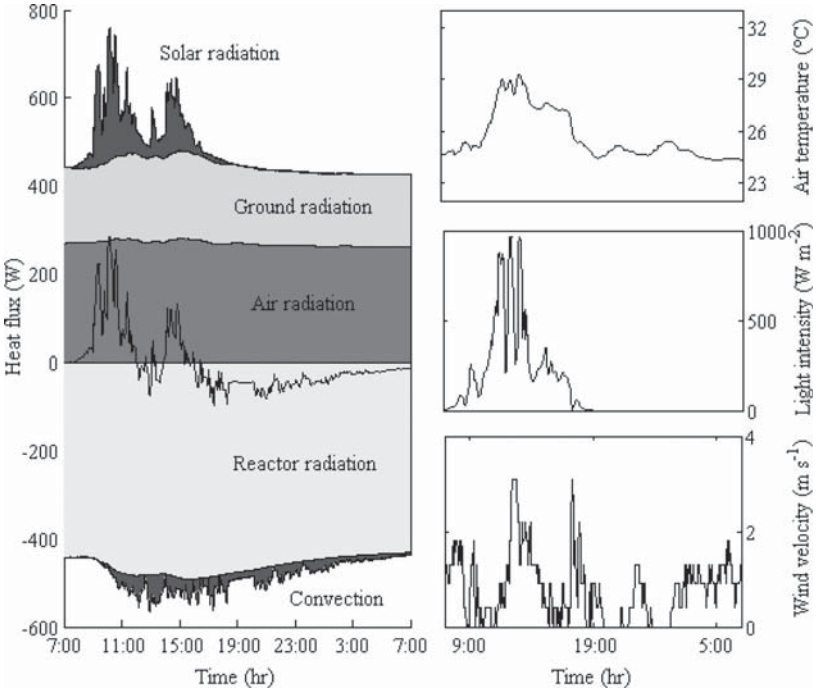

FIGURE 3. Daily changes in heat fluxes reaching a column photobioreactor liquid broth on August 22, 2008, Singapore. The bold plain line represents the total heat flux.

TABLE 1. Sensitivity of Key Parameters

parameter	variation permitted to maintain accuracy of 3 °C	common range (*13, 14*)
fixed		
τ	0.69−0.99	0.7−1.0
r_g	0.02−0.28	0−0.4
K_d	0−0.34	0.1−0.3
$\rho_g Cp_g I_g$	>2 × 10^3 J m^{-2} K^{-1}	2 × 10^5 to 1 × 10^6 J m^{-2} K^{-1}
$T_{g,ref}$	11−27 °C	10−25 °C (generally average air temperature of the year)
$l_{cond,g}$	<0.4 m	0.2−0.5 m
$f(t)$	±60 min	-
variable		
H_g	±8%	-
v_w	±0.2 m s^{-1}	-
T_a	±0.9 °C	-

perature were mainly due to significant fluctuations in solar radiation (0−200 W) and convective flux (−30 to 50 W), the latter being correlated to the difference between the air and the reactor temperatures. Losses from convection could not compensate the solar heat flux during daytime, which caused temperature to increase. However, convection was the main flux contributing to temperature decrease at night.

On the basis of these observations, a simplified model was constructed using only solar radiation and convection in the heat balance (eq 1) and the model was fitted over the entire set of experimental data. The simplified model was able to predict temperature with an accuracy of 4.7 °C (S10). This approach underestimated cooling at night and the predicted temperature at sunrise of the following day was overestimated by 2 °C. This can be explained by the fact that the difference between the radiation from the surroundings (air and ground) and from the reactor is, although small, not negligible compared to convection at night.

Simulations. Because Singapore may not a particularly suitable location for large-scale algae cultivation due to space requirements, the model was also used to predict temperature changes in a hypothetical column photobioreactor located in Merced, California. Hourly solar irradiance and wind velocity as well as 5-min interval air temperature data were used to feed the model (other parameters are shown in S6). Temperature was simulated over a 1-year period of continuous operation and heat losses caused by periodical introduction of fresh water (to compensate for water evaporation and biomass harvesting) were accounted by introducing the following flux in the heat balance (eq 1):

$$Q_{i/o} = -((1 - RH)X_a F_b + F_h \rho_w) Cp_w (T_r - T_{g,ref}) \quad (32)$$

where F_h is the harvesting rate (10 L day^{-1} $reactor^{-1}$) and with the assumption that freshwater introduced was groundwater at temperature $T_{g,ref}$ (K).

The model predicted temperatures above 35 °C will be achieved during most of the year with peak daily temperatures above 40 °C during the warmest month (Figure 4), a value above the maximum temperature tolerated by most commercial microalgae species.

Modifications to the reactor design were tested and found to have limited impact on temperature changes although both increasing and reducing the reactor radius around 0.1 m were found to slightly reduce the maximum temperatures achieved in the photobioreactor (Figure 5). As the solar flux (in W) is roughly proportional to the reactor lateral surface and the thermal capacity (in J K^{-1}) to the broth volume, a higher reactor radius can indeed result in lower broth temperature. The decrease in peak temperature predicted when reducing the radius to 0.05 m from 0.1 m was therefore surprising but it is explained by to the fact forced convection increases when the radius decreases (eq 27). The reactor radius cannot practically be increased above 0.20 m to avoid the formation of a dark area in the center of the reactor because of intense mutual shading (*18*). An additional simulation showed the use of high-reflectivity ground material (such as concrete of sand) increases the maximum temperatures reached during daytime (S11).

Consequences for Photobioreactor Operation. It is clear from the modeling that broth temperature must be actively controlled in photobioreactors to avoid a significant productivity drop. In the case of a column reactor located in

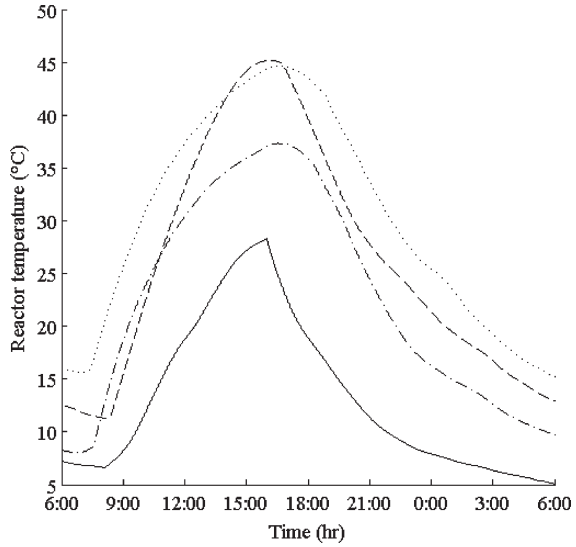

FIGURE 4. Predicted changes from July 23−24, 2009 (dotted line), October 25−26, 2008 (dashed line), January 25−26, 2009 (plain line), and April 25−26, 2009 (dot/dash line) in column photobioreactor broth temperature during outdoor cultivation in July in Merced, California.

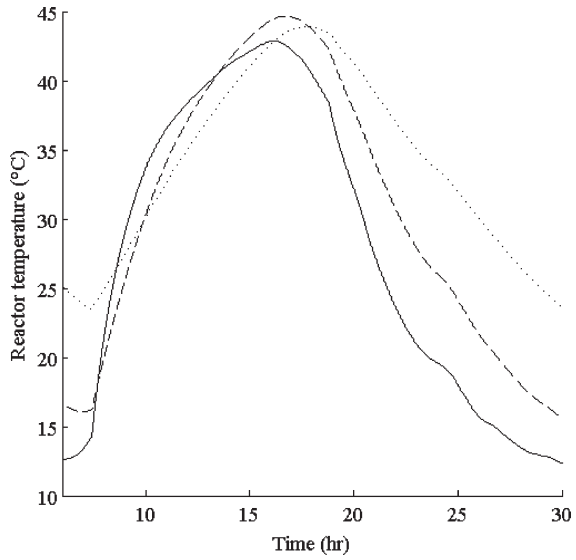

FIGURE 5. Predicted changes in 0.2 m (dotted line), 0.1 m (dashed line), and 0.05 m (plain line) radius column photobioreactor broth temperature during outdoor cultivation in July in Merced, California.

Merced, CA, 18 000 and 5500 GJ year^{-1} ha^{-1} of heat energy must be removed to keep broth temperature at or below 25 and 35 °C, respectively, assuming a density of one reactor per square meter (*19*). This was determined by calculating the energy (J) reaching the reactor during a time step of 1 s and resetting the temperature back to 25 or 35 °C at the end of each time step. The total energy computed over the 5-days data period was then considered representative of each season as shown in Table 2. Temperature control strategies such as water evaporation at the reactor surface or the use of heat exchangers circulating cool water (i.e., deep seawater) have been proposed (*2*). Not even considering cooling efficiency, evaporative cooling would require the distribution and consumption of 2400−8000 m^3 year^{-1} h^{-1} of high-quality groundwater or purified surface water over large arrays of individual photobioreactors (100 000 units for a 10 h production facility delivering, in our example, 365 tonnes of dried algae biomass per year). The use of heat exchangers is no less challenging as it would require significant capital and operation expenditures to supply and distribute cool water. Clearly, temperature control is a major issue that must be addressed when evaluating the technical feasibility, costs, and sustainability of mass algae production in photobioreactors.

TABLE 2. Daily Average Energy (MJ/m^2) Needed to Be Extracted to Maintain the Broth Temperature at T_{max} or Lower in a Column Photobioreactor Operated in Merced, California

season	T_{max} = 25 °C	T_{max} = 35 °C
autumn	4.8	1.6
winter	0.93	0.05
spring	3.0	0.02
summer	11	4.3
year	4.9	1.5

Acknowledgments

We acknowledge ALPHA Biofuels (Singapore), and especially Tan Hai Woon, Chief Technical Officer, for supporting the algae feasibility study that provided experimental data for validation. Dr. Wang Jing-Yuan and Dr. Lim Hock Beng are also gratefully acknowledged for great support at Nanyang Technological University, Singapore. We also thank Miss Qingxia Zhong is for her hard work during the feasibility study and Professor Yusuf Chisti (Massey University) for most valuable discussions on photobioreactors.

Supporting Information Available

S1, schematic representation of the photobioreactor and heat fluxes considered in the heat balance; S2, definition of geometrical parameters; S3, determination of θz and ωs; S4, Tg determination; S5, operation and monitoring of photobioreactor; S6, model input parameters; S7, comparison of predicted vs measured temperature over a 5-d period; S8, discussion of validity of assumptions; S9, temperature prediction using 12 h-averaged meteorological data; S10, temperature prediction using simplified model; S11, influence of ground reflectivity on broth temperature. This information is available free of charge via the Internet at http://pubs.acs.org/.

Literature Cited

(1) Pienkos, P. T.; Darzins, A. The promise and challenges of microalgal-derived biofuels. *Biofuels Bioprod. Biorefining* **2009**, *3* (4), 431–440; DOI 10.1002/bbb.

(2) Chisti, Y. Biodiesel from microalgae beats bioethanol. *Trends Biotechnol.* **2007**, *26* (3), 126–131; DOI 10.1016/j.tibtech.2007.12.002.

(3) Schenk, P. M.; Thomas-Hall, S. R.; Stephens, E.; Marx, U. C.; Mussgnug, J. H.; Posten, C.; Kruse, O.; Hankamer, B. Second Generation Biofuels: High-Efficiency Microalgae for Biodiesel Production. *Bioenergy Resour.* **2008**, *1* (1), 20–43; DOI 10.1007/s12155-008-9008-8.

(4) Dismukes, G. C.; Carrieri, D.; Bennette, N.; Ananyev, G. M.; Posewitz, M. C. Aquatic phototrophs: efficients alternatives to land-based crops for biofuels. *Curr. Opin. Biotechnol.* **2008**, *19* (3), 235–240; DOI 10.1016/j.copbio.2008.05.007.

(5) Packer, M. Algal capture of carbon dioxide; biomass generation as a tool for greenhouse gas mitigation with reference to New Zealand energy strategy and policy. *Energy Policy* **2009**, *37* (9), 3428–3437; DOI 10.1016/j.enpol.2008.12.025.

(6) Lardon, L.; Hélias, A.; Sialve, B.; Steyer, J.-P.; Bernard, O. Life-Cycle Assessment of Biodiesel Production from Microalgae. *Environ. Sci. Technol.* **2009**, *43* (17), 6475–6481; DOI 10.1021/es900705j.

(7) Walker, D. A. Biofuels, facts, fantasy, and feasibility. *J. Appl. Phyco.* **2009**, *21* (5), 509–517; DOI 10.1007/s10911-009-9446-5.

(8) Grobbelaar, J. U. Physiological and technological considerations for optimizing mass algal cultures. *J. Appl. Phyco.* **2000**, *12* (3−5), 201–206.
(9) Ugwu, C. U.; Aoyagi, H.; Uchiyama, H. Photobioreactors for mass cultivation of algae. *Bioresour. Technol.* **2008**, *99* (10), 4021–4028; DOI 10.1016/j.biortech.2007.01.046.
(10) Mata, M. T.; Martins, A. A.; Caetano, N. S. Microalgae for biodiesel production and other applications: A review. *Renew. Sust. Energy Rev.* **2009**, *14* (1), 217–232; DOI 10.1016/j.rser.2009.07.020.
(11) Morita, M.; Watanabe, Y.; Saiki, H. High Photosynthetic Productivity of Green Microalga *Chlorella sorokiniana*. *Appl. Biochem. Biotechnol.* **2000**, *87* (3), 203–218; DOI 10.1385/ABAB:87:3:203.
(12) Chisti, Y. Biodiesel from microalgae. *Biotechnol. Adv.* **2007**, *25* (3), 294–306; DOI 10.1016/j.biotechadv.2007.02.001.
(13) Howell, J. R.; Siegel, R. *Thermal Radiation Heat Transfer*, 4th ed; Taylor & Francis: New York, 2004.
(14) Liu, B. Y. H.; Jordan, R. C. The interrelationship and characteristic distribution of direct, diffuse and total solar radiation. *Sol. Energy* **1960**, *4* (3), 1–19.
(15) Jiji, L. M. *Heat Convection*; Springer: New York, 2006.
(16) Singapore. *National Weather Study Project*; http://nwsp.ntu.edu.sg/weather/new_portal_download_pre.htm.
(17) U.S. National Climatic Data Center Web site; http://www.ncdc.noaa.gov/crn/hourly.
(18) Posten, C. Design principles of photo-bioreactors for cultivation of microalgae. *Eng. Life Sci.* **2009**, *9* (3), 165–177; DOI: 10.1002/elsc.200900003.
(19) Sanchez Miron, A.; Contreras Gomez, A.; Garcia Camacho, F.; Molina Grima, E.; Chisti, Y. Comparative evaluation of compact photobioreactors for large-scale monoculture of microalgae. *J. Biotechnol.* **1999**, *70* (1), 249–270; DOI: 10.1016/S0168-1656(99)00079-6.

ES903214U

Supporting information

ES&T manuscript es-2009-03214u

Title: Mechanistic modelling of broth temperature in outdoor photobioreactors

Authors: Quentin Béchet, Andy Shilton, Oliver B. Fringer, Raul Munoz, Benoit Guieysse

8 Figures

1 Table

18 Pages

S1 - Schematic representation of the photobioreactor and heat fluxes considering in the heat balance.

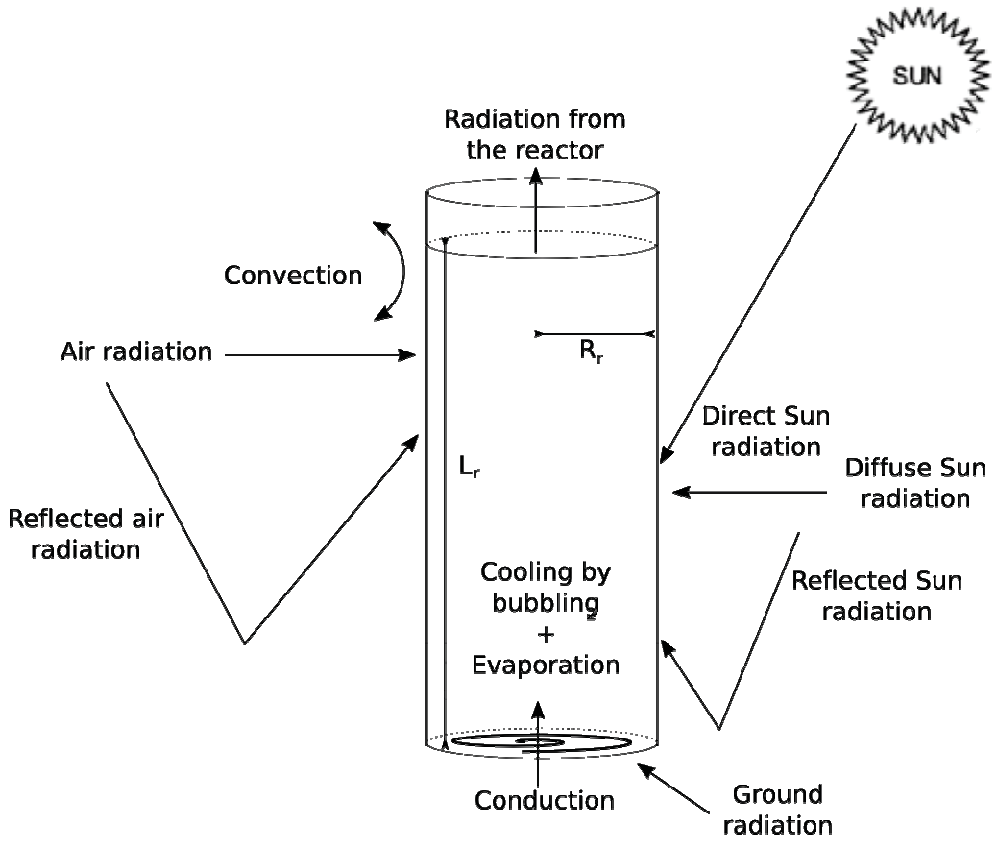

Figure S1: Schematic representation of the photobioreactor and heat fluxes considering in the heat balance.

S2 – Definition of geometrical parameters

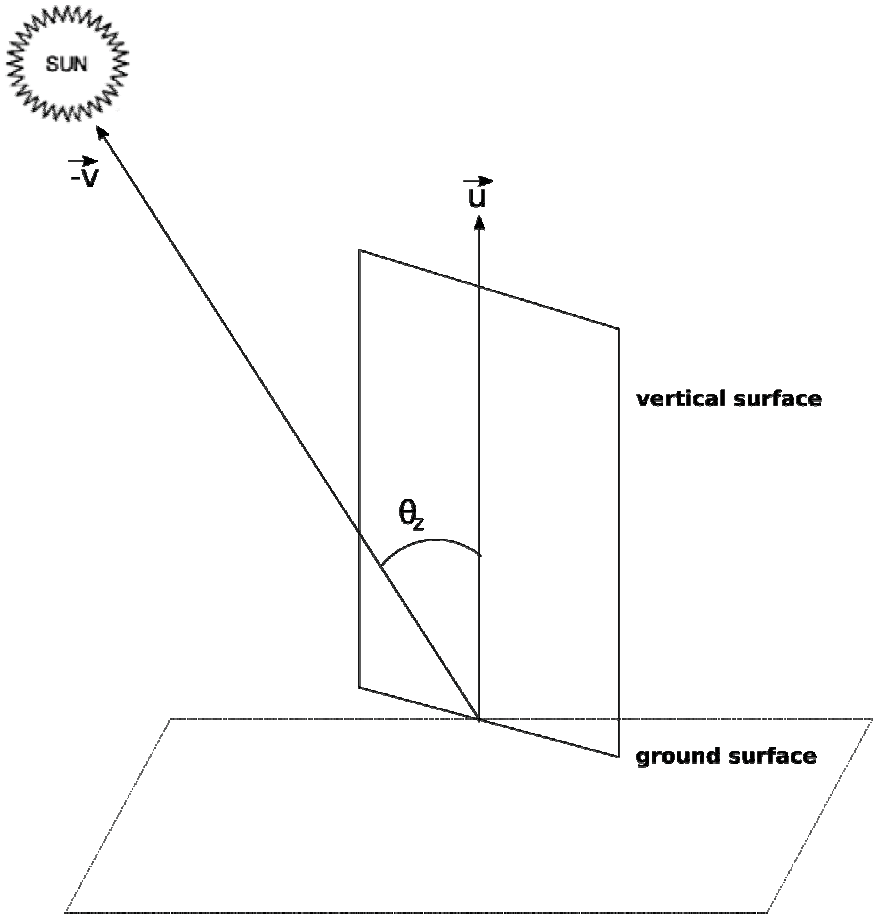

Figure S2-1: Definition of θ_z

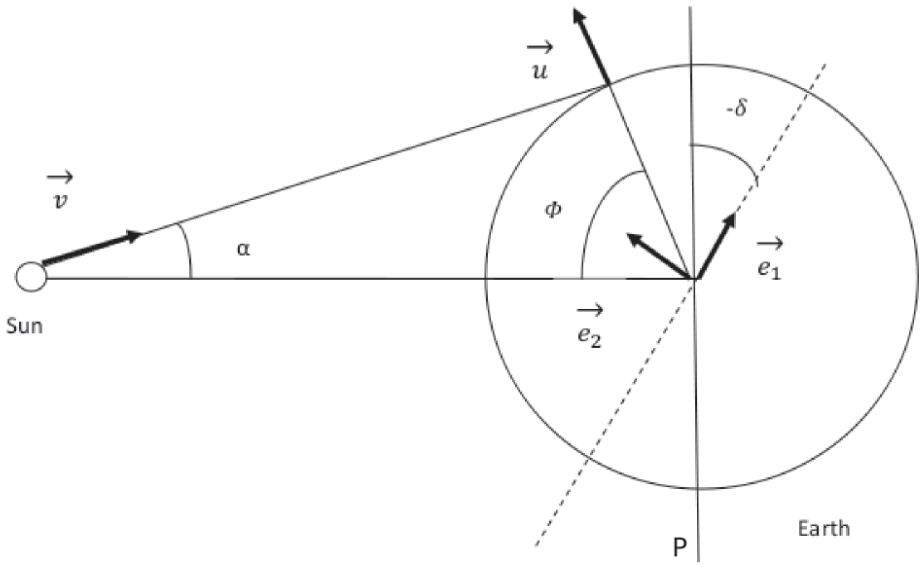

Figure S2-2: Definition of geometrical parameters – View from aside

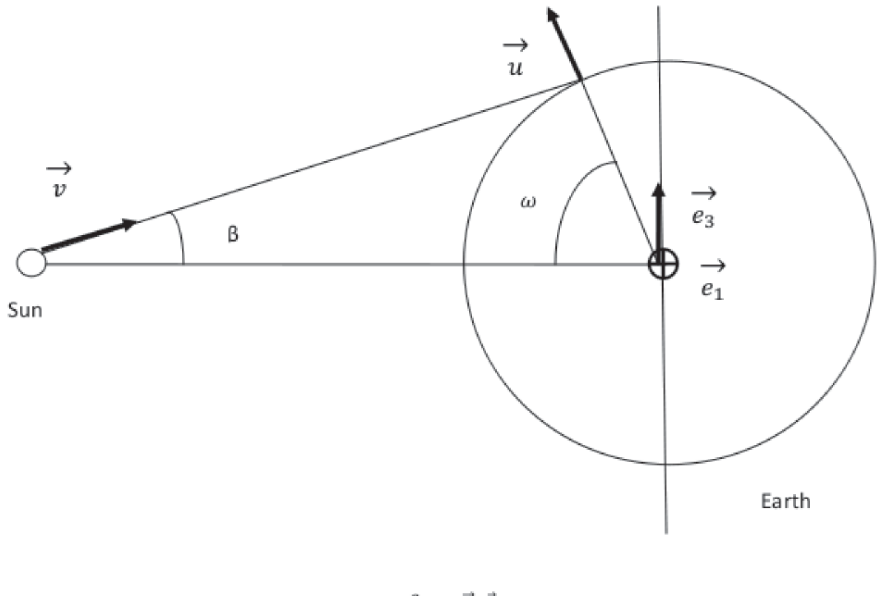

Figure S2-3: Definition of geometrical parameters – View from above

S3 - Determination of θ_z and ω_s

θ_z is a function of the latitude φ, the solar declination δ and the solar hour. First, we define the geometrical parameters $\vec{e}_1, \vec{e}_2, \vec{e}_3, \vec{u}, \alpha$ and β as shown in Figures S2-2 and S2-3. We first express the vectors $\vec{u}$ and $\vec{v}$ as a linear combination of $\vec{e}_1, \vec{e}_2$ and $\vec{e}_3$:

$$\vec{u} = \sin\varphi.\vec{e}_1 + \cos\varphi(\cos\omega.\vec{e}_2 + \sin\omega.\vec{e}_3) \quad \text{(S3-1)}$$

$$\vec{v} = \sin(\delta-\beta).\vec{e}_1 + \cos(\delta-\beta)(\cos\alpha.\vec{e}_2 + \sin\alpha.\vec{e}_3) \quad \text{(S3-2)}$$

As the Earth radius is negligible compared to the distance between the Earth and the Sun, we can consider that the angles α and β are close to 0. This yields:

$$\cos(\theta_z) = \vec{u}.\vec{v} = \sin\varphi\sin\delta + \cos\varphi\cos\delta\cos\omega \quad \text{(S3-3)}$$

ω varies along the day as a linear function of time which varies from $-\omega_s$ to ω_s, where ω_s is the angle at sunrise hour. When the Sun rises, the vector $\vec{u}$ is in the plane P (see Figure S2-2). A normal vector to the plane P is:

$$\vec{n} = -\sin\delta.\vec{e}_1 - \cos\delta.\vec{e}_2 \quad \text{(S3-4)}$$

When ω equals ω_s, $\vec{u}$ and $\vec{n}$ are perpendicular, which yields:

$$\cos\omega_s = -\tan\delta.\tan\varphi \quad \text{(S3-5)}$$

S4 - T_g **determination**

A heat balance on the ground surface can be use to derive the ground temperature as a function of time:

$$\rho_g Cp_g V_g \frac{dT_g}{dt} = (Q_{in,g} - Q_{out,g}) S_g \quad \text{(S4-1)}$$

Where ρ_g and Cp_g are the density and the heat capacity of the ground surface, respectively, $Q_{in,g}$ and $Q_{out,g}$ the incoming and outgoing fluxes, and V_g the volume of ground considered. Calling l_g the thickness of the ground layer, the heat balance becomes:

$$\rho_g Cp_g l_g \frac{dT_g}{dt} = Q_{in,g} - Q_{out,g} \quad \text{(S4-2)}$$

Five different heat fluxes are taken into account in the heat balance: radiation from the air, radiation from the Sun, radiation from the ground surface, convection and conduction with ground lower layers. The incoming and outgoing fluxes can be expressed as:

$$Q_{in,g} = \varepsilon_g \varepsilon_a \sigma T_a^4 + \varepsilon_g H_g \quad \text{(S4-3)}$$

$$Q_{out,g} = \varepsilon_g \sigma T_g^4 + h_{co,g}(T_g - T_a) + Q_{cond,g} \quad \text{(S4-4)}$$

Where $h_{co,g}$ is the convection coefficient between the air and the ground surface and $Q_{cond,g}$ the conductive flux with ground lower layers. $h_{co,g}$ is determined considering that two types of convection can occur: natural convection (no wind) and forced convection (wind).

Natural convection can be expressed as (Reference S4-1):

$$h_{co,g} = 0.27\frac{\lambda_a Ra_L^{1/4}}{L},\ 3.10^5 < Ra_L < 3.10^{10} \quad \text{(S4-5)}$$

Where λ_a is the air thermal conductivity and Ra_L is the Rayleigh Number defined as:

$$Ra_L = \frac{g\left|T_g - T_a\right|L^3}{a_a \nu_a T_a} \quad \text{(S4-6)}$$

Where L is a characteristic length for the ground; g is the gravity constant; v_a the air kinematics viscosity and a_a the air diffusivity.

In the case of forced convection, $h_{co,g}$ can be estimated as (Reference S4-1):

$$h_{co,g} = \lambda_a(0.664\,\mathrm{Re}_c + 0.037\left[\mathrm{Re}_L^{0.8} - \mathrm{Re}_c^{0.8}\right])\mathrm{Pr}^{1/3},\ \mathrm{Re}_L > \mathrm{Re}_c = 5.10^5 \quad \text{(S4-7)}$$

Where Pr is the Prandtl number for air (0.7 at 25°C) and Re_L the Reynolds number estimated for L as:

$$\mathrm{Re}_L = \frac{\rho_a L v_w}{\mu_a} \quad \text{(S4-8)}$$

Where ρ_a is the air density, v_w the wind velocity and μ_a the air viscosity.

$Q_{cond,g}$ can be determined using the Fourier's law, a conductive flux Q_{cond} (in W/m^2) in the vertical direction x according to:

$$Q_{cond} = -k\frac{dT}{dx} \quad \text{(S4-9)}$$

Where k is the conductivity of the media (i.e. the ground). Therefore, a characteristic length l_{cond} for the conduction in the ground is:

$$l_{cond} = k\frac{\Delta T}{F} \quad \text{(S4-10)}$$

Where ΔT is a characteristic temperature difference between the ground surface and a lower layer and F is a characteristic value for the flux reaching the ground surface. Knowing experimentally that the temperature of the ground surface can reach up to 50°C and that the temperature of lower ground layers $T_{g,ref}$ is close to the air temperature average (20°C), ΔT was taken equal to 30°C. Considering light irradiance (in average 500W/m^2) and convection (-100W/m^2) and assuming that the ground surface radiates more than the air because of its higher temperature (-100W), a correct order of magnitude for F is 300W/m^2. A common value for concrete conductivity is 2W/mK, which yields:

$$l_{cond,g} = 2\frac{30}{300} = 0.2m \quad \text{(S4-11)}$$

Assuming a linear temperature profile (and therefore a constant conductive flux) in the upper ground surface, the average conductive flux in the ground given by:

$$Q_{cond,g} = -k\frac{T_g - T_{g,ref}}{l_{cond,g}} \quad \text{(S4-12)}$$

Integration of the last expression over time yields values for T_g over time.

Reference S4-1:
Jiji, L. M. Heat Convection. Springer: New-York, 2006.

S5 - Operation and Monitoring of Photobioreactor

Rationale:

Pneumatically agitated reactors such as the bubble column reactor used in this study provide cost-efficient mass transfer and homogenous shear conditions, the latter being especially important for the cultivation of shear-sensitive microorganisms such as algae (Chisti 1998). We preferred the bubble column reactor over the airlift configuration because column reactors are simpler to design and operate.

Chlorella sorokiniana is suitable to produce biomass for biogas or oil from pyrolysis because of its fast growth rate and high temperature resistance (Morita et al, 2002; Cuaresmo et al. 2009). This latter property was especially useful in the context of our study because temperature resistance enabled to operate the reactor under temperature conditions that would have otherwise caused complete inhibition or death. Furthermore, for the purpose of modelling temperature, the individual characteristics of the algae (i.e. chlorophyll concentration) used are not relevant because they do not influence the temperature model under light-limiting conditions.

Chisti, Y. Pneumatically agitated bioreactors in industrial and environmental bioprocessing: hydrodynamics, hydraulics, and transport phenomena. *Appl. Mechanics Reviews,* **1998**, 51: 33-112.

Masahiko Morita, Yoshitomo Watanabe, Hiroshi Saiki. Photosynthetic productivity of conical helical tubular photobioreactor incorporating *Chlorella sorokiniana* under field conditions. *Biotechnol. Bioeng*., **2002**, 77(2), 155 – 162

María Cuaresma, Marcel Janssen, Carlos Vílchez, René H. Wijffels.

Productivity of *Chlorella sorokiniana* in a short light-path (SLP) panel photobioreactor under high irradiance. *Biotechnol. Bioeng*., **2009,** 104(2)0, 352 – 359.

Operation & Monitoring

CO_2-enriched air (2-3%) was continuously bubbled at a rate of approximately 1.2 $L.min^{-1}$. The air bubble size and residence time were approx 3 mm and 6 sec, respectively. The reactor was filled with BG-11 (Andersen et al. 2005) medium enriched P (0.90 g L^{-1}) and N (0.25 g L^{-1}) and inoculated with pure *Chlorella sorokiniana* to reach an initial concentration of 0.05- 0.10 g DW L^{-1}.

A typical operation cycle was as follows: After being thoroughly cleaned with pressurized water and 70% ethanol, the reactor was filled with approx. 40 L of tap water and aeration began. Nutrients were then added (from pure salts or stock solutions) to enriched obtained BG11 medium. The reactor was further aerated for a few minutes to remove potential chlorine from the tap water, dissolve the salt and homogenize the medium. The reactor was then inoculated with 1-2 L of pure *Chlorella sorokiniana* culture or 2-5 L of culture from a previous batch. Tap water was then added to reach a final gas-free liquid volume of 50L and a final working volume (gas bubble + liquid broth) of 51L (water height of 1.8 L; corresponding illuminated area of 1.0-1.1 m^2; gas hold up = 0.02).

To estimate the reactor transmittance and surface variations in light irradiance, Photosynthetically Active Radiation (PAR; μE m^{-2} s^{-1}) was frequently monitored at several points around the reactor by placing the sensor against the reactor wall (e.g.

vertically) or horizontally at the top of the reactor (LI 190 Quantum sensor and LI 250A light meter; LI-COR, USA). The air and CO_2 supply rates were routinely monitored and corrected (but were found very stable) and CO_2-enriched gas samples were taken after mixing to further monitor CO_2 concentration (GC-TCD). Air temperature outside the reactor (1.5 m height) was also monitored. For monitoring broth parameters, a multiprobe sensor (Cyberscan PD650, Eutech, Thermo Fisher) was inserted into the reactor (approx. 0.5 m bellow the culture broth surface) and allowed to equilibrate for 1-2 min before the values of dissolved oxygen concentration, pH, and the temperature inside the reactor were then recorded (samples for algae concentration monitoring were also taken but results will be presented elsewhere). After each batch, the entire reactor broth was removed before the reactor was cleaned.

Andersen, R. A.; Berges, J. A.; Harisson, P.J.; Watanabe, M. M. Appendix A-Recipes For Freshwater and Seawater Media. In *Algal Culturing Techniques*; Andersen, R. A; Elsevier Academic press: Singapore 2005; pp 429-530.

S6 – Model input parameters

Table S6: Constants and Parameters Values for the reactor in Singapore

Symbol	Definition	Unit	Value
Water constants			
ρ_w	Water density	kg m^{-3}	998
Cp_w	Water heat capacity	J kg^{-1} K^{-1}	$4.18.10^3$
L_w	Water latent heat	J kg^{-1}	$2.45.10^6$
V_r	Reactor working volume (gas-free liquid phase)	m^3	0.050
Ground constants			
r_g	Ground reflectivity	-	0.20
ε_g	Ground emissivity	-	0.80
Cp_g	Ground heat capacity	J kg^{-1} K^{-1}	$2.4.10^3$
ρ_g	Ground density	kg m^{-3}	4000
l_g	Ground thickness	m	0.02
L	Characteristic distance for ground surface	m	50
Air constants			
ε_a	Air emissivity	-	1
λ_a	Air conductivity	W m^{-1} K^{-1}	$2.63.10^{-2}$
Cp_a	Air heat capacity	J kg^{-1} K^{-1}	2.10^3
ρ_a	Air density	kg m^{-3}	1.2
K_d	Atmospheric diffusion coefficient	-	0.2
Reactor characteristics			
τ	Wall transmittance	-	0.9
ε_r	Reactor emissivity	-	0.97
R_r	Reactor radius	m	0.095
L_r	Reactor height	m	1.8
Cp_a	Air heat capacity	J kg^{-1} K^{-1}	2.10^3
ρ_a	Air density	kg m^{-3}	1.2
F_b	Air inflow rate	m^3 s^{-1}	$1.67.10^{-5}$
F_{ev}	Evaporation rate	m^3 s^{-1}	$9.26.10^{-10}$
L	Characteristic distance for ground surface	m	50
f_b	Air volume fraction as bubbles	-	0.02
$f(t)$	Shading function[a]	-	1 on [9:30am; 5:00pm], 0 elsewhere

a. $f(t)$ = 1 at all time for simulations using California climatic data.

S7 – Comparison of predicted vs measured temperature over a 5-d period.

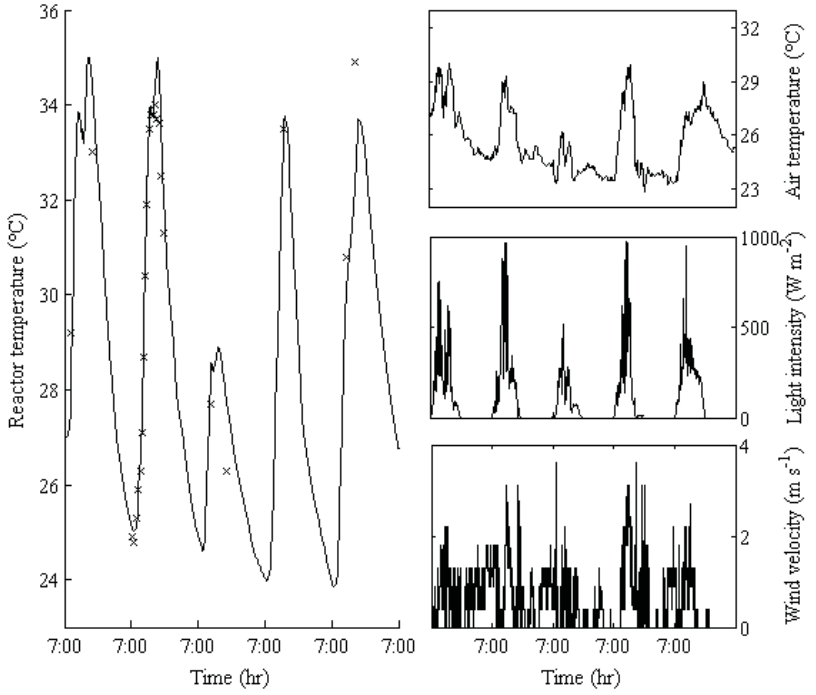

Figure S7-1: Change in experimental (crosses) and predicted (plain line) temperature inside a column photobioreactor (21-25 August 2008) Meteorological data is shown the right.

S8 – Discussing the validity of assumptions

S8.1. Effect of microbial activity on the heat balance:

Photosynthesis effect: Daily algae productivities around 0.2 g DW/L were recorded during experimentation, which corresponds to an energy conversion flux around 5.3 W over a period of 12 hr assuming an algae biomass heat value of 22.9 KJ/g. This flux is considerably lower than the 200W of solar irradiation causing temperature increase during day time. We can therefore confidently assume that neglecting this heat contribution will not significantly influence the model accuracy.

Heterotrophic decay: Up to 20% of the algae biomass can be lost at night due to microbial decay (this was however never observed in the present study). Thus, at an operating algae concentration of 1 g/L, a heat production of 5.3 W could occur at nigh (based on 12 hr and an algae heat value of 22.9 kJ/g). In reality, only a fraction of the chemical energy is actually released as heat, the remaining fraction being recovered as degradation products or new biomass. Even an optimistic contribution of 2-3 W cannot, in regards to the other fluxes involved, significantly slow down the rate of temperature decrease at night.

S8.2 Effect of algae characteristics

Algae concentration is always much lower than water activity in photobioreactors (0.38 ± 0.05 g/L in the present study; $p = 0.05$ and $n = 107$). Therefore, cell density does not significantly affect the broth emissivity. It can also be assumed that the value of the broth emissivity is that of water. Algae density can affect the transparency of the broth at low algae densities, when the reactor is not opaque and there is not light limitation. However, light limitation occurred during all experiments used to provide

temperature data for model validation and would indeed be expected during large-scale algae cultivation as explained in the manuscript.

S8.3. Effect the headspace volume:

The volume of air above the reactor is 5.7L. We assumed this air was at the broth temperature and therefore did not consider convection between the air and the liquid broth at the top surface. The air retention time in the headspace was short (5 min) so we believe the air temperature in the headspace did not differ significantly from the reactor broth temperature. Thus, during day time, this transparent air layer did not affect the heat balance. At night, there is no greenhouse effect because aeration was continued (no heat storage in the head space).

S9 – Temperature prediction using 12hr-averaged meteorological data.

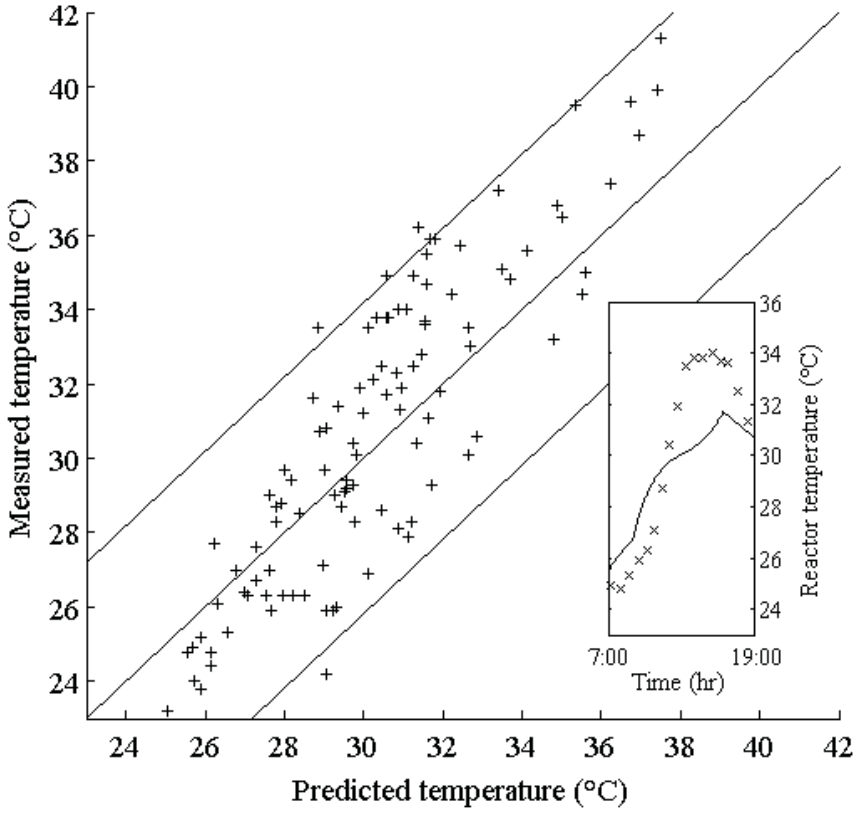

Figure S9.1: Comparison of experimental and predicted temperatures reached inside a column photobioreactor during outdoor cultivation in Singapore. Predicted temperatures were calculated using 12 hr day/night averaged meteorological data; other data used is shown in S6.

S10 – Temperature prediction using simplified model.

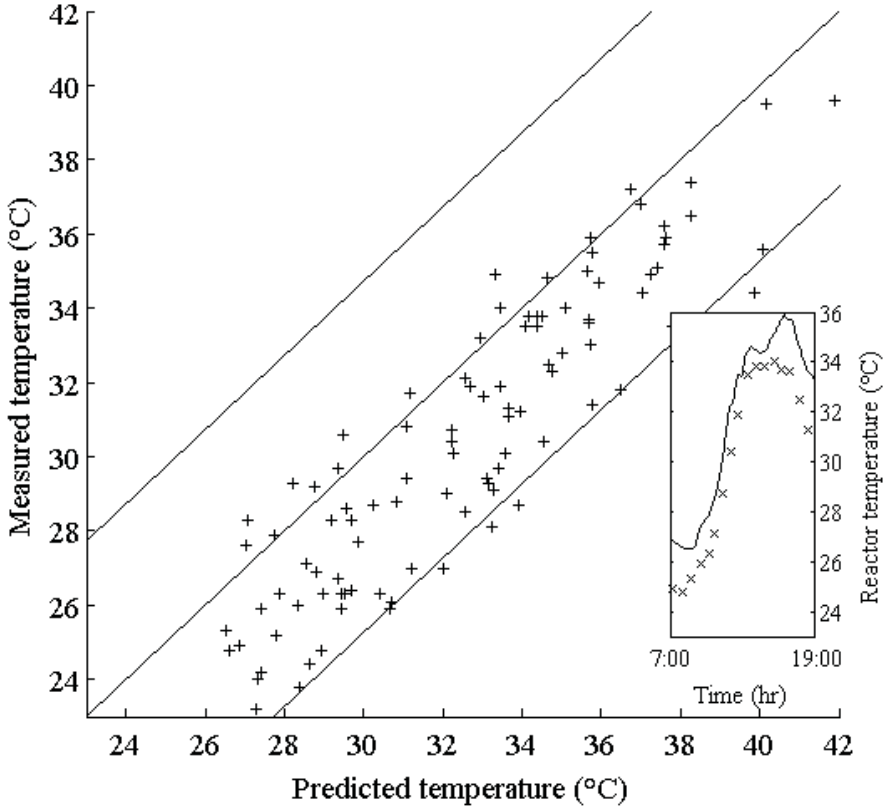

Figure S10.1: Experimental and predicted column photobioreactor temperature changes during outdoor cultivation in Singapore. Predicted temperatures were calculated using 5 min interval meteorological data; other data used is shown in S6.

S11 – Influence of ground reflectivity

A ground reflexivity coefficient of 0.20 was used for validation and simulations. This coefficient is more typical to soil (0.2) or grass cover (0.25) than new concrete (0.5). A value of 0.20 was used for validation to account for the fact the roof top concrete, where the reactor was located, was covered with a layer of dark dirt and mosses. For large-scale cultivation, an earth of grass cover is also more relevant to than concrete for economical reasons. A material reflectivity changes in time (depending on incident light angle, wetness and age) but the model accuracy could cope with changes in reflectivity within 0 - 0.4 (Table 1). Ground reflectivity has however a more significant impact on the maximum temperatures reached during day-time as seen below:

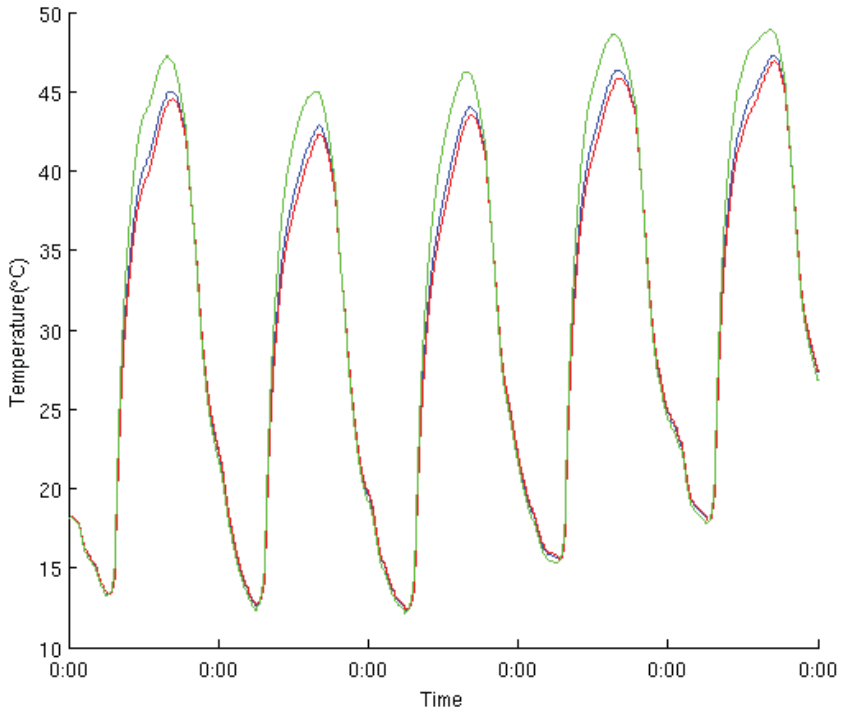

Figure S11-1: Predicted temperature changes in a 0.1 m radius column photobioreactor broth temperature during outdoor cultivation in July in Merced, California, USA at ground reflectivity values of 0.1 (red line); 0.2 (blue line), and 0.5 (green line).

Environmental Science & Technology

Addition/Correction

pubs.acs.org/est

Correction to Mechanistic Modeling of Broth Temperature in Outdoor Photobioreactors

Quentin Béchet, Andy Shilton, Oliver B. Fringer, Raul Muñoz, and Benoit Guieysse*

Environ. Sci. Technol. **2010**, *44*, 2197–2203; DOI: 10.1021/es903214u

The formula used to estimate the heat flux associated with the amount of diffuse solar radiation reaching the algae in the photobioreactor ($Q_{ra,d}$, W) was given as follows in the original article:

$$Q_{ra,d} = \tau\varepsilon_r(\pi R_r^2 + 2\pi R_r L_r)H_d \quad (10)$$

where τ is the wall transmittance (−), ε_r is the reactor emissivity (−), R_r and L_r are the reactor radius and height, respectively (m), and H_d is the intensity of the diffuse solar radiation reaching the ground surface (W m^{-2}). The first term of the sum represents the amount of diffuse radiation reaching the top surface of the reactor; and the second term represents the amount of diffuse solar radiation reaching the lateral surface of the reactor. The current expression of the second term does not account for the form factor between the reactor lateral surface and the atmosphere. As the diffuse lateral radiation reaching the lateral surface of the reactor only originates from above the reactor, the second term of the sum should be multiplied by a factor 0.5. Equation 10′ should therefore be corrected to:

$$Q_{ra,d} = \tau\varepsilon_r(\pi R_r^2 + \pi R_r L_r)H_d \quad (10')$$

The formula was erroneous only in the article but the code used to predict the results presented in the article was correct.

Published: October 29, 2013

ACS Publications © 2013 American Chemical Society

Article 4

MASSEY UNIVERSITY
GRADUATE RESEARCH SCHOOL

STATEMENT OF CONTRIBUTION TO DOCTORAL THESIS CONTAINING PUBLICATIONS

(To appear at the end of each thesis chapter/section/appendix submitted as an article/paper or collected as an appendix at the end of the thesis)

We, the candidate and the candidate's Principal Supervisor, certify that all co-authors have consented to their work being included in the thesis and they have accepted the candidate's contribution as indicated below in the *Statement of Originality*.

Name of Candidate: Quentin Béchet

Name/Title of Principal Supervisor: Prof. Benoit Guieysse

Name of Published Research Output and full reference:

Béchet Q, Chambonnière P, Shilton A, Guizard G, Guieysse B. Algal productivity modeling: a step toward accurate assessments of full-scale algal cultivation (submitted).

In which Chapter is the Published Work: 4

Please indicate either:

- The percentage of the Published Work that was contributed by the candidate:

  and / or

- Describe the contribution that the candidate has made to the Published Work:

  Q Béchet supervised the student P Chambonnière who performed most of the experimental work for model parameterization and the associated data analysis. Q Béchet did the experimental work for model validation and associated simulations. He also wrote most of the article.

Quentin Béchet — Digitally signed by Quentin Béchet DN: cn=Quentin Béchet, o=Massey University, ou=SEAT, email=q.bechet@massey.ac.nz, c=NZ Date: 2014.02.17 18:49:56 +13'00'

Candidate's Signature — 04/07/2014 — Date

Benoit Guieysse — Digitally signed by Benoit Guieysse DN: cn=Benoit Guieysse, o=Massey University, ou=SEAT, email=b.j.guieysse@massey.ac.nz, c=NZ Date: 2014.02.24 11:17:49 +13'00'

Principal Supervisor's signature — 07/07/2014 — Date

Algal productivity modeling: a step toward accurate assessments of full-scale algal cultivation

Journal:	*Biotechnology and Bioengineering*
Manuscript ID:	Draft
Wiley - Manuscript type:	Article
Date Submitted by the Author:	n/a
Complete List of Authors:	Béchet, Quentin; Massey University, Centre for Environmental Technology and Engineering Chambonnière, Paul; Massey University, School of Engineering and Advanced Technology Guizard, Guillaume; INRA, UR50 Laboratoire de Biotechnologie de l'Environnement Shilton, Andy; Massey University, Centre for Environmental Technology and Engineering Guieysse, Benoit; Massey University, SEAT
Key Words:	Chlorella vulgaris, Model, Light, Temperature, Biofuel, Photosynthesis

SCHOLARONE™
Manuscripts

For Review

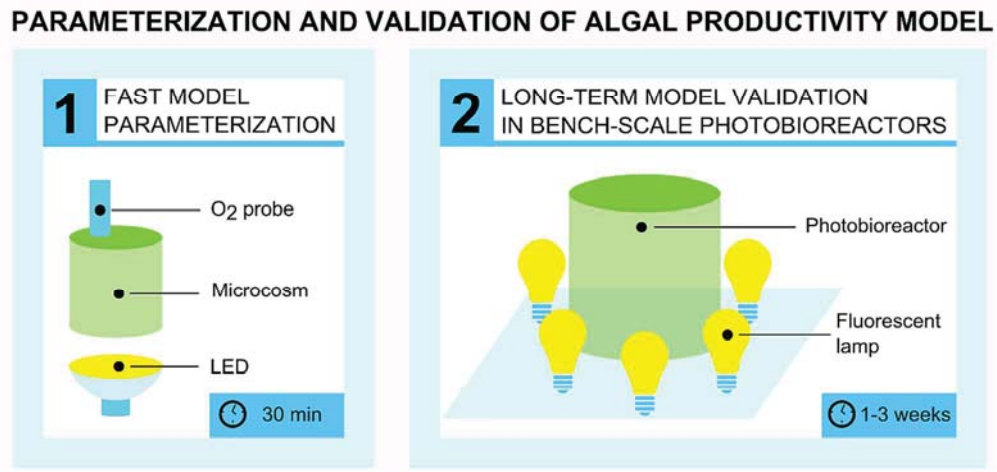

Graphical Abstract
98x48mm (300 x 300 DPI)

Peer Review

Algal productivity modeling: a step toward accurate assessments of full-scale algal cultivation

Quentin Béchet[a], Paul Chambonnière[a], Guillaume Guizard[b], Andy Shilton[a], Benoit Guieysse[a,*]

[a] School of Engineering and Advanced Technology, Massey University, Private Bag 11 222, Palmerston North 4442, New Zealand

[b] INRA, UR50 Laboratoire de Biotechnologie de l'Environnement, Avenue des Etangs, 11100 Narbonne, France

[*] Corresponding author

Telephone: +64 6 350 5841

Fax: +64 6 350 5604

Email: B.J.Guieysse@massey.ac.nz

Running title: Toward accurate algal productivity predictions

For Peer Review

Abstract

A new productivity model was parameterized for *Chlorella vulgaris* using short-term (<30 min) oxygen productivities from algal microcosms exposed to 6 light intensities (20-420 W/m^2) and 6 temperatures (5-42^oC). The model was then validated against experimental biomass productivities recorded in bench-scale photobioreactors operated under 4 light intensities (26.8-65.0 W/m^2) and 4 temperatures (10-30°C), yielding an accuracy of ± 13% over 163 days of cultivation. This modeling approach addresses major challenges associated with accurate predictions of algal productivity at full-scale. Firstly, while most prior modeling approaches have only considered the impact of light intensity on algal productivity, the model herein validated also accounts for the critical impact of temperature. Secondly, the new model addresses critical issues associated with parameterization using experimental data generated under conditions that are poorly representative of full-scale cultivation. In particular, this study validates a theoretical approach to convert oxygen productivities into biomass productivities and shows the impact of artificial lighting and light-acclimation can be neglected. Thirdly, the experimental methodology used has the practical advantage of only requiring one day of experimental work for complete model parameterization. The validation of this new modeling approach is therefore an important step for refining feasibility assessments of algae biotechnologies.

Key words: *Chlorella vulgaris*; Model; Light; Temperature; Biofuel; Photosynthesis

For Peer Review

1. Introduction

The ability to accurately predict algal productivity under a broad range of environmental conditions, reactor geometries and operational regimes is crucial to assess the feasibility of full-scale algal production. Among the numerous parameters to consider, light and temperature are the most important given their impact on photosynthesis and cellular respiration, and given the fact that these parameters cannot be easily controlled during full-scale cultivation. A recent review (Béchet et al. 2013a) revealed that most models predicting algal productivity have exclusively focused on the impact of light while neglecting temperature. Furthermore, few models have been validated against external data (i.e. an independent data set not in itself used for model parameterization). In their review, Béchet et al. (2013a) classified more than 40 productivity models into three categories based on the approach used to account for light intensity. This review concluded that Type-I models, predicting productivity as a function of the incident light intensity, are easy to construct and parameterized but are too specific to the system used for their development to enable broad use. Type-III models, which account for the light history of single cells, can accurately account for the complex biological mechanisms occurring in dense algae cultures but are limited by the complexity of the inputs required. Béchet et al. (2013a) thus concluded that Type-II models, which account only for light gradients within the culture broth, offer the best compromise between accurate description of biological mechanisms and practicability. To the best of our knowledge, there is currently no Type-II model of biomass productivity which also accounts for temperature. In this context, the main objective of this study was to develop and externally validate a Type-II model suitable to predict algal productivity under a broad range of light intensities and temperatures.

For Peer Review

Developing a Type-II model requires the generation of specific experimental data sets for parameterization given that light and temperature responses are species dependent (Bernard and Rémond, 2012; Butterwick et al., 2005; Falkowski and Owens, 1978; Ryther, 1956). In practice, parameterization always involves experimentation under well-controlled static conditions (i.e. indoor) that are poorly representative of outdoor cultivation conditions (Lucker et al., 2014). Inaccuracy may therefore originate from the impact of light spectrum on photosynthetic response (Jeon et al., 2005). Further to this, model parameterization can be time and resource consuming if a large number of light-temperature combinations must be evaluated. For example, the accurate measurement of biomass productivity from dry weight increments can require several days of experimentation (Collins and Boylen, 1982; Ogbonna et al., 1995). To circumvent this limitation, proxies such as dissolved oxygen production rates are commonly used for fast determination of kinetic parameters (Jeon et al., 2005; Yun and Park, 2003). However, the conversion of oxygen production rates into biomass productivities introduces uncertainty as the conversion factor can vary with cultivation conditions (Burris, 1981). In addition, a model developed using short-term experiments may inaccurately predict full-scale productivity since acclimation processes are expected to impact seasonal productivities (Bernard, 2011; Crill, 1977; Sakshaug et al., 1991). The second objective of this study was therefore to quantify the accuracy of a temperature-dependent Type-II model parameterized using short-term oxygen production rates. In order to reach this objective, the kinetic parameters of the productivity model were first determined using small algal microcosms exposed to six light intensities (20-420 W/m^2) and six temperatures (5-42^oC). The model predictions were then validated against direct measurements of biomass productivity in bench-scale photobioreactors operated under 4 light intensities and 4 temperatures for 7 to 21 days.

For Peer Review

2. Materials and methods

2.1. Mathematical expression of productivity model

Net algal productivity P_{net} (kg O_2/s) was expressed as the difference between the rate of photosynthesis P (kg O_2/s) and the rate of respiration ER (kg O_2/s) as:

$$P_{net} = P - ER \quad (1)$$

The rate of photosynthesis was expressed according to a Type-II model assuming that the rate of photosynthesis of a single algae cell is only a function of the light intensity the cell is exposed to, neglecting then the impact of light history (Béchet et al., 2013a). At a given temperature, the rate of photosynthesis P in a reactor was therefore computed by integrating the local rates of photosynthesis over the entire volume of the culture broth, which translates into the following mathematical expression:

$$P = \iiint_V P_{loc}\left(\sigma_X I_{loc}, T, X\right) \cdot dV \quad (2)$$

where P_{loc} is the local volumetric rate of photosynthesis (kg O_2/m^3-s), σ_X is the extinction coefficient (m^2/kg), I_{loc} is the local light intensity (W/m^2), T is the temperature (^oC), X is the algal concentration (kg/m^3), and V is the reactor volume (m^3). Three formulas are commonly used to express the local rate of photosynthesis P_{loc} as a function of the local light intensity I_{loc} (Table I). In the current lack of consensus on the best formula to use, each expression was used and compared (see Section 3.1).

The local light intensity was described by a modified Beer-Lambert law expressed as:

$$I_{loc}(l) = I_0 \exp\left(-\sigma_X X l\right) \quad (3)$$

where l is the light path between the considered position and the reactor external surface (m) and I_0 is the incident light intensity (W/m^2). The determination of σ_X is detailed in Section 2.5.

For Peer Review

The rate of respiration in the dark ER_{dark} (kg O_2/s) was assumed to obey first-order kinetics as:

$$ER_{dark} = \lambda XV \quad (4)$$

where λ is the respiration coefficient (kg O_2/kg-s). The expression of the rate of respiration in light conditions ER_{light} (in kg O_2/s) is discussed in the results and discussion section (Section 3.3). When the Monod formula is used, the net total productivity of the reactor P_{net} (kg O_2/s) can be expressed as follows:

$$P_{net} = \int_V P_m(T) \frac{\sigma I_{loc}}{K(T) + \sigma I_{loc}} X \cdot dV - ER(T, X) \quad (5)$$

2.2. Algae strain and preparation

Axenic *Chlorella vulgaris* was inoculated from single colonies maintained on solid medium. Liquid cultures were then prepared under sterile conditions in phosphate-buffered BG-11 as described in Béchet et al. (2013b) and incubated 7 days under the following conditions: temperature: 25°C; CO_2 concentration: 2%; light intensity: 14 W/m^2 (in photosynthetically active radiation, or PAR). The resulting cultures were then used to inoculate bench-scale photobioreactors as described below in Section 2.4.

2.3. Device used for the determination of model parameters

The model parameters were determined using six cylindrical vessels equipped with dissolved oxygen electrodes and placed above LED lamps (12V PHILIPS EnduraLED 10W MR16 Dimmable 4000K, Figure 1). The side and the top lid of the vessels were made of aluminum (i.e. opaque), while the bottom wall was made of a transparent plastic that did not impact the light spectrum. The light intensity entering each vessel was measured using a PAR sensor (Spectrum technologies #3668I, Plainfield IL) calibrated against actinometry measurements

For Peer Review

(Hatchard and Parker, 1956; see the supplementary information S7 for details). All incident light intensities are henceforth given as photosynthetically active radiation (PAR).

At the start of an experiment, aliquots were withdrawn from bench-scale photobioreactors described in Section 2.4 (30°C) and bubbled with 2% CO_2-enriched nitrogen gas to lower dissolved oxygen concentration to approximately 20% of saturation. Then, 76 mL of culture were immediately transferred into each vessel and the LED lamps were turned on. The rate of oxygen production was computed by linear regression of the dissolved oxygen concentration over time. The lights were turned off when the dissolved oxygen concentration reached more than 80 to 90% of the saturation value in any vessel (after 10 to 20 minutes). The consequential rate of oxygen consumption was then measured. Temperature was maintained constant (at approximately ± 1.5^{o}C) during the entire experiment by circulating air between the LED lamps and the vessels (Figure 1). Experiments were performed at different temperatures by controlling the ambient temperature.

2.4. Algal cultivation in the bench-scale photobioreactors for model validation

The four photobioreactors used for model validation were cylindrical reactors (height: 22 cm; diameter: 14 cm; Figure 2). Each of these four reactors was surrounded by 14 light bulbs with different light intensities (Osram Duluxstar Mini Twist Lumilux Daylight, Power 7W, 13W, 18W, and 23W respectively). The incident light intensity entering each reactor was measured using a lux meter (Extech 383274 data logger multimeter with the Light adapter Extech 401020) in the empty reactors at 4 heights and 20 angular positions on the reactor wall, representing a total of 80 measurement points. The incident light intensity reaching the four reactors was estimated at 26.8 W/m^2, 44.7 W/m^2, 49.9 W/m^2, and 65.0 W/m^2, respectively by assuming a conversion factor of 2.7 between klux and W/m^2 (Lang et al., 1981). Temperature was controlled in the four reactors by circulating water in a jacket around the reactors (Figure

For Peer Review

2). Temperature was shown not to differ across reactors by more than 1°C. Air enriched in CO_2 (2%) was bubbled in each reactor at a flow rate of 2.5 L/min in order to provide CO_2, remove oxygen and mix the reactor broth. No significant change of productivity was observed when doubling the nutrient concentrations and CO_2 supply during the experiment at 20°C, indicating that neither nutrients nor CO_2 limited the algal productivity.

At the beginning of each experiment, 1.5L of fresh medium were added into each reactor and aeration started at least 30 minutes before inoculation to allow the medium to reach the desired temperature. The liquid cultures used as inoculum were re-suspended in freshly prepared medium after centrifugation and 0.5L of this re-suspended algal solution was added in each reactor, making a total working volume of 2L in each reactor. Then reactors were operated on a batch mode until the concentration reached a level of around 1 g/L. The reactors were then operated on a semi-continuous mode by replacing a volume fraction of the cultivation broth by freshly prepared medium every day. In order to compensate for evaporation losses, reverse osmosis water was added in the reactors back up to 2L before sampling. During the cultivation, the dry weight concentration was measured daily as follows. Dry weight filters (Membrane filters, 0.45 µm, 47mm, MF-Millipore™, Merck Millipore, Billerica, MA, USA) were first dried at 105°C for 24 hours before being weighed. A known volume of broth was filtered before rinsing the filters with at least 5 mL of RO water to remove any dissolved salt from the filter. Then the filters were placed for 1 hour in the oven at 105°C before being weighted. The dry weight concentration was obtained by weight difference (duplicates were measured).

2.5. Light distribution

The extinction coefficient σ_X was experimentally determined for different algal concentrations X, by measuring the incident light intensity (I_0) and the light intensity

For Peer Review

transmitted by the vessels shown in Figure 1. σ_X was then expressed as a function of I_0 and X (as given by Equation 3) as follows:

$$\sigma_X = \frac{1}{HX} \ln\left(\frac{I_0}{I_{loc}(H)}\right) \quad (6)$$

where H is the height of the vessel (m). The measured extinction coefficient was observed to be dependent on the algal concentration as shown in supplementary information (S1). This dependence was experimentally observed in previous studies and was attributed to the diffusion of light by algae cells (Acién Fernández et al., 1997). The extinction coefficient was experimentally found to obey the following equation:

$$\sigma = AX^B \quad (7)$$

where A and B are empirical coefficients (A = 117.4 ± 1.6 m^2/kg; B = -0.200 ± 0.06). The light from the LED lamps used in the experiment was not emitted in a vertical direction but diffused in a cone of angle 36^o. In addition, due to the tendency of algae to scatter light (Acién Fernández et al., 1997), a fraction of the light entering the culture was absorbed by the side of the vessels. As Equation 3 does not account for this fraction, the extinction coefficient may be overestimated. In order to account for this effect, the value of the extinction coefficient was calculated by considering that either 1) I_0 in Equation 6 is the light intensity at the bottom of the vessel, or 2) I_0 in Equation 6 is the light intensity transmitted through the vessel when the vessel is filled with transparent medium. In the first case, the transmittance was overestimated as the absorption by the sides of the vessel was not accounted for. Conversely, in the second case, the transmittance was underestimated as the absorption by the sides of the vessel was overestimated. As a result, the "true" value of σ_X was between these two values, referred to as "lower" and "upper" values, respectively (see the supplementary information S1 for details).

For Peer Review

The determination of the light distribution in the bench-scale photobioreactors is detailed in supplementary information (S2). Due to the complexity of the equations describing the model, the productivity of the algal cultures studied here was calculated numerically. The numerical solving of these equations with MATLAB® is detailed in supplementary information (S3 and S4).

2.6. Conversion of oxygen productivity into biomass productivity

The model parameters P_m and λ were converted from oxygen-based units (kg O_2/kg-s) into biomass-based units (kg/kg-s) by assuming that 1) all the chemical energy generated through photosynthesis was used to synthetize glucose through the Calvin Cycle, and 2) the synthesized glucose was used as an energy source during respiration and/or as a carbon source during biomass synthesis. These assumptions enabled the determination of the following conversion coefficients (see the supplementary information S5 for more details):

- P_m' [kg/kg-s] = 0.76 (±0.09) P_m [kg O_2/kg-s]
- λ' [kg/kg-s] = 0.76 (±0.09) λ [kg O_2/kg-s] in light conditions
- λ' [kg/kg-s] = 0.94 λ [kg O_2/kg-s] in dark conditions

2.7. Fitting algorithm and Monte Carlo simulations

The model parameters K and P_m were obtained by fitting the values of oxygen production rates measured for different incident light intensities. A least-square algorithm was used in order to fit the model to experimental data, consisting of finding the parameters P_m and K minimizing the following sum:

$$S^2 = \sum_{I_0} \left(P_{\exp} - P_{theo}\left(I_0, P_m, K, X, \sigma_X\right)\right)^2 \quad (8)$$

where P_{exp} and P_{theo} are the measured and predicted oxygen productivities (kg O_2/s), I_0 are the six different incident light intensities (W/m^2), X is the cell concentration (kg/m^3), and σ_X is

For Peer Review

the extinction coefficient (m^2/kg). The fitting procedure is further detailed in supplementary information (S6).

Monte-Carlo simulations were used in order to quantify the impact of the uncertainty of measured variables on the fitted values of P_m, K, and λ. Four variables were considered in this uncertainty analysis:

1) The dissolved oxygen concentration measured by the electrodes which was found to be accurate at ± 5.4% (p = 0.05, N = 30);
2) The incident light intensity reaching the algae which was determined by actinometry and was accurate within ± 10% (see the supplementary information S7 for details);
3) The uncertainty on the extinction coefficient σ_X which was given by the upper and lower values of σ_X defined in Section 2.5;
4) The dry weight concentration which was found to be accurate within ± 7.0% and ± 7.9% in the two experiments used for model parameterization. This statistical analysis was based on the measurement of more than 200 dry weight measurements done in duplicate (see the supplementary information S6 for details).

When using the model to predict productivity in the bench-scale photobioreactors, the uncertainty on P_m, K, λ and model inputs caused inaccuracy on the model predictions. This level of inaccuracy was computed by performing Monte-Carlo simulations which are detailed in supplementary information (S6).

2.8. Overall accuracy

The overall accuracy of the model Δ was determined from the comparison of the model predictions to the experimental data collected in the bench-scale photobioreactors and was expressed as:

For Peer Review

$$\Delta = \frac{1}{N_I N_T} \frac{\sum_{I_0} \sum_{T} \left| P_{cumul,theo}(I_0,T) - P_{cumul,\exp}(I_0,T) \right|}{\sum_{I_0} \sum_{T} \left| P_{cumul,\exp}(I_0,T) \right|} \quad (9)$$

where $P_{cumul,theo}$ and $P_{cumul,exp}$ (kg) are the cumulative theoretical and measured productivities in the bench-scale photobioreactors over the entire period of cultivation, respectively, and N_I and N_T the number of incident light intensities and temperatures tested for, respectively.

3. Results and discussion

3.1. Model parameterization

The model was able to accurately describe the impact of the incident light intensity on oxygen production regardless of the formula used to express the local rate of photosynthesis (Figure 3). The values of the parameters K and P_m varied by up to ± 10% with the algae concentration and these variations could not be entirely explained by the error on the measured variables. The differences in P_m were unlikely due to the flashing-light effect or light-inhibition because the value of P_m (predicted productivity at high light intensities) tended to increase when the cell concentration was reduced. The observed variations of P_m with the algal concentration are most likely due to the modeling approach used to determine the light distribution in the culture broth described in Section 2.5. The level of inaccuracy of P_m is on the same order of magnitude of the level of inaccuracy reported by Cornet and Dussap (2009) who showed that a Type-II model was able to predict the rate of photosynthesis of *Spirulina platensis* in photobioreactors of different geometries with a level of accuracy of ± 15%.

No clear conclusion can be drawn on the best formula to represent the rate of photosynthesis. The study of Yun and Park (2005) showed that a Monod formula was able to predict the rate of photosynthesis of *Chlorella vulgaris* for different light intensities and algal concentrations. Consequently, the Monod formula will be used in the rest of this study.

For Peer Review

3.2. Evolution of the model parameters K and P_m with temperature

As shown in Figure 4, the values of K and P_m first increased with temperature before rapidly decreasing for temperatures higher than 38°C. As discussed by Bernard and Rémond (2012), the initial increase of the rate of photosynthesis with temperature is explained by the increasing activity of the key enzymes of the photosynthetic process. However, these enzymes are denatured at temperatures higher than a certain threshold (close to 38°C here), which results in the fast decrease of the rate of photosynthesis (Davison, 1991).

Previous results from the literature suggest that the rate of photosynthesis of single algae cells is not affected by temperature at low light intensities (Davison, 1991). When $\sigma I_{loc} << K$, the Monod formula can be simplified as:

$$P \cong \frac{P_m}{K} \sigma I_{loc} \quad (10)$$

This relationship implies that if the rate of photosynthesis of light-limited cells is temperature-independent, the ratio P_m/K should not depend on temperature. This was verified by our results as the values of P_m and K at different temperatures were close to linearly correlated (Figure 5).

3.3. Rate of endogenous respiration

The respiration coefficients λ in Equation 4 were determined from the 15-min respiration rates measured immediately after light exposure. Additional experiments showed that these rates were equal to the respiration rates recorded during several hours under darkness. Figure 4 shows that the evolution of the respiration coefficient λ with temperature is similar to the evolution of the other model parameters P_m and K with temperature. These trends are commonly reported in the literature (Collins and Boylen, 1982; Grobbelaar, 1990; Le Borgne

For Peer Review

and Pruvost, 2013) and are explained by the temperature-dependence of key enzymatic reactions.

While respiration in the dark has been modeled using first-order kinetics in most previous studies there is no consensus on the best modeling approach for respiration in light conditions (Béchet et al., 2013a). In the literature, the rate of respiration in light conditions is assumed to be either proportional to the rate of photosynthesis (e.g. Geider et al., 1997) or equal to the rate of respiration in the dark (e.g. Quinn et al., 2011). The 15-min respiration rate was not clearly correlated with the rate of photosynthesis during light exposure as demonstrated in supplementary information (S8). In the absence of correlation, it was assumed that rates of respiration in the dark and in light conditions were equal and the rate of respiration in light conditions was expressed as:

$$ER_{light} = \lambda XV \quad (11)$$

where the values of the respiration coefficients λ at various temperatures are listed in Table II. In the following the values of the model parameters P_m, K and λ at any temperature were determined by linear interpolation between values experimentally determined during model parameterization (Table II).

3.4. Model validation

In order to validate the productivity model against an external data set, biomass productivity was predicted in bench-scale photobioreactors by using the model parameters listed in Table II. Figure 6 shows the cumulative productivities in photobioreactors exposed to four light intensities and five temperatures. As can be seen, the model prediction (plain blue line) was overall in good agreement with the experimental data (red crosses) over the entire period of cultivation for temperatures lower than 30°C (the dash-lines represent the level of accuracy of model predictions due to uncertainty on model inputs). However, the model was unable to

For Peer Review

predict algal productivity for a period of time longer than 1 to 3 day(s) at a temperature of 35°C due to the subsequent culture collapse. This suggests that the optimal temperature for photosynthesis (around 38°C, Figure 4) differs from the optimal temperature for biomass production and highlights a limitation of the short-term model parameterization. This difference is explained by the fact that photosynthesis and biomass production are processes regulated by different enzymes (Madigan and Martinko, 2006). The experimental data at 35°C was therefore not used in the following assessment of the model accuracy.

The overall accuracy of the model was defined from the relative difference between the measured and predicted cumulative productivities in all the photobioreactors (in absolute value as described by Equation 9). Over the entire period of cultivation representing 163 days of operation, the model was able to predict productivity with an accuracy of ± 13% (see supplementary information S9 for details). To the best of our knowledge, this study presents the first quantification of the overall uncertainty of an algal productivity prediction resulting from the uncertainties in model inputs. This uncertainty analysis was used to determine if differences between experimental data and model predictions were caused by erroneous assumptions in the model development rather than experimental errors. As can be seen in Figure 6, the majority of the experimental data falls within the confidence interval of the model predictions (shown in dash lines), indicating that model inaccuracy likely originated from random measurement error (e.g. incident light intensity and temperature) and/or uncertainty in model kinetic parameters. This also implies that further improvement of the accuracy will be challenging because experimental error cannot be easily reduced further beyond the techniques used in this work. For example, the model could be refined by including the effect of cell history on the rate of photosynthesis as done in previous modeling studies (e.g. Duarte, 1995; Han, 2000; Wu and Merchuk, 2002). However, even if the model

For Peer Review

accuracy may be improved by such refinement, the overall uncertainty would also increase with the number of model parameters.

Few prior models have been validated against external data (e.g. data not used for parameterization), which is of significant concern considering the differences between the conditions used for model parameterization and full-scale conditions (Béchet et al., 2013a). The level of accuracy of ± 13% achieved by the productivity model however revealed that these differences did not significantly impact the model predictions in the bench-scale photobioreactors. The fitness of the model was indeed demonstrated under a broad range of light and temperature conditions (light intensity range: 26.8-65.0 W/m^2; temperature range: 10-30°C). In particular, the oxygen-biomass conversion factors and differences in the light sources used to parameterize and validate the model did not appear to significantly or systematically impact productivity. The ability of the model to accurately predict productivities over several weeks also suggests that light-acclimation did not significantly impact algal productivity over this timescale.

Of particular significance is the fact that the model presented in this study is able to account for the impact of temperature as prior literature has exclusively focused on the impact of light. The accuracy of the predictions within ± 13% demonstrates that the impact of temperature on productivity can be accurately predicted by expressing the parameters of a Type-II model (P_m and K) and the respiration coefficient λ as empirical functions of temperature. Furthermore, a practical advantage of the experimental methodology used to parameterize the model developed in this study only requires one day of experimental work. Indeed, the experiments performed to determine the values of P_m, K, and λ over the range of temperature 5-42^{o}C only represented one day of experimental work. In comparison, if the data collected from the bench-scale photobioreactors was to be used to parameterize the productivity model, around 2 months of continuous experimental work would be necessary.

For Peer Review

Given the ability of this model to accurately predict the impact of temperature on productivity and the rapidity of the methodology used for model parameterization, this modeling approach is an important step toward accurate feasibility assessments of full-scale algal cultivation.

4. Conclusions

- To the best of our knowledge, this study presents the first validation of a Type-II algal biomass productivity model which can account for light and temperature impacts.
- This model parameterized using short-term experiments in microcosms predicted biomass productivity from bench-scale photobioreactors operated under 4 light intensities (26.8-65.0 W/m^2) and 4 temperatures (10-30°C) with an accuracy of ± 13% over a total of 163 days of cultivation.
- The level of accuracy reported over a broad range of environmental conditions suggests that neither light-acclimation nor differences in light spectrums significantly impacted productivity. Likewise, potential variations in oxygen-biomass conversion factors did not introduce significant error in productivity predictions.
- In addition to provide accurate predictions of the impact of temperature on algal productivity, the associated methodology for model parameterization only requires one day of experimental work. The modeling approach presented in this study is therefore an important step toward accurate feasibility assessments of full-scale algal cultivation.

5. List of supplementary materials

S1: Determination of the extinction coefficient; S2: Determination of the light distribution in the bench-scale photobioreactors; S3: Expression of the total rate of photosynthesis in the device used for the determination of the model kinetic parameters; S4: Expression of the total rate of photosynthesis in the bench-scale photobioreactors used for model validation; S5: Conversion of oxygen productivity into biomass productivity; S6: Description of Monte-

For Peer Review

Carlo simulations used for treatment of uncertainties; S7: Actinometry; S8: Correlation between the rate of respiration and rate of photosynthesis; S9: Comparison of predicted and measured cumulative productivities in the bench-scale photobioreactors.

References

Acién Fernández FG, García Camacho F, Sánchez Pérez JA, Fernández Sevilla JM, Molina Grima E. 1997. A model for light distribution and average solar irradiance inside outdoor tubular photobioreactors for the microalgal mass culture. Biotechnol Bioeng 55(5):701-714.

Béchet Q, Shilton A, Guieysse B. 2013a. Modeling the effects of light and temperature on algae growth: State of the art and critical assessment for productivity prediction during outdoor cultivation. Biotechnol Adv 31(8):1648-1663.

Béchet Q, Muñoz R, Shilton A, Guieysse B. 2013b. Outdoor Cultivation of Temperature-Tolerant Chlorella sorokiniana in a Column Photobioreactor Under Low Power-Input. Bioeng Biotechnol 110(1):118-126.

Bernard O. 2011. Hurdles and challenges for modelling and control of microalgae for CO_2 mitigation and biofuel production. J Process Control 21:1378-1389.

Bernard O, Rémond B. 2012. Validation of a simple model accounting for light and temperature effect on microalgal growth. Biores Technol 123:520-527.

Bordel S, Guieysse B, Muñoz R. 2009. Mechanistic model for the reclamation of industrial wastewaters using algal-bacterial photobioreactors. Environ Sci Technol 43(9):3200–3207.

Burris JE. 1981. Effects of oxygen and inorganic carbon concentrations on the photosynthetic quotients of marine algae. Mar Biol 65:215-219.

Butterwick C, Heaney SI, Talling JF. 2005. Diversity in the influence of temperature on the growth rates of freshwater algae, and its ecological relevance. Freshw Biol 50:291-300.

For Peer Review

Carvahlo AP, Malcata FX. 2003. Kinetic modeling of the autotrophic growth of *Pavlova lutheri*: study of the combined influence of light and temperature. Biotechnol Prog 19:1128-1135.

Chalker BE. 1980. Modelling light saturation curves for photosynthesis: an exponential function. J Theor Biol 84:205-215.

Collins CD, Boylen CW. 1982. Physiological responses of *Anabaena variabilis* (cyanophyceae) to instantaneous exposure to various combinations of light intensity and temperature. J Phycol 18:206-211.

Cornet JF, Dussap CG, Gros JB. 1995. A simplified monodimensional approach for modeling coupling between radiant light transfer and growth kinetics in photobioreactors. Chem Eng Sci 50(9):1489-1500.

Cornet JF, Dussap CG. 2009. A simple and reliable formula for assessment of maximum volumetric productivities in photobioreactors. Biotechnol Prog 25(2):424-435.

Crill PA. 1977. The photosynthesis-light curve: a simple analog model. J Theor Biol 64:503-516.

Cullen JJ. 1990. On models of growth and photosynthesis in phytoplankton. Deep Sea Research 37(4):667-683.

Davison IR. 1990. Environmental effects of temperature on photosynthesis: temperature. J Phycol 27:2-8.

Duarte P. 1995. A mechanistic model of the effects of light and temperature o algal primary productivity. Ecol Model 82:151-160.

Evers EG. 1991. A model for light-limited continuous cultures: Growth, shading, and maintenance. Biotechnol Bioeng 38(3):254-259.

Falkowski PG, Owens TG. 1978. Effects of light intensity on photosynthesis and dark respiration in six species of marine phytoplankton. Marine Biol 45:289-295.

For Peer Review

Geider RJ. 1990. The relationship between steady state phytoplankton growth and photosynthesis. Limnol Oceanogr 35(4):971-972.

Geider RJ, MacIntyre HL. 1996. A dynamic model of photoadaptation in phytoplankton. Limnol Oceanogr 41(1):1-15.

Geider RJ, MacIntyre HL, Kana TM. 1997. Dynamic model of phytoplankton growth and acclimation: responses of the balanced growth rate and the chlorophyll *a*: carbon ratio to light, nutrient-limitation and temperature. Mar Ecol Prog Ser 148:187-200.

Geider RJ, MacIntyre HL, Kana TM. 1998. A dynamic regulatory model of phytoplanktonic acclimation to light, nutrients, and temperature. Limnol Oceanogr 43(3):679-694.

Grobbelaar JU. 1990. Modeling algal productivity in large outdoor cultures and waste treatment systems. Biomass 21:297-314.

Haario H, Kalachev L, Laine M. 2009. Reduced models of algae growth. Bull Math Biol 71:1626-1648.

Han BP, Virtanen M, Koponen J, Straškraba M. 2000. Effect of photoinhibition on algal photosynthesis: a dynamic model. J Plankton Res 22(5):865:885.

Hatchard CG, Parker CA. 1956. A new sensitive chemical actinometer. II. Potassium ferrioxalate as a standard chemical actinometer. Proc Royal Soc London Ser A Math Phys Sci 235(1203):518-536.

Jeon YC, Cho CW, Yun YS. 2005. Measurement of microalgal photosynthetic activity depending on light intensity and quality. Biochem Eng J 27:127-131.

Kiefer DA, Mitchell BG. 1983. A simple, steady-state description of phytoplankton growth based on absorption cross section and quantum efficiency. Limnol Oceanog 28(4):770-776.

Kurano N, Miyachi S. 2005. Selection of microalgal growth models for describing specific growth rate-light response using extended information criterion. J Biosci Bioeng 100 (4):403-408.

For Peer Review

Lang OL, Novel PB, Osmond B, Ziegler H. 1981. Photosynthetically active radiation. In: Physiological plant ecology. Vol. 12A, Encyclopedia of plant physiology (new series).

Le Borgne F, Pruvost J. 2013. Investigation and modeling of biomass decay rate in the dark and its potential influence on net productivity of solar photobioreactors for microalga *Chlamydomonas reinhardtii* and cyanobacterium *Arthrospira platensis*. Biores Technol 138: 271-276.

Lucker BF, Hall CC, Zegarac R, Kramer DM. 2014. The environmental photobioreactor (ePBR): an algal culturing platform for simulating dynamic natural environments. Algal Res (In press).

Madigan MT, Martinko JM. 2006. Brock – Biology of microorganisms. 11th Edition. Pearson Prentice Hall. Upper Saddle River, NJ 07458.

Ogbonna JC, Yada H, Tanaka H. 1995. Light-supply coefficient: a new engineering parameter for photobioreactor design. J Ferment Bioeng 80(4):369-376.

Pahlow, M. 2005. Linking chlorophyll-nutrient dynamics to the Redfield N:C ratio with a model of optimal phytoplankton growth. Mar Ecol Prog Ser 287:33-43.

Pahl-Wostl C, Imboden DM. 1990. DYPHORA – a dynamic model for the rate of photosynthesis of algae. J Plankton Res 12(6):1207-1221.

Pahl-Wostl C. 1992. Dynamic versus static models for photosynthesis. Hydrol 238:189-196.

Quinn J, de Winter L, Bradley T. 2011. Microalgae bulk growth model with application to industrial scale systems. Biores Technol 102, 5083-5092.

Ryther JH. 1956. Photosynthesis in the ocean as a function of light intensity. Limnol Oceanog 1(1):61-70.

Sakshaug E, Johnsen G, Andresen K, Vernet M. 1991. Modeling of light-dependent algal photosynthesis and growth: experiments with the Barents Sea diatoms *Thalassiosira nordenskioeldii* and *Chaetoceros furcellatus*. Deep-Sea Res 38(4):415-430.

For Peer Review

Wu X, Merchuk JC. 2002. Simulation of algae growth in a bench-scale bubble column reactor. Biotechnol Bioeng 80(2):156-168.

Yun YS, Park JM. 2003. Kinetic modeling of the light-dependent photosynthetic activity of the green microalga *Chlorella vulgaris*. Biotechnol Bioeng 83(3):303-311.

For Peer Review

List of figures

Figure 1: Device used for the determination of the model parameters.

Figure 2: Bench-scale photobioreactor used for model validation. The four reactors were surrounded by 14 light bulbs each, and temperature was controlled by re-circulating water in the double jacket.

Figure 3: Experimental (dots) and fitted oxygen productivities in the vessels used for model parameterization (Point-line: $X = 0.19$ kg/m^3; Plain line: $X = 0.43$ kg/m^3; Dash-line: $X = 0.64$ kg/m^3). The error bars represent the level of confidence on the measured rates of photosynthesis and light intensity (see the supplementary information S6 for details).

Figure 4: Values of P_m, K, and λ at different temperatures. The error bars represent the 95% confidence interval determined by Monte-Carlo simulations (see the supplementary information S6 for details).

Figure 5: P_m values vs. K values at different temperatures. The error bars represent the 95% confidence interval determined by Monte-Carlo simulations (see the supplementary information S6 for details).

Figure 6: Cumulative productivity in the bench-scale photobioreactors operated under different light intensities and temperatures (blue line: model prediction; dash-line: prediction inaccuracy due to uncertainty on inputs; red crosses: experimental data). The shaded area represents the period of time when the reactors were operated as batch systems.

For Peer Review

Table I: Mathematical formulas of the local rate of photosynthesis (P_{loc}, in kg O_2/m^3-s) as a function of the local light intensity (I_{loc}, in W/m^2) and the algal concentration X (kg/m^3). P_m (kg O_2/kg-s) represents the maximum specific rate of photosynthesis and K/σ (W/m^2) represents the half-saturating light intensity.

Formula	Equation	References
Monod	$P_{loc} = P_m \frac{\sigma I_{loc}}{K + \sigma I_{loc}} X$	Bordel et al. (2009) Carvahlo and Malcata (2003) Collins and Boylen (1982) Kiefer and Mitchell (1983) Cornet and Dussap (2009) Cornet et al. (1995) Evers (1991) Haario et al. (2009) Jeon et al (2005) Yun and Park (2003)
Poisson	$P_{loc} = P_m \left(1 - \exp\left(-\frac{\sigma I_{loc}}{K}\right)\right) X$	Cullen (1990) Geider (1990) Geider and McIntyre (1996) Geider et al. (1998) Palhow (2005) Sakshaug et al. (1991)
Tangent hyperbolic	$P_{loc} = P_m \tanh\left(\frac{\sigma I_{loc}}{K}\right) X$	Chalker (1980) Kurano and Miyachi (2005) Pahl-Wostl (1992) Pahl-Wostl and Imboden (1990)

For Peer Review

Table II: Values of the model parameters P_m, K and λ at different temperatures (values in parenthesis indicate the confidence interval at 95% computed through Monte-Carlo simulations).

Temperature (^oC)	5.5	14.1	21.7	29.3	37.8	42.3
P_m (10^{-5} kg O_2/kg-s)	1.04 (0.09)	3.11 (0.29)	4.97 (0.49)	6.44 (0.67)	8.37 (0.98)	0
K (W/kg)	598 (125)	1560 (260)	3750 (600)	4950 (900)	8170 (1620)	NA
λ (10^{-6} kg O_2/kg-s)	0	1.75 (0.17)	2.02 (0.19)	2.32 (0.22)	2.60 (0.25)	0

For Peer Review

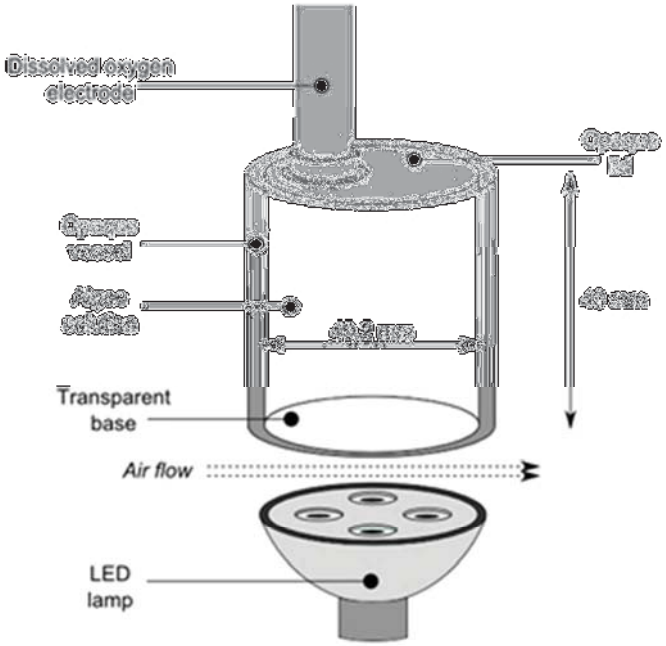

Figure 1: Device used for the determination of the model parameters.

Review

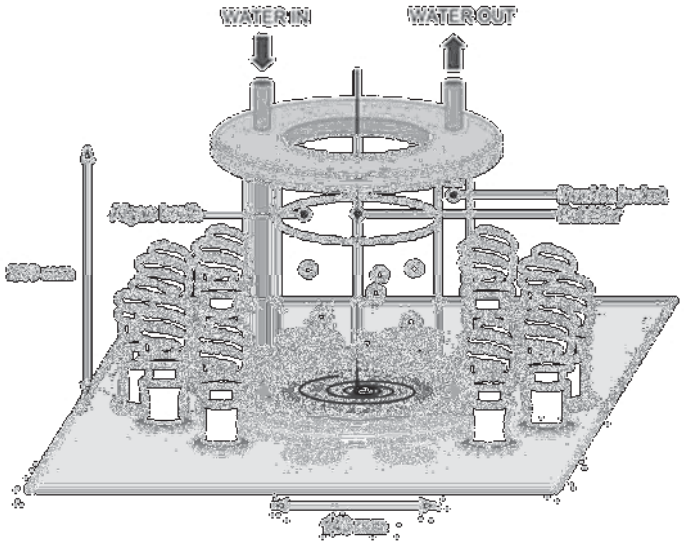

Figure 2: Bench-scale photobioreactor used for model validation. The four reactors were surrounded by 14 light bulbs each, and temperature was controlled by re-circulating water in the double jacket.

For Peer Review

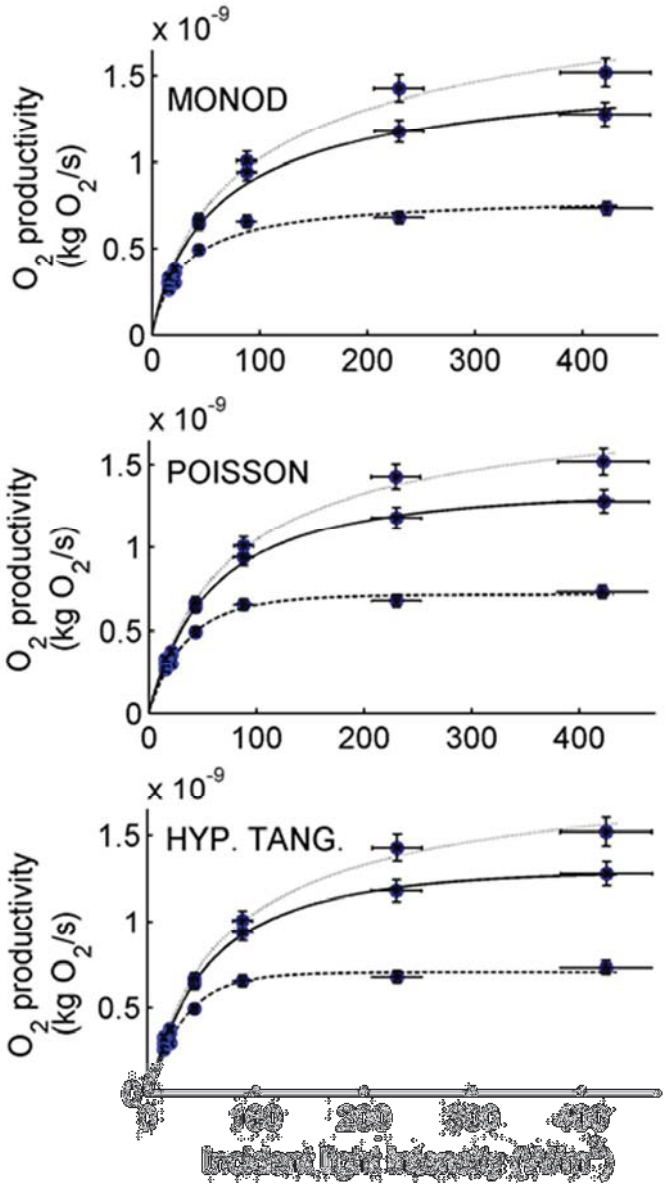

Figure 3: Experimental (dots) and fitted oxygen productivities in the vessels used for model parameterization (Point-line: X = 0.19 kg/m3; Plain line: X = 0.43 kg/m3; Dash-line: X = 0.64 kg/m3). The error bars represent the level of confidence on the measured rates of photosynthesis and light intensity (see the supplementary information S6 for details).

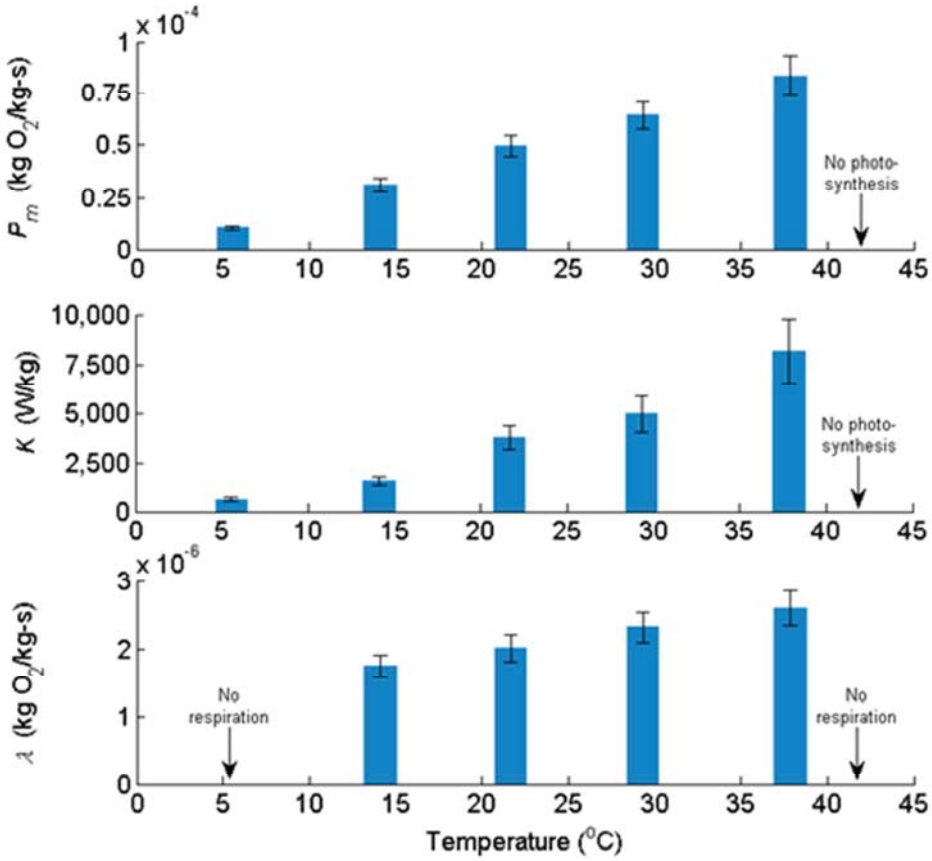

Figure 4: Values of Pm, K, and λ at different temperatures. The error bars represent the 95% confidence interval determined by Monte-Carlo simulations (see the supplementary information S6 for details).

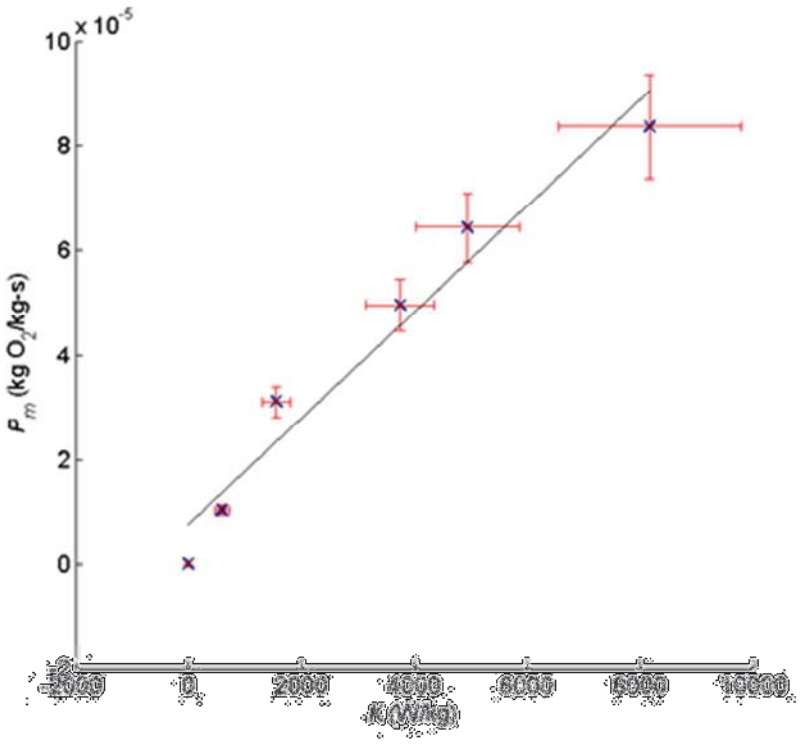

Figure 5: Pm values vs. K values at different temperatures. The error bars represent the 95% confidence interval determined by Monte-Carlo simulations (see the supplementary information S6 for details).

For Review

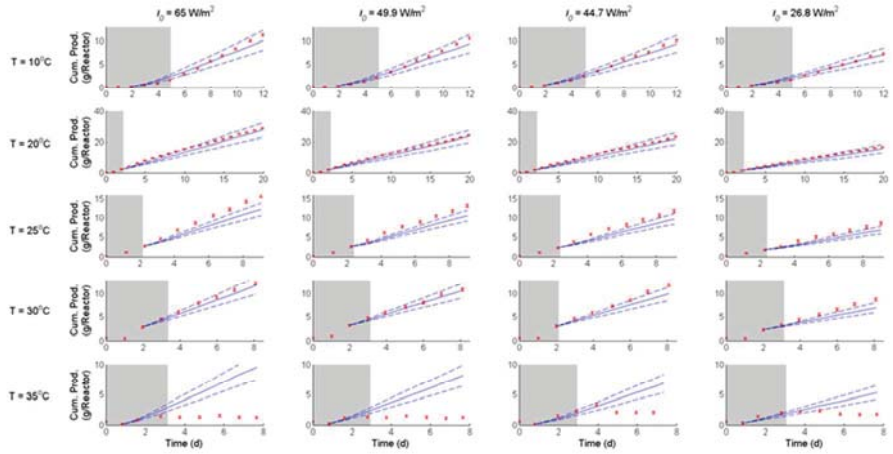

Figure 6: Cumulative productivity in the bench-scale photobioreactors operated under different light intensities and temperatures (blue line: model prediction; dash-line: prediction inaccuracy due to uncertainty on inputs; red crosses: experimental data). The shaded area represents the period of time when the reactors were operated as batch systems.

Peer Review

Algal productivity modeling: a step toward accurate assessments of full-scale algal cultivation – Supplementary information

Béchet Quentin, Chambonnière Paul, Shilton Andy, Guizard Guillaume, Guieysse Benoit

For Peer Review

S1: Determination of the extinction coefficient

Figure S1-1 shows how the extinction coefficient σ varies the cell concentration (the dash lines represent the error, calculated as described in the main manuscript).

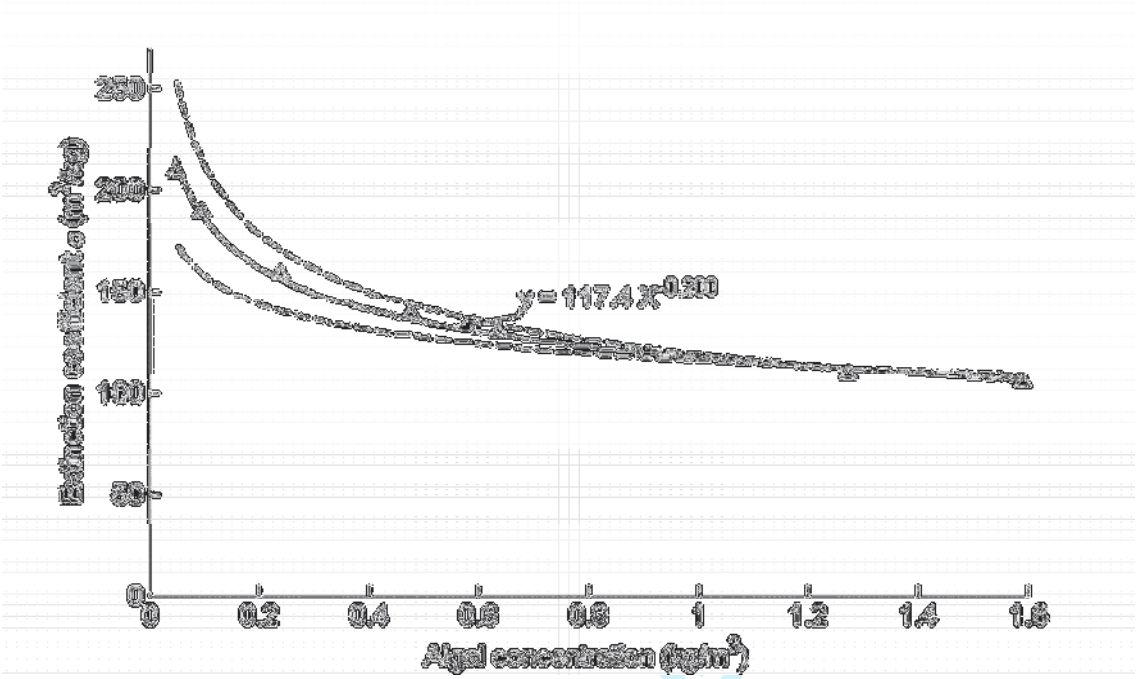

Figure S1-1: Relationship between the extinction coefficient σ_X and the algal concentration (plain line). The dash-lines represent the lower and upper values of σ_X (see main manuscript for details).

S2: Determination of the light distribution in the bench-scale photobioreactors

2.1. Introduction

The application of a Type II model requires determining the light distribution in the cultivation broth. The goal of this supplementary information is to explain how this calculation was performed in the indoor bench-scale photobioreactors shown in Figure 1 in the main manuscript.

The assumptions made to determine the light distribution are listed in the first section. The equations necessary to compute the local light intensity within the reactor are derived in the second section. Finally, the validity of the formulas and algorithms used in this study are checked in the last section by ensuring that basic conservation laws were respected. The light distribution in the reactors is illustrated in the two last sections.

2.2. Main assumptions

The determination of the light distribution in the reactors was carried under the following assumptions:

- The light propagation obeys the modified Beer-Lambert-law (which is equivalent to assuming that algae cells do not scatter light).
- The light source (light bulbs) emits diffuse radiation, meaning that the light emitted by the bulbs is not emitted in a preferential direction.
- The incident light intensity was measured inside the reactor when the reactor was empty. It was assumed that the amount of light going through the empty reactor was the same as the amount of light going through the full reactors.
- The incident light intensity varies with the height at which it was measured but does not depend on the angular position.

For Peer Review

2.3. Determining the light distribution in the bench-scale reactors

2.3.1. Equations used for the local light intensity

In order to determine the light intensity reaching an algae cell located in the reactor (located at the position M(r, z) on Figure S2-1), it is necessary to consider the amount of radiation coming from the entire external wall of the reactor:

$$I_{loc}(r,z) = \int_{\theta}\int_{z'} dI_{dS'\to M} \quad \text{(S2-1)}$$

where $I_{loc}(r,z)$ is the light intensity at the location M and $dI_{dS'->M}$ is the amount of radiation emitted by the surface dS' to the algae located at the position M (Figure S2-1). Using the modified Beer-Lambert law and the expression of the solid angle represented by an algae cell at M for the reactor infinitesimal surface dS', $dI_{dS'->M}$ can be expressed as:

$$dI_{dS'\to M} = I_0(z')\frac{\sigma\cdot\cos\alpha}{\pi r'^2}\exp(-\sigma X r')Rd\theta dz' \quad \text{(S2-2)}$$

where $I_0(\theta,z')$ is the incident radiation at the location $M'(\theta,z')$, σ is the extinction coefficient of the algae (m^2/kg)[1], α is the angle between the vector normal to the surface dS' and the line MM', r' is the distance between M and M' (m), X is the cell concentration (kg/m^3), and R is the reactor radius (m).

[1] Note that the extinction coefficient is a function of the cell concentration (see section 2.4 of the main manuscript). The extinction coefficient is noted σ instead of σ_X to simplify notations in all the supplementary information.

For Peer Review

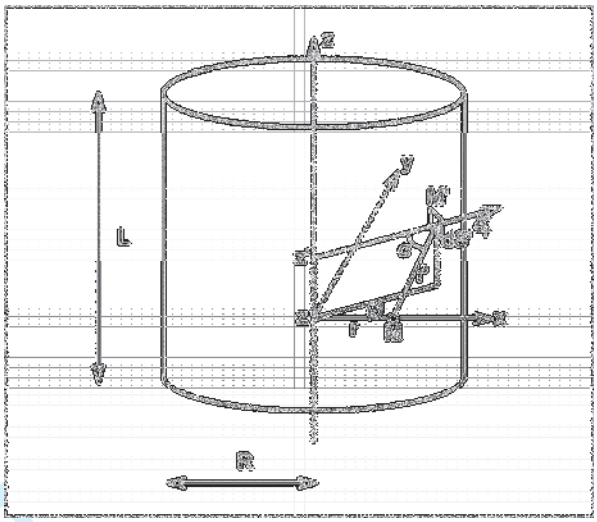

Figure S2-1

Figure S2-1: Bench-scale reactor (R: reactor radius; L: reactor height; M(r,z): position of the algae cell; $\boldsymbol{e}_r$: vector normal to the surface dS'; M'(θ,z'): position of the surface emitting light; r': distance between M and M').

Calculation of r'

The distance r' can be seen as the norm of the vector **MM'**, that can be decomposed as the sum of the vectors **–OM** and **OM'**:

$$r' = \left\| \overrightarrow{MM'} \right\| = \left\| -\overrightarrow{OM} + \overrightarrow{OM'} \right\| = \left\| -r\vec{e}_x + R\cos\theta\vec{e}_x + R\sin\theta\vec{e}_y + (z'-z)\vec{e}_z \right\| \quad \text{(S2-3)}$$

Equation (S2-3) leads to the following expression for r':

$$r' = \left(R^2 + r^2 - 2\cdot r\cdot R\cdot\cos\theta + (z-z')^2\right)^{1/2} \quad \text{(S2-4)}$$

Determination of the term cosα

cosα is the cosine of the angle between the vector $\boldsymbol{e}_r$ and the vector **MM'** (Figure S2-1):

$$\cos\alpha = \vec{e}_r \cdot \frac{\overrightarrow{MM'}}{\left\|\overrightarrow{MM'}\right\|} = \frac{1}{r'}\begin{vmatrix}\cos\theta \\ \sin\theta \\ 0\end{vmatrix} \cdot \begin{vmatrix}R\cos\theta - r \\ R\sin\theta \\ z'-z\end{vmatrix} = \frac{R - r\cos\theta}{r'} \quad \text{(S2-5)}$$

Finally, the following equation can be obtained for the local light distribution:

For Peer Review

$$I_{loc}(r,z)=\frac{\sigma R}{\pi}\int_{\theta}\int_{z'} I_0(z')\cdot\frac{(R-\cos\theta)\exp\left(-\sigma X\sqrt{R^2+r^2-2\cdot r\cdot R\cdot\cos\theta+(z-z')^2}\right)}{\sqrt{R^2+r^2-2\cdot r\cdot R\cdot\cos\theta+(z-z')^2}^{3}}\cdot d\theta dz' \quad \text{(S2-6)}$$

2.4. Numerical implementation of the equations

The calculation of the double integral in Equation S2-6 cannot easily be solved analytically and a numerical algorithm was therefore used to estimate the local intensity in the bench-scale reactors, using a trapezoidal formula. The external surface of the reactor was discretized in small surface elements (*dθdz'*, as shown by Equation S2-6). The number of these elements in the vertical (*dz'*) and angular direction (θ) will be referred to as N_z and N_θ in the rest of this document. For positions M relatively close to the reactor wall, the size of the infinitesimal surface *dS'* is too high for the solid angle to be expressed as:

$$\Omega_{dS'\to\sigma}=\frac{\sigma}{\pi r'^2}\cos\alpha \quad \text{(S2-7)}$$

(this formula requires that the distance *r'* is large compared with the characteristic length of the surface *dS'*). When the distance *r'* was too small compared with $Rd\theta$ (the width of *dS'*) or *dz'* (the height of *dS'*), the surface *dS'* was split in several smaller surfaces (Figure S2-2). In this specific case, the number of sub-divisions of each infinitesimal surface element *dS'* will be referred to as N_{lim}^2 in the following.

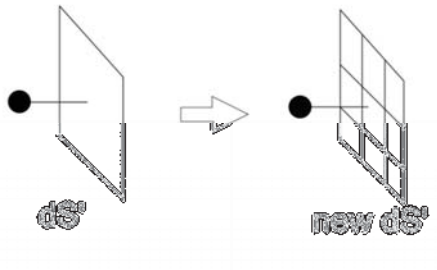

Figure S2-2: Splitting of the infinitesimal surface dS' when the algae cell considered (black circle) was too close to the reactor wall. This splitting was necessary for Equation S2-6 to remain valid.

For Peer Review

2.5. Validation: respect of the photon conservation

In order to verify the formula S2-6 and the corresponding algorithm used to determine the light distribution in the reactor, it was ensured that laws of conservation were respected. The flux of photons entering the reactor (I_{in}) was computed and compared to the sum of the fluxes of photons absorbed by the algae (I_{abs}) or going through the reactor (I_{th}). This section first explains how these three different components were calculated and then compares these fluxes to each other.

2.5.1. Photon flux going through the reactor (I_{th})

In the following, a small surface (dS) on the lateral surface of the reactor will be considered. As the incident light is assumed to be diffuse (section 2), a fraction of the radiation emitted by the surface dS goes through the top surface, the bottom surface or the top surface of the reactor (Figures S2-3 and S2-4a). Using the angles φ and θ defined by Figure S2-4c, the flux of photons emitted by dS in the direction (θ, φ) and going through the reactor is:

$$dI_{th}(\theta,\varphi) = dI(M)\frac{\cos\varphi\sin\varphi d\varphi d\theta}{\pi}\exp(-\sigma X r') \quad \text{(S2-8)}$$

where $dI(M)$ is the photon flux emitted by dS at the position M (W) and r' is the light path of the radiation emitted by dS before going out of the reactor (Figure S2-3).

For Peer Review

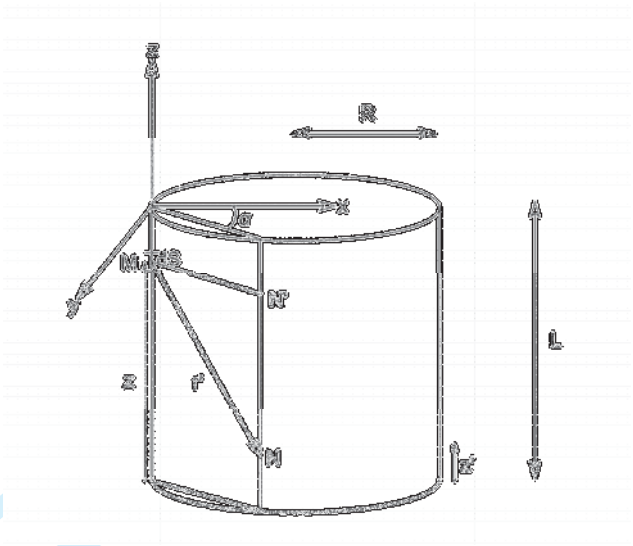

Figure S2-3: The surface considered is located at the position M and the radiation considered follows the direction MN. N is the position on the reactor lateral surface where the radiation considered goes out of the reactor.

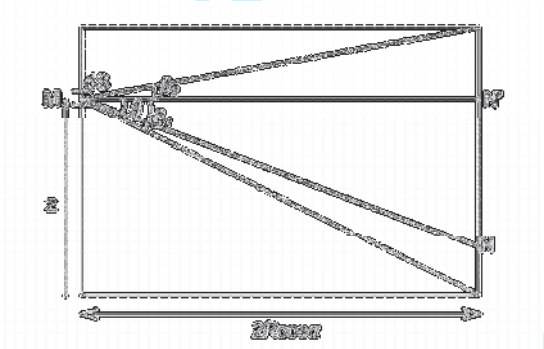

Figure S2-4a: Representation of the plane containing the points M, N, and N' shown in Figure S2-3. The angle β determines of the radiation considered goes through the top surface, the lateral surface or the bottom surface of the reactor.

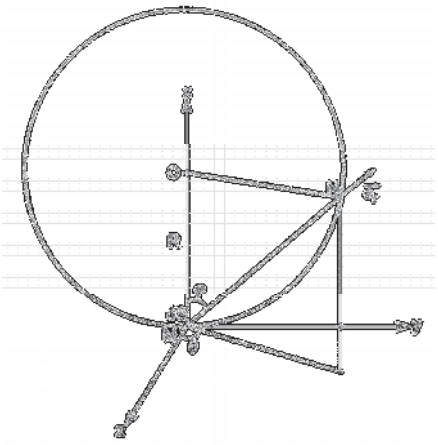

Figure S2-4b: Top view of the reactor. φ is the angle between the radiation considered and the x-axis. θ is the angle between the axis z and the projection of the direction of the radiation considered in the plane (y,z).

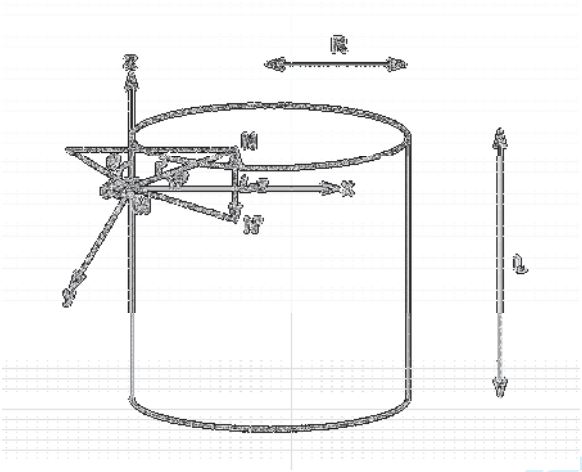

Figure S2-4c: Case where the radiation considered goes through the top surface of the reactor.

Figure S2-4b shows that three cases must be considered, depending on the angle β between a horizontal line passing through dS and the direction of light radiation (θ, φ):

- Case 1: $\beta > \beta_2$: the radiation goes through the top surface of the reactor
- Case 2: $\beta_2 > \beta > \beta_1$: The radiation goes through the lateral surface of the reactor
- Case 3: $\beta < \beta_1$: the radiation goes though the bottom surface of the reactor

Figure S2-2b shows that the angles β_1 and β_2 can be expressed as:

$$\beta_1 = \tan^{-1}\left(\frac{z}{2R\cos\alpha}\right) \quad \text{(S2-9)}$$

$$\beta_2 = \tan^{-1}\left(\frac{L-z}{2R\cos\alpha}\right) \quad \text{(S2-10)}$$

where α is angle indicating the orientation of the radiation in the plane (x,y). The cosine of this angle can be expressed as:

$$\cos\ \alpha\ = \frac{\left(\overrightarrow{e_r} - \left(\overrightarrow{e_r}.\overrightarrow{e_z}\right)\overrightarrow{e_z}\right)\overrightarrow{e_x}}{\left\|\left(\overrightarrow{e_r} - \left(\overrightarrow{e_r}.\overrightarrow{e_z}\right)\overrightarrow{e_z}\right)\overrightarrow{e_x}\right\|} \quad \text{(S2-11)}$$

where the vectors $\boldsymbol{e_r}$ and $\boldsymbol{e_z}$ are defined on Figure S2-4c. In the vector base ($\boldsymbol{e_x}$, $\boldsymbol{e_y}$, $\boldsymbol{e_z}$) shown by Figure S2-4b, the vector $\boldsymbol{e_r}$ can be decomposed as follows:

$$\overrightarrow{e_r} = \cos\varphi\overrightarrow{e_x} + \sin\varphi\sin\theta\overrightarrow{e_y} + \sin\varphi\cos\theta\overrightarrow{e_z} \quad \text{(S2-12)}$$

This leads to the following expression for the term cosα:

$$\cos\alpha = \frac{\cos\varphi}{\sqrt{\cos^2\varphi + \sin^2\varphi\sin^2\theta}} \quad \text{(S2-13)}$$

The angle β can be found by considering β is the angle between the vectors **MN'** (in the plane (x,y) and **MN**:

$$\sin\beta = \overrightarrow{e_r}\cdot\overrightarrow{e_z} = \sin\varphi\cos\theta \ \text{ and } \beta \in [-\pi/2;\ \pi/2] \quad \text{(S2-14)}$$

Case 1: $\beta > \beta 2$: The radiation goes through the top surface of the reactor

According to the definitions of the angles φ and θ, the vector **MN** can be expressed as:

$$\overrightarrow{MN} = r'\cdot\overrightarrow{e_r} = r'\cdot\left(\cos\varphi\overrightarrow{e_x} + \sin\varphi\cdot\sin\theta\overrightarrow{e_y} + \sin\varphi\cdot\cos\theta\overrightarrow{e_z}\right) \quad \text{(S2-15)}$$

In addition, the component of the vector **MN** in the vertical direction is L-z, which leads to following expression for r':

$$r' = \frac{L-z}{\sin\varphi\cdot\cos\theta} \quad \text{(S2-16)}$$

For Peer Review

Case 2: β2 > β > β1: The radiation goes through the lateral surface of the reactor

The distance NM (*r'*) can be expressed by using the theorem of Pythagoras in the triangle MNN':

$$r'^2 = (z - z')^2 + 4R^2 \cos^2 \alpha \quad \text{(S2-17)}$$

Figure S2-4b shows that the absolute value of the difference *z-z'* can be expressed as a function of the angles θ and φ as follows:

$$|z - z'| = r' \sin\varphi \cos\theta \quad \text{(S2-18)}$$

Equation S2-17 then can be written as:

$$r'^2 = r'^2 \sin^2 \varphi \cos^2 \theta + 4R^2 \cos^2 \alpha \quad \text{(S2-19)}$$

leading to the following expression for *r'*:

$$r' = \frac{2R\cos\varphi}{1 - \sin^2\varphi\cos^2\theta} \quad \text{(S2-20)}$$

Case 3: β < β1: The radiation goes through the bottom surface of the reactor

Similarly to the case where the radiation considered goes through the top surface of the reactor, the distance MN can be expressed as:

$$r' = -\frac{z}{\sin\varphi \cdot \cos\theta} \quad \text{(S2-21)}$$

Finally, in order to compute the total amount of radiation going through the reactor, the following integration needs to be performed:

$$I_{th} = 2\pi R \int_{z=0}^{L} I_0(z) \int_{\theta=0}^{2\pi} \int_{\varphi=0}^{\pi/2} \frac{\cos\varphi \sin\varphi \exp(-\sigma X r')}{\pi} d\varphi d\theta dz \quad \text{(S2-22)}$$

where the expression of *r'* must be adapted depending of the values of the angle β according to the three cases developed above.

For Peer Review

2.5.2. Photon flux absorbed by the algae in the reactor (I_{abs})

Using the formula obtained to calculate the local light intensity in the reactor (Equation S2-6), the flux of photons absorbed by the reactor can be computed as:

$$I_{abs} = \int_{r=0}^{R} \int_{\theta=0}^{2\pi} \int_{z=0}^{L} \sigma X I_{loc}(r,z) r \cdot dr \cdot d\theta \cdot dz = 2\pi\sigma X \int_{r=0}^{R} \int_{z=0}^{L} I_{loc}(r,z) r \cdot dr \cdot dz \quad \text{(S2-23)}$$

2.5.3. Photon flux entering the reactor (I_{in})

The flux of photons entering the reactor I_{in} can simply be expressed as a function of the incident light intensity as follows:

$$I_{in} = 2\pi R \int_{z=0}^{L} I_0(z) dz \quad \text{(S2-24)}$$

2.5.4. Conservation of photons

From the conservation of the photons entering the reactor, the sum of the radiation going through the reactor I_{th} (Equation S2-22) and the radiation absorbed by the reactor I_{abs} (Equation S2-23) should be equal to the radiation entering the reactor I_{in} (Equation S2-24):

$$I_{in} = I_{abs} + I_{th} \quad \text{(S2-25)}$$

Figure S2-5 shows that the radiation conservation is respected when using the formulas presented in this study.

For Peer Review

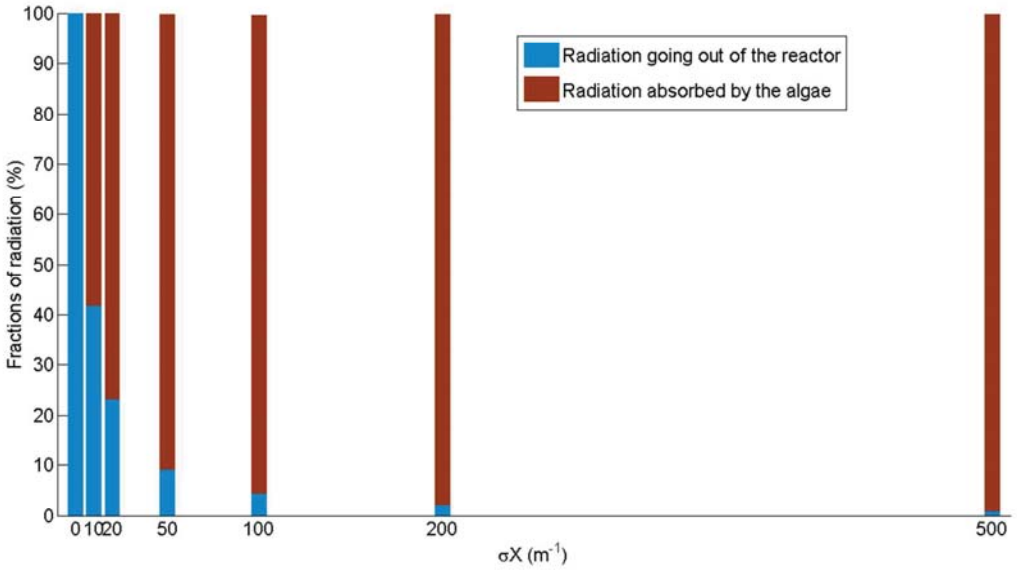

Figure S2-5: Fractions of the radiation absorbed by the reactor (red) and going out of the reactor (blue) for different optical properties of the algae. For these simulations, the following values were chosen (reactor radius: 0.1 m; reactor height: 0.1 m; homogenous incident light intensity of 100W/m^2; local light intensity computation: $N_\theta = 40$; $N_z = 40$; $N_{lim} = 10$; Fraction of radiation going out of the reactor: $N_r = 100$; $N_\theta = 100$; $N_z = 100$; Fraction of radiation absorbed by the algae in the reactor: $N_r = 50$; $N_z = 20$). For each algorithm, N_r, N_θ and N_z are the numbers of infinitesimal elements in the radial, angular, and vertical direction, respectively. N_{lim}^2 is the number of elements in which a small surface of the reactor is split when the algae considered is relatively close to the reactor wall (see Figure S2-3). As the light intensity in the center of the reactor is negligible compared with the incident light intensity, the amount of radiation absorbed by the reactor was computed in the volume fraction where the light intensity was higher than 0.1% of the incident light intensity.

2.6. Impact of algae optical properties on the light distribution

The objective of this section is to illustrate how the algal concentration and the pigment content affect the light distribution in the bench-scale reactors. For relatively high algal concentrations, most of the light entering the reactor is absorbed by the algae in the reactor (Figure S2-6).

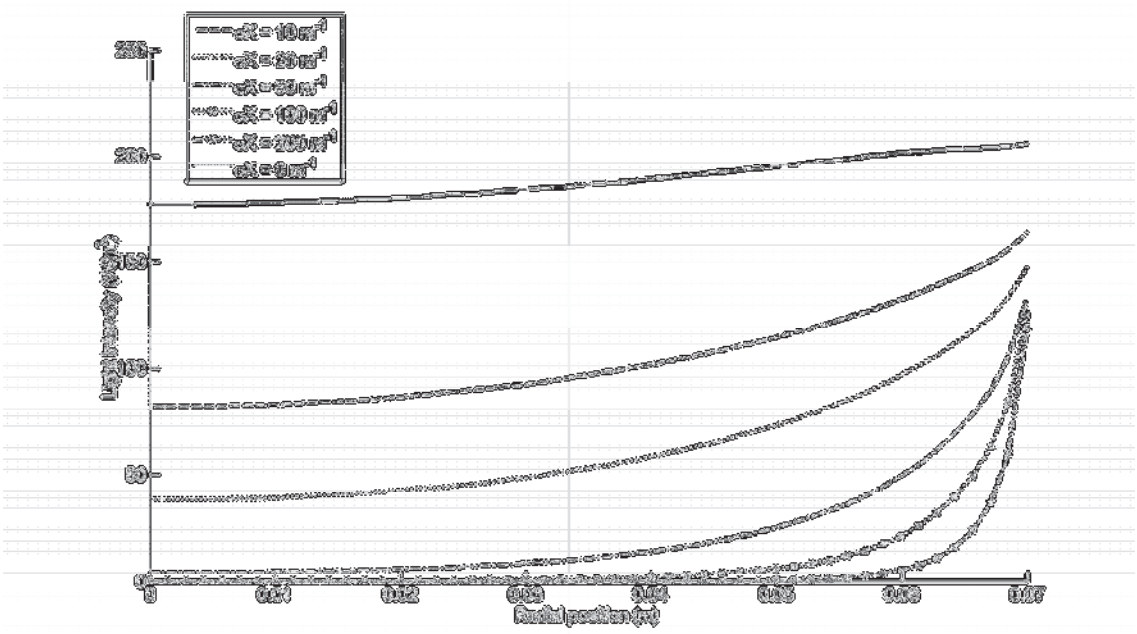

Figure S2-6: Light distribution in the reactor as a function of the radial position of the single algae cell in the Reactor 1 (R = 0.07 m; L = 0.1299 m; $z = L/2$).

2.7. Light distribution in the bench-scale photobioreactors

eer Review

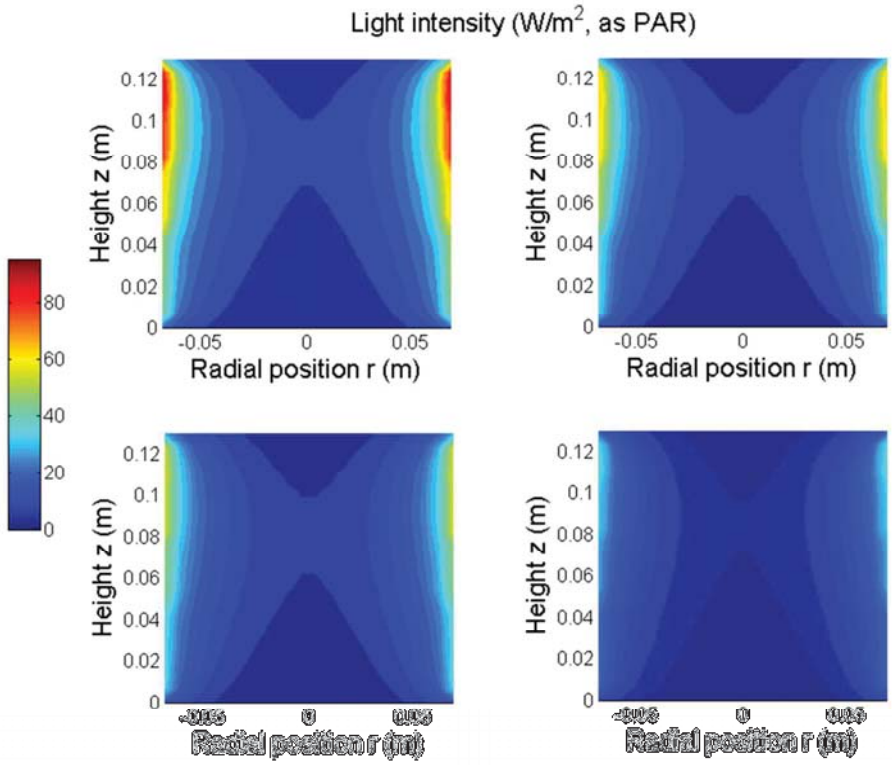

Figure S2-7: Light distribution in the bench-scale reactors determined using Equation S2-6. The average incident light intensities that the reactors were exposed to were (in PAR): Reactor 1: 65.0 W/m^2; Reactor 2: 49.9 W/m^2; Reactor 3: 44.7 W/m^2; Reactor 4: 26.8 W/m^2. The light path $1/\sigma X$ determining how far light penetrates in the cultivation broth was taken equal to 3.3 10^{-2} m ($\sigma X = 30$ m^{-1}).

For Peer Review

S3: Expression of the total rate of photosynthesis in the device used for the determination of the model kinetic parameters

3.1. Introduction

Type II models express the rate of photosynthesis of an entire algal culture by integrating the local rates of photosynthesis within the culture broth. The objective of this document is to explain how this integration was performed in practice.

3.2. Mathematical formulas used a Type II model

By definition of a Type II model, the total rate of photosynthesis P_{O2} (kg O_2/s) in the device used for the determination of the kinetic parameters (Figure 1 of the main manuscript) can be expressed as:

$$P_{O2} = \iiint_V P_{loc}(\sigma_X I_{loc}) \cdot dV \quad \text{(S3-1)}$$

where P_{loc} is the local volumetric rate of photosynthesis (kg O_2/m^3-s) in the volume dV (m^3), σ_X is the extinction coefficient (m^2/kg), and I_{loc} is the local light intensity (W/m^2). Three different mathematical formulas were used to express P_{loc} as a function of I_{loc} as can be seen in Table 1 in the main manuscript. For example, when using the Monod formula, Equation S3-1 becomes:

$$P_{O2} = \iiint_V P_m \frac{\sigma_X I_{loc}}{K + \sigma_X I_{loc}} X \cdot dV \quad \text{(S3-2)}$$

where P_m is the maximum rate of photosynthesis (kg O_2/kg-s), K is the half-saturating light intensity (W/kg) and X is the algal concentration (kg/m^3). By using the modified Beer-Lambert law discussed in the main manuscript (section 2.4), Equation S3-3 becomes:

$$P_{O2} = \int_L P_m \frac{\sigma I_0 \cdot \exp(-\sigma_X X z)}{K + \sigma I_0 \cdot \exp(-\sigma_X X z)} X \cdot S dz \quad \text{(S3-3)}$$

For Peer Review

where z is the depth in the vessel (in m, varying between 0 at the bottom of the vessel to L at the vessel top) and S is the vessel surface area (m^2). Integrating Equation S3-3 leads to:

$$P_{O2} = \frac{P_m S}{\sigma} \ln\left(\frac{K + \sigma_X I_0}{K + \sigma_X I_0 \cdot \exp(-\sigma_X XL)}\right) \quad \text{(S3-4)}$$

Equation S3-3 could not be solved analytically when the Poisson and the hyperbolic tangent formulas were used to express P_{loc} as a function of I_{loc}. The rates of photosynthesis when using these two other formulas were therefore computed numerically.

For Peer Review

S4: Expression of the total rate of photosynthesis in the bench-scale photobioreactors used for model validation

4.1. Introduction

Applying the model of Béchet et al. (2014) to predict the productivity of the bench-scale reactors overall several days of cultivation is computationally intensive. Indeed, these predictions theoretically require the numerical integration of the local productivity over the entire culture volume at each time step of the calculation. The objective of this document is to present the numerical strategies used during the implementation of the model.

4.2. Productivity model

The goal of this sub-section is to present in detail the mathematical expression of the model of Béchet et al. (2014). The total rate of photosynthesis in the bench-scale reactors is expressed as the sum of local productivities:

$$P_{tot} = \iiint_V P_{loc}(I_{loc}) \cdot dV \quad \text{(S4-1)}$$

where P_{tot} is the productivity of the entire cultivation system (kg/s), $P_{loc}(I_{loc})$ is the local volumetric productivity (kg/m^3-s) for the local light intensity I_{loc} (W/m^2), and dV is the volume of the infinitesimal elements (m^3). In this study, the productivity of one algae cell P_{loc} was assumed to follow a 'Monod-like' function of the local light intensity I_{loc}:

$$P_{loc} = P_m \frac{\sigma I_{loc}}{\sigma I_{loc} + K} \quad \text{(S4-2)}$$

where P_m is the maximum specific productivity (kg/kg-s), σ is the algal extinction coefficient (m^2/kg), and K is the half saturation constant (W/kg). The calculation of the local light intensity was described in S4. By introducing the cell concentration X (kg/m^3), the total productivity was calculated in the cylindrical reactors as:

For Peer Review

$$P_{tot} = \int_V P_m \frac{\sigma I_{loc}}{\sigma I_{loc} + K} X dV \quad \text{(S4-3)}$$

As the geometry of the bench-scale reactors was cylindrical and as the local light intensity I_{loc} was assumed to be independent on the radial position (see S4 for details), the total productivity was calculated as:

$$P = 2\pi P_m X \int_{z=0}^{L} \int_{r=0}^{R} \frac{\sigma I_{loc}(r,z)}{\sigma I_{loc}(r,z) + K} r dr dz \quad \text{(S4-4)}$$

where r and z are the radial position and the height of the location considered (m), and L and R the height and the radius of the reactor (m), respectively.

4.3. Calculation of the theoretical concentration over time

For a given couple (K, P_m), the following equation determines the evolution of the theoretical concentration over time:

$$V(t)\frac{dX}{dt} = P(P_m, K, t) \quad \text{(S4-5)}$$

where $V(t)$ is the reactor volume (m^3) and t is the time constant (s). In the numerical integration, the time step used set at 10,000 seconds.

4.4. Calculation of the reactor volume $V(t)$

The volume $V(t)$ was calculated as a function of the rate of evaporation in each in reactor R_{evap} (m^3/s) from the following equation:

$$\frac{dV}{dt} = -R_{evap} \quad \text{(S4-6)}$$

The reactor volume was adjusted daily by adding a certain volume of RO water to compensate for evaporation, which was considered in the calculation of the volume calculation (Figure S4-1). By noting the volume of RO water added in each reactor and by measuring the final volume of broth at the end of an experiment, the rate of evaporation (assumed constant during the experiment) was computed as follows:

For Peer Review

$$R_{evap} = \frac{V_{end} - V_{ini} + \sum V_{add}}{t_{end} - t_{ini}} \quad \text{(S4-7)}$$

where V_{end} is the final volume of the broth (m^3) at $t = t_{end}$ (s), V_{ini} is the initial broth volume (m^3) at t_{ini} (s), and V_{add} represents the volume of RO water added before each sampling (m^3). Table S4-1 shows the values of the rate of evaporation in the four reactors at different temperatures.

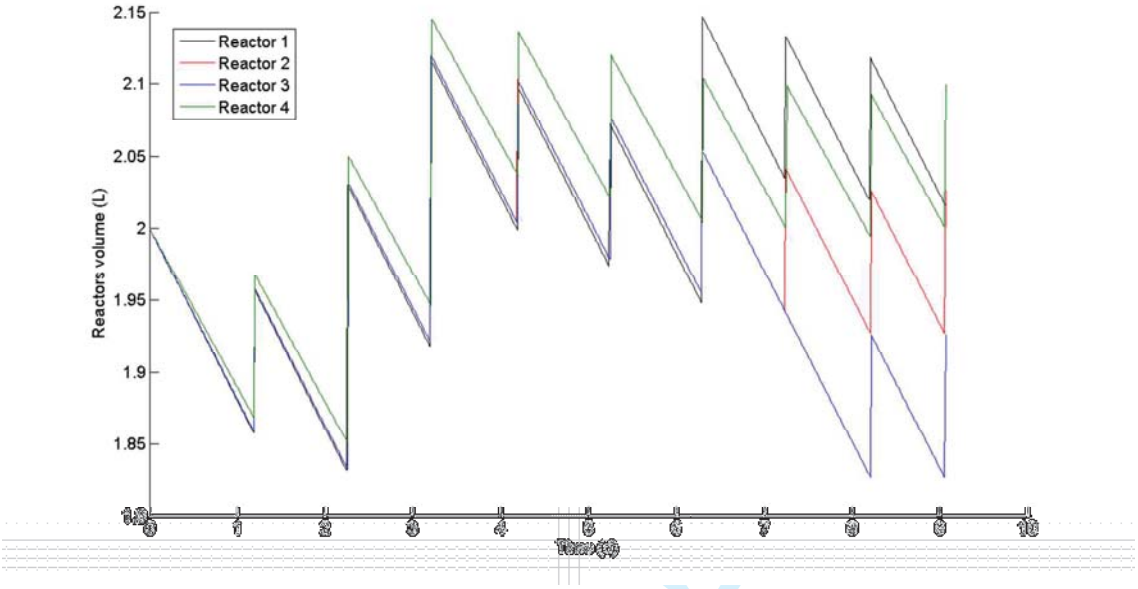

Figure S4-1: Evolution of the reactor volume over time in the four reactors maintained at a temperature of 25°C (The rates of evaporation are given in Table S4-1). The sudden increases of the volume are due to the small volumes of RO water added every day to compensate for evaporation.

Table S4-1: Evaporation rates in each reactor at different temperatures (in mL/d). The slight differences observed between reactors are mostly due to the fact that the temperature was not exactly the same in each reactor due to the differences in incident light intensities I_0 (expressed in average over the entire lateral surface of the reactor in PAR).

Temperature	10°C	20°C	25°C	30°C	35°C
Reactor 1 (I_0 = 65.0 W/m^2)	45.7	80.9	119.7	131.4	309.2
Reactor 2 (I_0 = 49.9 W/m^2)	43.4	75.9	118.6	123.9	307.7
Reactor 3 (I_0 = 44.7 W/m^2)	37.6	70.9	118.6	145.2	299.3
Reactor 4 (I_0 = 26.8 W/m^2)	34.1	73.6	110.4	121.7	293.2

4.5. Numerical implementation of the model

The bench-scale reactors were operated on a semi-continuous regime, and as a result the cell concentration constantly varied over time. As the cell concentration influences the light distribution, it was necessary to determine the light distribution and the total productivity (Equation 4) at each time step. As these calculations both involve a double integration over the entire reactor (see S4 for details), the computation of the algal concentration over time would be computationally intensive.

In order to minimize the computation time needed by the fitting algorithm, the calculation of the total productivity was performed for a large range of values for cell concentration, extinction coefficients, etc. These pre-calculated values of productivity were stored in a matrix of data points and the fitting algorithm determined at each time step the value of productivity by picking the right productivity value. By analyzing the formulas for the local light intensity and the total productivity, it can be demonstrated that the total productivity can be expressed as a function of the following parameters:

- σ: the extinction coefficient of the algae (m^2/kg)
- σX: the product of the extinction coefficient and the algal concentration (m^{-1})
- K: the half-saturating constant in the Monod model (W/kg)
- P_m: the maximal specific productivity (kg/kg-s)

Equation S4-4 can be re-written as:

For Peer Review

$$P = 2\pi P_m X \int_{z=0}^{L} \int_{r=0}^{R} \frac{\sigma I_{loc}(r,z)}{\sigma I_{loc}(r,z) + K} r dr dz = P_m f(\sigma, \sigma X, K) \quad \text{(S4-8)}$$

where the function f is defined as:

$$f(\sigma, \sigma X, K) = 2\pi\sigma X \int_{z=0}^{L} \int_{r=0}^{R} \frac{I_{loc}(r,z)}{\sigma I_{loc}(r,z) + K} r dr dz \quad \text{(S4-9)}$$

As the parameter P_m is only a multiplicative factor (Equation S4-8), the '*f*-matrix' contained values of the function f for the parameters σ, σX, and K. During the calculation of the algal concentration in the bench-scale reactors, the values of productivity for values of σ, σX or K that were not included in the *f*-matrices were obtained by linear interpolation. Figure S4-2 shows how the *f*-matrices were organized.

For Peer Review

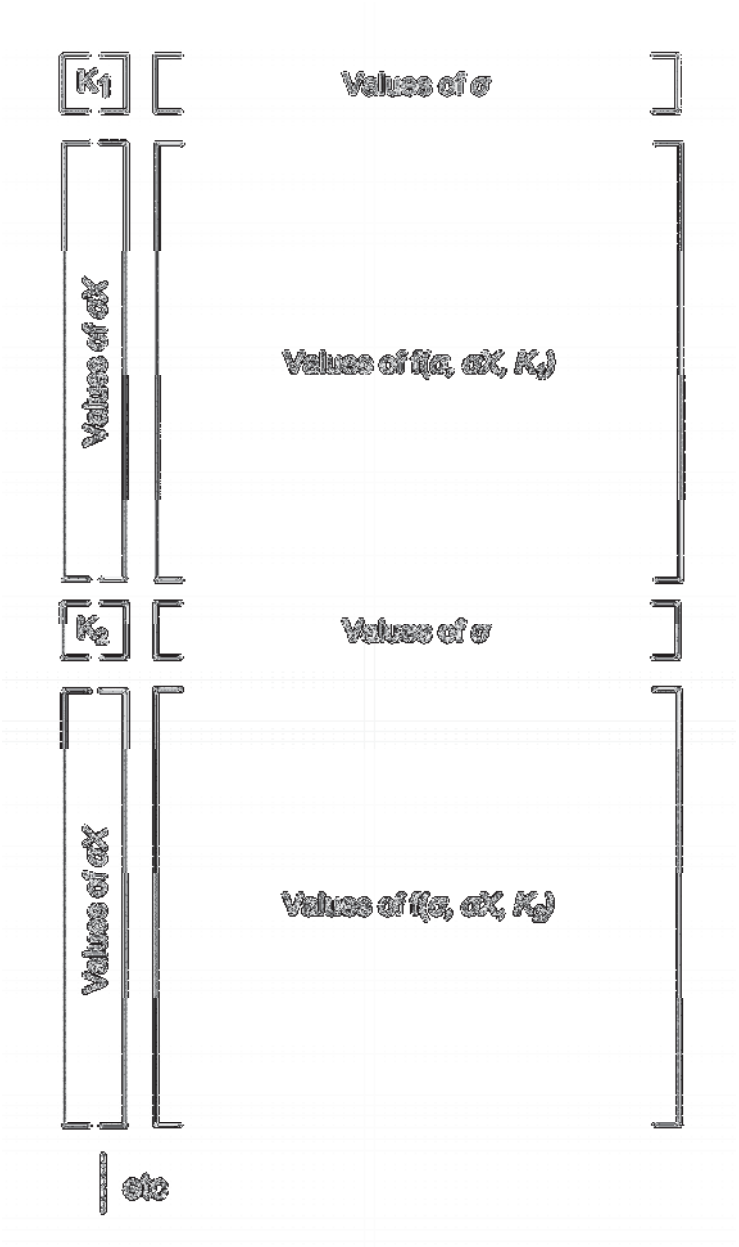

Figure S4-2: Organization of a '*f*-matrix' containing the values of the function *f* for different values of σ, σX, and K (Note that the values contained in this matrix needs to be multiplied by the multiplicative factor $2\pi P_m \sigma X$ to obtain the value of the total productivity P).

In order to further simplify the calculation of the terms of the *f*-matrix, it was noticed that for high values of σX, the light intensity in the central part of the reactor was relatively small. As a result, the function f can be approximated by the following expression:

$$f(\sigma,\sigma X,K)\approx 2\pi\sigma X\int_{z=0}^{L}\int_{r=R_{\min}}^{R}\frac{I_{loc}(r,z)}{\sigma I_{loc}(r,z)+K}rdrdz \quad \text{(S4-10)}$$

where R_{min} is defined as:

$$R_{\min}=R+\frac{\ln(0.001)}{\sigma X} \text{ if } R>-\frac{\ln(0.001)}{\sigma X} \quad \text{(S4-11a)}$$

$$R_{\min}=0 \text{ otherwise} \quad \text{(S4-11b)}$$

Validity of the values stored in the 'f-matrices'

In order to check the validity of the equations derived for the total productivity and their numerical implementation, the evolution of the predicted productivity in the four reactors as a function of the parameters σ, σX, and K is discussed in this section.

Figure S4-3 and S4-4 shows that above a certain value for σX, the total productivity of the bench-scale reactors reaches a plateau, which is due to the fact that the incident light is entirely captured by the algae. Figure S4-3 shows that the productivity is, as expected, an increasing function of the incident light intensity I_0. Finally, Figure S4-4 shows that the predicted productivity in the entire reactor is a decreasing function of K which is a direct consequence of the mathematical formulation of the Monod-function (Equation S4-2).

For Peer Review

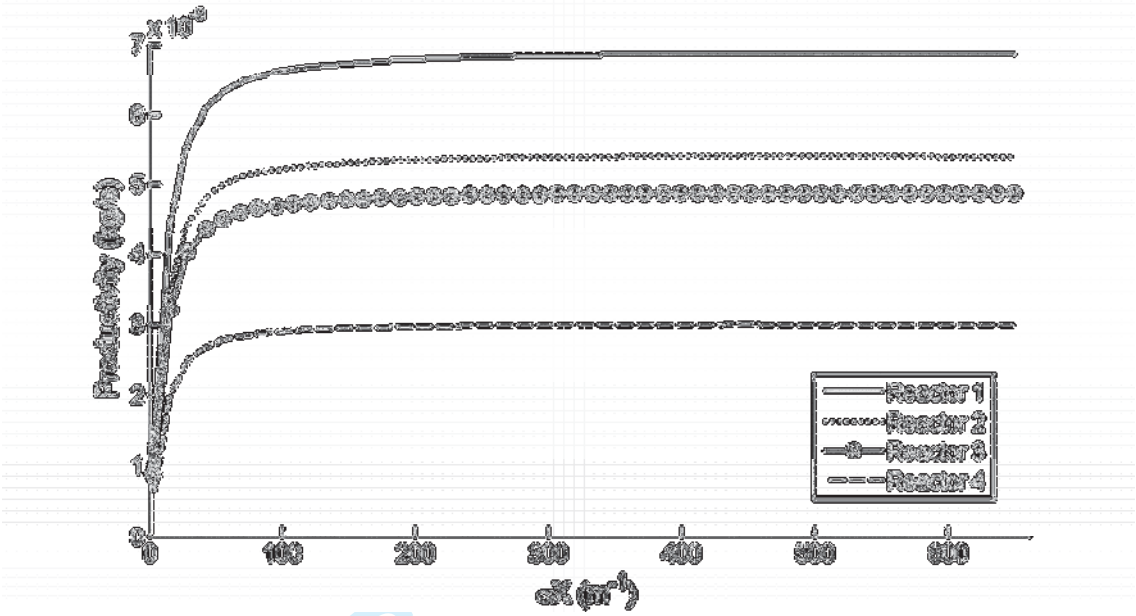

Figure S4-3: Evolution of the productivity of an entire reactor with the parameter σX for the four reactors (Reactor 1: I_0 = 65.0 W/m^2; Reactor 2: I_0 = 49.9 W/m^2; Reactor 3: I_0 = 47.4 W/m^2; Reactor 4: I_0 = 26.8 W/m^2; R = 0.07m; L = 0.1299m; σ = 100 m^2/kg; K = 5 10^4 W/kg; P_m = 10^{-4} kg/kg-s).

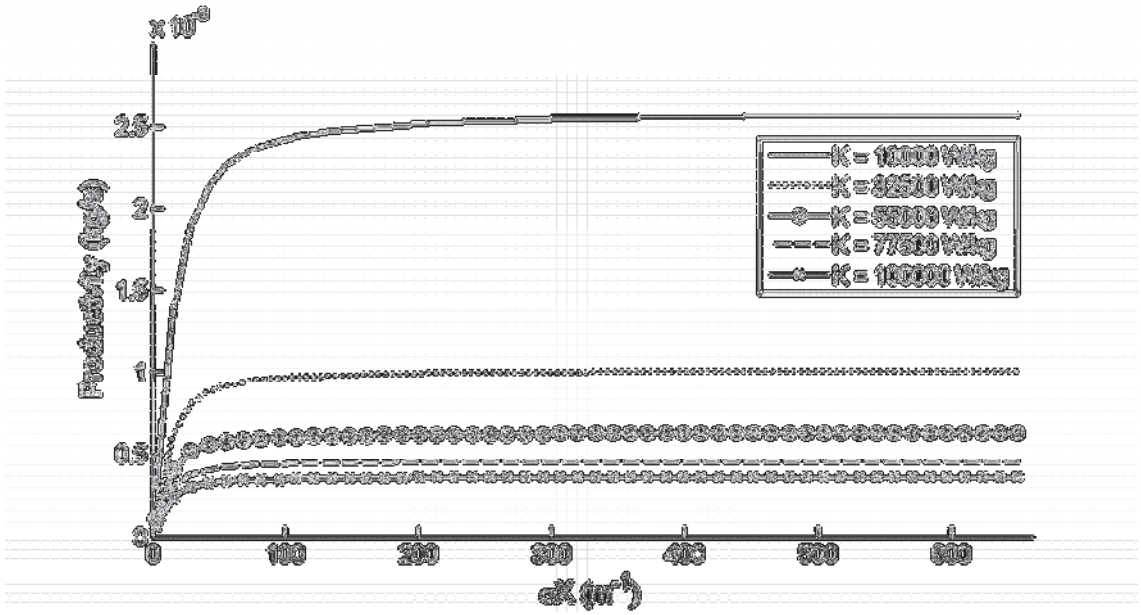

Figure S4-4: Evolution of the productivity of an entire reactor with the parameter σX for different values of K (Reactor 1: I_0 = 65.0 W/m^2; R = 0.07m; L = 0.1299m; σ = 100 m^2/kg; P_m = 10^{-4} kg/kg-s).

Another validation of the implementation of the formulas of the light distribution was performed by predicting the productivity in the reactors in the special case where $K = 0$ W/kg and $P_m = 1$ kg/kg-s. In this very specific case, the model should predict that productivity equals to:

$$P = 2\pi X \int_{z=0}^{L} \int_{r=R_{\min}}^{R} \frac{\sigma I_{loc}(r,z)}{\sigma I_{loc}(r,z)} r dr dz = \pi X L\left(R^2 - R_{\min}^2\right) \quad \text{(S4-12)}$$

Figure S4-5 shows that the model satisfies Equation S4-12 for any value of the extinction coefficient σ.

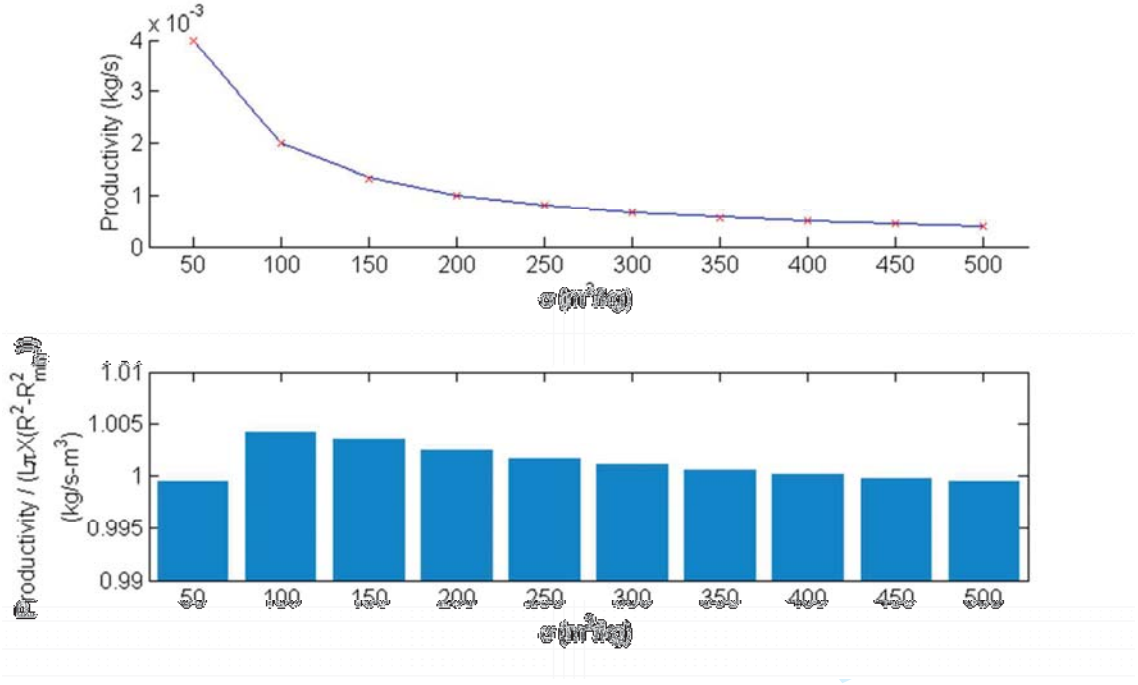

Figure S4-5: Top: Evolution of the productivity of the bench-scale reactors with the extinction coefficient; Bottom: Evolution of the ratio of the productivity and the right-hand term of Equation S4-12 (Reactor 1: $I_0 = 65.0$ W/m^2; $L = 0.1299$m; $R = 0.07$m; $\sigma X = 100$ m^{-1}, $K = 0$ W/kg; $P_m = 1$ kg/kg-s).

S5: Conversion of oxygen productivity into biomass productivity

When algae are exposed to light intensity, light energy is first converted into reducing power in the form of ATP and NADPH molecules through the Z-scheme (Madigan and Martinko, 2006). During this conversion, electrons originate from the oxidation of water, represented by the following half-equation:

$$\frac{1}{2}H_2O \rightarrow \frac{1}{4}O_2 + H^+ + e^- \quad \text{(S5-1)}$$

The resulting reducing power is then used to reduce CO_2 into glucose (Madigan and Martinko, 2006) through the Calvin Cycle, which can be represented by the following half-equation:

$$\frac{1}{4}CO_2 + H^+ + e^- \rightarrow \frac{1}{24}C_6H_{12}O_6 + \frac{1}{4}H_2O \quad \text{(S5-2)}$$

The gross production of glucose ($P_{glucose,gross}$, kg/s) can therefore be expressed as a function of the gross oxygen production rate ($P_{O2,gross}$, in kg O_2/s) as follows:

$$P_{glucose,gross} = \frac{180}{24}\frac{4}{32}P_{O_2,gross} = 0.94 \cdot P_{O_2,gross} \quad \text{(S5-3)}$$

The glucose generated through the Calvin Cycle was assumed to be used for three main purposes by the algae cells:

1) Respiration: glucose can be used as an energy source;
2) Synthesis of new cell material: glucose can also be used as a carbon source for the generation of new carbohydrate, lipids and proteins;
3) Glucose storage: glucose can be kept by algae cells for ulterior needs of energy (i.e. for maintenance and respiration at night-time).

The increase of biomass at day-time was therefore assumed to be the result of the synthesis of new cell material and the storage of glucose. Similarly, the biomass loss observed at night-time was assumed to be due to the respiration of glucose stored during the day.

For Peer Review

Glucose respiration

The use of glucose as an energy source during respiration leads to biomass loss, which can be expressed as follows:

$$R_{glucose} = \frac{4}{32}\frac{180}{24} R_{O_2} = 0.94 \cdot R_{O_2} \quad \text{(S5-4)}$$

where R_{O2} is the rate of oxygen consumption in the dark (kg O_2/s). As a result, the rate of glucose production available for biomass synthesis $P_{glucose,net}$ (kg/s) can obtained by subtracting Equations S5-3 and S5-4:

$$P_{glucose,net} = 0.94 \cdot \left(P_{O_2,gross} - R_{O_2}\right) \quad \text{(S5-5)}$$

Synthesis of new cell material

In order to determine the rate of new cell material synthesis from the oxygen production rate, it is necessary to determine the chemical composition of *C. vulgaris*. In the literature, the chemical composition of this algae species as carbohydrate/lipid/protein was determined in two different studies (Table S5-1). There is no clear consensus on the most representative composition during outdoor cultivation. For example, Wang et al. (2013) used the formula of Illman et al. (2000) to predict the nitrogen removal during outdoor algal production. Spolaore et al. (2006) uses the composition given by Becker (2007) for *Chlorella vulgaris* in their literature review. Sialve et al. (2009) uses the two compositions to estimate the methane yield of the anaerobic digestion of *C. vulgaris*. Because of this lack of consensus, the two compositions shown in Table S5-1were investigated in our study. Concerning the chemical formula of the carbohydrates, the proteins and the lipids, the same expressions were found in various studies (i.e. Sialve et al., 2009 and Wang et al., 2013; Table S5-2). The chemical formula of the proteins given in Table S5-2 was determined from the measurement of the fractions of the different amino-acids present in *Chlorella vulgaris* (Becker, 2007, Heaven et al., 2011).

Table S5-1: Chemical composition of *Chlorella vulgaris*. For the composition given by Becker (2007), the mid-range values were used in calculations. (Note: as the total of percentage does not equal 100%, it was assumed that the rest of the cell material was composed of ashes.)

For Peer Review

Study	Carbohydrate	Lipid	Protein
Illman et al., 2000	51%	18%	29%
Becker, 2007	12-17%	14-22%	51-58%

Table XXX-2: Chemical formula used for carbohydrates/lipids/proteins.

Carbohydrates	$C_5H_{10}O_5$
Lipids	$C_{57}H_{104}O_6$
Proteins	$C_{1.9}H_{3.8}O_1N_{0.5}$

From Table S5-1 and Table S5-2, the chemical formulas of *C vulgaris* were found to be $C_{416}H_{749}O_{228}N_{29}$ and $C_{379}H_{719}O_{167}N_{55}$ for the cell compositions given by Illman et al. (2000) and Becker (2007), respectively. In the following, the cell composition will be noted $C_aH_bO_cN_d$. Using this notation, the half equation representing the reduction of CO_2 into new cell material is:

$$\frac{a}{N_e}CO_2 + \frac{d}{N_e}NH_4^+ + \frac{b + 4a - 2c - 4d}{N_e}H^+ + e^- \rightarrow \frac{1}{N_e}C_aH_bO_cN_d + \frac{2a - c}{N_e}H_2O \quad \text{(S5-6)}$$

$$\text{where } N_e = b + 4a - 2c - 3d \quad \text{(S5-7)}$$

As the nitrogen source was nitrate during cultivation of *Chlorella vulgaris*, a fraction of the electrons released during glucose oxidation is used to reduce nitrate into ammonium. This reduction is represented by the following half-equation:

$$\frac{1}{4}CO_2 + \frac{1}{8}NO_3^- + H^+ + e^- \rightarrow \frac{1}{8}NH_4^+ + \frac{1}{4}HCO_3^- + \frac{1}{8}H_2O \quad \text{(S5-8)}$$

During synthesis of new cell material, the respective fractions of electrons used to reduce carbon (f_C) and nitrate (f_N) can be found using the stoichiometric coefficients in Equations S5-6 and S5-8 as follows:

$$f_C + f_N = 1 \quad \text{(S5-9a)}$$

$$\frac{d}{N_e}f_C = \frac{1}{8}f_N \quad \text{(S5-9b)}$$

For Peer Review

Solving this system of equations yields:

$$f_C = \frac{\mathrm{N_e}}{\mathrm{N_e} + 8\mathrm{d}} \quad \text{(S5-10)}$$

The use of 1 g of glucose by the cell for synthesis of new cell material therefore yields:

$$Y = f_C \cdot \frac{24}{180} \frac{MW_b}{\mathrm{N_e}} \frac{1}{f_{ash}} \text{ g biomass / g glucose used} \quad \text{(S5-11)}$$

Where MW_b is the molar weight of biomass (g/mol) and f_{ash} the fraction of cell ash (Table S5-1). Numerically, the yield was found equal to:

- $Y = 0.63$ for the cell composition of Illman et al. (2000)
- $Y = 0.61$ for the cell composition of Becker (2007).

As these two values do not differ significantly, a yield value of 0.62 was used in the following.

Total biomass production

In the study of Illman et al. (2000), the cell composition was measured on algal samples cultivated in a batch system when the net productivity was null (i.e. when algal concentration reached a plateau). As a result, it can be assumed that all the glucose produced by these cells was used for respiration. The cell composition given by Illman et al. (2000) is therefore likely to represent new cell material without any glucose storage. However, when algae were cultivated in the bench-scale photobioreactors used for model validation (see main manuscript), the light supply was up to 10 times higher than in the system of Illman et al (2000). As a result, the net biomass increase in the reactors was likely due to the generation of both new cell material and glucose storage. The rate of biomass production can therefore be expressed as follows:

$$P_{day} = P_{glucose,net} \cdot (1 - f_b) + P_{glucose,net} \cdot f_b \cdot 0.62 \quad \text{(S5-12)}$$

where f_b is the fraction of glucose used for the synthesis of new cell material. Equation S5-12 finally leads to the following expression:

$$P_{day} = 0.94 \cdot ((1 - f_b) + f_b \cdot 0.62) \cdot (P_{O_2,gross} - R_{O_2}) \quad \text{(S5-13)}$$

For Peer Review

It is challenging to estimate the fraction of glucose f_b as this fraction depends on multiple factors. For simplicity, it was assumed that this fraction was equal to 50%, leading to the following equation:

$$P_{day} = 0.76 \cdot \left(P_{O_2,gross} - R_{O_2}\right) \quad \text{(S5-13)}$$

In order to account for the fact that the fraction f_b may vary significantly depending on cultivation conditions, it was assumed in the uncertainty analysis that f_b can vary between 25% and 75%. As a result, the confidence interval for the conversion coefficient was 0.76 ± 0.09.

Night-time

At night-time, the rate of biomass loss can be assumed to be proportional to the rate of oxygen consumption as follows:

$$P_{night} = -0.94 \cdot R_{O_2} \quad \text{(S5-14)}$$

Summary: conversion coefficients

The conversion coefficients used to convert the model parameters P_m and λ from kg O_2/kg-s to kg/kg-s were therefore:

- At daytime:
  - P_m [kg/kg-s] = 0.76 (±0.09) P_m [kg O_2/kg-s]
  - λ [kg/kg-s] = 0.76 (±0.09) λ [kg O_2/kg-s]
- At night-time:
  - λ [kg/kg-s] = 0.94 λ [kg O_2/kg-s]

References

Becker, E.W. 2007. Micro-algae as a source of protein. Biotechnol. Adv. 25(2), 207–210.

For Peer Review

Heaven, S., Milledge, J., Zhang, Y. 2011. Comments on 'Anaerobic digestion of microalgae as a necessary step to make microalgal biodiesel sustainable'. Biotechnol. Adv. 29(1), 164-167.

Illman, A.M, Scragg, A.H., Shales, S.W. 2000. Increase in Chlorella strains calorific values when grown in low nitrogen medium. Enzym. Microb. Technol. 27, 631-635.

Madigan, M.T., Martinko, J.M. 2006. Brock – Biology of microorganisms. 11th Edition. Pearson Prentice Hall. Upper Saddle River, NJ 07458.

Sialve B., Bernet, N., Bernard, O. 2009. Anaerobic digestion of microalgae as a necessary step to make microalgal biodiesel sustainable. Biotechnol. Adv. 27, 409-416.

Spolaore, P., Joannis-Cassan, C., Duran, E., Isambert, A. 2006. Commercial applications of microalgae. J. Biosci. Bioeng. 101(2), 87-96.

Wang, T., Yabar, H., Higano, Y. 2013. Perspective assessment of algae-based biofuel production using recycled nutrient sources: the case of Japan. Biores. Technol. 128, 688-696.

For Peer Review

S6: Description of Monte-Carlo simulations used for treatment of uncertainties

6.1. Introduction

The values of the kinetic parameters of the model (P_m, K and λ) were determined by fitting the model to the measured rates of photosynthesis at different light intensities I_0. Uncertainty on the measured variables therefore generates inaccuracy on the model parameters. Similarly, the productivity predictions in the bench-scale photobioreactors were impacted by uncertainties on the model inputs. The objectives of this document are therefore to explain 1) how the level of inaccuracy on the model parameters was estimated and 2) how the inaccuracies on model parameters and other inputs impacted the model predictions in the bench-scale photobioreactors.

6.2. Inaccuracy on model parameters

6.2.1. Uncertainties on measured variables

The kinetic parameters P_m, K and λ were obtained by fitting the measured rates of photosynthesis at different light intensities. As the Type II model used in this study accounted for the light distribution in the culture broth, the values of P_m K and λ were determined from the measurement of a total of 4 variables:

- $P_{O2,\,data}$: The rate of dissolved oxygen production measured by the electrodes (kg O_2/m^3-s);

- I_0: The incident light intensity reaching the algae (W/m^2);

- σ: The extinction coefficient experimentally determined as explained in section 2.4 of the main manuscript (m^2/kg);

- X: The cell concentration in the reactors measured by dry weight measurement (kg/m^3).

For Peer Review

The uncertainty on the dissolved oxygen measurement was determined by measuring the dissolved oxygen concentration of a saturated solution (100%) 5 times with each of the 6 electrodes used during the experiment. The uncertainty on $P_{O2,Data}$ was then determined from the standard deviation of the resulting 30 measurements.

The determination of uncertainty on I_0 and σ are detailed in S1 and the main manuscript, respectively. Table S5-1 summarizes these levels of uncertainty.

The uncertainty on dry weight measurements was performed from 220 measurements performed in duplicate. Dry weight measurements were performed by weighing dry weight filters before and after filtration of a known volume of algal broth. The dry weight concentration of an algae sample was therefore calculated using the following formula:

$$C = \frac{m_a - m_b}{V_f} \quad \text{(S6-1)}$$

where m_a and m_b are the masses of the filters (mg) after and before filtration, respectively, and V_f the volume of the filtered sample (mL). The measured weight of filters was found to vary with different experimental factors: the time that filters spent in the dissector, the interactions between the atmospheric conditions and the balance, etc. It was indeed empirically observed that the mass difference in Equation (S6-1) could vary between replicates.

Figures S6-1 shows that the difference m_a-m_b between the duplicates (referred to as the '*m*-parameter' in the following) was distributed according to a normal distribution (indoor samples: μ = -0.1136, σ = 3.22, N = 220). It can also be noted that m-parameter was not correlated with the amount of biomass filtered (Figure S6-2). In order to verify that the mean was statistically close to 0, T-tests were performed as follows. Under the assumption ("H_0") that the mean of the distribution is 0, the following variable should be distributed according to a student distribution:

$$t = \frac{\mu_{\Delta m}}{s/\sqrt{n}} \sim T(n-1) \quad \text{(S6-2)}$$

where $\mu_{\Delta m}$ is the estimated mean of the variation between the two measured mass differences, s the estimated standard deviation, and N the sample size. For both samples, the T-tests did not allow to reject the null hypothesis (μ = 0). It is therefore unlikely that the statistical variable is not centered on 0.

For Peer Review

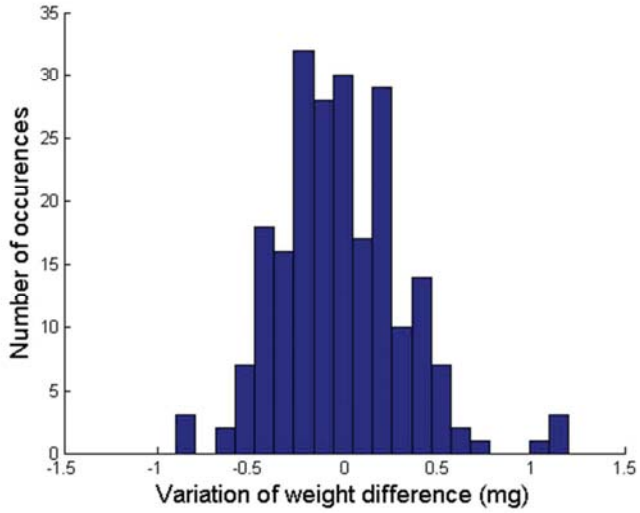

Figure S6-1: Distribution of the difference between the two measured mass variations measured as duplicates.

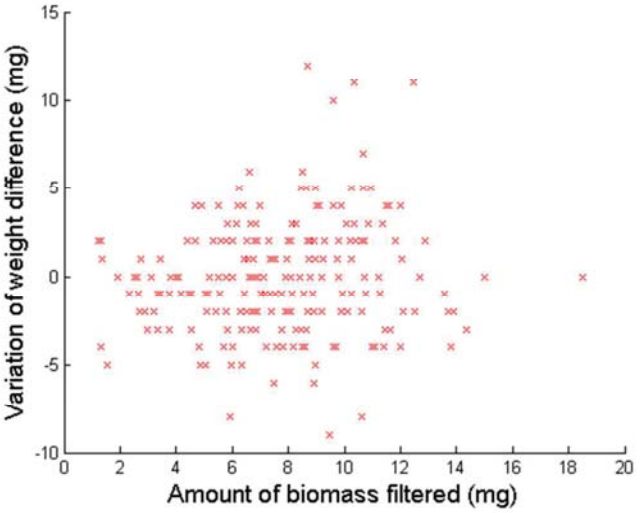

Figure S6-2: Difference between the two measured mass variations as a function of the amount of biomass filtered.

From this analysis, it was determined that the standard deviation of dry weight concentration (σ_{conc}, in kg DW/m^3) could be expressed as:

$$\sigma_{conc} = \frac{\sigma_{\Delta m}}{V_f} \quad \text{(S6-3)}$$

where $\sigma_{\Delta m}$ is the standard deviation of the amount of filtered biomass (mg) and V_f the volume of filtered sample (mL). The impact of the inaccuracy on this volume V_f was neglected on the error on the dry weight measurement. When cell concentration measurements were performed in duplicate, the actual standard deviation dry weight concentration was taken at:

$$\sigma_{conc,data} = \frac{\sigma_{conc}}{\sqrt{2}} = \frac{\sigma_{\Delta m}}{\sqrt{2}V_f} \quad \text{(S6-4)}$$

Table S6-1 summarizes the levels of uncertainty on the four measured variables considered in the Monte-Carlo analysis.

Table S6-1: Uncertainty of the measured variables at the 95% confidence interval.

Variable	Unit	Uncertainty
$P_{O2,data}$: Dissolved oxygen	kg O_2/m^3	+/- 5.4%
X: Cell concentration	kg/m^3	+/- 7.0%[a]
		+/- 7.9%[b]
I_0: Incident light intensity	W/m^2 (PAR)	+/- 10%
σ: Extinction coefficient	m^2/kg	See main manuscript

[a] For the experiments at different cell concentrations (see main manuscript).

[b] For the experiment at different temperatures (see main manuscript).

6.2.2. Description of Monte Carlo simulations

The experimental data used for model fitting was a set of six different rates of oxygen production at six different incident light intensities. A least-square fitting was used in order to express the values of kinetics parameters (P_m, K, and λ referred to α_i in this example) as a function of 1) the measured oxygen production rates (P_{O2}) 2) the measured light intensities (I_0), 3) the extinction coefficient (σ), and 4) the measured dry weight concentration (X). Mathematically, this fitting can be represented as:

For Peer Review

$$\alpha_i = f_i\left(P_{O2}, I_0, \sigma, X\right) \quad \text{(S6-1)}$$

Monte-Carlo simulations consisted on fitting the model parameters to the experimental data several times when a random combination of errors was added to the four measured variables. The random error was assumed to be normally distributed around 0 and with the confidence intervals at 95% showed in Table S6-1. At the end of these N simulations (2000 in this study), the fitted value and the associated level of inaccuracy on the model parameters (P_m, K, or λ) was obtained by computing the average and standard deviation of their fitted values.

Figure S6-3 illustrates the distribution of the values of P_m obtained in the different Monte-Carlo simulations.

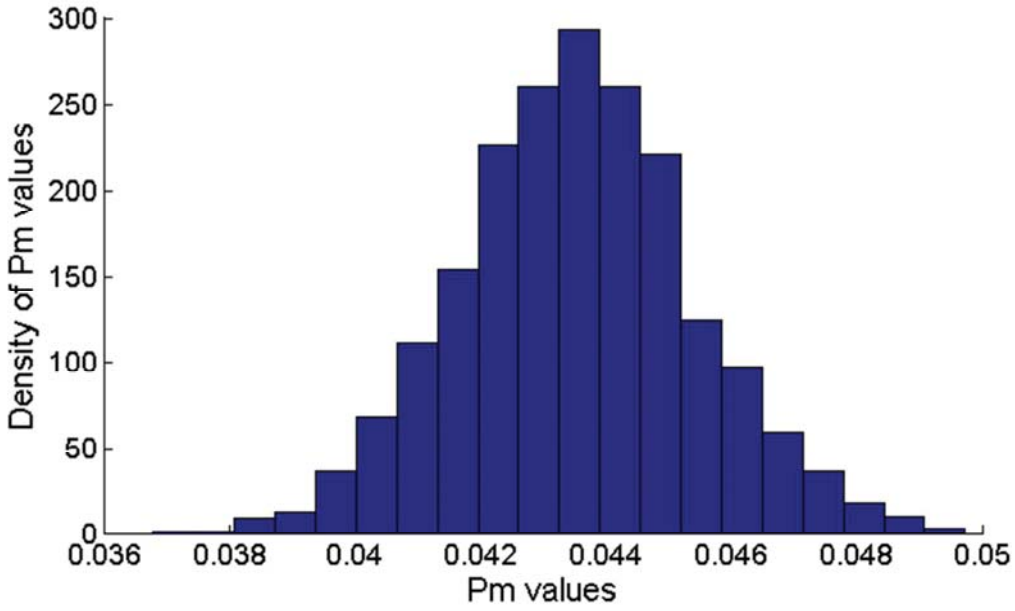

Figure S6-3: Distribution of P_m values obtained through the Monte-Carlo simulations (Experiment at 22°C for the algal concentration X = 0.47 kg/m^3).

6.2.3. Sensitivity analysis

The uncertainty on dissolved oxygen measurements has a relatively high impact on both the fitted values of P_m and K (Figure S6-4). The cell concentration has also an important influence on the fitted values of the parameters and especially on P_m. The incident light

intensity reaching the algae has a lower influence on P_m and K, which is due to the fact that the inaccuracy on I_0 was found to be relatively low. Finally, the inaccuracy on the extinction coefficient σ did not have a significant impact on the uncertainty on K and P_m, mostly due to the fact that the uncertainty of σ is relatively low for high cell concentrations (Figure 1 in the main manuscript).

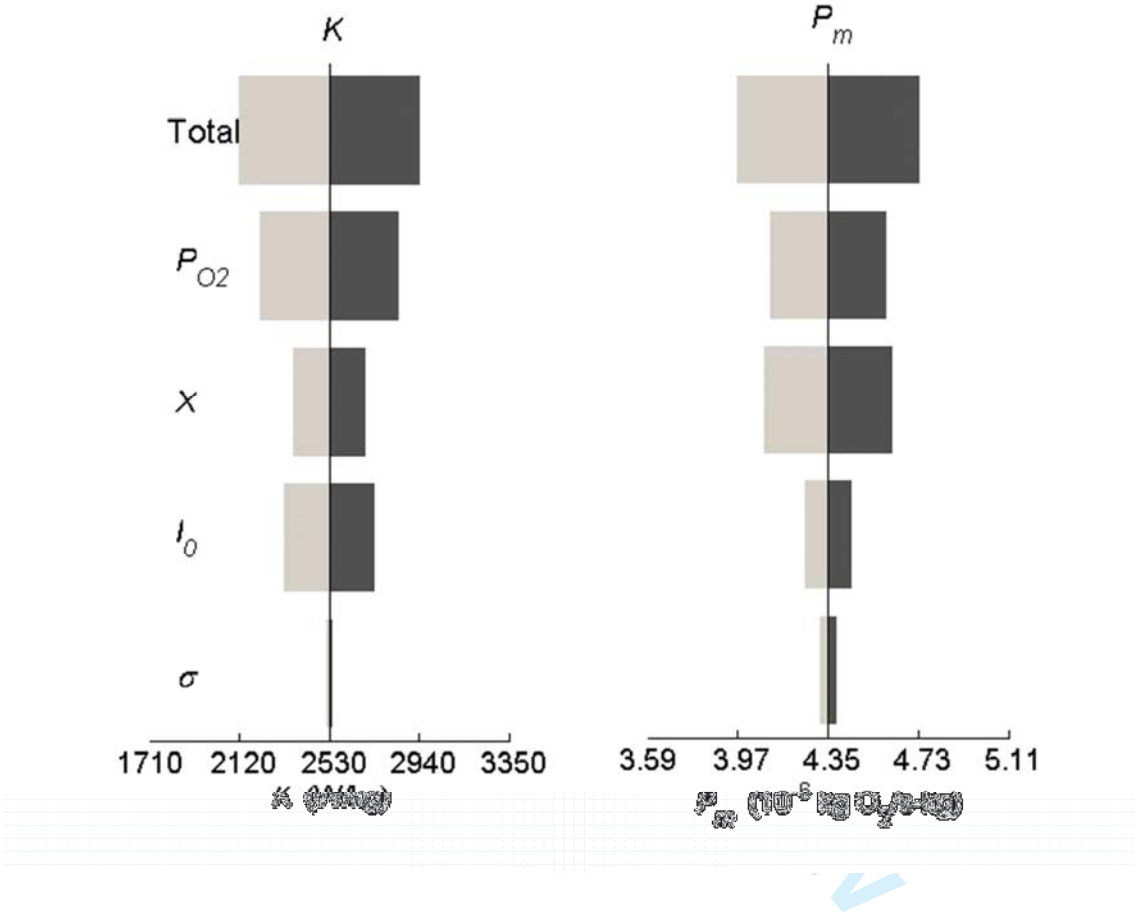

Figure S6-4: Variation of the fitted values of K and P_m caused by the uncertainty on each measured variables. The light/dark bar represents the variation of K and P_m for the lower and upper values of the measured variable, respectively. The confidence interval of each measured variable is given in Table S6-1.

6.3. Uncertainty on the model inputs in the bench-scale photobioreactors

Monte-Carlo simulations were used in order to determine how the uncertainty on model inputs impacted the productivity predictions in the bench-scale photobioreactors. Table S6-2 summarizes the levels of uncertainty on the different inputs of the model. The methodology followed to determine the inaccuracy of model productivity predictions in the bench-scale photobioreactors was similar to the approach described in the previous section.

Table S6-2: Uncertainty of the model inputs for application in the bench-scale photobioreactors at the 95% confidence interval.

Variable	Unit	Uncertainty
Pm, K, λ: Model kinetic parameters	-	See main manuscript
f_b: fraction of glucose converted into biomass	-	± 12% (See S5)
I_0: Incident light intensity	W/m^2 (PAR)	+/- 10%
σ: Extinction coefficient	m^2/kg	See main manuscript
T: Temperature	^oC	± 1^oC

For Peer Review

S7: Actinometry

7.1. Introduction

Actinometry was used to accurately quantify the amount of light reaching entering the vessels of the device used to determine the kinetic parameters of the model. This technique relies on the photo-chemical degradation Potassium Ferric Oxalate (PFO). When PFO is photo-degraded, iron ions (Fe^{2+}) are released in the solution (Hatchard and Parker, 1956). By measuring the evolution of the Fe^{2+} concentration in a solution exposed to light, the incident light intensity reaching the system can be determined. This document details the exact protocol followed in this study.

7.2. Chemical solutions

- 1N-H_2SO_4: 26.6 mL of pure sulfuric acid diluted in a volume of 1L with RO water.
- 0.1N-H_2SO_4: 100mL of 1N-H_2SO_4 diluted in a volume of 1L with RO water.
- 1N-NaAc: solution of sodium acetate concentrated at 1 mol/L (is sodium acetate is on the form $NaCH_3COO^-$, $3H_2O$, the corresponding mass concentration corresponds to 136 g/L)
- Buffer solution: This solution was prepared by mixing 600mL of the 1N-NaAc solution and 360mL of the 1N-H_2SO_4 solution and by diluting this solution to a volume of 1L with RO water.
- Indicator solution: 2.72 g of Phenanthroline monohydrate dissolved in 1L of RO water
- Potassium ferric oxalate solution (“PFOS”): 73.68 g of Potassium ferric oxalate (“PFO”) dissolved in 1L of 0.1N-H_2SO_4. Note that this solution must be prepared in dark conditions to avoid the degradation of the compound.
- Ferrous sulfate solution (“FSS”): 27.8 g $FeSO_4$, $8H_2O$ dissolved in 1L of RO water
- Iron calibration solution (“ICS”): 1.2 mL of the FSS diluted in 1L with 0.1-N H_2SO_4

For Peer Review

7.3. Calibration of the colorimetric indicator

The following solutions were poured in 6 different measuring cylinders:

- *X* mL of the ICS solution (*X* between equal to 0, 1, 2, 3, 4, or 5)
- 10-*X* mL of the 0.1 N-H_2SO_4 solution (for example, 6 mL of 0.1 N-H_2SO_4 solution for 4mL of the ICS solution)
- 2mL of the Indicator solution
- 5mL of the Buffer solution

Each measuring cylinder was filled up to 20mL with RO water. The solutions were let resting for 30 minutes before measuring optical density at 510nm. By calculating the molar concentration of Fe^{2+} in each of the 6 solutions, a calibration curve was obtained between the optical density and the Fe^{2+} concentration (mol/L) (Figure S7-1):

$$\left[Fe^{2+}\right] = 8.35 \cdot 10^{-5} OD_{510} \quad \text{(S7-1)}$$

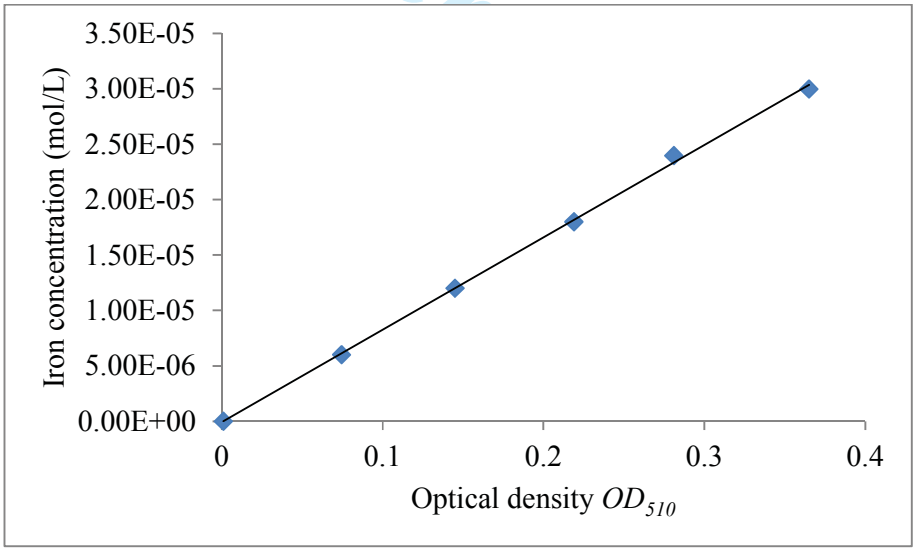

Figure S7-1: Ferric ions concentration versus optical density of the solution

7.4. Experimental protocol for the light measurement of light intensity in device used for model development

The vessels were filled with 76mL of PFOS solution. After turning on the lights, samples of 2mL of the PFOS solution were taken at regular time intervals. These samples were kept in the dark to avoid further degradation of the PFO. These 2mL samples were poured in a measuring cylinder to which were added:

- 8mL of the 0.1 N-H_2SO_4 solution
- 2mL of the Indicator solution
- 5mL of the Buffer solution
- RO water up to the 20mL mark

The optical density of the solution was measured after 30 minutes. By using the calibration curve determined previously, it was therefore possible to determine the rate of degradation of PFO over time β (in mol PFO/hr).

7.5. Calculation of the light intensity entering each vessel

The study of Hatchard and Parker (1956) showed that the efficiency of the photo-catalysis of PFO was around 1.21, meaning that 1/1.21 photons of visible light are needed to degrade one molecule of PFO. The energy of each of these photons (E, in J) can be determined by using Plank's law:

$$E = h\nu \quad \text{(S7-2)}$$

where h is the Plank constant (6.6 10^{-34} J.s) and ν is the photon frequency (s^{-1}), given as a function of the wavelength of the photon (λ, m) as:

$$\nu = \frac{c}{\lambda} \quad \text{(S7-3)}$$

where c is the speed of light ($3.10^8 m.s^{-1}$). For a monochromatic light, the light intensity (in W/m^2) can finally be expressed as follows:

$$I_0 = \frac{\beta}{1.21} N_A \frac{hc}{\lambda} \frac{1}{S} \quad \text{(S7-4)}$$

For Peer Review

S is the surface area of the system exposed to the light intensity I_0 (m^2), and N_A is the Avogadro number ($6.02.10^{23} mol^{-1}$).

However, the light source used in this study was not monochromatic as shown in Figure S7-2. It was therefore necessary to account for the spectral distribution of the light source in the calculations of the light intensity. In addition, the absorption of light by the PFO solution was found to be wavelength-dependent (Figure S7-3). Indeed, the PFO solution was found to only absorb light at wavelengths lower than 470nm.

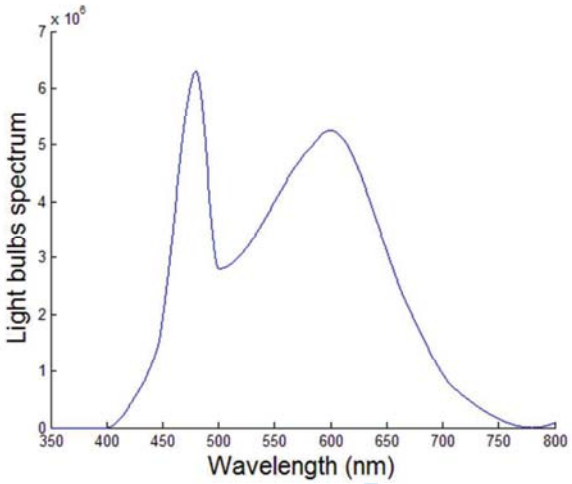

Figure S7-2: Spectral distribution of the light bulb used in this study (extracted from the datasheet of the light bulb).

Review

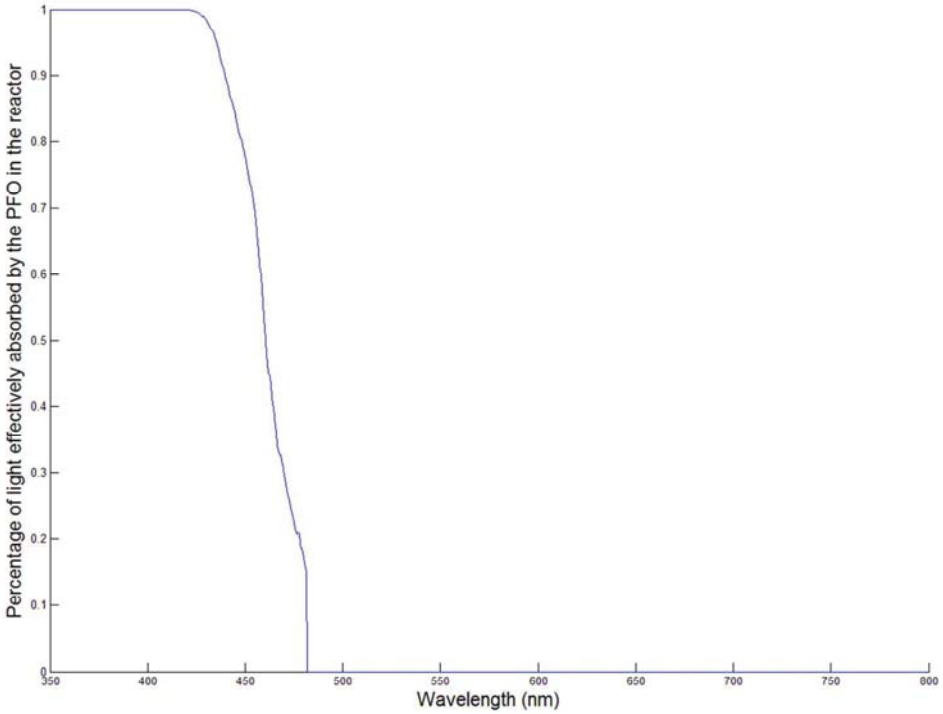

Figure S7-3: Absorbance of the actinometer in the reactor for different wavelengths.

The rate of photons dN_λ (mol photons/s) emitted by the light bulb for wavelengths between λ and $\lambda+d\lambda$ can be expressed as:

$$dN_\lambda = \lambda \frac{SI_0 \cdot f(\lambda) \cdot d\lambda}{hc} \quad \text{(S7-5)}$$

where S is the reactor bottom surface area (m^2), I_0 is the visible light intensity entering the reactors (W/m^2), $f(\lambda).d\lambda$ is the fraction of the light energy emitted by the light bulb between λ and $\lambda+d\lambda$. The rate of degradation of PFO in the reactor can therefore be expressed as:

$$\beta = \frac{1}{N_A} \int_\lambda 1.21 \cdot \lambda \frac{SI_0 \cdot f(\lambda) \cdot (1 - T_\lambda) d\lambda}{hc} \quad \text{(S7-6)}$$

where T_λ is the transmittance of the PFO solution for the wavelength λ. By reversing this last equation, the incident light intensity can be expressed as follows:

For Review

$$I_0 = \frac{\beta N_A}{\int_{\lambda} 1.21 \cdot \lambda \frac{S \cdot f(\lambda) \cdot (1 - T_\lambda) d\lambda}{hc}} \quad \text{(S7-7)}$$

Equation S7-7 was used to determine the light intensity entering the reactors for different light intensities. These computed values were then compared to experimental values obtained with a PAR sensor located at a distance of approximately 3 cm above the bottom surface of the vessels (Figure S7-4). Figure S7-4 shows that the light intensity measured by the light sensor was in average 13% lower than the light intensity entering the reactors estimated by actinometry. This underestimation is most likely due to the fact the PAR sensor was not in contact with the bottom surface of the vessels during the measurements.

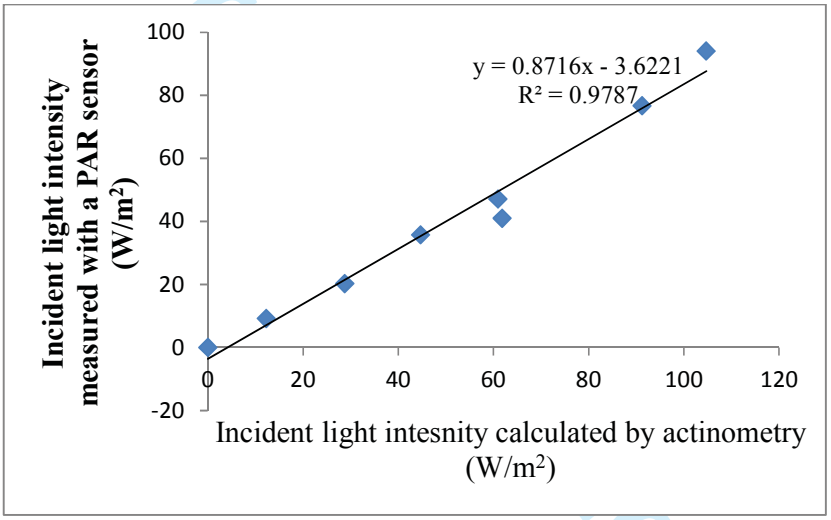

Figure S7-1: Direct PAR measurements versus actinometry measurements in the reactors.

7.6. Uncertainty on light measurement

In the conversion from degradation rates of PFO into light intensities (Equation S7-7), the main factor of uncertainty is the efficiency of the photo-catalysis of PFO taken equal to 1.21 in this analysis. Indeed, this value of 1.21 is only the average value reported by Hatchard and Parker (1956) and a variation of approximately +/- 10% was reported by the authors of this study. As a result, a level of +/- 10% on the values of I_0 used in the model fitting was taken to represent the level of uncertainty on I_0.

Reference

Hatchard, C.G., Parker, C.A. 1956. A new sensitive chemical actinometer. II. Potassium ferrioxalate as a standard chemical actinometer. Proc. Royal Soc. London Ser. A, Math. Phys. Sci. 235(1203), 518-536.

For Peer Review

S8: Correlation between the rate of respiration and rate of photosynthesis

Figure S8-1 shows that there is no clear correlation between the rate of photosynthesis and the rate of respiration immediately after light exposure.

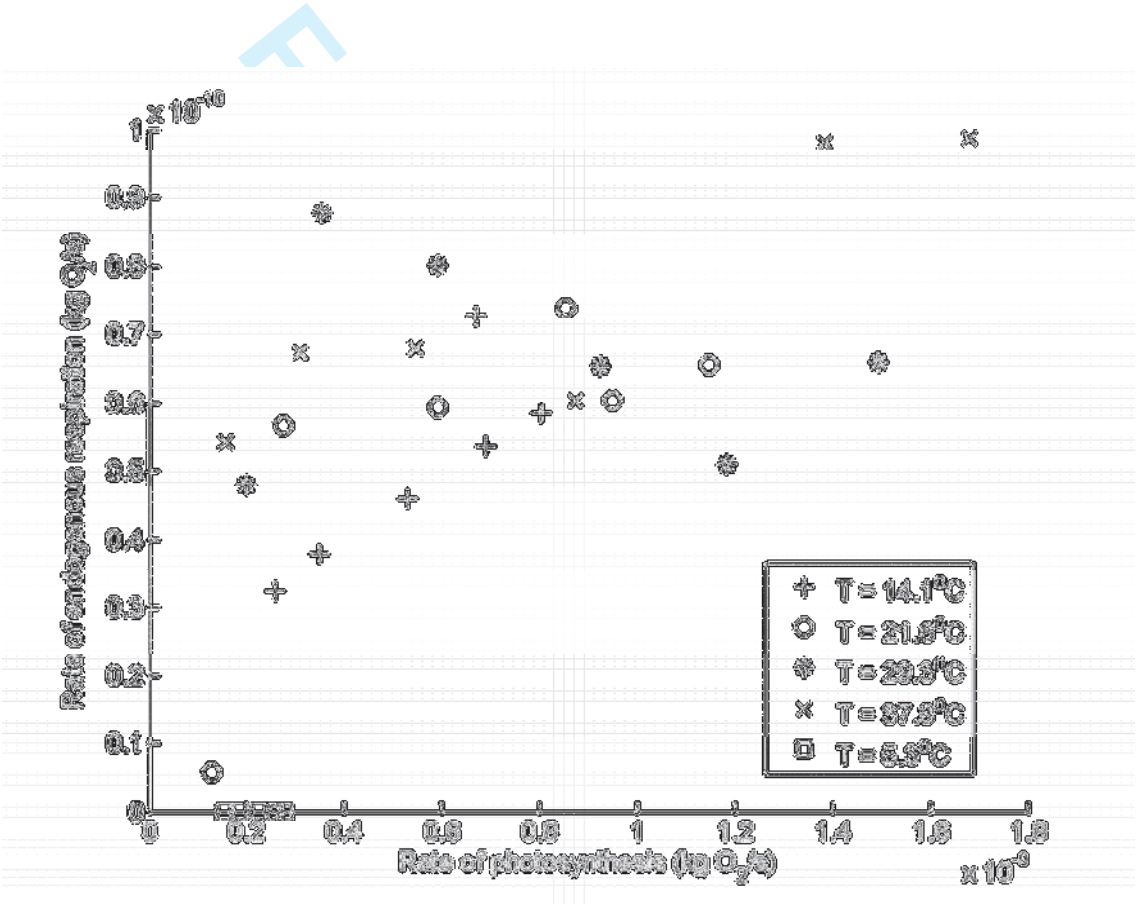

Figure S8-1: Measured rate of photosynthesis vs. Measured rate of respiration after light exposure in the vessels used during the determination of model kinetic parameters.

S9: Comparison of predicted and measured cumulative productivities in the bench-scale photobioreactors

Figure S9-1 directly compares the measured and predicted cumulative productivities in bench-scale photobioreactors operated under different light intensities and temperatures.

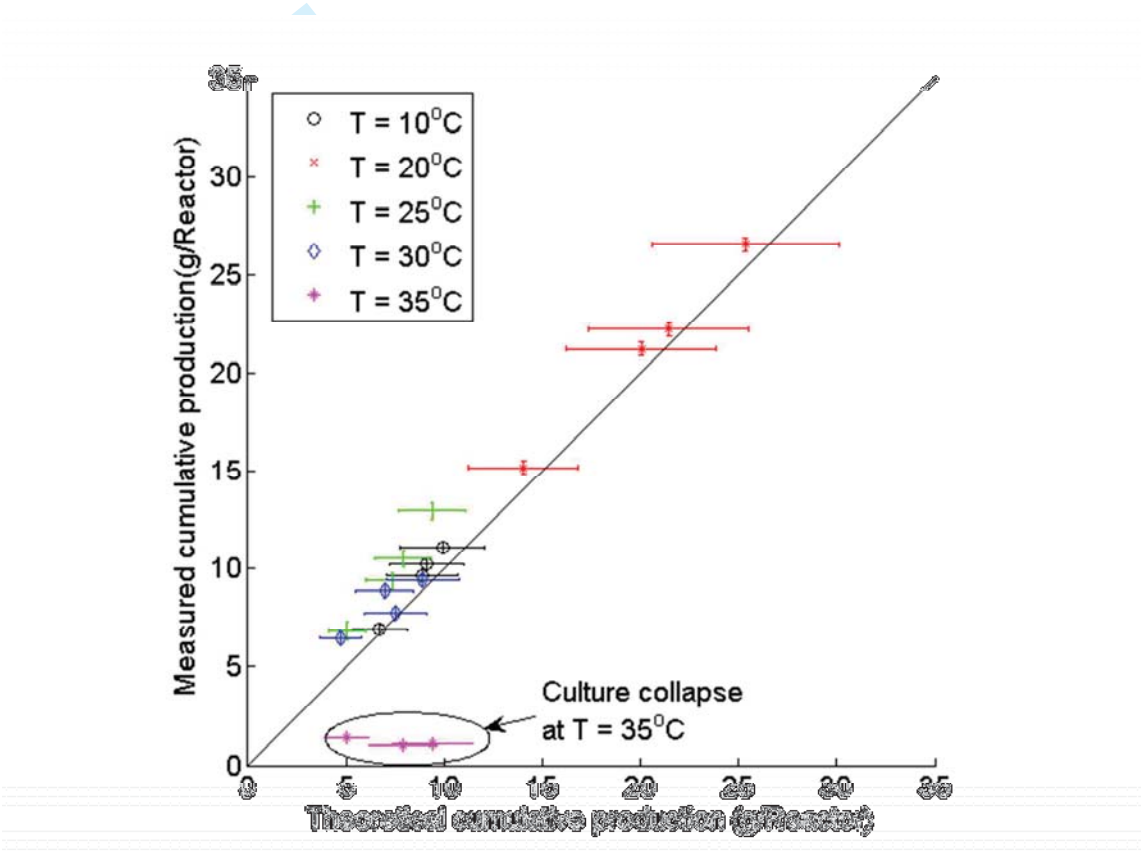

Figure S9-1: Predicted vs. measured cumulative productivities in the bench-scale reactors over the entire cultivation duration. The error bars represent the level of confidence at 95% (see S6 for details).

Article 5

MASSEY UNIVERSITY
GRADUATE RESEARCH SCHOOL

STATEMENT OF CONTRIBUTION TO DOCTORAL THESIS CONTAINING PUBLICATIONS

(To appear at the end of each thesis chapter/section/appendix submitted as an article/paper or collected as an appendix at the end of the thesis)

We, the candidate and the candidate's Principal Supervisor, certify that all co-authors have consented to their work being included in the thesis and they have accepted the candidate's contribution as indicated below in the *Statement of Originality*.

Name of Candidate: Quentin Béchet

Name/Title of Principal Supervisor: Prof. Benoit Guieysse

Name of Published Research Output and full reference:

Béchet Q, Shilton A, Guieysse B. Full-scale validation of a model of algal productivity (submitted).

In which Chapter is the Published Work: 4

Please indicate either:

- The percentage of the Published Work that was contributed by the candidate:

  and / or

- Describe the contribution that the candidate has made to the Published Work:

  Q Béchet was the main contributor of the article. He carried the experimental work and analyzed the results (including the numerical implementation of the model). He also wrote most of this article.

Quentin Béchet — Digitally signed by Quentin Béchet DN: cn=Quentin Béchet, o=Massey University, ou=SEAT, email=q.bechet@massey.ac.nz, c=NZ Date: 2014.02.17 18:49:56 +13'00'

Candidate's Signature — 04/07/2014 — Date

Benoit Guieysse — Digitally signed by Benoit Guieysse DN: cn=Benoit Guieysse, o=Massey University, ou=SEAT, email=b.j.guieysse@massey.ac.nz, c=NZ Date: 2014.02.24 11:17:49 +13'00'

Principal Supervisor's signature — 07/07/2014 — Date

This document is confidential and is proprietary to the American Chemical Society and its authors. Do not copy or disclose without written permission. If you have received this item in error, notify the sender and delete all copies.

Full-scale validation of a model of algal productivity

Journal:	*Environmental Science & Technology*
Manuscript ID:	es-2014-03204e
Manuscript Type:	Article
Date Submitted by the Author:	02-Jul-2014
Complete List of Authors:	Béchet, Quentin; Massey University, Guieysse, Benoit; Massey University, School of Engineering and Advanced TechnologyWater Shilton, Andrew; Massey University, Technology and Engineering

SCHOLARONE™
Manuscripts

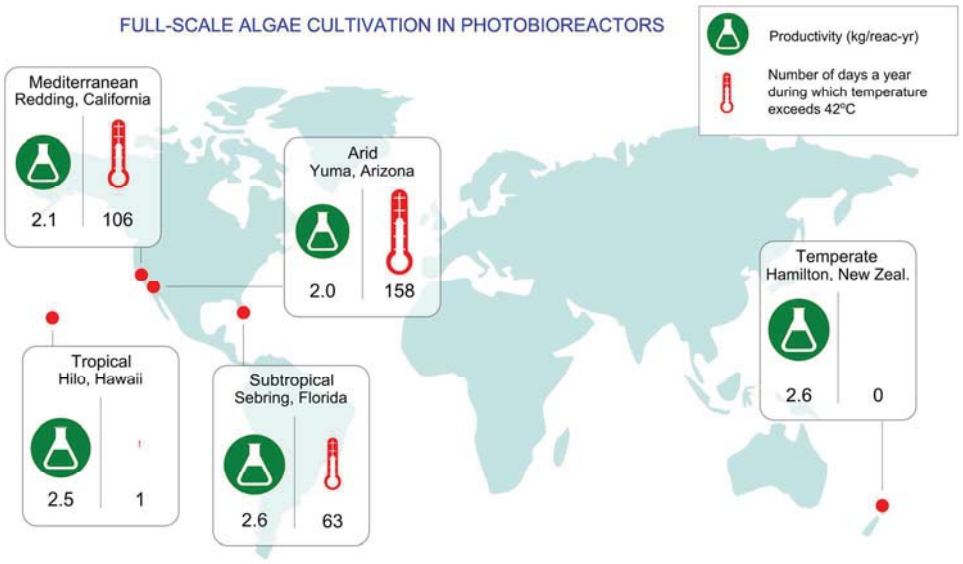

Graphical Abstract
171x97mm (300 x 300 DPI)

Full-scale validation of a model of algal productivity

Quentin Béchet[a], Andy Shilton[a], Benoit Guieysse[a,*]

[a]School of Engineering and Advanced Technology, Massey University, Private Bag 11 222, Palmerston North 4442, New Zealand

*Corresponding author:

Telephone: +64 6 350 5841

Fax: +64 6 350 5604

Email: B.J.Guieysse@massey.ac.nz

Abstract

While modeling algal productivity outdoors is crucial to assess the economic and environmental performance of full-scale cultivation, most of the models hitherto developed for this purpose have not been validated under fully relevant conditions, especially with regard to temperature variations. The objective of this study was to validate a model of algal biomass productivity accounting for both light and temperature and constructed using parameters experimentally derived using short-term indoor experiments. To do this, the accuracy of a model developed for *Chlorella vulgaris* was assessed against data collected from photobioreactors operated outdoor (New Zealand) over different seasons, years and operating conditions (temperature-control/no temperature-control, batch and fed-batch regimes). The model was able to predict the experimental productivities with an overall accuracy of ± 6.3% over 148 days of cultivation and this level of accuracy was observed. To the best of our knowledge, this is the first biomass productivity model to be validated against full-scale cultivation data. Considering the high level of accuracy of the productivity predictions, the model can help to significantly refine assessments of cost-efficiency and environmental impacts of full-scale algal cultivation. Simulations at five climatic locations demonstrated that temperature-control in outdoor photobioreactors would require tremendous amounts of energy without considerable increase of algal biomass. Prior assessments neglecting the impact of temperature variations on algal productivity in photobioreactors may therefore be erroneous.

1. Introduction

Billions of dollars have been invested in research on algal biofuels[1], based on various studies showing that algae biofuels could beat current biofuels in terms of areal productivity, costs, and environmental performance[2-5]. However, most of the published assessments of algae-based biofuels used algal productivity projections based on 'near-ideal' laboratory data or on models that have not been fully validated under field conditions, as further discussed below. The uncertainty associated with the use of such productivity estimates is a significant concern because overestimating full-scale productivity would significantly bias the estimated cost-efficiency (i.e. overestimation of projected revenues) and environmental performance[6].

A particularly neglected area of concern with regard to productivity predictions is the potential impact of broth temperature variations during full-scale cultivation. For example, (7) observed that the temperature of a flat-plate photobioreactor could vary between 20 and 44^{o}C in Japan while (8) reported daily temperature variations up to 15^{o}C in a column photobioreactor operated in Singapore. However, although large and frequent temperature fluctuations are well known to significantly impact productivity and even cause cellular death[9,10,7], most of the assessments of full-scale algal cultivation available in the literature have not considered the impact of temperature on productivity, as illustrated in Table 1. This is of particular concern as out of the 11 influential studies listed in Table 1, the three studies considering the impact of temperature predicted productivities 2 to 3 times lower than the other assessments. Accurate predictions of algal productivity accounting for the impact of temperature fluctuations are therefore critically needed.

A second concern with current productivity predictions is that most of the models described in the literature have been parameterized and validated using laboratory data generated under indoor conditions[25]. Using such models to predict full-scale productivity may lead to significant levels of inaccuracy because of light-acclimation processes[26], the use of proxies to quantify the productivity (e.g. oxygen instead of biomass[27]), and the differences between the spectrums of the light source used for model development and sunlight[28]. Recent studies have focused on the validation of productivity models using data generated during outdoor cultivation but these studies were performed under different schemes of temperature-control[29,30,14]. To the best of our knowledge, only (31) validated a productivity model on an outdoor non-temperature controlled system but this model only predicts oxygen productivity, which limits its use for engineering purposes.

The first objective of our study was to determine the accuracy of the productivity model developed indoors by (26) when applied to full-scale cultivation systems. This Type-II model, which predicts *Chlorella vulgaris* productivity as a function of light and temperature, was previously validated against indoor data collected in bench-scale reactors. In order to determine if the model could also generate accurate full-scale predictions, model predictions were validated against experimental data collected in photobioreactors operated outdoors under various conditions. Following this validation, the second objective of this study was to determine if the model can be used to refine prior assessments of biofuel production from microalgaeand quantify the impact of various temperature-control strategies on productivity.

2. Materials and methods

2.1. Algal cultivation in pilot-scale outdoor photobioreactors

A phosphate-buffered BG-11 was used for all cultures to avoid pH variations[33]. The protocol used for the maintenance of pure cultures and the preparation of inocula was described by (32). Pure liquid cultures were used to inoculate the outdoor vertical cylindrical photobioreactors shown in Figure 1 (inner diameter and height of 0.19 m and 2 m, respectively). Air enriched in CO_2 (5%) was continuously bubbled in the reactors to avoid high O_2 concentration or CO_2 limitation and to ensure good mixing conditions. The gas flow rates were controlled using rotameters (Air: Ki Air Instruments: 0-20 L/min; CO_2: Aalborg PMR 1-013799: 0-500mL/min) and adjusted when necessary. No algal sedimentation was observed and temperature was experimentally shown to be homogenous in the reactors. In order to investigate how well the productivity model could account for temperature variations, two of the reactors were equipped with heaters ensuring that the temperature of the culture broth was always higher than 18^{o}C (Winter 2012) and 22^{o}C (Fall 2014).

At the start of each new culture, a reactor was filled with approximately 40L of filtered tap water (1µm pore size) and immediately aerated to remove any residual chlorine. Dissolved mineral salts were then added followed by 0.5 L of freshly re-suspended algal inoculums (initial concentration in each reactor of around 0.1 g/L) and approximately 3 L of tap water was added to reach a final working volume of 50 L. All reactors were operated as batch systems until the algal concentration reached 0.5 g/L after which 5L of the culture broth was daily replaced with fresh medium. Evaporation never exceeded 50 mL/d and was not compensated for. A total of three distinct experiments were carried out as described in Table 2. An unexplained culture collapse was observed in one of the reactors operated in winter

2012 (Supplementary information S1) and the corresponding data was therefore excluded in the assessment of the model accuracy.

2.2. Sampling and analysis

The dry weight concentration and the optical density (at 683nm) were measured daily during Experiments 1 and 3 and twice a day at sunrise and sunset during Experiment 2 (winter 2012) in order to independently measure the biomass gain during day-time and biomass loss at night. In order to collect a sample representative of the entire culture, the broth of the photobioreactors was re-circulated for 5 minutes (Ebara pump, Type CDXM\A, Flow rate: approx. 25 L/min) and a sample was withdrawn from the recirculated fluid (any excess sample was immediately returned). The protocol for dry weight measurement was described by (32). In order to ensure that pH and dissolved oxygen concentration did not affect algal productivity, these two variables were continuously recorded in one of the reactors (non-temperature controlled). The pH was found to vary between 6.8 and 7.6 and the dissolved oxygen concentration was never observed to exceed 140% of saturation. Earlier experiments showed algal productivity was not limited by nutrient supply or CO_2 transfer under the conditions tested (32). Algal heat value was measured by centrifuging and re-suspending a volume of 5L of algae broth from the photobioreactors in around 10 mL of distilled water, drying this concentrate at 105^{o}C overnight, and quantifying the calorific value by bomb calorimetry.

2.3. Modeling productivity

The modeling approach used to determine the productivity of the outdoor reactors operated in New Zealand involved three integrated predictions:

1) The temperature of the reactors was determined using a refined version of the model of Béchet et al. (2010) for *Chlorella vulgaris*, as described below;
2) The light distribution in the reactors broth was determined using the modified Beer-Lambert law developed by (32);
3) From the determination of the reactors temperature (1) and the light distribution in the reactors (2), the instantaneous productivity was calculated using the model developed by (32).

Prediction of the reactors temperature

The temperature model described by (8) was used to predict the temperature in the outdoor reactors and refined for the calculations of the reactor wall transmittance and the fraction of the diffuse compound of the solar radiation as described in supplementary information (S2). In addition, the heat balance used in the original temperature model was modified in order to account for the heaters in the temperature-controlled reactors as described in supplementary information (S3). The model of (8) was originally developed to predict the temperature in a single photobioreactor but it was assumed that the interactions between the four reactors, which were spaced 1 meter apart, did not significantly impact the heat fluxes considered. The meteorological data used as inputs of the temperature model originated from a weather station located at a distance of approximately 1.5 km from the reactors (NIWA, Weather station number: 21963, -40.38195; 175.60915). The different parameters used in the temperature model are listed in supplementary information (S4). When compared against temperature data collected during the operation of the outdoor reactors in Singapore[8] and New Zealand, the accuracy of the temperature prediction was found to be +/- 4.0 ^{o}C ($p = 0.05$; $N = 6,995$). A level of uncertainty of +/- 4 ^{o}C on the temperature prediction was

151 therefore taken in the Monte-Carlo simulations performed to assess the impact of errors on
152 productivity predictions (see Section 2.5).
153
154 *Determination of light distribution*
155 Light distribution was determined using a modified Beer-Lambert expressed as:
156 $$I_{loc}(l) = I_0 \cdot \exp(-\sigma_X X l) \quad (1)$$
157 where I_{loc} is the local light intensity (W/m^2), l is the length of the light path between the
158 considered position and the reactor external surface (m), I_0 is the incident light intensity
159 (W/m^2, as photosynthetically active radiation, or PAR), σ_X is the extinction coefficient
160 (m^2/kg) and X is the algal concentration (kg/m^3). The light distribution in the outdoor reactors
161 was impacted by multiple factors such as the sun position, the ground reflectivity and the
162 reactor wall transmittance. The numerical determination of the light distribution in the
163 photobioreactors was therefore complex. In order to avoid mistakes in the numerical solving,
164 the algorithm was thoroughly verified through conversation laws such as photon
165 conservation. The determination of the light distribution in the outdoor reactors and the
166 associated verifications are fully detailed in supplementary information (S5).
167
168 *Calculation of the instantaneous productivity*
169 Net productivity (P_{net}, in kg/s) was expressed as the difference between the rate of
170 photosynthesis (P, in kg/s) and the rate of endogenous respiration (ER, in kg/s). Based on the
171 literature review of (25), the rate of photosynthesis (P, in kg/s) was expressed as a function of
172 light intensity and temperature, while the rate of endogenous respiration was solely expressed
173 as a function of temperature. P_{net} was thus expressed as:

$$P_{net} = \int_V P_m(T) \frac{\sigma_X I_{loc}}{K(T) + \sigma_X I_{loc}} X \cdot dV - \lambda(T) XV \quad (2)$$

where $P_m(T)$ is the maximal specific rate of photosynthesis at the temperature T (kg/kg-s), $K(T)$ is the half-saturation constant at the temperature T (W/kg), V is the reactor volume (m^3) and $\lambda(T)$ is the respiration coefficient at the temperature T (kg/kg-s). The values of the model parameters P_m, K and λ were measured at different temperatures by (32). Intermediate values of the model parameters were obtained by linear interpolation between measured values. Equation 2 was solved numerically by using a first-order Euler forward scheme with a time step of 1000s which did not cause any significant numerical error. At each time step, a discretization of the entire volume of the reactors was necessary to compute the productivity of the photobioreactor. In order to minimize the computational time, numerical simplifications were done and pre-calculations matrices were generated as fully described in supplementary information (S6).

2.4. Overall accuracy

The overall accuracy Δ of the model when compared to experimental data was defined as follows:

$$\Delta = \frac{\sum_{Exp} \sum_{Reac} \left| P_{cumul,theo} - P_{cumul,\exp} \right|}{\sum_{Exp} \sum_{Reac} \left| P_{cumul,\exp} \right|} \quad (3)$$

where $P_{cumul,theo}$ and $P_{cumul,exp}$ (kg) are the cumulative theoretical and measured productivities in the outdoor reactors over the period of cultivation.

194 2.5. Uncertainty analysis

195 Model predictions were based on various parameters and variables. Most of the model inputs
196 were well-known universal constants but others were specific to the cultivation conditions of
197 the experiments described in this study and were experimentally determined in situ (see
198 supplementary information S7). As a result, experimental error on these specific parameters
199 and variables may cause inaccuracy on the productivity predictions. Monte-Carlo simulations
200 were performed in order to quantify the impact of these experimental errors on the accuracy
201 of productivity predictions. These simulations were based on the assumption that
202 experimental error on model inputs were normally distributed around their measured values
203 (see supplementary information S7 for further details).

204

205 2.6. Data for simulations

206 The model was used to predict the theoretical productivity of outdoor reactors operated at
207 five distinct climatic locations. Meteorological data from Yuma (Arizona); Merced
208 (California), Sebring (Florida), Hilo (Hawaii) and Hamilton (New Zealand) were used to
209 represent arid, Mediterranean, sub-tropical, tropical, and temperate climates, respectively. For
210 the US locations, hourly solar irradiance, air temperature, wind speed, and rainfall, together
211 with monthly day-time and night-time relative humidity averages for the year 2009 (01-01-
212 2009 to 31-12-2009) were obtained from the National Climatic Data Center of the US
213 National Oceanic and Atmospheric Administration. Data for New Zealand was obtained from
214 the New Zealand Institute of Water and Atmospheric research (NIWA) over 2009. In all
215 simulations, the photobioreactors were operated by daily refreshing 10L of culture at 7 pm,
216 yielding a hydraulic retention time of 5 days, and the initial algal concentration was set at 0.1
217 g/L to allow rapid start-up and discourage contamination. (32) reported that *C. vulgaris*

218 photosynthesis and respiration were completely inhibited at temperatures higher than 42^{o}C,
219 mostly due to cellular death. For this reason, it was assumed that temperatures higher than
220 42^{o}C caused algae death and that the reactors had to be re-inoculated the next day at an initial
221 concentration of 0.1 g/L.
222
223 3. Results and discussion
224
225 3.1. Model validation
226 As can be seen in Figures 2 to 4, predicted cumulated productivities (blue plain lines) agreed
227 well with measured cumulative productivities (red dots) in all experiments and the model
228 achieved an overall accuracy of ± 6.3 % over 148 days of cultivation. More importantly, the
229 accuracy of the model prediction did not differ significantly across data sets collected at
230 different times of the year (Table 3), which evidences the ability of the model to account for
231 seasonal variations of temperature (-0.9 – 37.2^{o}C), solar irradiances (0-374 W/m^{2}, as PAR)
232 and solar angle (41.2^{o} – 90^{o}). Accurate predictions were also obtained for the reactors
233 operated with and without temperature-control (Figures 3 and 4) and under batch and fed-
234 batch operations at different hydraulic retention times. To the best of our knowledge, these
235 results provide the first published validation of an algal biomass productivity model
236 parameterized using indoor data and independently validated using data from long-term full-
237 scale cultivation. Although the accuracy of the modeling approach remains to be estimated
238 over a broader range of designs and operational conditions and for other algae species, this
239 study represents a critical milestone for the assessment and optimization of outdoor algae
240 cultivation, as demonstrated below.
241

As discussed in (32), most of the prior modeling studies in the field have not quantified the impact of the uncertainty of experimental parameters on the accuracy of productivity predictions. During model validation, uncertainty analysis is critical to determine if the prediction inaccuracies are due to the uncertainty of model inputs rather than erroneous model assumptions. In this study, the measured productivities were found to fall within the confidence intervals of the predicted productivities determined using Monte-Carlo simulations (represented by the dash-lines on Figures 2 to 4) for all the experiments. This indicates that the uncertainties on the model inputs can explain the inaccuracies of the productivity predictions. However, because the predicted net biomass gain is calculated as the results of two competitive processes, it is possible that the prediction of net biomass gain could be accurate even if both the rates of photosynthesis and respiration were systematically overestimated and underestimated, respectively, thereby cancelling out their respective errors. It was therefore necessary to validate the models for photosynthesis and respiration independently. For this purpose, algal concentration was measured at sunrise and sunset during Experiment 2 (winter 2012, see Table 2 for details), so that both biomass gain during day-time and biomass loss during night-time were measured. Figure 5 shows the predicted and measured cumulative biomass gains during daytime and biomass loss during night-time were not significantly different, thus validating the modeling approaches used to represent photosynthesis and respiration. The ability of the model to accurately predict respiration rates at night-time is critical to optimize the design and operation of full-scale cultivation systems as discussed in the modeling study of Le (34).

As outlined in Section 2.3 the model parameters were determined using the methodology described by (32). There were potentially three limitations to this approach: i) the

266 experiments used during model parameterization were of short duration (20 minutes); ii) the
267 light source used in these experiments had a spectrum different from the spectrum of natural
268 sunlight; iii) the model was based on the measurement of oxygen productivities rather than
269 direct measurement of biomass productivities. With regard to these potential shortcomings,
270 the accuracy of ± 6.3% herein reported indicates that algal acclimation processes, differences
271 in light spectrum between the LEDs used during model parameterization and natural sunlight,
272 and the uncertainty in the conversion coefficients between oxygen and biomass productivities
273 did not introduce any significant systematic error into the model predictions. This finding is
274 particularly relevant to the field of algal biotechnology because it demonstrates that the
275 experimental technique developed by (32) allows the rapid parameterization of models
276 accurately predicting full-scale productivity.
277
278 3.2. Is the accuracy of the model fit for the purpose of estimating economic feasibility and
279 environmental impacts?
280 As discussed in the introduction, there is considerable variability in the productivity
281 predictions used in past assessments of biofuel production from microalgae. This variability
282 bears the testimony of the large uncertainty associated with full-scale productivity prediction.
283 For example, (24) recently estimated the cost of algal biofuel production in open ponds to
284 $US 3.21/L by assuming a productivity of 5.5 kg/m^2-year. In a sensitivity analysis, the
285 authors assumed a productivity uncertainty of ± 33% and showed that this uncertainty
286 translated into an uncertainty on the biofuel cost of around ± $US 1.50/L. In comparison, the
287 level of accuracy of ± 6.3% obtained by the model herein validated would translate to an
288 uncertainty of ± $US 0.29 per liter. This uncertainty is comparable to the uncertainty caused
289 by the variability in the prices of CO_2 and nutrients[24]. The level of accuracy herein achieved

290 has therefore the potential to eliminate major sources of uncertainty in the assessment of the
291 economics of full-scale algal cultivation.
292
293 The model also aims to assist in the environmental impact assessment of full-scale algal
294 cultivation. For example, (35) estimated the amount of freshwater resources that would be
295 needed to cultivate algae in open ponds at 5.44 m^3/m^2-year in a Mediterranean climate. A
296 sensitivity analysis also revealed that the uncertainty of the optimal hydraulic retention time
297 (HRT) that would be used at full-scale caused an uncertainty of ± 3.3 m^3/m^2-year in the
298 estimation of this water demand[35]. The HRT defines what fraction of the pond liquid is
299 extracted for harvesting every day. During full-scale algae cultivation, the HRT can be
300 adjusted to maintain an optimal algal concentration X_{opt}, where any lower value would mean
301 higher water consumption while any higher value of HRT would increase biomass loss due to
302 respiration[36]. The optimal HRT value can be expressed as a function of the optimal
303 concentration as follows:

304 $$HRT = \frac{d \cdot X_{opt}}{P} \quad (4)$$

305 where d is the pond depth (m) and P is the productivity (kg/d). In the study of (35), the range
306 of HRT values used for the sensitivity analysis was necessarily large mostly to account for
307 uncertainties on productivity. However with the level of accuracy of ± 6.3% on productivity
308 prediction, the HRT range could be refined within ± 0.5 day (for an HRT value of
309 approximately 7 days according to Equation 4). As shown in (35), an uncertainty of ± 0.5 day
310 on the HRT causes an uncertainty on the water demand of ± 0.25 m^3/m^2-year, which is
311 comparable to the uncertainty caused by water leaks. The level of accuracy offered by the

312 productivity model herein validated has therefore the ability to significantly refine prior
313 assessments of the environmental impacts of full-scale algal cultivation.
314
315 3.3. Use of the model for assessing feasibility of temperature control
316 This section aims to demonstrate how the model can be applied to investigate practical
317 operation and assist design of full-scale systems. In this case-study, the viability of
318 engineered temperature-control in photobioreactors was investigated at five climatic
319 locations. The amount of energy required for temperature control was computed as the sum
320 of the amounts of energy that must be removed or added to the cultivation broth based on
321 energy balance. The efficiencies of three control strategies to boost productivity are discussed
322 below:
323 1. In the absence of temperature-control, productivity was predicted to be the lowest in
324 the sunniest arid and Mediterranean climates (Figure 6). This paradoxical result is due
325 to the frequent occurrence of high temperature causing cellular death (>42^{o}C) in arid
326 (158 days) and Mediterranean climates (106 days; Figure 6).
327 2. In order to minimize the energy demand of temperature-control, a 'temperature-range'
328 control strategy was also investigated, where temperature is only maintained between
329 20^{o}C and 35^{o}C during day-time. Figure 6 shows that this strategy significantly
330 increases productivity at hot locations but has a minimal impact at more temperate
331 locations where the temperature of photobioreactors is expected to be between 20^{o}C
332 and 35^{o}C at most times. However, the energy required for temperature-control relative
333 to the associated gain of biomass energy (henceforth defined as energy ratio)
334 exceeded 70 even in the arid and Mediterranean locations. This high energy ratio

indicates the excessive energy demand associated with this temperature-control strategy.

3. In a further attempt to minimize the energy ratio, an 'aggressive' temperature-control strategy was considered where temperature is maintained at 35°C at day-time to optimize productivity and at 5°C at night-time to minimize respiration. This strategy was predicted to boost productivity by 29 to 116% depending on climate (Figure 6) but its energy ratio was very high (240 – 740).

To further illustrate the potential environmental and economic implications of temperature-control, the feasibility of cooling the reactors using water evaporation at the surface of the reactor walls was investigated as this strategy is commonly proposed in the literature[37-39]. Using the relatively efficient 'temperature-range' control strategy, it would be necessary to evaporate 0.7 m^3 of freshwater at the reactor surface per year and per reactor in an arid location. By assuming a reactor density of 1-2 reactors/m^2 (33) the water demand for cooling would therefore represent 0.7-1.4 m^3/m^2-year, which is the equivalent of 13 to 26 years of rainfall at this location. In the alternative case where brackish water is used to cool down the photobioreactors, the cost of reverse osmosis (RO) to remove salts from water would represent a cost of US$ 0.17-0.34 per kg algae produced (based on the US$ 0.26-1.33 m^{-3} range for full-scale brackish water given by 40). Cooling by evaporation would therefore be uneconomical for algal biofuel feedstock production at the arid location since (3) estimated that the total cost of algae biomass cultivation should not exceed US$ 0.34 kg^{-1} to be competitive with oil at US$ 100 a barrel. Of course, it is not impossible that targeted temperature-control strategies may support significant productivity gain at affordable energy ratios under specific conditions. However, the energy ratio herein defined does not account

for inefficiencies in heat transfer and algal biofuel generation. In conclusion, temperature-control is unrealistic for low-value bulk algae products such as biofuels from photobioreactors.

3.4. The necessity of accounting for temperature fluctuations in feasibility assessments

Given it is not economically viable to control the temperature of photobioreactors at full-scale, accounting for the impact of temperature fluctuations is crucial for accurate productivity predictions. Yet, as shown in Table 1, most previous feasibility assessments were based on the assumption that temperature fluctuations did not impact productivity and outdoor productivities are commonly extrapolated from data obtained during indoor cultivation (i.e. at 25^{o}C). However, simulations based on the model developed in this study showed that the assumption that temperature can be controlled at 25^{o}C can have a significant impact on the accuracy of productivity predictions. For example, assuming that productivity in arid conditions is the same as productivity from cultivation undertaken at a constant 25^{o}C overestimates productivity by 58% in photobioreactors. As discussed in section 3.2, such level of inaccuracy can translate into relatively high inaccuracies on the estimated costs and environmental performance.

Most published assessments of biofuel production are based on cultivation in raceway ponds (Table 1) because these systems are generally considered to be more economical than closed photobioreactors. However, (41) demonstrated temperature fluctuations can also be significant in shallow ponds, with seasonal variations reaching 30^{o}C in a temperate climate. The results herein presented therefore suggest that temperature should also significantly impact algal productivity in raceway ponds and that, consequently, not accounting for its

383 effect may cause to overestimate cost-efficiency and environmental performance in these
384 systems. As the productivity model validated in this study was designed to be applicable to
385 any system geometry, coupling this productivity model with temperature predictions in open
386 ponds obtained from the validated model of (41) is the next logical step for refining
387 assessments of biofuel production from micro-algae.
388

389 4. Acknowledgments

390 Mégan Trémelot is thanked for experimental work during March-April 2014 (Experiment 3).
391 QB was supported by a Massey University Doctoral Scholarship. We also would like to
392 acknowledge Guillaume Guizard for his technical help with the design and construction of
393 the photobioreactors.

394

395 5. Supplementary information

396 S1: Culture collapse during Experiment 2 (winter 2012); S2: Temperature model –
397 Modifications from the model of Béchet et al. (2010); S3: Inclusion of the effect of the
398 heaters in the temperature model of Béchet et al. (2010); S4: Parameters value in the
399 temperature model; S5: Determination of the light distribution in the outdoor
400 photobioreactors; S6: Application of the Type II model to the outdoor photobioreactors; S7:
401 Monte-Carlo simulations.
402

403 References

404 1. Mascarelli, A.L. Algae: fuel of the future? *Environ. Sci. Technol.* **2009**, *43*(19), 7160–
405 7161.

406 2. Campbell, P.K.; Beer, T.; Batten, D. Life Cycle assessment of biodiesel production form
407 microalgae in ponds. *Bioresour. Technol.* **2011**, *102*, 50-56.

408 3. Chisti, Y. Biodiesel from microalgae beats bioethanol. *Trends Biotechnol.* **2008**, *26*(3):
409 126-131.

410 4. Lardon, L.; Helias, A.; Sialve, B.; Steyer, J.P.; Bernard, O. Life-cycle assessment of
411 biodiesel production from microalgae. *Environ. Sci. Technol*. **2009**, *43*, 6475–6481.

412 5. Stephenson, A.L.; Kazamia, E.; Dennis, J.S.; Howe, C.J.; Scott, S.A.; Smith, A. G. Life-
413 cycle assessment of potential algal biodiesel production in the United Kingdom: a
414 comparison of raceways and air-lift tubular bioreactors. *Energy Fuels* **2010**, 24, 4062–4077.

415 6. Walker, D.A. Biofuels, facts, fantasy, and feasibility. *J. Appl. Phycol*. **2009**, *21*, 509-517.

416 7. Zhang, K.; Kurano, N.; Miyachi, S. Outdoor culture of a cyanobacterium with a vertical
417 flat-plate photobioreactor: Effects on productivity of the reactor orientation, distance setting
418 between the plates, and culture temperature. *Appl. Microbiol. Biotechnol*. **1999**, *52*, 781–786.

419 8. Béchet, Q.; Shilton, A.; Fringer, O. B.; Muñoz, R.; Guieysse, B. Mechanistic modeling of
420 broth temperature in outdoor photobioreactors. *Environ. Sci. Technol.* **2010** *44*(6), 2197-
421 2203.

422 9. Borowitzka, M.A. Limits to growth. In Wong YS, Tam NFY (eds) Wastewater treatment
423 with algae. **1998**. Springer-Verlag Berlin pp 203-226.

10. Tredici, M. R.; Materassi, R. From open ponds to vertical alveolar panels: the Italian experience in the development of reactors for the mass cultivation of phototrophic microorganisms. *J. Appl. Phycol.* **1992**, *4*, 221-231.

11. Sun, A.; Davis, R.; Starbuck, M.; Ben-Amotz, A.; Pate, R., Pienkos, P. T. Comparative cost analysis of algal oil production for biofuels. *Energ*. **2011,** *36*, 5169-5179.

12. Slade, R.; Bauen, A. Micro-algae cultivation for biofuels: cost, energy balance, environmental impacts and future prospects. *Biomass Bioenergy* **2013**, 53, 29-38.

13. Batan, L.; Quinn, J. C.; Bradley, T.H. Analysis of water footprint of a photobioreactor microalgae biofuel production system from blue, green and lifecycle perspectives. *Algal Res.* **2013,** *2* (3), 196-203.

14. Quinn, J.; de Winter, L.; Bradley, T. Microalgae bulk growth model with application to industrial scale systems. *Biores. Technol*. **2011**, 102, 5083-5092.

15. Chisti, Y. Biodiesel from microalgae. *Biotechnol. Adv*. **2007**, *25*, 294-306.

16. Wigmosta, M. S.; Coleman, A. M.; Skaggs, R. J.; Huesemann, M. H; Lane, L. J. National microalgae biofuel production potential and resource demand. *Water Resour. Res.* **2011**, *47*, 3377–3388.

17. Weyer, K. M; Bush, D. R; Darzins A.; Willson, B. D. Theoretical maximal algal oil production. *Bioenerg. Res.* **2010**, *3*, 204-213.

18. Wang, T.; Yabar, H.; Higano, Y. Perspective assessment of algae-based biofuel production using recycled nutrient sources: the case of Japan. *Bioresour. Technol.* **2013**, *128*, 688-696.

445 19. Zemke, P.E.; Wood, B.D; Dye; D.J. Considerations for the maximum production rates of
446 triacylglycerol from microalgae. *Biomass Bioenerg.* **2010**, *34*, 145-151.

447 20. Illman, A.M, Scragg, A.H., Shales, S.W. Increase in Chlorella strains calorific values
448 when grown in low nitrogen medium. *Enzym. Microb. Technol.* **2000**, *27*, 631-635.

449 21. Benemann, J.R.; Oswald, W.J. Systems and economic analysis of microalgae ponds for
450 conversion of CO_2 to biomass. **1996**. Report to the Department of Energy, Department of
451 Civil Engineering, University of California, Berkeley.

452 22. Pate, R.; Klise, G.; Wu, B. Resource demand implications for US algae biofuels
453 production scale-up. *Appl. Energy* **2011**, *88*, 3377-3388.

454 23. Yang, J.; Xu, M.; Zhang, X.; Hu, Q.; Sommerfeld, M.; Chen, Y. Life-cycle analysis on
455 biodiesel production from microalgae: water footprint and nutrients balance. *Bioresour.*
456 *Technol.* **2011**, *102(1)*, 159-165.

457 24. Rogers, J. N.; Rosenberg, J. N.; Guzman, B. J.; Oh, V.H.; Mimbela, L. E.; Ghassemi, A.;
458 Betenbaugh, M.J.; Oyler, G.A.; Donohue, M.D. A critical analysis of paddlewheel-driven
459 raceway ponds for algal biofuel production at commercial scales. *Algal Research* **2013** (In
460 press)

461 25. Béchet, Q.; Shilton, A.; Guieysse, B. Modeling the effects of light and temperature on
462 algae growth: State of the art and critical assessment for productivity prediction during
463 outdoor cultivation. *Biotechnol. Adv.* **2013.** *31*(8):1648-1663.

464 26. Bernard, O. Hurdles and challenges for modelling and control of microalgae for CO_2
465 mitigation and biofuel production. *J. Process Control* **2011** *21*:1378-1389.

466 27. Burris, J.E. Effects of oxygen and inorganic carbon concentrations on the photosynthetic
467 quotients of marine algae. *Mar. Biol*. **1981**, *65*, 215-219.

468 28. Jeon, Y.C.; Cho, C.W., Yun,Y.S. Measurement of microalgal photosynthetic activity
469 depending on light intensity and quality. *Biochem. Eng. J.* **2005** *27*:127-131.

470 29. Bosma, R.; van Zessen E.; Reith, J.H.; Tramper, J.; Wijffels R.H. Prediction of
471 volumetric productivity of an outdoor photobioreactor. *Biotechnol. Bioeng.* **2007**, *97*(5),
472 1108-1120.

473 30. Ketheesan, B.; Nirmalakhandan N. Modeling microalgal growth in an airlift-driven
474 raceway reactor. *Biores. Technol*. **2013**, *136*, 689-696.

475 31. Costache, T.A.; Acién Fernández, F.G.A.; Morales, M.M.; Fernández-Sevilla, J.M.;
476 Stamatin, I.; Molina, E. Comprehensive model of microalgae photosynthesis rate as a
477 function of culture conditions in photobioreactors. *Appl. Microbiol. Biotechnol.* **2013**, *97*(17):
478 7627-7637.

479 32. Béchet, Q.; Chambonnière, P.; Shilton, A.; Guizard, G.; Guieysse, B. Algal productivity
480 modeling: a step toward accurate assessments of full-scale algal cultivation. **2014**.
481 (submitted)

482 33. Béchet, Q.; Muñoz, R.; Shilton, A.; Guieysse, B.Outdoor Cultivation of Temperature-
483 Tolerant Chlorella sorokiniana in a Column Photobioreactor Under Low Power-Input.
484 *Bioeng. Biotechnol.* **2013**, *110*(1), 118-126.

485 34. Le Borgne, F.; Pruvost, J. Investigation and modeling of biomass decay rate in the dark
486 and its potential influence on net productivity of solar photobioreactors for microalga

487 *Chlamydomonas reinhardtii* and cyanobacterium *Arthrospira platensis*. *Biores. Technol*.
488 **2013**, *138*:271-276.

489 35. Guieysse, B.; Béchet, Q.; Shilton A. Variability and uncertainty in water demand and
490 water footprint assessments of fresh algae cultivation based on case studies from five climatic
491 regions. *Biores. Technol*. **2013**, *128*, 317–323.

492 36. Muñoz-Tamayo, R.; Mairet, F.; Bernard, O. Optimizing microalgal production in raceway
493 systems. *Biotechnol. Prog.* **2013**, *29*(2), 543-552.

494 37. Singh, R.N.; Sharma, S. Development of suitable photobioreactor for algae production –
495 A review. *Renew. Sustain. Energ. Rev.* **2012**, *16*, 2347-2353.

496 38. Torzillo, G.; Pushparaj, B.; Bocci, F.; Balloni, W.; Materassi, R.; Florenzano, G.
497 Production of *Spirulina* Biomass in closed photobioreactors. *Biomass* **1986**, *11*, 61-74.

498 39. Tredici MR. 2004. Mass production of microalgae: photobioreactors. In Handbook of
499 microalgal culture: Biotechnology and Applied Phycology. Edited by Amos Richmond.
500 ISBN: 978-0-632-05953-9.

501 40. Karagiannis, I.; Soldatos, P.G. Water desalination cost literature: review and assessment.
502 *Desalination* **2008**, *223*,448-456.

503 41. Béchet, Q.; Shilton, A.; Park, J.B.K.; Craggs R.J.; Guieysse, B. Universal temperature
504 model for shallow algal ponds provides improved accuracy. *Environ. Sci. Technol.* **2011**
505 *45*(8), 3702-3709.

506

Figures

Figure 1: Four photobioreactors used for the outdoor validation of the model (May-June 2012). The reactors were positioned along an East-West axis to avoid mutual shading for this period of time.

Figure 2: Cumulative production in an outdoor photobioreactor between March and May 2011. Red dots: experimental data; blue plain line: prediction; blue dash-lines: upper and lower boundaries of the confidence intervals of the prediction. The grey shaded area represents the period of time over which the reactors were operated in batch regime. Error bars on data show confidence interval at 95% (see supplementary S7 for more details).

Figure 3: Cumulated production in outdoor photobioreactors between May and June 2012. Red dots: experimental data; blue plain line: prediction; blue dash-lines: upper and lower boundaries of the confidence intervals of the prediction. The grey shaded area represents the period of time over which the reactors were operated in batch regime. The data from the second reactor with no temperature control is shown in supplementary information (S1). Error bars on data show confidence interval at 95% (see supplementary S7 for more details).

Figure 4: Cumulated production in outdoor photobioreactors in March-April 2014. Red dots: experimental data; blue plain line: prediction; blue dash-lines: upper and lower boundaries of the confidence intervals of the prediction. The grey shaded area represents the period of time over which the reactors were operated in batch regime. Error bars on data show confidence interval at 95% (see supplementary S7 for more details).

Figure 5: Comparison of predicted and measured day-time productivities and night biomass losses in the reactors operated in winter 2012. The error bars represent the confidence intervals at 95% (calculated from statistical analysis and Monte-Carlo simulations described in supplementary information S7).

531 **Figure 6**: Top: Comparison of yearly biomass productivities at five climatic locations under
532 different temperature-control schemes (black: no temperature control; grey: 'temperature-
533 range' control; white: 'aggressive' temperature-control). The numbers on the bars represent
534 the number of days a year during which reactor temperature exceeds 42^{o}C. Middle: Amount
535 of energy (heating and cooling) necessary for temperature-control. Bottom: Ratio of the
536 energy needed for temperature-control over the gain of biomass as energy (assuming a
537 calorific value of 22 MJ/kg).

538 Figure 1

539

Figure 2

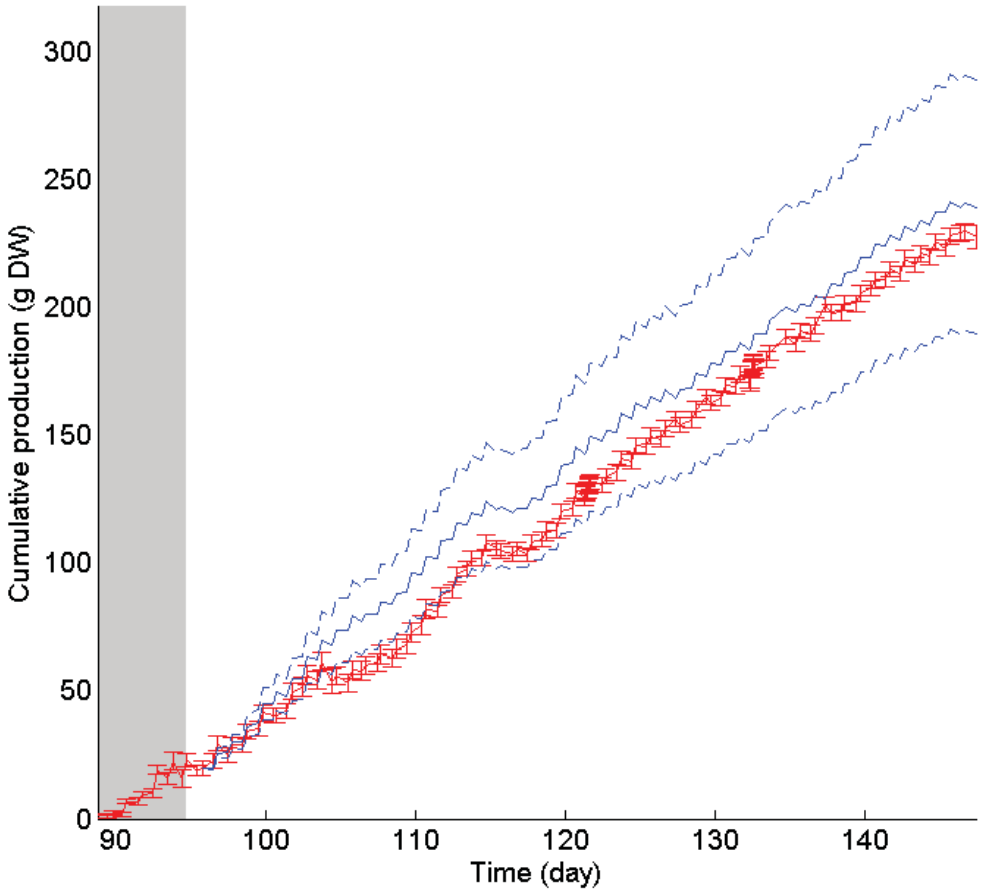
Cumulative production (g DW)
300
250
200
150
100
50
0
90
100
110
120
130
140
Time (day)

Figure 3

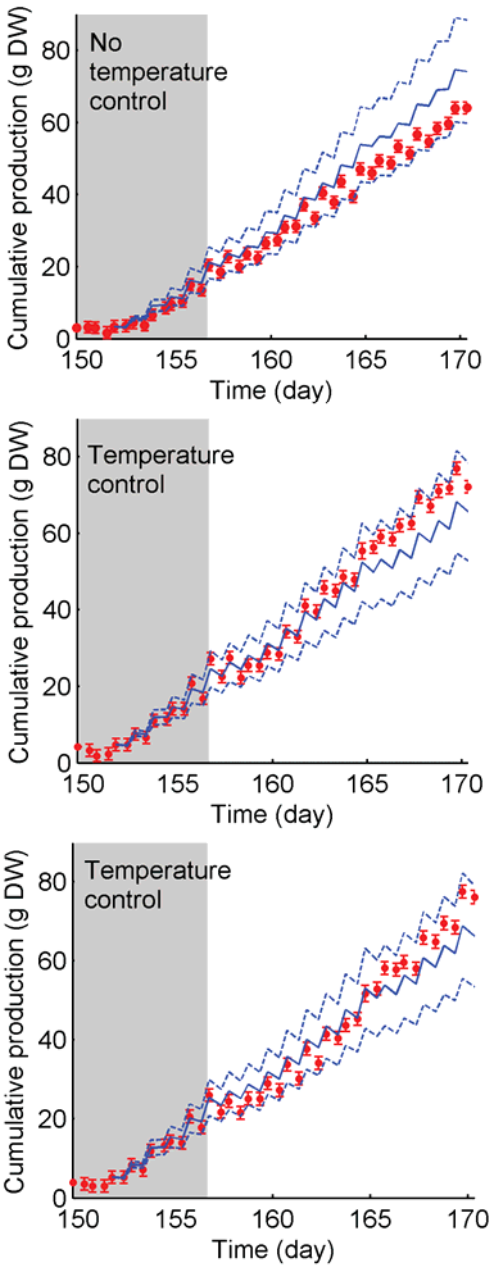
No temperature control
Temperature control
Temperature control
Cumulative production (g DW)
Time (day)
0
20
40
60
80
150
155
160
165
170

Figure 4

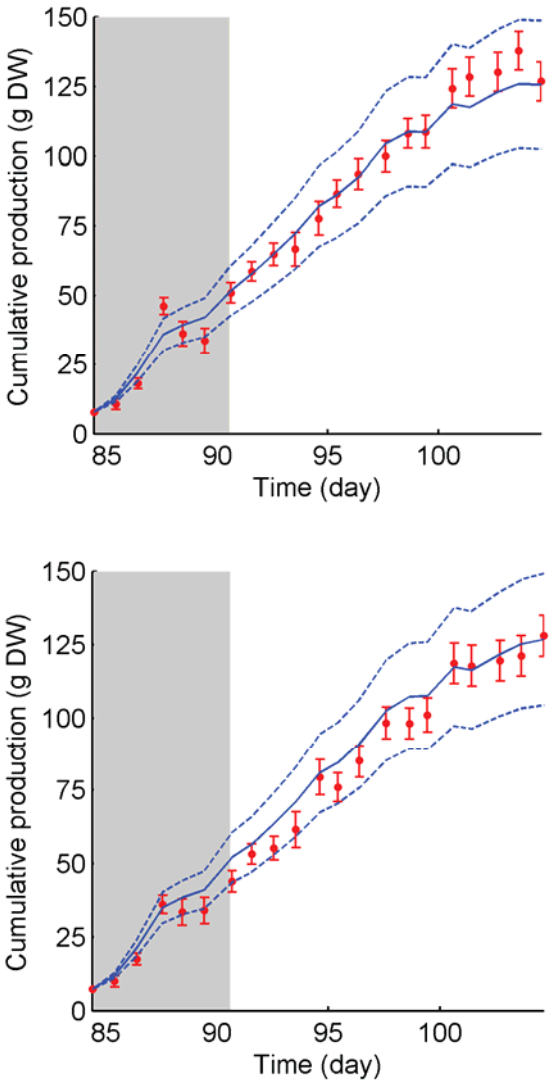
Cumulative production (g DW)
150
125
100
75
50
25
0
85
90
95
100
Time (day)
Cumulative production (g DW)
150
125
100
75
50
25
0
85
90
95
100
Time (day)

Figure 5

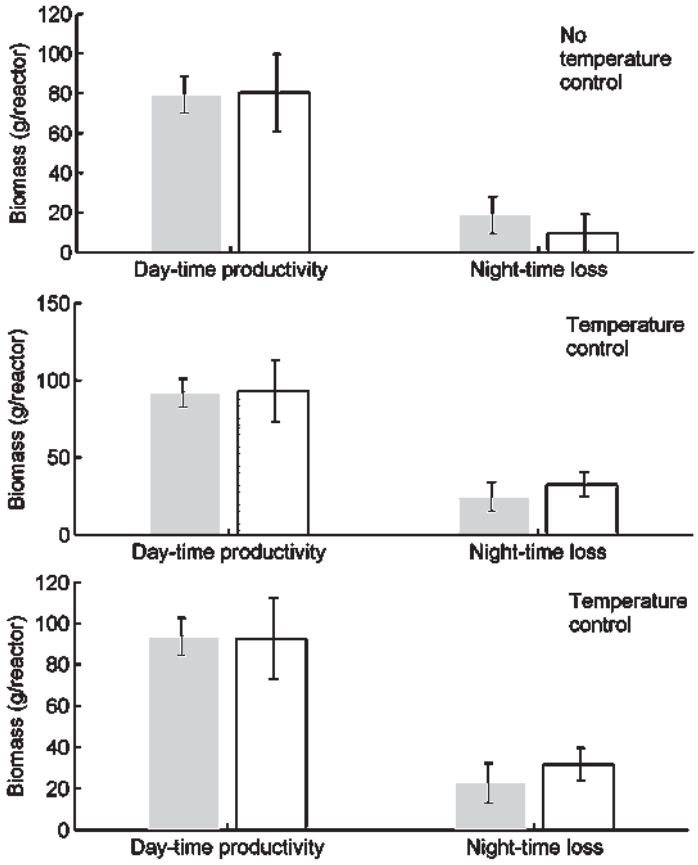
Biomass (g/reactor)
120
100
80
60
40
20
0
No temperature control
Day-time productivity
Night-time loss
Biomass (g/reactor)
150
100
50
0
Temperature control
Day-time productivity
Night-time loss
Biomass (g/reactor)
120
100
80
60
40
20
0
Temperature control
Day-time productivity
Night-time loss

Figure 6

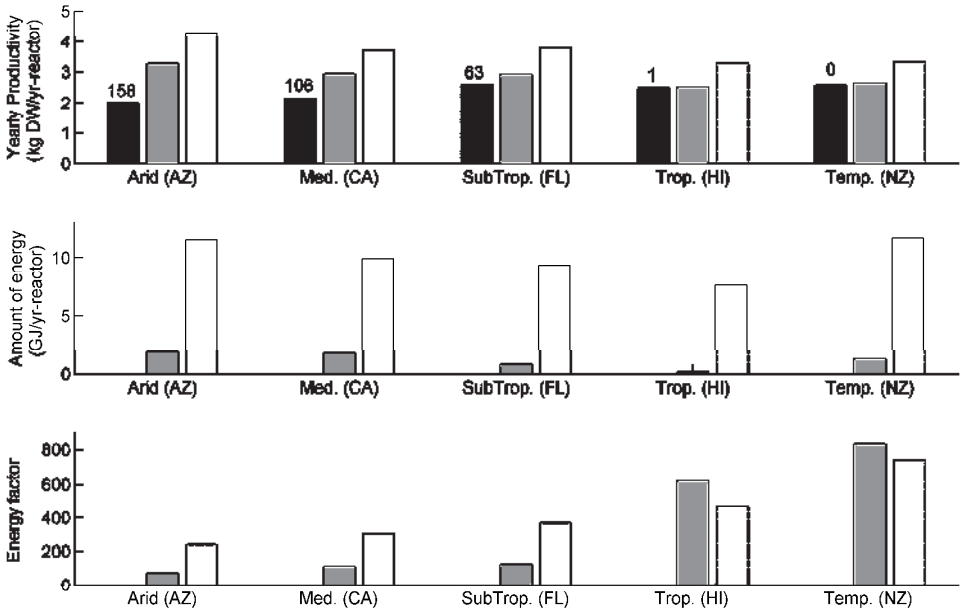
Yearly Productivity (kg DW/yr-reactor)
158
106
63
1
0
Arid (AZ)
Med. (CA)
SubTrop. (FL)
Trop. (HI)
Temp. (NZ)
Amount of energy (GJ/yr-reactor)
Energy factor

ecent assessments of full-scale algae cultivation for biofuel productions

	Algae species	Cultivation system	Location/Climate	Productivity (kg/m^2-year)	Origin of productivity value
	NS	Open pond	NS	7.3	Not specified
ty al tion	NS	Photobioreactor/ Open pond	NS	3.6 – 14.6	Open pond: "judgment and experience of the AQUAfuels partners" Photobioreactor: "experimental data incorporating future technical advances"
lgae	*Nannochloropsis salina*	Photobioreactor	Arizona California Colorado Montana Nebraska Nevada New Mexico Texas Utah Wyoming	5.3 5.3 3.6 2.9 3.4 3.8 4.7 4.7 3.9 3.3	Productivity modeled using the model of (14) accounting for the impact of temperature.
algal	*Chlorella vulgaris*	Photobioreactor/ Open pond	United Kingdom	10	Prediction by (15); unspecified assumptions.
e urce	NS	Open pond	United States	1.05 – 3.8	Model based on theoretical calculations assuming perfect efficiencies[17]. The model accounts for the impact of temperature (no clear origin of the formula).
d	*Chlorella vulgaris* *Botryococcus braunii*	Photobioreactor/ Open pond	Japan	14.2 – 27.8 23.7 – 31.6	Model based on theoretical calculations assuming perfect efficiencies[17,19]. The impacts of temperature and respiration were neglected.
	Chlorella vulgaris	Open pond	Mediterranean climate	7.3 – 11.0	Productivity values measured during indoor cultivation at 25°C[20]

	NS	Open pond	Australia	11.0	Prediction by (21); unspecified assumptions.
emand	NS	NS	Southwest of US Midwest of US Southeast of US Nineteen Lower-Tier State of US	11.3 7.0 7.7 9.1	Model based on theoretical calculations assuming perfect efficiencies[17]. The model neglects the impact of temperature.
diesel ae: nts	*Chlorella vulgaris*	Open pond	US (Average over 28 states) Arizona California Florida Hawaii	4.9 11.5 6.1 8.3 8.3	Productivity experimentally correlated with solar irradiance and pond temperature obtained from observations in South California.
fuels	NS	Open pond	New Mexico	5.5	Inaccessible reference

Table 2: Characteristics of the outdoor experiments used for model validation (TC: Temperature control)

	Number of reactors	Date of operation	Operation mode	Av./Max. Solar irradiance (W/m^2, PAR)	Reactor temperature range (^oC)
Exp. 1	1	29 Mar – 27 May 2011	Batch/Semi-continuous[a]	48/374	3.7 – 33.5
Exp. 2	4	25 May – 18 Jun 2012	Batch/Semi-continuous[a] TC in 2 reactors only[b]	31/202	No TC: -0.9 – 21.5 TC: 2.6 – 25.6
Exp. 3	2	24 March – 13 Apr 2014	Batch/Semi-continuous[a] TC in 1 reactor only[b]	61/352	No TC: 7.5 – 37.2 TC: 7.5 – 37.2

[a] 'Semi-continuous' means that a fraction of the cultivation broth was changed daily.
[b] The heaters used for temperature-control were turned on after 10 days of cultivation to minimize risks of contamination.

Table 3: Error on productivities calculated by dividing the difference between the predicted and the measured cumulative productivities over the entire period of cultivation. "TC" indicates temperature control

Experiment	Reactor	Length of cultivation (d)	Average productivity (g/reactor/d)	Average error (g/reactor-d)
1	1	51.7	4.0	0.23
2	1	18.6	3.3	0.54
	2 (TC)		3.6	0.35
	4 (TC)		3.8	0.53
3	1 (TC)	20.3	5.9	0.06
	2		6.0	0.06

Full-scale validation of model of algal productivity - Supplementary information

Quentin Béchet, Andy Shilton, Benoit Guieysse

S1: Culture collapse during Experiment 2 (winter 2012)

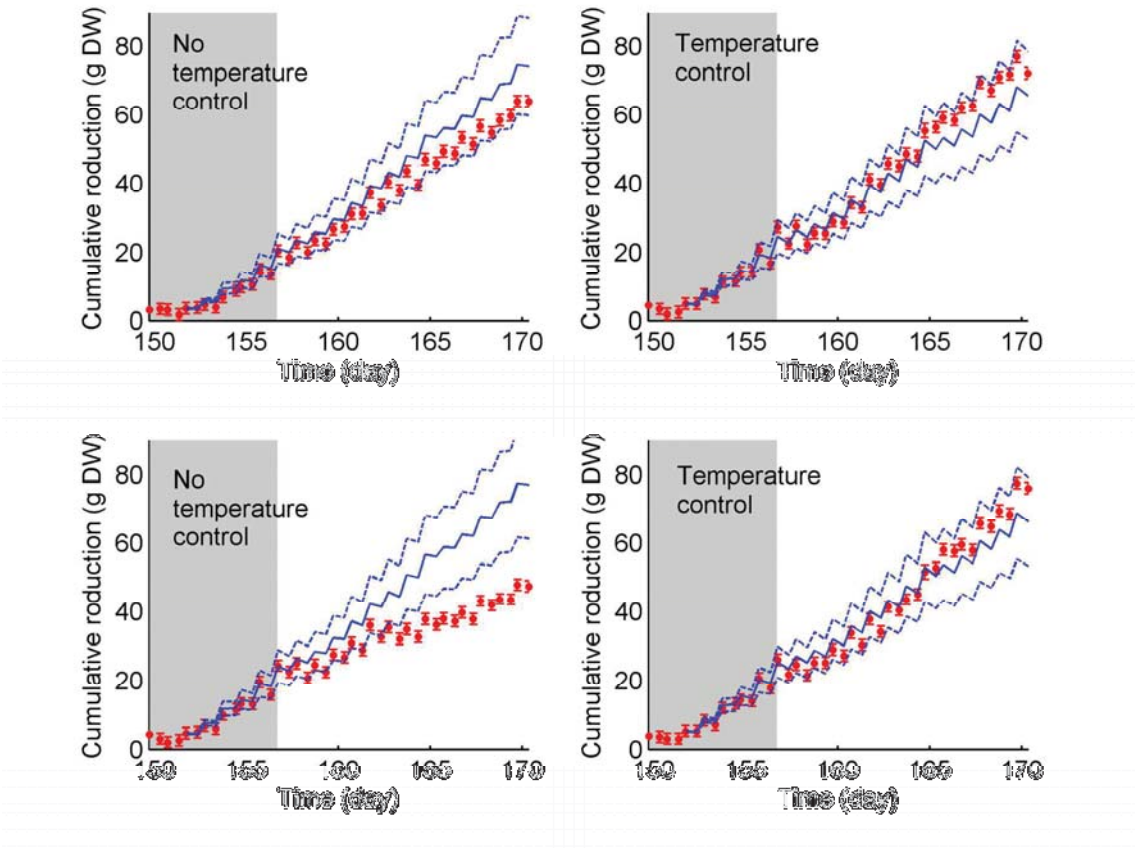

Figure S1-1: Complete data set for the Experiment 2 (winter 2012) – Culture collapse is clearly observed in Reactor 3 (bottom left).

S2: Temperature model – Modifications from the model of Béchet et al. (2010)

2.1. Introduction

The model initially developed in the study of Béchet et al. (2010) was used to predict the temperature in the outdoor photobioreactors used for model validation. The model is based on expressing the different heat fluxes reaching the reactor as a function of meteorological variables. In particular, the model is able to predict the amount of solar radiation reaching the algae under two main assumptions:

- The fraction of diffuse radiation in the solar radiation (K_d) was assumed to be constant over time and equal to 0.2, and;
- The transmittance of the reactor wall (τ) was taken equal to the measured value of 0.9.

First, a value of 0.2 for the coefficient K_d corresponds to clear-sky conditions that do not represent the meteorological conditions observed during the experimental studies carried in New Zealand. The Erbs correlation (Duffie and Beckman, 2006) for example predicts that K_d should vary between 0.165 and 1 depending on the cloud cover. Secondly, the transmittance value of the reactor wall was measured for radiation coming perpendicularly to the reactor wall surface and for an empty reactor. The value of the actual transmittance may therefore be different from 0.9. Even if these assumptions did not affect significantly the temperature prediction, the predicted amount of solar radiation reaching the algae (hence the productivity) is expected to be significantly affected by the inaccuracies on K_d and τ (Béchet et al, 2013). The objective of this document is to present how the values of these two parameters were calculated in the improved version of Béchet's temperature model.

2.2. Expression of the diffuse fraction of solar radiation (K_d)

The model used to calculate the fraction of diffuse radiation in the solar irradiance is the Erbs et al. correlation described in Duffie and Beckman (2006). Hourly values of K_d are given as a function of the hourly clearness index k_T as described by:

$$K_d = 1.0 - 0.09k_T \quad \text{for } k_T \leq 0.22 \quad \text{(S2-1a)}$$

$$K_d = 0.9511 - 0.1604k_T + 4.388k_T^2 - 16.638k_T^3 + 12.336k_T^4 \quad \text{for } 0.22 \leq k_T \leq 0.8 \quad \text{(S2-1b)}$$

$$K_d = 0.165 \quad \text{for } k_T \geq 0.8 \quad \text{(S2-1c)}$$

The hourly clearness index k_T is defined as the following ratio:

$$k_T = \frac{H_{g,hourly}}{H_{0,hourly}} \quad \text{(S2-2)}$$

where $H_{g,hourly}$ is the hourly amount of total solar radiation reaching horizontal ground surface (J/hour-m^2) and $H_{0,hourly}$ the hourly amount of solar radiation reaching the external surface of the atmosphere above the location considered (J/hour). $H_{0,hourly}$ can be calculated by integrating the intensity of the radiation reaching the external surface of the atmosphere at the location considered (H_0, W/m^2) over the hour considered. H_0 is given by:

$$H_0 = I_{sc}\left(1 + 0.033\cos\frac{360N}{365}\right)\cos\theta_z \quad \text{(S2-3)}$$

where I_{sc} is the solar constant (1367 W/m^2), N is the Julian day of the year ($N = 1$ for the 1st of January, etc.), and θ_z is the angle between the sun and a vertical axis at the location considered. The expression of θ_z as a function of time, day, and latitude can be found in Béchet et al. (2010).

2.3. Expression of the wall transmittance

In the model of Béchet et al. (2010), it was considered that the reactor wall had a constant transmittance of 0.9, meaning that only 90% of the radiation reaching the reactor would reach the algal broth. In addition, the algal broth was assumed to reflect 3% of the light reaching the reactor by analogy with the reflectivity of an air-water interface. In total, it was therefore assumed that the algae would absorb 87% of the incoming radiation. However, using the values of 0.9 for the wall transmittance and 0.03 for the algal broth reflectivity is limited for two reasons:

The values of transmittance and reflectivity are functions of the direction of incoming radiation. For example, the incident direction of the incoming direct solar radiation is a function of the sun position. At early morning or late evening, the direct sunlight reaches the reactor with almost a perpendicular angle to the reactor wall. The transmittance value is therefore close to 0.9. However, at midday when the sun is relatively high, the wall transmittance is lower than 0.9.

Both the values of transmittance and reflectivity are functions of the refraction indexes of the transparent mediums (air, polycarbonate, water). In the model of Béchet et al. (2010), the transmittance value of 0.9 was determined when the reactor was empty. Similarly, the water reflectivity of 0.03 was the reflectivity for an air-water interface. However, for incoming radiation to reach the algae, the radiation first goes through an air-polycarbonate-water interface.

The goal of this section is to refine the values of wall transmittance and water reflectivity to account for the incident direction of the radiation and the optical properties of the double interface air-polycarbonate-water. The first sub-section presents the calculation of the refraction index of the polycarbonate of the reactor walls. This refraction index value is then used in the second and third sections to determine the values of transmittance through the air-polycarbonate-water interface for direct and isotropic radiations. The last section describes how the expressions of the heat fluxes in the model of Béchet et al. (2010) were modified to account for these new transmittance values.

2.3.1. Refraction index of the reactor wall

The amount of radiation reflected by an interface between two mediums with different optical properties is given by the Fresnel equations (given here for non-polarized radiation, Bass et al., 2010):

$$R = \frac{R_s + R_p}{2} \quad \text{(S2-4a)}$$

$$R_s = \left(\frac{n_i \cos\theta_i - n_t \cos\theta_t}{n_i \cos\theta_i + n_t \cos\theta_t} \right)^2 \quad \text{(S2-4b)}$$

$$R_s = \left(\frac{n_i \cos\theta_t - n_t \cos\theta_i}{n_i \cos\theta_t + n_t \cos\theta_i} \right)^2 \quad \text{(S2-4c)}$$

where R is the reflectivity of a radiation coming with an incident angle θ_i, transmitted through the interface with an angle θ_t, n_i is the refraction index of the material before the interface, and n_t is the refraction index of the material after the interface (Figure S2-1). Knowing the angle θ_i, the transmitted angle θ_t can be calculated using the Snell-Descartes law:

$$n_i \sin(\theta_i) = n_t \sin(\theta_t) \quad \text{(S2-5)}$$

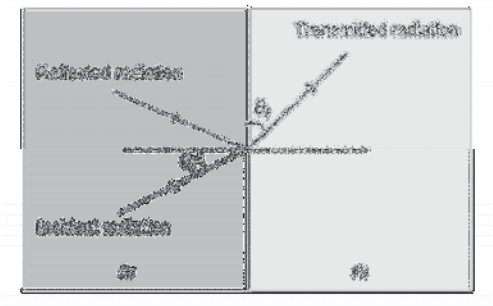

Figure S2-1: Reflected and transmitted radiation through an interface between two medium having different optical properties.

The transmittance of the reactor wall was measured by placing a piece of the reactor in a spectrophotometer cuvette. The incoming radiation emitted by the spectrophotometer lamp went through first an air-polycarbonate interface and then through a polycarbonate-air interface before reaching the light sensor of the spectrophotometer. This radiation came with a perpendicular direction to the surface of the polycarbonate wall ($\theta_i = 0^o$). Equation 8 gives that the transmitted angle is also 0^o in this case. When neglecting the multiple reflections in the piece of polycarbonate, the Fresnel equations yield the following expression for the transmittance:

$$T = \left(1 - \left(\frac{n_a - n_p}{n_a + n_p}\right)^2\right)\left(1 - \left(\frac{n_p - n_a}{n_p + n_a}\right)^2\right) = \left(1 - \left(\frac{n_a - n_p}{n_a + n_p}\right)^2\right)^2 \quad \text{(S2-6)}$$

Where n_a is the refraction index of air (1.00) and n_p the refraction index of the reactor wall. As the transmittance T was experimentally determined at 0.9, the refraction index was

determined to be equal to 1.58. This value is consistent with data found in the literature for polycarbonate materials. In the following, this value of 1.58 will be used for the refraction index n_p.

2.3.2. Different types of radiation

In the heat balance that was developed in the initial model of Béchet et al. (2010) to predict the temperature of the medium, 7 different heat fluxes were identified as radiative heat fluxes (Figure S2-2). With respect to the transmittance of the reactor wall, these radiative heat fluxes can be classified in three distinct categories:

- **Direct solar radiation** goes through the reactor wall with a given direction which is determined by the sun position.
- **Isotropic inward radiation** reaches the external wall of the reactor from any spatial direction and goes through an air-polycarbonate-water interface.
- **Isotropic outward radiation** reaches is radiation emitted by the algal broth in every direction and goes through a water-polycarbonate-air interface.

This subsection determines for these three types of radiation the corresponding transmittance value. The calculations presented below only apply to the radiation reaching the lateral surface of the reactor. The radiation reaching the top surface of the reactor represents only a small fraction of the total radiation and it will be assumed that the previous assumptions on the values of τ for this small fraction can be taken equal to 87% without a significant loss of accuracy.

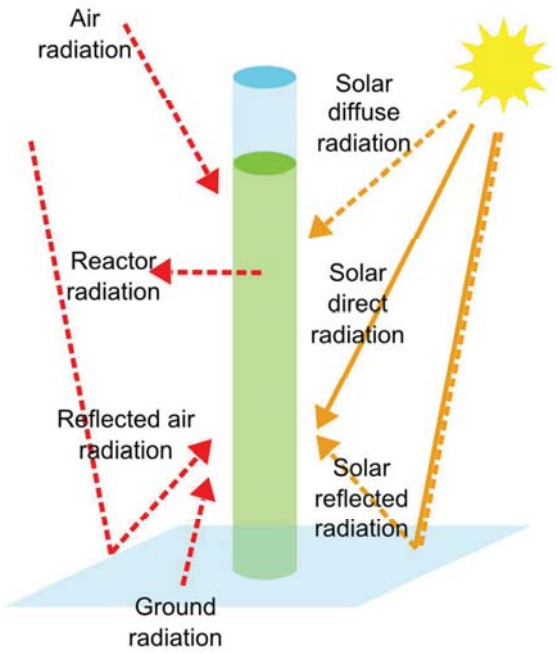

Figure S2-2: Radiative heat fluxes in the heat balance developed in the model of Béchet et al. (2010). The other heat fluxes resulting from conductive, convective or evaporative processes are not shown on this figure. (Red: long-wave heat fluxes; Orange: Short-wave heat fluxes; Plain line: direct radiation; Dash-line: Radiation assumed isotropic).

Transmittance for direct solar radiation

In the following, the sun position will be characterized by the angle θ_z between the sun and a vertical axis (Figure S2-3). The amount of direct solar radiation that is transmitted through the reactor wall is affected by θ_z, but also by the fact that the reactor is cylindrical. An integration of the amount of radiation going through the reactor therefore needs to be performed all around the reactor surface for angles ω going from 0 to 90^o (Figure S2-4).

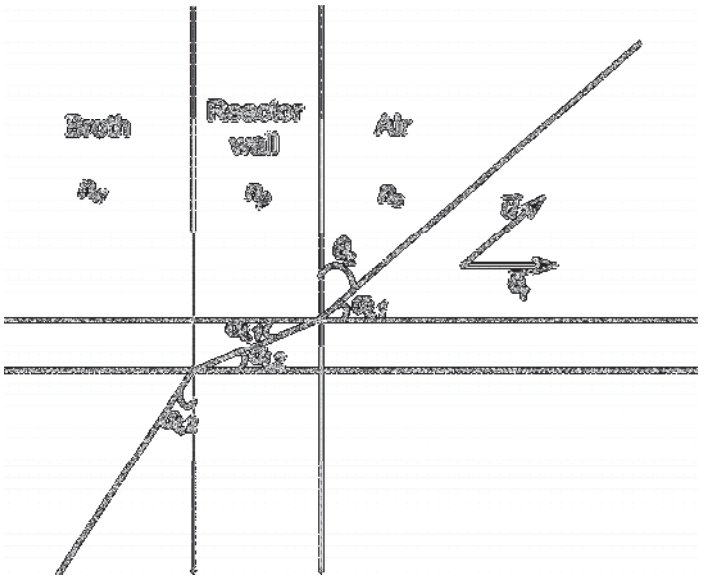

Figure S2-3: Side view of the reactor. θ_z is the angle between the incoming radiation and a vertical axis.

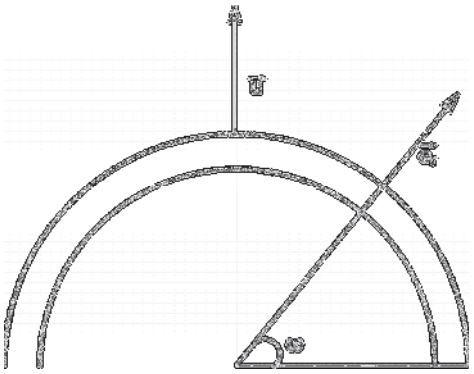

Figure S2-4: Top view of the reactor. The angle ω determines the position considered at the external surface of the reactor wall.

The incident angle between the incoming radiation and the perpendicular direction to the surface is given by the angle $\alpha_{i,1}$, which can be calculated as a function of ω and θ_z as follows:

$$\cos\alpha_{i,1} = \vec{u}.\vec{e}_r = \sin\omega\sin\theta_z \quad \text{(S2-7)}$$

where the vectors are defined in Figures S2-3 and S2-4. The amount of radiation reflected at each surface *dS* can therefore be calculated as a function of α using the Fresnel and Snell-Descartes equations (Equation S2-4a, S2-4b, S2-4c, and S2-5). Then the fraction of radiation that is transmitted through the first interface (air-polycarbonate) is partly transmitted through the second interface (polycarbonate-water). The transmittance through this second interface can be calculated using the same equations and a refraction index value for water of 1.33. From the calculation of these two transmittance values (T_1 and T_2), the total transmittance can be calculated as follows:

$$\tau_{dir}(\theta_z) = \int_0^{\pi/2} T_1(\alpha_1(\omega,\theta_z)) \cdot T_2(\alpha_2(\omega,\theta_z)) d\omega \quad \text{(S2-8)}$$

This integration was performed numerically with Matlab and Figure S2-5 shows the transmittance values for direct solar radiation as a function of the angle θ_z. When the incident radiation has a horizontal direction, the transmittance of the reactor wall is estimated to be close to 0.83 (Figure S2-5). This value lower than the 0.9 value experimentally measured in the spectrophotometer is due to the cylindrical geometry of the reactor.

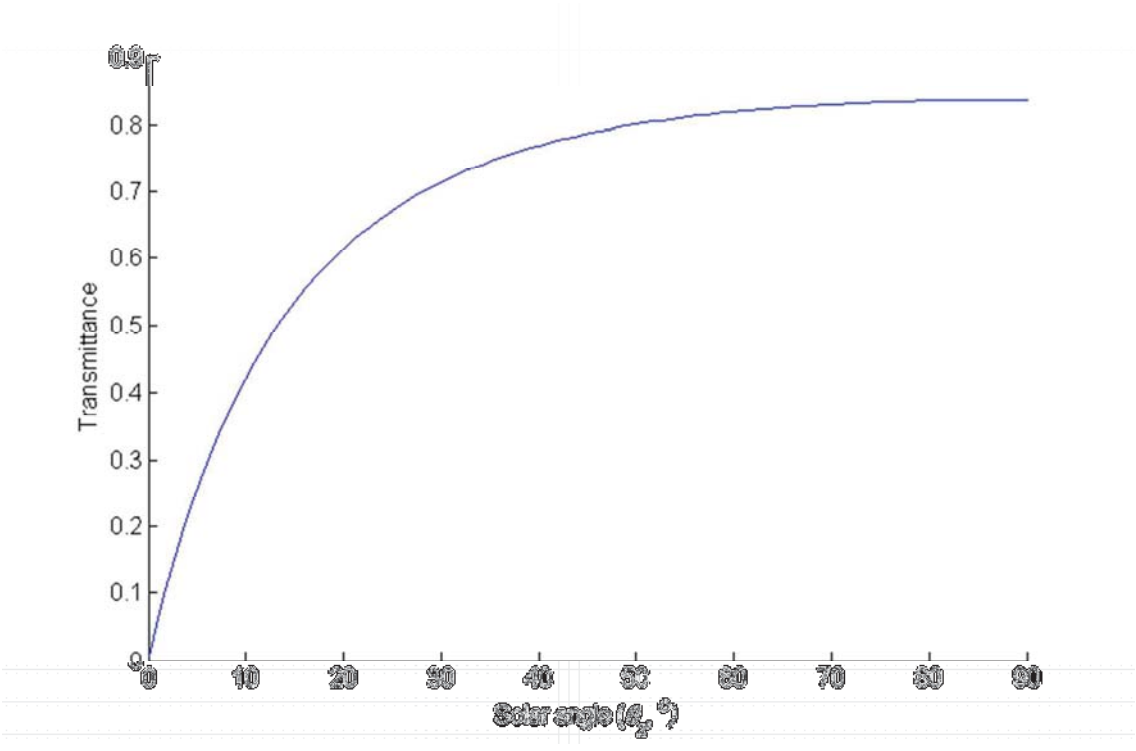

Figure S2-5: Transmittance value for direct solar radiation as a function of the solar angle θ_z as calculated by Equation S2-8.

Transmittance values for isotropic inward radiation

In the following, a vertical surface *dS'* at the water-polycarbonate interface will be considered (Figure S2-6). The first objective of this subsection is to determine the amount of isotropic radiation reaching *dS'*. In the case of diffuse radiation is emitted toward *dS'* from half a sphere, the usual way to calculate the amount of radiation is to consider a surface *dS* of this half sphere and to determine the amount of radiation that *dS* emits toward *dS'*. By using the parameters shown by Figure S2-6 to characterize the position of *dS*, the amount of radiation emitted by *dS* toward *dS'* is:

$$dF_{dS\to dS'} = \frac{F' dS \cos\alpha}{\pi} \quad \text{(S2-9)}$$

where *F'* is the radiation flux emitted by the surface *dS* (W/m^2), α is the angle between the direction of the incoming radiation (vector **u**, Figure S2-6) and the vector perpendicular to the surface *dS'*. α can be determined as follows:

$$\cos\alpha = \sin\varphi\cos\theta \quad \text{(S2-10)}$$

where ϕ and θ are defined on Figure S2-6. Similarly to the case of the direct solar radiation, the amount of radiation which is transmitted through the reactor wall can be determined using the Fresnel and Snell-Descartes equations through the two interfaces and the total transmittance can be calculated as a function of the two local transmittances T_1 and T_2:

$$\tau_{iso,in} = \frac{\int_0^{\pi/2}\int_0^{\pi/2}\left(T_1(\alpha(\varphi,\theta))\cdot T_2(\alpha(\varphi,\theta))\sin^2\varphi\cos\theta d\varphi d\theta\right)}{\pi/4} \quad \text{(S2-11)}$$

Numerically, the value of $\tau_{iso,in}$ was estimated at:

$$\tau_{iso,in} = 0.8887$$

It can be noted that this value of transmittance does not account for multiple reflections in the reactor wall. This assumption was justified by the fact that the incoming radiation reflected at the polycarbonate-water interface is more likely to be transmitted through the polycarbonate-air interface due to the values of the refraction indexes. This assumption is however limited in

the case of the outward isotropic radiation and multiple reflections will be accounted for in this case.

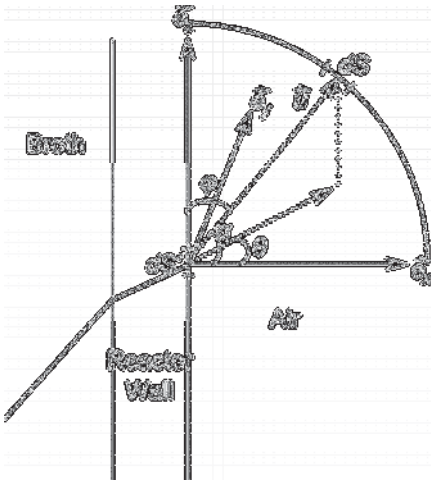

Figure S2-6: Side view of the reactor: estimation of the transmittance for diffuse incoming radiation

Transmittance for the isotropic outward radiation

Similarly to the previous approach, a vertical surface of broth will be considered. The radiation emitted by the broth will be assumed diffuse. By considering again half a sphere centered on the surface element considered dS, the amount of radiation emitted by dS though an element dS' of this half-sphere can be expressed as:

$$dF_{dS\to dS'} = FdS\sin\varphi d\varphi d\theta \quad \text{(S2-12)}$$

where F is the intensity of the radiation emitted by the surface dS and ϕ and θ are defined on Figure S2-7. Similarly to the calculation done in the two previous cases, the transmittance for the radiation emitted by dS to dS' was calculated using the Fresnel and Snell-Descartes equations. The main difference was that it is necessary to consider the double reflections in the reactor wall as explained in the previous subsection. By calling T_1, T_2, and T_3 the transmittances at the three interfaces as shown by Figure 12, the total reflectance for a radiation emitted with a direction u from the surface dS is:

$$T(\vec{u}) = T_1(\vec{u}) \cdot T_2(\vec{u}) \cdot \left(1 + (1 - T_3(\vec{u})) \cdot T_2(\vec{u}) + (1 - T_3(\vec{u}))^2 \cdot T_2(\vec{u})^2 + \ldots\right) = T_1(\vec{u}) \cdot T_2(\vec{u}) \cdot \frac{1}{1 - (1 - T_3(\vec{u})) \cdot T_2(\vec{u})}$$

(S2-13)

Then, the global transmittance for the diffuse radiation going out of the reactor was calculated by integrating the local transmittance as follows:

$$\tau_{iso,out} = \frac{\int_0^{\pi/2} \int_0^{\pi/2} T(\vec{u}(\varphi,\theta)) \cdot \sin\varphi d\varphi d\theta}{2/\pi} \quad \text{(S2-14)}$$

Numerically, the value of $T_{iso,out}$ was estimated at:

$$\tau_{iso,out} = 0.8627$$

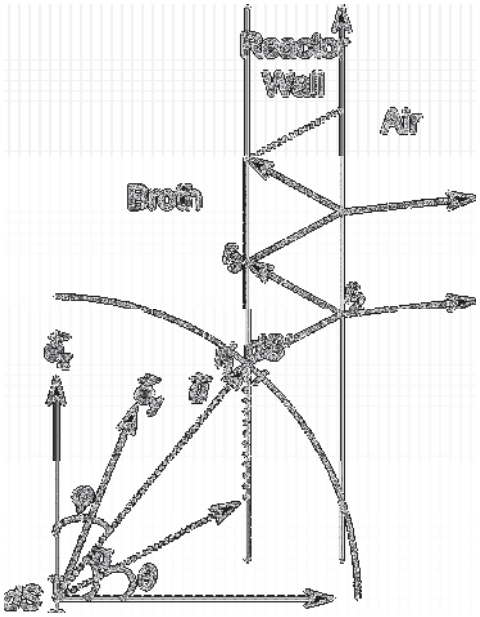

Figure S2-7: Side view of the reactor: estimation of the transmittance for diffuse outgoing radiation

2.3.3. Summary of equations expressing the radiative heat fluxes reaching the reactor.

Table S2-1: Updated expressions of the radiative heat fluxes reaching the algae in a photobioreactor. Note that the updated values of the reactor wall transmittance only apply to the lateral surface of the reactor. The transmittance value for the top surface is assumed to be

87% similarly to what was done in the study of Béchet et al. (2010). Symbols are defined in Béchet et al. (2010).

Heat flux	**Expression**
Radiation of the reactor ($Q_{ra,r}$)	$Q_{ra,r} = -\sigma\varepsilon_r T_r^4 \left(2\pi L_r R_r \tau_{iso,out} + \pi R_r^2 \tau\right)$
Direct solar radiation	
From the top surface ($Q_{ra,D,top}$)	$Q_{ra,D,top} = \varepsilon_r \tau H_D \pi R_r^2$
From the lateral surface ($Q_{ra,D,lat}$)	$Q_{ra,D,lat} = \tau_{dir}(\theta_z) H_D \tan(\theta_z) 2 R_r L_r$
Diffuse solar radiation ($Q_{ra,d}$)	$Q_{ra,d} = \varepsilon_r \tau H_d \pi R_r^2 + \tau_{iso,in} H_d \pi R_r L_r$
Reflected solar radiation ($Q_{re,s}$)	$Q_{re,s} = (1-\varepsilon_g) \tau_{iso,in} H_g \pi R_r L_r$
Air radiation ($Q_{ra,a}$)	$Q_{ra,a} = \varepsilon_a \sigma T_a^4 \left(\varepsilon_r \tau \pi R_r^2 + \tau_{iso,in} \pi R_r L_r\right)$
Reflection of the air radiation on the ground surface ($Q_{re,a}$)	$Q_{re,a} = (1-\varepsilon_g) \varepsilon_a \sigma T_a^4 \tau_{iso,in} \pi R_r L_r$
Radiation from the ground ($Q_{ra,g}$)	$Q_{ra,g} = \varepsilon_g \sigma T_g^4 \tau_{iso,in} \pi R_r L_r$

References

Bass, M.; Enoch, J.M; Decusatis, C.; Lakshminarayanan, V.; Li, G.; MacDonald, C.; Mahajan, V.N.; Van Stryland, E. Handbook of Optics: geometrical and physical optics, polarized light, components and instruments. 3rd, ed; McGraw-Hill, **2010**.

Béchet, Q.; Shilton, A.; Fringer, O.B.; Muñoz, R.; Guieysse, B.Mechanistic modeling of broth temperature in outdoor photobioreactors. *Environ. Sci. Technol.* **2010**, *44*, 2197–2203.

Béchet, Q.; Muñoz R.; Shilton A., Guieysse B. Outdoor cultivation of temperature-tolerant Chlorella sorokiniana in a column photobioreactor under low power-input. *Biotechnol. Bioengineer.***2013,** *110*, 118-126.

Duffie, J.A.; Beckman W.A. Solar engineering of thermal processes. 3rd, ed; Wiley, Hoboken, NJ, **2006**.

S3: Inclusion of the effect of the heaters in the temperature model of Béchet et al. (2010)

Two of the photobioreactors operated outdoors and used for model validation were temperature controlled after one week of cultivation. Heaters were placed in the reactors and operated as follows:

When the temperature was lower than a certain value ($T_{c,min}$), the heater automatically turned on until the temperature was higher that this threshold value;

If the heater was unable to compensate for the heat loss, the heater was constantly on.

The heat balance presented in Béchet et al. (2010) was modified to account for the effect of the heaters as follows:

$$\rho_w V_r Cp_w \frac{dT_r}{dt} = Q_{ra,r} + Q_{ra,d} + Q_{ra,D} + Q_{re,s} + Q_{ra,a} + Q_{re,a} + Q_{ra,g} + Q_c + Q_{ev} + Q_b + Q_{cond} + Q_h \quad \text{(S3-1)}$$

where T_r is the reactor broth temperature (K), ρ_w and Cp_w are the density (kg/m^3) and the specific heat capacity (J/kg-K) of water, respectively, V_r is the volume of the broth (m^3), $Q_{ra,r}$ is the radiation from the reactor itself (W), $Q_{ra,D}$ is the direct solar radiation (W), $Q_{ra,d}$ is the diffuse solar radiation (W), $Q_{re,s}$ is the solar radiation reflected from the ground (W), $Q_{ra,a}$ is the radiation from the air surrounding the reactor (W), $Q_{re,a}$ is the air radiation reflected from the ground (W), $Q_{ra,g}$ is the radiation from the ground (W), Q_c is the convective flux (W), Q_{ev} is the evaporation flux (W), Q_b is heat flux into air bubbles (W), Q_{cond} is the conductive flux with the ground surface at the base surface (W), Q_h is the heat flux generated by the heater (W). Q_h was expressed as follows:

$Q_h = P_h$ for $T_r < T_{c,min}$ (S3-2a)

$Q_h = 0$ for $T_r > T_{c,min}$ (S3-2b)

where P_h is the heater power (W).

References

Béchet, Q.; Shilton, A.; Fringer, O.B.; Muñoz, R.; Guieysse, B.Mechanistic modeling of broth temperature in outdoor photobioreactors. *Environ. Sci. Technol.* **2010**, *44*, 2197–2203.

S4: Parameters value in the temperature model

Table S4-1: Constants and parameters values used in the temperature model in New Zealand

Symbol	Definition	Unit	Value
Algorithm constants			
dt	Time step in the numerical algorithm	s	1000
Environment around the reactor			
α	Power law exponent	-	0.29
z	Height at which the wind velocity is taken	m	0.9
L	Distance between the reactors and closer obstacle	m	10
Ground characteristics			
$T_{g,ref}$	Ground temperature far from the surface[1]	K	283.5
r_g	Ground reflectivity	-	0.2
ε_g	Ground emissivity	-	0.8
ρ_g	Ground density	kg/m^3	4000
Cp_g	Ground heat capacity	J/kg-K	2.4 10^3
l_g	Ground thickness affected by daily temperature changeS3	M	0.16
Reactor characteristics			
R_r	Reactor radius	m	0.095
L_r	Reactor height	M	1.8
τ	Transmittance of the top reactor surface	-	0.9
ε_r	Reactor (water) emissivity	-	0.97
l_{base}	Thickness of the reactor plastic base	M	0.05
λ_{base}	Thermal conductivity of the reactor plastic base	W/m-K	0.12
f_b	Air volume as fraction in the broth	-	0.02
F_b	Air inflow rate	m^3/s	1.73 10-5
$T_{c,min}$	Minimal temperature allowed by the heaters	K	296.65
P_h	Power of the heaters	W	270
Micro-algae characteristics			
f_{abs}	Fraction of the sunlight converted as chemical energy by the micro-algae	-	0.025
HV	Heat value of the dry biomass	kJ/g	2.2 10^4
Sunlight characteristics			
f_{PAR}	Fraction of photosynthetically active radiation in sunlight	-	0.47

[1]Calculated by average the air temperature at the location considered over one year

[2]Calculated from the formula: $l_g = \sqrt{t\alpha_g}$, where t is the time period considered (here 86400s) and α_g the ground thermal diffusivity (here 3.13 10^{-7}m^2/s). This formula is extracted from Taine et al. (2008).

References

Taine, J.; Iacona, E.; Petit, J. P. Transferts Thermiques—Introduction aux Transferts d'Energie, 4th ed; Dunod: Paris, **2008**.

S5: Determination of the light distribution in the outdoor photobioreactors

5.1. Introduction

The application of a Type II model requires the determination of the light distribution. This supplementary information presents how the modified Beer-Lambert equation was applied to the specific geometry of outdoor vertical column photobioreactors.

The first section presents the different components of solar radiation reaching an outdoor reactor, together with the main assumptions that were made on these different components. The second section presents how the intensity of these different light components was calculated. For each equation, a validation based on laws of conservation is presented. The last section illustrates how the sun position impacts the light distribution in the outdoor photobioreactors.

5.2. Different components of solar radiation reaching the outdoor photobioreactors and main assumptions

When exposed to outdoor conditions, the photobioreactors used in this study receive solar radiation from three main sources (Figure S5-1):

The direct solar radiation reaches the algae with a given direction which depends on the sun position (characterized by the angle θ_z, Figure S5-1)

The diffuse solar radiation reaches the algae after being scattered by the atmosphere.

The reflected solar radiation reaches the algae after being first reflected on the ground surface.

In order to determine how these three radiation components penetrate in the algal broth in the reactor, the following assumptions were made:

The light propagation in the cultivation broth is assumed to obey a modified Beer-Lambert-law as described in the main manuscript.

The reflectivity of the plastic wall is assumed to be independent on the angle between incident radiation and a vector normal to the reactor surface.

The reflected component of the visible radiation reaching the algae is assumed to be diffuse and isotropic.

The diffuse component of the visible radiation reaching the algae is also assumed to be isotropic.

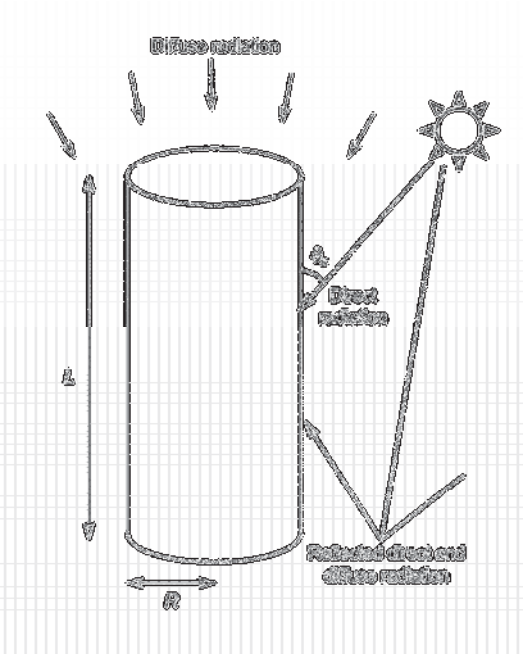

Figure S5-1: The three types of solar radiation reaching the algae in a vertical column photobioreactor

Box S5-1: Definition of key parameters

- $I_{0,dir}$: Intensity of the direct solar radiation reaching the horizontal ground surface (W/m^2, in PAR)
- $I_{0,dif}$: Intensity of the diffuse solar radiation reaching the horizontal ground surface (W/m^2, in PAR)

- $I_{0,ref}$: Intensity of the reflected solar radiation emitted by the horizontal ground surface (W/m^2, in PAR)
- σX: This parameter is the product of the algal concentration (X, kg/m^3) and the extinction coefficient (σ, m^2/kg). σX (m^{-1}) represents the level of opacity of the algal solution: the higher σX is, the lower the amount of radiation going through the reactor. Another way of describing this parameter is by noticing that $1/\sigma X$ represents the average light path of a photon entering the reactor.
- θ_z: Angle between a vertical axis and the sun (rad).
- R, L: Radius and height of the photobioreactor, respectively (m).

5.3. Derivation of the light intensity of the three different light components in the photobioreactors

In order to determine the local light intensity reaching a single algae cell in the reactor, it is necessary to determine the light intensities of the different components of light: the direct (I_{dir}), diffuse (I_{dif}) and reflected (I_{ref}) radiations. The local light intensity (I_{loc}) will finally be expressed as the sum of these three components:

$$I_{loc} = I_{dir} + I_{dif} + I_{ref} \quad \text{(S5-1)}$$

5.3.1. Direct light radiation

This section presents how the amount of direct radiation reaching an algae cell located at a point M in the cultivation broth (Figure S5-2a) was determined. Depending on the location M in the broth, the direct radiation can come from either the lateral or the top surface of the reactor. In the following N will be the location at which the direct radiation enters the reactor before reaching the location M (Figure S5-2a, S5-2b and S5-3). As the light propagation is

assumed to obey a modified Beer-Lambert law, the direct light intensity reaching the algae at the location M can be expressed as:

$$I_{dir}(r,\theta,z) = \frac{I_{0,dir}}{\cos\theta_z}\exp\left(-\sigma X \cdot MN\right) \quad \text{(S5-2)}$$

where (r, θ, z) are the cylindrical coordinates of the point M in the cultivation broth (Figures S5-2a and S5-2b).

Case where the direct radiation reaching M first goes through the lateral surface of the reactor

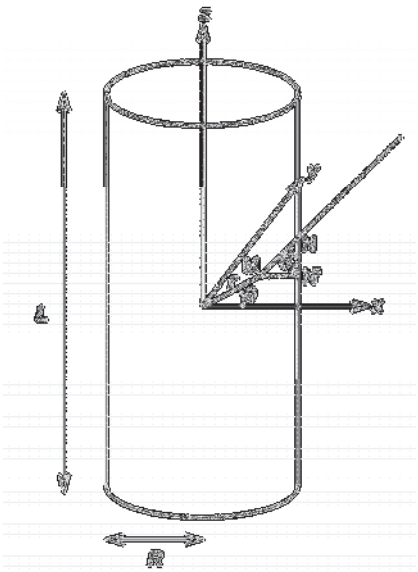

Figure S5-2a: Case where the direct radiation reaching the location M goes through the lateral surface of the photobioreactor – Side view. The x-axis is located in the same vertical plane as the direct radiation.

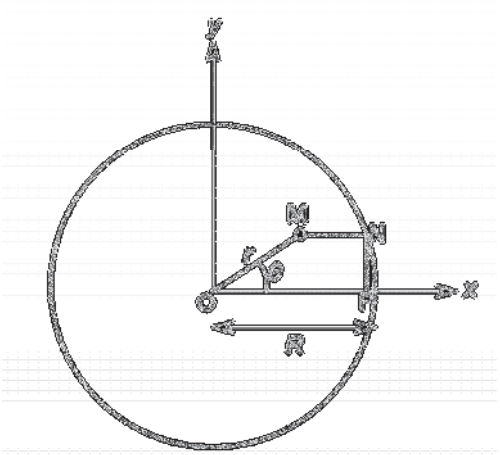

Figure S5-2b: Case where the direct radiation reaching the location M goes through the lateral surface of the photobioreactor – Top view.

In the triangle MNN' (Figure S5-2a), the distance MN can be expressed as:

$$MN = \frac{MN'}{\sin\theta_z} \quad \text{(S5-3)}$$

where N' is the projection of the point N on the horizontal plane containing the point M (Figure S5-2a).

The distance MN' can be expressed as:

$$MN' = \left| x_N - r\cos\theta \right| \quad \text{(S5-4)}$$

where x_N is the abscissa of the point N in the vector system (x,y,z) shown in Figures S5-2a and S5-2b. By applying the Pythagoras theorem in the triangle ONP (Figure S5-2b), x_N can be determined as:

$$x_N = \sqrt{R^2 - r^2\sin^2\theta} \quad \text{(S5-5)}$$

This last result leads to the final equation for the distance MN:

$$MN = \frac{\left| \sqrt{R^2 - r^2\sin^2\theta} - r\cos\theta \right|}{\sin\theta_z} \quad \text{(S5-6)}$$

Case where the direct radiation reaching M first goes through the top surface of the reactor

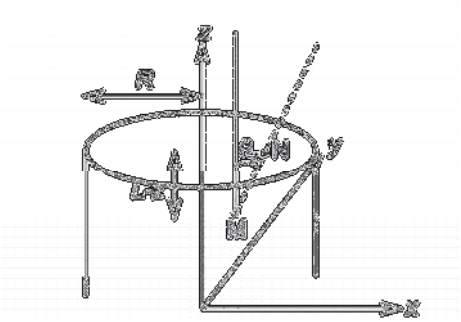

Figure S5-3: Case where the direct radiation reaching the location M first goes through the top surface of the photobioreactor

In this case, the distance MN can be easily expressed as (Figure S5-3):

$$MN = \frac{L - z}{\cos\theta_z} \quad \text{(S5-7)}$$

Determination of the origin of the direct radiation (top surface or lateral surface of the reactor)

In the following, a point M in the cultivation broth will be considered. If direct radiation reaches the point M by first going through the lateral surface of the reactor, then the distance NN' should respect the following condition:

$$z + NN' \leq L \quad \text{(S5-8)}$$

From Figure S5-2a, it can be demonstrated that:

$$NN' = \frac{MN'}{\tan\theta_z} \quad \text{(S5-9)}$$

This last equation leads to the following conditions:

If $z \le L - \frac{\sqrt{R^2 - r^2 \sin^2\theta} - r\cos\theta}{\tan\theta_z}$: the direct radiation reaching the point M enters the reactor through the lateral surface (Equation S5-5 to be applied for MN)

If $z \ge L - \frac{\sqrt{R^2 - r^2 \sin^2\theta} - r\cos\theta}{\tan\theta_z}$: the direct radiation reaching the point M enters the reactor through the top surface (Equation S5-6 to be applied for MN)

It can also be demonstrated that when the two conditions are respected simultaneously, Equations S5-5 and S5-6 yield the same expression for the distance MN.

Validation of the equations for the direct radiation

In order to check the equations derived to determine the local direct light intensity, the flux of direct radiation entering the reactor ($I_{0,dir,reac}$) was compared to the flux of direct radiation absorbed by the algae ($I_{abs,dir,reac}$). For high values of σX, these two quantities should be very close to each other as most of the radiation entering the reactor should be absorbed by the algae.

Amount of direct radiation entering the reactor $I_{0,dir,reac}$

$I_{0,dir,reac}$ can be expressed as the sum of direct radiation reaching the lateral surface and the direct radiation reaching the top surface:

$$I_{0,dir,reac} = I_{0,dir}\left(2RL\tan\theta_z + \pi R^2\right) \quad \text{(S5-10)}$$

where $I_{0,dir}$ is defined in Box S5-1.

Amount of radiation absorbed by the algae $I_{abs,dir,reac}$

$I_{abs,dir,reac}$ can be calculated by summing the amount of radiation absorbed by small volume elements in the reactor:

$$I_{abs,dir,reac} = \int_r \int_\theta \int_z \sigma X I_{loc}(r,\theta,z) \cdot r dr d\theta dz \quad \text{(S5-11)}$$

Figure S5-4 shows that when σX tends to high values the amount of radiation absorbed by the algae tends to the amount of light entering the reactor. In addition, Figure S5-4 shows that for low values of the angle θ_z, the amount of direct radiation absorbed is relatively low, which is due to the fact that the surface area of the reactor exposed to direct radiation is also relatively low.

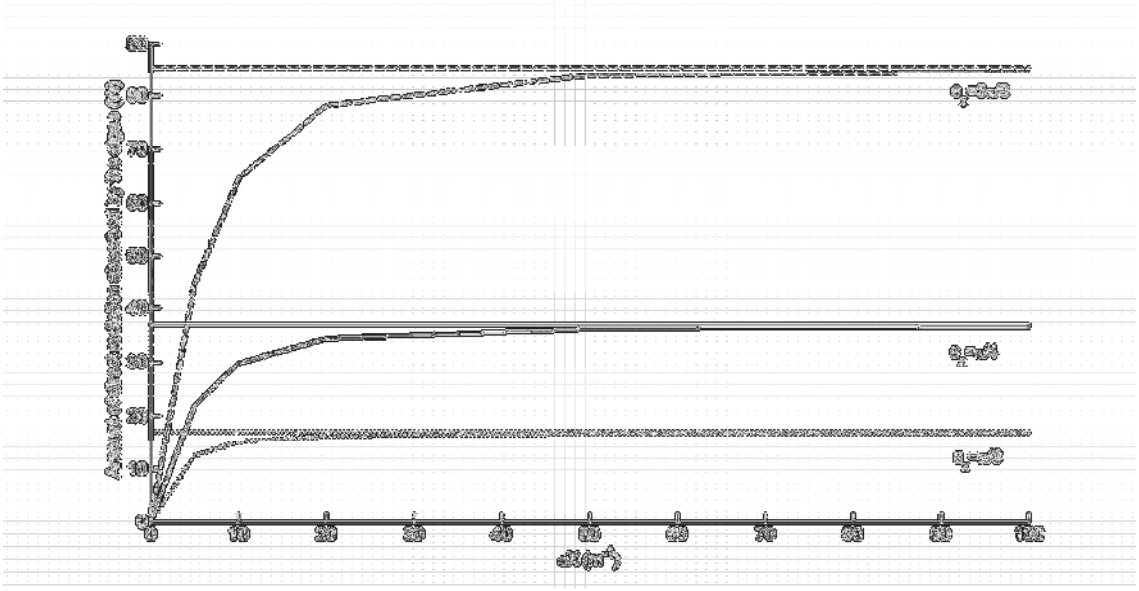

Figure S5-4: Amount of direct radiation absorbed by the algae as a function of the parameter σX (plain line). The horizontal line represents the amount of direct radiation reaching the external surface of the reactor (R = 0.095m, L = 1.8m, $I_{0,dir}$ = 100 W/m^2; Numerical constants used for the calculation of the absorbed radiation: N_r = 100, N_θ = 30, N_z = 30, where N_r, N_θ, and N_z are the number of infinitesimal elements in the radial, angular, and vertical direction, respectively). The amount of light absorbed by the algae was calculated only in the volume elements where the light intensity was higher than 0.5% of the incident light intensity.

5.3.2. Diffuse light radiation

The objective of this section is to estimate the amount of diffuse radiation reaching a single algae cell located in a given position M(r,θ,z) in the cultivation broth (Figure S5-5). By assuming that the diffuse radiation is isotropic, the diffuse radiation reaching the position M can have any incident direction. As a result, a fraction of the diffuse radiation reaching M first goes though the top surface of the reactor, while the other fraction first goes through the lateral surface of the reactor.

Amount of diffuse radiation entering the reactor through its lateral surface

Following the modified Beer-Lambert law for light propagation, the amount of diffuse radiation that first goes through a small surface *dS'* of the reactor wall to a single algae cell located at the position M can be expressed as:

$$dI_{dif,lat}(N'M) = I_{0,dif}\frac{\sigma}{\pi MN^2}\cos\alpha\cdot\exp\left(-\sigma X\cdot MN\right)dS' \quad \text{(S5-12)}$$

where $I_{0,dif}$ is the diffuse light intensity reaching the ground surface, N'(R,θ',z') is the position at which the ray of light considered goes through the reactor wall, α is the angle between a vector normal to the surface *dS'* and the direction N'M (Figure S5-5).

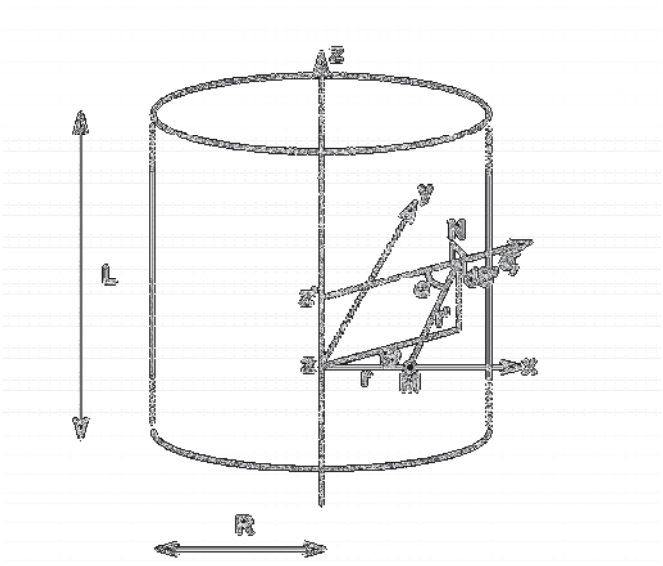

Figure S5-5: Diffuse radiation coming from the lateral surface of the reactor.

Similarly to the case of the indoor reactor (S2), the term *cosα* and the distance MN in Equation S5-11 can be expressed as:

$$\cos\alpha = \frac{R - r\cos\theta}{MN} \quad \text{(S5-13)}$$

$$MN = \sqrt{R^2 + r^2 - 2rR\cos\theta + \left(z'-z\right)^2} \quad \text{(S5-14)}$$

By integrating the amount of radiation $dI_{dif,lat}$ over the entire lateral surface of the reactor, the following expression can be obtained for the local diffuse light intensity entering the reactor through its lateral surface:

$$\sigma I_{loc,dif,lat}(r,z) = \frac{RI_{0,dif}\sigma}{\pi}\int_{z'=z}^{L}\int_{\theta'=0}^{2\pi}\frac{\left(R - r\cos\theta\right)}{\sqrt{R^2 + r^2 - 2rR\cos\theta + \left(z'-z\right)^2}^{3}}\exp\left(-\sigma X\cdot\sqrt{R^2 + r^2 - 2rR\cos\theta + \left(z'-z\right)^2}'\right)d\theta' dz' \quad \text{(S5-15)}$$

Amount of diffuse radiation entering the reactor through its top surface

Similarly to the previous case, the amount of diffuse radiation reaching the point M after going through a small surface *dS'* on the top surface of the reactor is:

$$dI_{dif,top}(N'M) = I_{0,dif}\frac{\sigma}{\pi MN'^2}\cos\alpha\cdot\exp\left(-\sigma X\cdot MN\right)\cdot dS' \quad \text{(S5-16)}$$

where the different symbols are defined similarly to the case of lateral diffuse radiation and are represented on Figure S5-6.

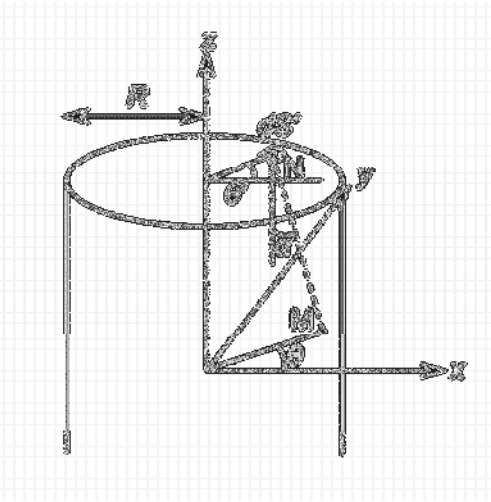

Figure S5-6: Diffuse radiation coming from the top surface of the reactor

Figure S5-6 shows that the x-axis is set parallel to the direction OM, so the coordinates of M and N in the vector system (*x*,*y*,*z*) shown in Figure S5-6 are:

$$M\begin{vmatrix} r \\ 0 \\ z \end{vmatrix} \text{ and } N\begin{vmatrix} r'\cos\theta' \\ r'\sin\theta' \\ L \end{vmatrix}$$

The distance MN can therefore be expressed as:

$$MN = \sqrt{r^2 + r'^2 - 2rr'\cos\theta' + (L-z)^2} \quad \text{(S5-17)}$$

Figure S5-6 shows that the term *cosα* can be expressed in this case as:

$$\cos\alpha = \frac{L-z}{MN} \quad \text{(S5-18)}$$

The total amount of diffuse radiation reaching a single algae cell at the position M and entering the reactor though its top surface can therefore be expressed as:

$$\sigma I_{loc,dif,top}(r,z) = \frac{I_{0,dif}\sigma}{\pi}\int_{r'=0}^{R}\int_{\theta'=0}^{2\pi}\frac{L-z}{\sqrt{r'^2+r^2-2rr'\cos\theta'+(L-z)^2}^3}\exp\left(-\sigma X\cdot\sqrt{r'^2+r^2-2rr'\cos\theta'+(L-z)^2}'\right)r'dr'd\theta' \quad \text{(S5-19)}$$

Validation of the equations for the diffuse radiation

In order to verify the equations derived to determine the local diffuse light intensity, the diffuse radiation entering the reactor ($I_{0,dif,reac}$) was compared to the diffuse radiation absorbed by the algae ($I_{abs,dif,reac}$). For high values of σX, most of the incoming light in the reactor should be absorbed by the algae and these two quantities should be very close to each other.

Amount of diffuse radiation entering the reactor $I_{0,dif,reac}$.

$I_{0,dif,reac}$ can be expressed as the sum of diffuse radiation reaching the lateral surface and the diffuse radiation reaching the top surface:

$$I_{0,dif,reac} = I_{0,dif}\left(\pi RL + \pi R^2\right) \quad \text{(S5-20)}$$

where $I_{0,dif}$ is defined in Box S5-1.

Amount of diffuse radiation absorbed by the algae $I_{abs,dif,reac}$

$I_{abs,dif,reac}$ can be calculated by integrating the amount of radiation absorbed by small volume elements in the reactor:

$$I_{abs,dif,reac} = 2\pi \int_{r=0}^{R} \int_{z=0}^{L} X\left(\sigma I_{dif,lat}(r,z) + \sigma I_{dif,top}(r,z)\right) \cdot r\,dr\,dz \quad \text{(S5-21)}$$

Figure S5-7 shows that the amount of diffuse light absorbed by the algae tends to the amount of diffuse radiation entering the reactor when the parameter σX tends to high values.

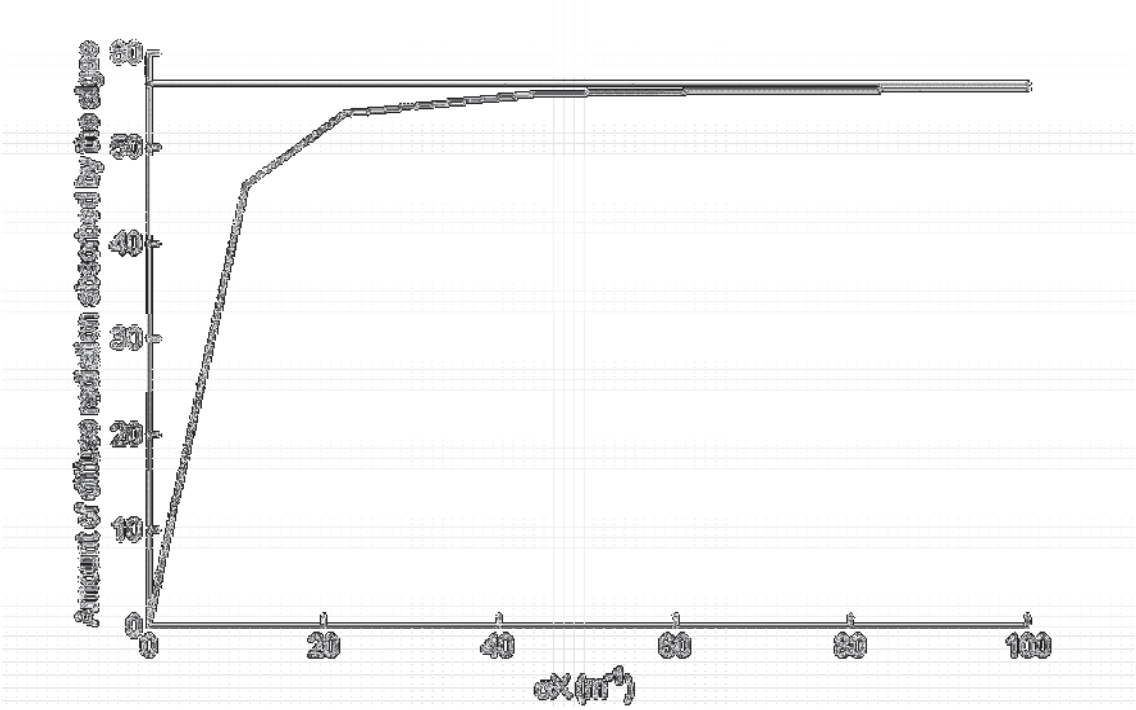

Figure S5-7: Amount of diffuse radiation absorbed by the algae as a function of the parameter σX. The horizontal line represents the amount of incident diffuse radiation reaching the reactor. (R = 0.095m, L = 1.8m, $I_{0,dif}$ = 100 W/m^2; Numerical constants used for the calculation of the absorbed and local radiations: N_r = 100, N_z = 50. N_r and N_z are the number of volume elements in the radial and vertical direction).The amount of light absorbed by the algae was calculated only in the volume elements where the light intensity was higher than 0.5% of the incident light intensity.

5.3.3. Reflected light radiation

As the radiation emitted by the ground surface is assumed to diffuse and isotropic, the calculation of the local reflected light intensity reaching a location M in the cultivation broth is similar to the calculation of the lateral diffuse radiation (section 3.2). This local light intensity can therefore be expressed as:

$$\sigma I_{loc,ref}(r,z) = \frac{R I_{0,ref}\sigma}{\pi} \int_{z'=0}^{z}\int_{\theta'=0}^{2\pi} \frac{(R - r\cos\theta)}{\sqrt{R^2 + r^2 - 2rR\cos\theta + (z'-z)^2}^{3}} \exp\left(-\sigma X \cdot \sqrt{R^2 + r^2 - 2rR\cos\theta + (z'-z)^2}'\right) d\theta' dz' \quad \text{(S5-22)}$$

In order to verify this formula, the amount of reflected radiation absorbed by the algae can be compared to the amount of reflected radiation entering the reactor. Similarly to the case of the diffuse lateral light radiation, the amount of incident reflected radiation can be expressed as:

$$I_{0,ref,reac} = I_{0,ref} \pi RL \quad \text{(S5-23)}$$

where $I_{0,ref}$ is defined in Box S5-1.

The amount of reflected light absorbed by the algae can be expressed as:

$$I_{abs,ref,reac} = 2\pi \int_{r=0}^{R} \int_{z=0}^{L} \sigma X I_{loc,ref}(r,z) \cdot r dr dz \quad \text{(S5-24)}$$

Figure S5-8 shows that when the parameter σX reaches relatively high values, the algae absorb, as expected, almost the entire reflected radiation entering the reactor.

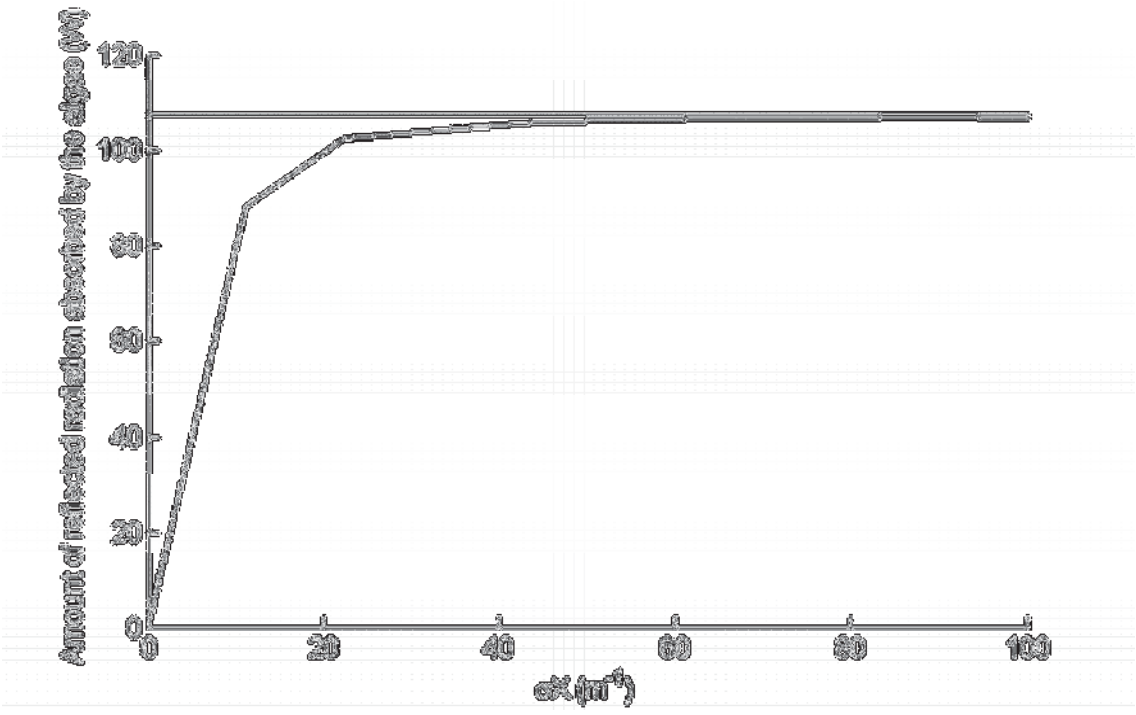

Figure S5-8: Amount of reflected radiation absorbed by the algae as a function of the parameter σX. The horizontal line represents the amount of incident reflected radiation reaching the reactor. (R = 0.095m, L = 1.8m, $I_{0,ref}$ = 200 W/m^2; Numerical constants used for the calculation of the absorbed and local radiations: N_r = 100, N_z = 50, N_θ = 50, $N_{lim,top}$ = 5,

$N_{lim,lat} = 5$. N_r, N_θ, and N_z are the number of infinitesimal elements in the radial, angular, and vertical direction and N_{lim}^2 is the number of elements in which an element dS' is split in the case where the location M is close to the reactor external surface, respectively. The amount of light absorbed by the algae was calculated only in the volume elements where the light intensity was higher than 0.5% of the incident light intensity.

5.4. Impact of the sun position on light distribution in the outdoor photobioreactors

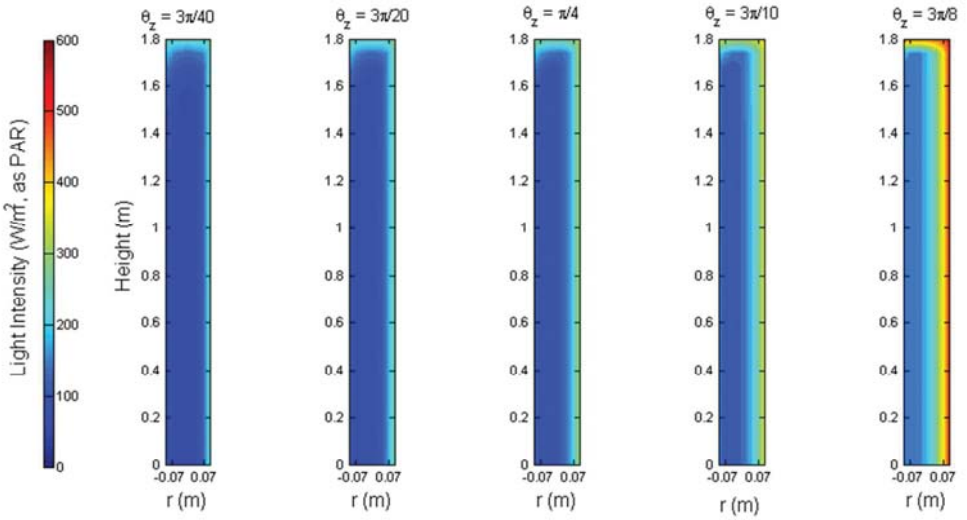

Figure S5-9: Light distribution in outdoor photobioreactors. θ_z is the angle between a vertical axis and the sun position . (Other parameters $\sigma X = 10$ m^{-1}; reactor radius $R = 0.095$m; reactor height: $L = 1.8$m; Direct solar radiation reaching the ground surface (PAR): $I_{0,dir} = 300$ W/m^2; Diffuse solar radiation reaching the ground surface: $I_{0,dif} = 100$ W/m^2; Intensity of the solar radiation reflected onto the ground surface: $I_{0,ref} = 100$ W/m^2).

S6: Application of the Type II model to the outdoor photobioreactors

6.1. Introduction

The application of Type II models to an outdoor photobioreactor is relatively complex as the light distribution in the algal broth is a function of changing variables: the sun position, the fraction of diffuse radiation in the solar radiation, etc. In order to model the productivity of an outdoor photobioreactor over time, the light distribution in the reactor broth needs to be determined at each time step of the calculation. Predicting productivity over large period of times (months to years) may therefore require extensive computational time. It is therefore necessary to find numerical strategies to minimize the computational time needed to determine the productivity at each time step. The goal of this supplementary information is to describe how the productivity model was numerically implemented in this study in order to minimize the computational time needed for each simulation.

The first section summarizes the relevant equations involved in the Type II model of productivity. In the second section, the numerical implementation of the Type II model is presented. The last section aims to verify the numerical implementation of the model equations though the verification of simple conservation laws.

6.2. Productivity model: equations

At daytime, the productivity is assumed to obey a Monod-like relationship with local light intensity:

$$P_{loc}(r,\theta,z,t) = P_m \frac{\sigma(t) I_{loc}(r,\theta,z,t)}{K + \sigma(t) I_{loc}(r,\theta,z,t)} \quad \text{(S6-1)}$$

where P_{loc} is the local productivity (kg/kg-s) at the position (r,θ,z) in the reactor and at the time t, P_m is the maximum specific productivity (kg/kg-s), σ is the extinction coefficient of the algae (m^2/kg) at the time t, I_{loc} is the local light intensity at the position (r,θ,z) in the reactor and at the time t, and K is the half-saturating constant for light intensity (W/kg). The

rate of endogenous respiration *ER* (kg/s) at daytime and night time is assumed to follow first-order kinetics, which is described by:

$$ER = \lambda(t)X(t)V \quad \text{(S6-2)}$$

where λ is the decay coefficient (s^{-1}) at the time t, X is the algal concentration (kg/m^3) at the time t, and V is the reactor volume (m^3).

The algal concentration X can be therefore expressed by integrating the following equation over time:

$$V\frac{dX}{dt}(t) = \int_r \int_\theta \int_z P_m X(t) \frac{\sigma(t) I_{loc}(r,\theta,z,t)}{K + \sigma(t) I_{loc}(r,\theta,z,t)} \cdot r \cdot dr \cdot d\theta \cdot dz - \lambda(t)X(t)V \quad \text{(S6-3)}$$

where X is the algal concentration (kg/m^3) at time t and V is the reactor volume (m^3).

The local light intensity at the position (r,θ,z) in the reactor can be expressed as the sum of four different components (Figure S6-1):

$$I_{loc}(r,\theta,z,t) = I_{loc,dir}(r,\theta,z,\sigma X(t),\theta_z(t)) + I_{loc,dif,top}(r,z,\sigma X(t)) + I_{loc,dif,lat}(r,z,\sigma X(t)) + I_{loc,ref}(r,z,\sigma X(t)) \quad \text{(S6-4)}$$

where:

- $I_{loc,dir}$ is the direct component of the local light intensity. This component is a function of the position (r,θ,z) in the reactor, the product σX (m^{-1}), and the angle between the sun and a vertical axis θ_z.
- $I_{loc,dif,top}$ is the intensity of the diffuse radiation going through the top surface of the reactor before reaching the location (r,θ,z) in the reactor. This component does not depend on the angular position of the considered location.
- $I_{loc,dif,lat}$ is the intensity of the diffuse radiation going through the lateral surface of the reactor before reaching the location (r,θ,z) in the reactor. This component does not depend on the angular position of the considered location.
- $I_{loc,ref}$ is the intensity of the reflected radiation going through the lateral surface of the reactor before reaching the location (r,θ,z) in the reactor. This component does not depend on the angular position of the considered location.

As already demonstrated in the supplementary information on light distribution in the outdoor photobioreactors (S6), these different light components can be expressed as follows:

$$I_{dir}(r,\theta,z)=\frac{I_{0,dir}}{\cos\theta_z}\exp\left(-\sigma X\cdot l(r,\theta,z)\right) \quad \text{(S6-5)}$$

$$I_{loc,dif,top}(r,z,\sigma X)=\frac{I_{0,dif}}{\pi}\int_{r'=0}^{R}\int_{\theta'=0}^{2\pi}\frac{L-z}{\sqrt{r'^2+r^2-2rr'\cos\theta'+(L-z)^2}^{3}}\exp\left(-\sigma X\cdot\sqrt{r'^2+r^2-2rr'\cos\theta'+(L-z)^2}\right)r'\,dr'\,d\theta' \quad \text{(S6-6)}$$

$$I_{loc,dif,lat}(r,z,\sigma X)=\frac{RI_{0,dif}}{\pi}\int_{z'=z}^{L}\int_{\theta'=0}^{2\pi}\frac{(R-r\cos\theta)}{\sqrt{R^2+r^2-2rR\cos\theta+(z'-z)^2}^{3}}\exp\left(-\sigma X\cdot\sqrt{R^2+r^2-2rR\cos\theta+(z'-z)^2}\right)d\theta'\,dz' \quad \text{(S6-7)}$$

$$I_{loc,ref}(r,z,\sigma X)=\frac{RI_{0,ref}}{\pi}\int_{z'=0}^{z}\int_{\theta'=0}^{2\pi}\frac{(R-r\cos\theta)}{\sqrt{R^2+r^2-2rR\cos\theta+(z'-z)^2}^{3}}\exp\left(-\sigma X\cdot\sqrt{R^2+r^2-2rR\cos\theta+(z'-z)^2}\right)d\theta'\,dz' \quad \text{(S6-8)}$$

where $I_{0,dir}$ is the intensity of the direct radiation reaching the horizontal ground surface (W/m^2, in PAR), l is the light path of the direct light in the algal broth before reaching the considered location (r,θ,z), R is the reactor radius (m), L is the reactor height (m), $I_{0,dif}$ is the intensity of the diffuse radiation reaching one squared meter of horizontal ground surface (W/m^2, in PAR), and $I_{0,ref}$ is the intensity of the reflected radiation expressed per square meter of horizontal ground surface (W/m^2, in PAR).

6.3. Numerical implementation

6.3.1. Reduction of the number of relevant variables

From Equations S6-3 to 8, the total instant productivity ($P(t)$, in kg/s) can be expressed as follows:

$$P(t)=P_m X(t)\iiint_{r\,\theta\,z}\frac{f(r,\theta,z,\sigma X(t),\theta_z(t))+\alpha\cdot g(r,z,\sigma X(t))+\beta h(r,z,\sigma X(t))}{K'(t)+f(r,\theta,z,\sigma X(t),\theta_z(t))+\alpha\cdot g(r,z,\sigma X(t))+\beta h(r,z,\sigma X(t))}\cdot r\cdot dr\cdot d\theta\cdot dz \quad \text{(S6-9)}$$

where the functions *f*, *g*, and *h* and the coefficients α and β are defined by the following relationships:

$$I_{loc,dir}(r,\theta,z,t) = I_{0,dir} f(r,\theta,z,\sigma X,\theta_z) \quad \text{(S6-10)}$$

$$I_{loc,dif,top}(r,\theta,z,t) = I_{0,dif} g(r,z,\sigma X) \quad \text{(S6-11)}$$

$$I_{loc,dif,lat}(r,\theta,z,t) = I_{0,dif} h(r,z,\sigma X) \text{ and } I_{loc,ref}(r,\theta,z,t) = I_{0,ref} h(r,z,\sigma X) \quad \text{(S6-12)}$$

$$\alpha = \frac{I_{0,dif}}{I_{0,dir}} \quad \text{(S6-13)}$$

$$\beta = \frac{I_{0,dif} + I_{0,ref}}{I_{0,dir}} \quad \text{(S6-14)}$$

$$K' = \frac{K}{\sigma I_{0,dir}} \quad \text{(S6-15)}$$

For a given geometry, the instant productivity of a reactor can therefore be expressed as a function of five different variables: σX, θ_z, α, β and K'.

6.3.2. Generation of a matrix of data

In order to minimize the computational time needed for simulations of productivity over long periods of time, the following strategy was followed. As demonstrated in the previous subsection, the instantaneous productivity can be expressed as a set of five variables: σX, θ_z, α, β and K'. The first step of the numerical strategy therefore consisted on pre-calculating the values of productivity over the entire range of these variables. These productivity values were then stored in a matrix of values (referred to as 'productivity matrix'). During a simulation of productivity over a long period of time, the value of the instant productivity at each time step was obtained by linear interpolation from the values extracted from the productivity matrix. This subsection presents how this productivity matrix was generated.

First, in order to minimize the computation of the productivity, it can be noticed that due to mutual shading, light does not penetrate deeply in the reactor. In the following, it will be assumed that light penetrates in the reactor over the following distance:

$$r_{\min} = R + \frac{\ln(0.01)}{\sigma X} \text{ in the radial direction;} \quad \text{(S6-16)}$$

$$z_{\min} = L + \frac{\ln(0.01)}{\sigma X} \text{ in the vertical direction.} \quad \text{(S6-17)}$$

The expression of the instant productivity can therefore be approximated at the sum of two integrals:

$$P(t) \cong P_m X(t) \cdot \left(\int_{z=z_{\min}}^{L} \int_{\theta=0}^{2\pi} \int_{r=0}^{r_{\min}} F(r,\theta,z,\sigma X,\theta_z,K',\alpha,\beta) \cdot r \cdot dr \cdot d\theta \cdot dz + \int_{z=0}^{L} \int_{\theta=0}^{2\pi} \int_{r=r_{\min}}^{R} F(r,\theta,z,\sigma X,\theta_z,K',\alpha,\beta) \cdot r \cdot dr \cdot d\theta \cdot dz \right) \quad \text{(S6-18)}$$

where F is defined as:

$$F(r,\theta,z,\sigma X,\theta_z,K',\alpha,\beta) = \frac{f(r,\theta,z,\sigma X(t),\theta_z(t)) + \alpha \cdot g(r,z,\sigma X(t)) + \beta h(r,z,\sigma X(t))}{K'(t) + f(r,\theta,z,\sigma X(t),\theta_z(t)) + \alpha \cdot g(r,z,\sigma X(t)) + \beta h(r,z,\sigma X(t))} \quad \text{(S6-19)}$$

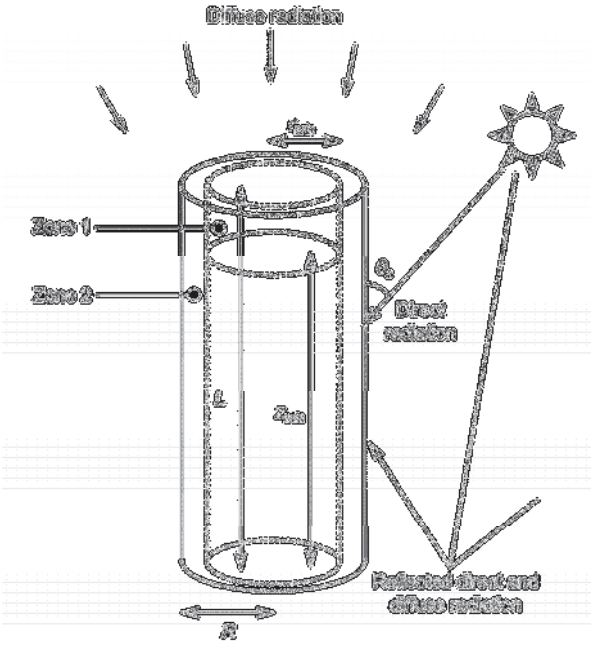

Figure S6-1: Splitting of the reactor into two zones for the calculation of the productivity.

By noticing that the light intensity in the central top volume fraction of the reactor (zone 1, Figure S6-1) originating from the lateral surface of the reactor is negligible compared with the intensity of the direct and top diffuse radiation, the previous integration can be split in two components:

$$P(t) \cong P_m X(t)\left(p_{top}(\sigma X, \theta_z, \alpha, K') + p_{lat}(\sigma X, \theta_z, \alpha, \beta, K')\right) \quad \text{(S6-20)}$$

where the top and lateral components p_{top} (zone 1, Figure S6-1) and p_{lat} (zone 2, Figure S6-1) are respectively defined by:

$$p_{top}(\sigma X, \theta_z, \alpha, K') = \int_{z=z_{\min}}^{L} \int_{\theta=0}^{2\pi} \int_{r=0}^{r_{\min}} \frac{f(r,\theta,z,\sigma X(t),\theta_z(t)) + \alpha \cdot g(r,z,\sigma X(t))}{K'(t) + f(r,\theta,z,\sigma X(t),\theta_z(t)) + \alpha \cdot g(r,z,\sigma X(t))} \cdot r \cdot dr \cdot d\theta \cdot dz \quad \text{(S6-21)}$$

$$p_{lat}(\sigma X, \theta_z, \alpha, \beta, K') = \int_{z=0}^{L} \int_{\theta=0}^{2\pi} \int_{r=r_{\min}}^{R} \frac{f(r,\theta,z,\sigma X(t),\theta_z(t)) + \alpha \cdot g(r,z,\sigma X(t)) + \beta h(r,z,\sigma X(t))}{K'(t) + f(r,\theta,z,\sigma X(t),\theta_z(t)) + \alpha \cdot g(r,z,\sigma X(t)) + \beta h(r,z,\sigma X(t))} \cdot r \cdot dr \cdot d\theta \cdot dz \quad \text{(S6-22)}$$

By finally noticing that the intensity of the diffuse radiation coming through the top surface of the reactor in zone 2 (Figure S6-1) of the reactor can be assumed to be negligible compared to the intensities of the diffuse lateral, reflected and direct components, the expression of p_{lat} becomes:

$$p_{lat}(\sigma X, \theta_z, \beta, K') = \int_{z=z_{\min}}^{L} \int_{\theta=0}^{2\pi} \int_{r=r_{\min}}^{R} \frac{f(r,\theta,z,\sigma X(t),\theta_z(t)) + \beta h(r,z,\sigma X(t))}{K'(t) + f(r,\theta,z,\sigma X(t),\theta_z(t)) + \beta h(r,z,\sigma X(t))} r \cdot dr \cdot d\theta \cdot dz \quad \text{(S6-23)}$$

The values of p_{lat} and p_{top} were calculated and stored in two different matrices organized as described by Figure S6-2.

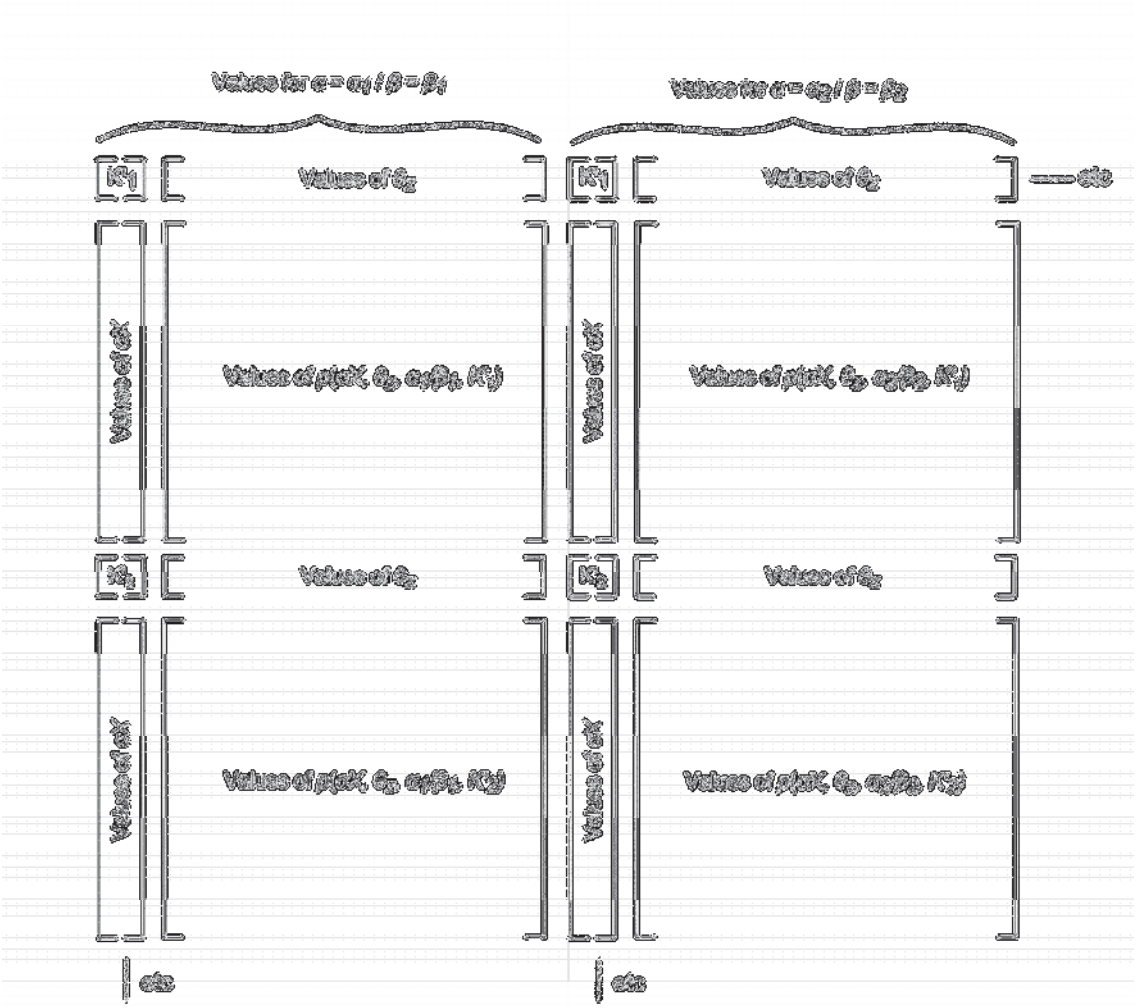

Figure S6-2: Organization of the matrix containing the values of the two components of the productivity p_{lat} and p_{top} (Note that the values contained in these matrices need to be multiplied by $P_m X$ to obtain a value of productivity in kg/s).

Further minimization of the computational time

In order to minimize the time necessary to generate the productivity matrices p_{lat} and p_{top}, the values of the two functions *f* and *g* were also stored in matrices of data. These two matrices, referred to as "*f*-matrix" and "*g*-matrix", contain values of *f* and *g* at different locations *r* and *z* in the reactor and for different values of the parameter σX (Figure S6-3). The values of *f* and *g* for intermediate values of *r*, *z*, and σX were obtained by linear interpolation between pre-calculated values.

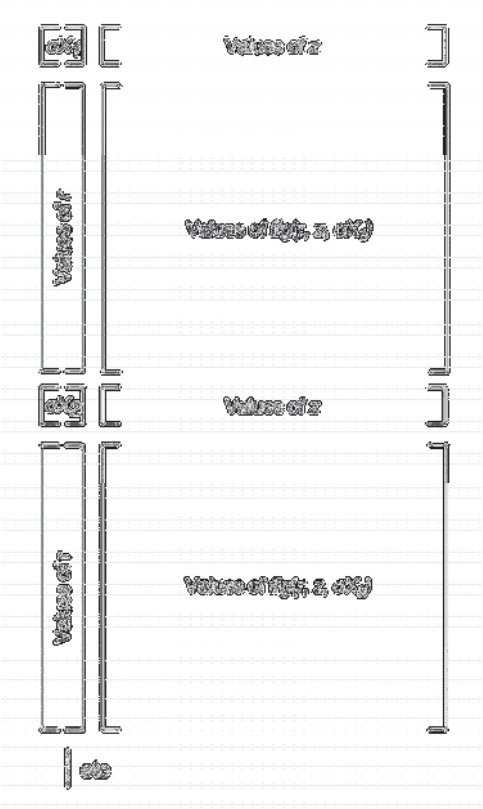

Figure S6-3: Organization of the *f*-Matrix and *g*-Matrix containing the values of the *f* and *g* functions (see Equations S6-11 and S6-12), respectively.

6.4. Verification of the different matrices and functions

This last section aims to verify the implementation of the different matrices used to calculate the productivity in outdoor photobioreactors. The verification of the *f*-function, the *g*-Matrix and the *h*-matrix are based on the fact that for high cell concentrations, all the radiation entering the reactor is absorbed by the cells. The amount of radiation absorbed by the algae can be calculated by integrating the local light intensity over the entire reactor volume (using the *h*-function or the values stored in the *g* and *h* matrices). The amount of radiation entering the reactors can be calculated by simple geometric considerations.

The validation of the different productivity matrices p_{top} and p_{lat} was performed by simulating the productivity in special cases.

6.4.1. Verification of the function *f*

In order to verify the values of the function *f*, the amount of direct radiation absorbed by the photobioreactor should converge to the amount of direct radiation absorbed by the photobioreactor when the algal concentration reaches relatively high values.

The amount of direct radiation reaching the reactor ($I_{dir,reac}$, W) can be expressed as:

$$I_{dir,reac} = I_{0,dir}\left(2RL\tan\theta_z + \pi R^2\right) \quad \text{(S6-24)}$$

where $I_{0,dir}$ is the intensity of the direct radiation per unit ground surface (W/m^2), R is the reactor radius (m), L is the reactor height (m) and θ_z is the angle between a vertical axis and the sun position.

The amount of absorbed radiation $I_{dir,abs}$ can be expressed as:

$$I_{dir,abs} = \int_{r=0}^{R}\int_{\theta=0}^{2\pi}\int_{z=0}^{H} \sigma X \cdot I_{0,dir} \cdot f\left(r,z,\theta,\theta_z,\sigma X\right)\cdot r \cdot dr \cdot d\theta \cdot dz \quad \text{(S6-25)}$$

Figure S6-4 compares the amount of direct radiation absorbed by the photobioreactor to the amount of direct radiation reaching the external surface of the photobioreactor. Figure S6-4 shows that these two variables are close to each other for high values of algal concentration, which validates the implementation of the *f*-function.

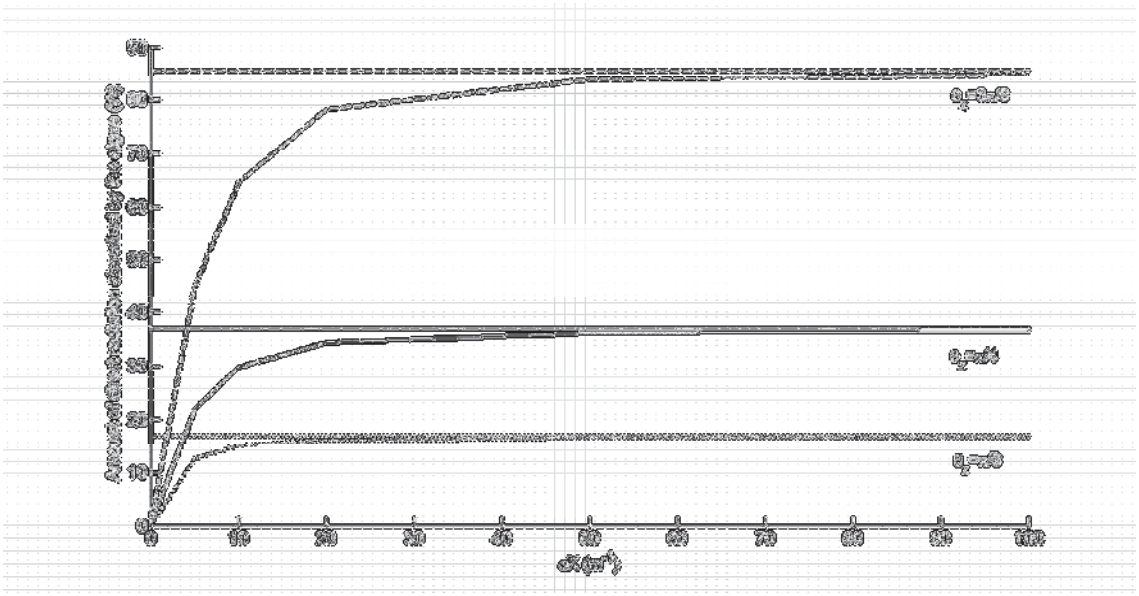

Figure S6-4: Amount of direct radiation absorbed by the algae as a function of the parameter σX (plain line). The horizontal line represents the amount of direct radiation reaching the external surface of the reactor (R = 0.095m, L = 1.8m, $I_{0,dir}$ = 100 W/m^2; Numerical constants used for the calculation of the absorbed radiation: N_r = 100, N_θ = 30, N_z = 30, where N_r, N_θ, and N_z are the number of infinitesimal elements in the radial, angular, and vertical direction, respectively). The amount of light absorbed by the algae was calculated only in the volume elements where the light intensity was higher than 0.5% of the incident light intensity.

6.4.2. Verification of the *g*-matrix

Similarly to the case of the direct radiation, the values of the g-Matrix were verified by calculating the fraction of diffuse radiation coming from the top surface of the photobioreactor absorbed by the algae.

The amount of diffuse radiation reaching the top surface of the reactor is:

$$I_{top,dif,reac} = I_{0,dif} \cdot \pi R^2 \quad \text{(S6-26)}$$

The fraction of this radiation that is absorbed by the algae is a function of the parameter σX and can be calculated as follows:

$$I_{top,dif,abs} = \int_{r=0}^{R} \int_{\theta=0}^{2\pi} \int_{z=0}^{H} \sigma X \cdot I_{0,dif} \cdot g(r,z,\sigma X) \cdot r \cdot dr \cdot d\theta \cdot dz \quad \text{(S6-27)}$$

Figure S6-5 shows that almost all the amount of top diffuse radiation entering the photobioreactor is absorbed by the algae for high values of cell concentration, which validates the implementation of the *g*-matrix.

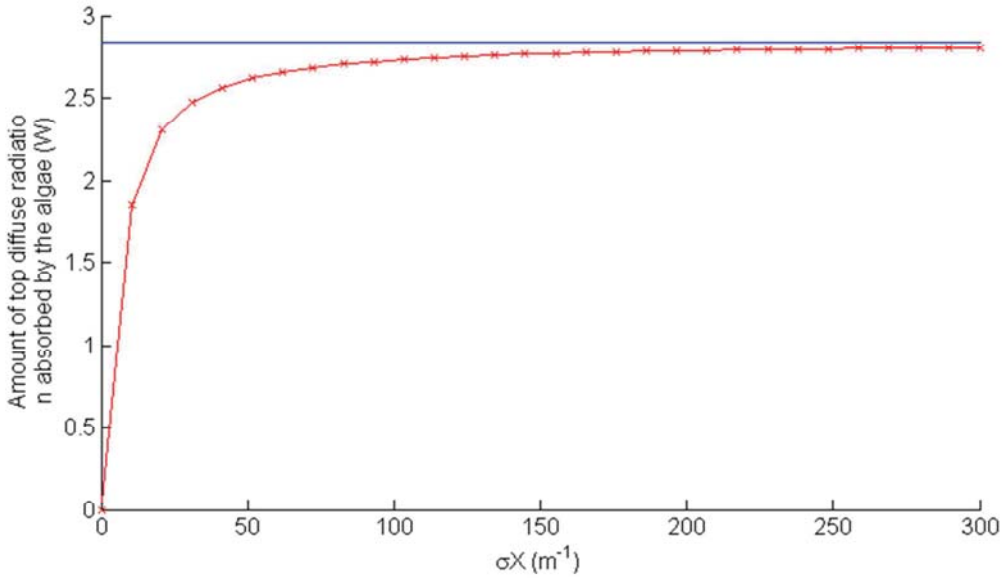

Figure S6-5: Evolution of the amount of the top diffuse radiation absorbed by the algae with the parameter σX (red line with crosses). The horizontal blue line represents the amount of top diffuse radiation entering the photobioreactor (R = 0.095m, L = 1.8m, $I_{0,dif}$ = 100 W/m^2, N_r = 100, N_z = 50).

6.4.3. Verification of the *h*-matrix

In order to verify the values of the *h*-matrix, the amount of lateral diffuse radiation absorbed by the algae was compared to the part of this radiation entering the photobioreactor.

The amount of diffuse radiation entering though the lateral surface of the photobioreactor can be expressed as:

$$I_{lat,dif,reac} = I_{0,dif} \cdot \pi RL \quad \text{(S6-28)}$$

The part of this radiation absorbed by the algae is:

$$I_{lat,dif,abs} = \int_{r=0}^{R} \int_{\theta=0}^{2\pi} \int_{z=0}^{H} \sigma X \cdot I_{0,dif} \cdot h(r,z,\sigma X) \cdot r \cdot dr d\theta dz \quad \text{(S6-29)}$$

Figure S6-6 compares the amount of lateral diffuse radiation absorbed by the algae as calculated by using the *g*-matrix to the amount of lateral diffuse radiation entering the reactor for high values of σX. Figure S6-6 shows that these two quantities are close to each other for high algae concentrations, which validates the implementation of the *h*-matrix.

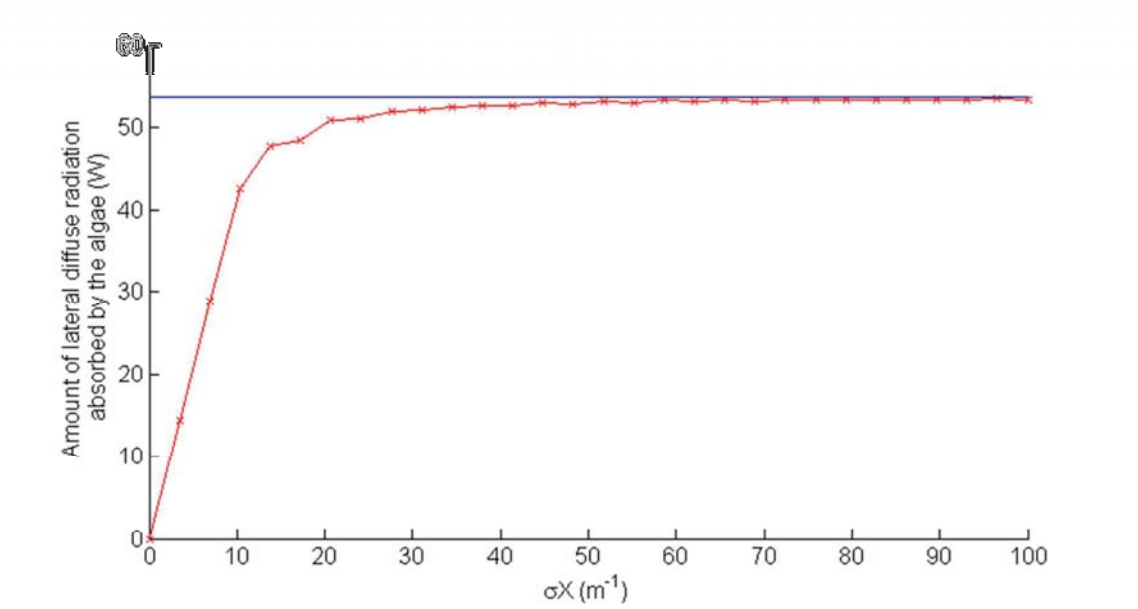

Figure S6-6: Evolution of the amount of the lateral diffuse radiation absorbed by the algae with the parameter σX (red line with crosses). The horizontal blue line represents the amount of top diffuse radiation entering the photobioreactor (R = 0.095m, L = 1.8m, $I_{0,dif}$ = 100 W/m^2, N_r = 100, N_z = 50). The "wriggles" are due to numerical error.

6.4.4. Verification of the p_{top} and p_{lat} Matrices

Special case: K = 0 W/kg; P_m = 1 kg/kg-s; X = 1 kg/m^3

For the specific case where K = 0 W/kg, P_m = 1 kg/kg-s and X = 1 kg/m^3, Equation S6-9 becomes:

$$P \cong \left(\int_{z=z_{\min}}^{L} \int_{\theta=0}^{2\pi} \int_{r=0}^{r_{\min}} r \cdot dr \cdot d\theta \cdot dz + \int_{z=0}^{L} \int_{\theta=0}^{2\pi} \int_{r=r_{\min}}^{R} r \cdot dr \cdot d\theta \cdot dz \right) = \pi R_{\min}^2 \left(L - z_{\min} \right) + L\pi \left(R^2 - R_{\min}^2 \right) \quad \text{(S6-30)}$$

Figure S6-7 shows that the calculation of the productivity in this special case using the matrices p_{top} and p_{lat} yields the same results as Equation S6-30.

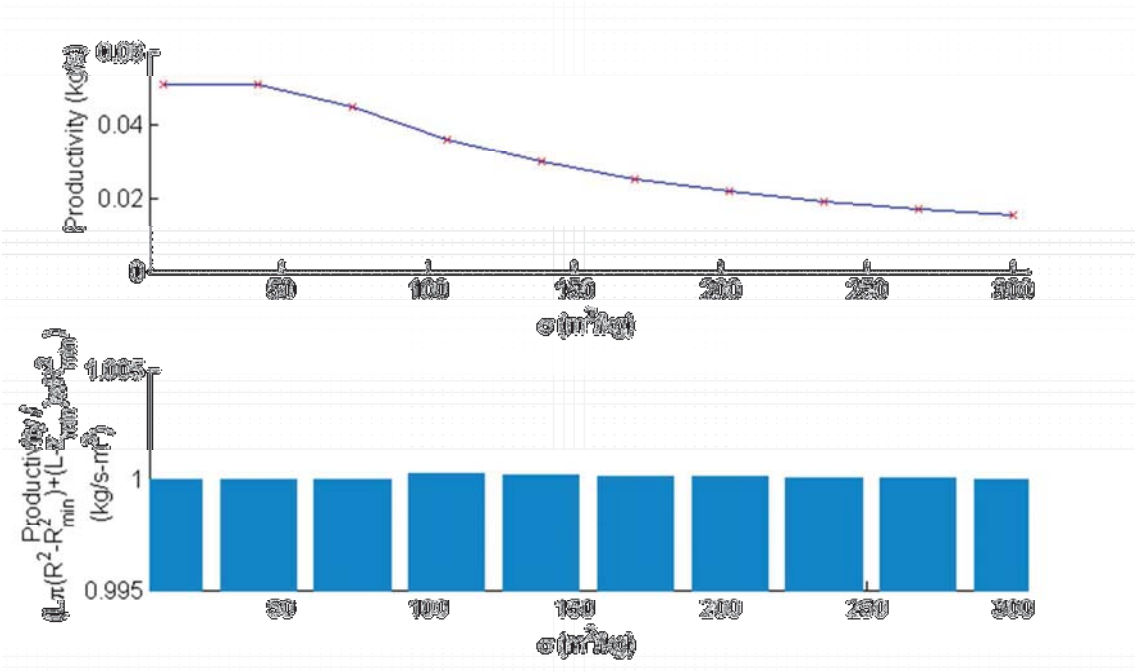

Figure S6-7: Evolution of the productivity with the extinction coefficient σ in the special case: K = 0 W/kg, P_m = 1 kg/kg-s, X = 1 kg/m^3 (Top: blue line: calculated productivity; Red crosses: volume of the reactor exposed to light; Bottom: ratio between the two last quantities). The small variations of this ratio are only due to numerical errors ($I_{0,dir}$ = 200 W/m^2; $I_{0,dif}$ = 100 W/m^2; $I_{0,ref}$ = 50 W/m^2, $\theta_z = \pi/4$).

Case where K/σ is very high

In the case where K/σ is relatively high compared with the incident light intensity, the total productivity can be approximated to:

$$P \cong P_m \int_r \int_\theta \int_z \frac{\sigma X I_{loc}(r,\theta,z,t)}{K} r \cdot dr \cdot d\theta \cdot dz = \frac{P_m}{K} I_{abs} \quad \text{(S6-31)}$$

where I_{abs} is the amount of solar radiation absorbed by the photobioreactor. For high values of the coefficient σX, the amount of solar radiation absorbed by the algae can be approximated by the amount of incident solar radiation (Figures 4, 5, 6), expressed as:

$$I_{abs} = I_{0,dir}\left(2RL\tan\theta_z + \pi R^2\right) + \left(I_{0,dif} + I_{0,ref}\right)\pi RL + I_{0,dif}\left(\pi R^2\right) \quad \text{(S6-32)}$$

Figure S6-8 shows that for very high values of K, the productivity tends to the expression given by Equation S6-32. The decrease of productivity with the increase of K observed in Figure S6-8 is explained by the mathematical expression of the Monod-like model (K is at the denominator).

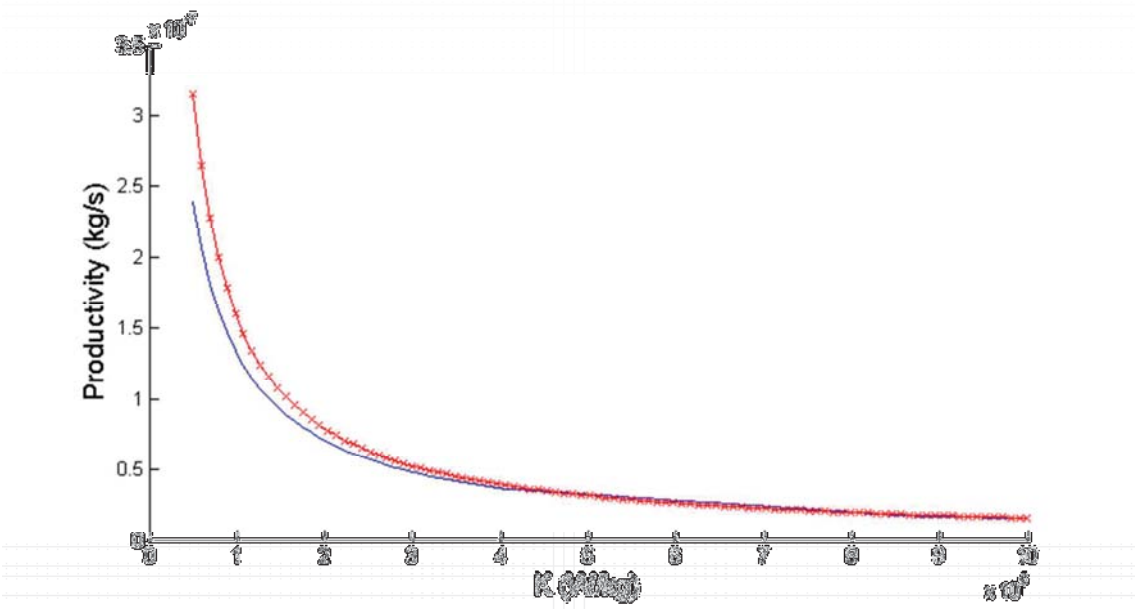

Figure S6-8: Evolution of the productivity with the parameter K (Blue line: Calculated productivity; Red crossed-line: Approximated productivity from Equations S6-31 and 32). (P_m = 10^{-4} kg/kg-s, X = 1 kg/m^3, σ = 100 m^2/kg; $I_{0,dir}$ = 200 W/m^2; $I_{0,dif}$ = 100 W/m^2; $I_{0,ref}$ = 50 W/m^2, θ_z = π/4).

Evolution of productivity with the algal concentration X

Figure S6-9 shows that the productivity does not significantly change with the algal concentration X by more than 1-2% for relatively high algal concentrations. This is consistent

with the fact that for σX values higher than 100 m^{-1}, almost all the solar radiation entering the reactor is absorbed by the algae (Figures 4, 5, and 6).

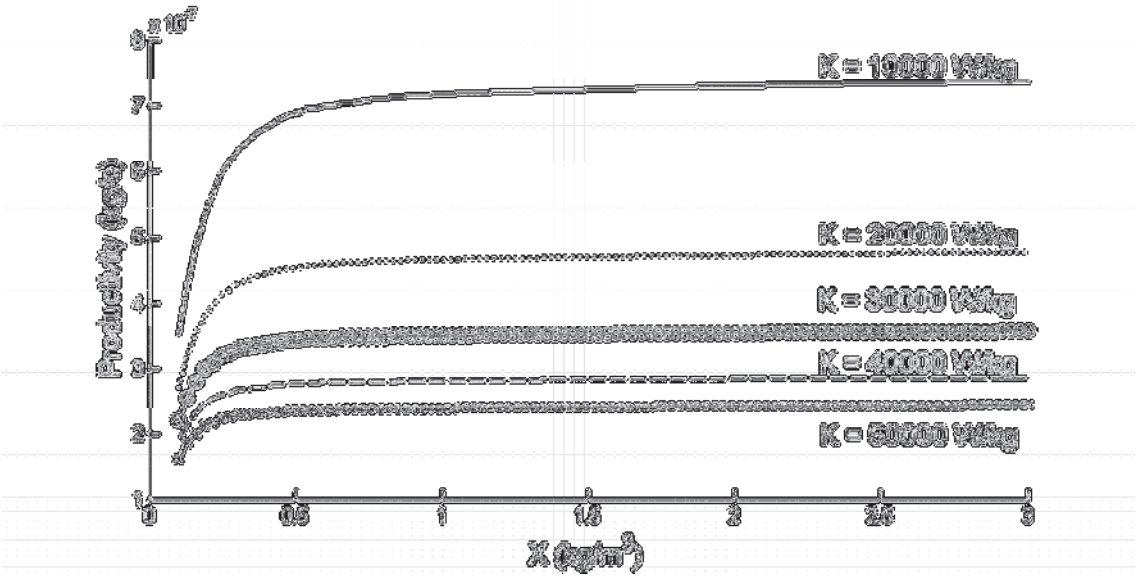

Figure S6-9: Evolution of the productivity with the algal concentration for different values of K (P_m = 10^{-4} kg/kg-s, σ = 100 m^2/kg; $I_{0,dir}$ = 200 W/m^2; $I_{0,dif}$ = 100 W/m^2; $I_{0,ref}$ = 50 W/m^2, θ_z = π/4).

Evolution of the productivity with the direct light intensity $I_{0,dir}$

Figure S6-10 shows that the predicted productivity increases with the direct light intensity as expected. The fact that the productivity is not null when the direct light intensity is equal to 0 is due to the fact that the diffuse and reflected radiations were assumed to be different from 0. In addition, the higher the sun is (the lower θ_z), the lower the surface area of the photobioreactor exposed to the direct radiation, hence the decrease of the productivity with the decrease of the angle θ_z (Figure S6-10, Figure S6-11).

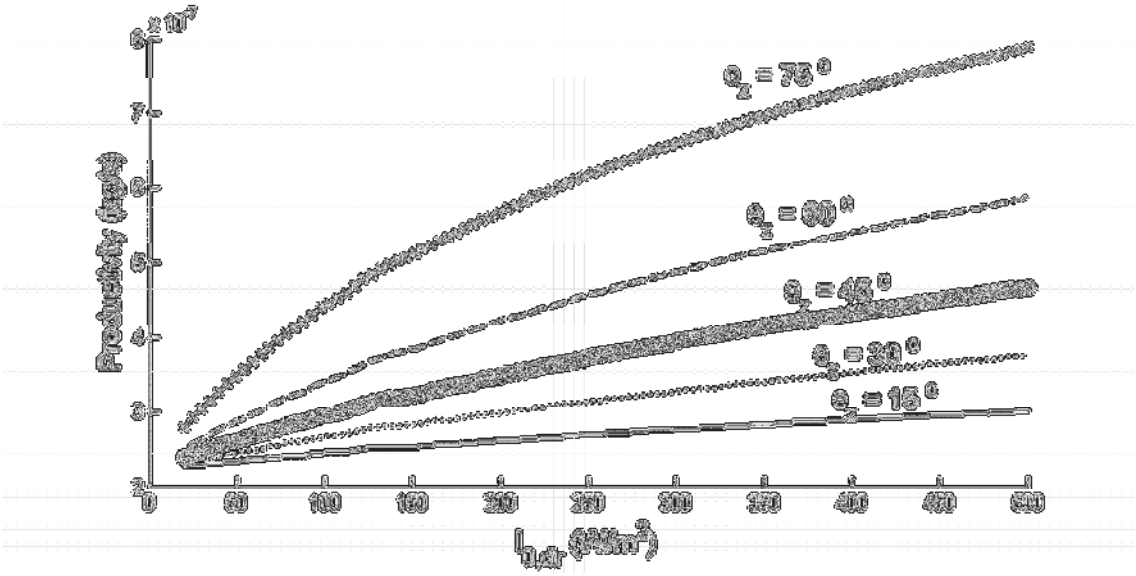

Figure S6-10: Evolution of the productivity of the reactor with the incident direct light intensity (P_m = 10^{-4} kg/kg-s, σ = 100 m^2/kg; X = 1kg/m^3; $I_{0,dif}$ = 100 W/m^2; $I_{0,ref}$ = 50 W/m^2, K = 30,000 W/kg).

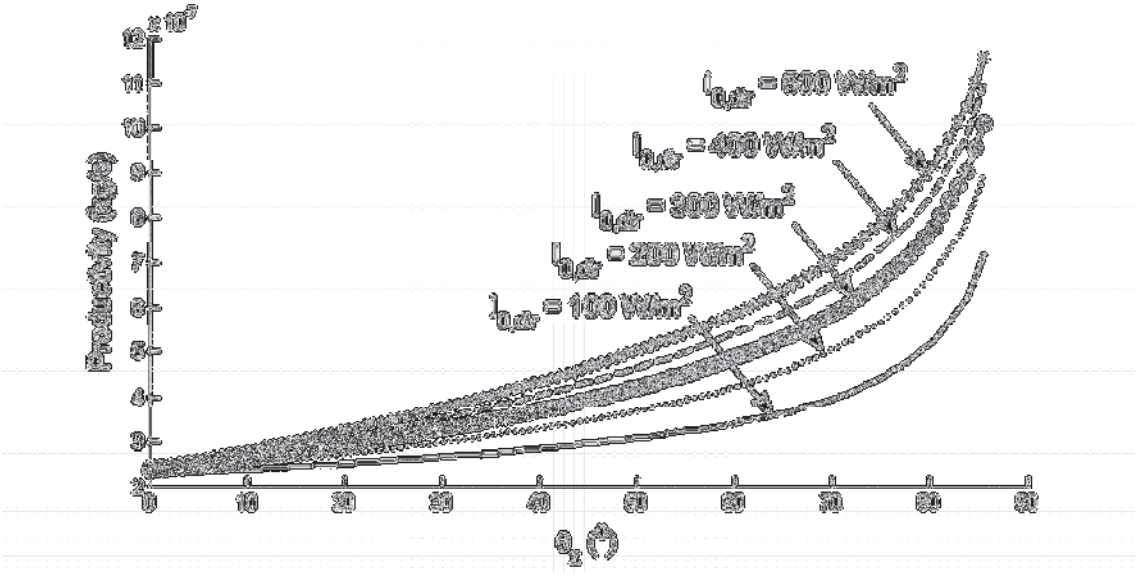

Figure S6-11: Evolution of the productivity of the reactor with the sun position (P_m = 10^{-4} kg/kg-s, σ = 100 m^2/kg; X = 1kg/m^3; $I_{0,dir}$ = 200; $I_{0,dif}$ = 100 W/m^2; $I_{0,ref}$ = 50 W/m^2, K = 30,000 W/kg).

Evolution of the productivity with the diffuse and reflected light intensities $I_{0,dif}$ and $I_{0,ref}$

Figures S6-12 and S6-13 show that the productivity increases with the amount of diffuse and reflected radiation entering the photobioreactor, which is in agreement with the theory. In addition, the productivity is a decreasing function of the half-saturation constant K which is again a direct consequence of the mathematical expression of the local productivity (Monod-like formula).

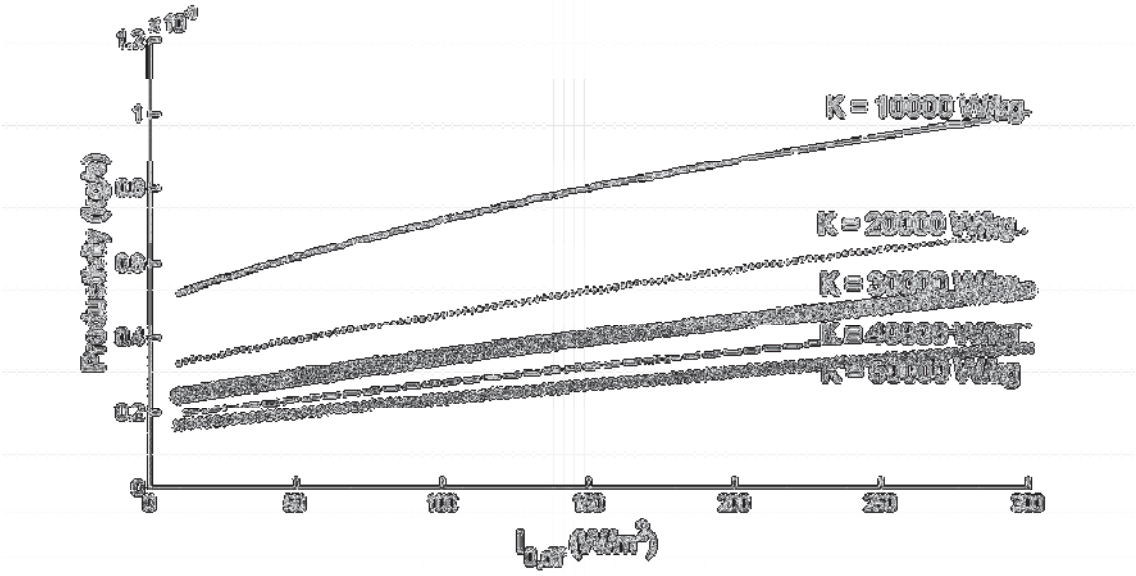

Figure S6-12: Evolution of the productivity of the reactor with the incident diffuse light intensity (P_m = 10^{-4} kg/kg-s, σ = 100 m^2/kg; X = 1kg/m^3; $I_{0,dir}$ = 200 W/m^2; $I_{0,ref}$= 50 W/m^2, θ_z = π/4).

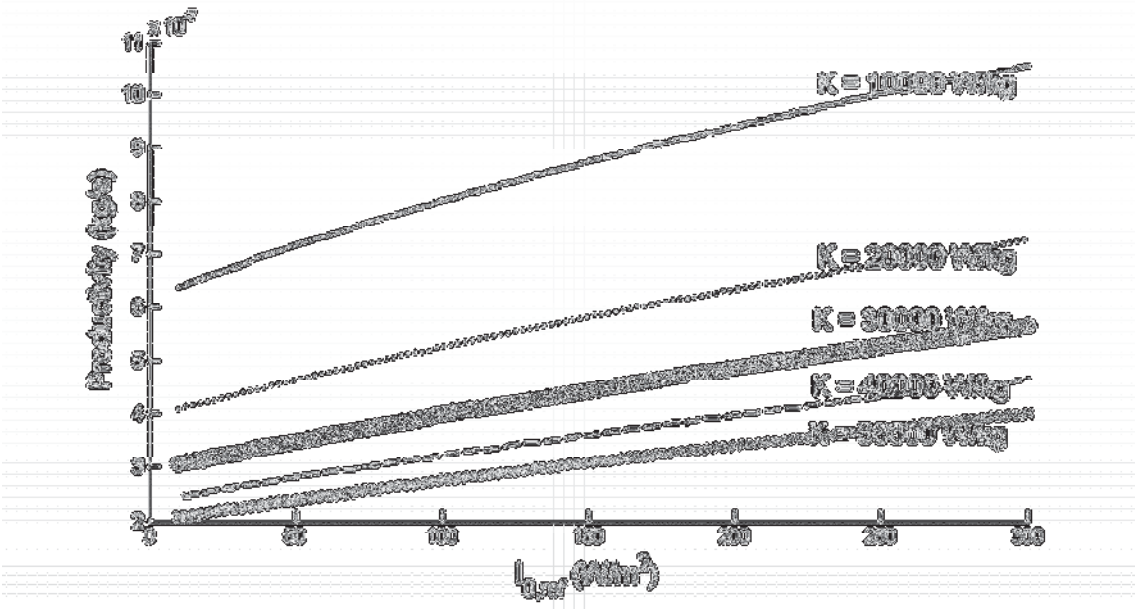

Figure S6-13: Evolution of the productivity of the reactor with the incident reflected light intensity (P_m = 10^{-4} kg/kg-s, σ = 600 m^2/kg; X = 1kg/m^3; $I_{0,dir}$ = 200 W/m^2; $I_{0,dif}$ = 100 W/m^2, $\theta_z = \pi/4$).

6.5. Constants used in the numerical integrations

In order to compute the productivity in the photobioreactor ($p_{lat} + p_{top}$, Equation S6-20), the volume of the photobioreactor was discretized in small volume elements. For the two matrices p_{lat} and p_{top}, the number of volume elements in the radial (N_r), angular (N_θ), and vertical (N_z) directions were 50, 20, and 50, respectively.

The function f and g were also computed from integrating numerically the amount of radiation coming from the external surface of the reactor to the considered location in the reactor. This calculation thus required to perform integrations over the external surface of the reactor. For the numerical integration associated with the calculation of the g function, the number of top surface elements in the radial (N_r) and angular (N_θ) were 100 and 20, respectively (and N_{lim} = 5, see the document on the light distribution in the indoor reactor for the definition of N_{lim}). For the numerical integration associated with the calculation of the h function, the number of surface elements in the angular (N_θ) and vertical (N_z) directions were 20 and 20, respectively (and N_{lim} = 5).

Table S6-1 also summarizes the number of elements for which the different functions (g, h, p_{top}, and p_{lat}) were calculated and the corresponding parameter ranges.

Table S6-1: Numerical constants used for the determination of the different productivity matrices

g-Matrix		
	Number of elements	Range
σX	40	10 – 300 (m^{-1})
r	50	0 – R
z	50	z_{lim} – L
h-Matrix		
	Number of elements	Range
σX	40	10 – 300 (m^{-1})
r	50	R_{min} – R
z	50	0 – L
p_{top}-Matrix		
	Number of elements	Range
σX	50	10-300 (m^{-1})
θ_z	30	0 – $\pi/2$
K'	101	0 – 600
α	75	0 – 100
p_{lat}-Matrix		
	Number of elements	Range
σX	50	10-300 (m^{-1})
θ_z	30	0 – $\pi/2$
K'	101	0 - 600
β	75	0 – 100

S7: Monte-Carlo simulations

The productivity predictions in the indoor and outdoor reactors made in this study were based on multiple input parameters. Due to the uncertainty on these experimentally measured model inputs, productivity predictions were inaccurate. Monte-Carlo simulations were performed in order to quantify how these uncertainties impact the accuracy of the model predictions similarly to the study of Béchet et al. (submitted). Figure S7-1 details what model inputs were considered and their associated levels of uncertainty.

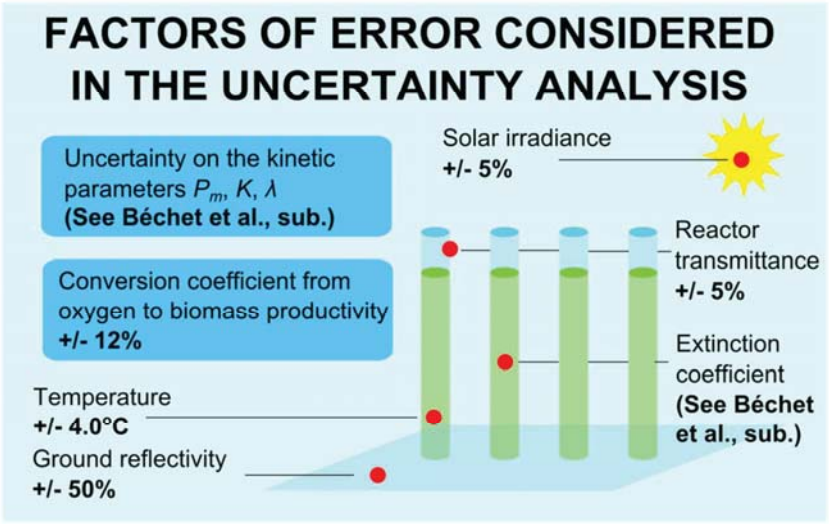

Figure S7-1: summary of the different sources of uncertainty in the model development and validation.

Reference

Béchet, Q.; Chambonnière, P.; Shilton, A.; Guizard, G.; Guieysse, B. Algal productivity modeling: a step toward accurate assessments of full-scale algal cultivation. **2014**. (submitted)

Article 6

MASSEY UNIVERSITY
GRADUATE RESEARCH SCHOOL

STATEMENT OF CONTRIBUTION TO DOCTORAL THESIS CONTAINING PUBLICATIONS

(To appear at the end of each thesis chapter/section/appendix submitted as an article/paper or collected as an appendix at the end of the thesis)

We, the candidate and the candidate's Principal Supervisor, certify that all co-authors have consented to their work being included in the thesis and they have accepted the candidate's contribution as indicated below in the *Statement of Originality*.

Name of Candidate: Quentin Béchet

Name/Title of Principal Supervisor: Prof Benoit Guieysse

Name of Published Research Output and full reference:

Guieysse B, Béchet Q, Shilton A. 2013. Variability and uncertainty in water demand and water footprint assessments of fresh algae cultivation based on case studies from five climatic regions. Biores Technol 128: 317–323.

In which Chapter is the Published Work: 5

Please indicate either:

- The percentage of the Published Work that was contributed by the candidate:

  and / or

- Describe the contribution that the candidate has made to the Published Work:

  Q Béchet performed the calculations of water demand and water footprint of algal cultivation in open ponds by using the code he developed for Article 2.

Quentin Béchet
Digitally signed by Quentin Béchet
DN: cn=Quentin Béchet, o=Massey University, ou=SEAT, email=q.bechet@massey.ac.nz, c=NZ
Date: 2014.02.17 18:49:56 +13'00'

Candidate's Signature

17/02/2014
Date

Benoit Guieysse
Digitally signed by Benoit Guieysse
DN: cn=Benoit Guieysse, o=Massey University, ou=SEAT, email=b.j.guieysse@massey.ac.nz, c=NZ
Date: 2014.02.24 11:17:49 +13'00'

Principal Supervisor's signature

24/02/2014
Date

Bioresource Technology 128 (2013) 317–323

Contents lists available at SciVerse ScienceDirect

Bioresource Technology

journal homepage: www.elsevier.com/locate/biortech

Variability and uncertainty in water demand and water footprint assessments of fresh algae cultivation based on case studies from five climatic regions

Benoit Guieysse *, Quentin Béchet, Andy Shilton

School of Engineering and Advanced Technology, Massey University, Private Bag 11 222, Palmerston North 4442, New Zealand

HIGHLIGHTS

- The water demand (WD) of algae cultivation for five case studies was quantified.
- Considerable variability and uncertainty regarding WD were found.
- The water footprint metric had poor geographical resolution and was biased towards high-productivity arid locations.

GRAPHICAL ABSTRACT

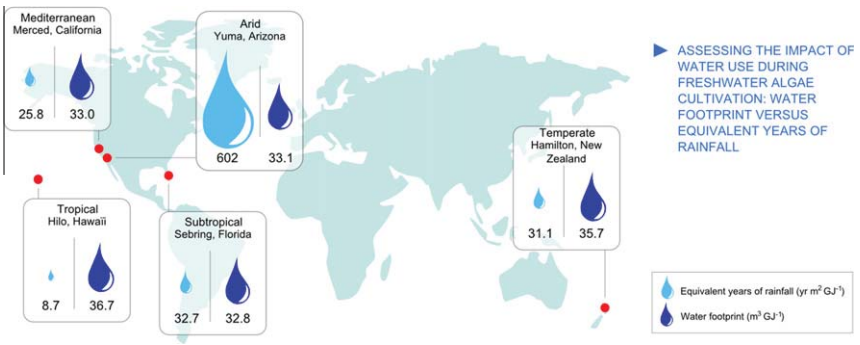

ARTICLE INFO

Article history:
Received 24 May 2012
Received in revised form 18 October 2012
Accepted 23 October 2012
Available online 1 November 2012

Keywords:
Algal biofuel
Climatic region
Fresh water algae
Raceway pond
Water demand

ABSTRACT

Using case studies from five typical climatic locations, this study revealed that current quantification of water demand (WD) and water footprint (WF) of freshwater algae cultivation in raceway ponds suffer from uncertainty and variability in the methodologies and assumptions used. Of particular concern, the WF metric had an intrinsically poor geographical resolution and could be biased towards high-productivity arid locations because local levels of water stress are not accounted for. Applying current methodologies could therefore cause the selection of locations that are neither economically viable nor environmentally sustainable. An improved methodology should utilize more accurate evaporation models, determine realistic limits for the maximum hydraulic retention times and process water recycling ratios, and apply weighting to the WF to reflect localized water stress or use an alternative metric such as the equivalent years of rainfall required to support a productivity of 1 GJ m^{-2}.

© 2012 Elsevier Ltd. All rights reserved.

1. Introduction

Despite the vast potential of algae biotechnologies to provide food, animal feed, bioactive compounds, biofuels, and new capabilities for pollution control (Dismukes et al., 2008; Spolaore et al., 2006; Singh et al., 2011), commercial algae cultivation remains expensive and difficult to scale up due to issues such as nutrient availability, CO_2 supply and delivery, land availability, process stability, biomass separation, and environment impacts (Murphy and Allen, 2011; Clarens et al., 2010; Singh and Olsen, 2011). Therefore, if algal biofuels are to become a commercial reality, the fundamental issues associated with large-scale algae cultivation must be addressed. Since more than 1 metric ton of process water must be handled for each kg of algae biomass produced (Murphy and Allen, 2011), water use represents a challenge of particular significance.

Water use can be assessed in terms of the water demand (WD) required for operating the process, which has direct economic and technological relevance, and the water footprint (WF), which reflects the amount of freshwater resource that the ecosystem is deprived of and which is essentially a policy tool. Different methods and assumptions have been used in the literature to estimate the amount of water used during algae cultivation (S1) and these differences may have led to conflicting conclusions. For example,

* Corresponding author. Tel.: +64 6 350 5841; fax: +64 6 350 5604.
E-mail address: B.J.Guieysse@massey.ac.nz (B. Guieysse).

0960-8524/$ - see front matter © 2012 Elsevier Ltd. All rights reserved.
http://dx.doi.org/10.1016/j.biortech.2012.10.096

Clarens et al. (2010) reported that the impact of water use during algae cultivation at three different locations in the USA was not sensitive to location, whereas Yang et al. (2011) and Wigmosta et al. (2011) found significant differences across the USA. Diverging conclusions are not uncommon in Life Cycle Assessments (LCAs) (Reap et al., 2008; Williams et al., 2009). Liu et al. (2012) demonstrated that considerable differences in the net energy ratio and carbon footprint of algae biodiesel production were attributable to differences in modeling methodologies and assumptions.

While refinement of full LCAs is necessary, the need for accurate estimation of water use is particularly pressing, not just for impact assessment but to simply allow accurate feasibility assessment of appropriate locations and process economics. With this perspective, the objective of this paper was to rigorously examine the impacts of assumptions and methods used in the literature on the accuracy and variability of the WD and WF of freshwater algae cultivation in open ponds, to determine where further experimental investigation is most needed, and to propose any necessary corrections or alternatives. The paper focuses on the application of WF to compare the feasibility of cultivating microalgae at different locations and does not benchmark freshwater algae cultivation in open ponds against technical alternatives.

2. Methods

2.1. Background

Many authors have highlighted that evaporation has a critical impact on the economics and sustainability of algae mass cultivation in open ponds (Pienkos and Darzins, 2009; Wijffels and Barbosa, 2010); therefore, and because the rate of free-surface evaporation from ponds is highly dependent on local meteorological conditions, emphasis was given to estimating the geographic variability of the WD and WF. For this purpose, algae cultivation was compared over five distinct climatic zones.

The indirect WF accounts for water consumption remote from the algae cultivation site such as, for example, water consumed during production of fertilizers needed to support algal growth (Clarens et al., 2010). Unless a component of the indirect footprint involves the same water basin used to supply water needed for algae cultivation, the indirect footprint should not be included in the comparison of the impacts of algae cultivation on local water resources. This component was therefore not considered in the comparative assessment.

For simplicity, biomass processing was excluded from the system boundary (Fig. 1). This approach is acceptable when focusing on direct water use because the WD associated with biomass processing is negligible: 2–10 L L^{-1} of biodiesel (Yang et al., 2011), or 0.06–0.28 m^3 GJ^{-1} assuming a biodiesel density and heat value of 0.92 kg L^{-1} and 38 kJ g^{-1}, respectively (Wigmosta et al., 2011). Furthermore, expressing the functional unit per GJ of biomass cultivated eliminates potential variability and uncertainty associated with parameters that are not strictly necessary for the purpose of comparing the geographic variability of the WD across different climatic regions (e.g. biomass separation efficiency, lipid extraction and biodiesel synthesis, and biomass heat value used for conversion).

Emphasis was given to variability and uncertainty in WD and WF assessments of freshwater algae cultivation in open ponds because this production system has been extensively discussed (Cooney et al., 2011; Lardon et al., 2009; Wigmosta et al., 2011; Yang et al., 2011). Algae cultivation in closed photobioreactors and the use of wastewater or saline water as a growth medium have undoubtedly great potential to significantly reduce freshwater consumption (Clarens et al., 2010; Pate et al., 2011); however, this paper will not benchmark freshwater algae cultivation in open ponds against these alternatives because such a comparison would require the assessments of all environmental impacts (e.g. climate change, eutrophication, etc.) in order to consider potential trade-offs (Clarens et al., 2010; Lardon et al., 2009; Murphy and Allen, 2011). In addition, computing the WD and WF of algae cultivation for alternative process configurations may be challenging due to limitations arising from, for example, freshwater requirements for cooling closed photobioreactors (e.g. 0.24–0.8 m^3 m^{-2} yr^{-1} in a Mediterranean climate) (Béchet et al., 2010).

2.2. Water demand

Within the system boundary (Fig. 1), the WD (m^3 m^{-2} yr^{-1}) can be calculated as the sum of the amount of freshwater required to make up for evaporation losses (Q_{ev}, m^3 m^{-2} yr^{-1}), leak losses (Q_{leak}, m^3 m^{-2} yr^{-1}) and the process water that is not recycled into the pond (Q_{pw}, m^3 m^{-2} yr^{-1}). The amounts of water consumed during the reaction of photosynthesis and evaporated during CO_2 supply are negligible (S2).

Leak rates of 0.0011–0.0036 m^3 m^{-2} yr^{-1}have been reported by Weissman et al. (1989) for lined ponds and this range was used in the sensitivity analysis with the median value of 0.00235 m^3 m^{-2} yr^{-1} used as base case.

Most of the approaches that have either been used to predict evaporation losses from algal ponds are based on empirical data or empirically-derived formulas that may be too site-specific to be universally applicable (S3). While not yet experimentally validated for algal ponds (and therefore still unproven as the most accurate), the evaporation model of Béchet et al. (2011) (S3) used in the base-case studies is based on a theoretical approach recommended by Sartori (2000) in his comprehensive review of

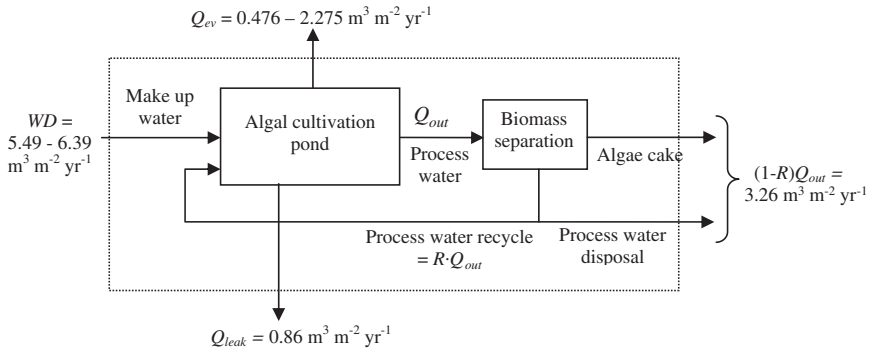

Fig. 1. Schematic representation of the water fluxes considered when computing the water demand (WD) of algae biomass cultivation. Numbers show the data computed in the base case scenario.

free-surface water evaporation formula (S3). Because Béchet's evaporation formula requires the input of the pond water temperature (and because pond temperature also depends on evaporation), the pond temperature was simultaneously simulated using the temperature model developed by the same authors (Béchet et al., 2011). This model has been specifically validated for high-rate algal ponds and predicts temperature at a time step of 200 s from hourly meteorological data.

Complete process water recycling is not possible during algae cultivation due to the 'blowdown' requirement for controlling salinity in the pond, frequent drainage and refill for maintenance (Murphy and Allen, 2011), and because process water is withdrawn with the algae cake harvested (Fig. 1). The yearly amount of freshwater required to make up for process water that is not recycled into the pond expressed per unit of pond area, Q_{pw}, can be calculated as:

$$Q_{pw} = \frac{(1-R)\cdot T\cdot V}{HRT\cdot A} = \frac{(1-R)\cdot T\cdot d}{HRT} \quad (1)$$

where R is the fraction of the process water that is recycled into the pond, T is the number of operational days per year (d yr^{-1}), HRT is the mean hydraulic retention time in the pond (d), V is the working volume of the cultivation system (m^3), A is the pond area (m^2) and d is the liquid depth in the pond (m). In the case studies, the ponds were assumed to be operated during the entire year (T = 365 d yr^{-1}).

2.3. Water footprint

Following the approach of Gerbens-Leenes et al. (2009), the WF (m^3 GJ^{-1}) was calculated as the sum of the blue-green WF which is a function of the amount of freshwater lost by evaporation (Yang et al., 2011), and the gray WF which is a function of the "amount of water needed to dilute pollutants discharged into the natural water system to the extent that the quality of the ambient water remains above agreed water quality standards" (Gerbens-Leenes et al., 2009). The option used for process water disposal is therefore critical to the WF and two scenarios were considered. In the first scenario, process water that is not recycled back into the pond was discharged to the local ecosystem, whereas in the second scenario this effluent was evaporated onsite using an evaporation pond.

In the first scenario the blue-green WF ($bgWF$, m^3 GJ^{-1}) can be calculated as:

$$bgWF = \frac{Q_{ev}}{P_{algae}} \quad (2)$$

where P_{algae} is the biomass productivity (GJ m^{-2} yr^{-1}).

Under the assumption that the process water leaking or disposed (i.e. not recycled) from the pond is not lost by the ecosystem, the gray WF ($grWF$, m^3 GJ^{-1}) can be determined as:

$$grWF = \frac{D\cdot(1-R)\cdot T\cdot d}{P_{algae}\cdot HRT} + \frac{D\cdot Q_{leak}}{P_{algae}} \quad (3)$$

where D is a multiplier used to compute the amount of local freshwater resource needed to dilute/absorb the pollutants present in the disposed process water to acceptable concentrations in the ecosystem (D = 0 when the pollutants are already below the relevant water quality standards). For the purpose of completing a precise assessment of the WF at a particular location, the details of the disposal option must be determined and the local water quality standards must be considered before the appropriate D can be determined. Treatment prior to discharge has the potential to reduce the dilution required but is highly site-specific. This paper focuses on the application of WF to compare the feasibility of cultivating microalgae at different locations. With this perspective, it is necessary to assume equivalent options for disposal and equivalent water quality standards across locations. In other words an equivalent D must be maintained or the assessment can be biased by local regulations. Yang et al. (2011) used a D ratio equal to 1 at all locations considered and the same assumption was adopted in this study.

In the second scenario (use of evaporation ponds), the blue-green WF can be calculated as:

$$bgWF = \frac{1}{P_{algae}}\left[Q_{ev} + \frac{(1-R)\cdot T\cdot d}{P_{algae}\cdot HRT}\right] \quad (4)$$

And the gray WF can be calculated as

$$grWF = \frac{D\cdot Q_{leak}}{P_{algae}} \quad (5)$$

Under the assumption that D = 1, the total WF is identical for the two disposal scenarios considered and can simply be calculated as the ratio of the WD to the algal productivity (P_{algae}). The use of Eq. (4) implies that the water removed with the algae cake was assumed to generate a gray WF in the first scenario or a blue-green WF in the second scenario. These assumptions have no impact on the total WF in either scenario (D = 1) and only a very minor impact on the individual contributions of the blue-green WF and gray WF because in the case studies, an algae cake containing 20% of solids (Cooney et al., 2011) only generates a water consumption equivalent to approximately 0.5% of the WD.

The biomass productivity from the pond (P_{algae}, GJ m^{-2} yr^{-1}) was calculated based on the global solar irradiance at the ground surface (I_0, GJ m^{-2} yr^{-1}) assuming a uniform photosynthetic efficiency (PE, %) across all locations (S4):

$$P_{algae} = I_0\cdot\left(\frac{PE}{100}\right) \quad (6)$$

2.4. Sensitivity/uncertainity analysis

Nine methodologies were compared in order to estimate the uncertainty of evaporation predictions (see S3 for complete description of models, results and further discussion). In the first approach, the rates of evaporation from the raceway pond were assumed to be equal to the observed pan-evaporation recorded at each location (Sander and Murthy, 2010). In the eight remaining approaches, evaporation rates were respectively computed using a semi-empirical lake evaporation model (estimating evaporation rates as 75% of the pan-evaporation data) (Yang et al., 2011; Frank et al., 2011); the "Penman" model (Clarens et al., 2010), and six evaporation formulas used in combination with a high temporal resolution temperature model (including the model used by Wigmosta et al. (2011)). The sensitivities of the WD and WF to the accuracy of evaporation predictions and key parameters (HRT, R, d, PE) were then assessed for each case study.

2.5. Case studies

2.5.1. Climatic locations

Five typical climatic zones were selected as case studies for the determination of the WD and WF. These included locations representative of arid (Yuma, Arizona, USA), tropical (Hilo, Hawaii, USA), sub-tropical (Sebring, Florida, USA), Mediterranean (Merced, California, USA) and temperate (Hamilton, New Zealand) climates or, more specifically, the respective classifications of BWh, Af, Am, Csa, Cfb under the Updated Köppen–Geiger Classification (Peel et al., 2007).

2.5.2. Meteorological data

Meteorological data for the temperate climate location was obtained from the New Zealand Institute of Water and Atmospheric Research. Solar irradiance, air temperature, wind velocity, rainfall, and relative humidity were collected hourly for the entire year 2008. For the other four climates, hourly solar irradiance, air temperature, wind speed, and rainfall, together with monthly daytime and nighttime relative humidity averages for the year 2009 were obtained from the National Climatic Data Center of the US National Oceanic and Atmospheric Administration.

2.5.3. Pond design

Pond depths varied from 0.2 to 0.3 m in the sensitivity analysis (the median value of 0.25 m being used as the base case), based on the values used in prior LCAs (Clarens et al., 2010; Cooney et al., 2011; Lardon et al., 2009; Murphy and Allen, 2011; Stephenson et al., 2010; Weissman et al., 1989; Wigmosta et al., 2011; Yang et al., 2011). While the sides of a pond may be sloped in practice, the sides were assumed vertical when calculating the pond working area as the effect of this assumption on the area is minor given the shallow depth relative to the width of a full scale pond.

2.5.4. Pond operation

Although *HRT* values ranging from 2 to 33 days have been proposed during algae cultivation (Cooney et al., 2011), a narrower range of 4–10 days was used in the sensitivity analysis to maintain yearly-averaged algae effluent concentrations within operational guidelines (S5). The median value of 7 days was used as base case. By accounting for a blowdown equivalent to 14% of evaporation losses (Weissman and Goebel, 1987) (this represents 0.07–0.32 $m^3\ m^{-2}\ yr^{-1}$ in the base case scenario), harvesting losses of 0.02–0.03 $m^3\ m^{-2}\ yr^{-1}$ assuming a solid content of 20% after separation (Cooney et al., 2011; Lardon et al., 2009), and process shutdown (the pond must be emptied and refilled with fresh medium four times per year (Murphy and Allen, 2011), which generates a WD of 1.0 $m^3\ m^{-2}\ yr^{-1}$ in the base case scenario), the maximum recycling efficiency achievable during algae cultivation at a 7-d *HRT* was estimated at 90% ($R = 0.9$). While there appears to be no research conducted on process water recycling in algal ponds, salt accumulation restricts WD savings from recycling to just 25–50% in horticulture (Massa et al., 2010). Based on these data, an *R* value of 0.75 was used as base case because this value predicted potential savings in WD of 60–68%. While higher than the horticultural savings, this range seems appropriate because unlike terrestrial plants, algae do not transpire. The minimum *R* ratio was set to 0.5 in the sensitivity analysis.

2.5.5. Photosynthetic efficiency (PE)

A *PE* range of 2–3% (the median value of 2.5% being used as base case) was used to estimate biomass productivity of 11.1–25.7 $g\ m^{-2}\ d^{-1}$. These values are comparable to the productivities achieved during commercial outdoor algae cultivation in open ponds (Park et al., 2011) (S4). An algal biomass heat value of 24.7 $kJ\ g^{-1}$ dried weight (Williams and Laurens, 2010), corresponding to a lipid content of 25% (total mass), was used to convert biomass productivities into $g\ m^{-2}\ d^{-1}$.

3. Quantification of water demand

The WD of algae cultivation ranged from 4.59 $m^3\ m^{-2}\ yr^{-1}$ in a tropical climate to 6.39 $m^3\ m^{-2}\ yr^{-1}$ in an arid climate (Fig. 2). Under the assumptions used in the present study (uniform Q_{leak}, *HRT* and *R* values across all locations), these variations in WD across climates were driven by variations in evaporation rates ranging from 0.476 $m^3\ m^{-2}\ yr^{-1}$in a tropical climate to 2.275 $m^3\ m^{-2}\ yr^{-1}$ in an arid climate. However, in addition to evaporative losses, both leaks and process water disposal contributed significantly to the WD which is surprising given that very little consideration has previously been given to these components.

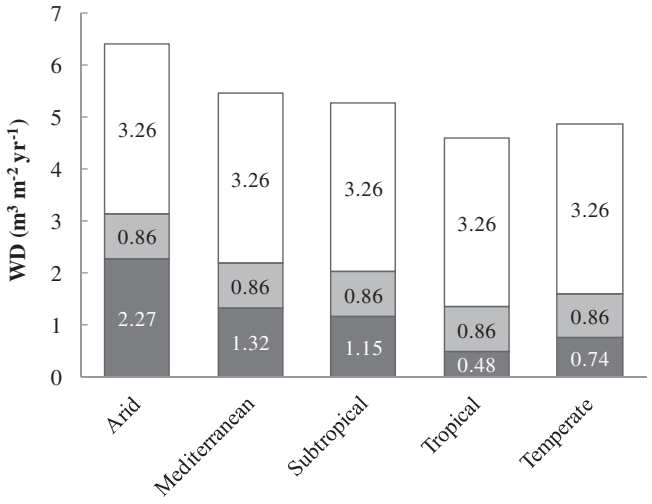

Fig. 2. Contribution of evaporation (dark gray), leak losses (light gray) and process water disposal (white) to the water demand (WD) of algae cultivation under five climatic conditions (base case). Numbers show data in $m^3\ m^{-2}\ yr^{-1}$.

3.1. Accuracy of evaporation: consequences on the quantification of the WD

The comparative analysis of nine methodologies revealed large variations in evaporation predictions across all locations (relative standard deviations of 17–44%, S3). In addition, the sensitivity analysis on the evaporation model used in the base case studies showed that considerable uncertainty was introduced from the air emissivity (up to 54% in a tropical climate). Based on these results, the uncertainty of evaporation estimates was set to 50% in the sensitivity analysis of the WD. This caused WD inaccuracies that could have a significant impact on the economic feasibility of algae cultivation. For example, an inaccuracy of 50% equates to $\pm 1.14\ m^3\ m^{-2}\ yr^{-1}$ in an arid climate, which represents more than 21 years of precipitation at the location considered. It may therefore be concluded that algae bioengineering must make use of accurate evaporation models to ensure accurate assessment of technical feasibility and process economics.

3.2. Impact of process operation on the quantification of the WD

Process operation (*HRT*, *R*) had the greatest impact on the sensitivity of the WD of algae cultivation over all the climates considered (Fig. 3). Increasing the *HRT* directly reduces the amount of process water disposed from the pond and, therefore, the WD of algae cultivation. Unfortunately biomass losses caused by dark respiration and/or predation may become significant at high *HRT* (S5). These limitations not withstanding, it would seem feasible to increase the *HRT* to some reasonable degree to minimize the WD of algae cultivation. Surprisingly, this operational approach to minimize WD has apparently not been addressed previously. Pond depth only had a relatively small impact on the WD within the range studied (Fig. 3), which is explained by the fact that light utilization efficiency (dark respiration at large depths) limits the range of pond depth suitable for algae cultivation; however, the modest WD gains that can be achieved through process design may be significant in arid areas, and this potential strategy to minimize WD should be experimentally demonstrated.

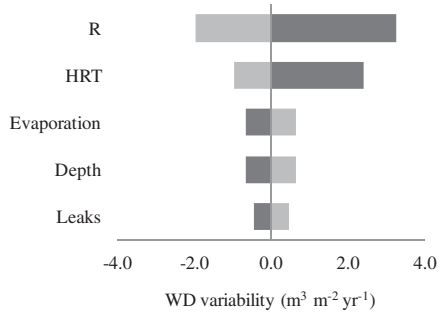

Fig. 3. Sensitivity of water demand (WD, $m^3\ m^{-2}\ yr^{-1}$) to operation (*HRT*, *R*), pond depth, leak losses and evaporation prediction in a Mediterranean climate. For each parameter, the light bar represents the variation in WD when the upper value of the range is used in the simulation, while the dark bar corresponds to the lower value of the range. The ranges for each parameter were: *R*, 0.5–0.9; *HRT*, 4–10 d; evaporation, ±50%; *d*, 0.2–0.3 m; and leaks, 0.0011–0.0036 $m^3\ m^{-2}\ yr^{-1}$. The sensitivity of the WD to evaporation ranged from ±0.24 $m^3\ m^{-2}\ yr^{-1}$ in a tropical climate to ±1.14 $m^3\ m^{-2}\ yr^{-1}$ in an arid climate whereas sensitivity to other parameters was uniform across the climates considered.

Fig. 3 illustrates how an efficient means to reduce the WD is to recycle process water back into the pond after biomass separation; however, while complete recycling ($R = 1$, S1) was assumed to be feasible in a large number of LCAs of algae biofuels, water quality degrades with use due, in particular, to the accumulation of salts and microorganisms pathogenic to microalgae (Stephenson et al., 2010). In order to account for this degradation of water quality, Murphy and Allen (2011) computed the WD associated with the blowdown requirement and frequent pond drainage for maintenance and cleaning. Based on these authors, the maximum achievable *R* value was estimated to be approximately 0.9 in the case studies; however, there is no experimental evidence that such high recycling efficiency can indeed be achieved without impacting productivity. Instead, the known detrimental impact of the accumulation of growth-inhibiting salt concentrations during horticulture suggests that the use of a lower recycling ratio should represent a more pragmatic assumption in the absence of specific data for algae. This is a particular concern given the drastic impact of recycling on the magnitude of the WD.

It could be argued that process water could simply be treated to a high enough standard before being recycled back to the pond. Unfortunately, there is again a lack of research into how this could actually be done. Since excess salts introduced from the water supply will eventually build up, reverse osmosis (RO) would be the logical treatment choice for this purpose and this process would also remove pathogens; however, RO is costly, energy intensive and cannot reclaim 100% of the water it treats. For example, treating a fraction of the process water by RO in order to raise the recycling efficiency from 75% to 95% could consume the equivalent of 10–16% of the algal biofuel-energy produced and generate 0.65 $m^3\ m^{-2}\ yr^{-1}$ of highly polluted RO water concentrate assuming a biomass-energy to biofuel-energy efficiency of 60%, an RO energy demand of 3.6 MJ m^{-3}, and an RO treatment recovery of 80% based on published data for full-scale RO of brackish water (Karagiannis and Soldatos, 2008). Moreover, with a cost of US \$0.26–0.41 kg^{-1} of algal biomass produced, RO treatment would be uneconomical for water recycling during freshwater algae cultivation since Chisti (2008) estimated that the total cost of algae biomass cultivation would need to be lower than US \$0.34 kg^{-1} for algal biofuels to compete with oil at US \$100 per barrel (considering an RO cost of US \$0.8 m^{-3} based on the US \$0.26–1.33 m^{-3} range for full-scale brackish water given by Karagiannis and Soldatos, 2008). In view of this, it appears that treating process water to minimize WD is unlikely to be feasible in full scale commercial operations. This also means that studies based on the assumption of complete recycling may have underestimated some of the technical and economic implications of water use during algae cultivation.

4. Quantification of water footprint

The WF of algae cultivation ranged from 33.0 $m^3\ GJ^{-1}$ in a Mediterranean climate to 36.7 $m^3\ GJ^{-1}$ in a tropical climate (Table 1). Both evaporation losses and process water disposal contributed significantly to the total WF, which explains the large sensitivity of the WF metric to process operation (*HRT*), process water recycling (*R*), and evaporation predictions (Fig. 4). Logically, the WF was also highly sensitive to the value of the photosynthetic efficiency used in the computation of the productivity. Overall, the WF could vary three-fold from as little as 20.7 $m^3\ GJ^{-1}$ in a tropical climate with high water recycling ($R = 0.9$) up to 62.7 $m^3\ GJ^{-1}$ in a tropical climate with low water recycling ($R = 0.5$). These predictions show that freshwater algae cultivation has the potential to have large impacts on local water resources, which underscores the case for water-efficient alternatives such as the use of wastewater, saline water or photobioreactors. The large variability of the WF seen above implies that further research is needed to determine if the uncertainty associated with the WF of freshwater algae cultivation is also significant for the broad comparative LCAs of these technological alternatives.

4.1. Uncertainty from process operation

The high sensitivity of the WF to hydraulic retention time and recycling ratio is explained by the sensitivity of the WD to these parameters; however, if water supply and disposal have significant impacts on production costs, a pond located in water-stressed areas will likely be operated at higher *HRT* and *R* values than a pond located in water-rich areas. Unfortunately, because it is currently not possible to accurately predict commercial operational values for *HRT* and *R* under given climatic conditions (and the impact of this tailored operation on productivity), a great uncertainty is generated from the assumption that process operation is uniform across all the locations considered.

4.2. Uncertainty from productivity predictions

As in the cases of the hydraulic retention time and recycling ratio, significant uncertainty arises from the selection of the value for photosynthetic efficiency (PE) and, more importantly for comparative assessment, the assumption that this value is uniform across the locations considered. The PE is indeed sensitive to climatic conditions, process design and operation, and biology (Williams and Laurens, 2010) and thus it is difficult to accurately predict this parameter.

4.3. Uncertainty from evaporation predictions

Although the uncertainty arising from the evaporation prediction appears to be rather limited (Fig. 4), it is of special concern because evaporation losses are the main driver for the differences in WF across different climatic regions. The simulations showed that the use of different evaporation methodologies could yield diverging conclusions as to the most sustainable location for algae cultivation in regards to water use. For example, algae cultivation in an arid climate had the lowest WF when the semi-empirical lake evaporation model was used, while cultivation in a Mediterranean climate had the lowest WF when using prediction generated with Béchet's model (Béchet et al., 2011).

Table 1
Water demand (WD) and water footprint (WF) of algae cultivation under five climatic conditions (base case).

Climate	Evaporation ($m^3\ m^{-2}\ yr^{-1}$)	WD ($m^3\ m^{-2}\ yr^{-1}$)	Solar irradiance ($GJ\ m^2\ yr^{-1}$)	Productivity ($GJ\ m^{-2}\ yr^{-1}$)	WF ($m^3\ GJ^{-1}$)	Rain fall ($m^3\ m^{-2}\ yr^{-1}$)	Years of rain fall [a] to produce 1 $GJ\ m^{-2}$
Arid	2.275	6.39	7.73	0.193	33.1	0.0549	602
Mediterranean	1.324	5.44	6.59	0.165	33.0	1.28	25.8
Subtropical	1.150	5.27	6.41	0.160	32.8	1.01	32.7
Temperate	0.737	4.85	5.44	0.136	35.7	1.15	31.1
Tropical	0.476	4.59	5.01	0.125	36.7	4.20	8.7

[a] These values are calculated by dividing the WD by the amounts of yearly rain fall and biomass productivity.

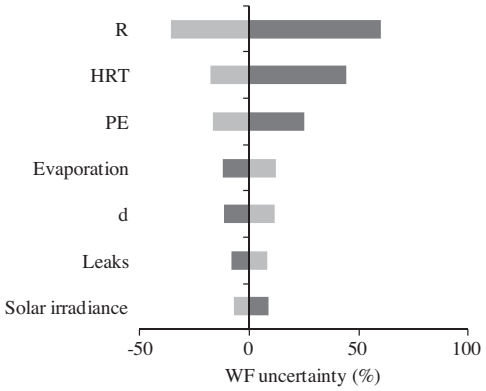

Fig. 4. Relative sensitivity of water footprint (WF) to operation (*HRT*, *R*), design (*d*), leak losses, productivity modeling (*PE*, solar irradiance) and evaporation prediction in a Mediterranean climate. For each parameter, the light bar represents the variation of the WF when the upper value of the range is used in the simulation, while the dark bar corresponds to the lower value of the range. The ranges for each parameter were: *R*, 0.5–0.9; *HRT*, 4–10 d; *PE*, 2–3%; evaporation, ±50%; *d*, 0.2–0.3 m; leaks, 0.0011–0.0036 $m^3\ m^{-2}\ yr^{-1}$; and solar irradiance, ±10%. The sensitivity of the WF to the selected parameters was similar across the five climates considered (full data set available in S3).

4.4. Geographical resolution

Interestingly, the WFs across the locations considered differed little despite significant variations in evaporation between these five climates (Table 1). This low geographical variation can be explained by the high sunlight intensities driving both high evaporation rates and high algal productivities. This 'productivity effect' counterbalances the significance of evaporation and, because the relative contribution of process water disposal is high, explains why the impacts of algae cultivation on local water resources counter-intuitively appear lower in arid than in water-rich regions.

To contrast against this WF bias, an alternative metric was defined as to the number of years of local rainfall required to support a productivity of 1 GJ of biomass energy per m^2 of pond area. These calculations show that cultivation of algae in an arid climate would require the equivalent of 602 years of locally available rainfall to enable 1 GJ of biomass energy to be produced per m^2 of pond against 26 years for a Mediterranean climate (Table 1). This simple comparison suggests that, despite having very similar WFs, algae cultivation has a potentially far greater impact on local water resources in an arid than a Mediterranean climate. Although basin-scale water resources should be considered when assessing the impacts of water use, the present study underscores that using WF ratios as a tool for comparing the impact of water use during algae cultivation may erroneously favor selection of arid locations. The critical point that must be recognized when undertaking any comparison of the impacts of algae cultivation on local water resources across locations is that 1 m^3 of freshwater resource in the desert is obviously not of equal economic and environmental values as 1 m^3 of freshwater in a temperate climate. While practitioners using WF in other fields have cited the importance of accounting for localized water stress (Berger and Finkbeiner, 2010; Ridoutt and Pfister, 2010; Pfister et al., 2009), to date this has not been done when using WF to compare locations for algal biofuel production.

It therefore appears that the algal biofuel industry has not yet adequately addressed the fundamental question of water use. Failure to get such basic issues addressed before rushing to full scale runs the risk of repeating the debacle of Jatropha cultivation for bio-energy production due to what Kant and Wu (2011) refer to issues that "were nothing out of ordinary and should have been anticipated". At this point in time, the present study suggests that a simple alternative to WF such as 'equivalent years of rain fall' at a water basin scale could be more meaningful. Comparing this metric leads to a dramatically different and a potentially more realistic perspective of which locations are suitable for algal biofuel production, as shown in Table 1.

5. Conclusions

The evaluation of WD during algae cultivation suffers from uncertainties in evaporation predictions and significant variability arising from process operation (*HRT*, *R*). Further issues arise when the analysis is extended to the determination of the WF, a metric that is naturally biased toward high-productivity arid locations, has a low geographical resolution, and is highly sensitive to poorly predictable parameters (*HRT*, *R*, evaporation, *PE*). Most critically however, the current WF methodology ignores the pragmatic fact that consuming water in an arid region has a far greater impact than consuming water in a region abundant in freshwater resources.

Further research is needed to develop models that accurately predict evaporation from algal ponds, to determine a realistic limit on the maximum hydraulic retention time and the maximum recycling ratio achievable under specific climatic conditions, and to apply a weighting to reflect the degree of localized water stress when using WF as a measure of water use impact.

Acknowledgements

Q.B. is supported by a Massey University Doctoral Scholarship. This sponsor had no involvement in this study design; the collection and interpretation of data; the writing of this paper; and the decision to submit this research for publication. The authors thank Dr. Ranvir Singh from Massey University, New Zealand, for valuable discussions about WF methodologies.

Appendix A. Supplementary data

S1, prior methodologies used to determine the water demand and water footprint of algae biomass/biofuel; S2, neglecting water losses caused by photosynthesis and CO_2 supply; S3, modeling evaporation from algal ponds; S4, modeling productivity during

algae cultivation; S5, influence of HRT on algal productivity in ponds. Supplementary data associated with this article can be found, in the online version, at http://dx.doi.org/10.1016/j.biortech.2012.10.096.

References

Béchet, Q., Shilton, A., Fringer, O., Munoz, R., Guieysse, B., 2010. Mechanistic modelling of broth temperature in outdoor photobioreactors. Environ. Sci. Technol. 44, 2197–2203.

Béchet, Q., Shilton, A., Park, J.B., Craggs, R.J., Guieysse, B., 2011. Universal temperature model for shallow algal ponds provides improved accuracy. Environ. Sci. Technol. 45, 3702–3709.

Berger, M., Finkbeiner, M., 2010. Water footprinting: how to address water use in life cycle assessment? Sustainability 2, 919–944.

Chisti, Y., 2008. Biodiesel from microalgae beats bioethanol. Trends Biotechnol. 26, 126–131.

Clarens, A.F., Resurreccion, E.P., White, M.A., Colosi, L.M., 2010. Environmental life cycle comparison of algae to other bioenergy feedstocks. Environ. Sci. Technol. 44, 1813–1819.

Cooney, M.J., Young, G., Pate, R., 2011. Bio-oil from photosynthetic microalgae: case study. Bioresour. Technol. 102, 166–177.

Dismukes, G.C., Carrieri, D., Bennette, N., Ananyev, G.M., Posewitz, M.C., 2008. Aquatic phototrophs: efficient alternatives to land-based crops for biofuels. Curr. Opin. Biotechnol. 19, 235–240.

Frank, E.D., Han, J., Palou-Rivera, I., Elgowainy, A., Wang, M.Q., 2011. Life Cycle Analysis of Algal Lipid Fuels with the GREET Model. Argonne National Laboratory, US Department of Energy.

Gerbens-Leenes, W., Hoekstra, A.Y., van der Meer, T.H., 2009. The water footprint of bioenergy. Proc. Natl. Acad. Sci. USA 106, 10219–10223.

Kant, P., Wu, S., 2011. The extraordinary collapse of jatropha as a global biofuel. Environ. Sci. Technol. 45, 7114–7115.

Karagiannis, I., Soldatos, P.G., 2008. Water desalination cost literature: review and assessment. Desalination 223, 448–456.

Lardon, L., Helias, A., Sialve, B., Steyer, J.P., Bernard, O., 2009. Life-cycle assessment of biodiesel production from microalgae. Environ. Sci. Technol. 43, 6475–6481.

Liu, X., Clarens, A.F., Colosi, L.M., 2012. Algae biodiesel has potential despite inconclusive results to date. Bioresour. Technol. 104, 803–806.

Massa, D., Incrocci, L., Maggini, R., Carmassi, G., Campiotti, C.A., Pardossi, A., 2010. Strategies to decrease water drainage and nitrate emission from soilless cultures of greenhouse tomato. Agr. Water Manage. 97, 971–980.

Murphy, C.C., Allen, D.T., 2011. Energy-water nexus for mass cultivation of algae. Environ. Sci. Technol. 45, 5861–5868.

Park, J.B.K., Craggs, R.J., Shilton, A.N., 2011. Wastewater treatment in high rate algal ponds for biofuel production. Bioresour. Technol. 102, 35–42.

Pate, R., Klise, G., Wu, B., 2011. Resource demand implications for US algae biofuels production scale-up. Appl. Energy 88, 3377–3388.

Peel, M.C., Finlayson, B.L., McMahon, T.A., 2007. Updated world map of the Köppen–Geiger climate classification. Hydrol. Earth Syst. Sci. 11, 1633–1644.

Pfister, S., Koehler, A., Hellweg, S., 2009. Assessing the environmental impacts of freshwater consumption in LCA. Environ. Sci. Technol. 43, 4098–4104.

Pienkos, P.T., Darzins, A., 2009. The promise and challenges of microalgal-derived biofuels. Biofuels Bioprod. Biorefining 3, 431–440.

Reap, J., Roman, F., Duncan, S., Bras, B., 2008. A survey of unresolved problems in life cycle assessment. Part 2: impact assessment and interpretation. Int. J. Life Cycle Assess. 13, 374–388.

Ridoutt, B.G., Pfister, S., 2010. A revised approach to water footprinting to make transparent the impacts of consumption and production on global freshwater scarcity. Global Environ. Change 20, 113–120.

Sander, K., Murthy, G.S., 2010. Life cycle analysis of algae biodiesel. Int. J. Life Cycle Assess. 15, 704–714.

Sartori, E., 2000. A critical review on equations employed for the calculation of the evaporation rate from free water surfaces. Sol. Energy 68, 77–89.

Singh, A., Nigam, P.S., Murphy, J.D., 2011. Mechanism and challenges in commercialization of algal biofuels. Bioresour. Technol. 102, 26–34.

Singh, A., Olsen, S.I., 2011. A critical review of biochemical conversion, sustainability and life cycle assessment of algal biofuels. Appl. Energy 88, 3548–3555.

Spolaore, P., Joannis-Cassan, C., Duran, E., Isambert, A., 2006. Commercial applications of microalgae. J. Biosci. Bioeng. 101, 86–87.

Stephenson, A.L., Kazamia, E., Dennis, J.S., Howe, C.J., Scott, S.A., Smith, A.G., 2010. Life-cycle assessment of potential algal biodiesel production in the United Kingdom: a comparison of raceways and air-lift tubular bioreactors. Energy Fuels 24, 4062–4077.

Weissman, J.C., Goebel, R.P., 1987. Design and Analysis of Microalgal Open Pond Systems for the Purpose of Producing Fuels, SERI/SP-231-2840. Solar Energy Research Institute, Golden, Colorado.

Weissman, J.C., Tillett, D.T., Goebel, R.P., 1989. Design and Operation of an Outdoor Microalgae Test Facility: Final Subcontract Report, SERI/ STR-232-3569. Solar Energy Research Institute, Golden, Colorado.

Wigmosta, M.S., Coleman, A.M., Skaggs, R.J., Huesemann, M.H., Lane, L.J., 2011. National microalgae biofuel production potential and resource demand. Water Resour. Res. 47, W00H04. http://dx.doi.org/10.1029/2010WR009966.

Wijffels, R.H., Barbosa, M.J., 2010. An outlook on microalgal biofuels. Science 329, 796–799.

Williams, E.D., Weber, C.L., Hawkins, T.R., 2009. Hybrid framework for managing uncertainty in life cycle inventories. J. Ind. Ecol. 13, 928–944.

Williams, P.J. le B., Laurens, L.M.L., 2010. Microalgae as biodiesel & biomass feedstocks: review & analysis of the biochemistry, energetics, & economics. Energy Environ. Sci. 3, 554–590.

Yang, J., Xu, M., Zhang, X., Hu, Q., Sommerfeld, M., Chen, Y., 2011. Life-cycle analysis on biodiesel production from microalgae water footprint and nutrients balance. Bioresour. Technol. 102, 159–165.

Web references

New Zealand Institute of Water and Atmospheric Research. <http://cliflo.niwa.co.nz> (accessed 23.05.12).

National Climatic Data Center of the US National Oceanic and Atmospheric Administration. <http://www.ncdc.noaa.gov/crn/report> (accessed 23.05.12).

Supporting information

Title: Variability and uncertainty in water demand and water footprint assessments of fresh algae cultivation based on case studies from five climatic regions

Authors: Benoit Guieysse, Quentin Béchet, Andy Shilton

S1 – Prior methodologies used to determine the water demand and water footprint of algae biomass/biofuel production

S2 – Neglecting water losses caused by photosynthesis and CO_2 supply

S3 – Modeling evaporation from algal ponds

S4 – Modeling productivity during algae cultivation

S5 – Influence of HRT on algal productivity in ponds

2 Figures

5 Tables

34 Pages

S1 - Prior methodologies used to determine the water demand and water footprint of algae biomass/biofuel production

Table S1-1: Water demand (WD) and water footprint (WF) of algae cultivation in the literature. Where the authors of the studies cited considered complete process water recycle (recycling ratio R = 1), we calculated the corresponding WF as the ratio of WD (or netWD) to the biomass or biodiesel productivity.

R	WD m^3/m^2-yr	netWD	WF	Reference
R = 1			379 ± 76 m^3/GJ biomass	Clarens et al., 2010
R = 1		0.3	10 m^3/GJ biomass[a]	Lardon et al., 2009
R = 1	1.6		20.4 m^3/GJ biodiesel	Sander and Murthy, 2010
R = 0 - 1	0.6-1.8		14.8-91.3 m^3/GJ biodiesel[b]	Yang et al., 2011
R = 0 - 1		0	0.1-43.8 m^3/GJ biodiesel[c]	Stephenson et al., 2010
R = 1		<0.1-2.1	40.6 m^3/GJ biodiesel[d]	Wigmosta et al. 2011
R = 0.9	5.4		31.7 m^3/GJ biomass[e]	Murphy and Allen, 2011
R = 0.95			13.4 m^3/GJ biomass[f]	Frank et al., 2011
R = 0 - 0.99[g]	0.5-22.3[g]		0.96 – 74.0 m^3/GJ biodiesel[g]	Cooney et al., 2011

(a) Net evaporation losses generated a WF of 0.24 m^3/kg algae (corrected from the original manuscript in agreement with Dr Lardon). An algal biomass high heat value (HHV) of 24 MJ/kg was used for conversion according to Clarens et al. (2010).

(b) The WD fluctuated depending on location. A total WF of 591-3650 kg/kg biodiesel was associated to a blue-green WF of 399 kg/kg biodiesel, depending on the ratio of process water recycling. A biodiesel HHV of 40 MJ/kg was used for conversion.

(c) Based on a negative net evaporation in the UK (evaporation = 1.1 m^3/m^2-yr and precipitation of 1.126 m^3/m^2-yr), the authors estimated the WD of algae cultivation to 3.8-1750 m^3/t biodiesel depending on the recycle ratio. A biodiesel HHV of 40MJ/kg was used for conversion.

(d) Based on the average WF value for the USA (1421 L water/L biodiesel), the biodiesel density of 0.92 kg/L and the energy value of 38 MJ/kg reported by the authors. Assuming R = 1, the authors computed the WF as the ratio of netWD to areal productivity.

(e) Because these authors considered saline algae cultivation, the equivalent WD for freshwater algae was computed as the sum of the amount of freshwater (1.0 m^3/m^2-yr) and saline water (4.4 m^3/m^2-yr) needed for supporting the process (US average data). Biomass productivity (GJ/m^2-yr) was estimated from the annualized growth yield of 18.9 g/m^2-d reported by the authors (US average) using a biomass heat value of 24.7 kJ/g according to Williams and Laurens (2010).

(f) Based on evaporation losses and process water disposal of 0.23 L/g-biomass (Arizona) and 0.1 L/g-biomass, respectively. A biomass heat value of 24.7 kJ/g was used for conversion according to Williams and Laurens (2010).

(g) Based on a productivity of 60 g/m^2-d, a pond depth of 0.2 m, and a HRT of 3.33 days, the authors reported WD of 0.5 m^3/m^2-yr (R = 0.99 using membrane separation followed by centrifugation) to 22.3 m^3/m^2-d (no recycling). This demand generated a WF of 234.5 - 2589 m^3/m^3-biodiesel (converted by assuming a biodiesel density of 0.92 kg/L and an energy value of 38 MJ/kg according to Wigmosta et al., 2011). When only the filtrate water from the membrane separation step was recycled back into the pond, the recycling efficiency was 90% (R = 0.9), and the WD and WF were estimated to 2.2 m^3/m^2-yr and 7.95 m^3/GJ-biodiesel, respectively. Evaporation losses were estimated to 0.423 m^3/m^2-yr, a value considered as an underestimate by the authors.

As can be seen in Table S1-1, there is a large variance in the WF estimates found in the literature. This variance underscores the variations in the methods and assumptions used to generate this data, as discussed below.

Use of indirect WF: The largest WF value shown in Table S1-1 was reported by Clarens et al. (2010). It can be explained by the fact that these authors included the indirect water use for energy generation, alum production (the chemical used for biomass flocculation), CO_2 generation and the production of the fertilizers superphosphate and urea. As explained in the manuscript, this contribution to the WF should normally not be considered when comparing the impact of water use across different locations.

Process water disposal: As seen in Table S1-1, most life cycle assessments (LCAs) of algae biofuels have assumed that complete ($R = 1$) or near complete ($R \geq 0.9$) recycling is feasible. To our knowledge, only Yang et al. (2011) have hitherto considered the environmental impact of process water discharge. These authors calculated the gray WF of algae biodiesel production as the ratio of the amount of process water discharged per biodiesel productivity. Therefore, under the definition conventionally associated with the gray WF, Yang et al. (2011) considered that the pollutants found in the process water discharged needed to be diluted with an equivalent volume of freshwater to respect local water quality criteria.

Evaporation: As further discussed in S3, various methods have been used to compute evaporation losses from algal ponds: Clarens et al. (2010) used the "Penman" model fed with on-site meteorological data; Sander and Murthy (2010) used pan-evaporation estimates; both Yang et al. (2011) and Frank et al. (2011) used semi-empirical lake evaporation rates estimated as 75% of the pan-evaporation data (known as the "Lake evaporation formula") while Murphy and Allen (2011) used a conversion factor of 0.7 for shallow lakes; Lardon et al. (2009) estimated net evaporation losses to 0.3 m^3/m^2-yr in a Mediterranean climate; Stephenson et al. (2010) used an net evaporation loss of 1.1 m^3/m^2-yr for the UK; Cooney et al. (2011) used a "conservative" estimate of 0.42 m^3/m^2-yr (based on the reported daily rate

57,955 m^3/d for a 50,000,000 m^2 pond, and assuming 365 days of operation per year) based on predictions from the evaporation model from the American Society of Heating, Refrigeration, and Air Conditioning; and Wigmosta et al. (2011) used a high resolution model accounting for pond temperature and fed with onsite meteorological data.

Process operation and design: Pond depth values ranging from 0.2 m (Cooney et al., 2011) to 0.3 m (Lardon et al., 2009; Murphy and Allen 2011; Yang et al, 2011) have been used in the LCA literature. The WD has then been estimated based on either the average operational Hydraulic Retention Time (HRT, Murphy and Allen, 2011; Cooney et al. 2011) or the average algae concentration at harvesting (Yang et al., 2011; Lardon et al., 2009; see S5). While both approaches are acceptable for calculating the yearly WD and WF (the HRT has little impact on evaporation losses, as see in S3), a thorough analysis of technical feasibility and production costs would require considering a realistic operational scenario (variable HRT and/or algae concentration at harvesting) in order to compute the WD and netWD with a high temporal resolution. Yearly-averaged algae concentrations have ranged from 210 g/m^3 (Murphy and Allen, 2011) up to 1000 g/m^3 (Yang et al., 2011; Stephenson et al., 2010) and HRT values have ranged from 2 d (Murphy and Allen, 2011) up to 33 d (Cooney et al., 2011).

Blowdown and shutdown: Based on estimates from Weissman and Goebel (1987), Murphy and Allen (2011) estimated blow-down contribution as 14% of the evaporation rates, whilst the Lundquist et al. (2010) computed the blow-down as 3% of the pond effluent flow rate. There is little published information available about process shutdown requirement for maintenance (e.g. for species control) and Murphy and Allen (2011) considered that the cultivation pond needs to be entirely emptied and refilled 4 times each year.

WD versus netWD: Various authors have estimated the direct WF of algae cultivation from the difference between the evaporation and precipitation rates, or netWD when $R = 1$ (Lardon et al, 2009; Stephenson et al., 2010; Clarens et al., 2010, Wigmosta et al., 2011). While the validity of this method for computing the WF is debatable (rainwater is "removed" from the ecosystem if it is collected and subsequently evaporated), the netWD can be systematically underestimated if it is not calculated with the proper temporal resolution (Wigmosta et al., 2011). This effect is explained by the fact that 1) most precipitation occurs during periods when surface evaporation is low (excess rain water cannot be retained to any significant extent in a shallow pond) whereas 2) most evaporative losses occur during dry periods (and would cause a significant drop in cultivation volume if freshwater was not actively supplied.)

Productivity: Various methods have been used in the literature to compare algal biomass (or biofuel) productivity across different locations: Clarens et al. (2010) used locally-based empirical estimates of the photosynthetic efficiency (PE); Wigmosta et al. (2011) used a PE-based model accounting for light saturation and temperature influence; while Murphy and Allen (2011) computed productivity as 43% of the empirical projections of Williams and Laurens (2010) to account for productivity losses (due to e.g. cloudy days and shutdown for maintenance) and considered that growth was only possible during days when the minimum air temperature was greater than 5°C and the maximum air temperature was lower than 35°C. In another study, Yang et al. (2010) calculated productivity as

$$AGR = k \cdot TR \cdot T \qquad \text{(S1-3)}$$

Where AGR is the algal growth rate (g/m^2-d), k is the temperature-dependant PE (g/kWh-°C), TR is the yearly averaged daily radiation at the location considered (kWh/m^2-d) and T is the 1961-1990 average annual air temperature at the location considered (°C).

References:

Clarens, A. F.; Resurreccion, E. P.; White, M. A.; Colosi, L. M. Environmental life cycle comparison of algae to other bioenergy feedstocks. *Environ. Sci. Technol*. **2010**; *44* (5), 1813-1819.

Cooney, M. J.; Young, G.; Pate, R. Bio-oil from photosynthetic microalgae: Case study. *Bioresour. Technol*. **2011**. *102*, 166-177.

Frank, E. D.; Han, J.; Palou-Rivera, I.; Elgowainy, A.; Wang, M. Q. Life Cycle Analysis of Algal Lipid Fuels with the GREET Model, 2011. Argonne National Laboratory,

Lardon, L.; Helias, A.; Sialve, B.; Steyer, J. P.; Bernard, O. Life-cycle assessment of biodiesel production from microalgae. *Environ. Sci. Technol.* **2009**, *43* (17), 6475-6481.

Lundquist, T. J.; Woertz, I. C.; Quinn, N. W. T.; Benemann, J. R. A Realistic Technology and Engineering Assessment of Algae Biofuel Production. Energy Biosciences Institute, University of California Berkeley, **2010**. http://digitalcommons.calpoly.edu/cenv_fac/188/

Murphy, C. C.; Allen D. T. Energy-water nexus for mass cultivation of algae. *Environ. Sci. Technol.* **2011**, *45* (13), 5861-5868.

Sander, K.; Murthy, G. S. Life cycle analysis of algae biodiesel. *Int. J. Life Cycle Assess*. **2010**, *15*, 704-714.

Stephenson, A. L.; Kazamia, E.; Dennis, J. S.; Howe, C. J.; Scott, S. A.; Smith, A. G. Life-cycle assessment of potential algal biodiesel production in the United Kingdom: a comparison of raceways and air-lift tubular bioreactors. *Energy Fuels* **2010**, *24* (7) 4062–4077.

Wigmosta, M. S.; Coleman, A. M.; Skaggs, R. J.; Huesemann, M. H.; Lane, L. J. National microalgae biofuel production potential and resource demand. *Water Resour. Res.* **2011**, *47*, W00H04; doi:10.1029/2010WR009966

Weissman, J. C.; Goebel, R. P. Design and Analysis of Microalgal Open Pond Systems for the Purpose of Producing Fuels, SERI/SP-231-2840;Solar Energy Research Institute: Golden, CO, 1987.

Williams, P. J.; le, B.; Laurens, L. M. L. Microalgae as biodiesel & biomass feedstocks: Review & analysis of the biochemistry, energetics, & economics. *Energy Environ. Sci.* **2010**, *3* (5), 554–590.

Yang, J.; Xu, M.; Zhang, X.; Hu, Q.; Sommerfeld, M.; Chen, Y. Life-cycle analysis on biodiesel production from microalgae: water footprint and nutrients balance. *Bioresour. Technol.* **2011**, *102* (1), 159-165.

S2 – Neglecting water losses caused by photosynthesis and CO_2 supply

Photosynthesis: Water serves as electron donor during photosynthesis and the reaction of photosynthesis yielding carbohydrate can be approximated as:

$2n\ CO_2 + 2n\ H_2O + photons \rightarrow 2(CH_2O)_n + 2n\ O_2$

meaning that approximately 0.6×10^{-3} m^3 of water is consumed for each kg of carbohydrate synthesized. Assuming a carbohydrate heat value of 17.3 MJ/kg (Gerbens-Leenes et al., 2009), this consumption yields a negligible water demand of 0.0035-0.0052 m^3/m^2-yr in our case studies.

CO_2 supply: The injection of CO_2-enriched air is often necessary during episodes of vigorous algae growth in order to provide CO_2, control pH, and remove O_2. The amount of water loss through aeration Q''_{ev} (m^3/d) can be calculated by assuming that the gas leaving the reactor is saturated with water and at the reactor broth temperature:

$$Q''_{ev} = \frac{(1 - RH) \cdot W_g \cdot Q_g \cdot d}{\rho_w} \qquad \text{(S3-1)}$$

where RH is the relative humidity in the gas injected, W_g is the concentration of water in saturated air (assumed constant and equal to 23×10^{-3} kg water/m^3 at 25°C and 1 bar), Q_g is the gas flow rate (m^3/m^3-d), d is the pond depth (m), and ρ_w is the water density at the reactor temperature (assumed constant and equal to 997 kg/m^3).

In closed photobioreactors, aeration also serves to mix the liquid bulk and is generally applied at a rate of 0.1 - 0.2 vvm (144 - 288 m^3/m^3-d). Thus, as a worse-case scenario, by assuming that CO_2-enriched air is supplied at a high rate of 0.1 vvm during 6 hours per day in the raceway pond, CO_2 supply would only cause an evaporation loss of 0.02-0.05 m^3/m^2-yr in

our case studies, which was much lower than the free surface evaporation rates predicted and was therefore neglected. The supply rate of 0.1 vvm for 6 hr is really high for open pond because CO_2 is mainly provided through atmospheric diffusion. For example, Stephenson et al. (2010) used a value of 0.003 vvm during 8 hr (1445 m^3/d in a pond during 8 hr/d with a working volume of 924 m^3).

References:

Gerbens-Leenes, W.; Hoekstra, A. Y.; van der Meer, T. H. The water footprint of bioenergy. Proc. Natl. Acad. Sci. USA **2009**, *106* (25), 10219-10223.

Stephenson, A. L.; Kazamia, E.; Dennis, J. S.; Howe, C. J.; Scott, S. A.; Smith, A. G. Life-cycle assessment of potential algal biodiesel production in the United Kingdom: a comparison of raceways and air-lift tubular bioreactors. *Energy Fuels* **2010**, *24* (7) 4062–4077.

S3 – Modeling evaporation from algal ponds

The need for a high temporal resolution: The rate of evaporation from an open pond surface is mainly a function of water temperature, air temperature, relative humidity, and wind velocity. These parameters exhibit significant daily variations. Of particular relevance to evaporation, water temperature in shallow algal ponds can easily vary by 10 °C in summer under a temperate climate (Béchet et al., 2011). This relatively high temperature variation is due to the combination of the low thermal inertia of shallow ponds, the high intensities of heat fluxes, and the optical properties of the algal broth (because the broth is opaque, all the visible light energy reaching the broth, except the small fraction used in photosynthesis, contributes to heat generation). Solar radiation can reach 1000 W/m^2 during day time in summer and can therefore increase the water temperature by several degrees Celsius per hour. At night, the combined effects of radiation, evaporation, and convection allows the water temperature to equilibrate with the air temperature. Similarly to water temperature, air temperature, wind velocity and relative humidity usually vary significantly on a daily timescale. Consequently, it is necessary to determine the evaporation rate at a high temporal resolution (1 hour) to generate accurate predictions.

Various models have been developed to predict the evaporation rate from a free water surface. As discussed by Sartori (2000), these models generate different results. The choice of the model is therefore crucial in order to accurately predict the rate of evaporation from an open pond. For example, using an evaporation model determined for a lake would not be appropriate because while ponds are shallow (max 0.3 m) and well mixed, most lakes have a much greater depth (and therefore a higher thermal inertia) and experience thermal

stratification (which slows heat transfer). We invite readers to consult the paper of Béchet et al. (2011) for further discussion on the topic.

The model used to estimate evaporation in this study was developed using a theoretical approach (see Béchet et al., 2011 for more details) and the rate of evaporation m_e (kg/s-m^2) was expressed as:

$$m_e = K\left(\frac{P_w}{T_p} - \frac{RHP_a}{T_a}\right)\frac{M_w}{R_g} \quad \text{(S3-1)}$$

where K is the mass transfer coefficient (m/s); P_a and P_w the saturated vapor pressure (Pa) at the air temperature T_a and the pond temperature T_p (K), respectively; RH is the relative humidity of the air over the pond surface; M_w is the molecular weight of water (kg/mol) and; R_g the ideal gas constant (Pa-m^3/mol-K). The mass transfer coefficient K can be calculated from the Sherwood number Sh_L:

$$Sh_L = \frac{KL}{D_{w,a}} \quad \text{(S3-2)}$$

where L is a characteristic length of the pond (m); and $D_{w,a}$ the diffusivity of water vapor in air (m^2/s). The Sherwood number can be expressed as a function of the Reynolds and the Schmidt numbers as follows:

$$Sh_L = 0.035\left(\mathrm{Re}_L\right)^{0.8}\left(Sch_L\right)^{1/3}, \text{ for } \mathrm{Re}_L > 5.10^5 \text{ (turbulent flow)} \quad \text{(S3-3)}$$

$$Sh_L = 0.628\left(\mathrm{Re}_L\right)^{0.5}\left(Sch_L\right)^{1/3}, \text{ for } \mathrm{Re}_L < 3.10^5 \text{ (laminar flow)} \quad \text{(S3-4)}$$

The Reynolds and the Schmidt numbers are defined as:

$$Sch = \frac{\nu_a}{D_{w,a}} \quad \text{(S3-5)}$$

$$Re_L = \frac{L\nu}{\nu_a} \quad \text{(S3-6)}$$

where v_a is the air kinematic viscosity (m^2/s) and; v is the wind velocity (m/s) at an elevation of 0.5 m from the pond surface. P_a and P_w can be determined using:

$$P_a = 3385.5 \exp\left(-8.0929 + 0.97608\left(T_a + 42.607 - 273.15\right)^{0.5}\right) \quad \text{(S3-7)}$$

$$P_w = 3385.5 \exp\left(-8.0929 + 0.97608\left(T_w + 42.607 - 273.15\right)^{0.5}\right) \quad \text{(S3-8)}$$

In order to estimate evaporation losses, water temperature and evaporation were simultaneously predicted using the temperature model validated by Béchet et al. (2011).

Sensitivity analysis

As discussed in the introduction, the rate of evaporation from the surface of an open water body depends on the water temperature. There is a level of uncertainty in the water temperature prediction by the model of Béchet et al. (2011) due to first, inaccuracy in measurement of the meteorological variables; and second, the uncertainty on input parameters needed for predicting temperature. The objective of this sensitivity analysis was to quantify the influence of these inaccuracies and uncertainties on the predicted rate of evaporation.

The temperature (and hence, the rate of evaporation) is a function of five different meteorological parameters: solar irradiance, air temperature, wind velocity, relative humidity, and precipitation rate. As seen in Figure S3-1, inaccuracy on solar irradiance measurement has a considerable impact on the uncertainly of evaporation prediction, which is logical given that water temperature changes are mainly driven by solar irradiation (Béchet et al, 2011). Wind velocity also significantly influences the rate of evaporation, as shown by equations S3-3,4, and 6, which explains the high sensitivity of this variable shown in Figure S3-1. The

other meteorological variables have a relatively low impact on evaporation due to their low influence on the water temperature.

The input parameters tested in the sensitivity analysis were:

- Air emissivity: this parameter characterizes the amount of long-wave radiation emitted by the atmosphere to the open pond (base case value: 0.8);
- Wind height: the height above the water surface at which the wind velocity must be measured (base case value: 0.5 m);
- Power law exponent: the exponent in the power law used to calculate the wind velocity at the height considered in the evaporation formula (base case value: 0.2);
- Inflow temperature: the temperature of the inflow (base case value: yearly average of the air temperature);
- Pond depth: the working depth of the water column (base case value: 0.25 m);
- PE: photosynthetic efficiency (base case value: 2.5%, expressed as % total radiation);
- HRT: hydraulic retention time (base case value: 7 d);
- Soil characteristics: as the pond is in contact with the ground, heat transfer occurs between the water body and the ground below the pond. This transfer is characterized by the soil specific heat, density, and conductivity (base case values: 1250 J/K-kg, 1900 kg/m^3, 1.7 W/m-K, respectively).

As seen in Figure S3-1, air emissivity has a considerable impact on the rate of evaporation and this is mainly explained because this property has a significant influence on water temperature (Béchet et al, 2011). The power law exponent and the wind height considerably influence the rate of evaporation and this is essentially explained by the impact of the wind velocity on the water saturation above the pond, as can be seen in equations S3-3, 4, and 6.

Interestingly, the pond depth does not significantly impact the evaporation rate (Figure S3-1) despite the significant impact of this parameter on the pond temperature (Béchet et al., 2011). This is explained by a counterbalancing effect on the diurnal and nocturnal rates of evaporation. Indeed, the thermal mass of the pond increases with the water column depth. Therefore, at daytime, the temperature of the pond is lower in a relatively deep pond (e.g. d = 0.4 m) than in a shallow pond (e.g. d = 0.2 m). Consequently, the diurnal rate of evaporation decreases with depth. However, at nighttime, the temperature of water decreases more slowly in the deep pond, explaining why the nocturnal rate of evaporation increases with depth. This however only applied to shallow well mixed (i.e. not stratified) water bodies and the effect of depth on a lake would likely be different. The other parameters tested in this sensitivity analysis have a minor impact on the rate of evaporation, in agreement with their limited impact on the temperature prediction (Béchet et al., 2010). Hence, assuming uniform PE, HRT and soil properties across different location generates little uncertainty on evaporation predictions.

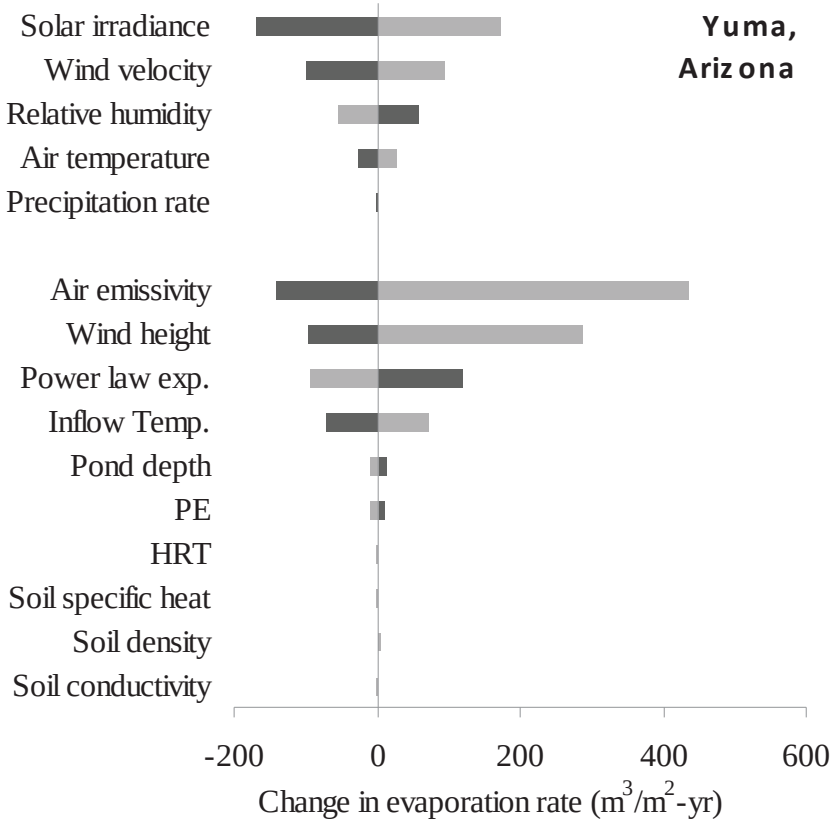
Yuma, Arizona
Solar irradiance
Wind velocity
Relative humidity
Air temperature
Precipitation rate
Air emissivity
Wind height
Power law exp.
Inflow Temp.
Pond depth
PE
HRT
Soil specific heat
Soil density
Soil conductivity
-200
0
200
400
600
Change in evaporation rate (m3/m2-yr)

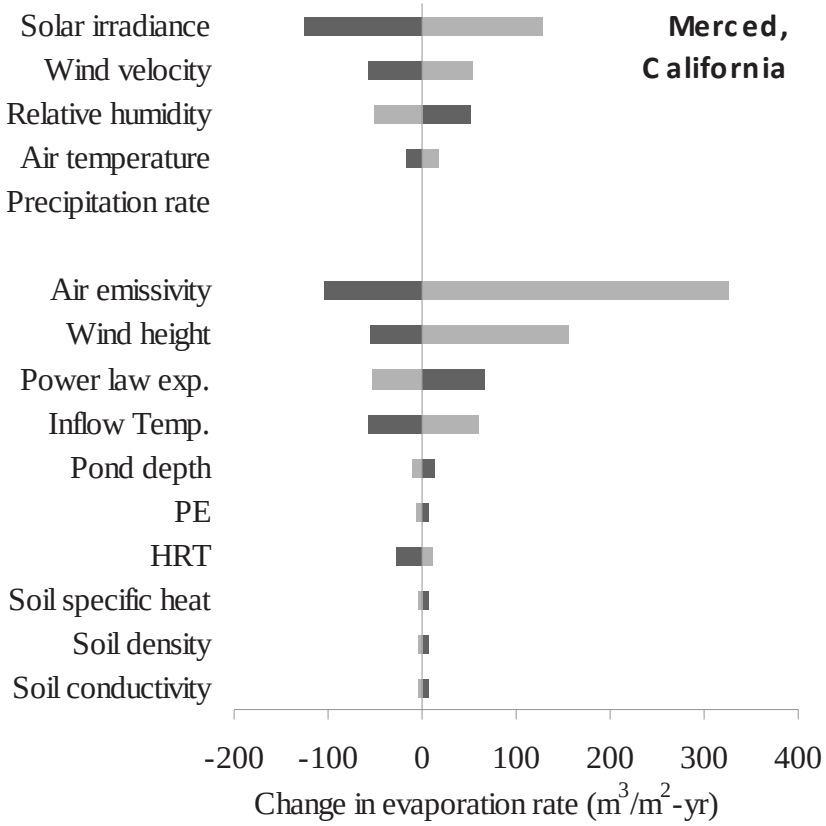
Merced, California
Solar irradiance
Wind velocity
Relative humidity
Air temperature
Precipitation rate
Air emissivity
Wind height
Power law exp.
Inflow Temp.
Pond depth
PE
HRT
Soil specific heat
Soil density
Soil conductivity
-200
-100
0
100
200
300
400
Change in evaporation rate (m3/m2-yr)

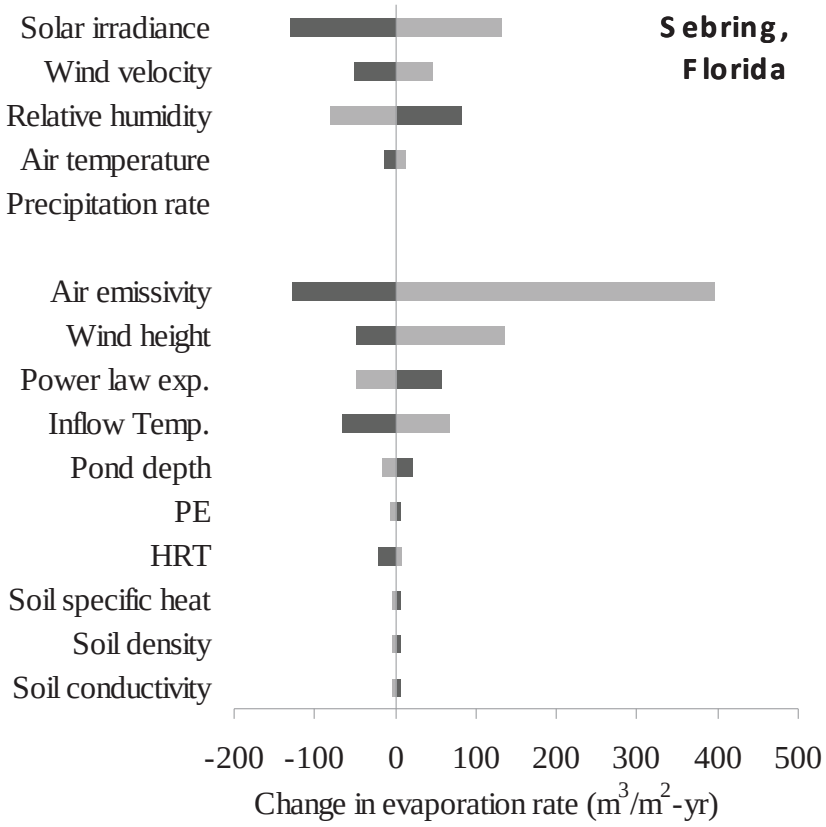
Sebring, Florida
Solar irradiance
Wind velocity
Relative humidity
Air temperature
Precipitation rate
Air emissivity
Wind height
Power law exp.
Inflow Temp.
Pond depth
PE
HRT
Soil specific heat
Soil density
Soil conductivity
-200 -100 0 100 200 300 400 500
Change in evaporation rate (m3/m2-yr)

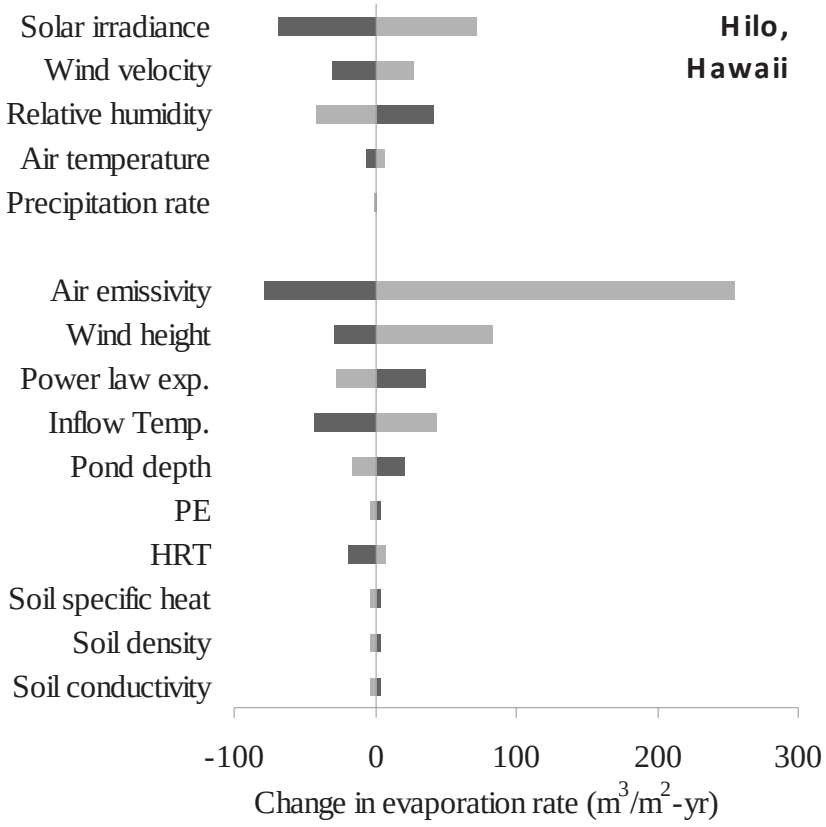
Hilo, Hawaii
Solar irradiance
Wind velocity
Relative humidity
Air temperature
Precipitation rate
Air emissivity
Wind height
Power law exp.
Inflow Temp.
Pond depth
PE
HRT
Soil specific heat
Soil density
Soil conductivity
-100 0 100 200 300
Change in evaporation rate (m3/m2-yr)

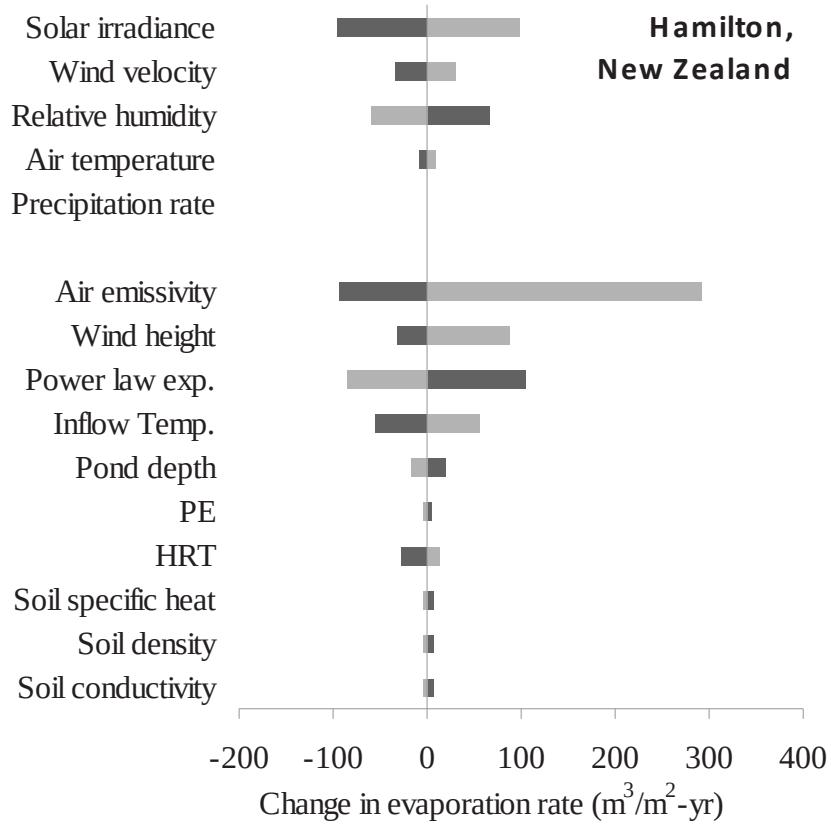

Figure S3-1: Sensitivity analysis of the rate of evaporation computed with the temperature model of Béchet et al. (2011) at the five climatic locations. For each parameter, the light bar represents the change of evaporation rate for the upper value of the variable/parameter and the dark bar represents the change of evaporation rate for the lower value of the variable/parameter. Ranges for the meteorological variables: Solar radiation, ± 10%; Air temperature, ± 0.5 °C; Wind velocity, ± 10%; Relative humidity, ± 10% (maximized at 100%); Precipitation rate, ± 10%. Range for the input parameters: Air emissivity, 0.75 - 0.95; Wind height, 0.3 - 2 m; Power law exponent, 0.09 - 0.29; Inflow temperature, ± 5°C; Pond depth, 0.2 - 0.3 m; PE, 2 to 3 %; HRT, 4 - 10 d; Soil characteristics, ± 50. When the variations are indicated as %, the upper and lower values were calculated as % variations from the base case values.

Past approaches for computing evaporation losses during algae cultivation

As highlighted in S1, various approaches have been used to estimate evaporation losses during algae cultivation in raceway ponds. To quantify the variation generated by the selection of the evaporation method, evaporation rates were predicted using 9 different methods:

Pan-evaporation*:* There are several reasons why the evaporation rate from an algal pond should differ from pan evaporation recorded at the same location. First, a lower amount of the visible light reaching the water is converted into heat in the Class A pan than in the algal pond because the water used in Class-A pans is clear. Secondly, the edges of Class-A pans shelter the water surface from wind, which reduces evaporation. Thirdly, the small size of Class-A pans influences the rate of evaporation because the relative humidity of the layer of air above the water surface varies with the surface area. Pan evaporation data was extracted from the Farnsworth tables (Farnswoth and Edwin, 1982). When the data was unavailable at the exact climatic locations used in our comparative study, the nearest location was selected in the Farnsworth tables (Arizona: Yuma Springs; California: Shasta Dam; Florida: Vero Beach; Hawaii: Hilo Airport; New Zealand: Hamilton).

Lake evaporation model*:* In the studies of Yang et al. (2011) and Frank et al. (2011), the evaporation from algal ponds is assumed to be directly proportional to the pan evaporation:

$$m_e = 0.75 m_{e,PAN} \quad \text{(S3-9)}$$

, where $m_{e,PAN}$ is the rate of evaporation in a Class-A pan (m^3/m^2-yr). This formula was derived originally for lake evaporation and is henceforth named ‘Lake evaporation formula’. This formula is limited because a typical lake has far more thermal inertia than a shallow pond and is often thermically stratified and, consequently, experiences lower temporal

temperature variations. This inertia reduces peak evaporation rates because the lake temperature will most likely never reach the high values experienced in algal ponds.

***Penman equation*:** Penman (1948) derived a semi-empirical formula in order to predict the rate of evaporation from shallow water bodies as a function of meteorological variables. This model was used by Clarens et al. (2010) in their life cycle comparison of algae biofuel production at various locations. Evaporation was thus computed as:

$$m_e = \frac{\Delta I_0 + \gamma \lambda_v \rho_w K_E v\left(P_w - RHP_a\right)}{\lambda_v \rho_w \left(\Delta + \gamma\right)} \quad \text{(S3-10)}$$

where Δ is the slope of the saturated vapor pressure versus temperature curve (Pa/°C), I_0 the solar irradiance (W/m^2), γ the psychometric constant (Pa/°C), λ_v the latent heat of vaporization of water (J/kg), ρ_w the water density (kg/m^3), and K_E a mass transfer coefficient determined empirically (Pa^{-1}). This formula, which includes the solar irradiance in its expression to account for the fact that sun radiation increases water temperature, should be more appropriate to describe evaporation from a free water surface than pan or lake evaporation data. However, its application to an algal pond remains unproven.

Semi-empirical formula accounting for pond temperature

As discussed above, the water temperature of water bodies fluctuates over time and various semi-empirical formulas suitable to predict evaporation rates as a function of the water body temperature are available in the literature. Consequently, applying this type of formula to determine the rate of evaporation from an open water body requires the measurement or prediction of the water temperature. In our comparative analysis we used the temperature model of Béchet et al. (2011) in which alternative expressions of the evaporative heat flux were used.

Model 1 is the formula used by Béchet et al. (2011) described above and used in the computation of evaporation losses in our case studies (equations S3-1 to S3-8).

Model 2: By recording wind velocity, air temperature, relative humidity, water temperature and the rate of evaporation from a small open pond, Tang and Etzion (2004) developed the following empirical relationship:

$$m_e = \frac{\left(0.2253 + 0.24644 v_{0.55}\right)\left(P_w - RHP_a\right)^{0.82}}{L_w} \quad \text{(S3-11)}$$

where L_w is the latent heat of vaporization of water (J/kg). The empirical correlation coefficients are likely specific to the system used for validation (location, design, operation etc) and, given the fact that this formula was validated with a small pond (1.16 m × 1.16 m × 0.22 m), may not be representative of large cultivation systems operated under different climatic conditions.

Model 3: This formula (which exact origin could not be tracked down) was used in a temperature model developed by Klemetson and Rogers (1985) for an aquaculture pond. Evaporation was calculated as:

$$m_e = 4.34.10^{-8}\left(1 + 0.22 v_{8.2}\right)\left(P_w - RHP_a\right) \quad \text{(S3-12)}$$

This formula was derived from an empirical study. As in the case of Model 2, the empirical coefficients are specific to the system used for validation (location, design, operation etc) and there is therefore no certainty that this model can be used to describe evaporation across different locations.

Model 4: The following formula was derived from an experimental study on Lake Hefner (Harbeck, 1952):

$$m_e = \frac{0.038 v_2 \left(P_w - RHP_a\right)}{L_w} \qquad \text{(S3-13)}$$

This model was used in the temperature model developed by Losordo and Piedrahita (1991) for shallow aquaculture ponds. The applicability of this formula is limited by the same aspects discussed above concerning the Lake evaporation formula.

Model 5: This formula was used to model the temperature of aeration basins (Talati and Strenstrom, 1990). The formula, which exact source could not be found, is written as:

$$m_e = \frac{4.8.10^{-5}\left(1.15.10^6\left(1-RH\right)+6.86.10^4\left(T_w - T_a\right)\right)e^{0.0604(T_a-273.15)} S_p{}^{-0.05} v_6}{L_w} \qquad \text{(S3-14)}$$

where S_p is the pond surface (m^2). The main limitation of this formula is that it is based on empirical correlation coefficients.

Model 6: Brady et al. (1969) proposed the following formula for predicting evaporation at the surface of an open water body:

$$m_e = \frac{\left(9.2 + 0.46 v_7{}^2\right)\left(P_w - RHP_a\right)}{L_w} \qquad \text{(S3-15)}$$

This formula was extracted from the study of Edinger et al. (1974) on heat transfer across the surface of large water bodies. It was recently used in combinations with the "EFDC temperature model" for predicting the hydrodynamics and temperature of algal ponds (Scott and Boriah, 2010); and the MASS2 model for predicting the temperature of large bodies of water and used by Wigmosta et al. (2011) in their LCA of algae biodiesel. The main limitation of this formula is that it is based on empirical correlation coefficients.

Results:

As can be seen in Table S3-1, there is a large variation in the magnitudes of evaporation rates predicted at different locations and no model was found to systematically underestimate or overestimate evaporation losses against the others. Interestingly, and although this should be confirmed with a more extensive analysis, the predictions from the 'high-resolution' models seemed less scattered than the predictions from the other approaches. This trend may be explained by the fact that the high-resolution models are based on similar theoretical considerations and inputs (e.g. pond temperature). The lake evaporation model predicted significantly lower evaporation rates in an arid climate than all the other approaches compared, and this is likely explained by the fact that this model does not account for the impact of the high pond temperatures experienced in arid climates. The large variability predicted under tropic climate may be explained by the difficulty to predict air emissivity in the presence of clouds.

Table S3-1: Rate of evaporation from an open pond using nine models over five climatic zones.

Evaporation (m^3/m^2-yr)	**Pan**	**Lake model**	**Penman**	**Model 1**	**Model 2**	**Model 3**	**Model 4**	**Model 5**	**Model 6**	**E_{max} [a]**	**RSD (%) [b]**
Yuma, AZ	2.14	1.50	2.72	2.27	2.97	3.06	2.30	2.91	2.88	1.56	20
Merced, CA	1.86	1.30	1.96	1.32	1.85	1.85	1.26	1.74	1.62	0.70	17
Sebring, FL	1.66	1.16	1.98	1.15	1.62	1.62	1.14	1.53	1.49	0.84	19
Hilo, HI	1.79	1.26	1.46	0.48	0.96	1.02	0.48	0.71	0.92	1.32	44
Hamilton, NZ	0.88	0.62	1.39	0.74	1.12	1.06	0.73	1.02	0.96	0.78	25

[a] E_{max} represents the maximum error reported (difference between highest and lowest evaporation prediction)

[b] RSD = Relative Standard Deviation = 100×SD/Average

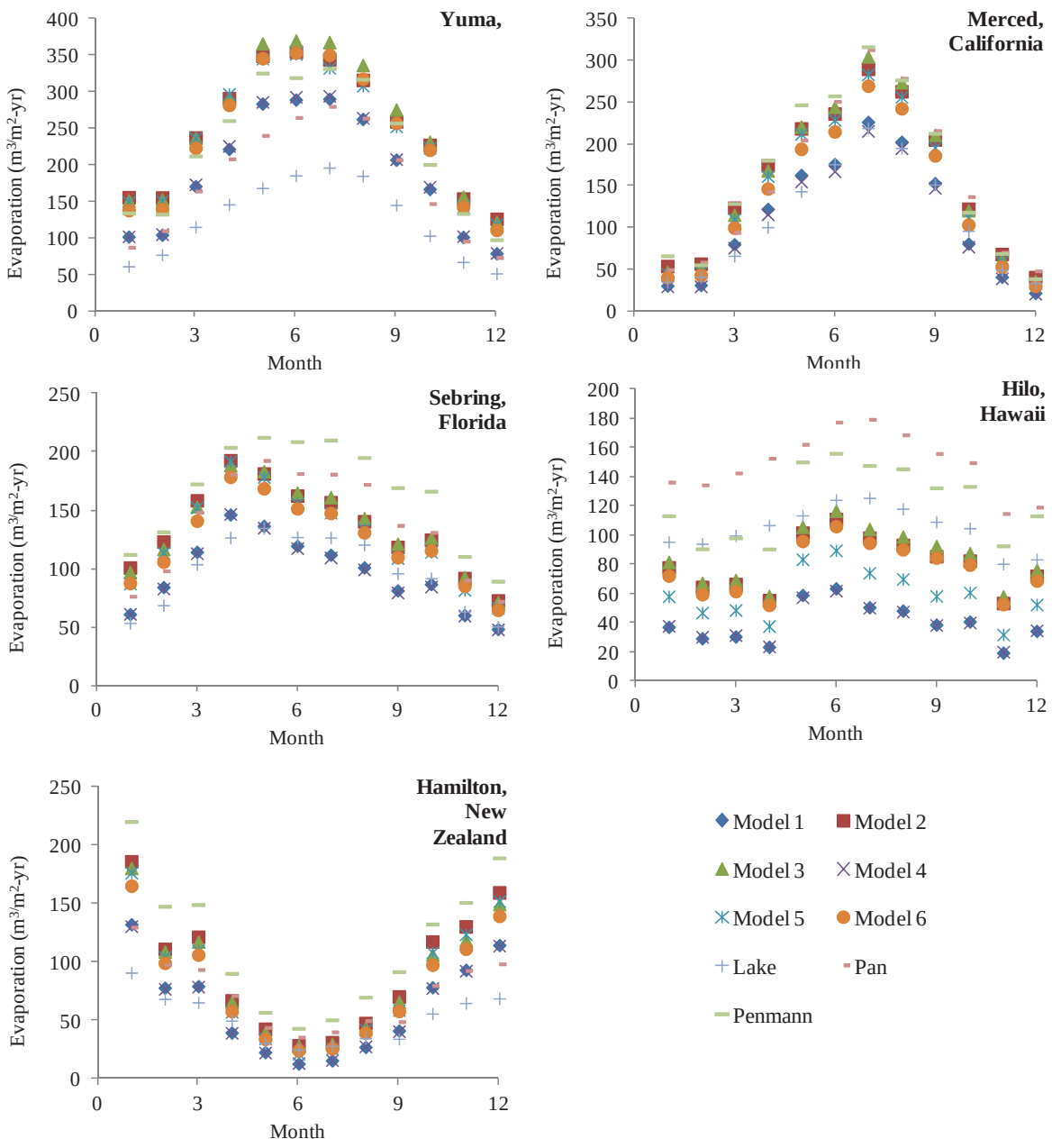

Figure S3-2: Monthly evaporation rates predicted at five different climatic zones using different models.

References

Béchet, Q.; Shilton, A.; Park, J. B.; Craggs, R. J.; Guieysse, B. Universal temperature model for shallow algal ponds provides improved accuracy. *Environ. Sci. Technol*. **2011**, *45* (8), 3702-3709.

Brady, D. K.; Graves, W.L.; Geyer, J.C. **1969**.Surface Heat Exchange at Power Plant Cooling Lakes - Report #5, Edison Electric Institute Publication #69-901, New York, NY.

Clarens, A. F.; Resurreccion, E. P.; White, M. A.; Colosi, L. M. Environmental life cycle comparison of algae to other bioenergy feedstocks. *Environ. Sci. Technol*. **2010**; *44* (5), 1813-1819.

Edinger J.E.; Brady, D.K.; Geyer, J.C. Heat Exchange and transport in the environment – Report #14, Edison Electric Institute Publication, New York, NY.

Farnsworth, R. K.; Edwin S.T. Mean Monthly, seasonal, and annual pan evaporation for the United States. USDC, NOAA, National Weather Service. **1982;** NOAA Technical Report NWS 34.

Frank, E. D.; Han, J.; Palou-Rivera, I.; Elgowainy, A.; Wang, M. Q. Life Cycle Analysis of Algal Lipid Fuels with the GREET Model. **2011**. Argonne National Laboratory, US Department of Energy.

Klemetson, S. L; Rogers, G., L. Aquaculture pond temperature modelling. *Aquac. Eng.* **1985**, *4*, 191-208.

Losordo, T. M.; Piedrahita, R. H. Modelling temperature variation and thermal stratification in shallow aquaculture ponds. *Ecol. Modell.* **1991**, *54*, 189-226.

Penman, H.L. Natural evaporation from open water, bare soil and grass. Proc. Roy. Soc. London **1948**; A(194), 120-145.

Perkins, W.A.; Richmond M.C. MASS2, Modular Aquatic Simulation System in Two Dimensions, Theory and Numerical Methods. **2004** PNNL-14820-1, Pacific Northwest National Laboratory, Richland, Washington 99352.

Rosati, A.; Miyakoda, K. A general circulation model for upper ocean simulation. *J Phys. Ocean.* **1988**, *18*, 1601-1626.

Sander, K.; Murthy, G. S. Life cycle analysis of algae biodiesel. *Int. J. Life Cycle Assess.* **2010**, *15*, 704-714.

Sartori, E. A critical review on equations employed for the calculation of the evaporation rate from free water surfaces. *Sol. Energy.* **2000**, *68* (1), 77-89.

Scott, C.J.; Boriah V. Modeling Algae Growth in an Open-Channel Raceway. J Comput. Biol. **2010**, *17(7)*, 895-906.

Talati, S. N.; Stenstrom, M. K. Aeration-basin heat loss. *J. Environ. Eng.* **1990**, *116* (1), 70-86.

Tang, R.; Etzion, Y. Comparative studies of the water evaporation rate from a wetted surface and that from a free water surface. *Build. Environ.* **2004**, *39*, 77-86.

Wigmosta, M.L. ; Coleman A. M., Skaggs, R.J.; Huesemann, M.H.; Lane, L.J. National microalgae biofuel production potential and resource demand. *Water. Res. Demand.* **2011,** *47*.

Yang, J.; Xu, M.; Zhang, X.; Hu, Q.; Sommerfeld, M.; Chen, Y. Life-cycle analysis on biodiesel production from microalgae: water footprint and nutrients balance. *Bioresour. Technol.* **2011**, *102* (1), 159-165.

S4 – Modeling productivity during algae cultivation

Predicting biomass productivity during outdoor algae cultivation in raceway ponds is challenging because the effect of light intensity and temperature on the light and dark reactions of photosynthesis are complex, interconnected and particularly difficult to predict under transient conditions.

Wigmosta et al. (2011) recently attempted to account for the effects of light saturation and temperature on algal productivity by using a light saturation function and setting the temperature range outside which algal growth becomes limited. Unfortunately, and although this approach may reasonably predict productivity for a specific location and algal species, algae response to light and temperature is likely location-dependent due to microbial acclimation during long-term cultivation and because different strains or species will likely be used at different locations to optimize productivity. Uncertainty is also introduced by considering that the threshold for light saturation is temperature independent.

We also refrained from the use of experimental productivity estimates (Clarens et al. 2010) for comparing the impacts of water use across locations because bias may be introduced if different species or operational practices have been used at the different locations considered. Instead, we assert that a more realistic approach is to use the assumption of a uniform photosynthetic efficiency (PE) across locations. The value of 2.5% was used in line with 'pragmatic' recommendations from Walker (2009). This approach yielded areal productivities well within the values reported during full-scale algae production, as shown in Table S4-1. For further comparison, Lardon et al. (2009) predicted productivities of 19.25-24.75 g/m^2-d in a Mediterranean climate; Frank et al. (2011) used a yearly averaged productivity of 25 g/m^2-d in Arizona; Lundquist et al. (2011) used a value of 22 g/m^2-d in

South California; and Park et al. (2011) cited productivities of 12.9 – 40 g/m^2-d during commercial algae production.

Table S4-1: Productivities predicted in the 5 cases studies versus productivities reported in the literature.

Climate	**Solar irradiance (GJ/m^2-yr)**	**Average productivity (g/m^2-d)**		
		This study	Murphy and Allen, 2011	Yang et al., 2010
Arid	7.73	21.4	22.10	31.4
Mediterranean	6.59	18.3	21.70	16.6
Subtropical	6.41	17.8	24.70	22.9
Tropical	5.01	13.9		22.9
Temperate	5.44	15.1	19.4[a]	16.0[a]

[a] Values for South Carolina

Unfortunately, assuming a constant PE across locations biases the comparison of WF ratios towards high-productivity locations, which are also often arid and semi-arid areas experiencing high water stress, as discussed in the main manuscript. This intrinsic 'productivity buffering effect' is compounded if biomass productivity is further linearly correlated with air temperature, as done by Yang et al. (2011), although there is no clear scientific foundation for this relationship.

References

Clarens, A. F.; Resurreccion, E. P.; White, M. A.; Colosi, L. M. Environmental life cycle comparison of algae to other bioenergy feedstocks. *Environ. Sci. Technol*. **2010**; *44* (5), 1813-1819.

Cooney, M. J.; Young, G.; Pate, R. Bio-oil from photosynthetic microalgae: Case study. *Bioresour. Technol*. **2011**. *102*, 166-177.

Frank, E. D.; Han, J.; Palou-Rivera, I.; Elgowainy, A.; Wang, M.Q. Life Cycle Analysis of Algal Lipid Fuels with the GREET Model. **2011**. Argonne National Laboratory, US Department of Energy.

Lardon, L.; Helias, A.; Sialve, B.; Steyer, J. P.; Bernard, O. Life-cycle assessment of biodiesel production from microalgae. *Environ. Sci. Technol.* **2009**, *43* (17), 6475-6481.

Lundquist, T.J.; Woertz, I.C.; Quinn, N.W.T.; Benemann, J.R. A Realistic Technology and Engineering Assessment of Algae Biofuel Production. Energy Biosciences Institute, University of California Berkeley, **2010**.

Park, J. B. K.; Craggs, R. J.; Shilton, A. N. Wastewater treatment in high rate algal ponds for biofuel production. *Bioresour. Technol*. **2011**, *102*, 35-42.

Wigmosta, M. S.; Coleman, A. M.; Skaggs, R. J.; Huesemann, M. H.; Lane, L. J. National microalgae biofuel production potential and resource demand. *Water Resour. Res.* **2011**, *47*, W00H04; doi:10.1029/2010WR009966

Yang, J.; Xu, M.; Zhang, X.; Hu, Q.; Sommerfeld, M.; Chen, Y. Life-cycle analysis on biodiesel production from microalgae: water footprint and nutrients balance. *Bioresour. Technol.* **2011**, *102* (1), 159-165.

Walker, D. Biofuels, facts, fantasy, and feasibility. *J. Appl. Phycol.* **2009**, *21* (5), 509-517.

S5 – Influence of HRT on algal productivity in ponds

As seen in the manuscript, the WD (m^3/m^2-yr) within the system boundary considered can be calculated as the sum of the amount of freshwater required to make up for evaporation losses (Q_{ev}, m^3/m^2-yr), leak losses (Q_{leak}, m^3/m^2-yr) and the process water that is not recycled back into the pond (Q_{pw}, m^3/m^2-yr). The 'process water' component Q_{pw} was then estimated by fixing the value of average hydraulic retention time (HRT) in accordance with operational guidelines, as done by Murphy and Allen, (2011) and Cooney et al. (2011). Thus, Q_{pw} was calculated as:

$$Q_{pw} = \frac{(1-R)\cdot T \cdot V}{HRT \cdot A} = \frac{(1-R)\cdot T \cdot d}{HRT} \qquad \text{(S5-1)}$$

where R is the fraction of the process water that is recycled into the pond, T is the number of operational days per year (d/yr), HRT is the yearly-averaged mean hydraulic retention time in the pond (d), V is the working volume of the cultivation system (m^3), A is the pond area (m^2) and d is the liquid depth in the pond (m).

Alternatively, Q_{pw} can be computed based on yearly-averaged biomass productivity by fixing the value of average algae concentration at harvesting (Yang et al., 2011; Lardon et al., 2009; Frank et al., 2011) and estimating the corresponding hydraulic retention time as:

$$HRT = \frac{d \cdot A}{P_{a\,lg\,ae}} \qquad \text{(S5-2)}$$

Where P_{algae} is the areal algae productivity (g/m^2-d).

If both methods are suitable for calculating the yearly WD, more realistic optional scenarios (e.g. seasonally adjusted HRT, number of operational days) must however be considered if a high-temporal accuracy is requested (Lundquist et al., 2011).

The ‘fixed HRT’ and ‘fixed concentration’ approaches should yield similar values to the process water component of the WD if similar considerations are given to the maximum algae growth rate (to determine a reasonable HRT, Murphy and Allen, 2011), light utilization efficiency (to determine the optimum algal biomass concentration in the pond for a given light regime), and harvesting costs. We used the ‘fixed HRT’ approach in this study because it removes the variability and uncertainly associated with the biomass heat value (kJ/g). However, while Cooney et al. (2011) considered an HRT range of 2-33 d in their sensitivity analysis, we reduced this range to 4-10 d in order to maintain the yearly-averaged concentrations within the 0.2-1.0 kg/m^3 guidelines for outdoor algae cultivation in open ponds (Stephenson et al., 2011; Lardon et al., 2009; Yang et al., 2011; Cooney et al., 2011; Murphy and Allen, 2011).

Table S5-1: Yearly averaged algae concentration predicted at each location (photosynthetic efficiency = 2.5% ,heat value = 24.7 kJ/g).

HRT	**4 days**	**7 days**	**10 days**
Arid	343	601	858
Mediterranean	293	512	731
Subtropical	285	498	711
Tropical	222	389	556
Temperate	241	423	604

Limit to increasing the HRT: In light-limited open ponds, algae productivity is mainly a function of the amount of light energy reaching the algae and subsequently converted into biochemical energy during photosynthesis. However, the HRT impacts productivity because

this parameter controls the algae concentration maintained in the pond and thereby, the 'dark' volume in the system (light does not penetrate below a certain depth). Thus, the more time the algae are kept in the system, the more time and space is given for dark respiration to occur, which reduces the overall productivity. The target HRT (or culture harvesting rate) should therefore depend on the climatic conditions experienced by the algae (solar irradiance influences light penetration and temperature influences the rate of dark respiration) as well as the type of algae cultivated, the target biomass composition (bio-oil and lipid synthesis typical requires nutrient deprivation and long cell age), and the desired algae concentration at harvesting. Hence, a high HRT could help reducing harvesting costs and water consumption, but it can also impact productivity.

Influence of climatic conditions of the HRT: In our case studies, biomass productivity was calculated by assuming that the HRT was uniform across all locations considered because it is currently impossible to predict how process operation will be controlled as a function of environmental parameters during large-scale algae cultivation. This assumption disregards the fact that a smaller HRT is needed to achieve the same biomass concentration at harvesting under high-productivity conditions (i.e. high light irradiance) than under low-productivity conditions, as seen in Table S5-2. It might therefore be preferable to reduce the HRT under high-productivity conditions if biomass loss at night (due to dark respiration) is a significant issue (e.g. it can consume up to 25% of the daily biomass output; Chisti, 2008). High HRT operation may also favor the accumulation of debris and bioproducts, with consequences on the efficiencies of light transmission, the efficiency of process water recycling, and predation/contamination risks.

Table S5-2: Average HRT (d) needed to maintain algae concentration of 500 g/m^2 (Frank et al, 2011) at harvesting (photosynthetic efficiency = 2.5%, algal biomass heat value = 24.7 kJ/g, pond depth = 0.25 m).

	Solar irradiance (GJ/yr)	**Productivity (g/m^2-d)**	**Average HRT (d)**	**WD m3/m2-yr**
Arid	7.73	21.4	5.8	5.19
Mediterranean	6.59	18.3	6.8	4.74
Subtropical	6.41	17.8	7.0	4.66
Tropical	5.01	13.9	9.0	4.97
Temperate	5.44	15.1	8.3	4.88

It is interesting to notice that maintaining an algae concentration of 1000 g/m^3, which has been proposed by Yang et al. (2010), would require operating ponds at HRT values of 11.7-18.0 d in our case studies. These values are significantly higher than the HRTs proposed by other authors in the field (e.g. 4-6 d for Lundquist et al., 2011; 3.33 d for Cooney et al., 2011; or 2 d for Murphy and Allen, 2011).

References:

Chisti, Y. Biodiesel from microalgae beats bioethanol. *Trends Biotechnol.* **2008**, *26* (3), 126-131.

Cooney, M. J.; Young, G.; Pate, R. Bio-oil from photosynthetic microalgae: Case study. *Bioresour. Technol*. **2011**. *102*, 166-177.

Frank, E. D.; Han, J.; Palou-Rivera, I.; Elgowainy, A.; Wang, M. Q. Life Cycle Analysis of Algal Lipid Fuels with the GREET Model, 2011. Argonne National Laboratory,

Lardon, L.; Helias, A.; Sialve, B.; Steyer, J. P.; Bernard, O. Life-cycle assessment of biodiesel production from microalgae. *Environ. Sci. Technol.* **2009**, *43* (17), 6475-6481.

Lundquist, T. J.; Woertz, I. C.; Quinn, N. W. T.; Benemann, J. R. A Realistic Technology and Engineering Assessment of Algae Biofuel Production. Energy Biosciences Institute, University of California Berkeley, **2010**. http://digitalcommons.calpoly.edu/cenv_fac/188/

Murphy, C. C.; Allen D. T. Energy-water nexus for mass cultivation of algae. *Environ. Sci. Technol.* **2011**, *45* (13), 5861-5868.

Stephenson, A. L.; Kazamia, E.; Dennis, J. S.; Howe, C. J.; Scott, S. A.; Smith, A. G. Life-cycle assessment of potential algal biodiesel production in the United Kingdom: a comparison of raceways and air-lift tubular bioreactors. *Energy Fuels* **2010**, *24* (7) 4062–4077.

Yang, J.; Xu, M.; Zhang, X.; Hu, Q.; Sommerfeld, M.; Chen, Y. Life-cycle analysis on biodiesel production from microalgae: water footprint and nutrients balance. *Bioresour. Technol.* **2011**, *102* (1), 159-165.